TARGETING PANCREATIC CANCER: STRATEGIES AND HOPES

EDITED BY: Kanjoormana Aryan Manu, Harikumar K. B. and Takatsugu Ishimoto

PUBLISHED IN: Frontiers in Oncology

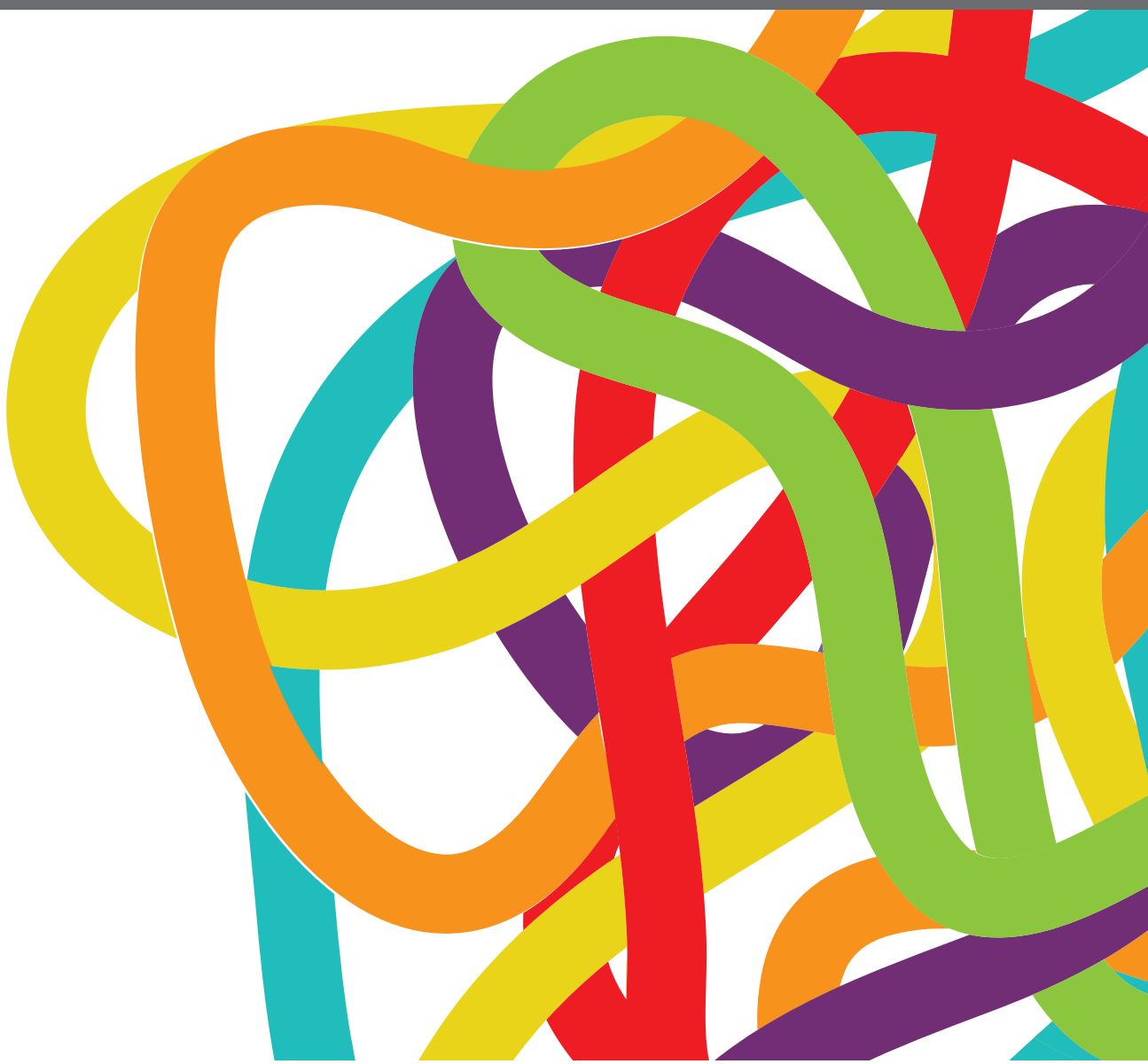

frontiers Research Topics

ISSN 1664-8714
ISBN 978-2-88974-991-1
DOI 10.3389/978-2-88974-991-1

About Frontiers

Frontiers is more than just an open-access publisher of scholarly articles: it is a pioneering approach to the world of academia, radically improving the way scholarly research is managed. The grand vision of Frontiers is a world where all people have an equal opportunity to seek, share and generate knowledge. Frontiers provides immediate and permanent online open access to all its publications, but this alone is not enough to realize our grand goals.

Frontiers Journal Series

The Frontiers Journal Series is a multi-tier and interdisciplinary set of open-access, online journals, promising a paradigm shift from the current review, selection and dissemination processes in academic publishing. All Frontiers journals are driven by researchers for researchers; therefore, they constitute a service to the scholarly community. At the same time, the Frontiers Journal Series operates on a revolutionary invention, the tiered publishing system, initially addressing specific communities of scholars, and gradually climbing up to broader public understanding, thus serving the interests of the lay society, too.

Dedication to Quality

Each Frontiers article is a landmark of the highest quality, thanks to genuinely collaborative interactions between authors and review editors, who include some of the world's best academicians. Research must be certified by peers before entering a stream of knowledge that may eventually reach the public - and shape society; therefore, Frontiers only applies the most rigorous and unbiased reviews.
Frontiers revolutionizes research publishing by freely delivering the most outstanding research, evaluated with no bias from both the academic and social point of view. By applying the most advanced information technologies, Frontiers is catapulting scholarly publishing into a new generation.

What are Frontiers Research Topics?

Frontiers Research Topics are very popular trademarks of the Frontiers Journals Series: they are collections of at least ten articles, all centered on a particular subject. With their unique mix of varied contributions from Original Research to Review Articles, Frontiers Research Topics unify the most influential researchers, the latest key findings and historical advances in a hot research area! Find out more on how to host your own Frontiers Research Topic or contribute to one as an author by contacting the Frontiers Editorial Office: frontiersin.org/about/contact

TARGETING PANCREATIC CANCER: STRATEGIES AND HOPES

Topic Editors:
Kanjoormana Aryan Manu, Amala Cancer Research Centre, India
Harikumar K. B., Rajiv Gandhi Centre for Biotechnology, India
Takatsugu Ishimoto, Kumamoto University, Japan

Citation: Manu, K. A., Harikumar, K. B., Ishimoto, T., eds. (2022). Targeting Pancreatic Cancer: Strategies and Hopes. Lausanne: Frontiers Media SA. doi: 10.3389/978-2-88974-991-1

Table of Contents

frontiers in Oncology

EDITORIAL
published: 31 March 2022
doi: 10.3389/fonc.2022.873682

Editorial: Targeting Pancreatic Cancer: Strategies and Hopes

Kanjoormana Aryan Manu[1*], *Kuzhuvelil B. Harikumar*[2] *and Takatsugu Ishimoto*[3]

[1] Department of Immunology, Amala Cancer Research Centre, Thrissur, India, [2] Cancer Research Program, Rajiv Gandhi Centre for Biotechnology (RGCB), Thiruvananthapuram, India, [3] Takatsugu Ishimoto, International Research Centre for Medical Sciences, Kumamoto University, Kumamoto, Japan

Keywords: pancreatic cancer, therapeutics, tumor microenvironment, metastasis, nomograms

Editorial on the Research

Targeting Pancreatic Cancer: Strategies and Hopes

Last couple of decades showed remarkable progress in the area of cancer research which improved the quality of diagnosis and treatment, resulted in substantial increase in cancer recovery rate. But the scenario is different for Pancreatic cancers, where the percentage of mortality is still as high as 95% which failed to decline. A study in 28 European countries, projected that pancreatic cancer will surpass breast cancer as the third leading cause of cancer death by 2025 (1). Surgical resection is the only possible treatment for pancreatic cancers which can be followed by adjuvant chemo therapies. To date there is no targeted therapy available for pancreatic cancers and it is the need of the hour to be more focused on pancreatic cancer and compile recent research outputs which help us to design our future directions. Our Research Topic was designed to look at the current and future strategies of pancreatic cancer treatments which may give hope to the patients. This Research Topic consists of 13 articles including 8 Original research articles, 4 reviews and 1 case report.

Development of early diagnosis and use of an effective personalised approach is one of the promising strategies to improve therapeutic outcome in pancreatic cancer patients. Miyabashi et al. have reviewed the promising details of combining genome-based medicine with drug screening based on personalized models which may direct to the use of precision medicine for pancreatic cancer. The liquid biopsy and use of three-dimensional organoid culture or patient-derived xenografts platforms also have been discussed in the review article.

Takahashi et al. have described the development of a novel method to detect pancreatic tumors using a tumor-specific enzyme-activatable fluorescence probe which helps rapid and real-time visualization of pancreatic cancer through the enzymatic activities of cancer tissues. This novel technique can accurately identify the extent of the tumor before and during surgery.

Use of bioinformatics tools and machine learning algorithms may be useful for predicting pancreatic cancer patient prognosis. Li et al. discussed the use of the 'Extreme gradient boosting classifier' (XGBoost) to predict CD8+ tumor-infiltrating lymphocyte expression levels in patients with pancreatic ductal adenocarcinoma (PDAC) using CT radiomic features. Tan et al. constructed a novel four genes signature to predict the prognosis of Stages III and IV PDAC patients by applying WGCNA and CIBERSORT algorithm scoring to transcriptome data different from traditional methods of filtrating for differential genes in cancer and healthy tissues. The findings may provide reference to predict survival and be beneficial for individualized management of advanced PDAC patients.

Pappalardo et al. published a review in this special issue on the current treatment scenario and new potential therapeutic approaches in early stage PDAC, from both preclinical and clinical point

OPEN ACCESS

Edited and reviewed by:
Liang Qiao,
Westmead Institute for Medical Research, Australia

***Correspondence:**
Kanjoormana Aryan Manu
manu.aryan@amalaims.org

Specialty section:
This article was submitted to Gastrointestinal Cancers: Hepato Pancreatic Biliary Cancers, a section of the journal Frontiers in Oncology

Received: *11 February 2022*
Accepted: *07 March 2022*
Published: *31 March 2022*

Citation:
Manu KA, Harikumar KB and Ishimoto T (2022) Editorial: Targeting Pancreatic Cancer: Strategies and Hopes. Front. Oncol. 12:873682. doi: 10.3389/fonc.2022.873682

of view. Lewis et al. published their new finding of a rabbit monoclonal antibody specific for human alternatively spliced tissue factor (asTF) and evaluated its binding characteristics and assessed its *in vivo* properties. Peng et al. evaluated the efficacy of hepatic artery infusion (HAI) of floxuridine (FUDR) in combination with systemic chemotherapy in patients with pancreatic cancer liver metastases (PCLM).

YAP1 is a transcriptional coactivator and a downstream effector of Hippo signaling (2). It has been reported to process a significant role in development of PDAC and progression (3). Gao et al. did a thorough study and showed that both YAP1-1 and YAP1-2 isoforms are important mediators in the EMT process of pancreatic cancer. Hayashi et al. reviewed the role of YAP in PDACs and summarised the biological significance of a dysregulated Hippo signaling pathway PDACs.

Tumor microenvironment consists cancer associated fibroblasts, $CD4^+$ T cells and myeloid cells, which are linked and can influence each other which contribute to cancer cell plasticity, invasiveness, metastasis, chemo-resistance, immunotherapy-resistance and radiotherapy-resistance (4). In a review, Du et al. characterized prevailing population of stromal cells in Pancreatic Ductal Adenocarcinoma tumors and how it interact with the other components of tumor microenvironment leading to tumor progression and described how the re-programming of tumor microenvironment improve treatment outcome for pancreatic cancer patients.

Lewis et al. described the pre-clinical evaluation of a humanized antibody targeting alternatively spliced tissue factor. It shows significant activity as a single agent and RNAseq analysis of tumors treated with this monoclonal antibody showed a significant decrease in the expression of genes associated with focal adhesion and cell cycle progression.

Identification of new targetable genes or proteins are important in developing novel therapeutics. Lack of targeted therapy is the major setback for pancreatic cancer treatment. In this Research Topic, Chen et al. reported identification of a novel miRNA hsa-mir-4772 and two novel genes (COL12A1 and COL5A2) associated with pancreatic cancer, which can be used as prognostic factors and therapeutic targets for pancreatic cancer.

Raoul et al. published a case study of a young woman with long term stabilization of a G2 metastatic pancreatic NET that, after pregnancy, suddenly progressed into one single liver metastasis corresponding to a transformation into G3 large-cell neuroendocrine cancer. Authors are raising a question for future research about the role of temozolomide which used in this patient in combination with capecitabine during G2 metastatic pancreatic NET treatment.

More focus has been required in pancreatic cancer research in order to develop early diagnosis methodologies and targeted medicines to tackle this disease and reduce mortality. Development of new liquid biopsy techniques give hopes for the people to get the disease diagnosed early which certainly improves the survival chance of patients. Use of personalised therapies, developing neoadjuvant treatments, combination therapies and identifying new molecular targets in cells and tumor microenvironment are also highly promising to give hope for patients. Parallel developments in the area of bioinformatics and new deep learning, data science and machine learning approaches and its application in pancreatic cancer research and therapy also gives ample hope for us. This Research Topic not only compiles research outputs in the field but also gives a real hope that 'the light of success' is not very far.

AUTHOR CONTRIBUTIONS

KM has written the editorial. HB and TI reviewed and edited the editorial. All authors contributed to the article and approved the submitted version.

REFERENCES

1. Sung H, Ferlay J, Siegel RL, Laversanne M, Soerjomataram I, Jemal A, et al. Global Cancer Statistics 2020: Globocan Estimates of Incidence and Mortality Worldwide for 36 Cancers in 185 Countries. *CA Cancer J Clin* (2021) 71 (3):209–49. doi: 10.3322/caac.21660
2. Moroishi T, Hansen CG, Guan KL. The Emerging Roles of Yap and Taz in Cancer. *Nat Rev Cancer* (2015) 15(2):73–9. doi: 10.1038/nrc3876
3. Mao W, Mai J, Peng H, Wan J, Sun T. Yap in Pancreatic Cancer: Oncogenic Role and Therapeutic Strategy. *Theranostics* (2021) 11(4):1753–62. doi: 10.7150/thno.53438
4. Ho WJ, Jaffee EM, Zheng L. The Tumour Microenvironment in Pancreatic Cancer - Clinical Challenges and Opportunities. *Nat Rev Clin Oncol* (2020) 17 (9):527–40. doi: 10.1038/s41571-020-0363-5

Conflict of Interest: The authors declare that the research was conducted in the absence of any commercial or financial relationships that could be construed as a potential conflict of interest.

frontiers in Oncology

CASE REPORT
published: 31 March 2021
doi: 10.3389/fonc.2021.646992

Case Report: Grade 2 Metastatic Pancreatic Neuroendocrine Tumor With Progression of One Metastasis After Pregnancy to Grade 3 Large-Cell Neuroendocrine Carcinoma: One Case Cured by Resection With Genomic Characterization of the Two Components

Jean-Luc Raoul[1], Marie-Françoise Heymann[2], Frédéric Dumont[3], Alain Morel[4], Hélène Senellart[1] and François Bertucci[5]*

[1] Department of Medical Oncology, Institut de Cancérologie de l'Ouest, Saint-Herblain, France, [2] Department of Pathology, Institut de Cancérologie de l'Ouest, Saint-Herblain, France, [3] Department of Surgery, Institut de Cancérologie de l'Ouest, Saint-Herblain, France, [4] Department of Oncopharmacology, Institut de Cancérologie de l'Ouest, Angers, France, [5] Predictive Oncology Laboratory, Department of Medical Oncology, CRCM, Institut Paoli-Calmettes, Aix-Marseille Université, Marseille, France

Temporal and spatial tumor heterogeneity can be observed in pancreatic neuroendocrine tumor. We report the case of a young woman with long term stabilization of a G2 metastatic pancreatic NET that, after pregnancy, suddenly progressed into one single liver metastasis corresponding to a transformation into G3 large-cell neuroendocrine cancer. The patient underwent liver resection (the progressive and one dormant metastasis). With a 45 months follow-up the patient is without evolutive disease. Exome sequencing of the two metastases revealed completely different genomic signatures and gene alterations: the dormant metastasis was MSS without any gene alteration; the poorly differentiated tumor was MSI, with gain of many mutations including MEN1, BCL2, MLH1 and TP53 corresponding to a mutational signature 11. Could temozolomide play a role in this transformation?

Keywords: sporadic gastrinoma, metastases, surgery, genomics, MEN 1 gene, microsatellite instability, MLH1

OPEN ACCESS

Edited by:
Kanjoormana Aryan Manu, Amala Cancer Research Centre, India

Reviewed by:
Sunu Cyriac, Amala Institute of Medical Sciences, India
Aranzazu Fariña Sarasqueta, Amsterdam University Medical Center, Netherlands

****Correspondence:***
Jean-Luc Raoul
jean-luc.raoul@ico.unicancer.fr

Specialty section:
This article was submitted to Gastrointestinal Cancers, a section of the journal Frontiers in Oncology

Received: *28 December 2020*
Accepted: *16 March 2021*
Published: *31 March 2021*

Citation:
Raoul J-L, Heymann M-F, Dumont F, Morel A, Senellart H and Bertucci F (2021) Case Report: Grade 2 Metastatic Pancreatic Neuroendocrine Tumor With Progression of One Metastasis After Pregnancy to Grade 3 Large-Cell Neuroendocrine Carcinoma: One Case Cured by Resection With Genomic Characterization of the Two Components. Front. Oncol. 11:646992. doi: 10.3389/fonc.2021.646992

INTRODUCTION

Gastroenteropancreatic neuroendocrine neoplasia (NEN) are low in incidence but high in prevalence due to their usual good prognosis even when metastatic (1). They represent a very heterogeneous group of tumors, particularly regarding their behavior. The pathological features, mainly based on proliferation index (assessed by Ki67 immunohistochemistry labeling) and

differentiation, have a major prognostic value (2). The WHO 2017 grading classification for pancreatic NEN (3) endorses the WHO 2010 principles. Neuroendocrine tumors (NETs) are well differentiated and composed of three grades (G): G1 (Ki67 <3%), G2 (Ki67 3%–20%), and G3 (>20%). Neuroendocrine carcinomas (NEC) correspond to poorly differentiated tumors, by default G3, and can involve large-cell or small-cell types. They differ from NETs with respect to clinical and biological features, outcome, and treatment. Yet some problems remain, including temporal and spatial tumor heterogeneity. The disease can evolve with time from grades G1–G2 to G3 and eventually toward a poorly differentiated NEC. The grade can differ between different sites in the same tumor and the same patient, and heterogeneity is even more frequent between the primary and the metastases, particularly when metachronous (4). A molecular classification will certainly be helpful in the near future (5).

Here, we report the case of a young woman with very long-term stabilization of a G2 metastatic pancreatic NET that, after pregnancy, suddenly progressed into one single liver metastasis corresponding to a transformation into G3 large-cell NEC. The patient underwent liver resection (the progressive and one dormant metastases). Exome sequencing of the two metastases revealed completely different genomic signatures and gene alterations.

CASE REPORT

Written informed consent for publication of her clinical details and images was obtained from the patient.

A 22-year-old female patient was seen in October 2009 for chronic diarrhea and weight loss (-8 kg). Colonoscopy was normal, but upper endoscopy revealed esophageal and duodenal ulcerations. CT scan disclosed a 4-cm tumor of the pancreatic tail associated with 10 minute (<1 cm) liver metastases. On endoscopic ultrasound, the pancreatic tumor was unique, and tumor cytology found well-differentiated neuroendocrine tumor cells (low Ki67 at 1%). Serum gastrin and chromogranin A (CgA) levels were elevated (2446 UI and 1455 UI respectively); Neuron-Specific Enolase (NSE), glucagon, insulin, and VIP serum levels were normal. Proton-pump inhibitors (PPIs) treatment was initiated. An oncogenic workup did not find any other familial case and the *MEN 1* gene was not mutated. The diagnosis of sporadic metastatic pancreatic gastrinoma was retained. After Multidisciplinary Tumor Board discussion, a spleno-pancreatectomy with lymphadenectomy and radiofrequency ablation of three metastases located in the right liver were performed in December 2009. Pathological analysis found a pancreatic G2 well-differentiated NET of 7 cm with 3/41 metastatic lymph nodes, a Ki67 index of 10%, and a low mitotic rate (4 mitoses/10 high-power fields). Postoperative serum gastrin and CgA levels remained stable (1104 UI and 1164 UI respectively). On somatostatin receptor scintigraphy, five liver metastases were clearly seen, with no other foci. The patient then received, in combination with PPIs, monthly intramuscular injections of 20 mg octreotide long-acting release (LAR) with a rapid fall in serum tumor markers.

Three months later, liver magnetic resonance imaging (MRI) found liver progression with the appearance of new lesions. A systemic chemotherapy regimen (6) combining capecitabine (750 mg/m^2 orally twice a day on days 1–14) and temozolomide (200 mg/m^2 orally once a day on days 10–14) was given for six 28-day cycles. A total body CT scan and a liver MRI then showed a partial response, and tumor markers returned to normal values. Monthly octreotide LAR was continued with a three-month follow-up liver MRI. On January 2014, the total body CT scan and liver MRI confirmed the partial response (most lesions remained centimetric) (**Figure 1A**), and a ^{68}Ga-DOTATOC PET scan did not demonstrate any activity. On January 2015, octreotide LAR was voluntarily stopped because this 28-year-old woman became pregnant.

On December 2015, two months after a normal delivery, an ultrasound scan showed a liver progression with one lesion increasing from 15 mm to 55 mm in diameter. Octreotide LAR

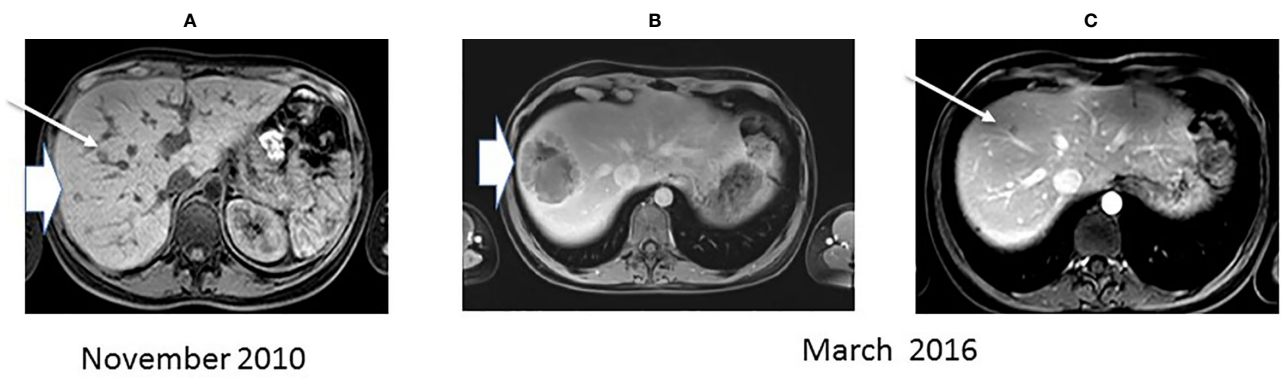

FIGURE 1 | MRI. MRI imaging of the liver in 2010 showing two minute tumors (**A** one progressed (arrowhead) **B**) in March 2016 while the other (thin arrow) **(C)** remained stable.

was reintroduced, but three months later MRI showed a further increase in the size of the larger lesion with a necrotic appearance (**Figure 1B**), while the other hepatic nodules remained stable (**Figure 1C**). ^{18}Fluorodeoxyglucose PET scan showed major hypermetabolism of this nodule (standardized uptake value 22.8) with no activity elsewhere (**Figure 2**). Biopsy was performed on this progressing liver metastasis and showed a well- to moderately differentiated component with a Ki67 index of 14% (G2) surrounding a poorly differentiated NEC with large cells and a Ki67 index of 60%, suggesting a transformation from low-grade NET to high-grade large-cell NEC. The NSE level then began to rise. The combination of capecitabine and temozolomide was reintroduced but failed. After right portal vein embolization, a right hepatectomy was performed in January 2017. The pathological examination identified two tumors separated by more than 20 mm: one was necrotic and measured 75 mm, and the second measured 23 mm. Macroscopically, there were two hepatic tumors, which measured 75 mm and 23 mm in diameter respectively. Both tumors were white colored, with a necrotic consistency for the largest one. The histologic study showed two neuroendocrine proliferations with different differentiations (**Figures 3** and **4**). The larger metastases was poorly differentiated with compact architecture: clumps of tumor cells expressed CD56, TTF-1, p53, and partly Chromogranin A and synaptophysin in some areas. The mitotic index was higher than 20 mitoses per 2 mm^2 (Ki67 index >80%). The other tumor was well differentiated and characterized by a glandular proliferation expressing the three neuroendocrine markers and by the absence of mitosis. The Ki67 index was low (<1%).

In June 2020, 41 months after resection, the imaging remained stable with no sign of progression.

MOLECULAR ANALYSIS

We extended the comparison of these two resected metastases at the molecular level by performing exome next-generation sequencing (FoundationOne® CDx, Foundation Medicine) on each lesion. The pathologically and radiologically dormant liver metastasis showed a Microsatellite Stable (MSS) status with a low tumor mutational burden (TMB; three mutations per Mb). No major gene alteration was seen, with only six variants of unknown significance detected on *BRCA2* (K2791N), *FOXL2* (V14I), *KDR* (R1229Q), *KLHL6* (M313I), *MAP3K13* (R458H), and *NOTCH1* (N280S). In contrast, the mutational profile of the poorly differentiated tissue of the progressing metastasis revealed many alterations, including Microsatellite Instable (MSI) status, very high TMB (153 mutations per Mb), and many gene mutations. The later notably involved *MEN1* splice site (927 + 1G>A), *BCL2* (E165K), *BCORL1* (Q606*), *DAXX* splice site (1039 + 1G>A), *ERBB4* (R50H), *HNF1A* (G292fs*25), *KDM5C* (R68fs*5), *MLH1* splice site (207 + 1G>A, Q510*), *MLL2* splice site (5645-1G>A), *PPP2R2A* splice site (180 + 1G>A), and *TP53* (P191del, R280K).

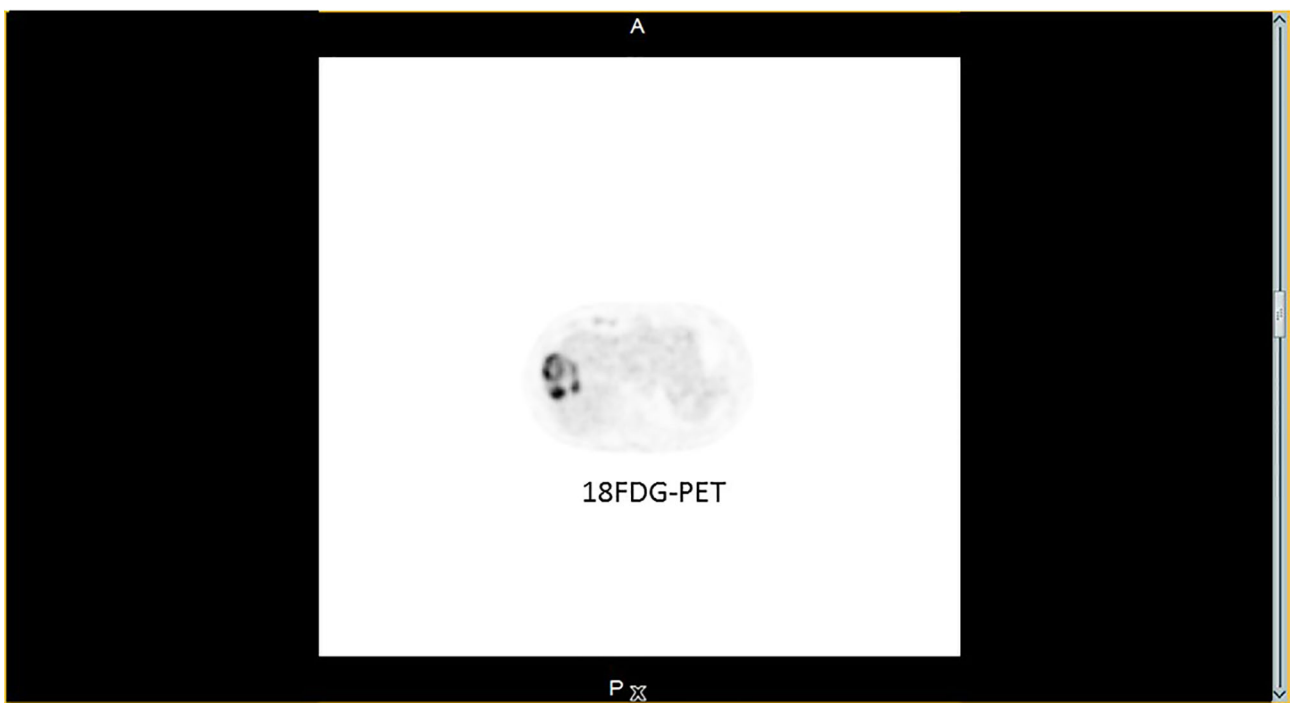

FIGURE 2 | ^{18}FDG-PET. ^{18}FDG-PET image from March 2016: major uptake in the progressing lesion; no other suspect foci was seen.

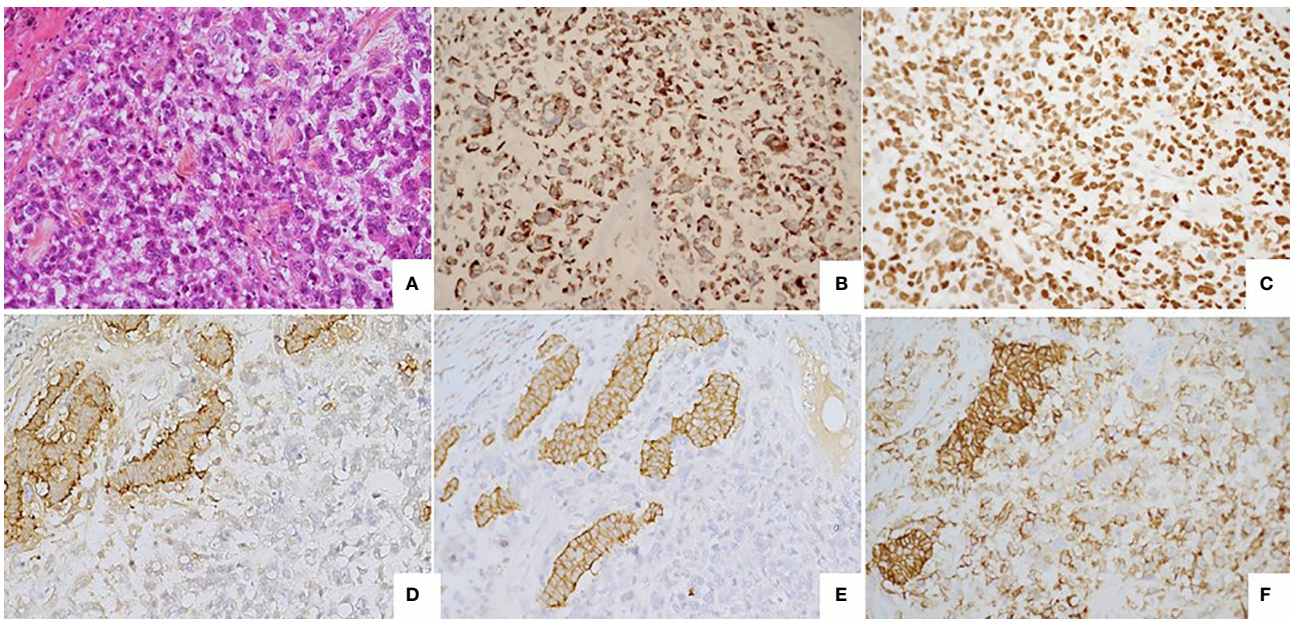

FIGURE 3 | Poorly differentiated tumor **(A)** Large cell neuroendocrine carcinoma composed by large cells with high mitotic index (> 20 mitoses/2mm^2). HES, x20. **(B)** Immunostaining CKAE1/AE3, monoclonal antibody, clone AE1/AE3/PCK26, Ventana, x20. **(C)** Immunostaining KI67 : high nuclear expression (> 70%) monoclonal antibody, clone MIB1, Agilent Dako, x20. **(D)** Immunostaining Chromogranin A, monoclonal antibody, clone LK2H10, Ventana, X20. **(E)** Immunostaining Synaptophysin, monoclonal antibody, clone SP11, Ventana, X20. **(F)** Immunostaining CD56, monoclonal antibody, clone MRQ-42, Ventana/Cell marque, X20.

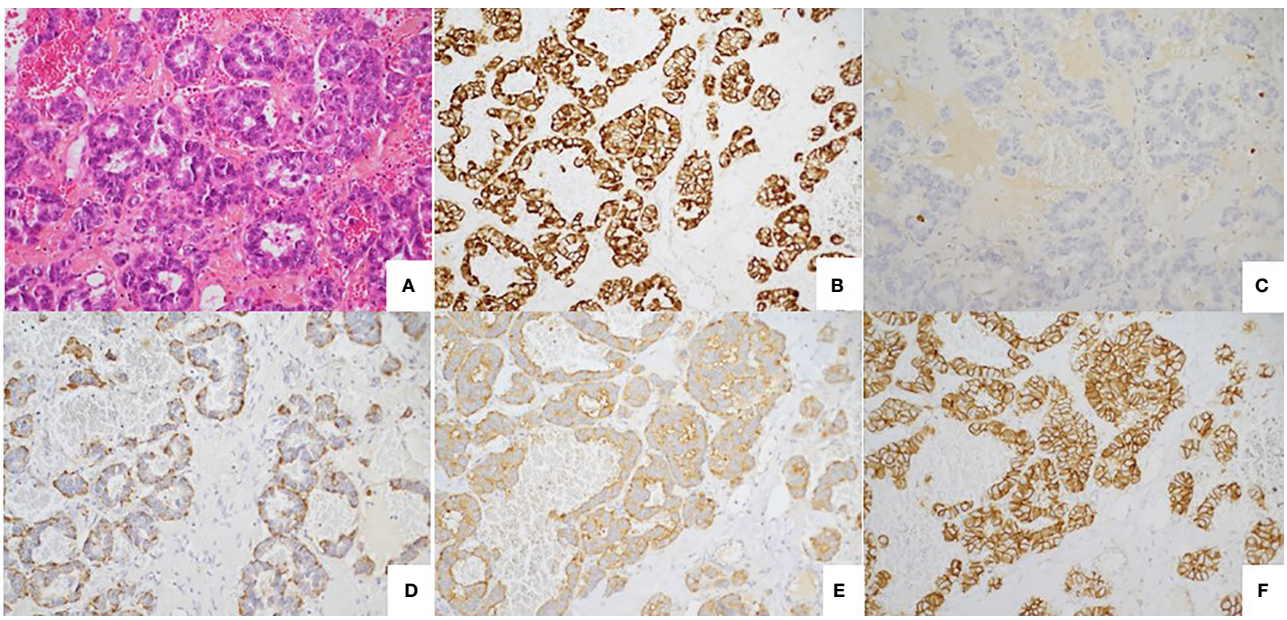

FIGURE 4 | Well differentiated tumor. **(A)** Well-differentiated neuroendocrine tumour with glandular architecture. HES, x 20. **(B)** Immunostaining CKAE1/AE3, monoclonal antibody, clone AE1/AE3/PCK26, Ventana, x20. **(C)** Immunostaining KI67: low nuclear expression (< 1%) monoclonal antibody, clone MIB1, Agilent Dako, x20. **(D)** Immunostaining Chromogranin A, monoclonal antibody, clone LK2H10, Ventana, X20. **(E)** Immunostaining Synaptophysin, monoclonal antibody, clone SP11, Ventana, X20. **(F)** Immunostaining CD56, monoclonal antibody, clone MRQ-42, Ventana/Cell marque, X20.

DISCUSSION

This case demonstrates that, after a long follow-up, a liver metastasis of a G2 functional (gastrinoma) pancreatic NET can dedifferentiate to a poorly differentiated G3 NEC, perhaps stimulated by a pregnancy.

The influence of pregnancy on the evolution of NETs is poorly understood, but these tumors may be sensitive to hormones and proteins produced in excess during the pregnancy. Pancreas NETs frequently express progesterone receptor (PR), and less often estrogen receptor (ER) (7, 8). Recently it was demonstrated (9) that placental growth factor, a member of the VEGF family (10), stimulates the growth of NETs. In the relationship between cancer and pregnancy, many factors are involved, and particularly immune modulations (11). It has also been reported that breast cancers observed during pregnancy frequently have more aggressive clinical behavior, perhaps related to molecular differences (12). Yet the impact of pregnancy on a slow-growing cancer like NET, obviously a rare event, is not described, to the best of our knowledge, in the literature.

If modification from a G1 to G2 NET is not unusual, progression of a G1 or G2 NET to a poorly differentiated NEC has seldom been described. A retrospective series reported 31 cases of well-differentiated digestive tract NETs (at least 50% of the tumor) with a separable component of high-grade NEC (13), including 21 pancreatic NETs. The high-grade part was reported either within the primary tumor (48%) or at metastatic sites (52%), and in most cases constituted at least 20% of the tumor. The high-grade component had no features of small-cell carcinoma in any of these cases but there were sometimes histologic overlaps with large-cell NEC. The prognosis of these patients remained good, closer to that of patients with well-differentiated NETs, and far better than observed in purely high-grade NEC. p53 positivity by IHC, a surrogate for *TP53* mutations, has never been reported in well-differentiated NETs or in these 21 transformed pancreatic NETs, but is found in most poorly differentiated pancreatic NEC and in our case. *DAXX*/*ATRX*/*MEN1* mutations were detected at similar frequency in the high-grade component and the lower-grade equivalent of pancreatic well-differentiated NETs, but never in a series of poorly differentiated pancreatic NEC. The contrary was observed for *RB1* mutations. For the authors, these parts of poorly differentiated NEC are, from a histogenetic point of view, closer to conventional carcinoma (from squamous or glandular cell origin) than to a conventional well-differentiated NET. For others (14), higher-grade regions in epithelial neoplasms reflect neoplastic progression due to additional molecular and genetic events. An alternative explanation is that regional variations in morphology reflect epigenetic variations or multiclonality.

Comparison of the exomes of the two tumor components in our patient gave some important information.

No gene alteration has been described in the well-differentiated part of the tumor. In contrast, the poorly differentiated part was MSI-h with a very high (153 muts/Mb) mutational burden, and many gene mutations, mostly G>A. This tumor was MSI-h, with a MLH1-acquired mutation. Such MLH1-acquired mutations can be found in MSI-h cancers from the Lynch spectrum without germline mutations (or hypermethylations) (15); MLH1 inactivation leads to increased mutational burden resulting in microsatellite instability. Only one case of pancreatic NEC (Ki67 = 60%) with such mismatched repair deficiency and loss of expression of MLH1 and PMS2 in tumor cells without gene promoter methylation has been reported (16); the outcome was surprisingly good. In a series of 89 gastroenteropancreatic NEC or mixed adenoneuroendocrine carcinomas with no familial history of Lynch syndrome, 12.4% had a MSI phenotype (essentially those with a primary located in the stomach or small intestine), usually due to methylation-mediated silencing of the MLH1 gene (17). Their prognosis was good. MLH1 mutation is rare in NEC, reported in less than 1% of small-cell lung carcinomas, in less than 1% of pancreatic NETs, and never in intestinal carcinoids; a few cases of pancreatic NEC with MSI-h in a Lynch syndrome due to germinal MLH1 mutation have been described (18).

MEN1, a tumor-suppressor gene that encodes the protein menin, is frequently mutated in neuroendocrine tumors. Germline mutations are associated with multiple endocrine neoplasia type 1 with frequently pancreatic NETs. Somatic mutations are observed in one third of pancreatic NETs (5) and in only a few cases of pancreatic adenocarcinomas. In our case, at diagnosis, MEN1 germline testing was negative and no alteration of MEN1 was described in the well-differentiated part of the removed tumor. In contrast, MEN1 alteration was found in the second component. The MEN1 splice site 927 + 1G>A has been described on germline allele and considered as likely pathogenic (ClinVar). This loss of menin, an epigenetic regulator, leads to the inactivation of p53/Rb pathways and triggers aberrant DNA damage response (19). DAXX mutations, observed in 20% of pancreatic NETs, are usually correlated with a poor prognosis; they can be driver mutations (5) and play a role in chromosomal instability (5). Other mutations described in our patients are infrequently found in NETs: never for BCL2 mutations, in many other cancers (gastric, prostate cancers, and melanoma) for ERBB4 mutations (coding for a member of the ErbB receptor family), and in endometrial tumors and in liver adenomas for HNF1A mutations.

In our case, most gene mutations were single-base substitution, essentially G>A; this mutational signature (signature 11) is particularly observed in glioblastoma and melanoma resistant to the alkylating agent, temozolomide (20), and our patient received such treatment. More recently, in gliomas with a high tumor burden, two main pathways have led to hypermutation: a *de novo* pathway and more commonly a post-treatment pathway associated with acquired resistance driven by MMR defects after treatment by temozolomide. This signature 11 may be caused, in gliomas, by temozolomide exposure and by MMR deficiency (21), and not by "pure" temozolomide signature. In such hypermutated MMR-deficient glioblastomas, the efficacy of PD-1 blockade seems infrequent (21).

Yet the debate is still open. Lung neuroendocrine carcinoids are being considered as opposed to large-cell NEC or small-cell lung carcinoma. In a recent series, 148 resected lung-neuroendocrine tumors (22), 53 typical carcinoids, 35 atypical carcinoids, 27 large-cell NEC, and 33 small-cell NEC were

investigated by NGS. Six histology-independent tumor clusters were found. Based on these results, the authors consider that typical carcinoids have the potential to evolve into high-grade tumors directly or indirectly, perhaps smoking-related. They consider that this phenomenon is inherent to all NETs and so not rare.

Treatment of such local progression is unclear. Local treatment seems appropriate to destroy this aggressive tumor, which differs from other low-grade and stable metastases. A series of 69 patients who received local treatment for focal progression was reported from three NET referral centers (14). The primary was pancreas in 55% of the cases. Most patients had low-grade well-differentiated tumors and none of the resected specimens had a poorly differentiated appearance. Locoregional treatments included tumor ablation (n=19), resection (n=18), embolization (n=16), and external beam radiation (n=16). The site of focal progression was the liver in 75% of the cases. The outcome was good with median progression-free survival of 17 months, and a median time to new systemic therapy of 21 months (for resected patients).

In conclusion, our case confirms that focal progression in metastatic NETs can correspond to a transformation of indolent low-grade tumor into high-grade poorly differentiated tumor, and that local treatment (here surgical resection) can reset the prognosis. Our case also confirms that ^{18}Fluoroglucose PET scans (23) can be useful to distinguish these transformed metastases from indolent metastases. Comparison of the exomes of both components shows impressive differences: no major abnormalities in the well-differentiated component, while in the poorly differentiated component the tumor was MSI with a very high tumor burden, somatic mutations in MEN1, MLH1, p53. Could temozolomide played a role in such tumor transformations?

PATIENT PERSPECTIVE

In case of a major progression limited to one metastases in a metastatic well differentiated NET, surgery may be an excellent therapeutic option even if this progressive tumor is poorly differentiated on biopsy. An exome next generation sequencing may be useful; in case of MSI tumor the use of check-point inhibitors blockade is not always of interest.

DATA AVAILABILITY STATEMENT

The raw data supporting the conclusions of this article will be made available by the authors, without undue reservation.

ETHICS STATEMENT

Ethical review and approval was not required for the study on human participants in accordance with the local legislation and institutional requirements. The patients/participants provided their written informed consent to participate in this study.

AUTHOR CONTRIBUTIONS

J-LR, FB, and HS participated in the conception and writing of the study. FB, J-LR, and AM to the interpretation of the data. HS, M-FH, and FD participated in the acquisition of the data. All authors contributed to the article and approved the submitted version.

REFERENCES

1. Lepage C, Bouvier AM, Phelip JM, Hatem C, Vernet C, Faivre J. Incidence and management of malignant digestive endocrine tumours in a well defined French population. *Gut* (2004) 53(4):549–53. doi: 10.1136/gut.2003.026401
2. Kidd M, Modlin I, Oberg K. Towards a new classification of gastroenteropancreatic neuroendocrine neoplasms. *Nat Rev Clin Oncol* (2016) 13(11):691–705. doi: 10.1038/nrclinonc.2016.85
3. Inzani F, Petrone G, Rindi G. The New World Health Organization Classification for Pancreatic Neuroendocrine Neoplasia. *Endocrinol Metab Clin North Am* (2018) 47(3):463–70. doi: 10.1016/j.ecl.2018.04.008
4. Grillo F, Albertelli M, Brisigotti MP, Borra T, Boschetti M, Fiocca R, et al. Grade Increases in Gastroenteropancreatic Neuroendocrine Tumor Metastases Compared to the Primary Tumor. *Neuroendocrinology* (2016) 103(5):452–9. doi: 10.1159/000439434
5. Scarpa A, Chang DK, Nones K, Corbo V, Patch AM, Bailey P, et al. Whole-genome landscape of pancreatic neuroendocrine tumours. *Nature* (2017) 543 (7643):65–71. doi: 10.1038/nature21063
6. Ramirez RA, Beyer DT, Chauhan A, Boudreaux JP, Wang YZ, Woltering EA. The Role of Capecitabine/Temozolomide in Metastatic Neuroendocrine Tumors. *Oncologist* (2016) 21(6):671–5. doi: 10.1634/theoncologist.2015-0470
7. Zimmermann N, Lazar-Karsten P, Keck T, Billmann F, Schmid S, Brabant G, et al. Expression Pattern of CDX2, Estrogen and Progesterone Receptors in Primary Gastroenteropancreatic Neuroendocrine Tumors and Metastases. *Anticancer Res* (2016) 36(3):921–4.
8. Estrella JS, Ma LT, Milton DR, Yao JC, Wang H, Rashid A, et al. Expression of estrogen-induced genes and estrogen receptor beta in pancreatic neuroendocrine tumors: implications for targeted therapy. *Pancreas* (2014) 43(7):996–1002. doi: 10.1097/MPA.0000000000000203
9. Hilfenhaus G, Gohrig A, Pape UF, Neumann T, Jann H, Zdunek D, et al. Placental growth factor supports neuroendocrine tumor growth and predicts disease prognosis in patients. *Endocr Relat Cancer* (2013) 20(3):305–19. doi: 10.1530/ERC-12-0223
10. Dewerchin M, Carmeliet P. Placental growth factor in cancer. *Expert Opin Ther Targets* (2014) 18(11):1339–54. doi: 10.1517/14728222.2014.948420
11. Holtan SG, Creedon DJ, Haluska P, Markovic SN. Cancer and pregnancy: parallels in growth, invasion, and immune modulation and implications for cancer therapeutic agents. *Mayo Clin Proc* (2009) 84(11):985–1000. doi: 10.4065/84.11.985
12. Nguyen B, Venet D, Azim HA Jr, Brown D, Desmedt C, Lambertini M, et al. Breast cancer diagnosed during pregnancy is associated with enrichment of non-silent mutations, mismatch repair deficiency signature and mucin mutations. *NPJ Breast Cancer* (2018) 4:23. doi: 10.1038/s41523-018-0077-3
13. Tang LH, Untch BR, Reidy DL, O'Reilly E, Dhall D, Jih L, et al. Well-Differentiated Neuroendocrine Tumors with a Morphologically Apparent High-Grade Component: A Pathway Distinct from Poorly Differentiated Neuroendocrine Carcinomas. *Clin Cancer Res* (2016) 22(4):1011–7. doi: 10.1158/1078-0432.CCR-15-0548
14. Al-Toubah T, Partelli S, Cives M, Andreasi V, Silvestris F, Falconi M, et al. Local treatment for focal progression in metastatic neuroendocrine tumors. *Endocr Relat Cancer* (2019) 26:405–9. doi: 10.1530/ERC-18-0462

15. Haraldsdottir S, Hampel H, Tomsic J, Frankel WL, Pearlman R, de la Chapelle A, et al. Colon and endometrial cancers with mismatch repair deficiency can arise from somatic, rather than germline, mutations. *Gastroenterology* (2014) 147(6):1308–16.e1. doi: 10.1053/j.gastro.2014.08.041
16. Vanoli A, Perfetti V, Furlan D, Neri G, Viglio A, Sessa F, et al. Long Survival and Prolonged Remission after Surgery and Chemotherapy in a Metastatic Mismatch Repair Deficient Pancreatic Neuroendocrine Carcinoma with MLH1/PMS2 Immunodeficiency and Minimal Microsatellite Shift. *Endocr Pathol* (2020) 31:411–7. doi: 10.1007/s12022-020-09622-5
17. Sahnane N, Furlan D, Monti M, Romualdi C, Vanoli A, Vicari E, et al. Microsatellite unstable gastrointestinal neuroendocrine carcinomas: a new clinicopathologic entity. *Endocr Relat Cancer* (2015) 22(1):35–45. doi: 10.1530/ERC-14-0410
18. Serracant Barrera A, Serra Pla S, Blazquez Mana CM, Salas RC, Garcia Monforte N, Bejarano Gonzalez N, et al. Pancreatic non-functioning neuroendocrine tumor: a new entity genetically related to Lynch syndrome. *J Gastrointest Oncol* (2017) 8(5):E73–E9. doi: 10.21037/jgo.2017.07.02
19. Qiu H, Jin BM, Wang ZF, Xu B, Zheng QF, Zhang L, et al. MEN1 deficiency leads to neuroendocrine differentiation of lung cancer and disrupts the DNA damage response. *Nat Commun* (2020) 11(1):1009. doi: 10.1038/s41467-020-14614-4
20. Alexandrov LB, Nik-Zainal S, Wedge DC, Aparicio SA, Behjati S, Biankin AV, et al. Signatures of mutational processes in human cancer. *Nature* (2013) 500 (7463):415–21. doi: 10.1038/nature12477
21. Touat M, Li YY, Boynton AN, Spurr LF, Iorgulescu JB, Bohrson CL, et al. Mechanisms and therapeutic implications of hypermutation in gliomas. *Nature* (2020) 580(7804):517–23. doi: 10.1038/s41586-020-2209-9
22. Pelosi G, Bianchi F, Dama E, Simbolo M, Mafficini A, Sonzogni A, et al. Most high-grade neuroendocrine tumours of the lung are likely to secondarily develop from pre-existing carcinoids: innovative findings skipping the current pathogenesis paradigm. *Virchows Arch* (2018) 472(4):567–77. doi: 10.1007/s00428-018-2307-3
23. Bahri H, Laurence L, Edeline J, Leghzali H, Devillers A, Raoul JL, et al. High prognostic value of 18F-FDG PET for metastatic gastroenteropancreatic neuroendocrine tumors: a long-term evaluation. *J Nucl Med* (2014) 55 (11):1786–90. doi: 10.2967/jnumed.114.144386

Conflict of Interest: The authors declare that the research was conducted in the absence of any commercial or financial relationships that could be construed as a potential conflict of interest.

frontiers in Oncology

ORIGINAL RESEARCH
published: 23 April 2021
doi: 10.3389/fonc.2021.646082

Construction and Validation of Novel Nomograms for Predicting Prognosis of Pancreatic Ductal Adenocarcinoma After Surgery According to Different Primary Cancer Locations

Ge Li[1,2†], Cheng-Yu Liao[3†], Jiang-Zhi Chen[1,2†], Long Huang[3], Can Yang[3], Yi-Feng Tian[3], Yi-Ting Wang[4], Qiang Du[1,2], Qian Zhan[5], Yan-Ling Chen[1,2*] and Shi Chen[3*]*

[1] Department of Hepatobiliary Surgery and Fujian Institute of Hepatobiliary Surgery, Fujian Medical University Union Hospital, Fuzhou, China, [2] Key Laboratory of The Ministry of Education for Gastrointestinal Cancer, Fujian Medical University, Fuzhou, China, [3] Shengli Clinical Medical College of Fujian Medical University, Fujian Medical University, Fujian Provincial Hospital, Fuzhou, China, [4] Fujian Provincial Key Laboratory on Hematology, Fujian Institute of Hematology, Fujian Medical University Union Hospital, Fuzhou, China, [5] Pancreatic Disease Center, Department of General Surgery, Ruijin Hospital, Research Institute of Pancreatic Diseases, Shanghai Jiao Tong University School of Medicine, Shanghai, China

Background/Aims: Pancreatic ductal adenocarcinoma (PDAC) can occur in different parts of the pancreas. This study aimed to identify clinicopathological characteristics independently correlated with the prognosis of PDAC of the pancreatic head/uncinate (PHC) or body-tail (PBTC), and to develop novel nomograms for predicting cancer-specific survival (CSS) according to different primary cancer locations.

Methods: 1160 PDAC patients were retrospectively enrolled and assigned to training and test sets with each set divided into PHC and PBTC groups. Comparative analysis of clinicopathologic characteristics, survival analysis, and multivariate analysis were performed. Independent factors were identified and used for constructing nomograms. The performance of the nomograms was validated in the test set.

Results: Primary tumor location was an independent risk factor for prognosis of PDAC after surgery. Specially, gender, fasting blood glucose, and preoperative cancer antigen 19-9 were significantly associated with prognosis of PHC, whereas age, body mass index, and lymph nodes were significantly correlated with the prognosis of PBTC. A significant difference in prognosis was found between PHC and PBTC in stage Ia and stage III. Three nomograms were established for predicting the prognosis for PDAC, PHC, and PBTC. Notably, these nomograms were calibrated modestly (c-indexes of 0.690 for PDAC, 0.669 for PHC, and 0.704 for PBTC), presented better accuracy and reliability than the 8th AJCC staging system, and achieved clinical validity.

Conclusions: PHC and PBTC share the differential clinical-pathological characteristics and survival. The nomograms show good performance for predicting prognosis in PHC

OPEN ACCESS

Edited by:
Kanjoormana Aryan Manu, Amala Cancer Research Centre, India

Reviewed by:
Benedict Kinny-Köster, Johns Hopkins Medicine, United States
Ming Cui, Peking Union Medical College Hospital (CAMS), China
Jishu Wei, Nanjing Medical University, China

****Correspondence:***
Shi Chen
wawljwalj@fjmu.edu.cn
Yan-Ling Chen
drchenyl@126.com
Qian Zhan
zhanxi80@126.com

†These authors have contributed equally to this work and share first authorship

Specialty section:
This article was submitted to Gastrointestinal Cancers, a section of the journal Frontiers in Oncology

Received: *24 December 2020*
Accepted: *06 April 2021*
Published: *23 April 2021*

Citation:
Li G, Liao C-Y, Chen J-Z, Huang L, Yang C, Tian Y-F, Wang Y-T, Du Q, Zhan Q, Chen Y-L and Chen S (2021) Construction and Validation of Novel Nomograms for Predicting Prognosis of Pancreatic Ductal Adenocarcinoma After Surgery According to Different Primary Cancer Locations. Front. Oncol. 11:646082. doi: 10.3389/fonc.2021.646082

and PBTC. Therefore, these nomograms hold potential as novel approaches for predicting survival of PHC and PBTC patients after surgery.

Keywords: pancreatic ductal adenocarcinoma, nomogram, cancer-specific survival (CSS), decision curve analysis, AJCC 8

INTRODUCTION

Pancreatic ductal adenocarcinoma (PDAC), a predominate type of pancreatic cancer (PC), is among the leading causes of cancer-related death, accounting for approximately 260,000 deaths worldwide annually (1). It has been recognized in recent decades that PDAC has an extremely poor prognosis with a 5-year survival rate of less than 10%. For PDAC patients eligible for surgical treatment, curative-intent surgical resection followed by adjuvant chemotherapy is considered the only curative treatment option (2). Although substantial progress has been made in the diagnosis and treatment of PDAC, early relapse after pancreatectomy commonly occurs in PDAC patients. Thus, an accurate prognostic method is urgently required for the precise stratification of patients to guide appropriate clinical management and follow-up plans.

Currently, the stratification of patients mainly relies on the American Joint Committee on Cancer (AJCC) staging system, in which tumor size and the histological characteristics are considered as the major factors for evaluation. However, many significant factors, such as cancer antigen 19-9 (CA19-9) level, tumor differentiation, histological grade, and genomic analysis, have been proposed to be potential determinants of survival but have not been included in the AJCC staging system. Moreover, PDAC can occur in various parts of the pancreas (head, body or tail) of the pancreas, and the risk factors influencing the prognosis of PDAC according to different primary locations have not been thoroughly investigated.

A number of previous studies have indicated that tumor location is closely related to the prognosis of PC, with primary tumor location at the body/tail of the pancreas (PBTC) tending to have a poorer prognosis compared with that at the head of the pancreas (3–6). Additionally, resected PBTC has shown more aggressive tumor biology than PDAC at the head of the pancreas. On the contrary, some previous studies demonstrated that PBTC had a better outcome than PDAC at the head of the pancreas for patients at the early stage (7), and Winer et al. (8) found that patients with pancreatic head cancer had worse overall survival (OS) than patients with PC at either the body or tail locations for all stages when analyzing the National Cancer Database. Nevertheless, van Erning et al. (9) indicated that OS for PDAC at different tumor locations does not differ significantly according to the database in the Netherlands. Thus, the findings regarding the prognosis of PDAC at different primary tumor locations remain inconsistent and even conflicting. Use of the TNM staging system for stratifying PDAC patients in order to determine the precise prognosis is questionable (10). Until now, research of the survival difference for PDAC at different locations after curative-intent surgical resection has been rare.

In the present study, we aimed to identify clinicopathological characteristics independently correlated with the prognosis of PDAC at the pancreatic head/uncinate (PHC) versus the PBTC and to develop and validate novel nomograms for predicting the cancer-specific survival (CSS) of PDAC cases according to different primary cancer locations after curative-intent resection. The findings of this study may provide a novel prognostic tool for managing PDAC cases with different primary tumor locations.

METHODS

Patients and Study Design

A total of 1160 PDAC patients who underwent curative-intent pancreatic resection at multiple centers, including Fujian Medical University Union Hospital, Fujian Provincial Hospital, and Shanghai Ruijin Hospital, spanning the period between January 2014 and March 2017 were retrospectively enrolled in this study. PDAC was histopathologically diagnosed and confirmed. Of 1160 enrolled patients, 813 enrolled from Fujian Medical University Union Hospital and Fujian Provincial Hospital were assigned to the training group, while 347 from Shanghai Ruijin Hospital were assigned to the test group for external validation. During enrollment, the following inclusion criteria were used: (1) histologically confirmed PDAC; (2) no prior receipt of other curative treatment including radiotherapy, immunogene and target therapy; (3) curatively resectable PDAC as preoperatively assessed by imaging, even with peripancreatic invasion or artery (hepatic, superior mesenteric and celiac artery) or vein (portal or superior and inferior mesenteric vein) that could be completely resected and constructed; (4) negative for intraoperative frozen section analysis; (5) only the single metastatic lesion in liver for patients with stage IV disease after 8-12 times paclitaxel-albumin or gemcitabine chemotherapy. PDAC patients with the following conditions were excluded from this study: (1) absent or incomplete information for important clinical characteristics needed for this study; (2) unresected tumors, based on bypass surgery, exploratory operation, or microscopic residual tumor in the resection margin; (3) death within 30 days after the surgery; and (4) causes of death other than PDAC and its complications.

This study was approved by the ethics committees of the institutional review boards of the participating hospitals, Fujian Medical University Union Hospital, Fujian Provincial Hospital, and Shanghai Ruijin Hospital. The need for written consent was waived due to the retrospective nature of this study.

Follow-Up

The patients were followed up by the operating surgeons at 1 month after surgery and every 3 months thereafter. The last follow-up was conducted in March 2020.

Statistical Analysis

Categorical variables were compared between groups using the chi square test. Continuous variables were analyzed using the independent-samples T test. To assess an association between various prognostic predictors and CSS, univariate and multivariate analyses were conducted using the Cox regression model, and hazard ratios (HRs) and 95% confidence intervals (CIs) were calculated. Goodness of fit was maximized using the log-likelihood, while information loss was minimized with the Akaike information criterion (AIC) (11). Based on the AIC of the Cox proportional hazards model, variables were selected in a backward stepwise manner. Nomograms were constructed on the basis of the independent variables identified by the multivariate analysis in the training cohort.

Nomogram performance was assessed using the Harrell's concordance index (c-index). The maximum c-index value of 1.0 represents a perfect discrimination. whereas 0.5 indicates no discriminative capacity. Calibration was made to graphically evaluate the performance of the model by comparing the means of predicted survival with those of actual survival. To reduce potential bias, 200-sample bootstrap validation was performed for internal validation. The values of c-indexes were compared using the compare C package (12). The precision of the 1-, 2-, and 3-year survival rates predicted by the nomograms was evaluated with time-dependent receiver operating characteristic (ROC) curve analysis using the time ROC package (13).

The ranges of threshold probabilities were finalized by decision curve analysis (DCA) (14) to assess the clinical validity of the nomograms. The Kaplan–Meier survival curve was utilized for comparing the nomograms with the latest edition of the 8th AJCC staging system (revised in 2018) by risk classification and stratification (15). For risk stratification, the accumulated nomogram scores were ranked by deciles to develop 10 risk groups, which composed the new nomo stages. Accordingly, each 8thAJCC substage was divided by nomo stages to derive three prognostic strata: low-, median-, and high-risk.

RESULTS

Baseline Demographic and Clinical Characteristics of PDAC Patients

A total of 1160 patients with PDAC were enrolled from three participating hospitals, of which 813 (467 PHC cases and 346 PBTC cases) recruited from Fujian Medical University Union Hospital and Fujian Provincial Hospital were assigned to the training set. The baseline demographic and clinical characteristics of the PHC and PBTC patients are summarized in **Table 1**. The age and gender of patients were comparable between the training and test cohorts in both PHC and PBTC groups (**Suppl. Tables 1**, **2**). It was noted that a majority of PDAC patients (PHC and PBTC groups) were men, with a greater male predominance in the PHC group (64.67% males and 35.33% females) than in the PBTC group (p=0.001). Comparison of clinical features revealed that patients in the PHC group showed a higher proportion of symptoms (e.g., jaundice, abdominal pain; p<0.001), thus leading to more timely medical intervention for PHC patients than PBTC patients. It was of note that PHC patients presented the earlier T and AJCC stage and less hepatic metastasis compared with PBTC patients (p<0.001). In addition, PHC patients exhibited a higher number of harvested lymph nodes confirmed by postoperative pathology, which described as lymph node count (LNC) afterward, than PBTC patients (11.27 and 4.86 for PHC and PBTC, respectively). The number of lymph nodes dissected during operation might be enough, but many of them were confirmed as adipose tissue by postoperative pathology, which could be the reason for that LNC in this study was lower than the number of 8th AJCC or ISGPS (International Study Group of Pancreatic Surgery) recommend. Lymph node metastasis occurred more frequently in the PHC group compared with the PBTC group (261 vs 219 in N0, 161 vs 108 in N1, 45 vs 19 in N2, p<0.001). Notably, the PBTC group had better tumor differentiation, less intraoperative blood loss, and higher values for lymph node ratio (LNR), albumin, carcino-embryonic antigen (CEA) and cancer antigen 125 (CA125) compared with the PHC group. The demographic and clinical characteristics were comparable among the patients in the training and test groups.

The median survival was 20 months (range, 1–74 months) and the 1-, 2-, and 3-year survival rates were 66.5%, 45.1%, and 32.2% in the PHC group, respectively. For patients with PBTC, the median survival was 14 months (range, 1–74 months), and the 1-, 2-, and 3-year survival rates were 58.9%, 31.2%, and 18.6%, respectively. Notably, PBTC patients had a significantly worse CSS compared with PHC patients (p<0.001).

Survival Analysis for Patients With PHC and PBTC

Survival rates were compared between the PHC and PBTC groups according to the AJCC stages (**Figure 1**). As a result, significant differences in survival were found in stage Ia and stage III, and patients in the PHC group had poorer clinical outcomes than those in the PBTC group (p=0.007 and <0.001 in stage Ia and stage III, respectively). The differences in clinical characteristics between the PHC and PBTC groups in stage Ia and stage III are summarized in **Suppl. Tables 3**, **4**. In stage Ia, patients with PBTC showed significantly worse tumor differentiation (p=0.012) and a lower LNC (p=0.001) compared to patients with PHC. In stage III, patients in the PBTC group had a significantly larger tumor size (p=0.004) and later T stage (p<0.001) than patients in the PHC group, while the PHC group showed significantly more lymph nodes metastasis (p=0.015) and later N stage (p<0.001), with a higher LNC (p<0.001) than the PBTC group.

Identification of Independent Prognostic Factors for PHC and PBTC After Curative-Intent Surgical Resection

Univariate and multivariate analyses were conducted to identify prognostic factors that correlate with different primary cancer locations of PDAC, including PHC and PBTC, and detailed results are listed in **Tables 2**–**4**. In all enrolled PDAC patients

TABLE 1 | Baseline demographic and clinical characteristics of the patients.

Variables	PHC		PBTC		p
	n=467		n=346		
Gender, n, (%)					0.001
Female	165	(35.33)	166	(47.98)	
Male	302	(64.67)	180	(52.02)	
Age (years), median, IQR	62.00	56.00, 69.00	63.00	57.00, 70.00	0.074
BMI (kg/m^2), mean, SD	22.88	3.44	22.83	3.20	0.831
Symptoms, (%)					<0.001
Yes (including abdominal pain/ gastrointestinal symptoms)	350	(74.95)	218	(63.01)	
No	117	(25.05)	128	(36.99)	
TBIL (umol/L), mean, SD	97.24	94.03	15.28	5.90	<0.001
ALB (g/L), mean, SD	36.58	5.25	39.42	4.32	<0.001
Fasting blood glucose (mmol/L), mean, SD	6.42	2.24	6.85	4.99	0.104
CA125, (%)					0.002
Normal	396	(84.80)	264	(76.30)	
Elevated	71	(15.20)	82	(23.70)	
CA19-9, (%)					0.492
Normal	108	(23.13)	73	(21.10)	
Elevated	359	(76.87)	273	(78.90)	
CEA, (%)					<0.001
Normal	351	(75.16)	216	(62.43)	
Elevated	116	(24.84)	130	(37.57)	
Smoking history, (%)					0.549
Yes	122	(26.12)	84	(24.28)	
No	345	(73.88)	262	(75.72)	
Drinking history, (%)					0.638
Yes	87	(18.63)	69	(19.94)	
No	380	(81.37)	277	(80.06)	
Histology, n, (%)					<0.001
Well differentiated	18	(3.85)	44	(12.72)	
Moderately differentiated	232	(49.68)	143	(41.33)	
Poorly differentiated	217	(46.47)	159	(45.95)	
Intraoperative blood loss (ml), mean, SD	613.19	488.26	505.00	487.05	0.002
Tumor size (cm), mean, SD	3.23	1.30	4.44	1.88	<0.001
Perineuronal invasion n, (%)					0.332
Yes	295	(63.17)	207	(59.83)	
No	172	(36.83)	139	(40.17)	
pT stage, n, (%)					<0.001
pT1	102	(21.84)	25	(7.23)	
pT2	281	(60.17)	163	(47.11)	
pT3	77	(16.49)	120	(34.68)	
pT4	7	(1.50)	38	(10.98)	
pN stage, n, (%)					0.033
N0	261	(55.89)	219	(63.29)	
N1	161	(34.48)	108	(31.21)	
N2	45	(9.64)	19	(5.49)	
LNC, mean, SD	11.27	8.51	4.86	5.17	<0.001
LNR, mean, SD	0.11	0.19	0.18	0.32	<0.001
LNM, mean SD	1.16	1.96	0.92	2.29	0.109
Metastasis, n, (%)					<0.001
M0	442	(94.65)	293	(84.68)	
M1	25	(5.35)	53	(15.32)	
8th AJCC stage, n, (%)					<0.001
Ia	64	(13.70)	18	(5.20)	
Ib	150	(32.12)	96	(27.75)	
IIa	35	(7.49)	64	(18.50)	
IIb	147	(31.48)	72	(20.81)	
III	46	(9.85)	43	(12.43)	
IV	25	(5.35)	53	(15.32)	
Neoadjuvant chemotherapy, n, (%)					0.722
Yes	131	(28.05)	101	(29.19)	
No	336	(71.95)	245	(70.81)	
1-year cumulative survival	0.665		0.589		<0.001
2-year cumulative survival	0.451		0.312		
3-year cumulative survival	0.322		0.186		

PHC, pancreatic head/uncinate ductal adenocarcinoma; PBTC, pancreatic body/tail ductal adenocarcinoma; IQR, interquartile range; SD, standard deviation; BMI, body mass index; TBIL, total bilirubin; ALB, albumin; LNC, lymph node count; LNM, lymph node metastasis; LNR, lymph node ratio; CA125, cancer antigen 125; CA19-9, cancer antigen 19-9; CEA, carcino-embryonic antigen.

with any primary cancer location, tumor location, gender, age, BMI, histological grade, symptoms, fasting blood glucose, tumor size, perineuronal invasion, T category, N category, hepatic metastasis, LNR, lymph node metastasis (LNM), and preoperative levels of CA19-9, CA125, and CEA were identified to be significantly associated with survival (**Table 2**). Further, multivariate analysis revealed that primary tumor location was an independent prognostic factor (PBTC: hazard ratio [HR] 1.443, 95% CI, 1.225–1.699, p<0.0001). In addition, gender, BMI, histological grade, symptoms, fasting blood glucose, tumor size, perineuronal invasion, M category, LNR, LNM, and preoperative CA19-9 and CEA levels were also independent prognostic factors for PDAC (**Table 2**).

The PDAC at different locations (PHC and PBTC) shared common independent prognostic factors: histological grade, tumor size, LNR, perineuronal invasion, M category and symptoms (**Table 4**). Notably, gender, fasting blood glucose, and preoperative CA19-9 level were significantly associated with the prognosis of PHC only, whereas age, BMI, and LNC were significantly correlated with the prognosis of PBTC only (**Table 4**), reflecting differences in independent prognostic factors between PHC and PBTC.

Construction and Validation of Prognostic Nomograms for PHC and PBTC

The identified independent risk factors influencing the prognosis of PHC and PBTC were used to construct prognostic nomograms for PHC and PBTC. As shown in **Figure 2**, covariates were selected on the basis of the AIC and likelihood rather than statistical significance (p value) to balance model complexity and performance. Points in the nomogram could be summed to calculate the probability of individual survival. The labels and points in the nomogram are presented in detail in **Suppl. Tables 5**, **6**.

Calibration plots were generated for the probabilities of 1-, 2-, and 3-year CSS of PDAC, PHC, and PBTC, and favorable consistency was illustrated by the survival predicted by the nomograms and the corresponding Kaplan–Meier estimates in both the training and test cohorts (**Figures 3**, **4**), indicating that the established nomograms were reliable for predicting survival.

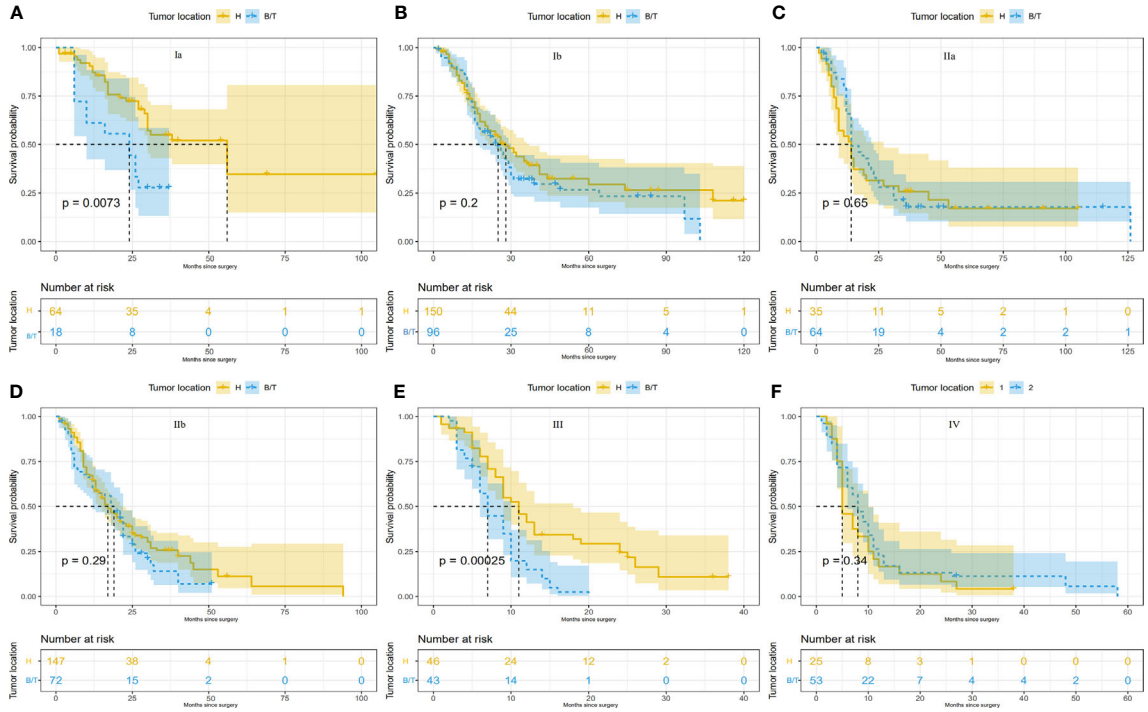

FIGURE 1 | Comparison of survival differences between PHC and PBTC according to the 8thAJCC system. Comparison between PHC and PBTC in **(A)** stage Ia; **(B)** stage Ib; **(C)** stage IIa; **(D)** stage IIb; **(E)** stage III; and **(F)** stage IV. Significant differences were observed in Ia and III (p=0.0073 and 0.00025, respectively).

TABLE 2 | Univariate and multivariate Cox regression analyses of prognostic factors in PDAC patients with curative-intent surgical resection.

Variables	Univariate analysis			Multivariate analysis		
	HR	95%CI	p	HR	95%CI	p
Tumor location						
Head	ref			ref		
Body/Tail	1.443	1.225-1.699	<0.0001	1.273	1.057-1.535	0.011
Gender						
Male	ref			ref		
Female	0.842	0.712-0.996	0.044	0.776	0.653-0.924	0.004
Age	1.009	1.000-1.018	0.041	1.006	0.997-1.016	0.173
BMI	0.975	0.951-0.999	0.038	0.958	0.935-0.983	0.001
Symptoms						
No	ref			ref		
Yes	1.283	1.069-1.539	0.007	1.231	1.020-1.488	0.030
TBIL	1.000	0.999-1.001	0.936	–		
ALB	0.992	0.976-1.008	0.329	–		
Fasting blood glucose	1.059	1.036-1.082	<0.0001	1.038	1.013-1.063	0.003
CA125						
Normal	ref			ref		
Elevated	1.698	1.392-2.073	<0.0001	1.213	0.968-1.520	0.093
CA19-9						
Normal	ref			ref		
Elevated	1.404	1.145-1.720	0.001	1.324	1.077-1.629	0.008
CEA						
Normal	ref			ref		
Elevated	1.210	1.016-1.441	0.03	1.110	1.013-1.209	0.026
Smoking history						
No	ref			–		
Yes	1.092	0.908-1.313	0.35	–		
Drinking history						
No				–		
Yes	1.060	0.863-1.302	0.58	–		
Histology						
Poorly differentiated	ref			ref		
Moderately differentiated	0.635	0.534-0.754	<0.0001	0.722	0.605-0.861	0.0002
Well differentiated	0.656	0.478-0.901	0.009	0.656	0.472-0.913	0.012
Intraoperative blood loss	1.000	0.999-1.000	0.121	–		
Tumor size	1.179	1.127-1.233	<0.0001	1.123	1.070-1.184	<0.0001
Perineuronal invasion						
No	ref			ref		
Yes	1.572	1.322-1.869	<0.0001	1.417	1.184-1.697	0.0001
pT stage						
pT1	ref			–		
pT2	1.357	1.050-1.753	0.019	–		
pT3	2.017	1.528-2.661	<0.0001	–		
pT4	9.600	6.439-14.312	<0.0001	–		
pN stage						
N0	ref			–		
N1	1.594	1.334-1.905	<0.0001	–		
N2	2.444	1.824-3.274	<0.0001	–		
LNC	0.995	0.984-1.006	0.358	–		
LNR	2.067	1.604-2.664	<0.0001	1.527	1.093-2.132	0.012
LNM	1.088	1.059-1.118	<0.0001	1.055	1.020-1.092	0.002
Metastasis						
M0	ref			ref		
M1	2.940	2.296-3.764	<0.0001	2.115	1.572-2.847	<0.0001
8^{th} AJCC stage						
Ia	ref			–		
Ib	1.342	0.946-1.902	0.099	–		
IIa	2.076	1.416-3.042	0.0001	–		
IIb	2.167	1.530-3.069	<0.0001	–		
III	4.853	3.297-7.145	<0.0001	–		
IV	5.456	3.702-8.043	<0.0001	–		
Neoadjuvant chemotherapy						
No	ref			ref		
Yes	0.832	0.691-1.001	0.05	0.787	0.651-0.952	0.013

PDAC, pancreatic ductal adenocarcinoma; BMI, body mass index; TBIL, total bilirubin; ALB, albumin; LNC, lymph node count; LNM, lymph node metastasis; LNR, lymph node ratio; CA125, cancer antigen 125; CA19-9, cancer antigen 19-9; CEA, carcino-embryonic antigen.

TABLE 3 | Univariate Cox regression analysis of prognostic factors in PHC and PBTC patients with curative-intent surgical resection.

Variables	Univariate analysis for PHC			Univariate analysis for PBTC		
	HR	95%CI	p	HR	95%CI	p
Gender						
Male	ref			ref		
Female	0.718	0.564-0.916	0.008	0.907	0.714-1.154	0.428
Age	1.002	0.990-1.015	0.699	1.016	1.003-1.029	<0.0001
BMI	0.990	0.959-1.022	0.522	0.948	0.912-0.985	0.006
Symptoms						
No	ref			ref		
Yes	1.229	0.944-1.601	0.126	1.528	1.185-1.971	0.001
TBIL	1.002	1.000-1.003	0.008	1.006	0.986-1.027	0.569
ALB	0.983	0.962-1.004	0.113	0.972	0.943-1.002	0.071
Fasting blood glucose	1.066	1.019-1.115	0.005	1.054	1.025-1.083	0.0002
CA125						
Normal	ref			ref		
Elevated	1.465	1.092-1.967	0.011	1.840	1.399-2.421	<0.0001
CA19-9						
Normal	ref			ref		
Elevated	1.509	1.140-1.997	0.004	1.276	0.948-1.717	0.109
CEA						
Normal	ref			ref		
Elevated	1.014	0.786-1.311	0.920	1.355	1.063-1.728	0.014
Smoking history						
No	ref			ref		
Yes	0.983	0.764-1.265	0.896	1.337	1.018-1.756	0.037
Drinking history						
No	ref			ref		
Yes	1.058	0.796-1.406	0.700	1.051	0.779-1.417	0.744
Histology						
Poorly differentiated	ref			ref		
Moderately differentiated	0.691	0.372-1.210	0.185	0.564	0.435-0.734	<0.0001
Well differentiated	0.671	0.549-0.871	0.001	0.528	0.359-0.776	0.001
Intraoperative blood loss	1.000	1.000-1.000	0.006	1.000	0.999-1.000	0.927
Tumor size	1.205	1.110-1.309	<0.0001	1.131	1.064-1.202	<0.0001
Perineuronal invasion						
No	ref			ref		
Yes	1.678	1.317-2.138	<0.0001	1.493	1.164-1.916	0.001
pT stage						
pT1	ref			ref		
pT2	1.414	1.041-1.922	0.027	1.073	0.667-1.726	0.772
pT3	2.021	1.401-2.915	0.0001	1.569	0.968-2.543	0.067
pT4	14.900	6.607-33.604	<0.0001	7.252	4.036-13.029	<0.0001
pN stage						
N0	ref			ref		
N1	1.683	1.320-2.146	<0.0001	1.622	1.244-2.115	0.0003
N2	2.484	1.711-3.607	<0.0001	3.272	2.014-5.317	<0.0001
LNC	0.996	0.983-1.010	0.602	1.043	1.019-1.066	0.0003
LNR	3.418	2.148-5.438	<0.0001	1.523	1.109-2.090	0.009
LNM	1.133	1.080-1.189	<0.0001	1.070	1.035-1.107	<0.0001
Metastasis						
M0	ref			ref		
M1	4.034	2.623-6.205	<0.0001	2.296	1.685-3.127	<0.0001
8th AJCC stage						
Ia	ref			ref		
Ib	1.517	0.983-2.339	0.060	0.797	0.438-1.448	0.456
IIa	2.624	1.542-4.466	0.0003	1.072	0.581-1.981	0.822
IIb	2.499	1.635-3.819	<0.0001	1.299	0.706-2.389	0.399
III	4.057	2.452-6.711	<0.0001	4.620	2.436-8.759	<0.0001
IV	8.046	4.585-14.117	<0.0001	2.794	1.513-5.158	0.001
Neoadjuvant chemotherapy						
No	ref			ref		
Yes	0.814	0.628-1.055	0.120	0.824	0.632-1.074	0.152

PHC, pancreatic head/uncinate ductal adenocarcinoma; PBTC, pancreatic body/tail ductal adenocarcinoma; BMI, body mass index; TBIL, total bilirubin; ALB, albumin; LNC, lymph node count; LNM, lymph node metastasis; LNR, lymph node ratio; CA125, cancer antigen 125; CA19-9, cancer antigen 19-9; CEA, carcino-embryonic antigen.

TABLE 4 | Multivariate Cox regression analysis of prognostic factors for PHC and PBTC patients with curative-intent surgical resection.

Variables	Multivariate analysis of PHC			Variables	Multivariate analysis of PBTC		
	HR	95% CI	p		HR	95% CI	p
Gender				Age	1.018	1.004-1.032	0.013
Male	ref			BMI	0.933	0.898-0.970	0.0004
Female	0.761	0.595-0.973	0.029	Fasting blood glucose	1.031	0.999-1.064	0.052
Fasting blood glucose	1.051	1.001-1.103	0.047	Smoking history			
Intraoperative blood loss	1.000	0.999-1.000	0.143	No	ref		
Histology				Yes	1.368	1.028-1.821	0.031
Poorly differentiated	ref			Histology			
Moderately differentiated	0.963	0.500-1.685	0.782	Poorly differentiated	ref		
Well differentiated	0.775	0.608-0.988	0.04	Moderately differentiated	0.644	0.493-0.841	0.001
Tumor size	1.112	1.017-1.216	0.019	Well differentiated	0.524	0.352-0.781	0.001
Perineuronal invasion				Tumor size	1.112	1.043-1.187	0.001
No	ref			Perineuronal invasion			
Yes	1.447	1.125-1.862	0.004	No	ref		
LNR	2.281	1.167-4.457	0.015	Yes	1.492	1.148-1.939	0.002
LNM	1.062	0.989-1.140	0.096	LNR	1.588	1.113-2.266	0.011
Metastasis				LNC	1.035	1.010-1.059	0.005
M0	ref			Metastasis			
M1	2.991	1.907-4.693	<0.0001	M0	ref		
CA125				M1	2.174	1.521-3.109	<0.0001
Normal	ref			Symptoms	0.905	0.835-0.981	0.044
Elevated	1.277	0.939-1.736	0.119	No	ref		
CA19-9				Yes	1.338	1.032-1.736	0.028
Normal	ref			CEA			
Elevated	1.612	1.204-2.157	0.001	Normal	ref		
				Elevated	1.388	1.193-1.647	0.101

PHC, pancreatic head/uncinate ductal adenocarcinoma; PBTC, pancreatic body/tail ductal adenocarcinoma; BMI, body mass index; LNC, lymph node count; LNM, lymph node metastasis; LNR, lymph node ratio; CA125, cancer antigen 125; CA19-9, cancer antigen 19-9; CEA, carcino-embryonic antigen.

The bootstrap-corrected c-indexes in the training cohort were 0.690 (95% CI 0.667–0.712) for PDCA, 0.669 (95% CI 0.636–0.702) for PHC, and 0.704 (95% CI 0.672–0.735) for PBTC. In the test cohort, the c-indexes were 0.669 (95% CI 0.634–0.704) for PDCA, 0.636 (95% CI 0.585–0.688) for PHC, and 0.643 (95% CI 0.588–0.699) for PBTC (**Table 5**).

Performance Comparison Between the Nomograms and 8th Edition TNM Staging Systems

In comparison to the AJCC 8TH staging system, the nomograms showed greater log-likelihoods and c-indexes, together with smaller values of AIC for CSS in the PDAC, PHC, and PBTC groups (**Table 5**), indicating that the newly established nomograms were more robust for survival prediction than the AJCC stages. Additionally, instead of the six stages classified by 8th AJCC system, the new models stratified patients into 10 nomo stages, providing better discriminative ability (**Figure 5**). As shown in **Suppl. Table 7**, the HRs for the Nomo stages also confirmed the classification ability of the nomograms. Further analysis (**Figure 6**) showed a good ability for risk stratification using the nomograms by stratifying the AJCC 8th stages into the low-, medium-, and high-risk groups. The mosaic plots intuitively demonstrated the dramatic survival heterogeneity between the 8th edition AJCC stages and the nomo stages (**Figure 7**). Finally, the ROC curve showed the superior sensitivity and specificity of nomograms compared with the 8th edition AJCC stages (**Suppl. Figure 1**), and DCA demonstrated that the net benefit was consistently enhanced in all cohorts of the nomograms with wide ranges of threshold probabilities compared with the TNM stages, suggesting the favorable clinical applicability of the nomograms for predicting survival (**Figure 8**).

Comparative Analysis of the Predictive Performance Among Three Nomograms

The PBTC nomogram had optimal AUCs in both the training cohort and test cohort, while the AUCs for the PDAC nomogram were higher than those of the PHC nomogram (**Table 6**). The aforementioned criteria (c-index) were consistent with the results of ROC curves (**Table 5**), indicating that the nomogram for PBTC performed best and the nomogram for PDAC was more robust for survival prediction compared with that for PHC.

DISCUSSION

PDAC can occur in different regions of the pancreas, and the influence of primary cancer location on the prognosis of PDAC has not been fully elucidated. Several nomograms had been established before to demonstrated their superiority over 8thAJCC system, some for the PBTC (16, 17), others for the PHC (18). However, this is the first study, to the best of our knowledge, developed three nomograms simultaneously based on the heterogeneous clinicopathological characteristics identified between PHC and PBTC. The novel major findings of this study are summarized as follows: (1) the primary cancer location was an independent factor for prognosis of patients with

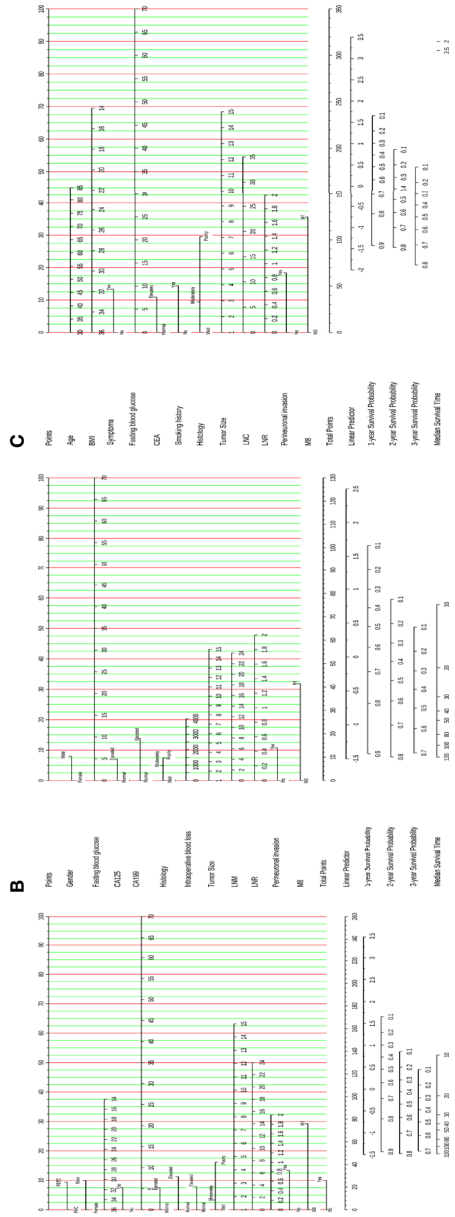

FIGURE 2 | Nomograms for survival prediction in PDAC, PHC and PBTC patients after surgery. **(A)** 1-, 2-, and 3-year CSS of PDAC; **(B)** 1-, 2-, and 3-year CSS of PHC; **(C)** 1-, 2-, and 3-year CSS of PBTC. The total points for the nomograms were calculated according to the points for each covariate. A higher total number of points represented a higher possibility of unfavorable expected survival. CSS, cancer-specific survival.

PDAC after surgery; (2) differential independent risk factors according to different primary tumor locations were identified to be significantly correlated with a poor prognosis; (3) three nomograms for the prediction of prognosis in PDAC, PHC, and PBTC were constructed on the basis of the identified independent prognosis factors; (4) these nomograms performed and calibrated well, with c-indexes of 0.690 (95% CI 0.667–0.712) for PDCA, 0.669 (95% CI 0.636–0.702) for PHC, and 0.704 (95% CI 0.672–0.735) for PBTC; and (5) performance comparison suggested that the newly established nomograms offer greater clinical net benefits than the 8th edition AJCC staging system. As such, these nomograms have the potential to be novel and better approaches for predicting survival of PHC and PBTC patients after surgery.

In the present study, we identified that tumor location was an independent risk factor for poor prognosis in PDAC. The prognosis of patients with PHC was better than that of patients with PBTC. Previous studies have shown the primary tumor location may have a significant impact on prognosis in colorectal and gastric cancer (19, 20), whereas its influence in PDAC remains controversial. Some previous studies have demonstrated that differences existed in the biological and oncological behavior and prognosis between head/uncinate and body/tail PC (6, 7, 21–25), while other studies (9, 26, 27) identified no significant correlation between primary tumor location and OS. Huang et al. (27) analyzed 11,837 patients with chemotherapy and surgical resection from five different countries, indicating that tumor location had no influence on survival. Nevertheless, they recruited the patients of stage I and II from 2003 to 2014, and the AJCC staging system was less accurate in early years. In contrast, we included patients from all stages based on their resectability, and the differences of prognosis between PHC and PBTC mainly occurred in stage Ia and III. It has been recognized that the head of the pancreas and the tail of pancreas arise from different embryonic anlagen, with the anterior domain of the pancreatic head together with the body and tail of pancreas derived from the dorsal primordia, while the ventral primordia formed inferior portions of the pancreatic head and uncinate process. Due to their differential embryological origins and differences in histology and cytology (28, 29), Dreyer et al. (24) reported that tumors in body and tail more likely were of the squamous subtype and were enriched for gene programs associated with tumor invasion and poor antitumor immune response. Hence, worse survival was observed with tumors in PBTC, consistent with the findings of some other studies (3, 18, 30). However, other studies proposed conclusion contrarily (8, 31).

The number of metastatic lymph nodes was not an independent risk factor as compared with other important clinical indicators such as tumor size and LNR. The 8th AJCC staging system overestimated the weight of lymph nodes, and it was inappropriate to classify all N2 stage cases as stage III (32, 33). We further compared the risk factors for PHC and PBTC and obtained some interesting findings. First, PHC and PBTC were found to have some unique independent risk factors, which indicated that their clinical-pathological behaviors might be

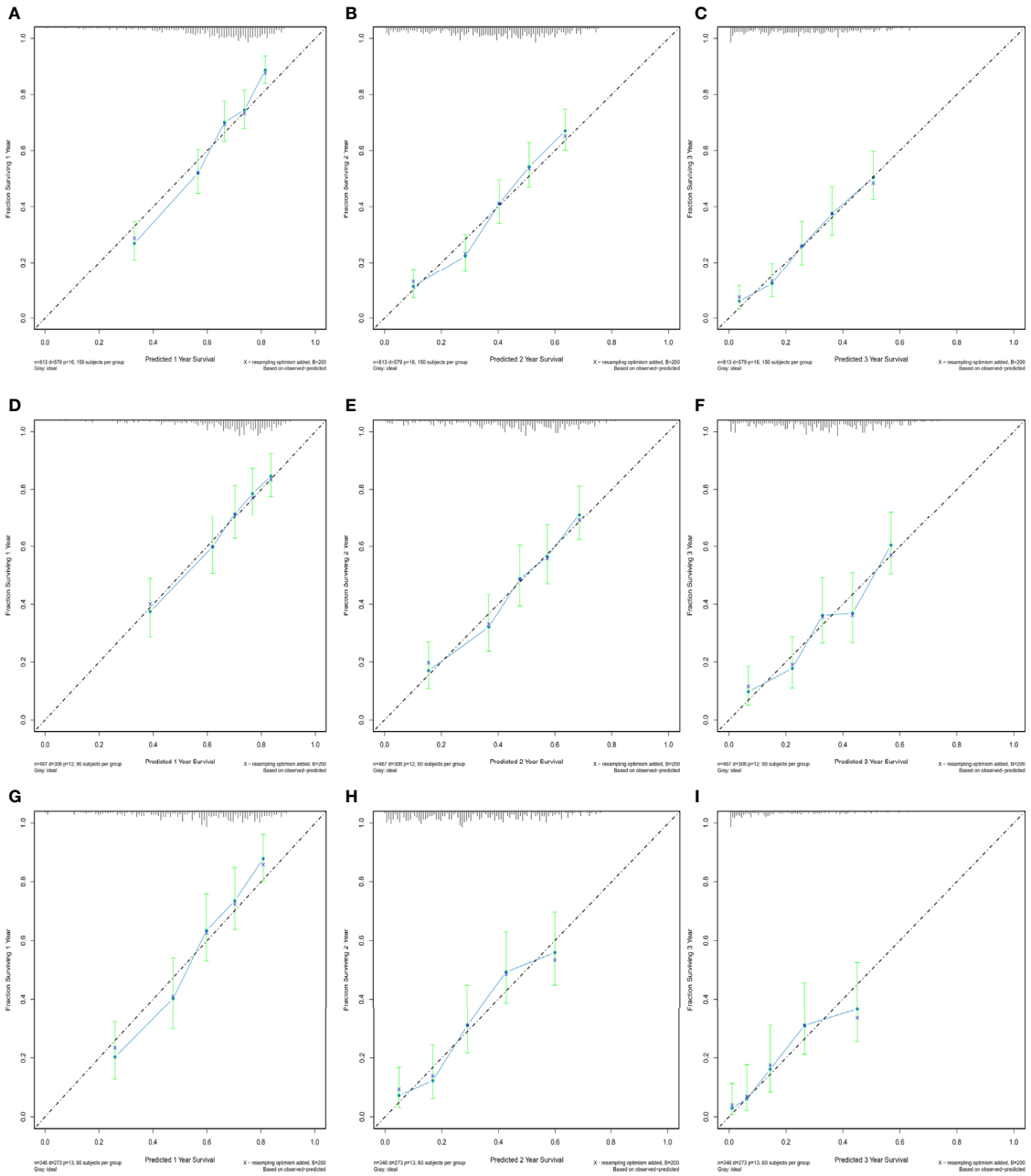

FIGURE 3 | Bootstrap calibrations of the nomograms in the training cohorts. Bootstrap calibrations of the nomograms for predicting **(A)** 1-year CSS, **(B)** 2-year CSS, and **(C)** 3-year CSS in PDAC group; **(D)** 1-year CSS, **(E)** 2-year CSS, and **(F)** 3-year CSS in the PHC group; and **(G)** 1-year CSS, **(H)** 2-year CSS, and **(I)** 3-year CSS in the PBTC group. The predictions were well correlated with the actual survival probabilities.

different. Secondly, tumor size, LNR, tumor differentiation degree, nerve invasion, and distant metastasis were all independent prognostic factors both for PHC and PBTC, which was consistent with previous reports (34–37). Third, the LNR in both groups exhibited independent predictive significance while LNM not. Some studies (38, 39) showed that the LNR had the strongest prediction ability compared with LNC and the 8th N stage. He et al. (40) identified the LNR as an independent predictive factor. Shi et al. (41) and Slidell et al. (42) found that LNC was as important as LNR, especially in node-negative disease. Similarly, in our study, negative lymph nodes were found more often in patients with PBTC, which might explain the strong correlation between LNC and the prognosis of PBTC. Fourth, hyperglycemia was found to an independent risk

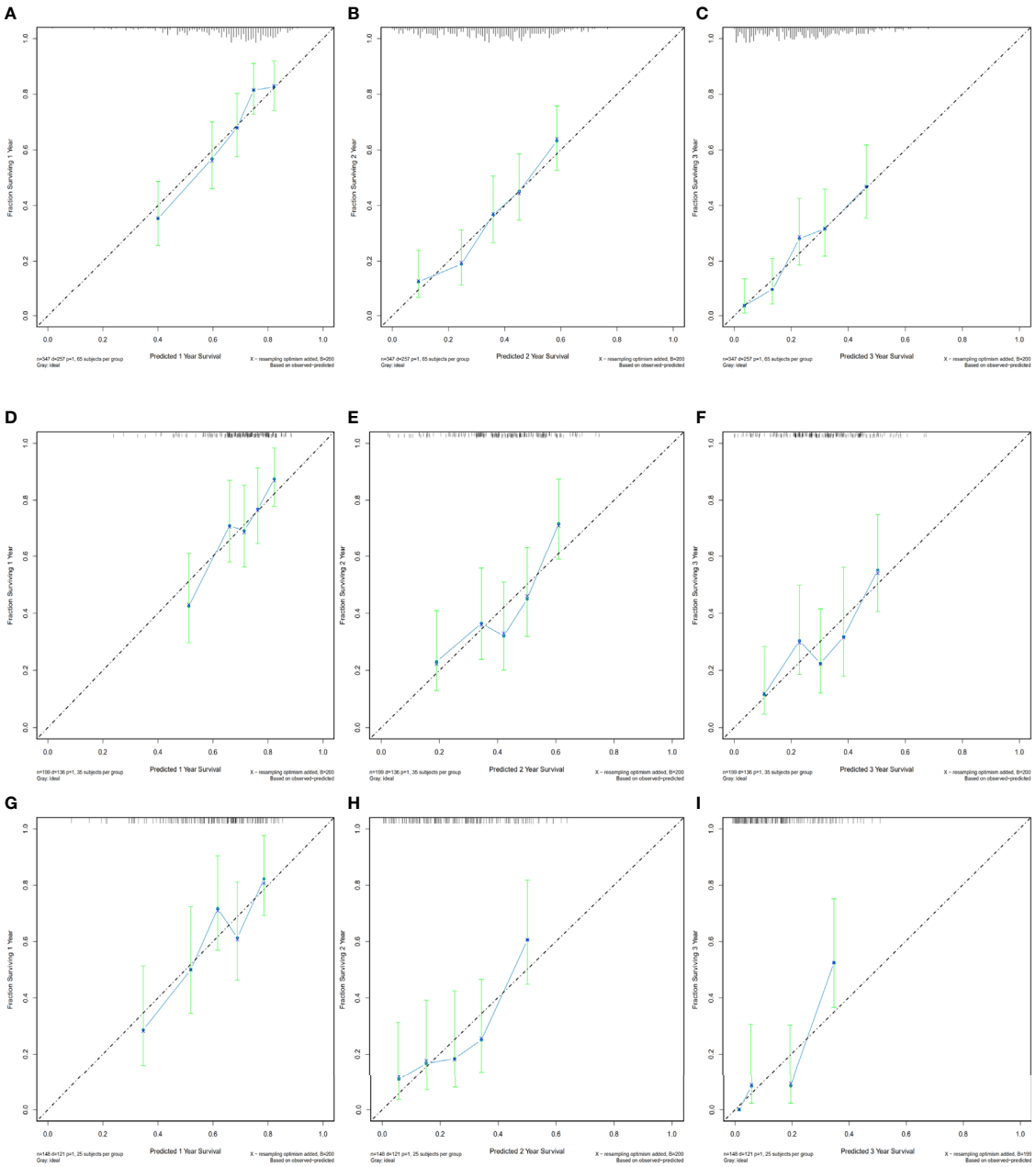

FIGURE 4 | Bootstrap calibration of nomograms in the test cohorts. The nomograms were externally validated in the test cohorts by predicting **(A)** 1-year CSS, **(B)** 2-year CSS, and **(C)** 3-year CSS in the PDAC group; **(D)** 1-year CSS, **(E)** 2-year CSS, and **(F)** 3-year CSS in the PHC group; and **(G)** 1-year CSS, **(H)** 2-year CSS, and **(I)** 3-year CSS in the PBTC group. All results showed good validation.

factor for PHC but not PBTC. Previous research (43–47) had shown that hyperglycemia is associated with worse survival of PC, but only a few studies focused on whether hyperglycemia affects the postoperative prognosis of PDAC. Raghavan et al. (44) reported that the prognosis of PDAC patients with hyperglycemia after surgery is poor, and the mechanism may be related to the Warburg effect. Li et al. (45) suggested that hyperglycemia might correlate with EMT. To date, there has been no report on whether hyperglycemia has distinctive impacts on pancreatic tumors in different locations. The above results demonstrated that the factors for prognosis of PDAC in different regions were heterogeneous, and the ability of 8th AJCC staging system to predict the outcome of PDAC remained mediocre as it defines PHC and PBTC as the same tumor.

We established nomograms on the basis of the differences in independent risk factors for PDAC, PHC and PBTC, and they

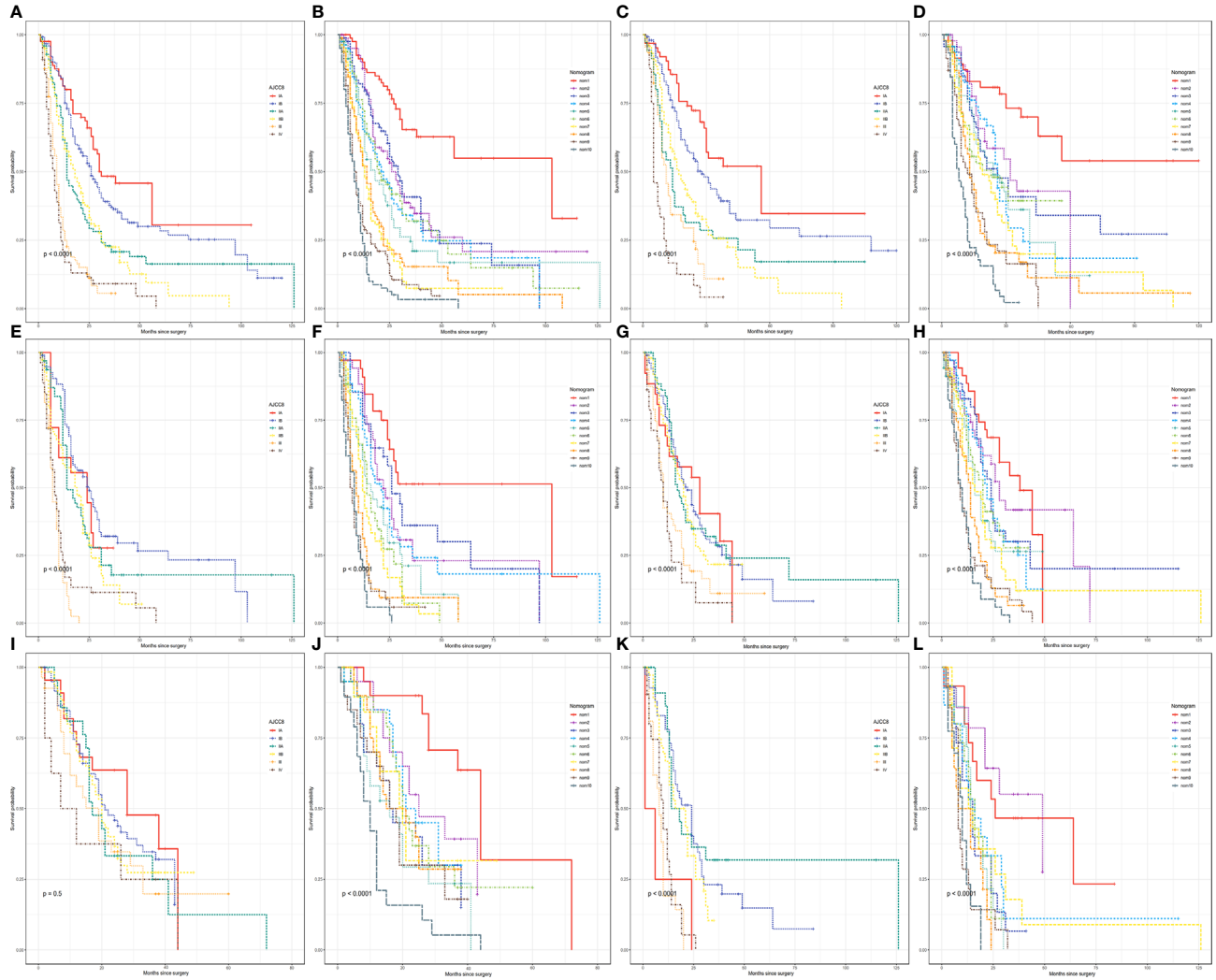

FIGURE 5 | Kaplan–Meier curve analysis of risk classification. Risk classification of the **(A, B)** PDAC group, **(C, D)** PHC group, and **(E, F)** PBTC group in the training cohort. Risk classification of the **(G, H)** PDAC group, **(I, J)** PHC group, and **(K, L)** PBTC group in the test cohort. All log-rank p values for trends were <0.0001, except p=0.5 for **(I)**.

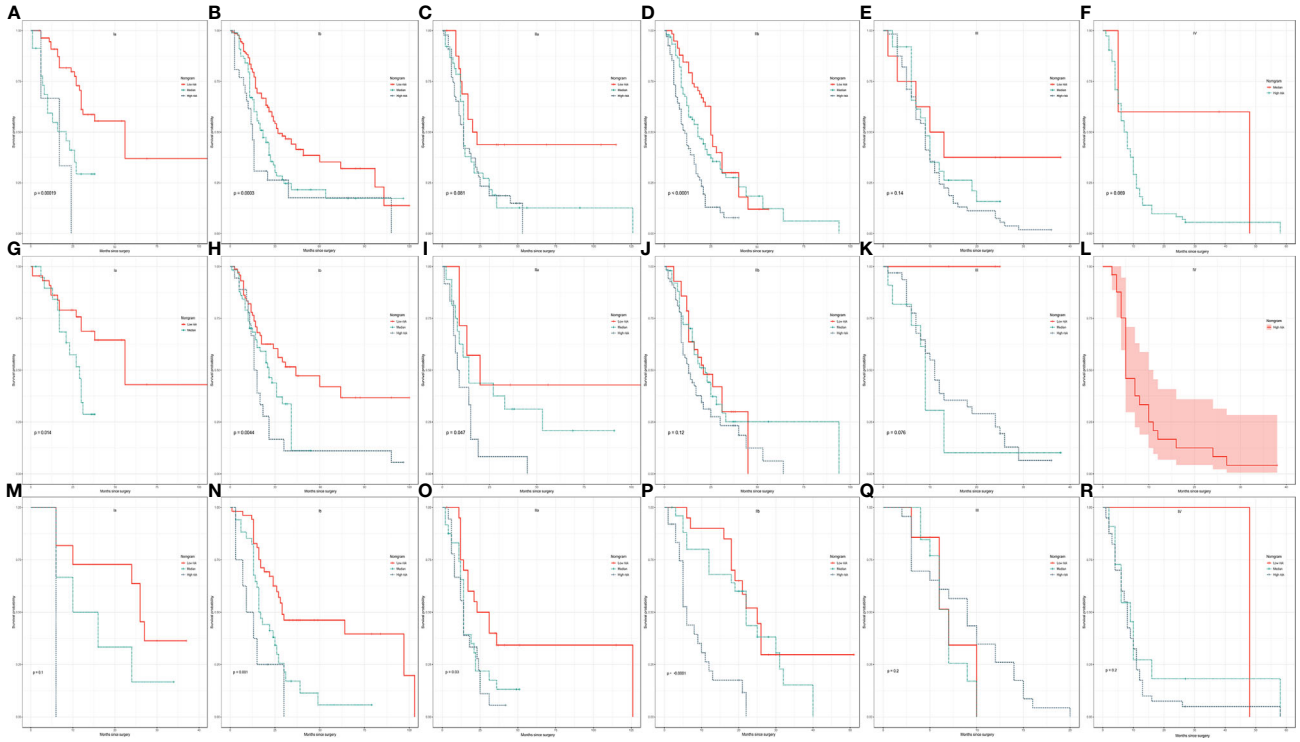

FIGURE 6 | Kaplan–Meier curve analysis of risk stratification. Risk stratification in the training cohort for each 8th AJCC substage in the **(A–F)** PDAC group, **(G–L)** PHC group, and **(M–R)** PBTC group. The log-rank p values were <0.05 for **(A, B, D, G, H, I, N–P)**.

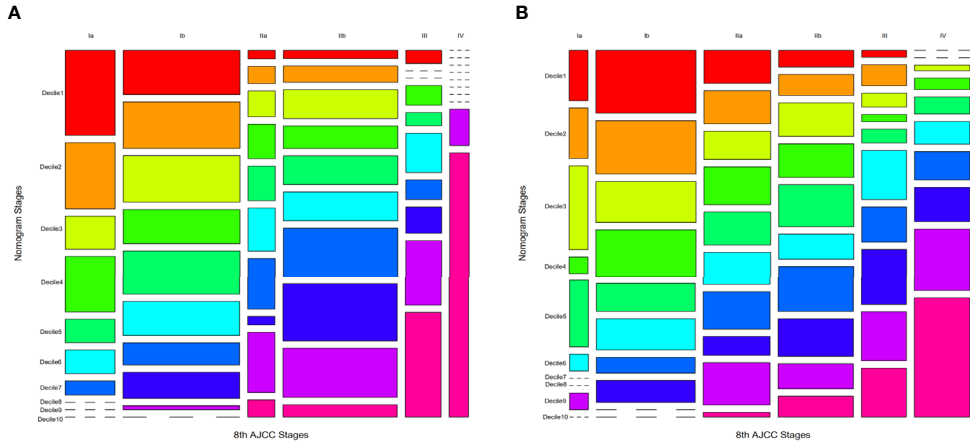

FIGURE 7 | Mosaic plots using the training cohort. **(A)** Mosaic plots for PHC and **(B)** PBTC in which each of the 10 deciles was represented by 1 of 10 consecutive rainbow colors. The area of the individual mosaics represents the represents the proportions of corresponding patients. The short-segmented lines indicate a frequency of zero.

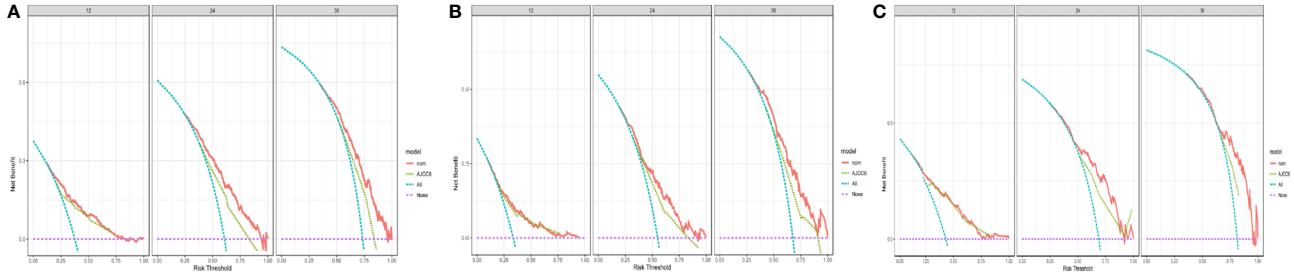

FIGURE 8 | Decision curve analysis and comparison of the nomograms with the 8thAJCC stages. Decision curve analysis (DCA) of the nomograms for predicting **(A)** 1-, 2-, and 3-year survival in the PDAC group; **(B)** 1-, 2-, and 3-year survival in the PHC; and **(C)** 1-, 2-, and 3-year survival in the PBTC group.

TABLE 5 | Comparison of nomograms with the AJCC staging system.

			Nomogram score	8th AJCC stage	p
Training cohort	PDAC	AIC	6734.785	6803.814	
		loglikelihood	-3366.392	-3396.907	
		c-index	0.690(0.667-0.712)	0.652(0.629-0.676)	0.002
	PHC	AIC	3266.077	3307.219	
		loglikelihood	-1632.038	-1648.609	
		c-index	0.669(0.636-0.702)	0.640(0.608-0.672)	0.04
	PBTC	AIC	2649.604	2684.392	
		loglikelihood	-1323.802	-1337.196	
		c-index	0.704(0.672-0.735)	0.656(0.622-0.690)	0.009
Test cohort	PDAC	AIC	2569.793	2625.635	
		loglikelihood	-1283.896	-1307.817	
		c-index	0.669(0.634-0.704)	0.591(0.550-0.631)	<0.0001
	PHC	AIC	1236.191	1266.524	
		loglikelihood	-617.095	-628.262	
		c-index	0.636(0.585-0.688)	0.558(0.502-0.614)	0.0008
	PBTC	AIC	989.924	989.506	
		loglikelihood	-493.962	-489.753	
		c-index	0.643(0.588-0.699)	0.618(0.562-0.674)	0.3

PDAC, pancreatic ductal adenocarcinoma; AIC, Akaike information criterion; PHC, pancreatic head/uncinate ductal adenocarcinoma; PBTC, pancreatic body/tail ductal adenocarcinoma.

TABLE 6 | Time-dependent ROC curve analysis.

	Training cohort AUC (%)						Test cohort AUC (%)					
Study cohort	**1 year**	**95% CI**	**2 year**	**95% CI**	**3 year**	**95% CI**	**1 year**	**95% CI**	**2 year**	**95% CI**	**3 year**	**95% CI**
PDAC	76.30	72.78-79.83	74.72	71.02-78.43	73.16	68.4-77.93	72.07	66.12-78.03	73.81	67.99-79.64	73.39	66.31-80.49
PHC	72.32	67.16-77.5	71.34	66.29-76.39	72.58	66.6-78.57	66.06	57.34-74.79	66.28	57.71-74.85	64.81	54.08-75.54
PBTC	80.00	75.07-84.92	77.33	71.67-82.98	76.97	69.45-84.49	69.69	60.69-78.7	76.63	67.22-86.06	83.70	71.85-95.56

showed high accuracy and reliability in the prognostic prediction of PHC and PBTC. Notably, our results support that the performance of these nomograms was superior to the latest edition 8th AJCC staging system. Furthermore, the newly established nomograms were able to stratify PDAC into 10 nomo stages in comparison with only three prognostic subgroups by each 8th AJCC stage, achieving more robust risk classification and stratification. Although there were many stages, clinicians only need the scores of patients according to nomograms, and the scores had one-to-one correspondence with the corresponding stage. Given that the better classification and stratification abilities can classify patients more precisely, the nomograms developed in this study may better help clinicians to identify high-risk patients and thereby promote personalized treatment planning. In addition, DCA verified the favorable clinical validity of the nomograms with consistently enhanced net benefits compared with the latest AJCC staging system. Among the three new models, the nomogram for PBTC had the best performance, as evidenced by the highest c-index and AUC value, while the nomogram for PDAC was slightly better than that for PHC. Therefore, we suggest that the nomogram for PDAC can be used in PHC patients to achieve more accurate survival prediction.

The present study has several potential limitations. First, PDAC patients were retrospectively recruited from three medical centers in China, the information of some impactful predictors such as cancer recurrence, neoadjuvant and adjuvant chemotherapy was incomplete, and differences in surgical procedure and postoperative pathological examinations may have existed, these might be the reasons for the moderate c-indexes, and thus, a prospective study is needed to validate the performance of the nomograms. Second, the enrolled patients included mainly individuals of Chinese ethnic population; thus, the nomograms established in this study will need to be verified in other ethnic populations. Third, this study enrolled patients with M1 stage; however, these were the patients with hepatic metastasis who showed a survival benefit following hepatic metastasis resection for PDAC, as reported by two small single-center series (48, 49). Fourth, genetic factors were not integrated into the analysis of risk factors for prognosis, as they might influence the prognosis.

In summary, the present study shows the differential clinical-pathological characteristics and after-surgery outcomes between PHC and PBTC, and demonstrates the prognosis of them should be evaluated by different staging systems, which have been successfully constructed in this study. The results show that these nomograms perform well and are well calibrated, and therefore, they hold potential to be used as novel and improved tools for the prediction of survival among PHC and PBTC patients after surgical treatment.

DATA AVAILABILITY STATEMENT

The original contributions presented in the study are included in the article/**Supplementary Material**. Further inquiries can be directed to the corresponding authors.

ETHICS STATEMENT

The studies involving human participants were reviewed and approved by the ethics committee of Fujian Medical University Union Hospital, Fujian Provincial Hospital, Ruijin Hospital. The patients/participants provided their written informed consent to participate in this study. Written informed consent was obtained from the individual(s) for the publication of any potentially identifiable images or data included in this article.

AUTHOR CONTRIBUTIONS

GL, C-YL and J-ZC: carried out the concepts, design, definition of intellectual content, literature search, data acquisition, data analysis and manuscript preparation. LH, CY, and Y-FT: helped perform the analysis with constructive discussions. QD and Y-TW: provided assistance for data acquisition, data analysis and statistical analysis. SC, QZ, and Y-LC: contributed to the conception of the study and performed manuscript review. All authors contributed to the article and approved the submitted version.

FUNDING

This work was supported by the high-level hospital foster grants from Fujian Provincial Hospital (#2019HSJJ13 to SC), the Natural Science Foundation for Distinguished Young Scholars of Fujian Province (#2018J06020 to SC), the Education and Scientific Research Foundation of Fujian Province (#2060402 to SC), the joint Funds for the innovation of science and technology, Fujian Province (#2018Y9098 to SC), the Fujian Provincial Health and Family Planning Research Medical Innovation Project (2019-cx-3 to SC), the Natural Science Foundation of Fujian Province (#2017J01206 to QD), the Startup Fund for scientific research, Fujian Medical University (#2019QH1036 to GL) and Fujian Province Educational Research Project for Youths (#JAT190185 to GL).

SUPPLEMENTARY MATERIAL

The Supplementary Material for this article can be found online at: https://www.frontiersin.org/articles/10.3389/fonc.2021.646082/full#supplementary-material

Supplementary Figure 1 | ROC curve analysis and comparison of the nomograms with the 8thAJCC stages. ROC curve analysis of the nomograms for predicting **(A)** 1-, 2-, and 3-year survival in the PDAC group; **(B)** 1-, 2-, and 3-year survival in the PHC; and **(C)** 1-, 2-, and 3-year survival in the PBTC group.

REFERENCES

1. Bray F, Ferlay J, Soerjomataram I, Siegel RL, Torre LA, Jemal A. Global Cancer Statistics 2018: GLOBOCAN Estimates of Incidence and Mortality Worldwide for 36 Cancers in 185 Countries. *CA Cancer J Clin* (2018) 68:394–424. doi: 10.3322/caac.21492
2. Neoptolemos JP, Palmer DH, Ghaneh P, Psarelli EE, Valle JW, Halloran CM, et al. Comparison of Adjuvant Gemcitabine and Capecitabine With Gemcitabine Monotherapy in Patients With Resected Pancreatic Cancer (ESPAC-4): A Multicentre, Open-Label, Randomised, Phase 3 Trial. *Lancet (London England)* (2017) 389:1011–24. doi: 10.1016/s0140-6736(16)32409-6
3. Artinyan A, Soriano PA, Prendergast C, Low T, Ellenhorn JD, Kim J. The Anatomic Location of Pancreatic Cancer is a Prognostic Factor for Survival. *HPB (Oxford)* (2008) 10:371–6. doi: 10.1080/13651820802291233
4. Brennan MF, Moccia RD, Klimstra D. Management of Adenocarcinoma of the Body and Tail of the Pancreas. *Ann Surg* (1996) 223:506–11; discussion 11-2. doi: 10.1097/00000658-199605000-00006
5. Watanabe I, Sasaki S, Konishi M, Nakagohri T, Inoue K, Oda T, et al. Onset Symptoms and Tumor Locations as Prognostic Factors of Pancreatic Cancer. *Pancreas* (2004) 28:160–5. doi: 10.1097/00006676-200403000-00007
6. Lau MK, Davila JA, Shaib YH. Incidence and Survival of Pancreatic Head and Body and Tail Cancers: A Population-Based Study in the United States. *Pancreas* (2010) 39:458–62. doi: 10.1097/MPA.0b013e3181bd6489
7. Zheng Z, Wang M, Tan C, Chen Y, Ping J, Wang R, et al. Disparities in Survival by Stage After Surgery Between Pancreatic Head and Body/Tail in Patients With Nonmetastatic Pancreatic Cancer. *PloS One* (2019) 14: e0226726. doi: 10.1371/journal.pone.0226726
8. Winer LK, Dhar VK, Wima K, Morris MC, Lee TC, Shah SA, et al. The Impact of Tumor Location on Resection and Survival for Pancreatic Ductal Adenocarcinoma. *J Surg Res* (2019) 239:60–6. doi: 10.1016/j.jss.2019.01.061
9. van Erning FN, Mackay TM, van der Geest LGM, Groot Koerkamp B, van Laarhoven HWM, Bonsing BA, et al. Association of the Location of Pancreatic Ductal Adenocarcinoma (Head, Body, Tail) With Tumor Stage, Treatment, and Survival: A Population-Based Analysis. *Acta Oncol (Stockholm Sweden)* (2018) 57:1655–62. doi: 10.1080/0284186x.2018.1518593
10. Li G, Chen JZ, Chen S, Lin SZ, Pan W, Meng ZW, et al. Development and Validation of Novel Nomograms for Predicting the Survival of Patients After Surgical Resection of Pancreatic Ductal Adenocarcinoma. *Cancer Med* (2020) 9:3353–70. doi: 10.1002/cam4.2959
11. Harrell F. *Regression Modeling Strategies: With Applications to Linear Models, Logistic and Ordinal Regression, and Survival Analysis*. Verlag New York: Springer (2002).
12. Kang L, Chen W, Petrick NA, Gallas BD. Comparing Two Correlated C Indices With Right-Censored Survival Outcome: A One-Shot Nonparametric Approach. *Stat Med* (2015) 34:685–703. doi: 10.1002/sim.6370
13. Hung H CC. Estimation Methods for Time-Dependent AUC Models With Survival Data. *Can J Stat* (2010) 38:8–26. doi: 10.2307/27805213
14. Vickers AJ, Elkin EB. Decision Curve Analysis: A Novel Method for Evaluating Prediction Models. *Med Decis Making* (2006) 26:565–74. doi: 10.1177/0272989x06295361
15. Allen PJ, Kuk D, Castillo CF, Basturk O, Wolfgang CL, Cameron JL, et al. Multi-Institutional Validation Study of the American Joint Commission on Cancer (8th Edition) Changes for T and N Staging in Patients With Pancreatic Adenocarcinoma. *Ann Surg* (2017) 265:185–91. doi: 10.1097/sla.0000000000001763
16. He C, Sun S, Zhang Y, Lin X, Li S. Score for the Overall Survival Probability of Patients With Pancreatic Adenocarcinoma of the Body and Tail After Surgery: A Novel Nomogram-Based Risk Assessment. *Front Oncol* (2020) 10:590. doi: 10.3389/fonc.2020.00590
17. Zou Y, Shi N, Ruan S, Jin L, Yin Z, Hang H, et al. Development of a Nomogram to Predict Diseasespecific Survival for Patients After Resection of a non-Metastatic Adenocarcinoma of the Pancreatic Body and Tail. *Front Oncol* (2020) 10:526602. doi: 10.3389/fonc.2020.526602
18. Li H-b, Zhou J, Zhao F-q. A Prognostic Nomogram for Disease-Specific Survival in Patients With Pancreatic Ductal Adenocarcinoma of the Head of

the Pancreas Following Pancreaticoduodenectomy. *Med Sci Monit* (2018) 24:6313–21. doi: 10.12659/MSM.909649
19. Petrelli F, Ghidini M, Barni S, Steccanella F, Sgroi G, Passalacqua R, et al. Prognostic Role of Primary Tumor Location in non-Metastatic Gastric Cancer: A Systematic Review and Meta-Analysis of 50 Studies. *Ann Surg Oncol* (2017) 24:2655–68. doi: 10.1245/s10434-017-5832-4
20. Petrelli F, Tomasello G, Borgonovo K, Ghidini M, Turati L, Dallera P, et al. Prognostic Survival Associated With Left-Sided vs Right-Sided Colon Cancer: A Systematic Review and Meta-Analysis. *JAMA Oncol* (2017) 3:211–9. doi: 10.1001/jamaoncol.2016.4227
21. Birnbaum DJ, Bertucci F, Finetti P, Birnbaum D, Mamessier E. Head and Body/Tail Pancreatic Carcinomas are Not the Same Tumors. *Cancers* (2019) 11:497. doi: 10.3390/cancers11040497
22. Mackay TM, van Erning FN, van der Geest LGM, de Groot JWB, Haj Mohammad N, Lemmens VE, et al. Association Between Primary Origin (Head, Body and Tail) of Metastasised Pancreatic Ductal Adenocarcinoma and Oncologic Outcome: A Population-Based Analysis. *Eur J Cancer (Oxford Engl 1990)* (2019) 106:99–105. doi: 10.1016/j.ejca.2018.10.008
23. Yin L, Xiao L, Gao Y, Wang G, Gao H, Peng Y, et al. Comparative Bioinformatical Analysis of Pancreatic Head Cancer and Pancreatic Body/Tail Cancer. *Med Oncol (Northwood London England)* (2020) 37:46. doi: 10.1007/s12032-020-01370-0
24. Dreyer SB, Jamieson NB, Upstill-Goddard R, Bailey PJ, McKay CJ, Biankin AV, et al. Defining the Molecular Pathology of Pancreatic Body and Tail Adenocarcinoma. *Br J Surg* (2018) 105:e183–e91. doi: 10.1002/bjs.10772
25. Lee M, Kwon W, Kim H, Byun Y, Han Y, Kang JS, et al. The Role of Location of Tumor in the Prognosis of the Pancreatic Cancer. *Cancers* (2020) 12:2036. doi: 10.3390/cancers12082036
26. Ruess DA, Makowiec F, Chikhladze S, Sick O, Riediger H, Hopt UT, et al. The Prognostic Influence of Intrapancreatic Tumor Location on Survival After Resection of Pancreatic Ductal Adenocarcinoma. *BMC Surg* (2015) 15:123. doi: 10.1186/s12893-015-0110-5
27. Huang L, Balavarca Y, van der Geest L, Lemmens V, Van Eycken L, De Schutter H, et al. Development and Validation of a Prognostic Model to Predict the Prognosis of Patients Who Underwent Chemotherapy and Resection of Pancreaticadenocarcinoma: A Large International Population-Based Cohort Study. *BMC Med* (2019) 17:66. doi: 10.1186/s12916-019-1304-y
28. Radi M, Gaubert J, Cristol-Gaubert R, Baecker V, Travo P, Prudhomme M, et al. A 3D Reconstruction of Pancreas Development in the Human Embryos During Embryonic Period (Carnegie Stages 15-23). *Surg Radiol Anat* (2010) 32:11–5. doi: 10.1007/s00276-009-0533-8
29. Tadokoro H, Kozu T, Toki F, Kobayashi M, Hayashi N. Embryological Fusion Between the Ducts of the Ventral and Dorsal Primordia of the Pancreas Occurs in Two Manners. *Pancreas* (1997) 14:407–14. doi: 10.1097/00006676-199705000-00012
30. Sheng W, Dong M, Wang G, Shi X, Gao W, Wang K, et al. The Diversity Between Curatively Resected Pancreatic Head and Body-Tail Cancers Based on the 8th Edition of AJCC Staging System: A Multicenter Cohort Study. *BMC Cancer* (2019) 19:981. doi: 10.1186/s12885-019-6178-z
31. Meng Z, Cao M, Zhang Y, Liu Z, Wu S, Wu H. Tumor Location as an Indicator of Survival in T1 Resectable Pancreatic Ductal Adenocarcinoma: A Propensity Score-Matched Analysis. *BMC Gastroenterol* (2019) 19:59. doi: 10.1186/s12876-019-0975-3
32. Shin DW, Lee JC, Kim J, Woo SM, Lee WJ, Han SS, et al. Validation of the American Joint Committee on Cancer 8th Edition Staging System for the Pancreatic Ductal Adenocarcinoma. *Eur J Surg Oncol* (2019) 45:2159–65. doi: 10.1016/j.ejso.2019.06.002
33. Song M, Yoon SB, Lee IS, Hong TH, Choi HJ, Choi MH, et al. Evaluation of the Prognostic Value of the New AJCC 8th Edition Staging System for Patients With Pancreatic Adenocarcinoma; A Need to Subclassify Stage III? *Eur J Cancer (Oxford Engl 1990)* (2018) 104:62–9. doi: 10.1016/j.ejca.2018.08.027
34. Yu FJ, Shih HY, Wu CY, Chuang YS, Lee JY, Li HP, et al. Enteral Nutrition and Quality of Life in Patients Undergoing Chemoradiotherapy for Esophageal Carcinoma: A Comparison of Nasogastric Tube, Esophageal Stent, and Ostomy Tube Feeding. *Gastrointest Endosc* (2018) 88:21–31.e4. doi: 10.1016/j.gie.2017.11.030
35. Pindak D, Tomas M, Dolnik J, Duchon R, Pavlendova J. Morbidity, Mortality and Long Term Survival in Patients With Vascular Resection in Pancreatic Cancer - Single Center Experience. *Neoplasma* (2017) 64:460–3. doi: 10.4149/neo_2017_318
36. Yamamoto T, Yagi S, Kinoshita H, Sakamoto Y, Okada K, Uryuhara K, et al. Long-Term Survival After Resection of Pancreatic Cancer: A Single-Center Retrospective Analysis. *World J Gastroenterol* (2015) 21:262–8. doi: 10.3748/wjg.v21.i1.262
37. Schorn S, Demir IE, Haller B, Scheufele F, Reyes CM, Tieftrunk E, et al. The Influence of Neural Invasion on Survival and Tumor Recurrence in Pancreatic Ductal Adenocarcinoma - A Systematic Review and Meta-Analysis. *Surg Oncol* (2017) 26:105–15. doi: 10.1016/j.suronc.2017.01.007
38. Riediger H, Keck T, Wellner U, zur Hausen A, Adam U, Hopt UT, et al. The Lymph Node Ratio is the Strongest Prognostic Factor After Resection of Pancreatic Cancer. *J Gastrointest Surg* (2009) 13:1337–44. doi: 10.1007/s11605-009-0919-2
39. Pawlik TM, Gleisner AL, Cameron JL, Winter JM, Assumpcao L, Lillemoe KD, et al. Prognostic Relevance of Lymph Node Ratio Following Pancreaticoduodenectomy for Pancreatic Cancer. *Surgery* (2007) 141:610–8. doi: 10.1016/j.surg.2006.12.013
40. He C, Zhang Y, Cai Z, Lin X, Li S. Overall Survival and Cancer-Specific Survival in Patients With Surgically Resected Pancreatic Head Adenocarcinoma: A Competing Risk Nomogram Analysis. *J Cancer* (2018) 9:3156–67. doi: 10.7150/jca.25494
41. Shi S, Hua J, Liang C, Meng Q, Liang D, Xu J, et al. Proposed Modification of the 8th Edition of the AJCC Staging System for Pancreatic Ductal Adenocarcinoma. *Ann Surg* (2019) 269:944–50. doi: 10.1097/sla.0000000000002668
42. Slidell MB, Chang DC, Cameron JL, Wolfgang C, Herman JM, Schulick RD, et al. Impact of Total Lymph Node Count and Lymph Node Ratio on Staging and Survival After Pancreatectomy for Pancreatic Adenocarcinoma: A Large, Population-Based Analysis. *Ann Surg Oncol* (2008) 15:165–74. doi: 10.1245/s10434-007-9587-1
43. Liao WC, Tu YK, Wu MS, Lin JT, Wang HP, Chien KL. Blood Glucose Concentration and Risk of Pancreatic Cancer: Systematic Review and Dose-Response Meta-Analysis. *BMJ (Clinical Res ed)* (2015) 350:g7371. doi: 10.1136/bmj.g7371
44. Raghavan SR, Ballehaninna UK, Chamberlain RS. The Impact of Perioperative Blood Glucose Levels on Pancreatic Cancer Prognosis and Surgical Outcomes: An Evidence-Based Review. *Pancreas* (2013) 42:1210–7. doi: 10.1097/MPA.0b013e3182a6db8e
45. Li W, Zhang L, Chen X, Jiang Z, Zong L, Ma Q. Hyperglycemia Promotes the Epithelial-Mesenchymal Transition of Pancreatic Cancer Via Hydrogen Peroxide. *Oxid Med Cell Longev* (2016) 2016:5190314. doi: 10.1155/2016/5190314
46. Sharma A, Smyrk TC, Levy MJ, Topazian MA, Chari ST. Fasting Blood Glucose Levels Provide Estimate of Duration and Progression of Pancreatic Cancer Before Diagnosis. *Gastroenterology* (2018) 155:490–500.e2. doi: 10.1053/j.gastro.2018.04.025
47. Nagai M, Murakami Y, Tamakoshi A, Kiyohara Y, Yamada M, Ukawa S, et al. Fasting But Not Casual Blood Glucose is Associated With Pancreatic Cancer Mortality in Japanese: EPOCH-JAPAN. *Cancer Causes Control* (2017) 28:625–33. doi: 10.1007/s10552-017-0884-0
48. Shrikhande SV, Kleeff J, Reiser C, Weitz J, Hinz U, Esposito I, et al. Pancreatic Resection for M1 Pancreatic Ductal Adenocarcinoma. *Ann Surg Oncol* (2007) 14:118–27. doi: 10.1245/s10434-006-9131-8
49. Yamada H, Hirano S, Tanaka E, Shichinohe T, Kondo S. Surgical Treatment of Liver Metastases From Pancreatic Cancer. *HPB (Oxford)* (2006) 8:85–8. doi: 10.1080/13651820500472200

Conflict of Interest: The authors declare that the research was conducted in the absence of any commercial or financial relationships that could be construed as a potential conflict of interest.

frontiers in Oncology

ORIGINAL RESEARCH
published: 28 April 2021
doi: 10.3389/fonc.2021.652426

Hepatic Artery Infusion of Floxuridine in Combination With Systemic Chemotherapy for Pancreatic Cancer Liver Metastasis: A Propensity Score-Matched Analysis in Two Centers

Changli Peng[1,2†], Bin Xu[3†], Juxiong Xiao[1†], Chunhui Zhou[1], Xiaodong Li[4], Hongbing Shi[4], Weiguang Qiang[4], Tianming Wang[1], Jiemin Zhao[4], Fei Liu[1], Gang Li[1], Haiping Li[1], Changyong Chen[1] and Liangrong Shi[1,2]*

[1] Interventional Radiology Center, Department of Radiology, Xiangya Hospital Central South University, Changsha, China, [2] Research Center for Geriatric Disorder, Xiangya Hospital Central South University, Changsha, China, [3] Department of Tumor Biological Treatment, The Third Affiliated Hospital, Soochow University, Changzhou, China, [4] Department of Oncology, The Third Affiliated Hospital of Soochow University, Changzhou, China

Aim: To evaluate the efficacy of hepatic artery infusion (HAI) of floxuridine (FUDR) in combination with systemic chemotherapy in patients with pancreatic cancer liver metastases (PCLM).

Patients and Methods: We retrospectively collected clinical data of 347 patients with PCLM who underwent first-line chemotherapy at two Chinese centers between 2012 and 2019. Propensity score matching between patients with and without HAI was performed to compensate for differences in baseline characteristics. Objective response rate (ORR) and overall survival (OS) between groups were compared. HAI pump functionality was recorded.

Results: Data of 258 patients (62 patients with HAI and 196 patients without HAI) were used for matching. After 1:1 ratio matching, 62 patients per group were included. The intrahepatic ORR was 66.1% in the HAI group and 22.6% in the non-HAI group ($P < 0.001$), and the extrahepatic ORR was 25.0 *versus* 28.9% ($P = 0.679$). The median OS was significantly longer in HAI group (14.0 *versus* 10.8 months, $P = 0.001$). Multivariance COX regression showed HAI led to a decrease in hazard ratio for death by 61.8% (HR = 0.382; 95% CI: 0.252–0.578; $P< 0.001$). Subgroup analysis revealed that patients without EHM, with higher intrahepatic tumor burden and with synchronous liver metastasis benefited more from HAI. Dysfunction of HAI pump occurred in 5.7% of patients during the period of follow-up.

OPEN ACCESS

Edited by:
Takatsugu Ishimoto, Kumamoto University, Japan

Reviewed by:
Alessandro Boscarelli, Institute for Maternal and Child Health Burlo Garofolo (IRCCS), Italy
Ali Coskun, Izmir Bozyaka Training and Research Hospital, Turkey

***Correspondence:**
Liangrong Shi
shiliangrong@csu.edu.cn

[†]These authors have contributed equally to this work

Specialty section:
This article was submitted to Gastrointestinal Cancers, a section of the journal Frontiers in Oncology

Received: 12 January 2021
Accepted: 06 April 2021
Published: 28 April 2021

Citation:
Peng C, Xu B, Xiao J, Zhou C, Li X, Shi H, Qiang W, Wang T, Zhao J, Liu F, Li G, Li H, Chen C and Shi L (2021) Hepatic Artery Infusion of Floxuridine in Combination With Systemic Chemotherapy for Pancreatic Cancer Liver Metastasis: A Propensity Score-Matched Analysis in Two Centers. Front. Oncol. 11:652426. doi: 10.3389/fonc.2021.652426

Conclusions: In patients with PCLM, first-line treatment with HAI FUDR plus SCT resulted in higher intrahepatic response and better OS.

Keywords: pancreatic cancer, liver metastasis, hepatic artery infusion, floxuridine, propensity score

INTRODUCTION

Pancreatic cancer is the seventh leading cause of global cancer deaths in industrialized countries (1). The majority of patients present with locally advanced or metastatic disease at initial diagnosis (2, 3), which leads to poor prognosis and a 5-year survival at 7% (4). Although the clinical outcome is still limited, chemotherapy remains the primary treatment modality for patients with metastatic pancreatic cancer (5). Given liver metastasis is most frequent situation and primarily responsible for the high mortality of pancreatic cancer (6), robust management of intrahepatic lesions may provide survival benefit.

Hepatic artery infusion (HAI) chemotherapy provides high drug exposure of the tumor at first passage, which offers theoretical advantages over systemic administration of drugs (7, 8). Floxuridine (FUDR), a deoxyribonucleoside derivative of 5-Fu, is an ideal agent for HAI due to its short half-life and extensive first pass extraction (9). Commonly, FUDR was administered continuously at low dose *via* HAI pump in combination with standard systemic chemotherapy (SCT). We and others have demonstrated that HAI plus SCT is effective in improving hepatic response and prolonging survival in colorectal cancer liver metastases (CRCLM) (10–13). Recently, HAI FUDR was also demonstrated to be effective in intrahepatic cholangiocarcinoma (IHC) (14).

Herein, we evaluate the efficacy of HAI FUDR *via* a radiologically implanted pump in patients who had pancreatic cancer liver metastases (PCLM) in two centers. The primary aim was to compare overall survival (OS) from HAI plus SCT *versus* SCT alone. The second aims were to evaluate the short-term effect and functionality of HAI pump system.

PATIENTS AND METHODS

Patients

From 2012 to 2019, consecutive histologically confirmed PCLM patients who received first-line chemotherapy were included from prospectively maintained databases in two Chinese centers (Xiangya Hospital, Central South University; the Third Affiliated Hospital of Soochow University). Patients with metachronous metastasis were included if the interval between the occurrence of liver metastasis and the end of adjuvant chemotherapy is more than 6 months. Patients who received concurrent radiotherapy were excluded. The cohort was divided into two groups according to whether the patients received HAI FUDR therapy. This study was approved by the Medical Ethics Committee of the Xiangya Hospital and the Ethics Committee of the Third Affiliated Hospital of Soochow University.

The following clinical and pathologic data were collected: age, gender, performance status, primary tumor location, time to liver metastasis, the number of liver lesion, presence of extrahepatic metastasis, baseline level of serum CA19-9, diabetes, chemotherapy regimen, objective response (assessed with CT-enhanced scan according to RECIST criteria version 1.1), and adverse events related to HAI pump system.

SCT and HAI

SCT regimens were determined by the oncologist on the basis of guidelines, chemotherapy history, and physical conditions of patients. Gemcitabine monotherapy, gemcitabine based dual drug regimen, and triple drug regimen FOLFIRINOX were acceptable.

HAI pump system (Celsite, B. Braun, Chasseneuil, France) was implanted under digital subtraction angiography (DSA) guidance using "side-hole" and "tip-fixation" technology as previously described (12, 15). The extrahepatic branches such as the right gastric artery and the dorsal pancreatic artery were embolized to prevent extrahepatic perfusion. When multiple arteries are involved in the liver blood supply, the catheter is placed in the dominant artery, and the non-dominant branches are embolized to ensure whole hepatic infusion.

FUDR was administrated immediately after HAI pump implantation, at 0.15 mg/kg/day with dexa-methasone (DXM) at 1 mg/m^2/day and low molecular heparin 3,200 U in saline, which lasted for 14 days respectively as described previously (16). This type of HAI regimen was administered by a Baxter infusor. SCT was started concurrently with HAI.

Dose reduction for systemic chemotherapy was made in the event of toxicity, which was assessed according to the National Cancer Institute-Common Terminology Criteria for Adverse Events (NCI-CTCAE) version 3.0. If an ulcer or gastro-duodenitis was documented, HAI therapy was held for 1 month to allow healing and the dosage of FUDR and DXM was reduced by 50% in subsequent therapies. The HAI therapy was terminated if intrahepatic progression was recorded or technical catheter-related problems and excessive toxicity related to HAI occurred.

Statistical Analysis

The primary aim, overall survival (OS), was defined as the time from diagnosis of liver metastasis to death or last follow-up. The secondary aims were objective response rate (ORR) and functionality of HAI pump.

A propensity score was computed using a multivariable logistic regression model, with the treatment groups as the dependent variables and potential confounding factors as covariates. The following five variables were included in the propensity score matching: age, female, number of liver

metastasis, synchronous liver metastasis, and with extrahepatic metastasis. All patients in the HAI group were matched 1:1 to patients in the non-HAI group, as reported previously.

Distribution difference of categorical variables was compared using Fisher's exact or χ^2 test. A Mann–Whitney test was used for intergroup comparisons of continuous variables. Survival curves were compared using the log-rank test. Cox proportional hazards regression model was used to adjust for age, gender, SCT regimen, number of liver lesion, time to hepatic metastasis, CA19-9 level, and presence of extrahepatic liver metastasis (EHM).

All statistical analyses were performed using the SPSS 22.0 software (SPSS Inc., Chicago, IL, USA). P <0.05 was considered statistically significant.

RESULTS

Patients

From 2012 to 2019, 347 patients with PDLM received first-line chemotherapy in Xiangya Hospital of Central South University and the Third Affiliated Hospital of Soochow University. Among them, 28 patients who had underwent chemoradiotherapy were excluded from this study. In addition, 61 patients (including 26 with obstructive jaundice and 35 with peritoneal carcinomatosis at baseline) receiving SCT alone were excluded for there were no matched patients in the HAI group. Finally, 258 patients (62 patients with HAI and 196 without HAI) were included. **Table 1** lists the comparisons of baseline characteristics between the HAI and non-HAI groups. In the whole population, there were significant differences in number of liver lesion, EHM, and CA19-9 level between the two groups. In the HAI group, patients who had liver lesions >10 and/or CA19-9 >800 ng/ml were significantly more than those in the unmatched non-HAI group. In contrast, more patients had EHM in the unmatched non-HAI group. After 1:1 ratio matching, 62 patients per group were included. The two groups were well matched in terms of age, gender, PS score, time to liver metastasis, and EHM. However, observed but not statistically significant difference existed in the number of liver lesion (P = 0.104) and CA19-9 level (P = 0.151).

ORR in the Matched Population

Table 2 lists the objective response in intrahepatic and extrahepatic lesions separately. For intrahepatic lesions, five CR (8.1%) and 36 PR (58.1%) were observed in patients treated with HAI. The intrahepatic ORR was 66.1% in the HAI group, which was significantly higher than 22.6% (0 CR and 14 PR) in the non-HAI group (P <0.001). In the HAI group, 44 patients had evaluable extrahepatic lesions (including intact primary tumor and extrahepatic metastasis) and 11 patients (25.0%) achieved PR. In the non-HAI group the extrahepatic ORR was 28.9% (13/45). There was no significant difference in extrahepatic ORR

TABLE 1 | Baseline clinical data.

Characteristic	All patients			Matched patients		
	non-HAI (n=196) (%)	HAI (n=62) (%)	*P* value	non-HAI (n=62) (%)	HAI (n=62) (%)	*P* value
Age [median(range)]	63.4 (38–75)	62.5 (42–75)	0.443	63.1 (38–75)	62.5 (42–75)	0.681
Age≥65	83 (42.3)	26 (41.9)	0.954	26 (41.9)	26 (41.9)	1.000
Female	88 (44.9)	24 (38.7)	0.392	24 (38.7)	24 (38.7)	1.000
ECOG score			0.154			0.983
0	76 (38.8)	28 (45.2)		27 (43.5)	28 (45.2)	
1	98 (50.0)	32 (51.6)		33 (53.2)	32 (51.6)	
2	22 (11.2)	2 (3.2)		2 (3.2)	2 (3.2)	
Tumor location			0.311			0.607
Head	78 (39.8)	18 (29.0)		23 (37.1)	18 (29.0)	
Body	64 (32.6)	24 (38.7)		20 (32.3)	24 (38.7)	
Tail	54 (27.6)	20 (32.3)		19 (30.6)	20 (32.3)	
SCLM	117 (59.7)	39 (62.9)	0.593	39 (62.9)	39 (62.9)	1.000
No. of LM			0.008			0.104
<10	112 (57.1)	23 (37.1)		33 (53.2)	23 (37.1)	
≥10	84 (42.9)	39 (62.9)		29 (46.8)	39 (62.9)	
EHM	82 9 (41.8)	16 (25.8)	0.006	16 (25.8)	16 (25.8)	1.000
CA19-9 (U/ml)			0.026			0.151
>800	120 (61.2)	28 (45.2)		36 (58.1)	28 (45.2)	
≥800	76 (38.8)	34 (54.8)		26 (41.9)	34 (54.8)	
Diabetes	87 (44.4)	27 (43.5)	0.908	30 (48.4)	28 (45.2)	0.719
ACT	65 (35.7)	16 (25.8)	0.277	19 (30.6)	16 (25.8)	0.549
SCT			0.113			0.407
GEM	10 (5.1)	4 (6.5)		3 (4.8)	4 (6.5)	
GC	68 (34.7)	32 (51.6)		23 (37.1)	32 (51.6)	
GEMOX	41 (20.9)	14 (22.6)		16 (25.8)	14 (22.6)	
GEMNP	45 (23.0)	8 (12.9)		15 (24.2)	8 (12.9)	
FOLFIRINOX	25 (12.8)	4 (6.5)		5 (8.1)	4 (6.5)	

ECOG, Eastern Cooperative Oncology Group; SCLM, synchronous liver metastasis; LM, liver metastasis; EHM, extrahepatic metastasis; ACT, adjuvant chemotherapy; SCT, systemic chemotherapy; GME, gemcitabine monotherapy; GBDC, gemcitabine-based dual-drug chemotherapy.

TABLE 2 | Objective response rate n (%).

	Extrahepatic lesion*			Intrahepatic lesions		
	non-HAI (n=45)	HAI (n=44)	*P* value	non-HAI (N=62)	HAI (N=62)	*P* value
ORR	13 (28.8)	11 (25.0)	0.679	16 (25.8)	41 (66.1)	<0.001
CR	0	0	–	0	5 (8.1))	0.057
PR	13 (28.8)	11 (25.0)	0.679	16 (25.8)	36 (58.1)	<0.001
SD	16 (35.6)	19 (43.2)	0.461	24 (38.7)	19 (29.0)	0.451
PD	16 (35.6)	14 (31.8)	0.709	22 (35.5)	2 (3.2)	<0.001

**evaluation for unresectable primary cancer and extrahepatic metastases.*

(P = 0.679). **Figure 1** demonstrates CT and DSA images of a patient who achieved PR with SCT and HAI.

Thirty-six patients (58.1%) in the HAI group and 39 patients (62.9%) in the non-HAI group underwent second-line SCT (P = 0.714). In the HAI group, HAI was continuously administrated for median four cycles (range 2–7) in combination with second-line SCT in 17 patients who developed extrahepatic disease progression but had disease control in the liver. In addition, eight patients received HAI (median four cycles, range 2–6) in second-line treatment in the non-HAI group.

OS in the Matched Population

By the end of follow-up, 57 patients (91.9%) in the HAI group and 60 patients (95.2%) in the non-HAI group died. The 1- and 2-year survival rate was 71.0 and 24.2% in the HAI group and 46.8 and 9.7% in the non-HAI group, respectively. Median OS was 14.0 months (95% CI: 12.5–15.5) for patients treated with HAI and 10.8 months (95% CI: 8.7–12.9) for patients without HAI. OS for patients with HAI was better than patients without HAI (P = 0.001) (**Figure 2**). After adjustment for age, gender, SCT regimen, number of liver lesion, time to hepatic metastasis, CA19-9 level, and presence of EHM, HAI led to a decrease in hazard ratio for death by 61.8% (HR = 0.382; 95% CI: 0.252–0.578; P <0.001).

Figure 3 shows the difference in median OS between patients with or without HAI by subgroup analysis. HAI was associated with a better OS in all subgroups including patients with extrahepatic metastasis (**Figure 4**). Notedly, the difference was greater in subgroups without EHM, with higher tumor burden in the liver with synchronous liver metastasis. In these subgroups, HAI led to an increase of median OS more than 4 months.

HAI Pump Implantation and Functionality

The HAI pump system was implanted successfully in all 70 patients (including eight patients who received HAI in a second-line treatment). Four patients (5.7%) discontinued HAI due to dysfunction of HAI pump. Catheter occlusion occurred in one patient after three cycles of HAI therapy. One patient had hepatic artery occlusion at 11 months. Two patients developed local abscess at the pump implant site, and the pumps were removed at 4 and 7 months. It should be noted that these two patients had insulin-resistant diabetes. No patient discontinued HAI due to liver injury caused by FUDR.

DISCUSSION

In the last decade, HAI was repositioned as part of a comprehensive treatment for advanced liver tumors (17), and administrated in combination with standard systemic therapy. In this study, we showed that HAI FUDR in combination with SCT

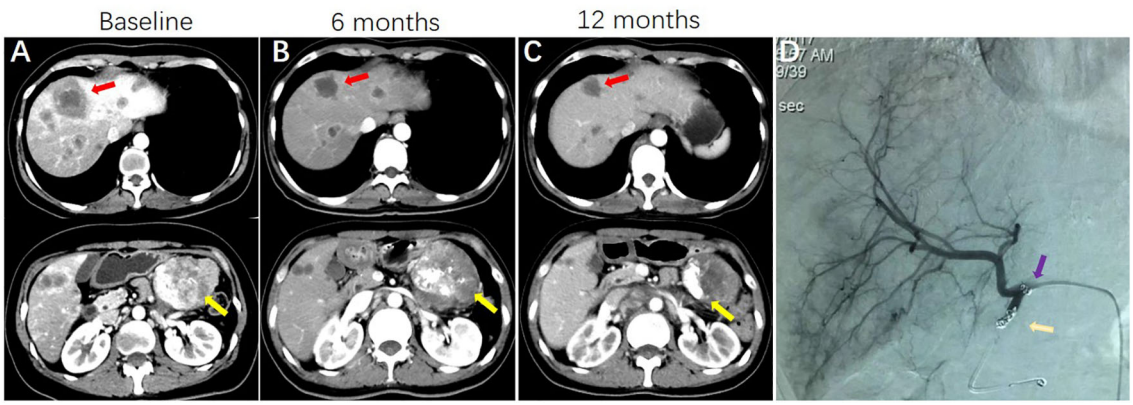

FIGURE 1 | A patient with pancreatic cancer and synchronous liver metastases, who was treated with systemic GC HAI FUDR. **(A)** CT images showing the presence of pancreatic cancer (yellow arrows indicate) and synchronous liver metastases (red arrows indicate) at baseline. **(B)** CT images show primary cancer and liver metastases are shrinking at 6 months. **(C)** images show sustained response of liver metastases and primary cancer. **(D)** Hepatic arteriography shows HAI pump functionality at 12 months (purple arrow indicates side hole of the catheter; gold arrow indicates the tip of the catheter, which was located in the occluded gastroduodenal artery).

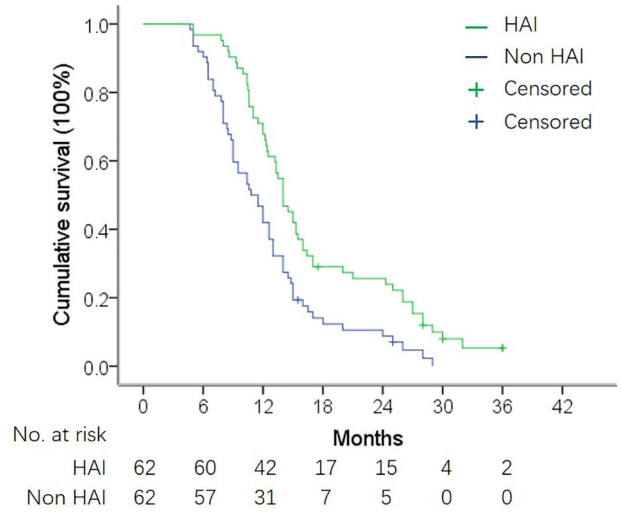

FIGURE 2 | OS in matched HAI and non-HAI group. Median OS was 14.0 months *vs.* 10.8 months in patients with and without HAI (log-rank test, $P = 0.001$).

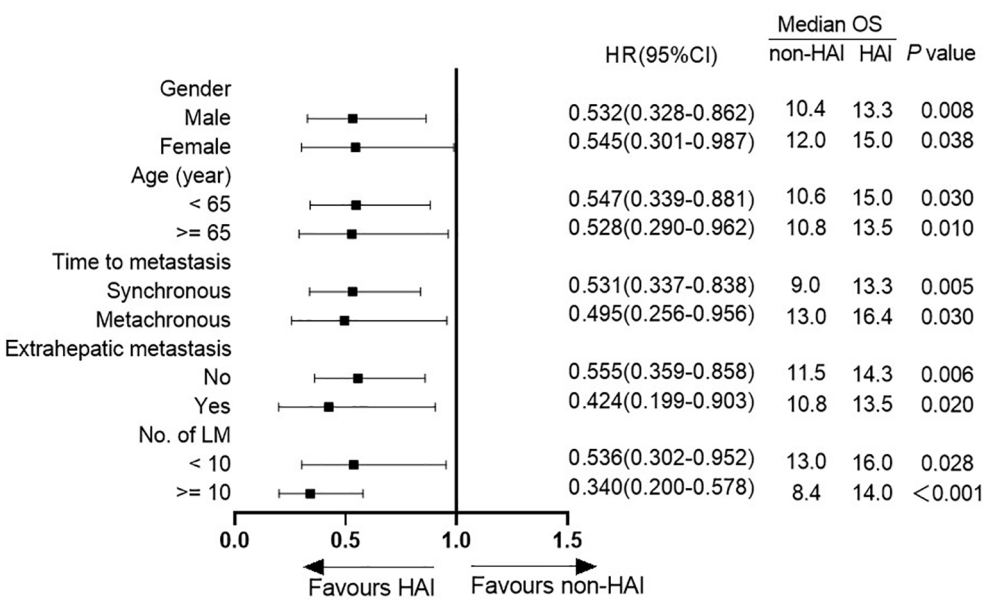

FIGURE 3 | Forest plot of subgroup analysis.

was associated with an improvement in survival in patients with PCLM. The median OS was 14.0 months for patients treated with HAI as compared with 10.8 months for patients without HAI after propensity score matching ($P = 0.008$). Although the extrahepatic ORR was similar, the intrahepatic ORR was significantly higher in the HAI group (66.1 *vs* 25.8%, $P < 0.001$).

In this cohort, patients with liver-predominant metastases were more likely to accept HAI therapy. Over 60% of patients receiving HAI had more than 10 liver lesions. In contrast, less patients with EHM were treated with HAI. In addition, a higher serum CA19-9 level was found in HAI-treated patients. Due to the significant imbalance of these radical factors between patients with and without HAI, propensity score matching analysis was introduced in this study. In order to reduce the number of confounding variance, patients with obstructive jaundice or peritoneal carcinomatosis, which is associated with poor prognosis in pancreatic cancer (3, 18), were excluded from the propensity score matching because they were not selected for

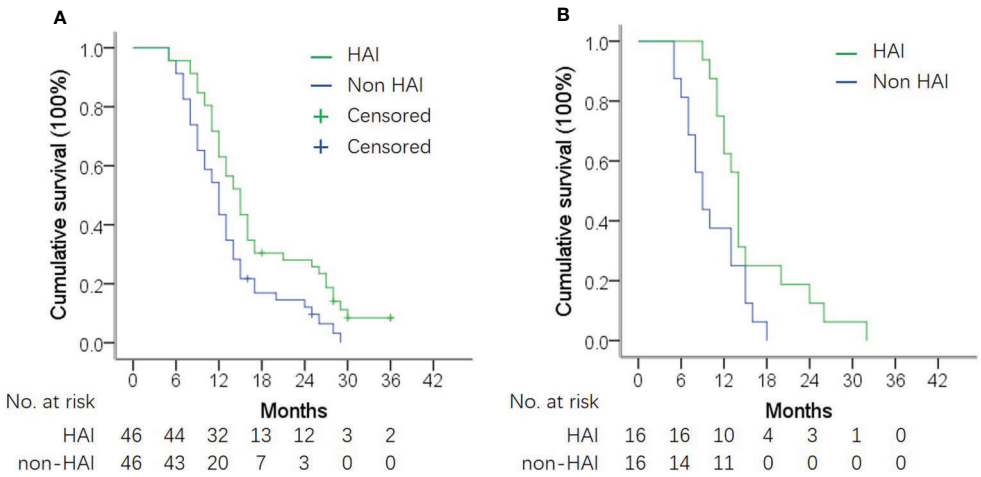

FIGURE 4 | OS in subgroup analysis according to presence of extrahepatic metastasis (EHM). **(A)** OS in patients without EHM. Median OS was 14.3 *vs.* 11.5 months in patients with and without HAI (log-rank test, $P = 0.006$). **(B)** OS in patients with EHM. Median OS was 10.8 *vs.* 13.5 months in patients with and without HAI (log-rank test, $P = 0.020$).

HAI in this study. Following matching, observed differences in the number of liver lesions and CA19-9 level still existed between the two groups. In addition, the distribution of SCT regimens was not completely balanced. To eliminate the potential impacts of these radical confounders, we established multivariance Cox regression model and confirmed that HAI reduced the risk of death by 61.8% (HR = 0.382; $P < 0.001$).

Nowadays, GEM/nab-paclitaxel and FOLFIRINOX are preferred regimens for patients with locally advanced or metastatic pancreatic cancer. A randomized phase III study on GEM plus nab-paclitaxel showed that the ORR was 23% in patients with advanced pancreatic cancer (19). In 2013, another phase III study showed that 31.6% of patients achieved PR after treatment with more intensive regimen FOLFIRINOX (20). In addition, the ORR varied from 15 to 30% in patients treated with other recommended regimens, for example, GEM monotherapy, GC and GEMOX, in previous studies (21–24). As listed above, the efficacy of SCT for advanced pancreatic cancer is still unsatisfactory. In the present study, most patients (87.1% in non-HAI group and 93.5% in HAI group) received GEM-based dual-drug combinations. In the non-HAI group, the ORR was 25.8%. This result was consistent with published data on modern SCT. In the HAI group, the extrahepatic ORR was similar to that of the non-HAI group, suggesting HAI with low-dose of FUDR does not help to improve extrahepatic response.

In this study, a low dose of FUDR was administrated continuously *via* HAI pump. FUDR is a suitable agent for HAI due to its unique characteristics as compared with 5-Fu, such as shorter half-life, higher systemic clearance rate, and higher liver extraction rate (25). We and others reported HAI rapidly reduced tumor burden and promoted more than 50% of unresectable CRCLM to convert into resectable disease (12, 26, 27). Recently, HAI was reported to have efficacy in IHC, a more progressive and refractory disease as compared with CRCLM. In a single arm phase II study, 58% of patients achieved and sustained PR on treatment with HAI FUDR plus systemic GEMOX (14). Four patients (10.5%) underwent resection after treatment. In the present study, 97.8% of patients (60/62) achieved intrahepatic disease control, including 67.7% PR and 8.1% CR. Although no patients underwent resection, the sustained intrahepatic response helped to prevent liver-related complications, which may immediately threaten the patient's life (7, 14). This may explain why patients with extensive liver metastases achieved greater survival advantage in the HAI group, and patients with extrahepatic metastasis also benefit from HAI.

In this study, HAI pump system was implanted by two different teams, with modified radiological techniques as described previously (15). Similar catheter functionality was achieved in the two centers. HAI pump dysfunction occurred in four patients (5.7%), including one catheter occlusion, one hepatic artery occlusion, and two infections, but none of them happened within the first 3 months. For HAI therapy, many research studies prefer surgery rather than radiological procedure to implant HAI pump system (11, 14), due to concerns about frequent dislodgement and extrahepatic infusion related to radiologically implanted catheter. In fact, these shortcomings of radiological procedure may be overcome by introducing modified techniques (12, 15, 28, 29). First, the rate of catheter displacement could be reduced to less than 5% by "tip-fix" technique (28, 30). In addition, under the guidance of DSA, extrahepatic branches can be accurately identified and embolized so as to reduce complications related to extrahepatic infusion (15). In addition, radiological implantation is performed under local anesthesia with minimal trauma, which allows the planned HAI and SCT to start immediately. This is a notable advantage over surgical procedure, especially for patients with progressive disease in the liver.

This study has several limitations. Foremost, it was designed as a retrospective observational study. The data were collected from the prospectively maintained databases with good integrity, which is favorable for propensity matching analysis. However, several factors

that can influence survival did not reach complete matching, due to the relatively small size of the whole population. Furthermore, the distribution of SCT regimen was not well balanced ($P = 0.407$). The proportion of patients receiving GC in the HAI group was relatively higher (51.6 *vs*. 37.1%). Although the Cox model analysis confirmed that HAI significantly reduced the risk of death after adjustment for confounding factors including SCT regimen, the limitation of no definite SCT regimen should not be ignored.

CONCLUSIONS

HAI FUDR was associated with higher intrahepatic ORR and longer OS patients with PCLM. However, this is a retrospective study with a relatively small sample size. The superiority of HAI in combination with standard SCT required further justification by multi-center randomized studies.

DATA AVAILABILITY STATEMENT

The raw data supporting the conclusions of this article will be made available by the authors, without undue reservation.

ETHICS STATEMENT

The studies involving human participants were reviewed and approved by the Medical Ethics Committee of the Xiangya Hospital and the Ethics Committee of the Third Affiliated Hospital of Soochow University. Written informed consent for participation was not required for this study in accordance with the national legislation and the institutional requirements.

AUTHOR CONTRIBUTIONS

All authors listed have made a substantial, direct, and intellectual contribution to the work, and approved it for publication.

FUNDING

This work was supported by grants from the National Natural Science Foundation of China (No. 81773234) and Scientific Research Project of Hunan Health and Health Commission (No. C2019189).

REFERENCES

1. Bray F, Ferlay J, Soerjomataram I, Siegel RL, Torre LA, Jemal A. Global Cancer Statistics 2018: GLOBOCAN Estimates of Incidence and Mortality Worldwide for 36 Cancers in 185 Countries. *CA Cancer J Clin* (2018) 68:394–424. doi: 10.3322/caac.21492
2. Stathis A, Moore MJ. Advanced Pancreatic Carcinoma: Current Treatment and Future Challenges. *Nat Rev Clin Oncol* (2010) 7:163–72. doi: 10.1038/nrclinonc.2009.236
3. Mizrahi JD, Surana R, Valle JW, Shroff RT. Pancreatic Cancer. *Lancet* (2020) 395:2008–20. doi: 10.1016/S0140-6736(20)30974-0
4. Siegel RL, Miller KD, Jemal A. Cancer Statistics, 2019. *CA Cancer J Clin* (2019) 69:7–34. doi: 10.3322/caac.21551
5. Conroy T, Bachet JB, Ayav A, Huguet F, Lambert A, Caramella C, et al. Current Standards and New Innovative Approaches for Treatment of Pancreatic Cancer. *Eur J Cancer* (2016) 57:10–22. doi: 10.1016/j.ejca.2015.12.026
6. Ryan DP, Hong TS, Bardeesy N. Pancreatic Adenocarcinoma. *N Engl J Med* (2014) 371:1039–49. doi: 10.1056/NEJMra1404198
7. Bouchahda M, Levi F, Adam R, Rougier P. Modern Insights Into Hepatic Arterial Infusion for Liver Metastases From Colorectal Cancer. *Eur J Cancer* (2011) 47:2681–90. doi: 10.1016/j.ejca.2011.06.037
8. Lyu N, Kong Y, Mu L, Lin Y, Li J, Liu Y, et al. Hepatic Arterial Infusion of Oxaliplatin Plus Fluorouracil/Leucovorin vs. Sorafenib for Advanced Hepatocellular Carcinoma. *J Hepatol* (2018) 69:60–9. doi: 10.1016/j.jhep.2018.02.008
9. Ensminger WD, Rosowsky A, Raso V, Levin DC, Glode M, Come S, et al. A Clinical-Pharmacological Evaluation of Hepatic Arterial Infusions of 5-Fluoro-2'-Deoxyuridine and 5-Fluorouracil. *Cancer Res* (1978) 38:3784–92.
10. Pak LM, Kemeny NE, Capanu M, Chou JF, Boucher T, Cercek A, et al. Prospective Phase II Trial of Combination Hepatic Artery Infusion and Systemic Chemotherapy for Unresectable Colorectal Liver Metastases: Long Term Results and Curative Potential. *J Surg Oncol* (2018) 117:634–43. doi: 10.1002/jso.24898
11. Groot Koerkamp B, Sadot E, Kemeny NE, Gonen M, Leal JN, Allen PJ, et al. Perioperative Hepatic Arterial Infusion Pump Chemotherapy is Associated With Longer Survival After Resection of Colorectal Liver Metastases: A Propensity Score Analysis. *J Clin Oncol* (2017) 35:1938–44. doi: 10.1200/JCO.2016.71.8346
12. Shi L, Zhao J, Lu Q, Chen X, Wang H, Jiang Y, et al. Initial Hepatic Artery Infusion and Systemic Chemotherapy for Asymptomatic Colorectal Cancer With Un-Resectable Liver Metastasis. *Int J Clin Exp Med* (2015) 8:1000–8.
13. Li X, Shi L, Wu J, Ji M, Zhao J, Qiang W, et al. First-Line Treatment With Hepatic Arterial Infusion Plus Capecitabine vs Capecitabine Alone for Elderly Patients With Unresectable Colorectal Liver Metastases. *Cancer Biol Ther* (2016) 17:14–9. doi: 10.1080/15384047.2015.1108487
14. Cercek A, Boerner T, Tan BR, Chou JF, Gonen M, Boucher TM, et al. Assessment of Hepatic Arterial Infusion of Floxuridine in Combination With Systemic Gemcitabine and Oxaliplatin in Patients With Unresectable Intrahepatic Cholangiocarcinoma: A Phase 2 Clinical Trial. *JAMA Oncol* (2019) 6(1):60–7. doi: 10.1001/jamaoncol.2019.3718
15. Deschamps F, Rao P, Teriitehau C, Hakime A, Malka D, Boige V, et al. Percutaneous Femoral Implantation of an Arterial Port Catheter for Intraarterial Chemotherapy: Feasibility and Predictive Factors of Long-Term Functionality. *J Vasc Interv Radiol* (2010) 21:1681–8. doi: 10.1016/j.jvir.2010.08.003
16. Kemeny N, Jarnagin W, Paty P, Gonen M, Schwartz L, Morse M, et al. Phase I Trial of Systemic Oxaliplatin Combination Chemotherapy With Hepatic Arterial Infusion in Patients With Unresectable Liver Metastases From Colorectal Cancer. *J Clin Oncol* (2005) 23:4888–96. doi: 10.1200/JCO.2005.07.100
17. Datta J, Narayan RR, Kemeny NE, D'Angelica MI. Role of Hepatic Artery Infusion Chemotherapy in Treatment of Initially Unresectable Colorectal Liver Metastases: A Review. *JAMA Surg* (2019) 154:768–76. doi: 10.1001/jamasurg.2019.1694
18. Tanaka M, Mihaljevic AL, Probst P, Heckler M, Klaiber U, Heger U, et al. Meta-Analysis of Recurrence Pattern After Resection for Pancreatic Cancer. *Br J Surg* (2019) 106:1590–601. doi: 10.1002/bjs.11295
19. Von Hoff DD, Ervin T, Arena FP, Chiorean EG, Infante J, Moore M, et al. Increased Survival in Pancreatic Cancer With Nab-Paclitaxel Plus Gemcitabine. *N Engl J Med* (2013) 369:1691–703. doi: 10.1056/NEJMoa1304369

20. Conroy T, Desseigne F, Ychou M, Bouche O, Guimbaud R, Becouarn Y, et al. FOLFIRINOX Versus Gemcitabine for Metastatic Pancreatic Cancer. *N Engl J Med* (2011) 364:1817–25. doi: 10.1056/NEJMoa1011923
21. Hess V, Salzberg M, Borner M, Morant R, Roth AD, Ludwig C, et al. Combining Capecitabine and Gemcitabine in Patients With Advanced Pancreatic Carcinoma: A Phase I/II Trial. *J Clin Oncol* (2003) 21:66–8. doi: 10.1200/JCO.2003.04.029
22. Cunningham D, Chau I, Stocken DD, Valle JW, Smith D, Steward W, et al. Phase III Randomized Comparison of Gemcitabine Versus Gemcitabine Plus Capecitabine in Patients With Advanced Pancreatic Cancer. *J Clin Oncol* (2009) 27:5513–8. doi: 10.1200/JCO.2009.24.2446
23. Louvet C, Labianca R, Hammel P, Lledo G, Zampino MG, Andre T, et al. Gemcitabine in Combination With Oxaliplatin Compared With Gemcitabine Alone in Locally Advanced or Metastatic Pancreatic Cancer: Results of a GERCOR and GISCAD Phase III Trial. *J Clin Oncol* (2005) 23:3509–16. doi: 10.1200/JCO.2005.06.023
24. Suker M, Beumer BR, Sadot E, Marthey L, Faris JE, Mellon EA, et al. FOLFIRINOX for Locally Advanced Pancreatic Cancer: A Systematic Review and Patient-Level Meta-Analysis. *Lancet Oncol* (2016) 17:801–10. doi: 10.1016/S1470-2045(16)00172-8
25. Power DG, Kemeny NE. The Role of Floxuridine in Metastatic Liver Disease. *Mol Cancer Ther* (2009) 8:1015–25. doi: 10.1158/1535-7163.MCT-08-0709
26. Gallagher DJ, Capanu M, Raggio G, Kemeny N. Hepatic Arterial Infusion Plus Systemic Irinotecan in Patients With Unresectable Hepatic Metastases From Colorectal Cancer Previously Treated With Systemic Oxaliplatin: A Retrospective Analysis. *Ann Oncol* (2007) 18:1995–9. doi: 10.1093/annonc/mdm405
27. Kemeny NE, Melendez FD, Capanu M, Paty PB, Fong Y, Schwartz LH, et al. Conversion to Resectability Using Hepatic Artery Infusion Plus Systemic Chemotherapy for the Treatment of Unresectable Liver Metastases From Colorectal Carcinoma. *J Clin Oncol* (2009) 27:3465–71. doi: 10.1200/JCO.2008.20.1301
28. Tanaka T, Arai Y, Inaba Y, Matsueda K, Aramaki T, Takeuchi Y, et al. Radiologic Placement of Side-Hole Catheter With Tip Fixation for Hepatic Arterial Infusion Chemotherapy. *J Vasc Interv Radiol* (2003) 14:63–8. doi: 10.1097/01.rvi.0000052292.26939.59
29. Peng C, Zhou C, Li G, Li H, Shi L. Hepatic Artery Infusion Pump for Nasopharyngeal Carcinoma With Liver Metastasis. *Clin Exp Metastasis* (2020) 37:333–9. doi: 10.1007/s10585-019-10015-0
30. Arai Y, Takeuchi Y, Inaba Y, Yamaura H, Sato Y, Aramaki T, et al. Percutaneous Catheter Placement for Hepatic Arterial Infusion Chemotherapy. *Tech Vasc Interv Radiol* (2007) 10:30–7. doi: 10.1053/j.tvir.2007.08.007

Conflict of Interest: The authors declare that the research was conducted in the absence of any commercial or financial relationships that could be construed as a potential conflict of interest.

frontiers in Oncology

ORIGINAL RESEARCH
published: 19 May 2021
doi: 10.3389/fonc.2021.671333

XGBoost Classifier Based on Computed Tomography Radiomics for Prediction of Tumor-Infiltrating CD8+ T-Cells in Patients With Pancreatic Ductal Adenocarcinoma

Jing Li[1†], Zhang Shi[1†], Fang Liu[1†], Xu Fang[1], Kai Cao[1], Yinghao Meng[1], Hao Zhang[1], Jieyu Yu[1], Xiaochen Feng[1], Qi Li[1], Yanfang Liu[2], Li Wang[1], Hui Jiang[2], Jianping Lu[1], Chengwei Shao[1] and Yun Bian[1*]*

[1] Department of Radiology, Changhai Hospital, Navy Medical University, Shanghai, China, [2] Department of Pathology, Changhai Hospital, Navy Medical University, Shanghai, China

Objectives: This study constructed and validated a machine learning model to predict CD8+ tumor-infiltrating lymphocyte expression levels in patients with pancreatic ductal adenocarcinoma (PDAC) using computed tomography (CT) radiomic features.

Materials and Methods: In this retrospective study, 184 PDAC patients were randomly assigned to a training dataset (n =137) and validation dataset (n =47). All patients were divided into CD8+ T-high and -low groups using X-tile plots. A total of 1409 radiomics features were extracted from the segmentation of regions of interest, based on preoperative CT images of each patient. The LASSO algorithm was applied to reduce the dimensionality of the data and select features. The extreme gradient boosting classifier (XGBoost) was developed using a training set consisting of 137 consecutive patients admitted between January 2017 and December 2017. The model was validated in 47 consecutive patients admitted between January 2018 and April 2018. The performance of the XGBoost classifier was determined by its discriminative ability, calibration, and clinical usefulness.

Results: The cut-off value of the CD8+ T-cell level was 18.69%, as determined by the X-tile program. A Kaplan–Meier analysis indicated a correlation between higher CD8+ T-cell levels and better overall survival (p = 0.001). The XGBoost classifier showed good discrimination in the training set (area under curve [AUC], 0.75; 95% confidence interval [CI]: 0.67–0.83) and validation set (AUC, 0.67; 95% CI: 0.51–0.83). Moreover, it showed a good calibration. The sensitivity, specificity, accuracy, positive and negative predictive values were 80.65%, 60.00%, 0.69, 0.63, and 0.79, respectively, for the training set, and 80.95%, 57.69%, 0.68, 0.61, and 0.79, respectively, for the validation set.

OPEN ACCESS

Edited by:
Kanjoormana Aryan Manu,
Amala Cancer Research Centre, India

Reviewed by:
Jinyang Li,
The Rockefeller University, United States
Yu H. Sun,
University of Rochester, United States
Antonella Argentiero,
Istituto Tumori Bari Giovanni Paolo II, Istituto Nazionale dei Tumori (IRCCS), Italy

***Correspondence:**
Yun Bian
bianyun2012@foxmail.com
Chengwei Shao
chenweishaoch@163.com

†These authors have contributed equally to this work and share first authorship

Specialty section:
This article was submitted to Gastrointestinal Cancers, a section of the journal Frontiers in Oncology

Received: 23 February 2021
Accepted: 26 April 2021
Published: 19 May 2021

Citation:
Li J, Shi Z, Liu F, Fang X, Cao K, Meng Y, Zhang H, Yu J, Feng X, Li Q, Liu Y, Wang L, Jiang H, Lu J, Shao C and Bian Y (2021) XGBoost Classifier Based on Computed Tomography Radiomics for Prediction of Tumor-Infiltrating CD8+ T-Cells in Patients With Pancreatic Ductal Adenocarcinoma. Front. Oncol. 11:671333. doi: 10.3389/fonc.2021.671333

Conclusions: We developed a CT-based XGBoost classifier to extrapolate the infiltration levels of $CD8^+$ T-cells in patients with PDAC. This method could be useful in identifying potential patients who can benefit from immunotherapies.

Keywords: pancreatic ductal adenocarcinoma, CD8 positive T lymphocytes, contrast-enhanced computed tomography images, radiomics, prognosis

INTRODUCTION

The microenvironment of pancreatic ductal adenocarcinoma (PDAC) is highly immunosuppressive and heterogeneous, characterized by an abundant desmoplastic stroma, inflammatory response, and neovascularization (1). Even with surgical resection, the radical resection rate is only approximately 18% (2), and the prognosis remains poor (3). Traditional chemotherapy is minimally effective, despite some recent success (4).

Tumors are a proliferation of abnormal cells that can escape immune eradication (5). The occurrence of immune escape is a key process in cancer progression. Immunotherapy, which aims to stimulate the body's immune system against tumor cells, can overcome this problem. The recent success of immunotherapy targeting immune checkpoint inhibitors (ICI), such as the programmed cell death protein 1 (PD1) and PD1 ligand (PD-L1) pathways, has shed new light on the treatment of patients with tumors (6, 7). Nonetheless, treatment with these drugs has failed to show significant clinical benefit in unselected patients with PDAC, whose objective response rate to ICI therapy has been approximately 5% in previous clinical trials (8, 9). Therefore, there is a clear need to develop related predictive biomarkers to identify subsets of patients who may benefit from ICI therapy. An effective ICI therapy prerequisite is a high level of $CD8^+$ tumor-infiltrating lymphocytes (TILs) in the tumor tissues, suggesting the importance of investigating $CD8^+$ TILs (10). Immunohistochemistry is the gold standard for evaluating $CD8^+$ TILs. However, the clinical application of immunohistochemistry is limited by its invasiveness, time consumption, tumor heterogeneity, and unrepeatability. In recent years, liquid biopsy is a hot spot of research. As a rapid and noninvasive alternative to tissue biopsy, liquid biopsy can capture circulating leukocytes to reflect cancer immunity (11). In general, cancer immunity consists of the local immunity in the tumor microenvironment and the systemic immunity in circulating peripheral blood (12). However, it is unclear whether systemic immune response always correlates with local immune response (12, 13). Takahiro Tsujikawa et al. have emphasized the utility of local immune monitoring for patient stratification, which could improve immunotherapy's success rate (14).

Computed tomography (CT) is widely used for tumor detection, staging, and treatment response monitoring in clinical practice. Recently, radiomic biomarkers have been of great interest. They may extract spatial and temporal features from images that are useful in predicting the underlying molecular mechanisms, the tumor-immune microenvironment, and clinical outcome. Studies dealing with glioma, esophagus, lung, and liver cancers have shown that several imaging features extracted by radiomics were closely related to $CD8^+$ TIL density (15–19). While reports are predicting clinicopathological results from tissue sections in PDAC (20–22), so far, there are no radiomic studies revealing the immune environment in PDAC. Subtyping of the immune microenvironment in PDAC will help design personalized immunotherapy for patients with PDAC.

Thus, we aimed to develop and validate a radiomic signature of immune infiltration in PDAC using radiomic data extracted from contrast-enhanced CT images in this study, which might help us identify the novel predictors of immunotherapy efficacy.

MATERIALS AND METHODS

Patients

This retrospective single-center cross-sectional study was reviewed and approved by the Biomedical Research Ethics Committee of our institution. The requirement for informed consent was waived by the Institutional Review Board. Data were obtained from consecutive patients treated for pancreatic cancer at our institution between January 2017 and April 2018 (**Figure 1**).

We included patients who (1) had undergone surgical treatment and (2) had pathologically confirmed PDAC. We excluded patients who (1) had undergone treatment of any type (radiotherapy, chemotherapy, or chemoradiotherapy) before the imaging studies, (2) did not undergo immunohistochemical $CD8^+$ staining, (3) were not evaluated by contrast-enhanced multidetector computed tomography (MDCT) within 1 week preoperatively, or (4) had pancreatic lesions that could not be visualized on MDCT. Consequently, 184 consecutive patients with PDAC, including 120 men (age: 60.75 ± 10.31 years; range: 27–81 years) and 64 women (age: 63.11 ± 7.99 years; range: 37–80 years), were included. The prediction model was developed for a primary set that consisted of 137 consecutive patients, including 93 men (age: 60.44 ± 10.16 years; range: 27–80 years) and 44 women (age: 63.32 ± 7.96 years; range: 37–80 years), admitted between January 2017 and December 2017. Thus, 47 consecutive patients, including 27 men (age: 61.81 ± 10.94 years; range: 42–81 years) and 20 women (age: 62.65 ± 8.25 years; range: 42–71 years), admitted between January 2018 and April 2018, constituted an independent validation set.

CT Scanning

Multiphasic CT was performed with a pancreas-specific protocol using 320-slice multidetector-row CT scanners (Aquilion ONE, Canon Medical Systems, Tokyo, Japan). The details are shown in **Appendix 1**.

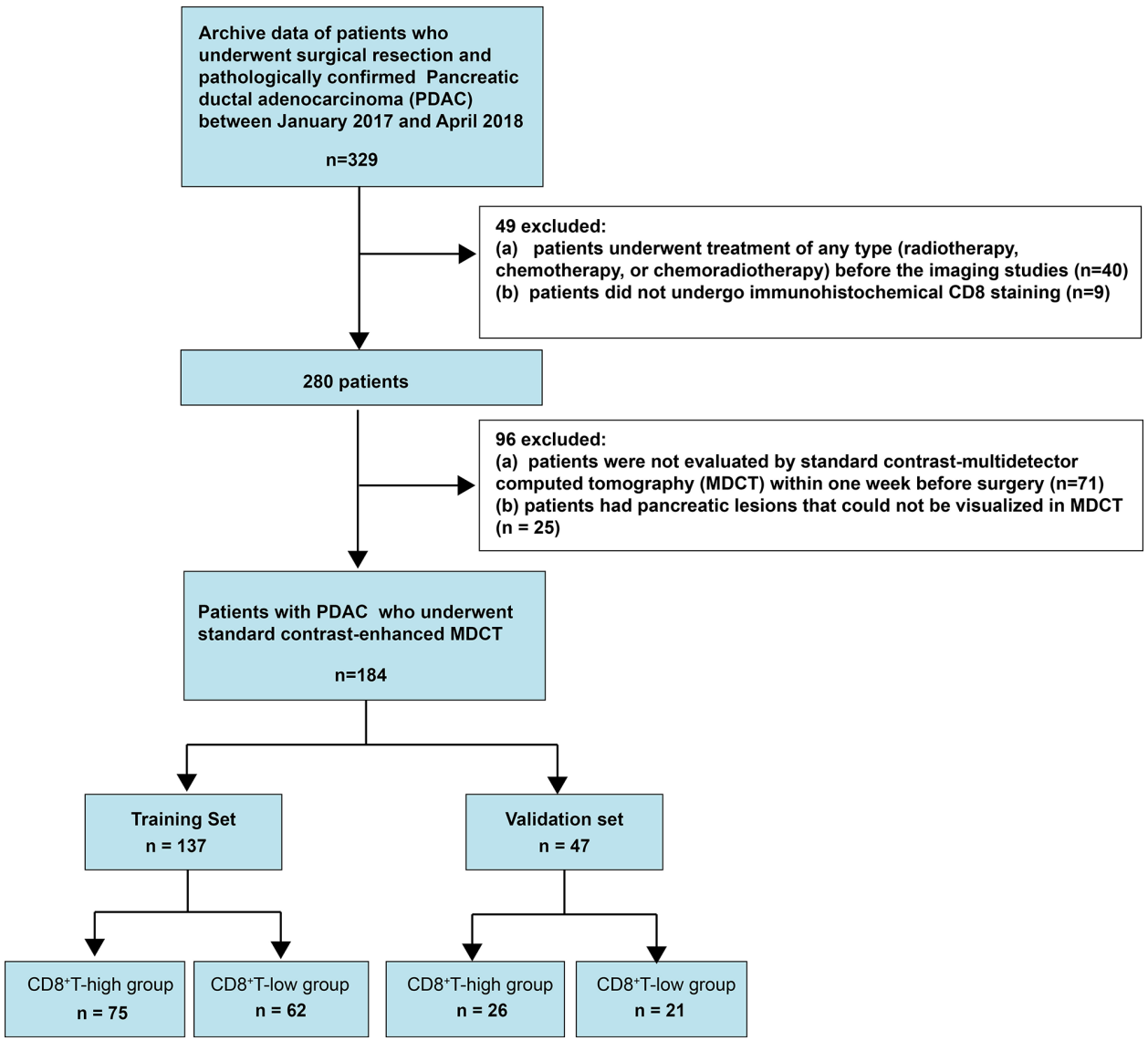

FIGURE 1 | Flow chart visualizing the patient selection process.

Pathological Image Analysis

All specimens were analyzed by two pathologists, one with 30 and the other with 20 years of experience in pancreatic pathology. Pathological examination and analysis were standardized as described previously (23). A CD8 antibody (DakoCytomation, Glostrup, Denmark) was used in pathological examinations. Each CD8-stained section was converted to digital pathological images by the scanner (NanoZoomer S60, Hamamatsu Healthcare, Japanese). The tumor boundaries were manually delineated, after which a customizable digital microscopy analysis platform (Visiopharm, Hørsholm, Denmark) was used to quantify CD8 in the tumor. The two pathologists examined the results, and the outcomes were determined by consensus. Subsequently, the proportion of the area of CD8 was calculated in the tumor.

All pathologic results for the following factors were recorded: (1) T and N stages, which were evaluated based on the American Joint Committee on Cancer TNM Staging Manual, 8th Edition (24); (2) grade of differentiation; (3) duodenal invasion; (4) common bile duct invasion; (5) lymphovascular space invasion (LVSI); and (6) peripancreatic nerve.

Radiological Imaging Analysis

The details are shown in **Appendix 1**.

Radiomics Workflow

The radiomics workflow included: (1) image segmentation, (2) feature extraction, and (3) feature reduction and selection. The detailed method is shown in **Figure 2**.

We used the draw tool, which is available in the Editor module of 3D Slicer version 4.8.1 (open source software; https://www.slicer.org/), to delineate the tumors in multiple slices. The details are shown in **Appendix 1**.

To assess interobserver reliability, ROI segmentation was performed in a blinded fashion by two radiologists (readers 1 and 2, respectively). To evaluate intraobserver reliability, reader 1 repeated the feature extraction twice during a week period. This reader completed the remaining image segmentations, and the readout sessions were conducted over 2 weeks period. Assessments of interobserver and intraobserver reliability were performed by obtaining the intraclass correlation coefficient (ICC). ICC values >0.75 were selected for subsequent investigation.

Statistical Analyses

Normal distribution and variance homogeneity tests were performed on all continuous variables. Those with normal distribution were expressed as mean and standard deviation, while those with non-normal distributions were expressed as medians and ranges. We evaluated the overall survival (OS). Deaths were set as events, and deaths attributed to other causes were set as censored observations. Survival times were calculated from surgery date to the time of death or the end of follow-up (August 1, 2020). First, the optimal cut-off CD8 level was determined with the help of X-tile (25). The X-tile program divided the patients into CD8-low and CD8-high groups, according to the optimal cut-off value. Kaplan–Meier estimates were applied to graph the survival curves, and the log-rank test was performed to analyze the differences between the curves. Second, we examined the differences in all variables between the CD8-low and CD8-high groups. Student's t-test (normal distribution), Kruskal–Wallis H test (skewed distribution), and the chi-square test (categorical variables) were used to determine the intergroup statistical differences. Third, univariate regression analysis was applied to estimate the effect size between all variables and the CD8 groups. Fourth, the prediction model was constructed using

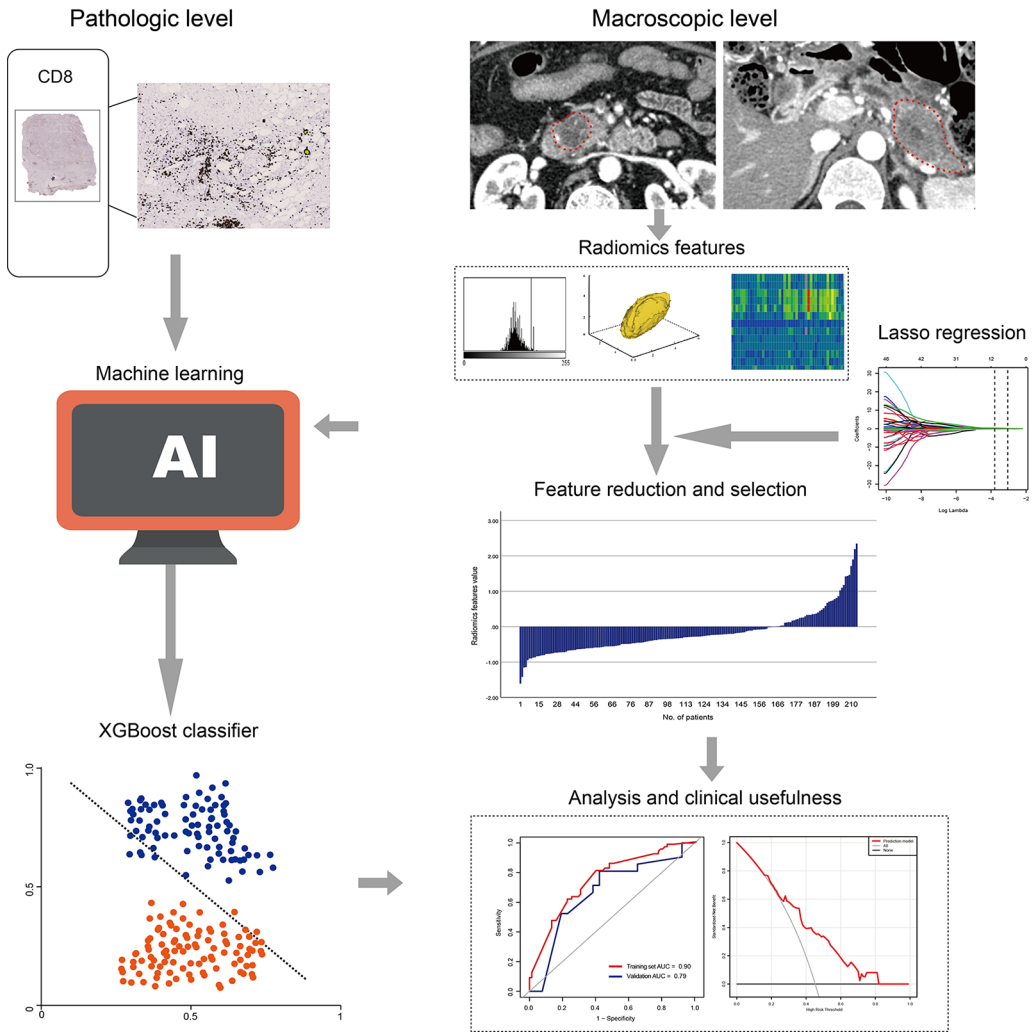

FIGURE 2 | Radiomics workflow.

an extreme gradient boosting classifier (XGBoost). XGBoost was performed using R software supplemented with the XGBoost package. The discrimination of the model was evaluated using a receiver operating characteristic (ROC) curve. The area under the curve (AUC) was calculated concurrently. The calibration of the model was assessed using the calibration curves and Hosmer–Lemeshow test. Finally, the model's clinical usefulness was tested with a decision-curve analysis (DCA) by quantifying the net benefit at different threshold probabilities.

A two-tailed p-value <0.05 was considered statistically significant. All analyses were performed using R software (version 3.3.3, The R Foundation for Statistical Computing, Vienna, Austria).

RESULTS

Clinical Characteristics

Based on the optimal CD8 level cut-off determined by X-tile (18.69%; **Figures 3A, B**), all patients were divided into CD8-high (CD8 >18.69%, n = 101; 54.89%) and CD8-low (CD8 ≤18.69%, n = 83; 45.10%) groups (**Figure 3C**). CD8 expression was 28.07 ± 9.12% and 14.17 ± 2.93% in the CD8-high and CD8-low groups, respectively. Forty-six patients in the CD8-high group and 48 patients in the CD8-low group died. The Kaplan–Meier curves of the two groups were significantly distinct (p = 0.001). A log-rank test showed that the survival duration in the CD8-high group (22.63 months, 95% CI: 20.20–36.20) was significantly longer than that in the CD8-low group (14.67 months, 95% CI: 12.13–22.37) (**Figure 3D**). Among the clinical, pathological, and imaging characteristics that we investigated, T and N stage in the training set differed significantly between the two groups. The patient characteristics are shown in **Table 1**.

Radiomics Analysis

A total of 1409 radiomics features were extracted from arterial and portal venous phases, respectively. The ICC interobserver and intraobserver were good, with 0.70–0.93 and 0.85–0.90, respectively.

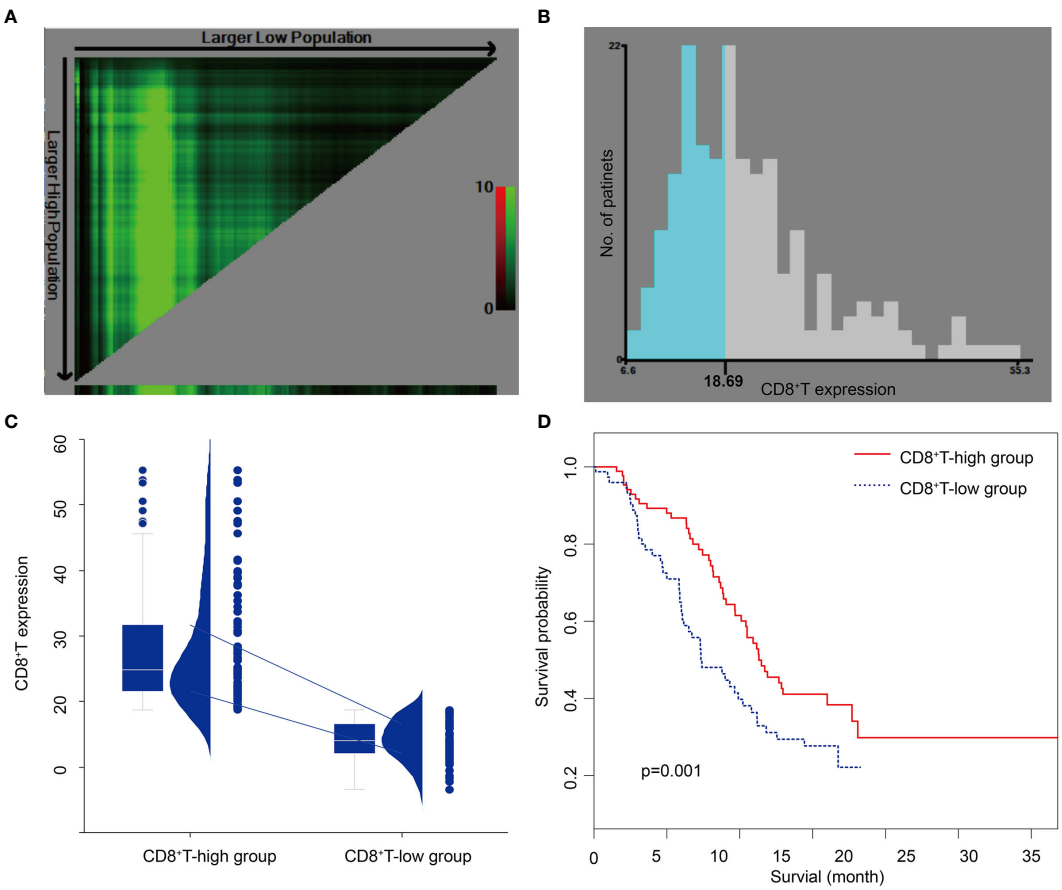

FIGURE 3 | X-tile analysis of survival data in patients with pancreatic ductal adenocarcinoma **(A, B)** The optimal cut-off CD8$^+$ T-cell level of 18.69%, determined by X-tile, is used to define the CD8$^+$ T-high and CD8$^+$ T-low groups. **(C)** CD8$^+$ T in the CD8$^+$ T-low group and the CD8$^+$ T-high group. The chart includes a box plot, density plot, and dot plot. The 25th and 75th percentiles are shown as connecting lines between groups. **(D)** The Kaplan-Meier curve and log-rank test suggest that patients in the CD8$^+$ T-high group survive significantly longer than those in the CD8$^+$ T-low group.

TABLE 1 | Baseline characteristics of patients with pancreatic cancer.

Characteristics	Training set			Validation set		
	$CD8^+T$-high (n=75)	$CD8^+T$ -low (n=62)	P-value	$CD8^+T$ -high (n=26)	$CD8^+T$ -low (n=21)	P-value
Clinical characteristics						
Sex, n (%)			0.48			0.97
Male	49 (65.33)	44 (70.97)		15 (57.69)	12 (57.14)	
Female	26 (34.67)	18 (29.03)		11 (42.31)	9 (42.86)	
Age, years (mean ± SD)	61.20 ± 9.96	61.56 ± 9.16	0.83	61.85 ± 9.78	62.57 ± 10.04	0.80
BMI, kg/m^2 (mean ± SD)	22.98 ± 2.81	23.16 ± 2.88	0.71	94.55 ± 369.17	23.10 ± 2.40	0.38
Operation, n (%)			0.12			0.48
Pancreaticoduodenectomy	41 (54.67)	42 (67.74)		16 (61.54)	15 (71.43)	
Distal pancreatectomy	34 (45.33)	20 (32.26)		10 (38.46)	6 (28.57)	
Pathological characteristics						
T stage, n (%)			0.007			0.12
T1	3 (4.00)	7 (11.29)		0	3 (14.29)	
T2	31 (41.33)	37 (59.68)		13 (50.00)	11 (52.38)	
T3-4	41 (54.67)	18 (29.03)		13 (50.00)	7 (33.33)	
N stage, n (%)			0.01			0.50
N0	33 (44.00)	23 (37.10)		12 (46.15)	7 (33.33)	
N1	26 (34.67)	35 (56.45)		9 (34.62)	7 (33.33)	
N2	16 (21.33)	4 (6.45)		5 (19.23)	7 (33.33)	
Grade of differentiation, n (%)			1.00			0.22
Well-moderately	53 (70.67)	44 (70.97)		17 (65.38)	10 (47.62)	
Poorly-undifferentiated	22 (29.33)	18 (29.03)		9 (34.62)	11 (52.38)	
Duodenum Invasion, n (%)			0.82			0.97
Negative	51 (68.00)	41 (66.13)		15 (57.69)	12 (57.14)	
Positive	24 (32.00)	21 (33.87)		11 (42.31)	9 (42.86)	
Bile Invasion, n (%)			0.29			0.13
Negative	49 (65.33)	35 (56.45)		18 (69.23)	10 (47.62)	
Positive	26 (34.67)	27 (43.55)		8 (30.77)	11 (52.38)	
LVSI n (%)			0.17			0.13
Negative	46 (61.33)	45 (72.58)		18 (69.23)	10 (47.62)	
Positive	29 (38.67)	17 (27.42)		8 (30.77)	11 (52.38)	
Perineural invasion, n (%)			0.73			1.00
Negative	5 (6.67)	3 (4.84)		2 (7.69)	1 (4.76)	
Positive	70 (93.33)	59 (95.16)		24 (92.31)	20 (95.24)	
CT characteristics						
Tumor size, cm (median, rang)	3.98 ± 1.72	3.44 ± 1.48	0.05	4.17 ± 1.73	3.24 ± 1.42	0.06
Location, n (%)			0.12			0.48
Head	41 (54.67)	42 (67.74)		16 (61.54)	15 (71.43)	
Body and tail	34 (45.33)	20 (32.26)		10 (38.46)	6 (28.57)	
Pancreatitis, n (%)			0.94			0.41
No	44 (58.67)	36 (58.06)		13 (50.00)	13 (61.90)	
Yes	31 (41.33)	26 (41.94)		13 (50.00)	8 (38.10)	
PD cutoff and dilation, n (%)			0.86			0.87
No	16 (21.33)	14 (22.58)		8 (30.77)	6 (28.57)	
Yes	59 (78.67)	48 (77.42)		18 (69.23)	15 (71.43)	
CBD cutoff and dilation, n (%)			0.60			0.72
No	48 (64.00)	37 (59.68)		15 (57.69)	11 (52.38)	
Yes	27 (36.00)	25 (40.32)		11 (42.31)	10 (47.62)	
Parenchymal atrophy, n (%)			0.30			0.92
No	32 (42.67)	32 (51.61)		12 (46.15)	10 (47.62)	
Yes	43 (57.33)	30 (48.39)		14 (53.85)	11 (52.38)	
Contour abnormality, n (%)			0.94			0.71
No	10 (13.33)	8 (12.90)		6 (23.08)	3 (14.29)	
Yes	65 (86.67)	54 (87.10)		20 (76.92)	18 (85.71)	
Cyst, n (%)			0.33			0.30
No	71 (94.67)	56 (90.32)		22 (84.62)	20 (95.24)	
Yes	4 (5.33)	6 (9.68)		4 (15.38)	1 (4.76)	
Vascular invasion, n (%)			0.47			0.63
No	54 (72.00)	48 (77.42)		19 (73.08)	14 (66.67)	
Yes	21 (28.00)	14 (22.58)		7 (26.92)	7 (33.33)	

BMI, body mass index; PD, pancreatic duct; CBD, common bile duct; LVSI, lymphvascular space invasion.

The radiomics features were reduced and selected in the arterial and portal venous phase images. The radiomics features that did not significantly differ between the groups or did not show significant correlations with CD8 expression were excluded. The remaining 67 radiomics features were further reduced using a LASSO logistic regression model. Finally, the radiomics characteristics were reduced to 10 features (**Supplemental Figures 1A, B**), and the LASSO logistic regression formula was used to obtain the rad-score (**Table 2**). The rad-score was significantly lower ($p < 0.001$) in the CD8-high group (median: -0.43; range: -1.61–1.42) than in the CD8-low group (median: -0.16; range: -1.16–2.35) (**Supplemental Figure 1C**).

Univariate Analysis

The results of the univariate analysis (**Table 3**) demonstrated that the rad-score and T stage were significantly associated with CD8 expression.

Development, Performance, and Validation of the Prediction Model

The performance of the prediction model combining radiomics features and tumor size is shown in **Figures 4** and **5**. The AUC values were 0.75 (95% CI: 0.67–0.83) and 0.67 (95% CI: 0.51–0.83) for the training and validation sets, respectively. The sensitivity, specificity, accuracy, positive predictive value, and negative predictive value for the training set were 80.65%, 60.00%, 0.69, 0.63, and 0.79, respectively, whereas those for the validation set were 80.95%, 57.69%, 0.68, 0.61, and 0.79, respectively. The calibration curve showed good calibration of the training ($p = 0.92$) and validation sets ($p = 0.23$).

TABLE 2 | The radiomics features selected by Lasso Regression.

Phase		Prediction model
Intercept	-0.1905	
	ß	Radiomics name
Arterial phase		
	-0.095	exponential_firstorder_Median
	0.028	exponential_firstorder_Variance
	0.0403	square_glszm_SmallAreaLowGrayLevelEmphasis
	-0.0705	wavelet-LHH_firstorder_Mean
	0.0965	wavelet-HLH_glszm_SizeZoneNonUniformity
	-0.1691	wavelet-HLH_glszm_LowGrayLevelZoneEmphasis
	0.2466	wavelet-HHH_firstorder_Mean
	0.1375	lbp-2D_firstorder_Skewness
Portal venous phase		
	-0.1429	wavelet-LLH_glszm_SmallAreaHighGrayLevelEmphasis
	-0.2314	wavelet-HHL_glszmSmallAreaEmphasis

Radiomics score = -0.1905 - 0.095 × exponential_firstorder_Median (Arterial phase).
+ 0.028 × exponential_firstorder_Variance (Arterial phase).
+ 0.0403 × square_glszm_SmallAreaLowGrayLevelEmphasis (Arterial phase).
- 0.0705 × wavelet-LHH_firstorder_Mean(Arterial phase).
+ 0.0965 × wavelet-HLH_glszm_SizeZoneNonUniformity(Arterial phase).
- 0.1691 × wavelet-HLH_glszm_LowGrayLevelZoneEmphasis (Arterial phase).
+ 0.2466 × wavelet-HHH_firstorder_Mean (Arterial phase).
+ 0.1375 × lbp-2D_firstorder_Skewness (Arterial phase).
- 0.1429 × wavelet-LLH_glszm_SmallAreaHighGrayLevelEmphasis (Portal phase).
- 0.2314 × wavelet-HHL_glszmSmallAreaEmphasis (Portal phase).

Clinical Utility of the Prediction Model

The decision curve of the rad-score is shown in **Figure 6**. The decision curves show that with a threshold probability >0.16, using the XGBoost classifier to predict $CD8^+$ T-cell added more benefit than the "treat all patients as high $CD8^+$ T-cell" scheme or the "treat none as low $CD8^+$ T-cell" scheme.

DISCUSSION

Immunotherapy has emerged as a promising treatment in cancer; assessing patients' different immune statuses with PDAC can better help physicians identify those who can benefit from immune therapies. Although relevant genetic subtypes have been identified (26, 27), clinicians still lack reproducible and biologically meaningful biomarkers to identify patients with favorable prognoses at initial diagnosis. We focused on the radiomic features extracted from the pancreatic protocol CT scan, which is widely used in practice, to identify such a biomarker. Compared with histopathologic and molecular biomarkers, radiomics has the potential to predict the molecular profiles of tumors from image phenotypes inexpensively, non-invasively, and easily. In this study, we observed that the infiltration of $CD8^+$ TILs is associated with the prognosis of patients with PDAC. Further, we established a CT-based radiomic score to extrapolate the tumor immune infiltration levels in patients with PDAC.

Cellular immunity is important for the immune system and plays a critical role in eliminating cancer and preventing inflammation. $CD8^+$ T-cells can lyse tumor cells directly that expose tumor-specific antigens in various cancers, including PDAC (28). Quantification of $CD8^+$ TILs, known as the immunoscore, was developed to evaluate the association between the infiltration level of $CD8^+$ TILs and patients with PDAC survival (27, 29–32), with results consistent with those in our study. Our study used X-tile plots (25), a new bioinformatics tool for biomarker assessment and outcome-based cut-point optimization, to provide a global assessment of every possible way of dividing the patients with PDAC into low- and high-level CD8 expression. All patients were divided into either CD8-high (CD8 >18.69%, n = 101; 54.89%) or CD8-low (CD8 ≤18.69%, n=83; 45.10%) groups, based on the optimal cut-off of CD8 level, as determined by x-tile (18.69%). Furthermore, a log-rank test showed that the survival duration in the CD8-high group (22.63 months, 95% CI: 20.20–36.20) was significantly longer than that in the CD8-low group (14.67 months, 95% CI: 12.13–22.37).

Compared to the immunoscore of surgical tissue samples, measuring the level of $CD8^+$ TILs by radiomics is more convenient, which is especially important in patients with unresectable PDAC. Sun et al. built a CT-based radiomic signature to assess $CD8^+$ TIL infiltration determined by RNA-seq data (33). More than fifteen types of tumors were included in this study, but not PDAC. We are the first to have investigated the possibility of extrapolating the infiltration levels of $CD8^+$ TILs in PDAC using radiomics based on CT in both a training

TABLE 3 | The result of univariate analysis.

Variables	Training set		Validation set	
	OR (95% CI)	*p*- Value	OR (95% CI)	*p*- Value
Rad-score	5.16 (2.10, 12.68)	0.0004	4.99 (1.47, 16.93)	0.01
Sex				
Male	1.0		1.0	
Female	0.77 (0.37, 1.59)	0.48	1.02 (0.32, 3.27)	0.97
Age	1.00 (0.97, 1.04)	0.82	1.01 (0.95, 1.07)	0.80
BMI	1.02 (0.91, 1.15)	0.71	1.00 (0.98, 1.01)	0.70
Operation				
Pancreaticoduodenectomy	1.0		1.0	
Distal pancreatectomy	0.57 (0.29, 1.16)	0.12	0.64 (0.19, 2.20)	0.48
T stage				
T1-2	1.0		1.0	
T3-4	0.34 (0.17, 0.69)	0.0029	0.50 (0.15,1.64)	0.25
N stage				
N0	1.0		1.0	
N1	1.93 (0.93, 4.03)	0.08	1.33 (0.34, 5.19)	0.68
N2	0.36 (0.11, 1.21)	0.10	2.40 (0.55, 10.53)	0.25
Grade of differentiation				
Well-moderately	1.0		1.0	
Poorly-undifferentiated	0.99 (0.47, 2.07)	0.97	2.08 (0.64, 6.74)	0.22
Duodenum Invasion				
Negative	1.0		1.0	
Positive	1.09 (0.53, 2.23)	0.82	1.02 (0.32, 3.27)	1.00
Bile Invasion				
Negative	1.0		1.0	
Positive	1.45 (0.73, 2.90)	0.29	2.47 (0.75, 8.17)	0.14
LVSI				
Negative	1.0		1.0	
Positive	0.60 (0.29, 1.24)	0.17	2.47 (0.75, 8.17)	0.14
Perineural invasion				
Negative	1.0		1.0	
Positive	1.40 (0.32, 6.13)	0.66	1.67 (0.14, 19.76)	0.69
Tumor size (cm, mean ± SD)	0.80 (0.64, 1.01)	0.06	0.66 (0.42, 1.04)	0.07
Location				
Head	1.0		1.0	
Body and tail	0.57 (0.29, 1.16)	0.12	0.64 (0.19, 2.20)	0.48
Parenchymal atrophy				
No	1.0		1.0	
Yes	0.70 (0.35, 1.37)	0.30	0.94 (0.30, 2.98)	0.92
PD cutoff and dilation				
No	1.0		1.0	
Yes	0.93 (0.41, 2.09)	0.86	1.11 (0.31, 3.92)	0.87
CBD cutoff and dilation				
No	1.0		1.0	
Yes	1.20 (0.60, 2.40)	0.60	1.24 (0.39, 3.94)	0.72
Pancreatitis				
No	1.0		1.0	
Yes	1.03 (0.52, 2.03)	0.94	0.62 (0.19, 1.98)	0.42
Contour abnormality				
No	1.0		1.0	
Yes	1.04 (0.38, 2.82)	0.94	1.80 (0.39, 8.27)	0.45
Cyst n (%)				
No	1.0		1.0	
Yes	1.90 (0.51, 7.07)	0.34	0.28 (0.03, 2.67)	0.27
Vascular invasion				
No	1.0		1.0	
Yes	0.75 (0.34, 1.64)	0.47	1.36 (0.39, 4.76)	0.63

OR, odds ratio; CI, confidence interval; Rad-score radiomics score; BMI, body mass index; LVSI, lymphvascular space invasion; PD, pancreatic duct; CBD, common bile duct; Rad-score, radiomics score.

and validation cohort. The rad score can reflect the infiltration level of $CD8^+$ TIL, and the association between lower rad scores and higher $CD8^+$ TIL infiltration can be observed, suggesting that the rad score may be an important prognosis biomarker for patients with PDAC. Furthermore, the DCA test showed that the rad-score could effectively facilitate clinical decision-making.

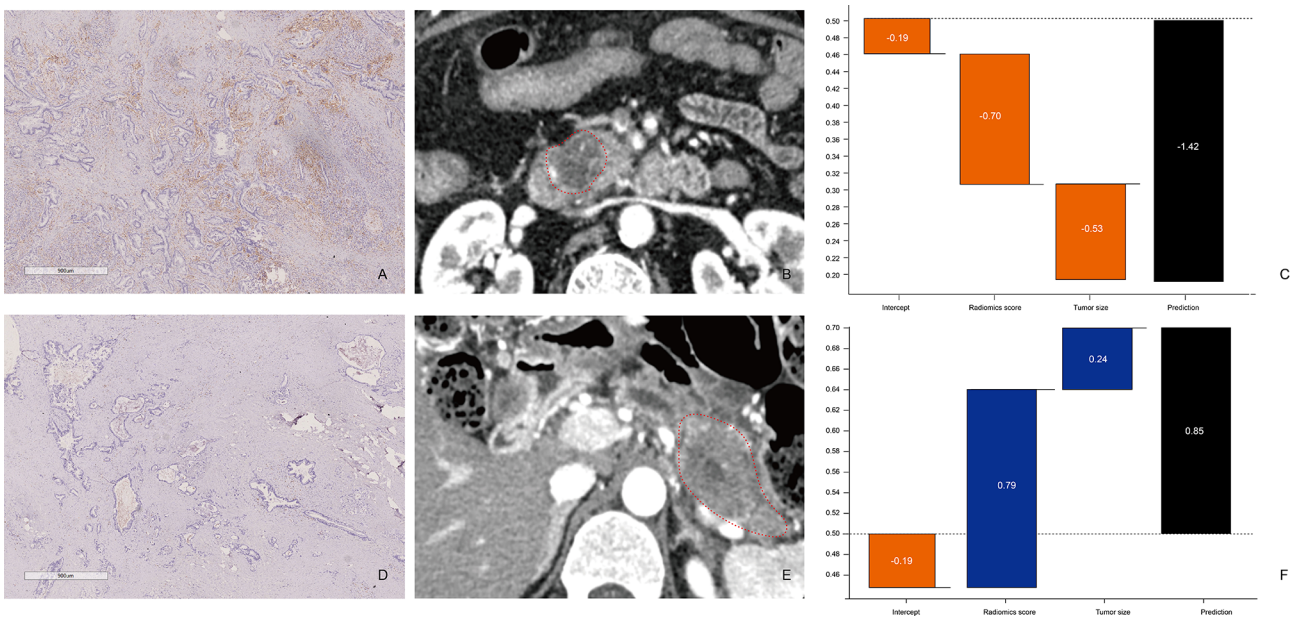

FIGURE 4 | Comparison between patients with low and high CD8$^+$ T-cell infiltration **(A–C)** Patient 1: A 65-year-old man with PDAC in the CD8$^+$ T-high group. **(A)** CD8$^+$ T-cell infiltration is high (×20). **(B)** The axial portal-phase CT image shows an infiltrative, low-attenuation mass (arrows) located at the pancreatic head. **(C)** The prediction probability of low CD8$^+$ T infiltration was 80.58% by XGBoost classifier. **(D–F)** Patient 2: A case of a 49-year-old man with PDAC in the CD8$^+$ T-low group. **(D)** CD8$^+$ T-cell infiltration is low (×20). **(E)** The axial portal-phase CT image shows an infiltrative, low-attenuation mass (arrows) located at the pancreatic body and tail. **(F)** The prediction probability of low CD8$^+$ T-cell infiltration is 70.07% by XGBoost classifier.

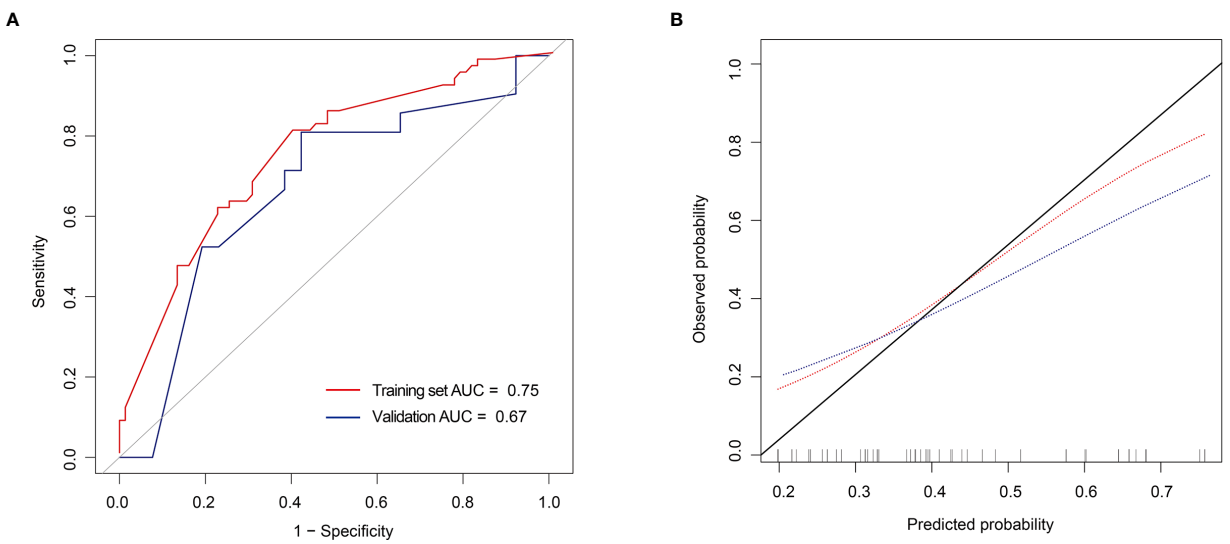

FIGURE 5 | Receiver operating characteristic (ROC) curves and calibration curves of the extreme gradient boosting (XGBoost) classifier **(A)** ROC curves of the XGBoost classifier in the training and validation set. **(B)** Calibration curves of the XGBoost classifier in the training and validation set.

The intra-tumor heterogeneity assessed by radiomics may reflect genomic heterogeneity, and tumors with more genomic heterogeneity are more likely to resist therapy and develop distant metastasis; thus, they tend to predict a worse prognosis (14, 34–36). Texture analysis is an objective mathematical method based on their gray levels and spatial relationships (37). The most widely used texture analysis methods are the gray-level co-occurrence matrix (GLCM) and gray-level run-length matrix (GLRLM) (38).

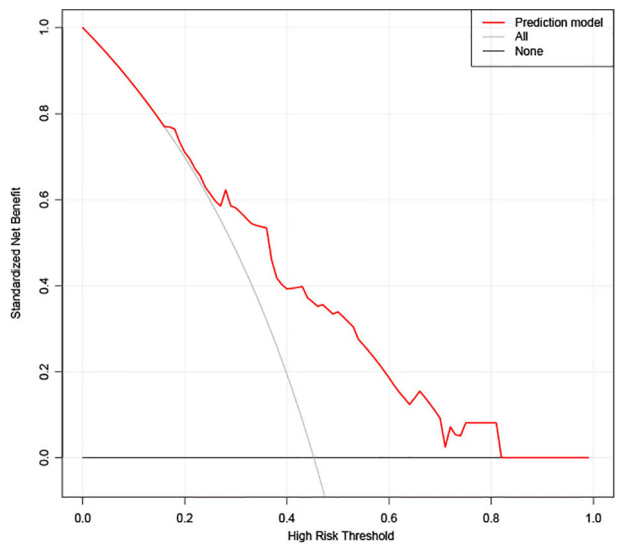

FIGURE 6 | Decision curve analysis (DCA) for the extreme gradient boosting (XGBoost) classifier. The y-axis represents the net benefit. The gray line represents the hypothesis that all patients had high $CD8^+$ T-cell infiltration. The black line shows the hypothesis that all patients had low $CD8^+$ T-cell infiltration. The x-axis shows the threshold probability, which is where the expected benefit of treatment is equal to the expected benefit of avoiding treatment. The decision curves show that with a threshold probability greater than 0.16, using the prediction model to predict $CD8^+$ T-cell infiltration adds more benefit than the treat-all-patients as high $CD8^+$ T-cell infiltration scheme or the treat-none as low $CD8^+$ T-cell infiltration scheme in the training set.

GLCM can describe the pixel distribution within a region and indicate the frequency of various combinations of grey values observed (38). GLRLM describes the relationships in linear one-dimensional terms (39). Chen et al. observed that highly immune infiltrated HCCs were more homogenous, explaining the high value of GLCM (17). Sun et al. observed that GLRLM could be representative of inflammatory infiltrate, which could reflect homogeneity or heterogeneity of an image (33). In our study, the radiomic signature comprised textural features from the gray-level size-zone matrix (GLSZM). GLSZM is an extended version of GLRLM that describes the size and intensity of voxels clusters in a region of interest (40), which has proven useful when the main characteristic is heterogeneity (40).

There are several limitations to this study. First, our validation cohort was from the same center as the training cohort, which restricts our findings' generalizability to other centers. Second, as a retrospective single-center study, the relatively small sample size may weaken our conclusion. The sample size should be increased to help draw a more reliable result. Third, a few studies have found the importance of joint analysis of PD-L1 expression with CD8 expression, which may explain the mechanism of the immunosuppressive microenvironment of PDAC (20, 41, 42). However, several studies (20, 41) have observed that the PD-$L1^-/CD8^{high}$ subtype had the best survival, whereas patients with low CD8 expression had similar survival regardless of PD-L1 status, which means the endogenous $CD8^+$ TIL-mediated antitumor immune response may play a key role in the prognosis of patients with PDAC. Therefore, evaluating CD8 infiltration levels should be prioritized in a limited timeframe. Fourth, a few recent studies have suggested that the combination of intratumoral and peritumoral radiomics is more effective in predicting therapeutic outcomes (17, 43). Therefore, in the future, further studies involving peritumoral radiomics in larger populations are needed. In addition, the prediction performance of XGBoost in this study is not fully satisfactory, so we will continue to explore other deep learning models to improve the diagnostic efficiency in the future.

CONCLUSION

In conclusion, our study established and validated an enhanced CT-based rad-score for predicting the infiltration level of $CD8^+$ TILs in patients with PDAC. This rad-score may be useful in the pretreatment prediction of individual patient immunoscores to guide accurate prognosis prediction and precision immunotherapy for patients with PDAC.

DATA AVAILABILITY STATEMENT

The original contributions presented in the study are included in the article/**Supplementary Material**. Further inquiries can be directed to the corresponding authors.

ETHICS STATEMENT

The studies involving human participants were reviewed and approved by Biomedical Research Ethics Committee of Changhai hospital. The patients/participants provided their written informed consent to participate in this study. Written informed consent was obtained from the individual(s) for the publication of any potentially identifiable images or data included in this article.

AUTHOR CONTRIBUTIONS

Guarantors of the integrity of entire study: YB and CW. Study design or data acquisition or data analysis/interpretation: all authors. Manuscript drafting or manuscript revision: JL, ZS, and FL. Approval of final version of submitted manuscript: all authors. Literature research: XCF, YM, HZ, XF, and QL. Clinical studies: JY, HJ, YL, LW, and CW. Statistical analysis: YB. Manuscript editing: JL and FL. Supervision: YB and JPL. All authors contributed to the article and approved the submitted version.

FUNDING

This work was supported in part by the National Science Foundation for Scientists of China (81871352), Clinical

Research Plan of SHDC (SHDC2020CR4073), 234 Platform Discipline Consolidation Foundation Project (2019YPT001), and Shanghai Science and Technology Innovation Action Plan Medical Innovation Research Project (20Y11912500).

SUPPLEMENTARY MATERIAL

The Supplementary Material for this article can be found online at: https://www.frontiersin.org/articles/10.3389/fonc.2021.671333/full#supplementary-material

Supplementary Figure 1 | Radiomic feature selection using a parametric method, the least absolute shrinkage and selection operator (LASSO). **(A)** Selection of the tuning parameter (λ) in the LASSO model via 10-fold cross validation based on minimum criteria. Binomial deviances from the LASSO regression cross-validation procedure have been plotted as a function of log (λ). The y-axis indicates binomial deviances. The lower x-axis indicates the log (λ). Numbers along the upper x-axis represent the average number of predictors. Red dots indicate the average deviance values for each model with a given λ, and vertical bars through the red dots show the upper and lower values of the deviances. The vertical black lines define the optimal values of λ, where the model provides its best fit to the data. The optimal λ value of 0.05 with log (λ) = -3.05 has been selected. **(B)** LASSO coefficient profiles of the 67 texture features. The dotted vertical line is plotted at the value selected using 10-fold cross-validation in A. The 10 resulting features with non-zero coefficients are indicated in the plot. **(C)** The error-bar chart of the 10 radiomics features and radiomics score.

REFERENCES

1. Topalovski M, Brekken RA. Matrix Control of Pancreatic Cancer: New Insights Into Fibronectin Signaling. *Cancer Lett* (2016) 381:252–8. doi: 10.1016/j.canlet.2015.12.027
2. Morganti AG, Massaccesi M, Torre GL, Caravatta L, Piscopo A, Tambaro R, et al. A Systematic Review of Resectability and Survival Afer Concurrent Chemoradiation in Primarily Unresectable Pancreatic Cancer. *Ann Surg Oncol* (2010) 17:194–205. doi: 10.1245/s10434-009-0762-4
3. Khorana AA, Mangu PB, Berlin J, Engebretson A, Hong TS, Maitra A, et al. Potentially Curable Pancreatic Cancer: American Society of Clinical Oncology Clinical Practice Guideline. *J Clin Oncol* (2016) 34:2541–56. doi: 10.1200/JCO.2016.67.5553
4. Conroy T, Desseigne F, Ychou M, Bouché O, Guimbaud R, Bécouarn Y, et al. FOLFIRINOX Versus Gemcitabine for Metastatic Pancreatic Cancer. *N Engl J Med* (2011) 364:1817–25. doi: 10.1056/NEJMoa1011923
5. Gonzalez H, Hagerling C, Werb Z. Roles of the Immune System in Cancer: From Tumor Initiation to Metastatic Progression. *Genes Dev* (2018) 32:1267–84. doi: 10.1101/gad.314617.118
6. Migden MR, Rischin D, Schmults CD, Guminski A, Hauschild A, Lewis KD, et al. Pd-1 Blockade With Cemiplimab in Advanced Cutaneous Squamous-Cell Carcinoma. *N Engl J Med* (2018) 379:341–51. doi: 10.1056/NEJMoa1805131
7. Reck M, Rodriguez-Abreu D, Robinson AG, Hui R, Csoszi T, Fulop A, et al. Pembrolizumab Versus Chemotherapy for PD-L1-Positive non-Small-Cell Lung Cancer. *N Engl J Med* (2016) 375:1823–33. doi: 10.1056/NEJMoa1606774
8. Royal RE, Levy C, Turner K, Mathur A, Hughes M, Kammula US, et al. Phase 2 Trial of Single Agent Ipilimumab (anti-CTLA-4) for Locally Advanced or Metastatic Pancreatic Adenocarcinoma. *J Immunother* (2010) 33:828–33. doi: 10.1097/CJI.0b013e3181eec14c
9. Brahmer JR, Tykodi SS, Chow LQM, Hwu W-J, Topalian SL, Hwu P, et al. Safety and Activity of anti-PD-L1 Antibody in Patients With Advanced Cancer. *N Engl J Med* (2012) 366:2455–65. doi: 10.1056/NEJMoa1200694
10. Tumeh PC, Harview CL, Yearley JH, Shintaku IP, Taylor EJM, Robert L, et al. PD-1 Blockade Induces Responses by Inhibiting Adaptive Immune Resistance. *Nature* (2014) 515:568–71. doi: 10.1038/nature13954
11. Russano M, Napolitano A, Ribelli G, Iuliani M, Simonetti S, Citarella F, et al. Liquid Biopsy and Tumor Heterogeneity in Metastatic Solid Tumors: The Potentiality of Blood Samples. *J Exp Clin Cancer Res* (2020) 39:95. doi: 10.1186/s13046-020-01601-2
12. Wargo JA, Reddy SM, Reuben A, Sharma P. Monitoring Immune Responses in the Tumor Microenvironment. *Curr Opin Immunol* (2016) 41:23–31. doi: 10.1016/j.coi.2016.05.006
13. Stroncek DF, Butterfield LH, Cannarile MA, Dhodapkar MV, Greten TF, Grivel JC, et al. Systematic Evaluation of Immune Regulation and Modulation. *J Immunother Cancer* (2017) 5:21. doi: 10.1186/s40425-017-0223-8
14. Tsujikawa T, Kumar S, Borkar RN, Azimi V, Thibault G, Chang YH, et al. Quantitative Multiplex Immunohistochemistry Reveals Myeloid-Inflamed Tumor-Immune Complexity Associated With Poor Prognosis. *Cell Rep* (2017) 19:203–17. doi: 10.1016/j.celrep.2017.03.037
15. Liao H, Zhang Z, Chen J, Liao M, Xu L, Wu Z, et al. Preoperative Radiomic Approach to Evaluate Tumor-Infltrating CD8+ T Cells in Hepatocellular Carcinoma Patients Using Contrast-Enhanced Computed Tomography. *Ann Surg Oncol* (2019) 26:4537–47. doi: 10.1245/s10434-019-07815-9
16. Mazzaschi G, Milanese G, Pagano P, Madeddu D, Gnetti L, Trentini F, et al. Integrated CT Imaging and Tissue Immune Features Disclose a Radio-Immune Signature With High Prognostic Impact on Surgically Resected NSCLC. *Lung Cancer* (2020) 144:30–9. doi: 10.1016/j.lungcan.2020.04.006
17. Chen S, Feng S, Wei J, Liu F, Li B, Li X, et al. Pretreatment Prediction of Immunoscore in Hepatocellular Cancer: A Radiomics-Based Clinical Model Based on Gd-EOB-DTPA-Enhanced MRI Imaging. *Eur Radiol* (2019) 29:4177–87. doi: 10.1007/s00330-018-5986-x
18. Wen Q, Yang Z, Zhu J, Qiu Q, Dai H, Feng A, et al. Pretreatment CT-Based Radiomics Signature as a Potential Imaging Biomarker for Predicting the Expression of PD-L1 and CD8+TILs in ESCC. *Onco Targets Ther* (2020) 13:12003–13. doi: 10.2147/OTT.S261068
19. Zhang X, Liu S, Zhao X, Shi X, Li J, Guo J, et al. Magnetic Resonance Imaging-Based Radiomic Features for Extrapolating Infiltration Levels of Immune Cells in Lower-Grade Gliomas. *Strahlenther Onkol.* (2020) 196:913–21. doi: 10.1007/s00066-020-01584-1
20. Danilova L, Ho WJ, Zhu Q, Vithayathil T, Jesus-Acosta AD, Azad NS, et al. Programmed Cell Death Ligand-1 (Pd-L1) and CD8 Expression Profiling Identify an Immunologic Subtype of Pancreatic Ductal Adenocarcinomas With Favorable Survival. *Cancer Immunol Res* (2019) 7:886–95. doi: 10.1158/2326-6066.CIR-18-0822
21. Miksch RC, Schoenberg MB, Weniger M, Bösch F, Ormanns S, Mayer B, et al. Prognostic Impact of Tumor-Infiltrating Lymphocytes and Neutrophils on Survival of Patients With Upfront Resection of Pancreatic Cancer. *Cancers (Basel)* (2019) 11:39. doi: 10.3390/cancers11010039
22. Tahkola K, Leppänen J, Ahtiainen M, Väyrynen J, Haapasaari K-M, Karttunen T, et al. Immune Cell Score in Pancreatic Cancer-Comparison of Hotspot and Whole-Section Techniques. *Virchows Arch* (2019) 474:691–9. doi: 10.1007/s00428-019-02549-1
23. Verbeke F, Verbeke CS. *Pathology of the Pancreas: A Practical Approach*. London: Springer-Verlag (2013).
24. Amin MB, Edge SB, Greene FL, Byrd DR, Brookland RK, Washington MK, et al. *Ajcc Cancer Staging Manual*. New York: Springer (2017). doi: 10.1007/978-3-319-40618-3
25. Camp RL, Dolled-Filhart M, Rimm DL. X-Tile: A New Bio-Informatics Tool for Biomarker Assessment and Outcome-Based Cut-Point Optimization. *Clin Cancer Res* (2004) 10:7252–9. doi: 10.1158/1078-0432.CCR-04-0713
26. Wartenberg M, Cibin S, Zlobec I, Vassella E, Eppenberger-Castori S, Terracciano L, et al. Integrated Genomic and Immunophenotypic Classification of Pancreatic Cancer Reveals Three Distinct Subtypes With Prognostic/Predictive Significance. *Clin Cancer Res* (2018) 24:4444–54. doi: 10.1158/1078-0432.CCR-17-3401
27. Balachandran VP, Łuksza M, Zhao JN, Makarov V, Moral JA, Remark R, et al. Identification of Unique Neoantigen Qualities in Long Term Pancreatic Cancer Survivors. *Nature* (2017) 551:512–6. doi: 10.1038/nature24462
28. Seo YD, Pillarisetty VG. T-Cell Programming in Pancreatic Adenocarcinoma: A Review. *Cancer Gene Ther* (2017) 24:106–13. doi: 10.1038/cgt.2016.66

29. Lianyuan T, Dianrong X, Chunhui Y, Zhaolai M, Bin J. The Predictive Value and Role of Stromal Tumor-Infiltrating Lymphocytes in Pancreatic Ductal Adenocarcinoma (PDAC). *Cancer Biol Ther* (2018) 19:296–305. doi: 10.1080/15384047.2017.1416932
30. Lohneis P, Sinn M, Bischoff S, Jühling A, Pelzer U, Wislocka L, et al. Cytotoxic Tumour-Infiltrating T Lymphocytes Influence Outcome in Resected Pancreatic Ductal Adenocarcinoma. *Eur J Cancer* (2017) 83:290–301. doi: 10.1016/j.ejca.2017.06.016
31. Foucher ED, Ghigo C, Chouaib S, Galon J, Iovanna J, Olive D. Pancreatic Ductal Adenocarcinoma: A Strong Imbalance of Good and Bad Immunological Cops in the Tumor Microenvironment. *Front Immunol* (2018) 9:1044. doi: 10.3389/fimmu.2018.01044
32. Vonderheide RH. The Immune Revolution: A Case for Priming, Not Checkpoint. *Cancer Cell* (2018) 33:563–9. doi: 10.1016/j.ccell.2018.03.008
33. Sun R, Limkin EJ, Vakalopoulou M, Dercle L, Champiat S, Han SR, et al. A Radiomics Approach to Assess Tumour-Infltrating CD8 Cells and Response to anti-PD-1 or anti-PD-L1 Immunotherapy: An Imaging Biomarker, Retrospective Multicohort Study. *Lancet Oncol* (2018) 19:1180–91. doi: 10.1016/S1470-2045(18)30413-3
34. Campbell PJ, Yachida S, Mudie LJ, Stephens PJ, Pleasance ED, Stebbings LA, et al. The Patterns and Dynamics of Genomic Instability in Metastatic Pancreatic Cancer. *Nature* (2010) 467:1109–13. doi: 10.1038/nature09460
35. Li J, Byrne KT, Yan F, Yamazoe T, Chen Z, Baslan T, et al. Tumor Cell-Intrinsic Factors Underlie Heterogeneity of Immune Cell Infiltration and Response to Immunotherapy. *Immunity* (2018) 49:178–93.e177. doi: 10.1016/j.immuni.2018.06.006
36. Balli D, Rech AJ, Stanger BZ, Vonderheide RH. Immune Cytolytic Activity Stratifies Molecular Subsets of Human Pancreatic Cancer. *Clin Cancer Res* (2017) 23:3129–38. doi: 10.1158/1078-0432.CCR-16-2128
37. Gurcan MN, Boucheron LE, Can A, Madabhushi A, Rajpoot NM, Yener B. Histopathological Image Analysis: A Review. *IEEE Rev BioMed Eng* (2009) 2:147–71. doi: 10.1109/RBME.2009.2034865
38. Haralick RM, Shanmugam K, Dinstein IH. Textural Features for Image Classification. *IEEE Trans Syst Man Cybern* (1973) 6:610–21. doi: 10.1109/TSMC.1973.4309314
39. Galloway MM. Texture Analysis Using Gray Level Run Lengths. *Comput Graphics Image Process* (1975) 4:172–9. doi: 10.1016/S0146-664X(75)80008-6
40. Thibault G, Fertil B, Navarro C, Pereira S, Cau P, Levy N, et al. Shape and Texture Indexes Application to Cell Nuclei Classification. *Int J Pattern Recogn Artif Intell* (2013) 27:1357002. doi: 10.1142/S0218001413570024
41. Hou Y-C, Chao Y-J, Hsieh M-H, Tung H-L, Wang H-C, Shan Y-S. Low CD8+ T Cell Infiltration and High Pd-L1 Expression are Associated With Level of CD44+/CD133+ Cancer Stem Cells and Predict an Unfavorable Prognosis in Pancreatic Cancer. *Cancers (Basel)* (2019) 11:541. doi: 10.3390/cancers11040541
42. Teng MWL, Ngiow SF, Ribas A, Smyth MJ. Classifying Cancers Based on T-cell Infiltration and PD-L1. *Cancer Res* (2015) 75:2139–45. doi: 10.1158/0008-5472.CAN-15-0255
43. Braman NM, Etesami M, Prasanna P, Dubchuk C, Gilmore H, Tiwari P, et al. Intratumoral and Peritumoral Radiomics for the Pretreatment Prediction of Pathological Complete Response to Neoadjuvant Chemotherapy Based on Breast DCE-MRI. *Breast Cancer Res* (2017) 19:80. doi: 10.1186/s13058-017-0846-1

Conflict of Interest: The authors declare that the research was conducted in the absence of any commercial or financial relationships that could be construed as a potential conflict of interest.

frontiers in Oncology

ORIGINAL RESEARCH
published: 19 May 2021
doi: 10.3389/fonc.2021.649290

Yap1-2 Isoform Is the Primary Mediator in TGF-β1 Induced EMT in Pancreatic Cancer

Chao Gao[1†], Mei-Yu Quan[2†], Qian-Jie Chen[3], Ruo Yang[4], Yuanyuan Wu[1], Jia-Yu Liu[1], Zhong-Yuan Lin[1], Xue Li[4], Jue-Ting Cai[4], Tian-Fang Jiang[5], Le Xu[6], Majid Mossahebi-Mohammadi[4], Qiang Guo[4] and Jin-San Zhang[1,4*]*

[1] Institute of Life Sciences, Wenzhou University, Wenzhou, China, [2] The Key Laboratory of Interventional Pulmonology of Zhejiang Province, The First Affiliated Hospital of Wenzhou Medical University, Wenzhou, China, [3] Department of Pharmacy, Cangnan Hospital Affiliated to Wenzhou Medical University, Wenzhou, China, [4] International Collaborative Center on Growth Factor Research, and School of Pharmaceutical Sciences, Wenzhou Medical University, Wenzhou, China, [5] Eye Hospital, Wenzhou Medical University, Wenzhou, China, [6] Division of Respiratory Medicine, Taizhou Enze Hospital, Taizhou, China

OPEN ACCESS

Edited by:
Takatsugu Ishimoto, Kumamoto University, Japan

Reviewed by:
Nissar Ahmad Wani, Central University of Kashmir, India
Kazumichi Kawakubo, Hokkaido University Hospital, Japan

***Correspondence:**
Jin-San Zhang
Zhang_jinsan@wmu.edu.cn
Qiang Guo
guoqiang_j@163.com

†These authors have contributed equally to this work and share first authorship

Specialty section:
This article was submitted to Gastrointestinal Cancers, a section of the journal Frontiers in Oncology

Received: *04 January 2021*
Accepted: *26 March 2021*
Published: *19 May 2021*

Citation:
Gao C, Quan M-Y, Chen Q-J, Yang R, Wu Y, Liu J-Y, Lin Z-Y, Li X, Cai J-T, Jiang T-F, Xu L, Mossahebi-Mohammadi M, Guo Q and Zhang J-S (2021) Yap1-2 Isoform Is the Primary Mediator in TGF-β1 Induced EMT in Pancreatic Cancer. Front. Oncol. 11:649290. doi: 10.3389/fonc.2021.649290

Pancreatic ductal adenocarcinoma (PDAC) is the most aggressive human malignancy and intrinsically resistant to conventional therapies. YAP1, as a key downstream effector of the Hippo pathway, plays an important role in tumorigenesis including PDAC. Alternative mRNA splicing of YAP1 results in at least 8 protein isoforms, which are divided into two subgroups (YAP1-1 and YAP1-2) based on the presence of either a single or double WW domains. We investigated the functions and regulatory mechanisms of YAP1-1 and YAP1-2 in PDAC cells induced by TGF-β to undergo epithelial-to-mesenchymal transition (EMT). CRISPR-Cas9 and shRNA were used to silence YAP1 expression in pancreatic cancer cells. Re-constituted lentivirus mediated overexpression of each single YAP1 isoform was generated in the parental knockout L3.6 cells. EMT was induced by treatment with TGF-β, EGF and bFGF in parental and the constructed stable cell lines. Western blot and qPCR were used to detect the expression of EMT markers. Scratch wound healing and transwell assays were used to detect cell migration. The stability and subcellular localization of YAP1 proteins were determined by Western blot analysis, immunofluorescence, as well as ubiquitination assays. We showed that TGF-β, EGF and bFGF all significantly promoted EMT in PDAC cells, which was inhibited by knockdown of YAP1 expression. Interestingly, YAP1-1 stable cells exhibited a stronger migratory ability than YAP1-2 cells under normal culture condition. However, upon TGF-β treatment, L3.6-YAP1-2 cells exhibited a stronger migratory ability than L3.6-YAP1-1 cells. Mechanistically, TGF-β treatment preferentially stabilizes YAP1-2 and enhances its nuclear localization. Furthermore, TGF-β-induced EMT and YAP1-2 activity were both blocked by inhibition of AKT signaling. Our results showed that both YAP1-1 and YAP1-2 isoforms are important mediators in the EMT process of pancreatic cancer. However, YAP1-2 is more important in mediating TGF-β-induced EMT, which requires AKT signaling.

Keywords: YAP1 isoforms, epithelial-mesenchymal transition, pancreatic cancer, TGF-β, AKT signaling

INTRODUCTION

Pancreatic ductal adenocarcinoma (PDAC), is highly fatal due to its aggressive biology nature and intrinsic resistance to conventional therapies (1). Yes-associated protein 1 (YAP1), together with WW domain-containing transcription regulator protein 1 (WWT1, also called TAZ), function as the main downstream effectors of the Hippo pathway. YAP1 plays critical roles in tissue homeostasis and regulation of organ size. The Hippo signaling is also a tumor suppressor pathway, while YAP1 has been identified as an oncogene in various malignancies associated with tumor progression and poor prognosis (2). YAP1 overexpression is detected in the early stages of pancreatic carcinogenesis (3). Interestingly, YAP1 has been shown to be involved in both oncogenic KRAS-dependent and KRAS-independent cancer-promoting activities (4, 5). In recent years, YAP1 has been reported to participate in Epithelial-to-mesenchymal transition (EMT) process of tumor cells (6, 7).

Through alternative mRNA splicing, the human *YAP1* gene generates at least eight isoforms that differ in the regions of the 2nd WW domain and the transcriptional activation domain (TAD) (8). These isoforms can be divided into YAP1-1, which contains one WW domain, and YAP1-2, which contains two WW domains (9). The WW domain consists of incomplete duplicates of 30-40 amino acid residues, of which two invariant tryptophan residues mediate specific interactions with partners with short proline-rich sequences (9, 10). The WW domain of YAP1 is involved in complex formation with PPxY motif-containing proteins (where P is proline, x is any amino acid and Y is tyrosine) (11), such as LATS1/2 (12), AMOT (13), PTCH1 (14), ZEB1 (15), etc. Previous studies, including our own, revealed that the presence of single or double WW domains could influence the interactions of YAP1 with these proteins such as LATS (16). Although the mRNA sequences encoding different isoforms have been reported, the biological and functional differences of various protein isoforms of YAP1 have just begun to be appreciated.

EMT is a cellular reprograming process during which cells lose their epithelial traits and gradually acquire mesenchymal characteristics (17), such as downregulation of E-Cadherin and upregulation of Vimentin, resulting in weakened adhesion and enhanced motility (18). During EMT, remodeling of cell-cell and cell-extracellular matrix interactions leads to the detachment of epithelial cells from their original sites. This is crucial to the early-stage dissemination of cancer cells and is pivotal for the invasion and metastasis. Moreover, EMT has been reported to confer increased chemoresistance in cancer cells, including PDAC (19, 20). Transforming growth factor-beta (TGF-β) (21), epidermal growth factor (EGF) (22), and fibroblast growth factor (FGF) (23), are all well-known cytokines that promote the EMT phenotype (24). TGF-β activates Smad2 and Smad3, which subsequently bind to Smad4 and then translocate to the nucleus to regulate gene expression (25). TGF-β can also activate the PI3K/AKT pathway to promote EMT (26). YAP1 plays a multitude of roles as the key downstream effector of Hippo signaling. It promotes tumor development and progression, as well as EMT and drug resistance in PDAC (27).

In this study, we investigated whether YAP1 contributes to TGF-β-induced EMT in PDAC cells and the potential difference between the YAP1 isoforms that mediate such activities. Our results indicated that, with TGF-β treatment, YAP1-2 exhibited stronger effects than YAP1-1 in promoting EMT in PDAC cells. Mechanistically, we showed that TGF-β treatment activates the AKT pathway to preferentially stabilize YAP1-2 and promote its nuclear localization.

MATERIALS AND METHODS

Cell Culture and Treatment

Human pancreatic cancer cell lines L3.6, PANC1, PATU89.88T, and rat pheochromocytoma cell line PC12 were obtained from ATCC. The human embryonic kidney cell line HEK293T was obtained from the Shanghai Cell Bank of the Chinese Academy of Sciences. All cells were cultured in RPMI 1640 (Gibco) or DMEM (Gibco) medium with 10% fetal bovine serum (FBS, Gibco) at 37°C in standard conditions (5% CO_2, 95% air).

Transwell Assays

A total of 1×10^5 L3.6 cells were seeded in the upper chamber of a transwell membrane (8 μm pore size) in 24-well plates. FBS medium (10%) was added to the lower chamber as an attractant, while 1% FBS medium was added to the upper chamber. After 24 h of incubation, the cells were fixed with paraformaldehyde (PFA) and stained with crystal violet dye. The number of stained cells was counted under a phase-contrast microscope (Leica, Germany).

Western Blot

Total protein was extracted from PDAC cells for Western blot analysis. The cells were lysed with lysis buffer (Beyotime, P0013) containing phosphatase inhibitors and phenylmethanesulfonyl fluoride (PMSF, Beyotime, ST506). The samples were fractionated by SDS-PAGE gels and transferred to microporous polyvinylidene difluoride (PVDF) membranes (Roche, 3010040001). The membranes were blocked with 5% skim milk for 1 h and incubated with primary antibodies overnight at 4°C. Antibodies against GAPDH (10494-1-AP) and anti-β-actin (20536-1-AP) were purchased from Proteintech. Other primary antibodies including anti-YAP (CST, 14074), anti-E-Cadherin (CST, 3195), anti-Vimentin (CST, 5741), anti-phospho-Smad2 (CST, 8828), anti-Smad2/3 (CST, 8685), anti-phospho AKT (CST, 4060), and anti-AKT (CST, 9272) were the products of Cell Signaling Technology. The membranes were then probed with secondary antibodies: goat anti-mouse IgG (H+L)-HRP or goat anti-rabbit IgG (H+L)-HRP (Bioworld).

Scratch Healing Assay

The cells were seeded in 6-well plates, and 10 μl pipette tips were used to make a scratch to assess regeneration and repair of the cells. The wound images were taken at 0 h, 24 h, 48 h, and 72 h, respectively.

Immunofluorescence

The cells were seeded in 24-well plates at the appropriate density for 12 h. They were fixed with 4% PFA for 15 min and permeabilized with 0.1% Triton X-100 for 7 min. They were then blocked with 5% normal sheep serum before incubating with primary antibody (1:100) for 2 h at room temperature followed by incubation with the secondary antibodies for 1 h at room temperature (Goat anti-Mouse IgG H&L, Abcam, 1:1000). After washes with PBS, the cells were mounted with Gold Antifade with DAPI (Invitrogen, P36931).

RNA Isolation, Real-Time PCR and YAP1 Isoform Detection

Total RNA was extracted with RNAiso Plus (TaKaRa, JPN). The PrimeScript RT Reagent Kit (TaKaRa, JPN) was used for cDNA synthesis. Real-time PCR was carried out with the CFX96 Real-Time System (Bio-Rad) and SYBR Premix Ex Taq (TaKaRa, JPN). The gene-specific primers used in this study were as follows: Vimentin (forward: 5'-GAGGATCTGGAATTCGG ATCC-3', reverse:5'- ACGCGTCGACTTATTCAAGGT-3'); E-Cadherin (forward: 5'-AATGCCGCCATCGCTTAC-3', reverse: 5'-ACCAGGGTATACGTAGGGAAACTCT-3'); and GAPDH (forward: 5'-ACATCGCTCAGACACCATG-3', reverse: 5'-TGTAGTTGAGGTCAATGAAGGG-3'). All values were normalized to GAPDH.

Lentiviral Packaging, Transduction, and Selection of Stable Cells

Lentiviral packaging, host cell infection and pLKO-shRNA stable PDAC cell selection with puromycin were performed as previously described (28). For the stable reconstituted expression of YAP1-specific isoforms, lentiviral particles carrying pLenti6.3-Flag-YAP1 cDNA encoding YAP1-1γ or YAP1-2γ were used to infect L3.6-KoYAP1 cells. The cells were then selected in culture medium supplemented with blasticidin (5 μg/ml), and the pooled blasticidin-resistant cells were used as stable overexpression cells.

Ubiquitination Assay

HEK293T cells were transfected with the *Flag-YAP1* and *HA-UbI* vectors and incubated with 20 μM MG132 for 4 h before harvesting. The cells were washed twice with prechilled PBS and lysed in 120 μL of lysis buffer (10% glycerol, 1% SDS, 62.5 mM Tris-HCl (pH 6.8), 1 mM iodoacetamide and 10 mM NEM). Cell lysates were boiled for 15 min and then diluted with NTEN lysis buffer freshly supplemented with protease and deubiquitination inhibitors at a 1:9 ratio. The cell lysates were immunoprecipitated with anti-Flag M2 agarose beads (Sigma, USA), and the immune complexes were subjected to Western blotting.

Statistical Analysis

Statistical analyses were performed using GraphPad Prism 8 (GraphPad Software, San Diego, CA, USA) and SPSS 19.0 software (SPSS, Inc., Chicago, USA). p values showing differences were calculated by an unpaired two-tailed t-test, and those showing no differences were calculated by a one-tailed t-test.

RESULTS

YAP1 Contributes to EMT Phenotype in PDAC Cells

We determined the role of YAP1 in the EMT of pancreatic cancer cells by examining the expression of EMT markers in a YAP1 knockout cell line previously generated in L3.6 (16). The Western blot results showed that deletion of YAP1 led to increased Vimentin, but decreased E-Cadherin expression (**Figure 1A**). Furthermore, wound healing and transwell assays indicated that the migratory and invasive potential were diminished in YAP1-KO cells (**Figures 1B–E**). We further verified that YAP1 knockdown was associated with reduced migration and invasion capabilities in PANC1 and PATU8988T cell lines. YAP1 knockdown led to increased Vimentin, but decreased E-Cadherin expression in PANC1 and PATU8988T (**Figure 1F**). Suppression of YAP1 expression in these cells were achieved by lenti shRNA, which also led to decreased migration and invasion based on wounding and transwell assays (**Figures 1G–J**). Therefore, YAP1 expression correlated with migration and invasion in three independent pancreatic cancer cell lines.

YAP1 Mediates Growth Factor-Induced EMT in L3.6 Cells

Given that YAP1 knockout or knockdown inhibited the invasion and migration of PDAC cells, we hypothesized that YAP1 may also play a role in growth factor-induced EMT. As shown in **Figures 2A, B**, treatment with TGF-β (20ng/ml), EGF (20ng/ml), and bFGF (20ng/ml) significantly promoted healing of parental L3.6 cells in the wounding assay, which were significantly inhibited in L3.6-KoYAP1 cells. Transwell assays confirmed these results (**Figures 2C, D**). Western blot analyses were used to detect the EMT-associated proteins E-Cadherin and Vimentin, and the results indicated that YAP1-KO effectively prevented the occurrence of EMT characteristics induced by these growth factors (**Figure 2E**). In summary, the results showed that YAP1 expression plays an important role in the EMT induced by different growth factors.

Identification of YAP1-2 as the Major Isoform in TGF-β-Induced EMT

The above results suggest YAP1 as an important mediator in these growth factor-induced EMT phenotype. We next wanted to determine if the YAP1 protein isoforms presented distinct or redundant roles in EMT process with a focus on TGF-β. Scratch assays were performed with L3.6-YAP1-1 and L3.6-YAP1-2 stable cells. These cells were generated in our previous study on YAP1 knockout L3.6 cells with reconstituted overexpression of single YAP1 isoforms (16). The results revealed that YAP1-1 has a stronger stimulatory effect on EMT than YAP1-2 in none treated cells. However, upon induction by TGF-β, L3.6-YAP1-2 cells exhibited stronger migration than L3.6-YAP1-1 cells (**Figures 3A, B**). SB431542, a TGF-β receptor inhibitor, largely abolished TGF-β-induced EMT in both L3.6-YAP1-1 and L3.6-YAP1-2 cells. Consistent results were obtained in the transwell assays (**Figures 3C, D**). Upon examining the TGF-β signaling and EMT markers, we found YAP1-2 cells possessed higher E-Cadherin

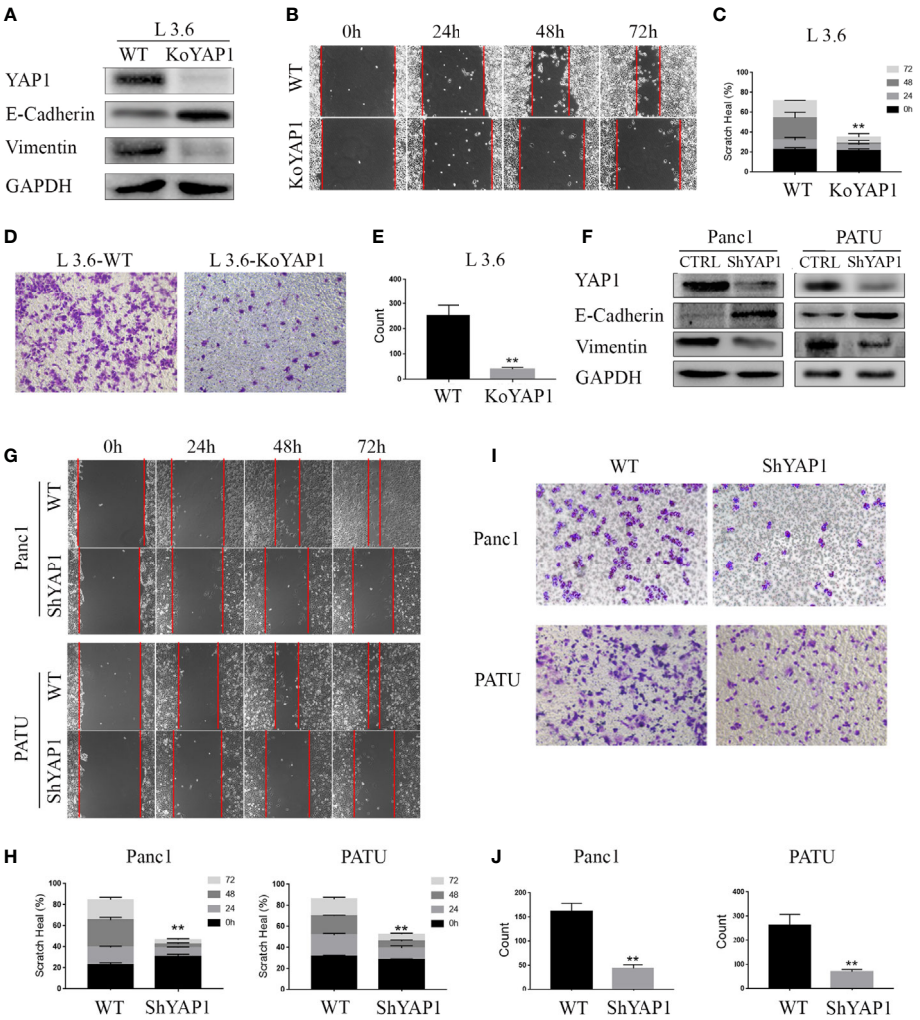

FIGURE 1 | YAP1 contributes to EMT phenotype in PDAC cells. **(A)** Western blot analysis of YAP1 and EMT marker expression in L3.6 wild type (WT) and YAP1 knockout cells (KoYAP1). **(B–E)** The migration and invasion ability of L3.6-WT and L3.6-KoYAP1 were detected by scratch healing assay **(B)** and transwell assay **(D)**. Statistical analysis of the scratch healing assay **(C)** and transwell assay **(E)**. **p < 0.001. **(F–J)** Different PADC cell lines were used to verify the effect of YAP1. EMT markers (E-Cadherin and Vimentin) and YAP1 knockdown efficiency were determined by western blot **(F)**, migration and invasion of the indicated cell lines were detected by scratch healing assay **(G)** and transwell assay(I). Statistical analysis of the scratch healing assay **(H)** and transwell assay **(J)**. **p < 0.001.

expression when untreated than YAP1-1. Interestingly, the E-Cadherin expression in YAP1-2 cells was significantly inhibited by TGF-β treatment, but that of YAP1-1 was minimally impacted. The trend of Vimentin was the opposite, and all changes were reversed by SB431542 (**Figures 3E–G**). Also, we showed that blocking YAP1 using Verteporfin, a YAP1 inhibitor, led to a significant change in the expression of E-Cadherin and Vimentin in L3.6-YAP1-2 cells (**Figure S2**). In short, the results proved that the YAP1-2 is more potent than YAP1-1 in mediating TGFβ-induced EMT in pancreatic cancer cells.

TGF-β Mainly Promotes YAP1-2 Stability and Its Nuclear Localization

YAP1 stability and nuclear translocation represent a key regulatory mechanism downstream of Hippo signaling. Western blot analysis revealed that the YAP1-1 protein was more stable than the YAP1-2 protein under normal conditions, but the stability of the YAP1-2 protein was preferentially improved after TGF-β treatment (**Figures 4A, B**). Immunoprecipitation assay results indicated that the ubiquitination level of YAP1-2 was significantly higher than that of YAP1-1. Although TGF-β treatment significantly decreased the ubiquitination levels of both isoforms, the gap between YAP1-1 and YAP1-2 was narrowed down significantly (**Figures 4C, D**), and TGF-β treatment also stabilized both YAP1-1 and YAP1-2 proteins induced by verteporfin (**Figure S2**). These results suggest that the stability of both proteins was upregulated after induction, but YAP1-2 changed more significantly than YAP1-1. Subsequently, we examined the subcellular localization of the different isoforms of YAP1 with

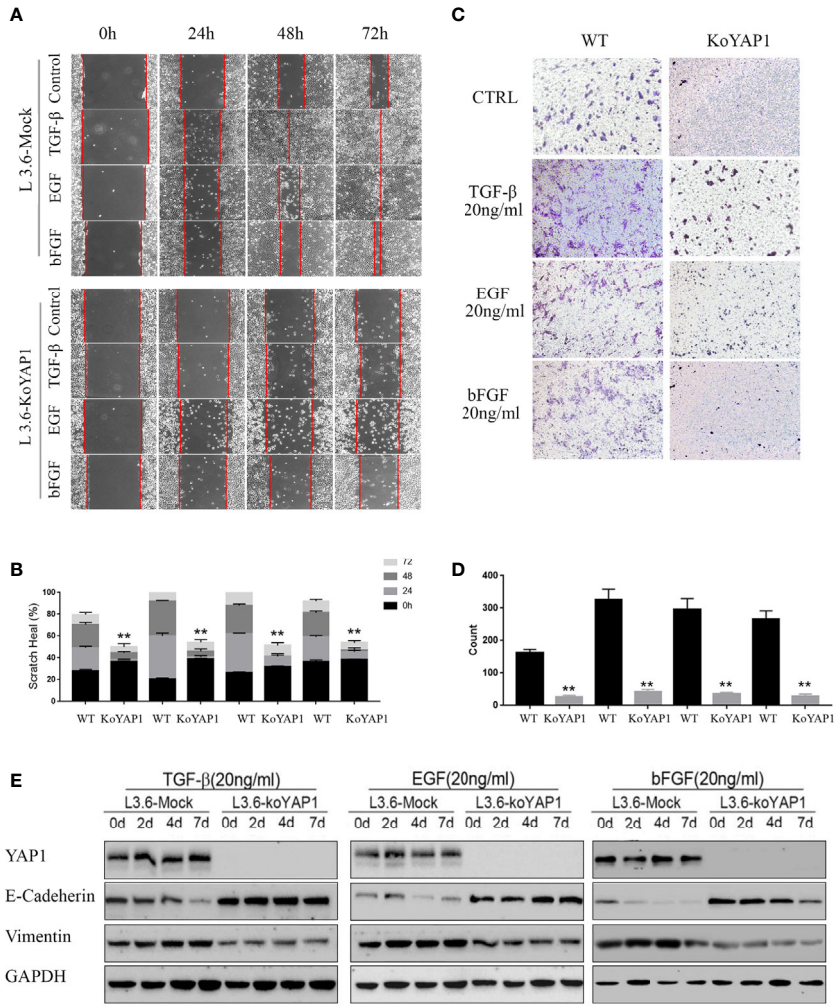

FIGURE 2 | Knockout of YAP1 blocks EMT phenotype induced by TGF-β, bFGF and EGF. L3.6-WT and L3.6-KoYAP1 cells were treated with TGF-β (20ng/ml), EGF (20ng/ml), and bFGF (20ng/ml), respectively, for 72 h. Cell migration and invasion were detected by scratch healing assay **(A)** and transwell assay **(C)** and the expression of EMT markers by western blot **(E)**. Statistical analysis of the scratch healing assay **(B)** and transwell assay **(D)**. **p < 0.001.

immunofluorescence. Increased nuclear translocation of YAP1-2 was observed after TGF-β treatment, and the process could be inhibited by SB431542, whereas the localization of YAP1-1 only changed slightly (**Figure 4E**). Western blot analysis confirmed that YAP1-2 protein expression was upregulated in both the nucleus and cytoplasm after induction, but was more prominent in the nucleus (**Figure 4F**). In summary, the data demonstrated that both the stability and location of YAP1-2 changed significantly after TGF-β induction.

AKT Inhibition Abolishes the Function of YAP1-2 in TGF-β-Induced EMT

In previous studies, it was reported that YAP1 activity closely correlates with the AKT signaling activation in fibrotic disease (29), wound healing (30), etc. Therefore, we evaluated the role of the AKT pathway in YAP1-related EMT by co-treatment of the cells with MK2206, an AKT phosphorylation inhibitor. As expected, Western blot analysis showed that the phosphorylation of AKT was significantly inhibited by MK2206 treatment (**Figures 5E**, **S1**). Scratch healing assay (**Figures 5A, B**) and transwell assay (**Figures 5C, D**) results indicated that MK2206 treatment significantly inhibited migration and invasion of both L3.6-YAP1-1 and L3.6-YAP1-2 cells with TGF-β-induced EMT. The Western blot and qRT-PCR results showed that MK2206 upregulated E-Cadherin and downregulated Vimentin at both the protein and mRNA levels in the L3.6-YAP1-1 and L3.6-YAP1-2 cells with TGF-β-induced EMT (**Figures 5E–G**, **S1**). Additionally, MK2206 treatment also decreased the protein levels of YAP1-1 and YAP1-2 (**Figures 5E**, **S1**). In summary, YAP1-2 is more important than YAP1-1 in mediating TGF-β-induced invasion and migration of L3.6 cells, a process relies on activation of the AKT pathway.

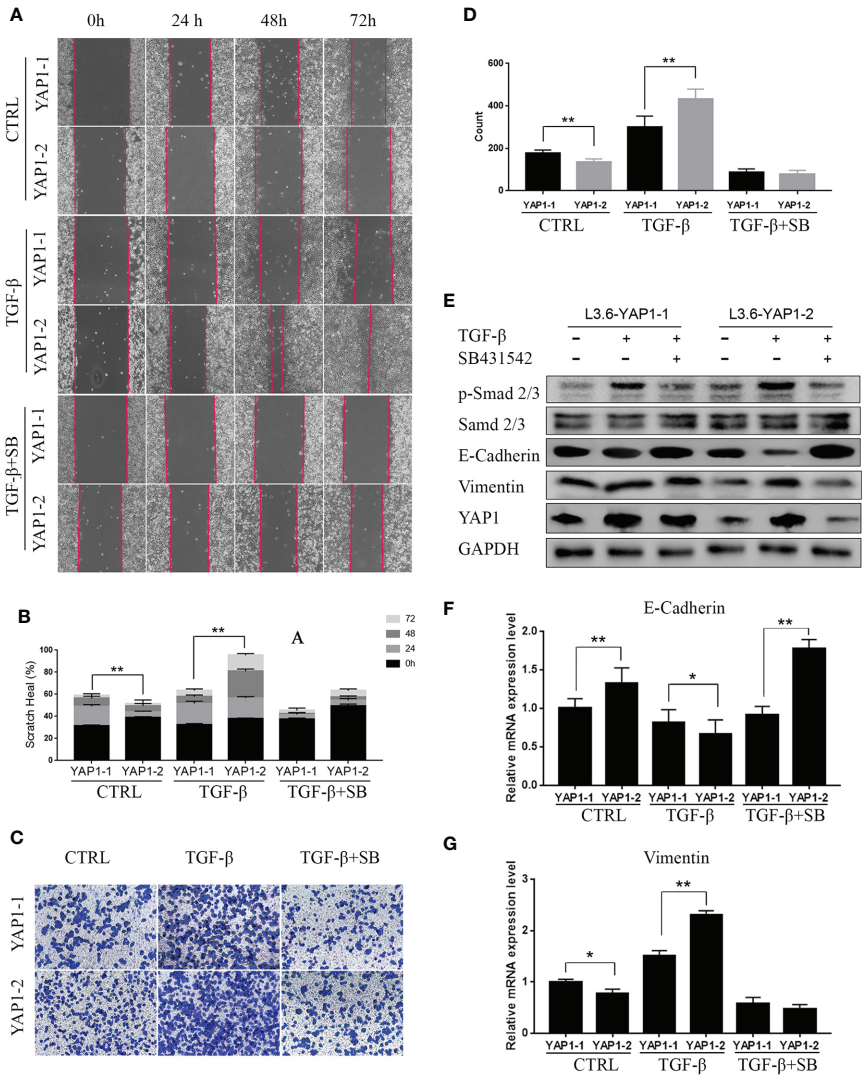

FIGURE 3 | YAP1-2 is the major functional isoform in mediating TGFβ-induced EMT. **(A, C)** Cells were pretreated with 20ng/ml TGF-β and 2.5μM SB431542 for 72 h, the scratch healing assay **(A)** and transwell assay **(C)** were performed to detect cell migration in L3.6-YAP1-1 and L3.6-YAP1-2 stable lines. **(B, D)** Statistical analysis of the scratch healing assay **(B)**, and transwell assay **(D)**. **p < 0.001. **(E–G)** Cells were treated with 20ng/ml TGF-β and 2.5μM SB431542 for 72 h, Western Blot **(E)** and qPCR **(F, G)** were performed to detect the expression of EMT related markers in L3.6-YAP1-1 and L3.6-YAP1-2 cells. SB431542 is abbreviated as "SB". *p < 0.05, **p < 0.001.

AKT Signaling Is Required for TGF-β-Induced YAP1 Stabilization and Nuclear Localization

We determined the potential differential impact of AKT signaling on YAP1 isoform stability and subcellular location in pancreatic cancer cells by examining their expression in response to TGF-β treatment, both with and without the AKT inhibitor. To this end, we chose previously generated L3.6-YAP1-1 and L3.6-YAP1-2 reconstituted expression stable cell lines (16). The cells were seeded at very low density (10^6 cells/10-cm dish) for 3 days and then trypsinized and replanted at high cell density ($2x10^6$ cells/3.5-cm dish) for TGF-β treatment with and without the AKT inhibitor. The results indicated that the stabilizing effect of TGF-β on both YAP1-1 and YAP1-2 were diminished, but much more prominent for YAP1-2 (**Figures 6A, B**). Similarly, inhibition of AKT phosphorylation largely blocked the nuclear localization of YAP1-2 (**Figure 6C**). Therefore, the activity of the AKT pathway is of critical importance for TGF-β promoted EMT, which is mainly mediated by YAP1-2. To further confirm the role of AKT in TGF- β induced EMT, the AKT- Kinase Dead (KD) mutant plasmid was co-transfected with YAP1-1 and YAP1-2, respectively, to PC12 cells. Analysis of fractionated proteins showed that nuclear-translocation of YAP1-2 was inhibited upon AKT-KD co-expression (**Figures 6D, E**).

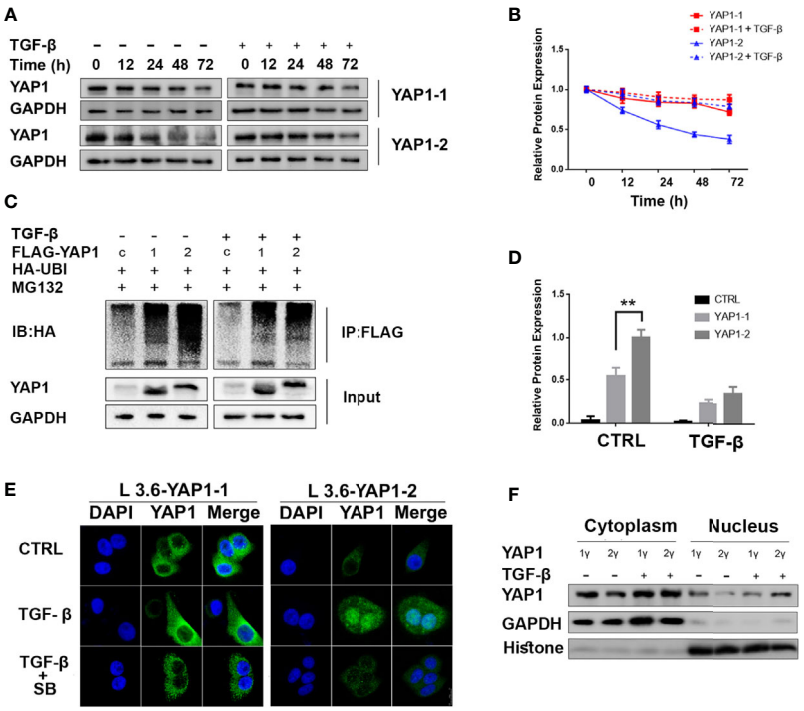

FIGURE 4 | TGF-β promotes YAP1-2 stability and nuclear localization. **(A)** L3.6-YAP1-1 and L3.6-YAP1-2 cells were cultured under the low-density condition for 3 days to accumulate YAP1 proteins with or without TGF-β (20ng/ml) treatment. The cells were then transferred to 3.5 cm dishes in high-density conditions to trigger YAP1 degradation. Whole-cell lysates from L3.6-YAP1-1 and L3.6-YAP1-2 cells were collected at indicated time points and subjected to Western blotting to detect the abundance of YAP1. **(B)** Statistical analysis of **(A)**. **(C)** HA-tagged ubiquitin was co-transfected with either Flag-YAP1-1 or YAP1-2 into HEK293T cells as indicated with Flag-YFP as a control. The transfected cells were treated with 20ng/ml TGF-β for 24 h. YAP1 ubiquitination was determined by immunoprecipitation (IP) for Flag and immunoblotting for HA. **(D)** Statistical analysis of **(C)**. **p< 0.001. **(E)** Cells were pretreated with 20ng/ml TGF-β and 2.5μM SB431542 for 72 h, immunofluorescence was performed to reveal the expression and subcellular localization of L3.6-YAP1-1 and L3.6-YAP1-2 cells. **(F)** Cells were pretreated with 20ng/ml TGF-β for 72 h, extraction of cytoplasmic and nuclear proteins was then performed to detect the distribution of YAP1 in L3.6-YAP1-1 and L3.6-YAP1-2 by immunoblot analysis.

DISCUSSION

YAP1 protein isoforms differ within the TAD and WW motifs, two key regions mediating their transcriptional activation and interaction with PPxY motif proteins (8). We recently reported the dichotomy between the mRNA and protein expression, as well as the distinct mechanism of regulation between the YAP1-1 and YAP1-2 isoforms in response to cell density. We proposed that YAP1-1 is more potent in promoting cancer cell malignancy in culture and primary tumor growth *in vivo*, whereas YAP1-2 has a more significant role in promoting metastasis due to its stabilization under low cell contact/density such as in the form of circulating tumor cells (16).

Consistent with our previous findings, the current study further demonstrated that the stability and nuclear localization of YAP1-1 proteins were higher than those of YAP1-2 under quiescent conditions, and correlates with stronger invasion and metastasis. Interestingly, YAP1-2 exhibited stronger promotion of the invasion and metastasis of PDAC cells than YAP1-1 in the process of TGF-β induced EMT, which was associated with a more robust increase in protein stability as well as nuclear localization of YAP1-2 than YAP1-1. Therefore, stabilization of YAP1 proteins, especially the YAP1-2 isoform, contributes to TGF-β induced EMT. However, we cannot rule out the possibility that other mechanisms may also be involved. We have previously demonstrated that the presence of the 2nd WW motif enhances the interactions of both YAP1-1 and YAP1-2 proteins with some PPXY proteins such as LATS1. Importantly, only YAP1-2 is capable of forming *de novo* complex with AMOT and PTPN14. Of note, the WW domain not only mediates binding to negative regulators mainly residing in the cytosol as mentioned above, but it also interacts with nuclear factors such as RUNX (31), ZEB1 (15), P73 (32, 33) and SMADs (34, 35) to alter the targets of YAP1. ZEB1 and SMADs are both important EMT regulators. During EMT, ZEB1 and SMADs are often increased, showing stronger nuclear localization and higher transcriptional activity, a process that we speculate may involve YAP1-2. It is also possible that, in response to TGF-β stimulation, activated YAP1-2 preferentially binds to EMT-related nuclear factors to facilitate their nuclear transport and transcriptional activities, which should be an interesting area for future investigation.

Our data highlight a critical role of activated AKT signaling for the stability of YAP1 in the context of TGF-β stimulation.

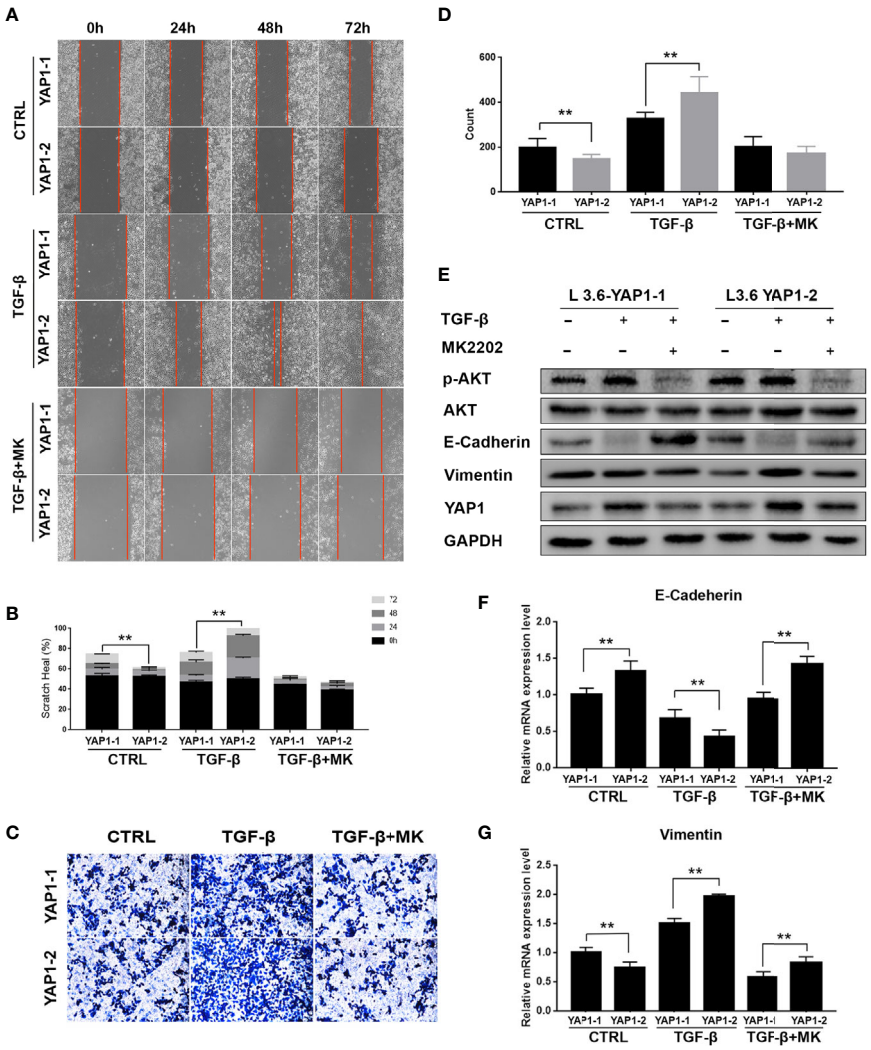

FIGURE 5 | Inhibition of AKT signaling abolishes the activity of YAP1-2 in TGF-β induced EMT. **(A, C)** L3.6-YAP1-1 and L3.6-YAP1-2 stable cells were pretreated with 20ng/ml TGF-β and 2.5μM MK2206 for 72 h, the scratch healing assay **(A)** and transwell assay **(C)** were performed to determine the migration ability of L3.6-YAP1-1 and L3.6-YAP1-2. **(B, D)** Statistical analysis of the scratch healing assay **(B)** and transwell assay **(D)**. **p < 0.001. **(E, F)** Cells were pretreated with 20ng/ml TGF-β for 72 h, and then with MK2206 (2.5μM) for another 24 h. Western Blot **(E)** and qPCR **(F, G)** were performed to detect the expression of EMT markers and AKT phosphorylation. MK2206 is abbreviated as "MK". **p < 0.001.

AKT has been shown to bind directly to YAP1 and enhance its stability. However, this molecule is not the only factor that regulates the stability of YAP1. The main regulation of YAP1 is from the upstream Hippo pathway, which is subjected to regulation by diverse stimuli such as cell-cell contact, mechanical cues, as well as EMT. When cells undergo EMT, they shrink, and cell contact becomes weaker. Under such circumstances, Hippo pathway is suppressed leading to YAP1 stabilization. Given that inhibition of the AKT pathway is known to strongly inhibit EMT phenotype, thus TGF-β stimulated AKT activation may contribute directly and indirectly to the stabilization and the nuclear localization of YAP1.

EMT is a crucial initiating step of tumor metastasis and correlates to the advanced stages of tumor progression. Our data suggest the existence of redundant and unique regulatory mechanisms underlying the functions of YAP1-1 and YAP1-2 in cancer development and progression. We propose that in the early stages, when cancer cells have a low level of malignancy, YAP1-1 is predominant due to its weaker binding with negative regulatory factors than YAP1-2 and mainly promotes cell proliferation. However, when the tumors progress to a higher degree of malignancy after undergoing EMT, YAP1-2 becomes preferentially stabilized, leading to increased nuclear localization and interactions with additional nuclear factors to promote tumor invasion and metastasis. The potential differential interactions of YAP1-2 from YAP1-1 with EMT-promoting nuclear factors, such as SMADs and ZEB1, should be an interesting line of research in the future.

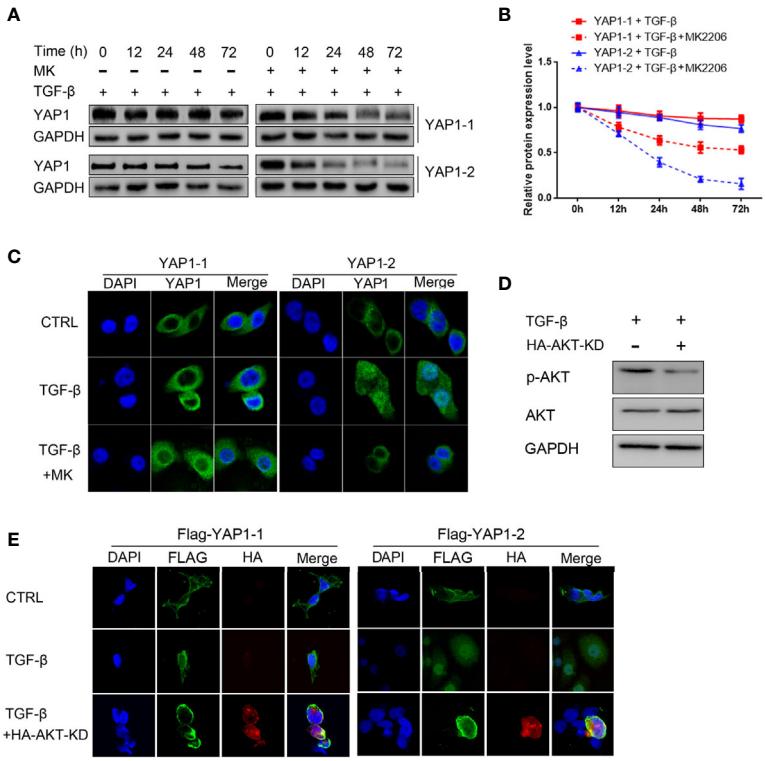

FIGURE 6 | AKT signaling is required for TGF-β induced YAP1 stabilization and nucleus localization. **(A)** L3.6-YAP1-1 and L3.6-YAP1-2 cells were cultured at low-density for 3 days to accumulate YAP1 proteins with or without 20ng/ml TGF-β and 2.5μM MK2206 treatment. The cells were then transferred to 3.5 cm dishes at high-density to trigger degradation. Whole cell lysates were collected at indicated time points and subjected to Western blotting to detect the abundance of YAP1. **(B)** Statistical analysis of **(A)**. **(C)** Cells were treated with 20ng/ml TGF-β and MK2206 for 72 h, immunofluorescence was performed to detect the expression and subcellular localization of YAP1 in L3.6-YAP1-1 and L3.6-YAP1-2 stable cells. **(D)** The HA-AKT(KD) mutant effectively inhibited activation of endogenous AKT. **(E)** HA- AKT(KD) was transfected to PC12 cells, and simultaneously treated with 20ng/ml TGF-β. Immunofluorescence was performed to detect the Tag (Flag) of exogenous YAP1. MK2206 is abbreviated as "MK".

Hippo signaling has emerged as an attractive target for cancer therapy including PDAC (27). YAP1 acts as a central node in relaying Hippo signaling to transcriptional regulation and cancer promotion. Our findings on the unique function and associated regulatory mechanisms between different YAP1 isoforms should facilitate more efficient and precise therapeutic targeting of this critical pathway for cancer therapy.

DATA AVAILABILITY STATEMENT

The raw data supporting the conclusions of this article will be made available by the authors, without undue reservation.

AUTHOR CONTRIBUTIONS

J-SZ and QG conceived the study. M-YQ, RY, CG, J-TC, Q-JC, Z-YL, XL, YW, J-YL, T-FJ, and LX: methodology, data acquisition, and analysis. CG and QG drafted the manuscript. MM-M and J-SZ edited and revised the manuscript. All authors have read and agreed to this version of the manuscript. All authors contributed to the article and approved the submitted version.

FUNDING

QG was funded by the National Natural Science Foundation of China (#81702912). J-SZ was partially supported by a start-up package from Wenzhou University.

SUPPLEMENTARY MATERIAL

The Supplementary Material for this article can be found online at: https://www.frontiersin.org/articles/10.3389/fonc.2021.649290/full#supplementary-material

Supplementary Figure 1 | MK2206 treatment of L3.6-YAP1-1 and L3.6-YAP1-2. MK2206 was added to L3.6-YAP1-1 and L3.6-YAP1-2 stable cells. The results showed that the EMT marker did not change after MK2206 treatment.

Supplementary Figure 2 | YAP1 inhibition affects the expression of EMT markers. L3.6-YAP1-1 and L3.6-YAP1-2 stable cell lines were treated with Verteporfin, YAP1 specific inhibitor, alone or in combination with TGF-β.

REFERENCES

1. Mizrahi J, Surana R, Valle J, Shroff R. Pancreatic Cancer. *Lancet (Lond Engl)* (2020) 395(10242):2008–20. doi: 10.1016/s0140-6736(20)30974-0
2. Yoo W, Lee J, Jun E, Noh K, Lee S, Jung D, et al. The YAP1-NMU Axis Is Associated With Pancreatic Cancer Progression and Poor Outcome: Identification of a Novel Diagnostic Biomarker and Therapeutic Target. *Cancers* (2019) 11(10):1477. doi: 10.3390/cancers11101477
3. Gruber R, Panayiotou R, Nye E, Spencer-Dene B, Stamp G, Behrens A. YAP1 and TAZ Control Pancreatic Cancer Initiation in Mice by Direct Up-Regulation of JAK-STAT3 Signaling. *Gastroenterology* (2016) 151(3):526–39. doi: 10.1053/j.gastro.2016.05.006
4. Mueller S, Engleitner T, Maresch R, Zukowska M, Lange S, Kaltenbacher T, et al. Evolutionary Routes and KRAS Dosage Define Pancreatic Cancer Phenotypes. *Nature* (2018) 554(7690):62–8. doi: 10.1038/nature25459
5. Kapoor A, Yao W, Ying H, Hua S, Liewen A, Wang Q, et al. Yap1 Activation Enables Bypass of Oncogenic Kras Addiction in Pancreatic Cancer. *Cell* (2014) 158(1):185–97. doi: 10.1016/j.cell.2014.06.003
6. Wang D, Luo Y, Wang G, Yang Q. CircATRNL1 Promotes Epithelial-Mesenchymal Transition in Endometriosis by Upregulating Yes-associated Protein 1. *vitro Cell Death Dis* (2020) 11(7):594. doi: 10.1038/s41419-020-02784-4
7. Ben Q, An W, Sun Y, Qian A, Liu J, Zou D, et al. A Nicotine-Induced Positive Feedback Loop Between HIF1A and YAP1 Contributes to Epithelial-to-Mesenchymal Transition in Pancreatic Ductal Adenocarcinoma. *J Exp Clin Cancer Res: CR* (2020) 39(1):181. doi: 10.1186/s13046-020-01689-6
8. Sudol M. YAP1 Oncogene and its Eight Isoforms. *Oncogene* (2013) 32 (33):3922. doi: 10.1038/onc.2012.520
9. Sudol M, Bork P, Einbond A, Kastury K, Druck T, Negrini M, et al. Characterization of the Mammalian YAP (Yes-Associated Protein) Gene and its Role in Defining a Novel Protein Module, the WW Domain. *J Biol Chem* (1995) 270(24):14733–41. doi: 10.1074/jbc.270.24.14733
10. Salah Z, Alian A, Aqeilan R. WW Domain-Containing Proteins: Retrospectives and the Future. *Front Biosci (Landmark Ed)* (2012) 17:331–48. doi: 10.2741/3930
11. Sudol M, Harvey KF. Modularity in the Hippo Signaling Pathway. *Trends Biochem Sci* (2010) 35(11):627–33. doi: 10.1016/j.tibs.2010.05.010
12. Pan D. The Hippo Signaling Pathway in Development and Cancer. *Dev Cell* (2010) 19(4):491–505. doi: 10.1016/j.devcel.2010.09.011
13. Leung CY, Zernicka-Goetz M. Angiomotin Prevents Pluripotent Lineage Differentiation in Mouse Embryos *via* Hippo pathway-dependent and -independent mechanisms. *Nat Commun* (2013) 4:2251. doi: 10.1038/ncomms3251
14. Iglesias-Bexiga M, Castillo F, Cobos ES, Oka T, Sudol M, Luque I. WW Domains of the Yes-Kinase-Associated-Protein (YAP) Transcriptional Regulator Behave as Independent Units With Different Binding Preferences for PPxY Motif-Containing Ligands. *PLoS One* (2015) 10(1):e0113828. doi: 10.1371/journal.pone.0113828
15. Lehmann W, Mossmann D, Kleemann J, Mock K, Meisinger C, Brummer T, et al. ZEB1 Turns Into a Transcriptional Activator by Interacting With YAP1 in Aggressive Cancer Types. *Nat Commun* (2016) 7:10498. doi: 10.1038/ncomms10498
16. Guo Q, Quan M, Dong J, Bai J, Wang J, Han R, et al. The WW Domains Dictate Isoform-Specific Regulation of YAP1 Stability and Pancreatic Cancer Cell Malignancy. *Theranostics* (2020) 10(10):4422–36. doi: 10.7150/thno.42795
17. Greenburg G, Hay ED. Epithelia Suspended in Collagen Gels can Lose Polarity and Express Characteristics of Migrating Mesenchymal Cells. *J Cell Biol* (1982) 95(1):333–9. doi: 10.1083/jcb.95.1.333
18. Zeisberg M, Neilson EG. Biomarkers for Epithelial-Mesenchymal Transitions. *J Clin Invest* (2009) 119(6):1429–37. doi: 10.1172/JCI36183
19. Zheng X, Carstens J, Kim J, Scheible M, Kaye J, Sugimoto H, et al. Epithelial-to-Mesenchymal Transition is Dispensable for Metastasis But Induces Chemoresistance in Pancreatic Cancer. *Nature* (2015) 527(7579):525–30. doi: 10.1038/nature16064
20. Kuwada K, Kagawa S, Yoshida R, Sakamoto S, Ito A, Watanabe M, et al. The Epithelial-to-Mesenchymal Transition Induced by Tumor-Associated Macrophages Confers Chemoresistance in Peritoneally Disseminated Pancreatic Cancer. *J Exp Clin Cancer Res: CR* (2018) 37(1):307. doi: 10.1186/s13046-018-0981-2
21. Heldin CH, Vanlandewijck M, Moustakas A. Regulation of EMT by TGFbeta in Cancer. *FEBS Lett* (2012) 586(14):1959–70. doi: 10.1016/j.febslet.2012.02.037
22. Sheng W, Shi X, Lin Y, Tang J, Jia C, Cao R, et al. Musashi2 Promotes EGF-induced EMT in Pancreatic Cancer *via* ZEB1-ERK/MAPK signaling. *J Exp Clin Cancer Res* (2020) 39(1):16. doi: 10.1186/s13046-020-1521-4
23. Katoh M, Nakagama H. FGF Receptors: Cancer Biology and Therapeutics. *Med Res Rev* (2014) 34(2):280–300. doi: 10.1002/med.21288
24. Massague J. Tgfbeta Signalling in Context. *Nat Rev Mol Cell Biol* (2012) 13 (10):616–30. doi: 10.1038/nrm3434
25. Mohd Faheem M, Rasool RU, Ahmad SM, Jamwal VL, Chakraborty S, Katoch A, et al. Par-4 Mediated Smad4 Induction in PDAC Cells Restores Canonical TGF-beta/Smad4 Axis Driving the Cells Towards Lethal EMT. *Eur J Cell Biol* (2020) 99(4):151076. doi: 10.1016/j.ejcb.2020.151076
26. Baek S, Ko J, Lee J, Kim C, Lee H, Nam D, et al. Ginkgolic Acid Inhibits Invasion and Migration and TGF-β-Induced EMT of Lung Cancer Cells Through PI3K/Akt/mTOR Inactivation. *J Cell Physiol* (2017) 232(2):346–54. doi: 10.1002/jcp.25426
27. Ansari D, Ohlsson H, Althini C, Bauden M, Zhou Q, Hu D, et al. The Hippo Signaling Pathway in Pancreatic Cancer. *Anticancer Res* (2019) 39(7):3317–21. doi: 10.21873/anticanres.13474
28. Zhang JS, Herreros-Villanueva M, Koenig A, Deng Z, De Narvajas AA, Gomez TS, et al. Differential Activity of GSK-3 Isoforms Regulates NF-kappaB and TRAIL- or TNFalpha Induced Apoptosis in Pancreatic Cancer Cells. *Cell Death Dis* (2014) 5:e1142. doi: 10.1038/cddis.2014.102
29. Zhang W, Kong Y. YAP is Essential for TGF-β-Induced Retinal Fibrosis in Diabetic Rats *via* promoting the fibrogenic activity of Müller cells. *J Cell Mol Med* (2020) 24(21):12390–400. doi: 10.1111/jcmm.15739
30. Wei F, Wang A, Wang Q, Han W, Rong R, Wang L, et al. Plasma Endothelial Cells-Derived Extracellular Vesicles Promote Wound Healing in Diabetes Through YAP and the PI3K/Akt/mTOR Pathway. *Aging* (2020) 12 (12):12002–18. doi: 10.18632/aging.103366
31. Vitolo MI, Anglin IE, Mahoney WMJr., Renoud KJ, Gartenhaus RB, Bachman KE, et al. The RUNX2 Transcription Factor Cooperates With the YES-associated Protein, YAP65, to Promote Cell Transformation. *Cancer Biol Ther* (2007) 6(6):856–63. doi: 10.4161/cbt.6.6.4241
32. Strano S, Munarriz E, Rossi M, Castagnoli L, Shaul Y, Sacchi A, et al. Physical Interaction With Yes-associated Protein Enhances p73 Transcriptional Activity. *J Biol Chem* (2001) 276(18):15164–73. doi: 10.1074/jbc.M010484200
33. Raj N, Bam R. Reciprocal Crosstalk Between YAP1/Hippo Pathway and the P53 Family Proteins: Mechanisms and Outcomes in Cancer. *Front Cell Dev Biol* (2019) 7:159. doi: 10.3389/fcell.2019.00159
34. Narimatsu M, Labibi B, Wrana JL, Attisano L. Analysis of Hippo and TGFbeta Signaling in Polarizing Epithelial Cells and Mouse Embryos. *Differentiation* (2016) 91(4-5):109–18. doi: 10.1016/j.diff.2016.01.003
35. Pefani DE, Pankova D, Abraham AG, Grawenda AM, Vlahov N, Scrace S, et al. TGF-Beta Targets the Hippo Pathway Scaffold RASSF1A to Facilitate Yap/Smad2 Nuclear Translocation. *Mol Cell* (2016) 63(1):156–66. doi: 10.1016/j.molcel.2016.05.012

Conflict of Interest: The authors declare that the research was conducted in the absence of any commercial or financial relationships that could be construed as a potential conflict of interest.

frontiers in Oncology

ORIGINAL RESEARCH
published: 20 May 2021
doi: 10.3389/fonc.2021.641289

Bioinformatics Analysis of a Prognostic miRNA Signature and Potential Key Genes in Pancreatic Cancer

Shuoling Chen[1,2†], *Chang Gao*[1,3†], *Tianyang Yu*[1,3†], *Yueyang Qu*[4], *Gary Guishan Xiao*[4*] *and Zunnan Huang*[1,3*]

[1] Key Laboratory of Big Data Mining and Precision Drug Design of Guangdong Medical University, Key Laboratory for Research and Development of Natural Drugs of Guangdong Province, School of Pharmacy, Guangdong Medical University, Dongguan, China, [2] The Second School of Clinical Medicine, Guangdong Medical University, Dongguan, China, [3] Southern Marine Science and Engineering Guangdong Laboratory (Zhanjiang), Zhanjiang, China, [4] School of Pharmaceutical Science and Technology, Dalian University of Technology, Dalian, China

OPEN ACCESS

Edited by:
Takatsugu Ishimoto,
Kumamoto University, Japan

Reviewed by:
Yuangen Yao,
Huazhong Agricultural University, China
Jian Tu,
University of South China, China

***Correspondence:**
Zunnan Huang
zn_huang@yahoo.com
Gary Guishan Xiao
gxiao@dlut.edu.cn

[†]These authors have contributed equally to this work

Specialty section:
This article was submitted to Gastrointestinal Cancers, a section of the journal Frontiers in Oncology

Received: 14 December 2020
Accepted: 31 March 2021
Published: 20 May 2021

Citation:
Chen S, Gao C, Yu T, Qu Y, Xiao GG and Huang Z (2021) Bioinformatics Analysis of a Prognostic miRNA Signature and Potential Key Genes in Pancreatic Cancer. Front. Oncol. 11:641289. doi: 10.3389/fonc.2021.641289

Background: In this study, miRNAs and their critical target genes related to the prognosis of pancreatic cancer were screened based on bioinformatics analysis to provide targets for the prognosis and treatment of pancreatic cancer.

Methods: R software was used to screen differentially expressed miRNAs (DEMs) and genes (DEGs) downloaded from The Cancer Genome Atlas (TCGA) and Gene Expression Omnibus (GEO) databases, respectively. A miRNA Cox proportional hazards regression model was constructed based on the miRNAs, and a miRNA prognostic model was generated. The target genes of the prognostic miRNAs were predicted using TargetScan and miRDB and then intersected with the DEGs to obtain common genes. The functions of the common genes were subjected to Kyoto Encyclopedia of Genes and Genomes (KEGG) and Gene Ontology (GO) analyses. A protein-protein interaction (PPI) network of the common genes was constructed with the STRING database and visualized with Cytoscape software. Key genes were also screened with the MCODE and cytoHubba plug-ins of Cytoscape. Finally, a prognostic model formed by the key gene was also established to help evaluate the reliability of this screening process.

Results: A prognostic model containing four downregulated miRNAs (hsa-mir-424, hsa-mir-3613, hsa-mir-4772 and hsa-mir-126) related to the prognosis of pancreatic cancer was constructed. A total of 118 common genes were enriched in two KEGG pathways and 33 GO functional annotations, including extracellular matrix (ECM)-receptor interaction and cell adhesion. Nine key genes related to pancreatic cancer were also obtained: MMP14, ITGA2, THBS2, COL1A1, COL3A1, COL11A1, COL6A3, COL12A1 and COL5A2. The prognostic model formed by nine key genes also possessed good prognostic ability.

Conclusions: The prognostic model consisting of four miRNAs can reliably predict the prognosis of patients with pancreatic cancer. In addition, the screened nine key genes,

which can also form a reliable prognostic model, are significantly related to the occurrence and development of pancreatic cancer. Among them, one novel miRNA (hsa-mir-4772) and two novel genes (COL12A1 and COL5A2) associated with pancreatic cancer have great potential to be used as prognostic factors and therapeutic targets for this tumor.

Keywords: pancreatic cancer, miRNAs, biomarkers, target genes, The Cancer Genome Atlas, Gene Expression Omnibus

BACKGROUND

Pancreatic cancer, also known as pancreatic ductal adenocarcinoma (PDAC), is a malignancy that frequently appears in the digestive system, and its incidence is on the rise worldwide (1). According to data published recently, PDAC has become the 10th most common malignant tumor, ranking 4th among the causes of death among malignant tumor patients (2). In China, PDAC is one of the major tumors whose both incidence and mortality are increasing (3).

The best and only radical treatment for PDAC is surgical resection (4). However, for many years, there has been no significant improvement in the surgical resection rate or annual survival rate after surgical treatment (5). Moreover, due to extensive metastasis at the time of diagnosis, most patients miss the optimal time for surgery, and PDAC is not sensitive to radiotherapy and chemotherapy. The lack of proper treatment methods highlights the importance of the identification of new therapeutic targets for PDAC. As the study of miRNAs has deepened in recent years, an increasing number of miRNAs have been confirmed to be related to the development of cancers, including PDAC (6, 7). Therefore, it is of great importance to further clarify how miRNAs affect the pathogenesis, invasion and metastasis of PDAC and to provide novel treatment methods.

In recent years, it has been reported that microRNAs (miRNAs, miRs) are influencing factors of PDAC. For example, He et al. (8) illustrated that overexpressed miR-371-5p is associated with a poor prognosis in PDAC patients, and miR-371-5p inhibitors suppress the proliferation of PDAC cells by blocking the cell cycle (8). Deng et al. (9) demonstrated that the downregulation of miR-26a in PDAC cells can inhibit cyclin E2 expression, decreasing the patient survival rate. Zhao et al. (10) found that increasing the expression of miR-148b can suppress the expression of its target gene AMP-activated protein kinase α1 (AMPKα1) to inhibit metastasis and invasion while improving the chemosensitivity of PDAC cells. Therefore, miRNAs can be used as potential biomarkers for PDAC, and the range of their application is broad.

However, the process by which novel miRNA biomarkers are experimentally identified is time consuming and laborious, and the results are not necessarily ideal. Therefore, bioinformatics methods have been proposed to mine such markers from clinical data stored on the internet. The Cancer Genome Atlas (TCGA, https://portal.gdc.cancer.gov/) (11), Gene Expression Omnibus (GEO, http://www.ncbi.nlm.nih.gov/geo) (12), Database for Annotation, Visualization and Integrated Discovery (DAVID, https://david.ncifcrf.gov/) (13), STRING (http://string-db.org/cgi/input.pl) (14), R software (https://www.r-project.org/) (15) and Cytoscape (https://cytoscape.org/) (16) are popular databases and tools that can be used for data download, functional enrichment and protein-protein interaction (PPI) analysis. In recent years, studies have used bioinformatics methods to screen PDAC markers. Ye et al. (17) demonstrated that miR-7 showed predictive ability for PDAC, and lower miR-7 expression levels in patients lead to tumors with a more advanced stage as well as a worse prognosis. Borgmästars et al. (18) revealed that hsa-miR-885-5p acts as a tumor suppressor by calculation and predicted that it can act as a biomarker to predict the prognosis of PDAC patients.

In this study, by analyzing data from the TCGA and GEO databases using bioinformatics methods, we screened prognostic miRNAs and genes related to PDAC. R language packages and Cytoscape plug-ins were applied for the discovery of key genes that affect the occurrence of PDAC. The prognostic miRNAs and key genes we obtained may exert considerable impact on the progression of PDAC, which enables them to become potential therapeutic targets and to be considered for future investigations on PDAC. Our study may provide new ideas for future research on PDAC treatment.

MATERIALS AND METHODS

Data Download and Differential Expression Analysis

The miRNA transcriptome data with the clinical information of 183 pancreatic-related samples (179 tumor tissues and 4 normal tissues) were downloaded from the TCGA database (https://portal.gdc.cancer.gov/) on April 1, 2020. The GSE28735 dataset was directly downloaded from the GEO database (https://www.ncbi.nlm.nih.gov/geo/query/acc.cgi?acc=GSE28735) on April 1, 2020, and includes 45 tumor samples and 45 normal samples. In addition, its relevant clinical survival data were further retrieved

Abbreviations: PDAC, pancreatic ductal adenocarcinoma; miRNA, microRNA; AMPKα1, AMP-activated protein kinase α1; TCGA, The Cancer Genome Atlas; GEO, Gene Expression Omnibus; DAVID, Database for Annotation, Visualization and Integrated Discovery; DEMs, differentially expressed miRNAs; DEGs, differentially expressed genes; PPI, protein-protein interaction; ADAM9, A disintegrin and metalloprotease 9; SOCS6, suppressor of cytokine signaling 6; MMP14, matrix metalloproteinase 14; ITGA2, integrin subunit alpha 2; THBS2, thrombospondin 2; COL1A1, collagen alpha-1(I) chain; COL3A1, collagen alpha-1(III) chain; COL11A1, collagen alpha-1(XI) chain, COL6A3, collagen alpha-3 (VI) chain; COL12A1, collagen alpha-1(XII) chain; COL5A2, collagen alpha-2(V) chain; ECM, extracellular matrix.

from GEO2R website (https://www.ncbi.nlm.nih.gov/geo/geo2r/?acc=GSE28735) of GEO database on March 13, 2021. TCGA data were analyzed with the edgeR package, gplots package and limma package for DEMs with the screening criteria $P < 0.05$ and $|\log2FC| > 1.0$. GEO data were analyzed by the limma package for DEGs with the same screening criteria.

Construction of the Cox Proportional Hazards Regression Model

Univariate Cox proportional hazards regression analysis was performed on DEMs with survival package of R software. Then, with the criteria $P < 0.05$, DEMs from univariate Cox were selected and multivariate Cox stepwise regression analysis was performed on them with survival package of R software. After multivariate Cox, prognostic miRNAs were obtained, and prognostic miRNAs with $P < 0.05$ were considered independent prognostic factors.

Establishment of a Prognostic Model

After the prognostic miRNAs were screened, a prognostic model based on the selected miRNAs was established, and we calculated the risk score of the model using the following formula: risk score = $\beta1 \times \text{Exp}(\text{miRNA}_1) + \beta2 \times \text{Exp}(\text{miRNA}_2) + \ldots + \beta n \times \text{Exp}(\text{miRNA}_n)$. Subsequently, on the basis of the median risk score, patients were assigned to two different groups: high risk and low risk. Then, survival analysis was performed to establish a miRNA prognostic model. A risk score curve was plotted to demonstrate the risk score differences according to the model. A survival status map was plotted to demonstrate the survival status of every cancer sample. A heatmap was plotted to demonstrate the expression level of the prognostic miRNAs in every cancer sample and a survival curve was plotted to demonstrate the 3-year survival in the high- and low-risk groups. We also drew the ROC curve of the model. The AUC value of the model shows the predictive capability, and AUC value > 0.7 indicates the model has strong prognostic ability.

Target Gene Prediction and Common Gene Acquisition

The online website databases TargetScan (http://www.targetscan.org/) (19) and miRDB (http://miRdb.org/) (20) were used to predict the target genes of the miRNAs from the prognostic model. To reduce the false positive rate, the target genes predicted by the two databases were intersected, and the overlapping genes from both databases were employed. Then, we intersected the target genes and the DEGs to obtain the common genes. At this time, the common genes were both the target genes of the prognostic miRNAs and the DEGs related to PDAC.

Kyoto Encyclopedia of Genes and Genomes (KEGG) Pathway and Gene Ontology (GO) Functional Analyses of Common Genes

To further clarify the roles that the common genes play in biological processes, we used the DAVID (https://david.ncifcrf.gov/) to perform KEGG pathway enrichment and GO functional annotation analyses. The enriched KEGG pathway and GO functional annotations with $P < 0.05$ were obtained. The pathways and annotations with smallest P values and largest counts were considered crucial pathways and annotations. GO annotation includes three categories: biological process (BP), cellular component (CC) and molecular function (MF).

Construction of the PPI Network and Screening of the Core Network

We used the online visualization tool STRING (http://string-db.org) to analyze interactions among the common genes. The PPI network was constructed with the common genes whose confidence score was greater than or equal to 0.400, and the disconnected genes were hidden. The network was then input into Cytoscape software (version 3.7.1, https://cytoscape.org/) for visualization. The logFC values of the genes in the network were also imported into Cytoscape. Key genes were screened using the MCC algorithm of the Cytoscape cytoHubba plug-in (21). Meanwhile, the functional modules of the common genes were scored and screened out using the Cytoscape MCODE plug-in with the following criteria: degree cut-off = 2, haircut on, node score cut-off = 0.2, k-core = 2, and max. depth = 100.

MiRNA-Gene-Pathway Network Visualization

The targeted relationship network between the miRNAs and common genes and the pathways and annotations enriched in the common genes were also established using Cytoscape. The regulatory relationships among the miRNAs, key genes and enriched pathways of the common genes in the KEGG pathway analysis with the minimum P value or the maximum count value and the GO functional annotations are presented.

Establish of a Prognostic Model Formed by Screened Key Genes

In order to evaluate the reliability of the key genes screened by Cytoscape, we directly established a prognostic gene model formed by those key genes. And the survival analysis of this new model was conducted, and the risk score curve, survival status map, heatmap and survival curve were plotted. The ROC curve was used as a criterion to show the predictive capability of this models and a AUC value > 0.7 also indicated a strong prognostic ability.

Cell Culture

A normal human pancreatic ductal epithelial cell line was purchased from RiboBio Co., Ltd. (Guangzhou, China), and the PDAC cell lines SW1990 and PANC-1 were purchased from Shanghai GeneChem Co., Ltd. (Shanghai, China). SW1990 and PANC-1 cells were cultured in DMEM (Gibco Company, USA). HPDE6C7 cells were cultured in MEM medium (Gibco, USA). Both media contained 10% inactivated fetal bovine serum (Gibco, USA). All cells were incubated in an incubator at 37°C and 5% CO_2.

RNA Isolation and Real-Time Quantitative PCR

Total RNA was isolated from cultured cells using TRIzol reagent (Thermo Fisher Scientific, USA). A miRNA reverse transcription kit (RiboBio Co., Ltd, Guangzhou, China) was used to generate cDNA. A real-time quantitative PCR kit was used to conduct quantitative analysis. U6 was used as an endogenous control. The relative expression was analyzed by the $2^{-\Delta\Delta Ct}$ method. The primers used were as follows: hsa-mir-424: 5'-GCGCAGCAG CAATTCATGT-3' and 5'-AGTGCAGGGTCCGAGGTATT-3'; and U6: 5'-CGCTTACGAATTTGCGTGTCAT-3' and 5'-CTC GCTTCGGCAGCACA-3'.

RESULTS

Differential Expression Analysis

22 DEMs were identified from 183 PDAC samples from the TCGA: 5 were upregulated, and 17 were downregulated (**Figure 1A**). A total of 402 DEGs were identified from the GSE28735 dataset of the GEO: 234 were upregulated, and 168 were downregulated (**Figure 1B**).

Construction of the Cox Proportional Hazards Regression Model

Six miRNAs associated with the survival of PDAC patients were identified ($P < 0.05$) (**Table 1**). Four downregulated prognostic miRNAs were further selected (hsa-mir-424, hsa-mir-126, hsa-mir-3613 and hsa-mir-4772) (**Table 2**). Among them, the *P* values of hsa-mir-424, hsa-mir-126 and hsa-mir-3613 were less than 0.05, indicating that they were independent prognostic factors. The prognostic miRNA risk score was calculated according to the following formula: risk score = (0.6006 × hsa-mir-424) + (-0.6601 × hsa-mir-126) + (-0.3851 × hsa-mir-3613) + (0.1819 × hsa-mir-4772). Then, the samples were divided into a high-risk group and a low-risk group based on the medium risk score. The risk score of the former group was significantly higher than that of the latter group (**Figure 2A**, top). A high risk score correlated with a poor prognosis. Survival analysis showed that the mortality rate increased as the risk score increased (**Figure 2A**, middle). The heatmap showed that as the risk score increased, the expression levels of hsa-mir-4772, hsa-mir-424 and hsa-mir-126 increased, indicating that they were high-risk miRNAs; the expression of hsa-mir-3613 decreased as the risk score increased, indicating that it was a low-risk miRNA (**Figure 2A**, bottom). Compared with high-risk group, low-risk group survival

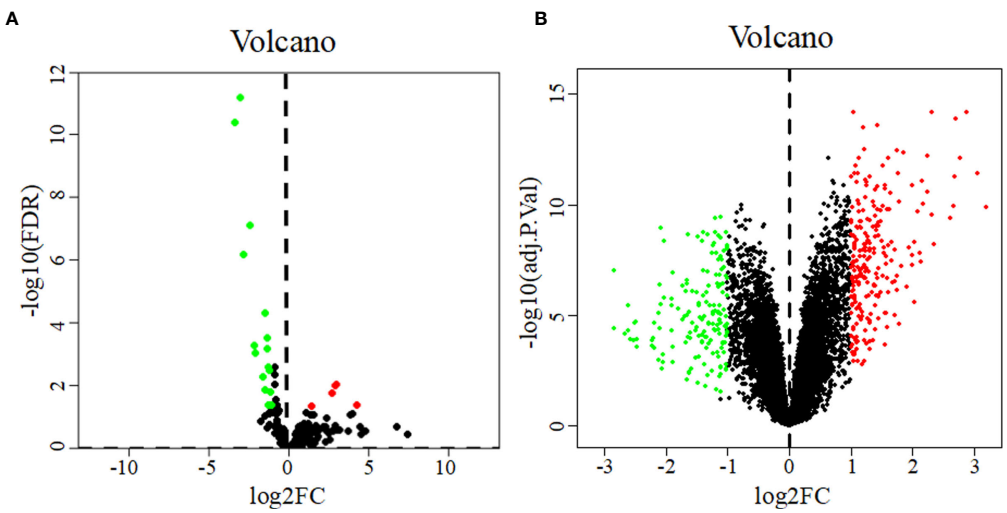

FIGURE 1 | Volcano diagrams of DEMs **(A)** and DEGs **(B)**. Volcano diagrams show the P value and the fold change of differentially expressed miRNAs and genes. Green and red circles represent downregulated and upregulated miRNAs or genes, respectively.

TABLE 1 | Univariate Cox proportional hazards regression analysis.

miRNA	LogFC	HR	z	*P*
hsa-mir-424	-1.47463701	1.731552246	3.781794216	0.000155702
hsa-mir-3613	-1.269297217	0.643105251	-2.819911816	0.004803685
hsa-mir-100	1.451158169	1.361225074	2.714421025	0.006639173
hsa-mir-139	-2.996528993	0.781057493	-2.595815983	0.009436659
hsa-mir-4772	-1.634160607	1.237295209	2.543043319	0.01098916
hsa-mir-126	-1.308472669	0.627370307	-2.527151064	0.011499203

Bold represents prognostic miRNAs.

TABLE 2 | Multivariate Cox proportional hazards regression analysis.

miRNA	Coef	Exp (Coef)	SE (Coef)	z	*P*
hsa-mir-424	0.6006	1.8232	0.1646	3.648	0.000264
hsa-mir-3613	-0.3851	0.6804	0.1733	-2.223	0.026234
hsa-mir-4772	0.1819	1.1995	0.1047	1.737	0.082428
hsa-mir-126	-0.6601	0.5168	0.2027	-3.257	0.001126

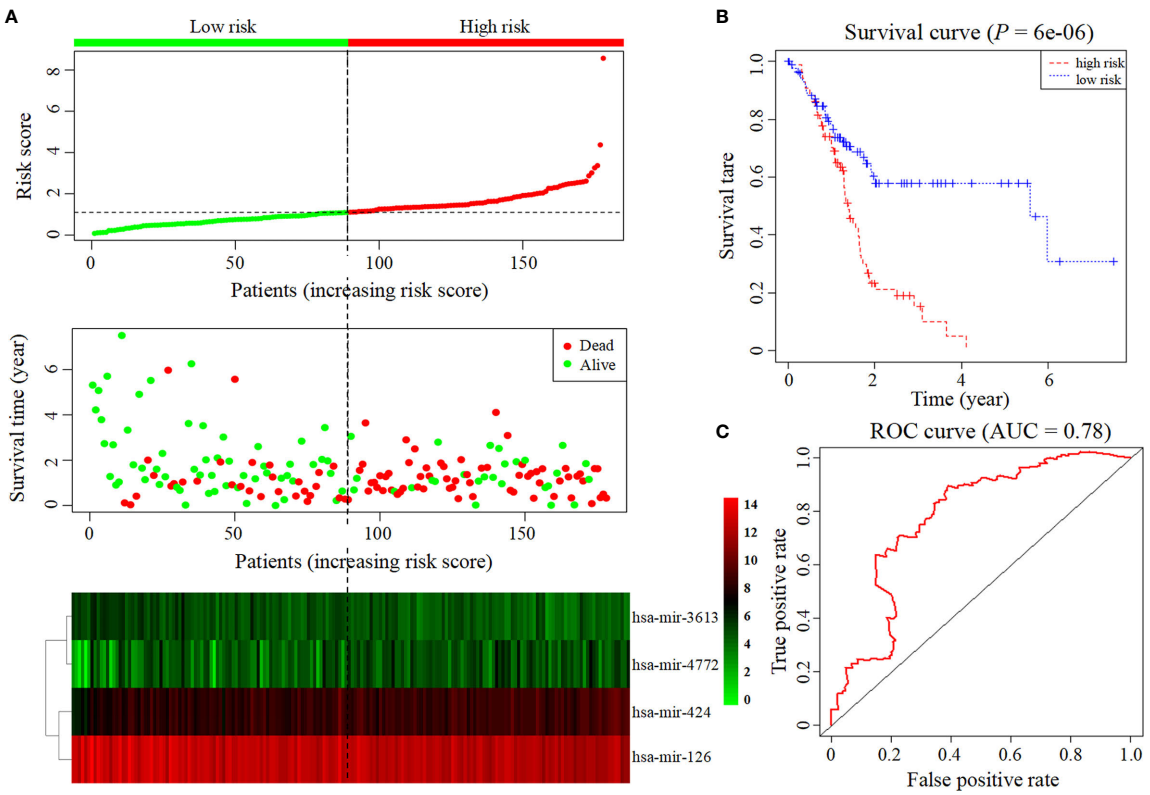

FIGURE 2 | Construction of prognostic model based on four prognostic miRNAs. **(A)** The risk score curve, survival status and heatmap are shown from top to bottom. **(B)** Survival curve. **(C)**. ROC curve of the prognostic model.

rate was notably higher (P = 6e-06; three-year survival rate, low-risk group: 57.90%, 95% CI = 46.60%-71.90%; high-risk group: 15.21%; 95% CI = 7.69%-30.1%) (**Figure 2B**). The AUC value of the ROC curve of the model was 0.78 (**Figure 2C**), which was greater than 0.7, indicating that the model was reliable.

Prediction of the Target Genes of the Prognostic miRNAs

The online tools TargetScan and miRDB were used to predict the target genes of the four prognostic miRNAs, and the intersecting genes predicted by both databases were considered candidate target genes. A total of 6521 target genes were obtained (1081 target genes of hsa-mir-424, 692 target genes of hsa-mir-4772, 1243 target genes of hsa-mir-126 and 3505 target genes of hsa-mir-3613). After excluding 1384 duplicate target genes that were jointly regulated by multiple miRNAs, the total number of target genes of the four miRNAs was 5137. Then, we took the intersection of the 5137 target genes and the DEGs, and 118 common genes were identified (**Table 3**).

Functional Enrichment Analysis of Common Genes

The DAVID database was applied for the KEGG pathway and GO functional annotation analyses of 118 common genes. Common genes were enriched in two KEGG pathways and 33 GO terms ($P < 0.05$) (**Figure 3**). The pathway with the smallest *P* value was ECM-receptor interaction (P = 1.04E-07), and the pathway with the largest count was focal adhesion (count = 10). In the BP category of GO, the common genes were mainly enriched in functional annotations such as cell adhesion,

TABLE 3 | Regulatory relationships between the prognostic miRNAs and common genes.

miRNA	Common gene				
mir-424	BTG2	PTPRR	EPB41L4B	PDCD4	KIF23
	KCNN4	SLC4A4	**COL12A1**	ESRRG	C2CD4B
	SLC7A2	AHNAK2	MTMR11	GLS2	ANLN
	PGM2L1	PDK4	TMC7	NRP2	BACE1
mir-3613	PTPRR	EPB41L4B	MET	LRRN1	**COL1A1**
	PDCD4	FNDC1	KIAA1324	EPHA4	LONRF2
	SDR16C5	OLR1	TRHDE	NR4A3	CD109
	LMO7	IAPP	**MMP14**	MCOLN3	MPP6
	GABRP	VCAN	ATRNL1	**COL11A1**	KCNJ16
	SLC4A4	AGR2	FOXQ1	DGKH	CCDC141
	SGIP1	ARNTL2	SV2B	UNC79	ITGB6
	SLC1A2	MATN3	GPRC5A	**COL3A1**	PRKAR2B
	INPP4B	NQO1	IFI44L	NR5A2	TNS4
	FLRT2	NRCAM	**COL6A3**	FBXO32	DPP10
	MTMR11	MBOAT2	SLC16A10	RTKN2	IGF2BP3
	PCDH7	SLC6A6	EDNRA	PROX1	**COL5A2**
	PDK4	IGFBP5	EFNA5	ADAM28	TMEM97
	SCG3	FAM129A	SCGN	NPR3	DCDC2
	ABHD17C	TMEM45B	ASPM	LIFR	**THBS2**
	PAIP2B	PLAC8	MMP9		
mir-4772	**ITGA2**	NR4A3	LMO7	SLC30A8	MMP6
	COL12A1	FOXQ1	SV2B	PAK3	F8
	PRKAR2B	FGD6	MBOAT2	RTKN2	ASAP2
	NPR3	FREM1			
mir-126	EPB41L4B	MLPH	TGFBI	DKK1	GJB2
	SCEL	REG3G	DCDC2	FAM129A	ETV1
	ANGPTL1	PKHD1	PGM2L1	PCDH7	TFPI2
	FABP4	FLRT2	ADAM9	ITGB6	SGIP1
	ESRRG	DGKH	BAIAP2L1	ESM1	ST6GALN
	COL12A1	KCNJ16	**COL11A1**	ADHFE1	AC1
	HOXB5	LONRF2	ACADL		

Bold represents key genes.

biological adhesion, skeleton system development, response to organic substance and sensory perception of mechanical stimulus. The annotation with the smallest *P* value in the BP category was cell adhesion (*P* = 3.72E-06), and the annotations with the largest count were cell adhesion (count = 19) and biological adhesion (count = 19). In the CC category, the common genes were mainly enriched in functional annotations such as proteinaceous extracellular matrix, extracellular matrix, extracellular region, intrinsic to plasma membrane and plasma membrane. The annotation with the smallest *P* value in the CC category was proteinaceous extracellular matrix (*P* = 2.30E-07), and the annotation with the largest count was plasma membrane (count = 42). In the MF category, the common genes were enriched in functional annotations such as extracellular matrix structural constituent, integrin binding and growth factor binding. The annotation with the smallest *P* value and the largest count in the MF category was extracellular matrix structural constituent (*P* = 2.65E-05, count = 7).

PPI Network Construction and Key Gene Acquisition

The STRING database was applied to construct an interaction network of the 118 common genes (**Figure 4A**). The network contained 60 nodes and 107 edges. Using the MCC algorithm of the cytoHubba plug-in, the top 15 genes were identified (**Figure 4B**). The MCODE plug-in revealed one important functional module in the interaction network (MCODE score = 7.500, **Figure 4C**) that included nine key genes: MMP14, ITGA2, THBS2, COL1A1, COL3A1, COL11A1, COL6A3, COL12A1 and COL5A2. All nine key genes were upregulated in PDAC.

Visualization of the miRNA-Gene-Pathway and Annotation Networks

The miRNA-gene-pathway and annotation networks demonstrated the regulatory relationships between the miRNAs and key genes, as well as the enriched pathways and annotations of the key genes (**Figure 5**). Among them, hsa-mir-424 regulated COL12A1; hsa-mir-3613 regulated COL11A1, COL6A3, COL5A2, COL3A1, COL1A1, MMP14 and TSBH2; hsa-mir-4772 regulated COL12A1 and ITGA2; hsa-miR-126 regulated COL12A1 and COL11A1. KEGG pathway analysis indicated that COL6A3, COL3A1, ITGA2, COL1A1, COL5A2, THBS2, and COL11A1 were involved in the ECM-receptor interaction pathway; and COL6A3, COL3A1, ITGA2, COL1A1, COL5A2, THBS2, and COL11A1 were involved in the focal adhesion pathway. Regarding the GO annotation, COL3A1, ITGA2, COL6A3, COL12A1, THBS2, and COL11A1 were enriched in the biological adhesion and cell adhesion (GO-BP); COL3A1, COL12A1, COL1A1, COL5A2, and

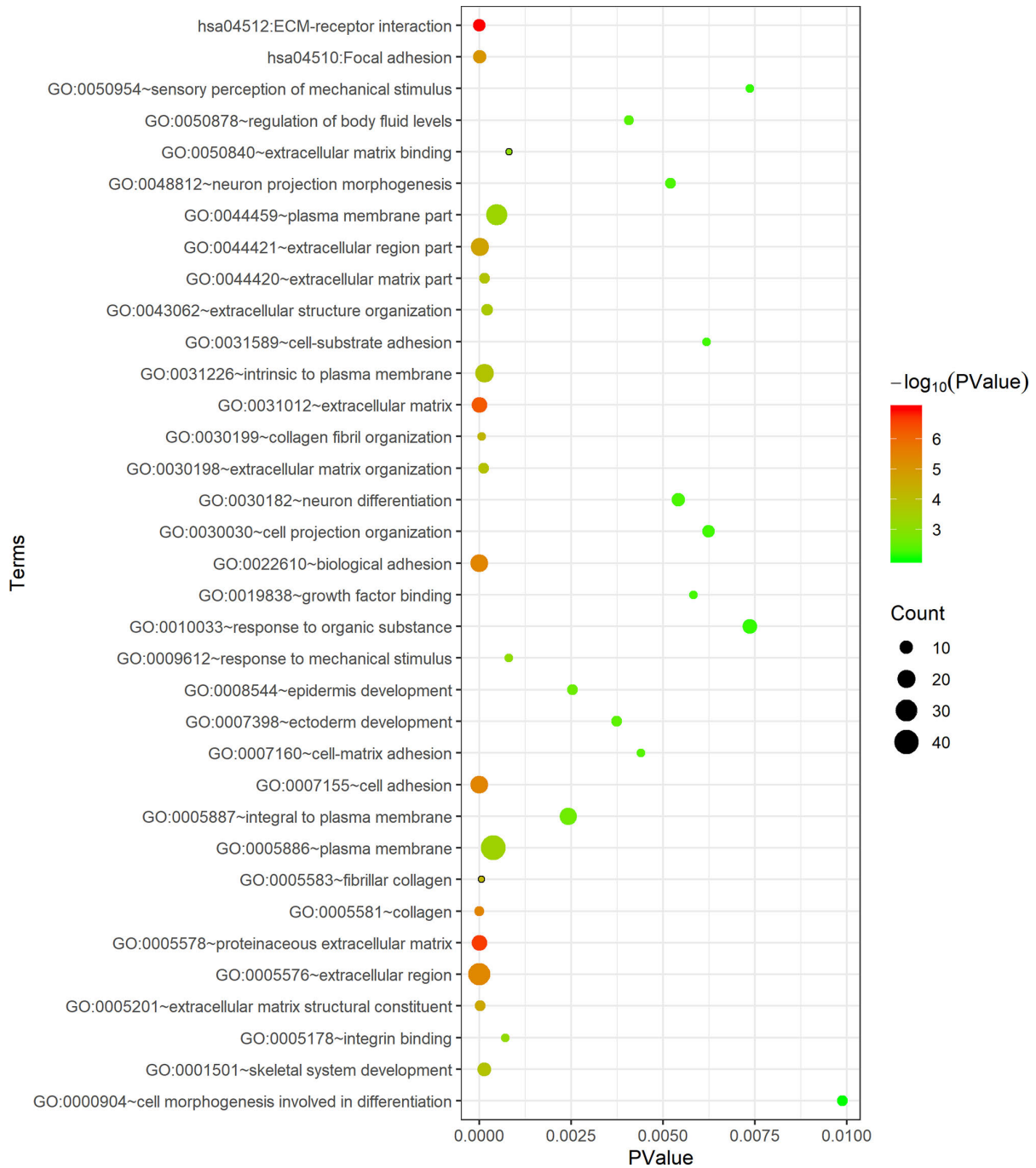

FIGURE 3 | Functional enrichment analysis of 118 common genes. The x-axis represents the *P* value, and the y-axis represents the pathways and annotations. The bubble size increases with the number of enriched genes.

COL11A1 were enriched in the extracellular matrix structural constituent (GO-MF); and COL6A3, MMP14, and COL1A1 were enriched on the plasma membrane (GO-CC); and COL3A1, MMP14, COL5A2, COL6A3, COL12A1, COL1A1, and COL11A1 were enriched on the proteinaceous extracellular matrix (GO-CC).

Establishment of Prognostic Model Based on the Key Genes

We further put the nine key genes into one prognostic model, and its prognostic risk score was calculated according to the following formula: Risk score = (-3.290e-01 × COL11A1) +

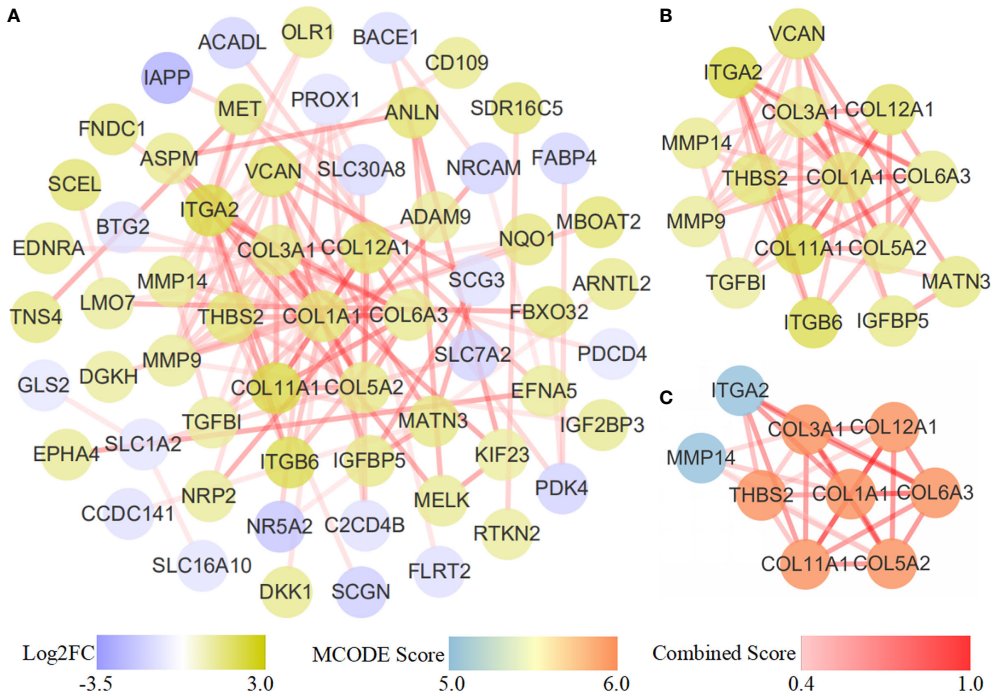

FIGURE 4 | PPI network diagram. **(A)** PPI network of 118 common genes. **(B)** Results of the cytoHubba topological analysis. Different node colors represent the logFC value of the DEGs. **(C)** MCODE network module diagram. The shade and shallowness of the red lines represent the combined score between proteins.

(-1.358e+00 × COL12A1) + (3.811e+00 × COL1A1) + (-1.293e+01 × COL3A1) + (3.860e+00 × COL5A2) + (1.044e+01 × COL6A3) + (-2.232e-01 × ITGA2) + (4.880e+00 × MMP14) + (-4.655e+00 × THBS2). Then, the samples were divided into a high-risk group and a low-risk group based on the medium risk score. The risk score curve, survival status map and heatmap were plotted (**Figure 6A**). High risk score correlated with a poor prognosis. Survival analysis showed that the mortality rate increased as the risk score increased. Compared with high-risk group, low-risk group survival rate was notably higher (P = 2.15e-05; three-year survival rate, low-risk group: 35.50%, 95% CI = 20.21%-62.30%; high-risk group: 9.52%; 95% CI = 2.75%-32.9%) (**Figure 6B**). The AUC value of the ROC curve of the model was 0.765 (**Figure 6C**), which also possessed strong prognostic ability, indicating that these nine key gene we screened out were quiet reliable.

DISCUSSION

PDAC is a fatal digestive tumor that is difficult to diagnose and treat and is associated with a very poor prognosis (22); therefore, it is very important to identify novel molecular biomarkers or therapeutic targets. MiRNAs collectively act on protein-coding genes and are the main regulators of vital biological processes, such as cell proliferation, apoptosis, virus infection and carcinogenesis. Therefore, miRNAs have also become the focus of research in the field of tumor development.

To identify new credible prognostic miRNAs and important regulatory genes of PDAC, we screened 22 DEMs and 402 DEGs related to PDAC from the TCGA and GEO databases. Using Cox proportional hazards regression analysis and survival analysis, we obtained four miRNAs that are closely related to PDAC (hsa-mir-424, hsa-mir-4772, hsa-mir-126 and hsa-mir-3613) and incorporated them into a four-miRNA prognostic model with an AUC value of the survival ROC curve of 0.78. Then, 5147 target genes of these miRNAs were obtained from TargetScan and miRDB prediction, and 118 genes in the intersection of the target genes and DEGs were defined as common genes. Finally, the common genes were analyzed with STRING and Cytoscape plug-ins, and nine key genes (MMP14, ITGA2, THBS2, COL1A1, COL3A1, COL11A1, COL6A3, COL12A1 and COL5A2) related to PDAC were further acquired. We also constructed a prognostic model formed by these nine key genes, and the AUC value of its survival ROC curve was 0.765, indicating that these nine key genes screened out were quite reliable.

All four prognostic miRNAs (hsa-mir-424, hsa-mir-3613, hsa-mir-4772 and hsa-mir-126) are downregulated in PDAC according to our analysis. Among them, hsa-mir-126, hsa-mir-3613 and hsa-mir-424 have been experimentally verified to be underexpressed in PDAC. However, the downregulation of hsa-mir-4772 in PDAC has yet to be experimentally confirmed.

Previous studies have already proven that downregulated mir-126 and mir-3613 are involved in the development of PDAC, which agrees with our prediction. Hamada et al. (23) illustrated that in pancreatic cancer tissues, miR-126 is notably downregulated, while

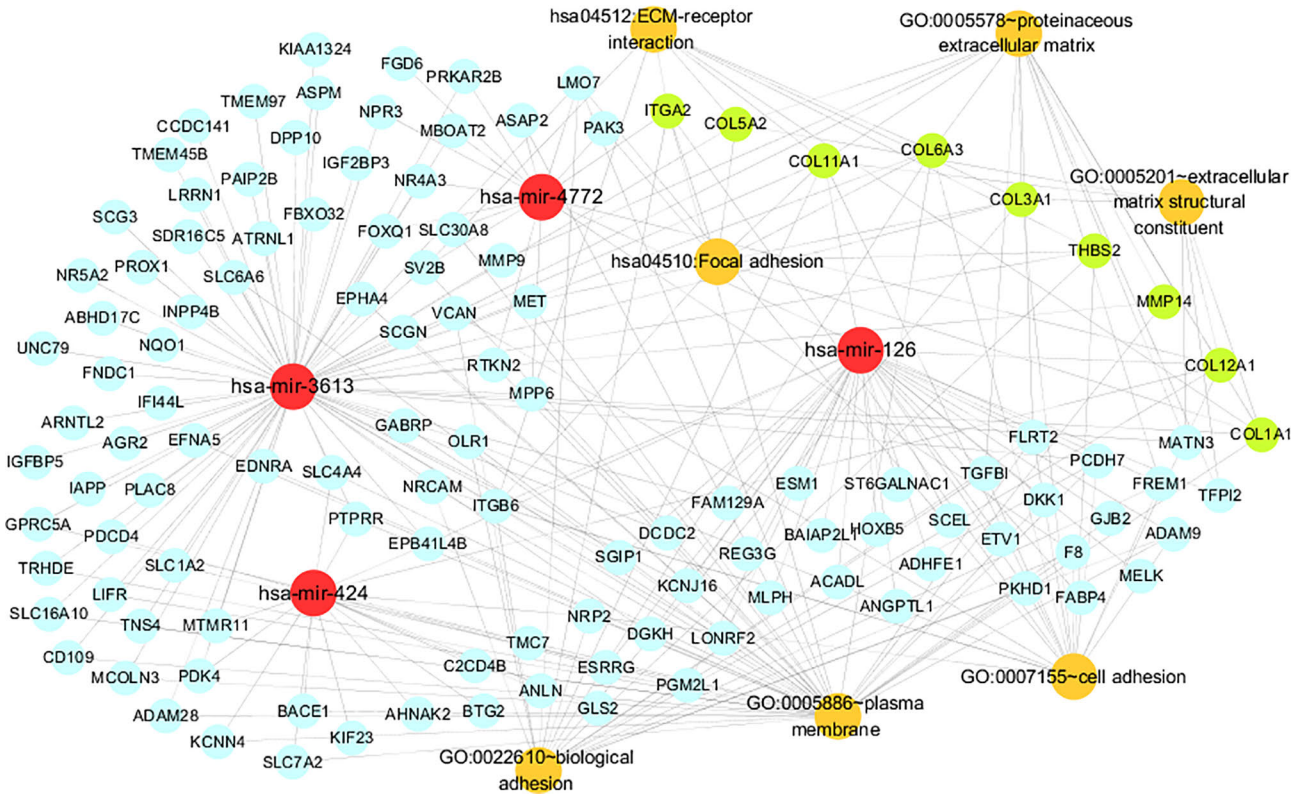

FIGURE 5 | The miRNA-gene pathway and annotation networks represent the relationships among miRNAs, common genes, key genes and gene enrichment results. MiRNAs, common genes, key genes and enrichment terms are represented by red, blue, green and orange circles, respectively.

ADAM9 (a disintegrin and metalloprotease 9), the target gene of miR-126, is significantly upregulated. miR-126 upregulation induces ADAM9 suppression to further repress the metastasis and invasion ability of PDAC cells (23). Jiao et al. (24) also demonstrated inhibited miR-126 expression in PDAC tissue, and by increasing miR-126 expression, its target gene KRAS was repressed, thereby inhibiting the occurrence and development of PDAC. Jiang et al. (25) showed that low miR-3613 expression leads to a poor prognosis in PDAC patients, and their functional experiments demonstrated that miR-3613-5p inhibits proliferation and enhances the apoptosis of PDAC cells, indicating that hsa-miR-3613 acts as a tumor suppressor gene (25). All these results prove that the low expression of hsa-mir-126 and hsa-miR-3613 in pancreatic cancer tissue is related to the carcinogenesis of pancreatic cancer, but the specific mechanisms involved need to be further studied.

It has also been reported that mir-424 is abnormally expressed in PDAC; the results indicate that miR-424 suppresses PDAC development, which is inconsistent with our prediction. Wu et al. (26) found that miR-424-5p is upregulated in PDAC tissue compared to that in normal pancreatic tissue. Overexpressed miR-424-5p suppresses its target gene SOCS6 (suppressor of cytokine signaling 6), which further inhibits the expression of BCL-2 and MCL-1 in the ERK1/2 pathway, while downregulating overexpressed miR-424-5p inhibits the proliferation, migration and invasion of PDAC cells and promotes their apoptosis (26). These findings were inconsistent with our predictions in PDAC; however, it has been reported that miR-424 is downregulated in other cancers, in agreement with our calculations. For example, Fang et al. (27) showed that miR-424 is downregulated in colorectal cancer cells and patient biopsy tissues and that the upregulation of miR-424 can lead to proliferation inhibition and apoptosis induction in colorectal cancer cells. Wang et al. (28) showed that miR-424-5p expression is repressed in both tissues and cell lines of basal breast cancer and that low miR-424-5p expression is significantly associated with an advanced malignant status; however, the upregulation of miR-424-5p inhibits the proliferation and motility of basal breast cancer cells. Piao et al. (29) illustrated that miR-424-5p levels were significantly lower in liver cancer tissues than in normal liver tissues, while an increase in miR-424-5p levels can inhibit the expression of its target gene YAP1, leading to proliferation inhibition and apoptosis induction. Dong et al. (30) demonstrated that miR-424 is downregulated in endometrial cancer tissues compared to normal tissues and that the overexpression of miR-424 inhibits invasion and sphere formation in endometrial cancer cells. The above research shows that hsa-mir-424 can act as a tumor suppressor. The disagreement concerning the role of hsa-mir-424 in PDAC and other cancers in the literature

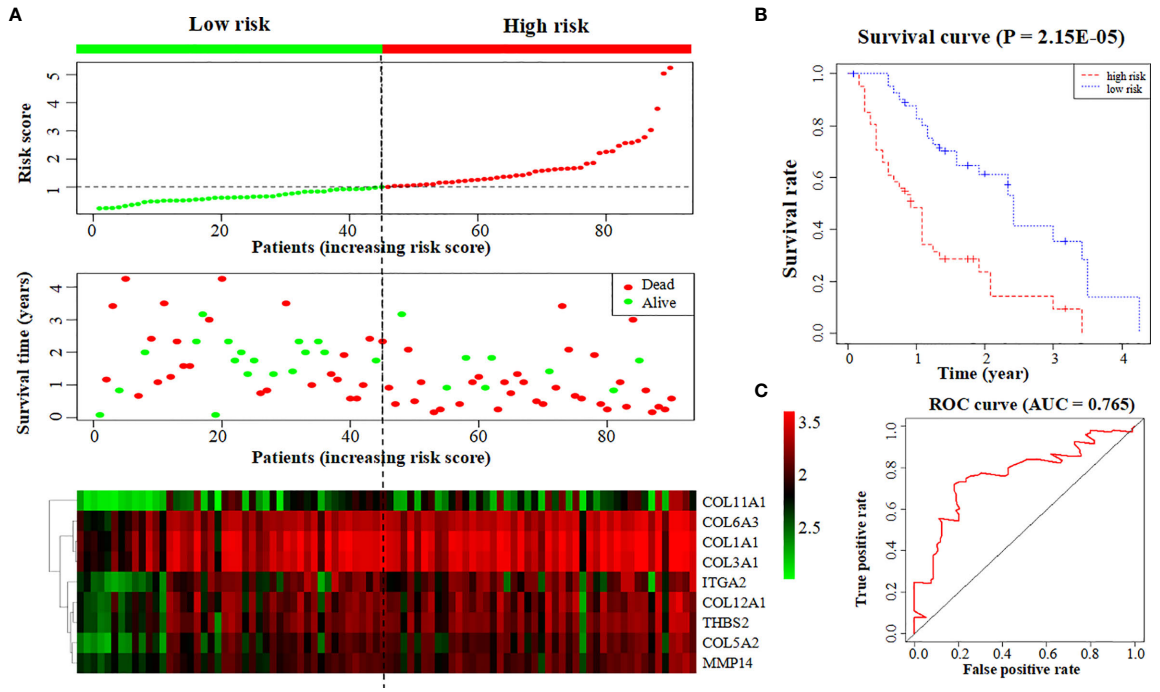

FIGURE 6 | Construction of a prognostic model based on nine key genes. **(A)** The risk score curve, survival status and heatmap are shown from top to bottom. **(B)** Survival curve. **(C)** ROC curve of the prognostic model.

aroused our interest. Thus, we carried out an experiment in which real-time quantitative PCR was applied to detect the expression level of mir-424 in the pancreatic cancer cell lines SW1990 and PANC-1 and the normal pancreatic epithelial cell line HPDE6C7. The experiments showed that hsa-mir-424 expression was significantly lower in PDAC cells than in normal cells (P<0.001), confirming our calculation (i.e., that hsa-mir-424 was indeed downregulated in PDAC cells; supplementary file, **Figure S1**). We cannot explain the difference between the results obtained by Wu et al. (26) and those obtained by us, but the expression of hsa-mir-424 in pancreatic cancer and its specific mechanism in the occurrence and development of pancreatic cancer are worthy of further investigation.

To date, no relevant experiment has proven that hsa-mir-4772 plays a role in PDAC; nevertheless, one bioinformatics study proposed that mir-4772 affects PDAC carcinogenesis, concordant with our results. Gupta et al. (31) illustrated the downregulation of miR-4772 in pancreatic cancer tissue through differential analysis and survival analysis of samples from the TCGA database and concluded that miR-4772 can be used as a prognostic marker to detect early pancreatic cancer. Thus, mir-4772 may suppress PDAC progression, bit its specific mechanism in PDAC is worthy of further exploration.

According to our prediction, the expression of nine key genes related to the prognosis of pancreatic cancer (MMP14, ITGA2, THBS2, COL1A1, COL3A1, COL11A1, COL6A3, COL12A1 and COL5A2) was upregulated. Among these proteins, the overexpression of MMP14, ITGA2, THBS2, COL1A1, COL3A1, COL11A1 and COL6A3 has been experimentally confirmed in PDAC, while that of COL12A1 and COL5A2 has been shown in other types of cancer. **Table 4** shows the expression of these nine key genes that have experimentally verified in PDAC and other cancers and whether they are consistent with our prediction results in PDAC.

MMP14 (matrix metalloproteinase 14), also known as MT1-MMP, was the first member of the MMP family identified as a transmembrane protein (32). MMP14 is a collagenase that causes ECM degradation and leads to metastasis (32). Haage et al. (33) found that in pancreatic cancer, MMP14 promotes local ECM degradation and mediates cancer cell migration and invasion by activating MMP-2/9, while the inhibition of MMP14 suppresses cell migration (33). Dangi-Garimella et al. (34) demonstrated that the overexpression of MMP14 upregulates HMGA2, which increases the resistance of PDAC cells to the anticancer drug gemcitabine,

TABLE 4 | Features of key genes in previous studies.

Gene	MMP14	ITGA2	THBS2	COL1A1	COL3A1
Feature	▲	▲	▲	▲	▲
Gene	COL11A1	COL6A3	COL12A1	COL5A2	
Feature	▲	▲	△	△	

▲ *These genes were experimentally determined to be upregulated in PDAC, and their expression was consistent with our prediction in PDAC.* △ *These genes were experimentally determined to be upregulated in other cancers, and their expression was consistent with our prediction in PDAC.*

subsequently leading to a poor prognosis. ITGA2 (integrin subunit alpha 2) is an important member of the integrin family (35). This gene encodes the transmembrane receptor alpha subunit of collagen and related proteins (35). ITGA2 affects cell proliferation, invasion, metastasis and angiogenesis in cancer. Ren et al. (36) demonstrated that ITGA2 is significantly upregulated in PDAC cells and tissues, and silencing overexpressed ITGA2 represses the progression of PDAC. They also demonstrated that ITGA2 upregulates the phosphorylation of STAT3, indicating that ITGA2 enhances proliferation and invasion by activating the STAT3 pathway (36). Gong et al. (37) illustrated that ITGA2 expression is elevated in PDAC cells, while miR-107 downregulates the expression of ITGA2 and suppresses the migration process by acting on the focal adhesion pathway. THBS2 (thrombospondin 2) is a member of the thrombospondin family (38). It is a disulfide-linked homotrimeric glycoprotein that mediates the interaction between cells and between cells and substrates (38). THBS2 is an effective inhibitor of tumor growth and angiogenesis. Kim et al. (39) showed that the THBS2 antigen is overexpressed in both cancer tissues and plasma of PDAC patients and might be related to the poor vascularization of PDAC. Le Large et al. (40)also revealed that THBS2 was significantly increased in pancreatic cancer tissues compared with normal tissues. In addition, both Kim (39) and Le Large (40) showed that the combined expression of THBS2 and CA19/9 in plasma can be used as a biomarker for PDAC patients. The above studies have shown that the overexpression of MMP14, ITGA2 and THBS2 promotes pancreatic cancer occurrence and development and indicate that they possess the ability to become therapeutic targets of PDAC.

COL1A1, COL3A1, COL11A1, COL6A3, COL12A1 and COL5A2 belong to the collagen family. The entire family contains 19 types of collagen and more than ten types of collagen-like proteins and is encoded by more than 30 different genes (41). Due to differences in its molecular structure, collagen can be divided into two categories: fibrogenic collagen and nonfibrogenic collagen (41). Types I, II, III, V, and IX collagen are fibrogenic (41). The extracellular matrix (ECM) is composed primarily of collagen, which is a macromolecular substance that supports the cell structure and regulates the physiological activities of the cell (42). ECM degradation is one of the most important steps that leads to cancer cell invasion and metastasis (43). Stably expressed collagen is necessary to maintain the normal functions of cells and tissues. However, the abnormal overexpression of collagen is associated with a variety of pathological processes, especially in malignant tumors.

COL1A1 is a member of the type I collagen family and encodes the pro-α 1 chains of type I collagen (44). Yang et al. (45) found that the miRNA sponge hsa-circRNA-0007334 inhibits hsa-mir-577 expression, leading to the overexpression of the mir-577 target gene COL1A1 and subsequently causing PDAC cell migration. They also demonstrated that high COL1A1 shortens the survival time of PDAC patients (45). COL3A1 is a type III collagenase whose lack causes perforation, tearing, fracture and even fragmentation of connective tissue-related structures in the body (46). Hall et al. (47) revealed that the overexpression of COL3A1 in patients with pancreatic cancer can be significantly downregulated after gemcitabine combined with EC359 treatment. COL11A1 is a specific type XI collagen cleavage fragment. This gene encodes one of the two α chains of type XI collagen (48). It comprises a major part of the ECM and affects the occurrence and development of a variety of cancers (49, 50). Kleinert et al. (51) reported that COL11A1 was significantly increased (by 5.52 times) in subjects with pancreatic cancer relative to those with normal chronic pancreatitis. Overexpression of the COL11A1 protein may be related to connective tissue proliferation events and can shorten the survival time of PDAC patients (51). García-Pravia et al. (52) also demonstrated that the COL11A1 gene was significantly overexpressed in subjects with pancreatic cancer relative to those with chronic pancreatitis, and they further revealed that the detection of proCOL11A1 by immunostaining can accurately distinguish PDAC from chronic pancreatitis. COL6A3, as a type VI collagen α chain, can interact with various components in the ECM (53). Its abnormal expression in various cancers suggests that COL6A3 affects cancer formation. Svoronos et al. (54) showed that in the PDAC stroma, COL6A3 is the major overexpressed gene, and overexpressed COL6A3 leads to a poor prognosis in PDAC. Arafat et al. (55) also showed that a high level of COL6A3 expression is found in the tissues of PDAC patients, especially those in later disease stages, and that patients in earlier stages present relatively low COL6A3 levels. The above experimental results indicate the oncogenic roles of COL1A1, COL3A1, COL11A1 and COL6A3 in PDAC formation and suggest that they may also possess potential as therapeutic targets of PDAC.

Although the upregulation of COL12A1 and COL5A2 has not been experimentally shown in pancreatic cancer, their abnormal overexpression has been experimentally shown in other cancer types. COL12A1 is encoded by a gene at chromosome position 6q12-q13 (56). COL12A1 connects fibers, and its mutation can cause muscle diseases (56). COL12A1 overexpression has been proven in several cancers, indicating its oncogenic role in human cancer. Jiang et al. (57) demonstrated that COL12A1 is upregulated in gastric cancer. The overexpression of COL12A1 is also associated with invasion, lymph node metastasis, distant metastasis and an advanced TNM stage of gastric cancer (57). Zhang et al. (58) first demonstrated COL12A1 overexpression in colorectal cancer cells using bioinformatics and then validated their results experimentally. The COL5A2 gene encodes a 46 kDa nuclear localization transcriptional inhibitor protein that has been reported to affect cancer progression (59). Fischer et al. (60) illustrated that in normal colon tissue, COL5A2 is not expressed, but in colon cancer tissues, COL5A2 is expressed. Chen et al. (61) showed that in osteosarcoma, COL5A2 expression can be repressed by the tumor suppressor gene NKX2-2. Thus, these two genes are upregulated in other cancers and have a great impact on the progression of those cancers, indicating that they may also affect the progression of PDAC in the same manner. However, the role and mechanism of COL12A1 and COL5A2 in PDAC deserve further study.

As shown in **Table 3**, there were 12 targeting relationships between the 4 prognostic miRNAs and 9 key genes. Specifically, COL12A1 is the target gene of hsa-mir-424; COL12A1 and COL11A1 are the target genes of hsa-mir-126; MMP14, TSBH2,

COL3A1, COL1A1, COL11A1, COL6A3 and COL5A2 are the target genes of hsa-miR-3613; and ITGA2 and COL12A1 are the target genes of hsa-mir-4772. To date, none of the abovementioned targeting relationships have been confirmed experimentally. Therefore, the targeting relationships between these miRNAs and their target genes need to be confirmed in future studies.

In the KEGG pathway analysis of the 9 key genes, the ECM-receptor interaction pathway was enriched, and there are reports that this pathway can affect cell proliferation and differentiation, adhesion and metastasis (62). MMP14 and COL family genes are involved in tumor ECM regulation, which is very important for the study of cancer lymph node metastasis (32, 63). Therefore, it can be boldly speculated that MMP14 and these key COL family genes affect metastasis by acting on the ECM-receptor interaction pathway in pancreatic cancer. Regarding the GO functional annotations, cell adhesion has a profound impact on tumor proliferation and metastasis. Cell adhesion and connection maintain the integrity of the endothelial barrier, and malignant cancer cells metastasize through the blood or lymphatic vessels as soon as endothelial cells are impaired (64). MMP14 and ITGA2 are involved in cell adhesion according to previous studies. Munaut et al. (65) revealed that overexpressed MMP14 promotes the migration and invasion of glioblastoma cells by activating MMP-2 and upregulating VEGF. Ren et al. (36) also noted that ITGA2 reduces the adhesion of malignant tumor cells by acting on the STAT3 signaling pathway. Therefore, by affecting cell adhesion, MMP14 and ITGA2 may cause lymph node metastasis in PDAC cells. In summary, ECM regulation and cell adhesion will become the key to studying the mechanism of PDAC.

We also conducted bioinformatics analysis of mature miRNAs related to pancreatic cancer in the TCGA database in the same manner described above (**Figure S2**, **Table S1**). Analysis of the mature miRNAs revealed three miRNAs that can be used to predict the prognosis of pancreatic cancer patients, namely, hsa-miR-126-3p, hsa-miR-424-5p, and hsa-miR-3613-5p (**Table S2**). The mature prognostic model basically correlates with the precursor prognostic model, which also includes hsa-miR-4772 as an independent prognostic factor, while the mature model can distinguish between the 3p and 5p arms of miRNAs. The AUC value of the ROC curve was 0.784, which indicated that the prognostic ability of the mature miRNA prognostic model was slightly better than that of the precursor model (AUC = 0.78 (**Figure S3**). A mature miRNA contains 3p and 5p arms, limiting the prediction of the target genes of mature miRNAs and reducing the number of target genes. Therefore, by intersecting the mature miRNA target genes and DEGs of the GSE28735 dataset, only 28 common genes were obtained (**Table S3**). STRING analysis of the common genes showed that they are not very closely related, so a PPI network was not formed; therefore, the key genes were not obtained. That is, in this scenario, the precursor miRNAs provide more information than mature miRNAs. However, although the use of precursor miRNAs to construct a prognostic model may not be as reasonable as the use of mature miRNAs, our research shows that, consistent with previous experimental studies, prognostic models of precursor miRNAs and key genes are also reliable and accurate.

CONCLUSIONS

In this study, by conducting a bioinformatics analysis on the miRNA and gene profiles of pancreatic cancer, we obtained a reliable four-miRNA (hsa-mir-424, hsa-mir-126, hsa-mir-3613 and hsa-mir-4772) prognostic model of PDAC. Further, nine key genes were identified: MMP14, ITGA2, THBS2, COL1A1, COL3A1, COL11A1, COL6A3, COL12A1 and COL5A2, which could also form an accurate prognostic model of PDAC. Among them, hsa-mir-4772, COL12A1 and COL5A2 were identified as novel PDAC biomarkers in PDAC that need to be experimentally proven. In addition, contrary to a previous study, mir-424 was confirmed to be downregulated in pancreatic cancer cells by qRT-PCR, agreeing with our prediction. These prognostic miRNAs and genes possess great potential as targets and biomarkers for PDAC treatment and prognosis. Our research can offer novel ideas for future diagnosis and treatment and may facilitate the development of new drugs.

DATA AVAILABILITY STATEMENT

The original contributions presented in the study are included in the article/**Supplementary Material**. Further inquiries can be directed to the corresponding authors.

AUTHOR CONTRIBUTIONS

ZH, GX, SC, and TY contributed to the design and conception of the study. SC, CG, TY, and YQ did information retrieval and analysis. SC, CG, and TY wrote the manuscript. SC, CG, TY, and YQ created tables and figures. ZH and GX guided manuscript writing and revision and provided financial support. All authors contributed to the article and approved the submitted version.

FUNDING

This work was supported by the National Natural Science Foundation of China [31770774], the Provincial Major Project of Basic or Applied Research in Natural Science, Guangdong Provincial Education Department [2016KZDXM038], and the Higher Education Reform Project of Guangdong Province [2019268].

ACKNOWLEDGMENTS

We thank American Journal Experts for their help in revising the English grammar.

SUPPLEMENTARY MATERIAL

The Supplementary Material for this article can be found online at: https://www.frontiersin.org/articles/10.3389/fonc.2021.641289/full#supplementary-material

REFERENCES

1. Siegel R, Naishadham D, Jemal A. Cancer Statistics, 2012. *CA Cancer J Clin* (2012) 62(1):10–29. doi: 10.3322/caac.20138
2. Rahib L, Smith BD, Aizenberg R, Rosenzweig AB, Fleshman JM, Matrisian LM. Projecting Cancer Incidence and Deaths to 2030: The Unexpected Burden of Thyroid, Liver, and Pancreas Cancers in the United States. *Cancer Res* (2014) 74(11):2913–21. doi: 10.1158/0008-5472.CAN-14-0155
3. Li HY, Cui ZM, Chen J, Guo XZ, Li YY. Pancreatic Cancer: Diagnosis and Treatments. *Tumour Biol* (2015) 36(3):1375–84. doi: 10.1007/s13277-015-3223-7
4. Gluth A, Werner J, Hartwig W. Surgical Resection Strategies for Locally Advanced Pancreatic Cancer. *Langenbecks Arch Surg* (2015) 400(7):757–65. doi: 10.1007/s00423-015-1318-7
5. Zheng L, Wolfgang CL. Which Patients With Resectable Pancreatic Cancer Truly Benefit From Oncological Resection: Is it Destiny or Biology? *Cancer Biol Ther* (2015) 16(3):360–2. doi: 10.1080/15384047.2014.1002699
6. Qadir MI, Faheem A. Mirna: A Diagnostic and Therapeutic Tool for Pancreatic Cancer. *Crit Rev Eukaryot Gene Expr* (2017) 27(3):197–204. doi: 10.1615/CritRevEukaryotGeneExpr.2017019494
7. Rupaimoole R, Slack FJ. MicroRNA Therapeutics: Towards a New Era for the Management of Cancer and Other Diseases. *Nat Rev Drug Discov* (2017) 16 (3):203–22. doi: 10.1038/nrd.2016.246
8. He D, Miao HL, Xu YM, Xiong LH, Wang Y, Xiang HX, et al. MiR-371-5p Facilitates Pancreatic Cancer Cell Proliferation and Decreases Patient Survival. *PLoS One* (2014) 9(11):e112930. doi: 10.1371/journal.pone.0112930
9. Deng JJ, He MX, Chen LZ, Chen C, Zheng JM, Cai ZL. The Loss of miR-26a-mediated Post-Transcriptional Regulation of Cyclin E2 in Pancreatic Cancer Cell Proliferation and Decreased Patient Survival. *PLoS One* (2013) 8(10): e76450. doi: 10.1371/journal.pone.0076450
10. Zhao G, Zhang JG, Liu Y, Qin Q, Wang B, Tian K, et al. miR-148b Functions as a Tumor Suppressor in Pancreatic Cancer by Targeting Ampkα1. *Mol Cancer Ther* (2013) 12(1):83–93. doi: 10.1158/1535-7163.MCT-12-0534-T
11. Tomczak K, Czerwińska P, Wiznerowicz M. The Cancer Genome Atlas (TCGA): An Immeasurable Source of Knowledge. *Contemp Oncol (Pozn)* (2015) 19(1A):A68–77. doi: 10.5114/wo.2014.47136
12. Barrett T, Edgar R. Gene Expression Omnibus: Microarray Data Storage, Submission, Retrieval, and Analysis. *Methods Enzymol* (2006) 411:352–69. doi: 10.1016/S0076-6879(06)11019-8
13. Dennis G, Sherman BT, Hosack DA, Yang J, Gao W, Lane HC, et al. David: Database for Annotation, Visualization, and Integrated Discovery. *Genome Biol* (2003) 4(5):P3. doi: 10.1186/gb-2003-4-9-r60
14. von Mering C, Huynen M, Jaeggi D, Schmidt S, Bork P, Snel B. STRING: A Database of Predicted Functional Associations Between Proteins. *Nucleic Acids Res* (2003) 31(1):258–61. doi: 10.1093/nar/gkg034
15. Jalal H, Pechlivanoglou P, Krijkamp E, Alarid-Escudero F, Enns E, Hunink MGM. An Overview of R in Health Decision Sciences. *Med Decis Making* (2017) 37(7):735–46. doi: 10.1177/0272989X16686559
16. Shannon P, Markiel A, Ozier O, Baliga NS, Wang JT, Ramage D, et al. Cytoscape: A Software Environment for Integrated Models of Biomolecular Interaction Networks. *Genome Res* (2003) 13(11):2498–504. doi: 10.1101/gr.1239303
17. Ye ZQ, Zou CL, Chen HB, Jiang MJ, Mei Z, Gu DN. MicroRNA-7 as a Potential Biomarker for Prognosis in Pancreatic Cancer. *Dis Markers* (2020) 2020:2782101. doi: 10.1155/2020/2782101
18. Borgmästars E, de Weerd HA, Lubovac-Pilav Z, Sund M. miRFA: An Automated Pipeline for microRNA Functional Analysis With Correlation Support From TCGA and TCPA Expression Data in Pancreatic Cancer. *BMC Bioinf* (2019) 20(1):393. doi: 10.1186/s12859-019-2974-3
19. Peterson SM, Thompson JA, Ufkin ML, Sathyanarayana P, Liaw L, Congdon CB. Common Features of microRNA Target Prediction Tools. *Front Genet* (2014) 5:23. doi: 10.3389/fgene.2014.00023
20. Rigden DJ, Fernández XM. The 27th Annual Nucleic Acids Research Database Issue and Molecular Biology Database Collection. *Nucleic Acids Res* (2020) 48 (D1):D1–8. doi: 10.1093/nar/gkz1161
21. Chin CH, Chen SH, Wu HH, Ho CW, Ko MT, Lin CY. cytoHubba: Identifying Hub Objects and Sub-Networks From Complex Interactome. *BMC Syst Biol* (2014) 8:S11. doi: 10.1186/1752-0509-8-S4-S11
22. Zhang LL, Sanagapalli S, Stoita A. Challenges in Diagnosis of Pancreatic Cancer. *World J Gastroenterol* (2018) 24(19):2047–60. doi: 10.3748/wjg.v24.i19.2047
23. Hamada S, Satoh K, Fujibuchi W, Hirota M, Kanno A, Unno J, et al. MiR-126 Acts as a Tumor Suppressor in Pancreatic Cancer Cells Via the Regulation of ADAM9. *Mol Cancer Res* (2012) 10(1):3–10. doi: 10.1158/1541-7786.MCR-11-0272
24. Jiao LR, Frampton AE, Jacob J, Pellegrino L, Krell J, Giamas G, et al. MicroRNAs Targeting Oncogenes are Down-Regulated in Pancreatic Malignant Transformation From Benign Tumors. *PLoS One* (2012) 7(2): e32068. doi: 10.1371/journal.pone.0032068
25. Jiang Q. The Expression and Role of miR-628-5p and miR-3613-5p in Pancreatic Ductal Adenocarcinoma/Risk Factors for Early-Onset Pancreatic Cancer Patients, and Survival Analysis. *Chin Acad Med Sci Peking Union Med Collage* (2017). (In Chinese).
26. Wu KM, Hu GH, He X, Zhou P, Li J, He B, et al. MicroRNA-424-5p Suppresses the Expression of SOCS6 in Pancreatic Cancer. *Pathol Oncol Res* (2013) 19(4):739–48. doi: 10.1007/s12253-013-9637-x
27. Fang YF, Liang X, Xu JF, Cai X. miR-424 Targets AKT3 and PSAT1 and has a Tumor-Suppressive Role in Human Colorectal Cancer. *Cancer Manag Res* (2018) 10:6537–47. doi: 10.2147/CMAR.S185789
28. Wang JL, Wang SB, Zhou JJ, Qian Q. miR-424-5p Regulates Cell Proliferation, Migration and Invasion by Targeting Doublecortin-Like Kinase 1 in Basal-Like Breast Cancer. *BioMed Pharmacother* (2018) 102:147–52. doi: 10.1016/j.biopha.2018.03.018
29. Piao LS, Wang F, Wang YY, Yang ZR, Li QW, Cui LF, et al. Mir-424-5p Regulates Hepatoma Cell Proliferation and Apoptosis. *Cancer Biother Radiopharm* (2019) 34(3):196–202. doi: 10.1089/cbr.2018.2625
30. Dong PX, Xiong Y, Yue JM, Hanley SJB, Watari H. miR-34a, miR-424 and miR-513 Inhibit MMSET Expression to Repress Endometrial Cancer Cell Invasion and Sphere Formation. *Oncotarget* (2018) 9(33):23253–63. doi: 10.18632/oncotarget.25298
31. Gupta MK, Sarojamma V, Reddy MR, Shaik JB, Vadde R. Computational Biology: Toward Early Detection of Pancreatic Cancer. *Crit Rev Oncog* (2019) 24(2):191–8. doi: 10.1615/CritRevOncog.2019031335
32. Gonzalez-Molina J, Gramolelli S, Liao ZH, Carlson JW, Ojala PM, Lehti K. MMP14 in Sarcoma: A Regulator of Tumor Microenvironment Communication in Connective Tissues. *Cells* (2019) 8(9):991. doi: 10.3390/cells8090991
33. Haage A, Nam DH, Ge X, Schneider IC. Matrix metalloproteinase-14 is a Mechanically Regulated Activator of Secreted MMPs and Invasion. *Biochem Biophys Res Commun* (2014) 450(1):213–8. doi: 10.1016/j.bbrc.2014.05.086
34. Dangi-Garimella S, Krantz SB, Barron MR, Shields MA, Heiferman MJ, Grippo PJ, et al. Three-Dimensional Collagen I Promotes Gemcitabine Resistance in Pancreatic Cancer Through MT1-MMP-mediated Expression of HMGA2. *Cancer Res* (2011) 71(3):1019–28. doi: 10.1158/0008-5472.CAN-10-1855
35. Adorno-Cruz V, Liu HP. Regulation and Functions of Integrin α2 in Cell Adhesion and Disease. *Genes Dis* (2019) 6(1):16–24. doi: 10.1016/j.gendis.2018.12.003
36. Ren DY, Zhao JY, Sun Y, Li D, Meng ZB, Wang B, et al. Overexpressed ITGA2 Promotes Malignant Tumor Aggression by Up-Regulating PD-L1 Expression Through the Activation of the STAT3 Signaling Pathway. *J Exp Clin Cancer Res* (2019) 38(1):485. doi: 10.1186/s13046-019-1496-1
37. Gong J, Lu XY, Xu J, Xiong W, Zhang H, Yu XJ. Coexpression of UCA1 and ITGA2 in Pancreatic Cancer Cells Target the Expression of miR-107 Through Focal Adhesion Pathway. *J Cell Physiol* (2019) 234(8):12884–96. doi: 10.1002/jcp.27953
38. Bornstein P, Kyriakides TR, Yang Z, Armstrong LC, Birk DE. Thrombospondin 2 Modulates Collagen Fibrillogenesis and Angiogenesis. *J Investig Dermatol Symp Proc* (2000) 5(1):61–6. doi: 10.1046/j.1087-0024.2000.00005.x
39. Kim J, Bamlet WR, Oberg AL, Chaffee KG, Donahue G, Cao XJ, et al. Detection of Early Pancreatic Ductal Adenocarcinoma With Thrombospondin-2 and CA19-9 Blood Markers. *Sci Transl Med* (2017) 9 (398):eaah5583. doi: 10.1126/scitranslmed.aah5583
40. Le Large TYS, Meijer LL, Paleckyte R, Boyd LNC, Kok B, Wurdinger T, et al. Combined Expression of Plasma Thrombospondin-2 and CA19-9 for Diagnosis of Pancreatic Cancer and Distal Cholangiocarcinoma: A Proteome Approach. *Oncologist* (2020) 25(4):e634–e43. doi: 10.1634/theoncologist.2019-0680

41. Prockop DJ, Kivirikko KI. Collagens: Molecular Biology, Diseases, and Potentials for Therapy. *Annu Rev Biochem* (1995) 64:403–34. doi: 10.1146/annurev.bi.64.070195.002155
42. Kehlet SN, Willumsen N, Armbrecht G, Dietzel R, Brix S, Henriksen K, et al. Age-Related Collagen Turnover of the Interstitial Matrix and Basement Membrane: Implications of Age- and Sex-Dependent Remodeling of the Extracellular Matrix. *PLoS One* (2018) 13(3):e0194458. doi: 10.1371/journal.pone.0194458
43. Najafi M, Farhood B, Mortezaee K. Extracellular Matrix (ECM) Stiffness and Degradation as Cancer Drivers. *J Cell Biochem* (2019) 120(3):2782–90. doi: 10.1002/jcb.27681
44. Maasalu K, Nikopensius T, Kõks S, Nõukas M, Kals M, Prans E, et al. Whole-Exome Sequencing Identifies De Novo Mutation in the COL1A1 Gene to Underlie the Severe Osteogenesis Imperfecta. *Hum Genomics* (2015) 9:6. doi: 10.1186/s40246-015-0028-0
45. Yang JH, Cong XL, Ren M, Sun HY, Liu T, Chen GY, et al. Circular RNA Hsa_circRNA_0007334 is Predicted to Promote MMP7 and COL1A1 Expression by Functioning as a Mirna Sponge in Pancreatic Ductal Adenocarcinoma. *J Oncol* (2019) 2019:7630894. doi: 10.1155/2019/7630894
46. Cortini F, Marinelli B, Romi S, Seresini A, Pesatori AC, Seia M, et al. A New Col3a1 Mutation in Ehlers-Danlos Syndrome Vascular Type With Different Phenotypes in the Same Family. *Vasc Endovasc Surg* (2017) 51(3):141–5. doi: 10.1177/1538574417692114
47. Hall BR, Cannon A, Thompson C, Santhamma B, Chavez-Riveros A, Bhatia R, et al. Utilizing Cell Line-Derived Organoids to Evaluate the Efficacy of a Novel LIFR-inhibitor, EC359 in Targeting Pancreatic Tumor Stroma. *Genes Cancer* (2019) 10(1-2):1–10. doi: 10.18632/genesandcancer.184
48. Booth KT, Askew JW, Talebizadeh Z, Huygen PLM, Eudy J, Kenyon J, et al. Splice-Altering Variant in COL11A1 as a Cause of Nonsyndromic Hearing Loss DFNA37. *Genet Med* (2019) 21(4):948–54. doi: 10.1038/s41436-018-0285-0
49. Prockop DJ, Kivirikko KI, Tuderman L, Guzman NA. The Biosynthesis of Collagen and its Disorders (First of Two Parts). *N Engl J Med* (1979) 301 (1):13–23. doi: 10.1056/NEJM197907053010104
50. Nimni M, Harkness R. Molecular Structures and Functions of Collagen. *Collagen* (1988) 1:1–77. doi: 10.1201/9781351070799
51. Kleinert R, Prenzel K, Stoecklein N, Alakus H, Bollschweiler E, Hölscher A, et al. Gene Expression of Col11A1 is a Marker Not Only for Pancreas Carcinoma But Also for Adenocarcinoma of the Papilla of Vater, Discriminating Between Carcinoma and Chronic Pancreatitis. *Anticancer Res* (2015) 35(11):6153–8.
52. García-Pravia C, Galván JA, Gutiérrez-Corral N, Solar-García L, García-Pérez E, García-Ocaña M, et al. Overexpression of COL11A1 by Cancer-Associated Fibroblasts: Clinical Relevance of a Stromal Marker in Pancreatic Cancer. *PLoS One* (2013) 8(10):e78327. doi: 10.1371/journal.pone.0078327
53. Yonekawa T, Nishino I. Ullrich Congenital Muscular Dystrophy: Clinicopathological Features, Natural History and Pathomechanism(s). *J Neurol Neurosurg Psychiatry* (2015) 86(3):280–7. doi: 10.1136/jnnp-2013-307052
54. Svoronos C, Tsoulfas G, Souvatzi M, Chatzitheoklitos E. Prognostic Value of COL6A3 in Pancreatic Adenocarcinoma. *Ann Hepatobil Pancreat Surg* (2020) 24(1):52–6. doi: 10.14701/ahbps.2020.24.1.52
55. Arafat H, Lazar M, Salem K, Chipitsyna G, Gong Q, Pan T-C, et al. Tumor-Specific Expression and Alternative Splicing of the COL6A3 Gene in Pancreatic Cancer. *Surgery* (2011) 150(2):306–15. doi: 10.1016/j.surg.2011.05.011
56. Gerecke DR, Olson PF, Koch M, Knoll JH, Taylor R, Hudson DL, et al. Complete Primary Structure of Two Splice Variants of Collagen XII, and Assignment of Alpha 1(XII) Collagen (COL12A1), Alpha 1(IX) Collagen (COL9A1), and Alpha 1(XIX) Collagen (COL19A1) to Human Chromosome 6q12-Q13. *Genomics* (1997) 41(2):236–42. doi: 10.1006/geno.1997.4638
57. Jiang XX, Wu MJ, Xu X, Zhang L, Huang YY, Xu ZZ, et al. COL12A1, a Novel Potential Prognostic Factor and Therapeutic Target in Gastric Cancer. *Mol Med Rep* (2019) 20(4):3103–12. doi: 10.3892/mmr.2019.10548
58. Zhang ST, Jin JJ, Tian XX, Wu LJ. hsa-miR-29c-3p Regulates Biological Function of Colorectal Cancer by Targeting SPARC. *Oncotarget* (2017) 8 (61):104508–24. doi: 10.18632/oncotarget.22356
59. Watanabe M, Nakagawa R, Naruto T, Kohmoto T, Suga K-I, Goji A, et al. A Novel Missense Mutation of COL5A2 in a Patient With Ehlers-Danlos Syndrome. *Hum Genome Var* (2016) 3:16030. doi: 10.1038/hgv.2016.30
60. Fischer H, Stenling R, Rubio C, Lindblom A. Colorectal Carcinogenesis is Associated With Stromal Expression of COL11A1 and COL5A2. *Carcinogenesis* (2001) 22(6):875–8. doi: 10.1093/carcin/22.6.875
61. Chen HM, Liu WQ, Zhong L, Liao D, Zhang RH, Kang TB, et al. Nkx2-2 Suppresses Osteosarcoma Metastasis and Proliferation by Downregulating Multiple Target Genes. *J Cancer* (2018) 9(17):3067–77. doi: 10.7150/jca.26382
62. Bao YL, Wang L, Shi L, Yun F, Liu X, Chen YX, et al. Transcriptome Profiling Revealed Multiple Genes and ECM-receptor Interaction Pathways That may be Associated With Breast Cancer. *Cell Mol Biol Lett* (2019) 24:38. doi: 10.1186/s11658-019-0162-0
63. Cortes-Reynosa P, Robledo T, Macias-Silva M, Wu SV, Salazar EP. Src Kinase Regulates Metalloproteinase-9 Secretion Induced by Type IV Collagen in MCF-7 Human Breast Cancer Cells. *Matrix Biol* (2008) 27(3):220–31. doi: 10.1016/j.matbio.2007.11.003
64. Mierke CT. Role of the Endothelium During Tumor Cell Metastasis: Is the Endothelium a Barrier or a Promoter for Cell Invasion and Metastasis? *J Biophys* (2008) 2008:183516. doi: 10.1155/2008/183516
65. Munaut C, Noël A, Hougrand O, Foidart J-M, Boniver J, Deprez M. Vascular Endothelial Growth Factor Expression Correlates With Matrix Metalloproteinases MT1-MMP, MMP-2 and MMP-9 in Human Glioblastomas. *Int J Cancer* (2003) 106(6):848–55. doi: 10.1002/ijc.11313

Conflict of Interest: The authors declare that the research was conducted in the absence of any commercial or financial relationships that could be construed as a potential conflict of interest.

frontiers in Oncology

REVIEW
published: 23 June 2021
doi: 10.3389/fonc.2021.682872

Molecular and Phenotypic Profiling for Precision Medicine in Pancreatic Cancer: Current Advances and Future Perspectives

Koji Miyabayashi, Hayato Nakagawa and Kazuhiko Koike*

Department of Gastroenterology, Graduate School of Medicine, The University of Tokyo, Tokyo, Japan

Pancreatic cancer is the most common lethal malignancy, with little improvement in patient outcomes over the decades. The development of early detection methods and effective therapeutic strategies are needed to improve the prognosis of patients with this disease. Recent advances in cancer genomics have revealed the genetic landscape of pancreatic cancer, and clinical trials are currently being conducted to match the treatment to underlying mutations. Liquid biopsy-based diagnosis is a promising method to start personalized treatment. In addition to genome-based medicine, personalized models have been studied as a tool to test candidate drugs to select the most efficacious treatment. The innovative three-dimensional organoid culture platform, as well as patient-derived xenografts can be used to conduct genomic and functional studies to enable personalized treatment approaches. Combining genome-based medicine with drug screening based on personalized models may fulfill the promise of precision medicine for pancreatic cancer.

Keywords: precision medicine, patient derived organoid, patient derived xenograft, liquid biopsy, molecular subtypes

OPEN ACCESS

Edited by:
Kanjoormana Aryan Manu, Amala Cancer Research Centre, India

Reviewed by:
Matthew Brendan O'Rourke, University of Technology Sydney, Australia
Aranzazu Fariña Sarasqueta, Amsterdam University Medical Center, Netherlands

****Correspondence:***
Hayato Nakagawa
hanakagawa-tky@umin.ac.jp

Specialty section:
This article was submitted to Gastrointestinal Cancers, a section of the journal Frontiers in Oncology

Received: *19 March 2021*
Accepted: *04 June 2021*
Published: *23 June 2021*

Citation:
Miyabayashi K, Nakagawa H and Koike K (2021) Molecular and Phenotypic Profiling for Precision Medicine in Pancreatic Cancer: Current Advances and Future Perspectives. Front. Oncol. 11:682872. doi: 10.3389/fonc.2021.682872

INTRODUCTION

Pancreatic ductal adenocarcinoma (PDAC) is one of the most lethal malignancies, with an average 5-year survival rate of less than 10% (1). More than half of patients are diagnosed with metastatic disease, which is associated with a 5-year survival rate of only 3% (1). Early detection methods and effective therapies need to be developed to improve the prognosis of PDAC (2). The recent revolutionary improvement in genetic analysis technology offers the promise of using genetic information for personalized medicine. In pancreatic cancer, a number of studies have described a genetic background characterized by a set of commonly mutated genes in core molecular pathways and significant intratumoral heterogeneity. Resistance to chemotherapeutic agents has also been attributed to difficulties in drug delivery through a rich stromal microenvironment, as well as the nature of the cancer itself. For these reasons, the development of therapeutics for pancreatic cancer has been challenging, and many promising drugs have failed in clinical trials.

Clinical trials are currently underway to tailor treatment to underlying mutations (3–5). Basically, three groups of pancreatic cancer patients benefit from personalized medicine (**Table 1**

TABLE 1 | Ongoing clinical trials.

Homologous reconbination deficiency (HRD) related therapies			
Targets	**Patients**	**Drugs**	**Trials**
HRD genes	metastatic PDAC with germline/somatic *BRCA, PALB2* mutations	Rucaparib	Phase 2 NCT03140670
	solid tumors with germline/somatic DDR gene mutations	Rucaparib	Phase 2 NCT041717000
	metastatic PDAC with DDR gene mutations	Rucaparib	Phase 2 NCT03337087
	metastatic PDAC with DDR gene mutations	Rucaparib	Phase 2 NCT02890355
	advanced PDAC with *BRCA1/2, PALB2, CHEK2 or ATM* mutations	Niraparib	Phase 2 NCT03601923, Phase 2 NCT03553004
	metastatic PDAC with DDR gene mutations	Niraparib	Phase 1b/2 NCT03404960
Mismatch repair deficiency (MMR-D) or microsatellite instability high (MSI-H)			
Targets	**Patients**	**Drugs**	**Trials**
PD-1	advanced/metastatic PDAC	Pembrolizumab	Phase 2 NCT04058964, Phase 2 NCT03331562, Phase 2 NCT03264404, Phase 2b NCT02907099, Phase 1 (Part B) NCT04007744
	advanced/metastatic PDAC	Nivolumab	Phase 2 NCT03697564
KRAS wild-type			
Targets	**Patients**	**Drugs**	**Trials**
NTRK fusion	advanced/metastatic solid tumors with *NTRK/ROS1/ ALK* gene rearrangements	Entrectinib	Phase 2 NCT02568267
ALK, ROS1 gene translocations	solid tumors with *ALK, ROS1* translocations	Crizotinib	Phase 2 NCT02465060(MATCH screening trial) Phase 2 NCT02465060(MATCH screening trial)
$BRAF^{V600E}$	solid tumors with $BRAF^{V600E/R/K/D}$	Dabrafenib	Phase 2 NCT02465060(MATCH screening trial)
HER2	advanced PDAC, biliary cancers	Afatinib	Phase 1b NCT02451553
	solid tumors with *NRG1* fusion	Zenocutuzumab	Phase 1/2 NCT02912949

and **Figure 1**). Patients with *BRCA1* and *BRCA2* mutations benefit from platinum-based therapy and poly (ADP-ribose) polymerase (PARP) inhibitors (3, 4, 6–9). Patients with microsatellite instability-high (MSI-H) benefit from immune checkpoint blockade (ICB) therapy (5, 10). Patients with wild-type *KRAS* ($KRAS^{WT}$) often carry other oncogenic mutations such as *BRAF* (3, 4), which can be candidates for small-molecule therapy. To enroll patients in genome-based precision medicine, recent reports have suggested that diagnosis by liquid biopsy is promising (11). However, the number of patients who can benefit from precision medicine is limited due to the limited number of mutations leading to precision medicine (3, 4).

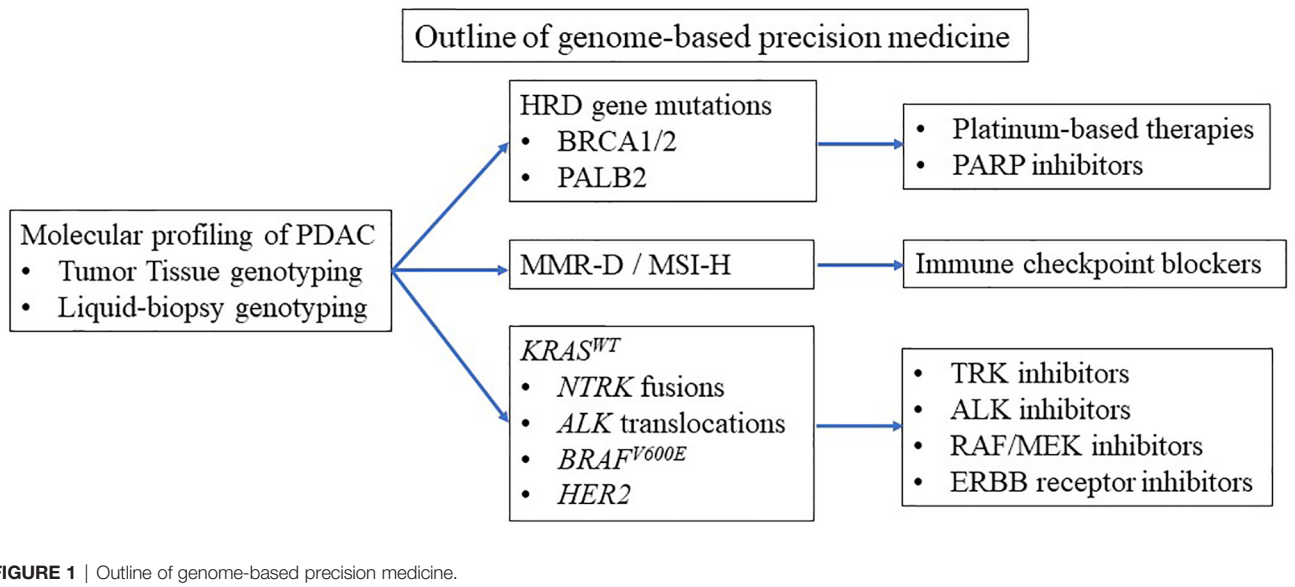

FIGURE 1 | Outline of genome-based precision medicine.

The recent identification of two major transcriptional subtypes of PDAC with characteristic histopathological features and different prognoses has provided a new perspective for developing therapies (12–15). These include a "basal-like" (or squamous) subtype, which is poorly differentiated and carries a worse prognosis, and a "classical" (or progenitor) subtype, which is well differentiated and has a better prognosis (13, 14, 16). Basal-like and classical subtypes can predict the response to chemotherapy (12, 17–19) and are associated with stromal subtypes. Stroma-targeted therapies have largely failed because of their complicated features and models which recapitulate the tumor microenvironment (TME), and drug responses to stroma-targeted therapies are needed. In addition to precision medicine based on molecular profiling, phenotypic profiling, such as drug screening using personalized models, is useful in the clinic. The patient-derived xenograft (PDX) has been established as a preclinical tool to improve drug screening and development; however, the PDX model requires sufficient tissue for transplantation, and failures are not uncommon (20–23). A recently described, organoid culture system can be exploited for molecular and phenotypic profiling to enable personalized therapeutics (24, 25). A variety of approaches using co-culture of organoids with stromal cells have been established and used for ICB therapy testing. Organoid technology may bridge the gap between cancer genetics and clinical trials, enabling personalized therapy.

Several studies have described the usefulness of precision medicine based on molecular profiling (3–5) and phenotypic profiling (24, 25). Approaches using both genome-based medicine and individualized model-based drug screening will be useful for achieving precision medicine for pancreatic cancer.

MOLECULAR SUBTYPES OF PANCREATIC CANCER

Genomic Subtypes

Recent genomic analyses have revealed the mutational landscape of PDAC (14, 26–28). More than 90% of PDAC harbor activating KRAS mutations. Mutations in KRAS are seen in all stages of pancreatic intraepithelial neoplasia (PanIN). The commonly accepted model of carcinogenesis describes a stepwise progression from normal pancreatic epithelium to PanIN and finally to adenocarcinoma due to accumulation of genetic alterations. Inactivation of tumor suppressor genes, such as *TP53*, SMAD family member 4, and cyclin-dependent kinase inhibitor 2A, is seen with progressive PanIN development and occurs in more than 50% (29, 30). The prevalence of recurrently mutated genes then decreases to ~10%, which aggregates into core molecular pathways, including KRAS, wingless and int (WNT), NOTCH, DNA damage repair, RNA processing, cell cycle regulation, transforming growth factor beta (TGF-β) signaling, switch/sucrose non-fermentable, chromatin regulation, and axonal guidance (14, 26–28). Pancreatic tumors exhibit a high frequency of chromosomal rearrangement (31), and a subset of PDAC tumors may progress *via* chromosomal rearrangements instead of stepwise progression *via* accumulation of genetic mutations (31). Chromosomal rearrangements and amplification of *KRAS* are reportedly linked to poor outcomes in PDAC patients (32).

Pathway analyses based on genetic changes have detected associations of various pathways with outcome in PDAC patients. DNA repair-associated pathways are associated with a poor prognosis, whereas beta-catenin signaling is associated with improved outcomes (33). Many of these pathways can be actionable therapeutic targets in preclinical models and in the clinic. Molecular profiling suggests that up to 25% (range 12–25%) of pancreatic cancers harbor actionable molecular changes (5). Three main groups, such as genetic changes in homologous recombination deficiency (HRD), mismatch repair deficiency (MMR-D)/high microsatellite instability (MSI-H), and oncogene alterations, such as *BRAF* mutation and *NTRK* gene fusions in $KRAS^{WT}$, are considered potential actionable mutations. In the American Society of Clinical Oncology (ASCO) guidelines, early testing for actionable genomic changes (both germline and somatic) is recommended for pancreatic cancer patients who are likely to be potential candidates for additional treatment after first-line therapy (34). Patients with *BRCA* mutations, MMR-D/MSI-H, and *NTRK* gene fusions can be given tailored therapies, such as PARP inhibitors, ICB therapy, and TRK fusion inhibitors, respectively. A retrospective analysis of the Know Your Tumor program testing matched therapies following molecular profiling revealed significantly longer overall survival (OS) after PARP inhibitor therapy in patient with *BRCA* mutations or after ICB therapy in those with MMR-D compared with patients who received unmatched therapies (2.58 *vs.* 1.51 years) or those without an actionable molecular change (2.58 *vs.* 1.32 years) (3). In this study, the most common actionable alteration was mutations in the DNA damage response (DDR) pathway, including *BRCA* mutations. These data suggest promise for this personalized approach.

HRD

Diverse defects in HR DNA repair genes, such as germline mutations in *BRCA1*, *BRCA2*, and *PALB2*, somatic mutations in *BRCA1* and *BRCA2*, and promoter methylation of *BRCA1*, have been reported in breast and ovarian cancers (35, 36). *BRCA* mutations are also associated with an increased risk for pancreatic cancer, and 4% to 7% of patients with pancreatic cancer have a germline *BRCA* mutation (8). *BRCA* genes encode for proteins involved in the HR repair of DNA double-stranded breaks. Cells with deficient HR repair are sensitive to PARP inhibition. PARP enzymes are key components in the repair of DNA single-stranded breaks and replication fork damage (37). PARP inhibition causes accumulation of such lesions through catalytic inhibition and trapping of PARP on DNA at the sites of single-stranded breaks. These processes eventually result in double-stranded breaks, which cannot be accurately repaired in tumors with HRD. Thus, PARP inhibitors cause accumulation of DNA damage and tumor-cell death. Accordingly, PARP

inhibitors are selectively effective for cells with HRD due to *BRCA1* or *BRCA2* mutations (38, 39).

Recent investigations of genomic profiling in large cohorts of PDAC have reported the significance of HRD in predicting sensitivity to platinum-based therapy and PARP inhibitors (3, 4, 6, 7). According to ASCO guidelines, treatment with platinum-based chemotherapy or the PARP inhibitor olaparib is recommended for patients who have a germline *BRCA1* or *BRCA2* mutation. A recent randomized phase III trial (POLO) demonstrated the efficacy of olaparib, a PARP inhibitor, in germline *BRCA*-mutated metastatic PDAC (8). Among the 154 enrolled patients, progression-free survival (PFS) was significantly longer in the olaparib group than the placebo group (7.4 *vs.* 3.8 months). Furthermore, another recent randomized phase II trial showed that patients with germline *BRCA1/2*- or *PALB2*-mutated PDAC benefit from first-line platinum chemotherapy, with median OS and PFS of 15.5 (14.6–19) and 7 (6.1–8.1) months, respectively. Patients with HRD had improved PFS compared with no HRD when treated with first-line platinum therapy but not with first-line non-platinum therapy (9). These results suggest that HRD can effectively be targeted in PDAC.

In addition to mutations in canonical HR genes, a comprehensive evaluation of HR gene mutations is needed beyond germline *BRCA* mutations to understand their sensitivity to DDR-targeted therapies, including platinum-based therapy. Multiple groups have identified a broader group of patients with HRD sensitive to DDR-targeted therapies (3, 4, 7). The concept of "BRCAness" was introduced to describe the clinical and biological features in some sporadic tumors shared with tumors harboring germline BRCA1/2 mutations. Polak et al. (40) explored signature 3, a mutational signature prevalent in tumors with BRCAness, and found altered expression of *PALB2* and *RAD51*, which are genes that are important in the HRR pathway. In addition, signature 3 has been found in tumors with both germline and somatic *BRCA1/2* mutations (40). Thus, signature 3 can be considered a potential biomarker that could lead to BRCAness-targeting therapies. O'Reilly and colleagues (7) evaluated the mutational status of HR genes and HRD genetic signatures to determine their benefit to platinum therapy. They observed that patients with HRD had significantly improved PFS when treated with first-line platinum-based therapy compared with those who received first-line non-platinum-based therapy. Subgroup analyses suggest that patients with either pathogenic somatic or germline *BRCA1*, *BRCA2*, or *PALB2* mutations, as well as biallelic loss of other rarer HR genes, such as *ATM* and *CHEK2*, could be recommended for platinum-based therapy. Aguirre and colleagues (4) observed four samples that did not have clear DNA changes or mRNA downregulation of *BRCA1*, *BRCA2*, *PALB2*, or *RAD51C* but nevertheless had enrichment of HRD/signature 3 compared with samples with HRD. These data suggest that signature 3 can be recommended for platinum-based therapy and PARP inhibitors. Furthermore, patients with biallelic HRD show higher tumor mutation burden (TMB), indicating the potential benefit from immunotherapy as shown in other types of cancer (41, 42).

MMR-D/MSI-H

Immune checkpoint inhibitors have been an effective therapy for MMR-D/MSI-H cancers regardless of tumor type, although activity may vary by tumor type. MMR-D occurs as a consequence of loss-of-function changes in MMR genes (*MLH1, PMS2, MSH2, MSH6*) because of the inherited germline mutations known as Lynch syndrome, or because of the biallelic somatic inactivation of MMR genes. In PDAC, approximately 1% of patients have MMR-D or MSI-H due to Lynch syndrome or somatic MMR gene mutations (43, 44). The normal MMR system can correct the process of DNA replication errors but MMR-D results in an inappropriate response to DNA mismatches, increasing the possibility of gene mutation. MMR-D causes MSI-H by missing or inserting one or more of the repeating units in the inappropriate process of DNA replication and repair. MMR-D and MSI-H are generally associated with high TMB. A high TMB increases the potential number of neoantigens, and these neoantigens can be presented by the tumor cell and recognized by host immune cells, which are also known as tumor-infiltrating lymphocytes (TILs) that migrate into TME (45, 46). TILs, particularly CD8+ cytotoxic T cells, orchestrate a significant antitumor response to eliminate tumor cells (45, 46). Detection of MMR-D and/or MSI-H was proposed as a biomarker of an immunogenic tumor and response to ICB therapy, such as anti-programmed cell death protein 1 (PD-1) inhibition. The immune checkpoint inhibitor pembrolizumab is currently approved for treatment of MMR-D/MSI-H cancer regardless of the histology. In ASCO guidelines, pembrolizumab is recommended as a second-line therapy for PDAC patients with MMR-D or MSI-H (34).

The recently published KEYNOTE 158 study (10) and NCI-MATCH study (5), which investigated the efficacy of ICB therapy in non-colorectal cancers, clearly suggested that MMR-D in solid tumors is a predictor of the response to ICB therapy. However, ICB therapy has low efficacy against pancreatic cancer, suggesting that cancer type-specific responses show variable clinical outcomes, and that disease-specific biological factors may have an independent impact on ICB response, regardless of MMR-D status. Regarding the underlying mechanisms, the degree of T-cell infiltration is critical for predicting the efficacy of ICB therapy in other types of cancers (47–52), and a small subset of patients with MSI-H tumors exhibit T-cell infiltration and sensitivity to immunotherapy (53). In pancreatic cancer, dense stroma with desmoplastic reaction may function as a physical barrier and affect the infiltration of myeloid-derived suppressor cells and T cells in tumor stroma (54, 55). In addition, PDAC exhibits substantial immunological heterogeneity, with tumors influencing T-cell infiltration (45, 56–58). For example, Stanger et al. (46) observed heterogeneity in the degree of T-cell infiltration in their cohort of 12 PDAC patients (none of whom were MSI-H), in line with prior reports for PDAC (45). The abundance of PD-1+CD8+ T cells was more predictive of immunotherapy response than was total CD8+ T cell infiltration alone. Furthermore, Leach and colleagues (59) identified mucin 16 neoantigens as T-cell targets in PDAC and as potential biomarkers of immunogenic tumors that may guide the application of immunotherapies (59). These results suggest that

both the quality and quantity of tumor-infiltrating CD8+ T cells are critical for predicting the immunotherapy response, and novel biomarkers are needed to predict the status of tumor-infiltrating CD8+ T cells.

Furthermore, the abovementioned results suggest that MMR-D status is not a perfect predictor of immunotherapy response. Loss-of-function changes in MMR genes can sometimes be a passenger mutation/change and responses to immune checkpoint inhibitor therapy could be affected by founder mutations that determine the molecular behavior of cancer (60). MSI-H and high TMB may be a better predictor of the immune checkpoint inhibitor response, as these markers are highly associated with MMR-D-driven carcinogenesis (61). The basis for these differences in T-cell infiltration is poorly understood in PDAC, where most tumors share the same oncogenic mutations. Further prospective studies are needed to evaluate the predictor role of characterization of T-cell infiltration on ICB response/resistance in cancer patients with MMR-D tumors.

KRAS^{WT}

KRAS mutation is a major driver mutation in pancreatic cancer and more than 90% of pancreatic cancer patients harbor *KRAS* mutation. Recently drugs targeting *KRAS*^{G12C} are available and clinical trials suggested promising results (62–64). However, *KRAS*^{G12D} and *KRAS*^{G12V} mutations are more common in pancreatic cancer, and these mutations are still undruggable. In *KRAS*^{WT} PDAC patients, *NTRK* fusions, *ALK* rearrangements, *ROS, NRG1* rearrangements, *BRAF, PIK3CA*, and a number of cancer-associated genes representing potential drivers have been identified (e.g., *ERBB2, STK11, GNAS, CHEK2*, and *RB1*), as potential targets.

Gene fusions involving *NTRK1, NTRK2*, or *NTRK3* (*TRK* fusions) are found in many pediatric and adult malignancies (65). *NTRK* fusions are rare in PDAC and are identified in less than 1% of tumors (66). Pishvaian et al. (67) reported a partial response to entrectinib, a potent TRK and ROS1 inhibitor in a subgroup of advanced PDAC patients. Larotrectinib, a highly selective small-molecule inhibitor of the TRK kinases, has shown efficacy in preclinical models and in patients with tumors harboring TRK fusions. In ASCO guidelines, in patients with tumors harboring *NTRK* fusions, treatment with larotrectinib or entrectinib is recommended as treatment options after first-line therapy such as FOLFIRINOX and gemcitabine plus nab-paclitaxel (GnP) (34). *NRG1* rearrangement contributes to susceptibility to ERBB inhibitors and anti-EGFR antibodies and clinical trials are ongoing (68, 69). *ALK* gene translocations have been reported in 0.16% of PDAC, and crizotinib is reportedly effective for a PDAC patient with *ALK* gene translocation (70).

BRAF^{V600E} mutations occurred at a frequency of 3% and were mutually exclusive with *KRAS* mutations. *BRAF*^{V600E} could be a driver event based on mouse models (71). Analyses of PDAC cells revealed that *BRAF*^{V600E} cells are sensitive to the FDA-approved BRAF inhibitor PLX-4032, while cells with *KRAS* mutations are resistant (33). These data suggest that a subset of patients may benefit from targeted therapy along the KRAS/BRAF axis. Aguirre et al. (4) reported the first therapeutic experience with mitogen-activated protein kinase (MAPK) inhibition in a patient harboring a *BRAF* in-frame deletion. The patient had a partial response to the MEK inhibitor trametinib. A second patient with rapidly progressive disease harboring a *BRAF* mutation was also treated with trametinib but failed to show a response. This heterogeneity in resistance mechanisms will require effective combination treatments with MAPK inhibitors. The Cancer Genome Atlas Research Network reported that the *KRAS*^{WT} tumors had significantly elevated tuberous sclerosis complex/mammalian target of rapamycin (TSC/mTOR) signaling pathway activity compared with *KRAS* mutant tumors, indicating that functional activation of the mTOR signaling pathway may be an alternative oncogenic driver in *KRAS*^{WT} pancreatic cancer (15).

These data suggest that larger multicenter clinical trials are needed to fully investigate the therapeutic efficacy of the inhibition of upstream and downstream signaling of RAS in *KRAS*^{WT} patients with other oncogenic mutations.

Liquid Biopsy

Although genome-based precision medicine, such as platinum-based therapy and PARP inhibition, in PDAC patients with HRD is promising, tissue-based genomic sequencing for first-line treatment decision making in PDAC remains challenging due to the turn-around time of obtaining sequencing results, which is 3 to 6 weeks. To enroll patients in genome-based precision medicine, recent reports have suggested that diagnosis by liquid biopsy with a short turn-around time has emerged. Liquid biopsy includes analyses of tumor materials obtained in a minimally invasive or noninvasive manner by collecting blood or other body fluids. Liquid biopsy samples are obtained from saliva, stool, or urine. They include circulating tumor cells (CTCs), circulating tumor DNA (ctDNA), extracellular vesicles, cell-free DNA, and microRNA. More recently, next-generation sequencing-based methods have enabled ctDNA profiling as an alternative to tumor tissue sequencing (72, 73). For example, the TARGET study recently reported the screening of 100 patients using ctDNA sequencing for trial enrollment (74). Most recently, Yoshino and colleagues (11) reported that ctDNA genotyping significantly shortened the screening duration (11 *vs.* 33 days; $P < 0.0001$) and improved the trial enrollment rate (9.5 *vs.* 4.1%; $P < 0.0001$) compared with tumor tissue sequencing. Overall, ctDNA was detected in 91.4% (1,438/1,573) of patients; however, the ctDNA detection rate of PDAC was the lowest (83.4% (304/363) compared with other types of cancers, such as esophageal squamous-cell carcinoma cancer (99.1% (107/108) and CRC (96.0%, 628/654). Overall, they detected multiple biomarkers relevant to the selection of treatment, including *KRAS, NRAS, BRAF*, and *PIK3CA* mutations; *ERBB2, FGFR1–2*, and *MET* amplifications; *FGFR2–3, ALK, NTRK1*, and *RET* fusions; and MSI. Liquid biopsy also enables the collection of repeated samples during the course of the treatment of patients and the collection of clones resistant to ongoing therapy. Thus, this technology has the potential to promote innovation in precision medicine.

Transcriptomic Subtypes

Cancer Cell Subtypes

Targeting drugs, according to tumor subtypes, have improved treatment outcomes in other cancers. Identification of therapeutic molecular subtypes in PDAC has been challenging. In addition to genomic subtypes, transcriptomic subtypes have been evaluated to understand the biology of pancreatic cancer. The recent identification of PDAC transcriptional subtypes has provided a new perspective relevant to the development of therapies. These include basal-like/squamous and classical/progenitor (hereafter referred to as basal-like and classical, respectively) (12–14, 75–77). Basal-like tumors are associated with poor outcomes and treatment resistance (12–14, 16–19, 75–77). Two independent clinical trials revealed that basal-like tumors are resistant to FOLFIRINOX-based regimens (19, 78). In those studies, RNA *in situ* hybridization or immunohistochemical analysis of GATA-binding protein 6 (GATA6) was used to differentiate basal-like and classical tumors. The resistance of basal-like tumors to FOLFIRINOX is supported by a recent report by Tiriac et al. (24), who showed that patient-derived organoid (PDO) chemotherapy signatures may predict treatment response. The signatures representing individual cytotoxic agents were applied to the COMPASS cohort, suggesting that basal-like tumors are most likely to have a non–oxaliplatin-sensitive signature (24). To apply molecular subtyping in treatment decision-making for PDAC patients, Rashid et al. (79) revealed that the tumor-intrinsic two-subtype schema of Moffitt et al. is the most replicable, and they developed the Purity Independent Subtyping of Tumors, a clinically usable single-sample classifier based on gene expression data obtained using multiple platforms, including microarrays, RNA sequencing, and NanoString.

The development of subtype-based therapies remains challenging because the genetic and epigenetic aberrations that promote the stable or dynamic regulation of subtypes are unknown. The basal-like subtype consists of small subgroups that are regulated by different mechanisms (14). The master regulators of the basal-like subtype have been identified, and the basal-like subtype is associated with the activation of genes involved in the epithelial–mesenchymal transition, activation of transcription factors such as MYC and TP63, and downregulation of markers for endoderm such as *HNF4A* and *GATA6* (12–14). In addition, expression of the ΔN isoform of TP63 (ΔNp63) and GLI2 promotes the basal-like identity in PDAC (80, 81). Several epigenetic regulator genes, including *KDM6A*, *KMT2C*, and *KMT2D*, are associated with the basal-like subtype (12, 14, 82). Mueller et al. (83) divided the basal-like subtype into the TP63-related transcriptional program with squamous differentiation and the RAS/epithelial–mesenchymal transition-related transcriptional program with undifferentiated cancers. Further characterization of the master regulators of molecular subtypes may lead to the identification of biomarkers and targets for tailored therapies.

Because *KRAS* is the most commonly mutated gene in PDAC, the association between KRAS addiction (KRAS dependency) and a molecular subtype has been debated. KRAS-addicted cells have been previously observed as more classical and epithelial in monolayer cell cultures (12). Collisson et al. (12) showed that classical PDAC cells are relatively more dependent on KRAS and more sensitive to erlotinib than basal-like PDAC cells. Conversely, basal-like PDAC lines are more sensitive to gemcitabine than classical PDAC (12). KRAS ablation induces a basal-like phenotype in surviving cells *in vivo* (80). A study of the inducible KrasG12D;Trp53-/- PDAC mouse model (84) revealed cancer cell-intrinsic mechanisms enabling bypass of KRAS dependency and tumor recurrence (85). Specifically, Yap1 amplification and overexpression enabled escape in approximately one-third of KRAS-negative recurrent PDAC tumors (85) and serves a similar role in lung cancer (86). However, allelic imbalance and elevated expression of mutant KRAS have been associated with aggressive and undifferentiated histological phenotypes in PDAC (32, 83). Furthermore, increased dosage of mutant KRAS is sufficient to induce basal-like features (32, 87). These results suggest that mutant *KRAS* plays an important role in oncogenesis in PDAC, but other epigenetic or microenvironmental factors are critical in regulating molecular phenotypes.

Stromal Subtypes

Pancreatic cancer is characterized histologically by a dense stromal reaction with desmoplasia, which creates a physical barrier around the tumor cells and prevents appropriate vascularization and delivery of chemotherapeutic agents (88). The surrounding desmoplasia was formerly considered to promote cancer, and a number of clinical trials targeting the stroma have been conducted to prove this. However, most of those trials failed, and the current understanding is that the stroma is multi-faceted (89–91). To reveal the heterogeneity of stromal components, studies based on single-cell RNA sequencing have been conducted (92–95). Cancer-associated fibroblasts (CAFs) play an important role in the TME, and cancer-derived IL-1 or TGF-β can stimulate the differentiation of surrounding fibroblasts into inflammatory and myofibroblastic CAFs, respectively (93). IL-6 secreted by inflammatory CAFs promote proliferation of the tumor, whereas myofibroblastic CAFs produce the surrounding stroma. Because cancer cells create an environment favorable to themselves, these stromal subtypes are linked to the cancer cell subtypes mentioned above. Mauer et al. (77) reported CAF subtypes using laser capture microdissection and RNA sequencing of pathologically verified PDAC epithelia and their adjacent stroma. The authors detected two subtypes reflecting ECM deposition and remodeling (ECM-rich) versus immune-related processes (immune-rich). There was a strong association between ECM-rich stroma and basal-like tumors, whereas immune-rich stroma occurred more often in association with classical tumors (77, 96). As such, the epithelial and stromal subtypes were partially linked, suggesting potential biomarkers for stroma-targeted therapies in PDAC.

As mentioned previously, TILs are associated with the response to immune checkpoint inhibitors. Therapeutic strategies targeting immune modulators have emerged. Bailey

et al. (14) identified an immunogenic cancer subtype, which shares many of the characteristics of classical tumors but is uniquely associated with significant immune-cell infiltration. This cancer cell subtype, as well as Mauer et al.'s immune-rich subtype, has potential as a biomarker for immune therapy. Furthermore, studies using mouse models have revealed potential targets such as colony-stimulating factor 1 receptor, cytotoxic T-lymphocyte-associated protein 4 (97, 98), and CXC chemokine receptor 2 (99, 100), which led to clinical trials. However, due to their complexity, TME-targeted therapies have largely failed (101, 102). Clinical trials of such therapies have been reviewed recently (103). Further investigations are warranted to discover effective TME-targeted therapies.

PATIENT-DERIVED MODELS

PDO

Organoids are three-dimensional structures that are grown *in vitro* and recapitulate many aspects of corresponding organs *in vivo*, providing many novel human cancer models. Theoretically, PDOs allow expansion of small tumor samples, enabling the analyses of cancer at any stage. Various human carcinomas have been established from resected specimens and biopsy samples (24, 104–116). Pancreatic tumors contain abundant stromal components and exhibit low neoplastic cellularity, which contribute to the low accuracy of genetic and transcriptional analyses of the neoplastic compartment in bulk tumor tissues. In organoid culture, only the epithelial component expands, thus providing high-quality research materials (24).

The organoid culture system is a powerful tool for personalized medicine and is used in co-clinical trials because the response of PDOs to drugs largely mimics the initial response of corresponding patients to the same drugs (24, 108, 111, 117, 118) (**Figure 2**). Tiriac et al. (24) established a biobank of 66 pancreatic cancer PDOs, from both biopsy samples and resected specimens, and compared the gene expression of those PDOs with responses to standard cytotoxic drugs and identified transcriptional gene signatures of responders to different chemotherapies. They found that the transcriptional gene signature reflects a drug response in an independent cohort of PDAC patients. Currently, clinical trials using PDOs are ongoing, and PDO can be used to select second-line or adjuvant treatments because the time required to generate and test PDOs is about 4–6 weeks (25). Pancreatic cancer frequently acquires resistance to chemotherapy. Tiriac et al. (24) reported their experience with longitudinal collection of organoids from the same patient undergoing chemotherapy. Interestingly, an organoid collected before the corresponding patient acquired resistance to FOLFIRINOX and gemcitabine/nab-paclitaxel regimens was sensitive to gemcitabine, paclitaxel, 5-FU, and oxaliplatin, whereas organoids collected after the chemoresistance developed were resistant to those chemotherapeutic agents. In addition, the first organoid collected was resistant to mTOR inhibition, whereas subsequent organoids were sensitive to mTOR inhibition. These results suggest that collecting organoids during chemotherapy enables drug selection according to chemosensitivity in PDAC patients. Collecting organoids from metastatic and recurrent sites is difficult. However, Gao et al. (119) demonstrated the feasibility of growing organoids from CTCs from a prostate cancer patient to overcome this shortcoming.

As mentioned, pancreatic cancer is characterized by a dense stromal reaction with desmoplasia. To mimic the tumor environment, co-culture systems have been developed. The co-culture system of pancreatic stellate cells, a resident mesenchymal cell, with pancreatic cancer PDOs, has been established (92). This system enables to produce the desmoplastic stroma and led to the specification of pancreatic CAF subtypes, including inflammatory CAFs and myofibroblastic CAFs (93). Several approaches of co-culturing PDOs with immune and fibroblastic components have been established to predict the efficacy of immune checkpoint inhibitors in other types of cancer (120) (121), which can be applicable to PDOs in PDAC. As with the PDX mouse model, organoid transplant mouse models are a powerful tool for drug screening and biological research. Boj et al. (122) reported that orthotopic transplantation of organoids led to the development of all stages of disease progression including early PanIN, late PanIN, invasive ductal adenocarcinoma, and metastasis. A recent study reported the usefulness of an intraductal transplantation mouse model of PDOs (87), which models the progressive switching of molecular subtypes. These models are promising tools to evaluate human PDAC at any stage to understand its fundamental biology and to identify biomarkers of early disease as well as biomarkers of subtype switching at later stages, contributing to discovery of novel therapeutic strategies.

PDX

PDXs have emerged as an important platform to discover novel therapeutic strategies and biomarkers (21, 22, 123). PDX models retain key features of donor tumors both histologically and biologically, and effectively recapitulate the chemosensitivity of corresponding patients compared with conventional two-dimensional cell-line-based xenograft models (124–127). Analyses of genetic profiles show good concordance between primary tumors and the tumors derived from PDX models, although there were differences in genes involved in the stromal and immune compartments due to the replacement of the human stroma by murine elements. The key characteristics and practical applications of PDXs can be found in recent reviews (20–23).

PDX models of PDAC patients have been reported (128–130), and one study found a good correlation between response to gemcitabine in PDXs and in PDAC patients (131). The drug response of PDX models remains stable across generations (up to 10 passages) (128, 132). Hidalgo et al. (133) performed an empirical treatment of PDX models with a panel of drugs while the patients were receiving first-line therapy and showed that GnP is effective in PDX models, which is correlated with the efficacy of this combination in the clinic (134). Similarly, lack of efficacy in preclinical studies with PDX predicted failure of the same therapies in the clinic, such as the SRC inhibitor saracatinib

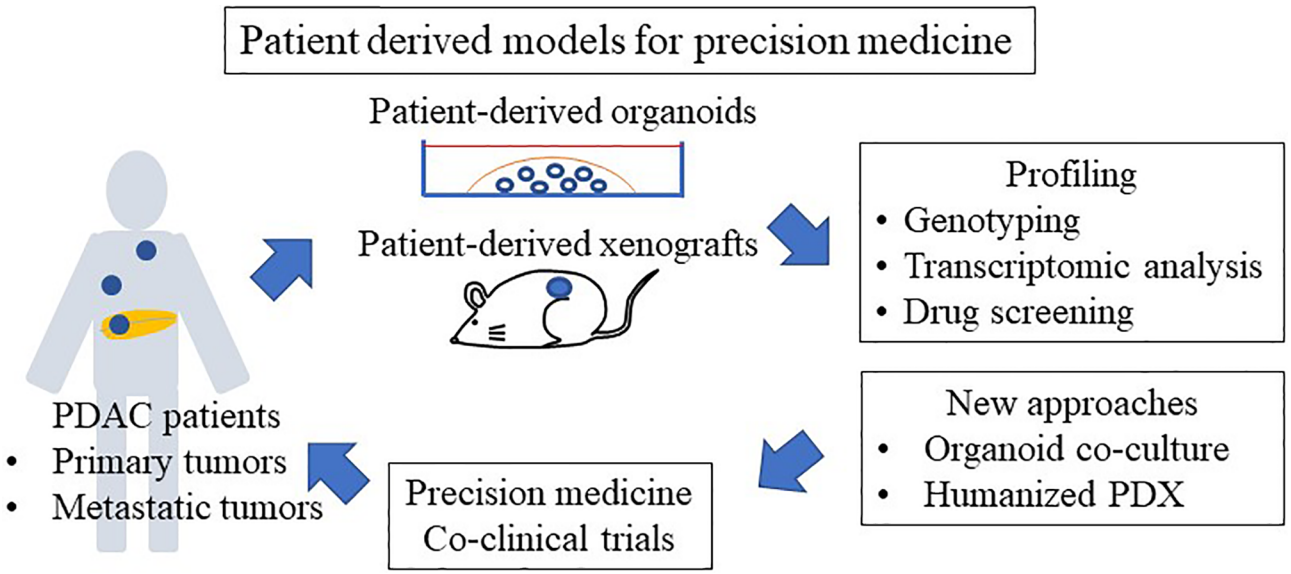

FIGURE 2 | Patient-derived models for precision medicine.

and the mTOR inhibitor sirolimus in PDAC (124, 135). Based on these data, PDX models are an essential part of the preclinical screening for new chemotherapeutic agents (**Figure 2**).

PDX models are also used in co-clinical trials, in which they are developed from patients enrolled in clinical trials and treated with the same experimental agents (**Figure 2**). These models are used to evaluate the clinical response based on appropriate endpoints such as response rate or tumor growth delay. PDX models are also powerful tools for simulating tolerance after exposure to therapies used in the clinical setting and to develop strategies for overcoming resistance (136, 137). Furthermore, biological and genetic comparisons between sensitive and resistant models could lead to the discovery of biomarkers of drug efficacy as well as biomarkers for inclusion in clinical studies. In PDAC, PDX studies using gemcitabine revealed expression of deoxycytidine kinase, the gemcitabine-activating enzyme, as a predictor of drug efficacy (128, 138). Similarly, PDX models have been used to determine metabolic and imaging biomarkers (139, 140). This strategy provides an interesting platform to evaluate drug response in the patients and PDX models simultaneously, and to investigate biomarkers of sensitivity and resistance, as well as new combination strategies to overcome emerging resistance pathways. These findings suggest that PDX models hold promise for precision medicine in PDAC.

Regarding the drawbacks, in most patients, obtaining individualized PDXs to guide treatment is not feasible because of the low success rate of engraftment, the discrepancy between the time needed for PDX expansion and treatment, and the rapidity of disease progression in patients (131, 133). PDX models are generally established from surgical specimens, which provide a large amount of tumor tissue. However, because most PDAC patients are inoperable, generating PDX from smaller samples, such as fine-needle aspiration for personalized therapy, is more useful. To resolve this problem, CTC-derived xenografts are now applied to evaluate other types of cancer such as breast cancer (141), prostate cancer (142), gastric cancer (143), small-cell lung cancer (SCLC) (144), and melanoma (145). A major obstacle is that PDX models require the use of immunocompromised mice, which prevents the evaluation of immunomodulators, such as vaccines, anti-PD-1, and anti-cluster of differentiation 40 (CD40) antibodies. Humanized mice with human immune system in which selected immune components have been introduced may solve the problems. However, human tumor stroma in the cancer specimens are rapidly replaced by mouse stromal cells including fibroblasts, inflammatory cells, blood vessels, and immune cells, and these elements are difficult to introduce in humanized mouse. As reported, expression profiling based on species-specific RNA sequencing of PDXs provides a unique opportunity to distinguish mouse stroma-derived transcripts from human cancer cell-derived transcripts without physically separating the two components prior to RNA extraction (87). Novel approaches, such as short-term primary cultures or organoids, are being developed and are expected to be applied to preclinical screening studies (24). Clinical trials using PDOs are ongoing (25), and PDX-derived organoids are useful for drug screening.

CONCLUSIONS

Integrated analyses of the genome, epigenome, and transcriptome are yielding biological insights with potential therapeutic relevance in PDAC. Genome-based therapies have led to paradigm-changing treatments for other cancers and have dramatically

improved survival and cure rates. Therapeutic strategies based on gene alterations in cancer cells, including HRD and MMR-D/MSI-H, have improved the survival of PDAC patients. In the You Know Tumor trial, the OS was significantly longer in patients who received a tailored therapy than in those without an actionable molecular change. However, this remains an unfulfilled promise in PDAC because of the limited number of patients and the rapidity of disease progression. The rapid analysis of genetic mutations using liquid biopsy and new biomarkers, such as BRCA-ness, signature3, and higher TMB, may allow more patients to be recruited for personalized therapy. In addition, the difficulty of drug delivery through the stromal barrier in tumors contributes to high resistance to available chemotherapeutic agents, and therapeutic strategies targeting stromal components have failed due to their complexity. In addition to genomic subtypes, transcriptomic analyses revealed the associations of cancer cell and CAF subtypes with immune cell components, providing biological insights relevant to the treatment of PDAC. Furthermore, phenotypic characterization of individualized models such as PDXs and PDOs will provide additional information for selecting tailored therapies for PDAC patients. Individualized PDXs have the potential to identify effective therapies; however, they have significant limitations, including long lead times and the need for large amounts of tumor tissue for testing. The PDO platform can be exploited for genomic and functional studies even during chemotherapy, with the possibility of selecting sensitive therapeutic agents after acquisition of chemoresistance. New approaches such as co-culture of PDOs with stromal components and humanized PDX may bridge the gap between cancer genetics and patient clinical trials and allow for personalized therapy, although further studies are needed to validate this approach. A multi-parameter approach that combines genome-based medicine with drug screening using individualized models will be key for precision medicine.

AUTHOR CONTRIBUTIONS

KM wrote the paper and prepared figures. HN revised manuscript and prepared figures. KK supervised the entire project. All authors contributed to the article and approved the submitted version.

FUNDING

This research was supported by Takeda Science Foundation, Ichiro Kanehara Foundation, MSD Life Science Foundation, The Naito Foundation, Kobayashi Foundation for Cancer Research, and Life Science Foundation of Japan.

REFERENCES

1. Siegel RL, Miller KD, Jemal A. Cancer Statistics, 2019. *CA Cancer J Clin* (2019) 69(1):7–34. doi: 10.3322/caac.21551
2. Hruban RH, Lillemoe KD. Screening for Pancreatic Cancer Gets a D, But the Student Is Improving. *JAMA Surg* (2019) 154(9):795–7. doi: 10.1001/jamasurg.2019.2832
3. Pishvaian MJ, Blais EM, Brody JR, Lyons E, DeArbeloa P, Hendifar A, et al. Overall Survival in Patients With Pancreatic Cancer Receiving Matched Therapies Following Molecular Profiling: A Retrospective Analysis of the Know Your Tumor Registry Trial. *Lancet Oncol* (2020) 21(4):508–18. doi: 10.1016/s1470-2045(20)30074-7
4. Aguirre AJ, Nowak JA, Camarda ND, Moffitt RA, Ghazani AA, Hazar-Rethinam M, et al. Real-Time Genomic Characterization of Advanced Pancreatic Cancer to Enable Precision Medicine. *Cancer Discovery* (2018) 8(9):1096–111. doi: 10.1158/2159-8290.CD-18-0275
5. Azad NS, Gray RJ, Overman MJ, Schoenfeld JD, Mitchell EP, Zwiebel JA, et al. Nivolumab Is Effective in Mismatch Repair-Deficient Noncolorectal Cancers: Results From Arm Z1d-a Subprotocol of the NCI-MATCH (Eay131) Study. *J Clin Oncol* (2020) 38(3):214–22. doi: 10.1200/JCO.19.00818
6. Pishvaian MJ, Bender RJ, Halverson D, Rahib L, Hendifar AE, Mikhail S, et al. Molecular Profiling of Patients With Pancreatic Cancer: Initial Results From the Know Your Tumor Initiative. *Clin Cancer Res* (2018) 24(20):5018–27. doi: 10.1158/1078-0432.CCR-18-0531
7. Park W, Chen J, Chou JF, Varghese AM, Yu KH, Wong W, et al. Genomic Methods Identify Homologous Recombination Deficiency in Pancreas Adenocarcinoma and Optimize Treatment Selection. *Clin Cancer Res* (2020) 26(13):3239–47. doi: 10.1158/1078-0432.CCR-20-0418
8. Golan T, Hammel P, Reni M, Van Cutsem E, Macarulla T, Hall MJ, et al. Maintenance Olaparib for Germline Brca-Mutated Metastatic Pancreatic Cancer. *N Engl J Med* (2019) 381(4):317–27. doi: 10.1056/NEJMoa1903387
9. O'Reilly EM, Lee JW, Zalupski M, Capanu M, Park J, Golan T, et al. Randomized, Multicenter, Phase II Trial of Gemcitabine and Cisplatin With or Without Veliparib in Patients With Pancreas Adenocarcinoma and a Germline Brca/Palb2 Mutation. *J Clin Oncol* (2020) 38(13):1378–88. doi: 10.1200/JCO.19.02931
10. Marabelle A, Le DT, Ascierto PA, Di Giacomo AM, De Jesus-Acosta A, Delord JP, et al. Efficacy of Pembrolizumab in Patients With Noncolorectal High Microsatellite Instability/Mismatch Repair-Deficient Cancer: Results From the Phase Ii KEYNOTE-158 Study. *J Clin Oncol* (2020) 38(1):1–10. doi: 10.1200/JCO.19.02105
11. Nakamura Y, Taniguchi H, Ikeda M, Bando H, Kato K, Morizane C, et al. Clinical Utility of Circulating Tumor DNA Sequencing in Advanced Gastrointestinal Cancer: SCRUM-Japan Gi-SCREEN and GOZILA Studies. *Nat Med* (2020) 26(12):1859–64. doi: 10.1038/s41591-020-1063-5
12. Collisson EA, Sadanandam A, Olson P, Gibb WJ, Truitt M, Gu S, et al. Subtypes of Pancreatic Ductal Adenocarcinoma and Their Differing Responses to Therapy. *Nat Med* (2011) 17(4):500–3. doi: 10.1038/nm.2344
13. Moffitt RA, Marayati R, Flate EL, Volmar KE, Loeza SG, Hoadley KA, et al. Virtual Microdissection Identifies Distinct Tumor- and Stroma-Specific Subtypes of Pancreatic Ductal Adenocarcinoma. *Nat Genet* (2015) 47(10):1168–78. doi: 10.1038/ng.3398
14. Bailey P, Chang DK, Nones K, Johns AL, Patch AM, Gingras MC, et al. Genomic Analyses Identify Molecular Subtypes of Pancreatic Cancer. *Nature* (2016) 531(7592):47–52. doi: 10.1038/nature16965
15. Cancer Genome Atlas Research Network. Electronic Address Aadhe, Cancer Genome Atlas Research N. Integrated Genomic Characterization of Pancreatic Ductal Adenocarcinoma. *Cancer Cell* (2017) 32(2):185–203.e13. doi: 10.1016/j.ccell.2017.07.007
16. NK S, Wilson GW, Grant RC, Seto M, O'Kane G, Vajpeyi R, et al. Morphological Classification of Pancreatic Ductal Adenocarcinoma That Predicts Molecular Subtypes and Correlates With Clinical Outcome. *Gut* (2020) 69(2):317–28. doi: 10.1136/gutjnl-2019-318217
17. Muckenhuber A, Berger AK, Schlitter AM, Steiger K, Konukiewitz B, Trumpp A, et al. Pancreatic Ductal Adenocarcinoma Subtyping Using the Biomarkers Hepatocyte Nuclear Factor-1A and Cytokeratin-81 Correlates With Outcome and Treatment Response. *Clin Cancer Res* (2018) 24(2):351–9. doi: 10.1158/1078-0432.Ccr-17-2180

18. Aung KL, Fischer SE, Denroche RE, Jang GH, Dodd A, Creighton S, et al. Genomics-Driven Precision Medicine for Advanced Pancreatic Cancer: Early Results From the COMPASS Trial. *Clin Cancer Res* (2018) 24 (6):1344–54. doi: 10.1158/1078-0432.CCR-17-2994
19. O'Kane GM, Grunwald BT, Jang GH, Masoomian M, Picardo S, Grant RC, et al. Gata6 Expression Distinguishes Classical and Basal-like Subtypes in Advanced Pancreatic Cancer. *Clin Cancer Res* (2020) 26(18):4901–10. doi: 10.1158/1078-0432.Ccr-19-3724
20. Hidalgo M, Amant F, Biankin AV, Budinska E, Byrne AT, Caldas C, et al. Patient-Derived Xenograft Models: An Emerging Platform for Translational Cancer Research. *Cancer Discov* (2014) 4(9):998–1013. doi: 10.1158/2159-8290.CD-14-0001
21. Siolas D, Hannon GJ. Patient-Derived Tumor Xenografts: Transforming Clinical Samples Into Mouse Models. *Cancer Res* (2013) 73(17):5315–9. doi: 10.1158/0008-5472.CAN-13-1069
22. Tentler JJ, Tan AC, Weekes CD, Jimeno A, Leong S, Pitts TM, et al. Patient-Derived Tumour Xenografts as Models for Oncology Drug Development. *Nat Rev Clin Oncol* (2012) 9(6):338–50. doi: 10.1038/nrclinonc.2012.61
23. Byrne AT, Alferez DG, Amant F, Annibali D, Arribas J, Biankin AV, et al. Interrogating Open Issues in Cancer Precision Medicine With Patient-Derived Xenografts. *Nat Rev Cancer* (2017) 17(4):254–68. doi: 10.1038/nrc.2016.140
24. Tiriac H, Belleau P, Engle DD, Plenker D, Deschenes A, Somerville TDD, et al. Organoid Profiling Identifies Common Responders to Chemotherapy in Pancreatic Cancer. *Cancer Discov* (2018) 8(9):1112–29. doi: 10.1158/2159-8290.CD-18-0349
25. Grossman JE, Huang L, Muthuswamy L, Perea S, Akshinthala D, Gonzalez R, et al. Abstract CT119: Organoid Sensitivity in Pancreatic Cancer Correlates With Clinical Response to Treatment and Reveals Utility for Reducing Toxicity: Preliminary Results From the HOPE Trial. *Cancer Res* (2020) 80(16 Supplement):CT119–CT. doi: 10.1158/1538-7445.Am2020-ct119
26. Jones S, Zhang X, Parsons DW, Lin JC, Leary RJ, Angenendt P, et al. Core Signaling Pathways in Human Pancreatic Cancers Revealed by Global Genomic Analyses. *Science* (2008) 321(5897):1801–6. doi: 10.1126/science.1164368
27. Biankin AV, Waddell N, Kassahn KS, Gingras MC, Muthuswamy LB, Johns AL, et al. Pancreatic Cancer Genomes Reveal Aberrations in Axon Guidance Pathway Genes. *Nature* (2012) 491(7424):399–405. doi: 10.1038/nature11547
28. Waddell N, Pajic M, Patch AM, Chang DK, Kassahn KS, Bailey P, et al. Whole Genomes Redefine the Mutational Landscape of Pancreatic Cancer. *Nature* (2015) 518(7540):495–501. doi: 10.1038/nature14169
29. Hruban RH, Goggins M, Parsons J, Kern SE. Progression Model for Pancreatic Cancer. *Clin Cancer Res* (2000) 6(8):2969–72.
30. Hosoda W, Chianchiano P, Griffin JF, Pittman ME, Brosens LA, Noe M, et al. Genetic Analyses of Isolated High-Grade Pancreatic Intraepithelial Neoplasia (HG-PanIN) Reveal Paucity of Alterations in TP53 and SMAD4. *J Pathol* (2017) 242(1):16–23. doi: 10.1002/path.4884
31. Notta F, Chan-Seng-Yue M, Lemire M, Li Y, Wilson GW, Connor AA, et al. A Renewed Model of Pancreatic Cancer Evolution Based on Genomic Rearrangement Patterns. *Nature* (2016) 538(7625):378–82. doi: 10.1038/nature19823
32. Chan-Seng-Yue M, Kim JC, Wilson GW, Ng K, Figueroa EF, O'Kane GM, et al. Transcription Phenotypes of Pancreatic Cancer are Driven by Genomic Events During Tumor Evolution. *Nat Genet* (2020) 52(2):231–40. doi: 10.1038/s41588-019-0566-9
33. Witkiewicz AK, McMillan EA, Balaji U, Baek G, Lin WC, Mansour J, et al. Whole-Exome Sequencing of Pancreatic Cancer Defines Genetic Diversity and Therapeutic Targets. *Nat Commun* (2015) 6:6744. doi: 10.1038/ncomms7744
34. Sohal DPS, Kennedy EB, Cinar P, Conroy T, Copur MS, Crane CH, et al. Metastatic Pancreatic Cancer: ASCO Guideline Update. *J Clin Oncol* (2020), JCO2001364. doi: 10.1200/JCO.20.01364
35. Robson M, Im SA, Senkus E, Xu B, Domchek SM, Masuda N, et al. Olaparib for Metastatic Breast Cancer in Patients With a Germline Brca Mutation. *N Engl J Med* (2017) 377(6):523–33. doi: 10.1056/NEJMoa1706450
36. Del Campo JM, Matulonis UA, Malander S, Provencher D, Mahner S, Follana P, et al. Niraparib Maintenance Therapy in Patients With Recurrent Ovarian Cancer After a Partial Response to the Last Platinum-Based Chemotherapy in the ENGOT-OV16/NOVA Trial. *J Clin Oncol* (2019) 37 (32):2968–73. doi: 10.1200/JCO.18.02238
37. Pommier Y, O'Connor MJ, de Bono J. Laying a Trap to Kill Cancer Cells: PARP Inhibitors and Their Mechanisms of Action. *Sci Transl Med* (2016) 8 (362):362ps17. doi: 10.1126/scitranslmed.aaf9246
38. Bryant HE, Schultz N, Thomas HD, Parker KM, Flower D, Lopez E, et al. Specific Killing of BRCA2-Deficient Tumours With Inhibitors of Poly(ADP-Ribose) Polymerase. *Nature* (2005) 434(7035):913–7. doi: 10.1038/nature03443
39. Farmer H, McCabe N, Lord CJ, Tutt AN, Johnson DA, Richardson TB, et al. Targeting the DNA Repair Defect in BRCA Mutant Cells as a Therapeutic Strategy. *Nature* (2005) 434(7035):917–21. doi: 10.1038/nature03445
40. Polak P, Kim J, Braunstein LZ, Karlic R, Haradhavala NJ, Tiao G, et al. A Mutational Signature Reveals Alterations Underlying Deficient Homologous Recombination Repair in Breast Cancer. *Nat Genet* (2017) 49(10):1476–86. doi: 10.1038/ng.3934
41. Konstantinopoulos PA, Waggoner S, Vidal GA, Mita M, Moroney JW, Holloway R, et al. Single-Arm Phases 1 and 2 Trial of Niraparib in Combination With Pembrolizumab in Patients With Recurrent Platinum-Resistant Ovarian Carcinoma. *JAMA Oncol* (2019) 5(8):1141–9. doi: 10.1001/jamaoncol.2019.1048
42. Vinayak S, Tolaney SM, Schwartzberg L, Mita M, McCann G, Tan AR, et al. Open-Label Clinical Trial of Niraparib Combined With Pembrolizumab for Treatment of Advanced or Metastatic Triple-Negative Breast Cancer. *JAMA Oncol* (2019) 5(8):1132–40. doi: 10.1001/jamaoncol.2019.1029
43. Hu ZI, Shia J, Stadler ZK, Varghese AM, Capanu M, Salo-Mullen E, et al. Evaluating Mismatch Repair Deficiency in Pancreatic Adenocarcinoma: Challenges and Recommendations. *Clin Cancer Res* (2018) 24(6):1326–36. doi: 10.1158/1078-0432.CCR-17-3099
44. Latham A, Srinivasan P, Kemel Y, Shia J, Bandlamudi C, Mandelker D, et al. Microsatellite Instability Is Associated With the Presence of Lynch Syndrome Pan-Cancer. *J Clin Oncol* (2019) 37(4):286–95. doi: 10.1200/JCO.18.00283
45. Stromnes IM, Hulbert A, Pierce RH, Greenberg PD, Hingorani SR. T-Cell Localization, Activation, and Clonal Expansion in Human Pancreatic Ductal Adenocarcinoma. *Cancer Immunol Res* (2017) 5(11):978–91. doi: 10.1158/2326-6066.CIR-16-0322
46. Li J, Byrne KT, Yan F, Yamazoe T, Chen Z, Baslan T, et al. Tumor Cell-Intrinsic Factors Underlie Heterogeneity of Immune Cell Infiltration and Response to Immunotherapy. *Immunity* (2018) 49(1):178–93.e7. doi: 10.1016/j.immuni.2018.06.006
47. Chen PL, Roh W, Reuben A, Cooper ZA, Spencer CN, Prieto PA, et al. Analysis of Immune Signatures in Longitudinal Tumor Samples Yields Insight Into Biomarkers of Response and Mechanisms of Resistance to Immune Checkpoint Blockade. *Cancer Discovery* (2016) 6(8):827–37. doi: 10.1158/2159-8290.CD-15-1545
48. Kortlever RM, Sodir NM, Wilson CH, Burkhart DL, Pellegrinet L, Brown Swigart L, et al. Myc Cooperates With Ras by Programming Inflammation and Immune Suppression. *Cell* (2017) 171(6):1301–15.e14. doi: 10.1016/j.cell.2017.11.013
49. Peng D, Kryczek I, Nagarsheth N, Zhao L, Wei S, Wang W, et al. Epigenetic Silencing of TH1-Type Chemokines Shapes Tumour Immunity and Immunotherapy. *Nature* (2015) 527(7577):249–53. doi: 10.1038/nature15520
50. Spranger S, Bao R, Gajewski TF. Melanoma-Intrinsic Beta-Catenin Signalling Prevents Anti-Tumour Immunity. *Nature* (2015) 523 (7559):231–5. doi: 10.1038/nature14404
51. Wang G, Lu X, Dey P, Deng P, Wu CC, Jiang S, et al. Targeting YAP-Dependent Mdsc Infiltration Impairs Tumor Progression. *Cancer Discovery* (2016) 6(1):80–95. doi: 10.1158/2159-8290.CD-15-0224
52. Welte T, Kim IS, Tian L, Gao X, Wang H, Li J, et al. Oncogenic mTOR Signalling Recruits Myeloid-Derived Suppressor Cells to Promote Tumour Initiation. *Nat Cell Biol* (2016) 18(6):632–44. doi: 10.1038/ncb3355
53. Le DT, Durham JN, Smith KN, Wang H, Bartlett BR, Aulakh LK, et al. Mismatch Repair Deficiency Predicts Response of Solid Tumors to PD-1 Blockade. *Science* (2017) 357(6349):409–13. doi: 10.1126/science.aan6733
54. Sahin IH, Askan G, Hu ZI, O'Reilly EM. Immunotherapy in Pancreatic Ductal Adenocarcinoma: An Emerging Entity? *Ann Oncol* (2017) 28 (12):2950–61. doi: 10.1093/annonc/mdx503

55. Uzunparmak B, Sahin IH. Pancreatic Cancer Microenvironment: A Current Dilemma. *Clin Transl Med* (2019) 8(1):2. doi: 10.1186/s40169-019-0221-1
56. Balli D, Rech AJ, Stanger BZ, Vonderheide RH. Immune Cytolytic Activity Stratifies Molecular Subsets of Human Pancreatic Cancer. *Clin Cancer Res* (2017) 23(12):3129–38. doi: 10.1158/1078-0432.CCR-16-2128
57. Bailey P, Chang DK, Forget MA, Lucas FA, Alvarez HA, Haymaker C, et al. Exploiting the Neoantigen Landscape for Immunotherapy of Pancreatic Ductal Adenocarcinoma. *Sci Rep* (2016) 6:35848. doi: 10.1038/srep35848
58. Gunderson AJ, Kaneda MM, Tsujikawa T, Nguyen AV, Affara NI, Ruffell B, et al. Bruton Tyrosine Kinase-Dependent Immune Cell Cross-talk Drives Pancreas Cancer. *Cancer Discovery* (2016) 6(3):270–85. doi: 10.1158/2159-8290.CD-15-0827
59. Balachandran VP, Luksza M, Zhao JN, Makarov V, Moral JA, Remark R, et al. Identification of Unique Neoantigen Qualities in Long-Term Survivors of Pancreatic Cancer. *Nature* (2017) 551(7681):512–6. doi: 10.1038/nature24462
60. Sahin IH, Akce M, Alese O, Shaib W, Lesinski GB, El-Rayes B, et al. Immune Checkpoint Inhibitors for the Treatment of MSI-H/MMR-D Colorectal Cancer and a Perspective on Resistance Mechanisms. *Br J Cancer* (2019) 121(10):809–18. doi: 10.1038/s41416-019-0599-y
61. Grant RC, Denroche R, Jang GH, Nowak KM, Zhang A, Borgida A, et al. Clinical and Genomic Characterisation of Mismatch Repair Deficient Pancreatic Adenocarcinoma. *Gut* (2020). doi: 10.1136/gutjnl-2020-320730
62. Ostrem JM, Peters U, Sos ML, Wells JA, Shokat KM. K-Ras(G12C) Inhibitors Allosterically Control GTP Affinity and Effector Interactions. *Nature* (2013) 503(7477):548–51. doi: 10.1038/nature12796
63. Canon J, Rex K, Saiki AY, Mohr C, Cooke K, Bagal D, et al. The Clinical KRAS(G12C) Inhibitor AMG 510 Drives Anti-Tumour Immunity. *Nature* (2019) 575(7781):217–23. doi: 10.1038/s41586-019-1694-1
64. Hallin J, Engstrom LD, Hargis L, Calinisan A, Aranda R, Briere DM, et al. The KRAS(G12C) Inhibitor MRTX849 Provides Insight Toward Therapeutic Susceptibility of KRAS-Mutant Cancers in Mouse Models and Patients. *Cancer Discovery* (2020) 10(1):54–71. doi: 10.1158/2159-8290.CD-19-1167
65. Laetsch TW, DuBois SG, Mascarenhas L, Turpin B, Federman N, Albert CM, et al. Larotrectinib for Paediatric Solid Tumours Harbouring NTRK Gene Fusions: Phase 1 Results From a Multicentre, Open-Label, Phase 1/2 Study. *Lancet Oncol* (2018) 19(5):705–14. doi: 10.1016/s1470-2045(18)30119-0
66. Nevala-Plagemann C, Hidalgo M, Garrido-Laguna I. From State-of-the-Art Treatments to Novel Therapies for Advanced-Stage Pancreatic Cancer. *Nat Rev Clin Oncol* (2020) 17(2):108–23. doi: 10.1038/s41571-019-0281-6
67. Pishvaian MJ, Rolfo CD, Liu SV, Multani PS, Chow Maneval E, Garrido-Laguna I. Clinical Benefit of Entrectinib for Patients With Metastatic Pancreatic Cancer Who Harbor NTRK and ROS1 Fusions. *J Clin Oncol* (2018) 36(4_suppl):521–. doi: 10.1200/JCO.2018.36.4_suppl.521
68. Heining C, Horak P, Uhrig S, Codo PL, Klink B, Hutter B, et al. Nrg1 Fusions in KRAS Wild-Type Pancreatic Cancer. *Cancer Discovery* (2018) 8(9):1087–95. doi: 10.1158/2159-8290.CD-18-0036
69. Jones MR, Williamson LM, Topham JT, Lee MKC, Goytain A, Ho J, et al. Nrg1 Gene Fusions Are Recurrent, Clinically Actionable Gene Rearrangements in KRAS Wild-Type Pancreatic Ductal Adenocarcinoma. *Clin Cancer Res* (2019) 25(15):4674–81. doi: 10.1158/1078-0432.CCR-19-0191
70. Tuli R, Lo S, Koo J, Pishvaian M, Bender RJ, Petricoin E, et al. Anaplastic Lymphoma Kinase Rearrangement and Response to Crizotinib in Pancreatic Ductal Adenocarcinoma. *JCO Precis Oncol* (2017) 1):1–5. doi: 10.1200/po.17.00016
71. Collisson EA, Trejo CL, Silva JM, Gu S, Korkola JE, Heiser LM, et al. A Central Role for RAF–>MEK–>ERK Signaling in the Genesis of Pancreatic Ductal Adenocarcinoma. *Cancer Discov* (2012) 2(8):685–93. doi: 10.1158/2159-8290.CD-11-0347
72. Nakamura Y, Yoshino T. Clinical Utility of Analyzing Circulating Tumor DNA in Patients With Metastatic Colorectal Cancer. *Oncologist* (2018) 23 (11):1310–8. doi: 10.1634/theoncologist.2017-0621
73. Nakamura Y, Shitara K. Development of Circulating Tumour DNA Analysis for Gastrointestinal Cancers. *ESMO Open* (2020) 5(Suppl 1):e000600. doi: 10.1136/esmoopen-2019-000600
74. Rothwell DG, Ayub M, Cook N, Thistlethwaite F, Carter L, Dean E, et al. Utility of ctDNA to Support Patient Selection for Early Phase Clinical Trials: The TARGET Study. *Nat Med* (2019) 25(5):738–43. doi: 10.1038/s41591-019-0380-z
75. Raphael BJ, Hruban RH, Aguirre AJ, Moffitt RA, Yeh JJ, Stewart C, et al. Integrated Genomic Characterization of Pancreatic Ductal Adenocarcinoma. *Cancer Cell* (2017) 32(2):185–203.e13. doi: 10.1016/j.ccell.2017.07.007
76. Puleo F, Nicolle R, Blum Y, Cros J, Marisa L, Demetter P, et al. Stratification of Pancreatic Ductal Adenocarcinomas Based on Tumor and Microenvironment Features. *Gastroenterology* (2018) 155(6):1999–2013.e3. doi: 10.1053/j.gastro.2018.08.033
77. Maurer C, Holmstrom SR, He J, Laise P, Su T, Ahmed A, et al. Experimental Microdissection Enables Functional Harmonisation of Pancreatic Cancer Subtypes. *Gut* (2019) 68(6):1034–43. doi: 10.1136/gutjnl-2018-317706
78. Martinelli P, Carrillo-de Santa Pau E, Cox T, Sainz BJr., Dusetti N, Greenhalf W, et al. GATA6 Regulates EMT and Tumour Dissemination, and is a Marker of Response to Adjuvant Chemotherapy in Pancreatic Cancer. *Gut* (2017) 66(9):1665–76. doi: 10.1136/gutjnl-2015-311256
79. Rashid NU, Peng XL, Jin C, Moffitt RA, Volmar KE, Belt BA, et al. Purity Independent Subtyping of Tumors (Purist), A Clinically Robust, Single-Sample Classifier for Tumor Subtyping in Pancreatic Cancer. *Clin Cancer Res* (2020) 26(1):82–92. doi: 10.1158/1078-0432.Ccr-19-1467
80. Adams CR, Htwe HH, Marsh T, Wang AL, Montoya ML, Subbaraj L, et al. Transcriptional Control of Subtype Switching Ensures Adaptation and Growth of Pancreatic Cancer. *Elife* (2019) 8:e45313. doi: 10.7554/eLife.45313
81. Somerville TDD, Xu Y, Miyabayashi K, Tiriac H, Cleary CR, Maia-Silva D, et al. Tp63-Mediated Enhancer Reprogramming Drives the Squamous Subtype of Pancreatic Ductal Adenocarcinoma. *Cell Rep* (2018) 25 (7):1741–55.e7. doi: 10.1016/j.celrep.2018.10.051
82. Andricovich J, Perkail S, Kai Y, Casasanta N, Peng W, Tzatsos A. Loss of KDM6A Activates Super-Enhancers to Induce Gender-Specific Squamous-like Pancreatic Cancer and Confers Sensitivity to BET Inhibitors. *Cancer Cell* (2018) 33(3):512–26.e8. doi: 10.1016/j.ccell.2018.02.003
83. Mueller S, Engleitner T, Maresch R, Zukowska M, Lange S, Kaltenbacher T, et al. Evolutionary Routes and KRAS Dosage Define Pancreatic Cancer Phenotypes. *Nature* (2018) 554(7690):62–8. doi: 10.1038/nature25459
84. Collins MA, Bednar F, Zhang Y, Brisset JC, Galban S, Galban CJ, et al. Oncogenic Kras is Required for Both the Initiation and Maintenance of Pancreatic Cancer in Mice. *J Clin Invest* (2012) 122(2):639–53. doi: 10.1172/JCI59227
85. Kapoor A, Yao W, Ying H, Hua S, Liewen A, Wang Q, et al. Yap1 Activation Enables Bypass of Oncogenic Kras Addiction in Pancreatic Cancer. *Cell* (2019) 179(5):1239. doi: 10.1016/j.cell.2019.10.037
86. Shao DD, Xue W, Krall EB, Bhutkar A, Piccioni F, Wang X, et al. KRAS and YAP1 Converge to Regulate EMT and Tumor Survival. *Cell* (2014) 158 (1):171–84. doi: 10.1016/j.cell.2014.06.004
87. Miyabayashi K, Baker LA, Deschenes A, Traub B, Caligiuri G, Plenker D, et al. Intraductal Transplantation Models of Human Pancreatic Ductal Adenocarcinoma Reveal Progressive Transition of Molecular Subtypes. *Cancer Discovery* (2020) 10(10):1566–89. doi: 10.1158/2159-8290.CD-20-0133
88. Provenzano PP, Cuevas C, Chang AE, Goel VK, Von Hoff DD, Hingorani SR. Enzymatic Targeting of the Stroma Ablates Physical Barriers to Treatment of Pancreatic Ductal Adenocarcinoma. *Cancer Cell* (2012) 21 (3):418–29. doi: 10.1016/j.ccr.2012.01.007
89. Catenacci DV, Junttila MR, Karrison T, Bahary N, Horiba MN, Nattam SR, et al. Randomized Phase Ib/Ii Study of Gemcitabine Plus Placebo or Vismodegib, a Hedgehog Pathway Inhibitor, in Patients With Metastatic Pancreatic Cancer. *J Clin Oncol* (2015) 33(36):4284–92. doi: 10.1200/JCO.2015.62.8719
90. De Jesus-Acosta A, Sugar EA, O'Dwyer PJ, Ramanathan RK, Von Hoff DD, Rasheed Z, et al. Phase 2 Study of Vismodegib, a Hedgehog Inhibitor, Combined With Gemcitabine and Nab-Paclitaxel in Patients With Untreated Metastatic Pancreatic Adenocarcinoma. *Br J Cancer* (2020) 122 (4):498–505. doi: 10.1038/s41416-019-0683-3
91. Van Cutsem E, Tempero MA, Sigal D, Oh DY, Fazio N, Macarulla T, et al. Randomized Phase Iii Trial of Pegvorhyaluronidase Alfa With Nab-Paclitaxel Plus Gemcitabine for Patients With Hyaluronan-High Metastatic Pancreatic Adenocarcinoma. *J Clin Oncol* (2020) 38(27):3185–94. doi: 10.1200/JCO.20.00590

92. Ohlund D, Handly-Santana A, Biffi G, Elyada E, Almeida AS, Ponz-Sarvise M, et al. Distinct Populations of Inflammatory Fibroblasts and Myofibroblasts in Pancreatic Cancer. *J Exp Med* (2017) 214(3):579–96. doi: 10.1084/jem.20162024
93. Biffi G, Oni TE, Spielman B, Hao Y, Elyada E, Park Y, et al. Il1-Induced JAK/STAT Signaling Is Antagonized by TGFbeta to Shape Caf Heterogeneity in Pancreatic Ductal Adenocarcinoma. *Cancer Discovery* (2019) 9(2):282–301. doi: 10.1158/2159-8290.CD-18-0710
94. Elyada E, Bolisetty M, Laise P, Flynn WF, Courtois ET, Burkhart RA, et al. Cross-Species Single-Cell Analysis of Pancreatic Ductal Adenocarcinoma Reveals Antigen-Presenting Cancer-Associated Fibroblasts. *Cancer Discovery* (2019) 9(8):1102–23. doi: 10.1158/2159-8290.CD-19-0094
95. Ligorio M, Sil S, Malagon-Lopez J, Nieman LT, Misale S, Di Pilato M, et al. Stromal Microenvironment Shapes the Intratumoral Architecture of Pancreatic Cancer. *Cell* (2019) 178(1):160–75.e27. doi: 10.1016/j.cell.2019.05.012
96. Nicolle R, Blum Y, Marisa L, Loncle C, Gayet O, Moutardier V, et al. Pancreatic Adenocarcinoma Therapeutic Targets Revealed by Tumor-Stroma Cross-Talk Analyses in Patient-Derived Xenografts. *Cell Rep* (2017) 21(9):2458–70. doi: 10.1016/j.celrep.2017.11.003
97. Zhu Y, Knolhoff BL, Meyer MA, Nywening TM, West BL, Luo J, et al. CSF1/CSF1R Blockade Reprograms Tumor-Infiltrating Macrophages and Improves Response to T-cell Checkpoint Immunotherapy in Pancreatic Cancer Models. *Cancer Res* (2014) 74(18):5057–69. doi: 10.1158/0008-5472.CAN-13-3723
98. Candido JB, Morton JP, Bailey P, Campbell AD, Karim SA, Jamieson T, et al. Csf1r(+) Macrophages Sustain Pancreatic Tumor Growth Through T Cell Suppression and Maintenance of Key Gene Programs That Define the Squamous Subtype. *Cell Rep* (2018) 23(5):1448–60. doi: 10.1016/j.celrep.2018.03.131
99. Nywening TM, Belt BA, Cullinan DR, Panni RZ, Han BJ, Sanford DE, et al. Targeting Both Tumour-Associated CXCR2(+) Neutrophils and CCR2(+) Macrophages Disrupts Myeloid Recruitment and Improves Chemotherapeutic Responses in Pancreatic Ductal Adenocarcinoma. *Gut* (2018) 67(6):1112–23. doi: 10.1136/gutjnl-2017-313738
100. Steele CW, Karim SA, Leach JDG, Bailey P, Upstill-Goddard R, Rishi L, et al. Cxcr2 Inhibition Profoundly Suppresses Metastases and Augments Immunotherapy in Pancreatic Ductal Adenocarcinoma. *Cancer Cell* (2016) 29(6):832–45. doi: 10.1016/j.ccell.2016.04.014
101. Ramanathan RK, McDonough SL, Philip PA, Hingorani SR, Lacy J, Kortmansky JS, et al. Phase IB/II Randomized Study of FOLFIRINOX Plus Pegylated Recombinant Human Hyaluronidase Versus Folfirinox Alone in Patients With Metastatic Pancreatic Adenocarcinoma: Swog S1313. *J Clin Oncol* (2019) 37(13):1062–9. doi: 10.1200/JCO.18.01295
102. Hingorani SR, Zheng L, Bullock AJ, Seery TE, Harris WP, Sigal DS, et al. Halo 202: Randomized Phase II Study of PEGPH20 Plus Nab-Paclitaxel/Gemcitabine Versus Nab-Paclitaxel/Gemcitabine in Patients With Untreated, Metastatic Pancreatic Ductal Adenocarcinoma. *J Clin Oncol* (2018) 36(4):359–66. doi: 10.1200/JCO.2017.74.9564
103. Ho WJ, Jaffee EM, Zheng L. The Tumour Microenvironment in Pancreatic Cancer - Clinical Challenges and Opportunities. *Nat Rev Clin Oncol* (2020) 17(9):527–40. doi: 10.1038/s41571-020-0363-5
104. Broutier L, Mastrogiovanni G, Verstegen MM, Francies HE, Gavarro LM, Bradshaw CR, et al. Human Primary Liver Cancer-Derived Organoid Cultures for Disease Modeling and Drug Screening. *Nat Med* (2017) 23(12):1424–35. doi: 10.1038/nm.4438
105. Nanki K, Toshimitsu K, Takano A, Fujii M, Shimokawa M, Ohta Y, et al. Divergent Routes Toward Wnt and R-spondin Niche Independency During Human Gastric Carcinogenesis. *Cell* (2018) 174(4):856–69.e17. doi: 10.1016/j.cell.2018.07.027
106. Yan HHN, Siu HC, Law S, Ho SL, Yue SSK, Tsui WY, et al. A Comprehensive Human Gastric Cancer Organoid Biobank Captures Tumor Subtype Heterogeneity and Enables Therapeutic Screening. *Cell Stem Cell* (2018) 23(6):882–97.e11. doi: 10.1016/j.stem.2018.09.016
107. Sachs N, de Ligt J, Kopper O, Gogola E, Bounova G, Weeber F, et al. A Living Biobank of Breast Cancer Organoids Captures Disease Heterogeneity. *Cell* (2018) 172(1-2):373–86.e10. doi: 10.1016/j.cell.2017.11.010
108. Lee SH, Hu W, Matulay JT, Silva MV, Owczarek TB, Kim K, et al. Tumor Evolution and Drug Response in Patient-Derived Organoid Models of Bladder Cancer. *Cell* (2018) 173(2):515–28.e17. doi: 10.1016/j.cell.2018.03.017
109. Mullenders J, de Jongh E, Brousali A, Roosen M, Blom JPA, Begthel H, et al. Mouse and Human Urothelial Cancer Organoids: A Tool for Bladder Cancer Research. *Proc Natl Acad Sci USA* (2019) 116(10):4567–74. doi: 10.1073/pnas.1803595116
110. Li X, Francies HE, Secrier M, Perner J, Miremadi A, Galeano-Dalmau N, et al. Organoid Cultures Recapitulate Esophageal Adenocarcinoma Heterogeneity Providing a Model for Clonality Studies and Precision Therapeutics. *Nat Commun* (2018) 9(1):2983. doi: 10.1038/s41467-018-05190-9
111. Hill SJ, Decker B, Roberts EA, Horowitz NS, Muto MG, Worley MJJr., et al. Prediction of DNA Repair Inhibitor Response in Short-Term Patient-Derived Ovarian Cancer Organoids. *Cancer Discovery* (2018) 8(11):1404–21. doi: 10.1158/2159-8290.CD-18-0474
112. Kopper O, de Witte CJ, Lohmussaar K, Valle-Inclan JE, Hami N, Kester L, et al. An Organoid Platform for Ovarian Cancer Captures Intra- and Interpatient Heterogeneity. *Nat Med* (2019) 25(5):838–49. doi: 10.1038/s41591-019-0422-6
113. Sachs N, Papaspyropoulos A, Zomer-van Ommen DD, Heo I, Bottinger L, Klay D, et al. Long-Term Expanding Human Airway Organoids for Disease Modeling. *EMBO J* (2019) 38(4):e100300. doi: 10.15252/embj.2018100300
114. Schutgens F, Rookmaaker MB, Margaritis T, Rios A, Ammerlaan C, Jansen J, et al. Tubuloids Derived From Human Adult Kidney and Urine for Personalized Disease Modeling. *Nat Biotechnol* (2019) 37(3):303–13. doi: 10.1038/s41587-019-0048-8
115. Nuciforo S, Fofana I, Matter MS, Blumer T, Calabrese D, Boldanova T, et al. Organoid Models of Human Liver Cancers Derived From Tumor Needle Biopsies. *Cell Rep* (2018) 24(5):1363–76. doi: 10.1016/j.celrep.2018.07.001
116. Weeber F, van de Wetering M, Hoogstraat M, Dijkstra KK, Krijgsman O, Kuilman T, et al. Preserved Genetic Diversity in Organoids Cultured From Biopsies of Human Colorectal Cancer Metastases. *Proc Natl Acad Sci USA* (2015) 112(43):13308–11. doi: 10.1073/pnas.1516689112
117. Vlachogiannis G, Hedayat S, Vatsiou A, Jamin Y, Fernandez-Mateos J, Khan K, et al. Patient-Derived Organoids Model Treatment Response of Metastatic Gastrointestinal Cancers. *Science* (2018) 359(6378):920–6. doi: 10.1126/science.aao2774
118. Pauli C, Hopkins BD, Prandi D, Shaw R, Fedrizzi T, Sboner A, et al. Personalized In Vitro and In Vivo Cancer Models to Guide Precision Medicine. *Cancer Discovery* (2017) 7(5):462–77. doi: 10.1158/2159-8290.CD-16-1154
119. Gao D, Vela I, Sboner A, Iaquinta PJ, Karthaus WR, Gopalan A, et al. Organoid Cultures Derived From Patients With Advanced Prostate Cancer. *Cell* (2014) 159(1):176–87. doi: 10.1016/j.cell.2014.08.016
120. Neal JT, Li X, Zhu J, Giangarra V, Grzeskowiak CL, Ju J, et al. Organoid Modeling of the Tumor Immune Microenvironment. *Cell* (2018) 175(7):1972–88.e16. doi: 10.1016/j.cell.2018.11.021
121. Dijkstra KK, Cattaneo CM, Weeber F, Chalabi M, van de Haar J, Fanchi LF, et al. Generation of Tumor-Reactive T Cells by Co-culture of Peripheral Blood Lymphocytes and Tumor Organoids. *Cell* (2018) 174(6):1586–98.e12. doi: 10.1016/j.cell.2018.07.009
122. Boj SF, Hwang CI, Baker LA, Chio II, Engle DD, Corbo V, et al. Organoid Models of Human and Mouse Ductal Pancreatic Cancer. *Cell* (2015) 160(1-2):324–38. doi: 10.1016/j.cell.2014.12.021
123. Calles A, Rubio-Viqueira B, Hidalgo M. Primary Human non-Small Cell Lung and Pancreatic Tumorgraft Models–Utility and Applications in Drug Discovery and Tumor Biology. *Curr Protoc Pharmacol* (2013) Chapter 14: Unit 14 26. doi: 10.1002/0471141755.ph1426s61
124. Garrido-Laguna I, Tan AC, Uson M, Angenendt M, Ma WW, Villaroel MC, et al. Integrated Preclinical and Clinical Development of mTOR Inhibitors in Pancreatic Cancer. *Br J Cancer* (2010) 103(5):649–55. doi: 10.1038/sj.bjc.6605819
125. Jimeno A, Amador ML, Kulesza P, Wang X, Rubio-Viqueira B, Zhang X, et al. Assessment of Celecoxib Pharmacodynamics in Pancreatic Cancer. *Mol Cancer Ther* (2006) 5(12):3240–7. doi: 10.1158/1535-7163.MCT-06-0565
126. Johnson JI, Decker S, Zaharevitz D, Rubinstein LV, Venditti JM, Schepartz S, et al. Relationships Between Drug Activity in NCI Preclinical *In Vitro* and *In Vivo* Models and Early Clinical Trials. *Br J Cancer* (2001) 84(10):1424–31. doi: 10.1054/bjoc.2001.1796

127. Daniel VC, Marchionni L, Hierman JS, Rhodes JT, Devereux WL, Rudin CM, et al. A Primary Xenograft Model of Small-Cell Lung Cancer Reveals Irreversible Changes in Gene Expression Imposed by Culture *In Vitro*. *Cancer Res* (2009) 69(8):3364–73. doi: 10.1158/0008-5472.CAN-08-4210
128. Rubio-Viqueira B, Jimeno A, Cusatis G, Zhang X, Iacobuzio-Donahue C, Karikari C, et al. An *In Vivo* Platform for Translational Drug Development in Pancreatic Cancer. *Clin Cancer Res* (2006) 12(15):4652–61. doi: 10.1158/1078-0432.CCR-06-0113
129. Bertotti A, Migliardi G, Galimi F, Sassi F, Torti D, Isella C, et al. A Molecularly Annotated Platform of Patient-Derived Xenografts ("Xenopatients") Identifies HER2 as an Effective Therapeutic Target in Cetuximab-Resistant Colorectal Cancer. *Cancer Discovery* (2011) 1(6):508–23. doi: 10.1158/2159-8290.CD-11-0109
130. Julien S, Merino-Trigo A, Lacroix L, Pocard M, Goere D, Mariani P, et al. Characterization of a Large Panel of Patient-Derived Tumor Xenografts Representing the Clinical Heterogeneity of Human Colorectal Cancer. *Clin Cancer Res* (2012) 18(19):5314–28. doi: 10.1158/1078-0432.CCR-12-0372
131. Garrido-Laguna I, Uson M, Rajeshkumar NV, Tan AC, de Oliveira E, Karikari C, et al. Tumor Engraftment in Nude Mice and Enrichment in Stroma- Related Gene Pathways Predict Poor Survival and Resistance to Gemcitabine in Patients With Pancreatic Cancer. *Clin Cancer Res* (2011) 17 (17):5793–800. doi: 10.1158/1078-0432.CCR-11-0341
132. Keysar SB, Astling DP, Anderson RT, Vogler BW, Bowles DW, Morton JJ, et al. A Patient Tumor Transplant Model of Squamous Cell Cancer Identifies PI3K Inhibitors as Candidate Therapeutics in Defined Molecular Bins. *Mol Oncol* (2013) 7(4):776–90. doi: 10.1016/j.molonc.2013.03.004
133. Hidalgo M, Bruckheimer E, Rajeshkumar NV, Garrido-Laguna I, De Oliveira E, Rubio-Viqueira B, et al. A Pilot Clinical Study of Treatment Guided by Personalized Tumorgrafts in Patients With Advanced Cancer. *Mol Cancer Ther* (2011) 10(8):1311–6. doi: 10.1158/1535-7163.MCT-11-0233
134. Von Hoff DD, Ervin T, Arena FP, Chiorean EG, Infante J, Moore M, et al. Increased Survival in Pancreatic Cancer With Nab-Paclitaxel Plus Gemcitabine. *N Engl J Med* (2013) 369(18):1691–703. doi: 10.1056/NEJMoa1304369
135. Nam HJ, Im SA, Oh DY, Elvin P, Kim HP, Yoon YK, et al. Antitumor Activity of Saracatinib (AZD0530), A c-Src/Abl Kinase Inhibitor, Alone or in Combination With Chemotherapeutic Agents in Gastric Cancer. *Mol Cancer Ther* (2013) 12(1):16–26. doi: 10.1158/1535-7163.MCT-12-0109
136. Vidal A, Munoz C, Guillen MJ, Moreto J, Puertas S, Martinez-Iniesta M, et al. Lurbinectedin (PM01183), a New DNA Minor Groove Binder, Inhibits Growth of Orthotopic Primary Graft of Cisplatin-Resistant Epithelial Ovarian Cancer. *Clin Cancer Res* (2012) 18(19):5399–411. doi: 10.1158/1078-0432.CCR-12-1513
137. Das Thakur M, Salangsang F, Landman AS, Sellers WR, Pryer NK, Levesque MP, et al. Modelling Vemurafenib Resistance in Melanoma Reveals a Strategy to Forestall Drug Resistance. *Nature* (2013) 494(7436):251–5. doi: 10.1038/nature11814
138. Sebastiani V, Ricci F, Rubio-Viqueira B, Kulesza P, Yeo CJ, Hidalgo M, et al. Immunohistochemical and Genetic Evaluation of Deoxycytidine Kinase in Pancreatic Cancer: Relationship to Molecular Mechanisms of Gemcitabine Resistance and Survival. *Clin Cancer Res* (2006) 12(8):2492–7. doi: 10.1158/1078-0432.CCR-05-2655
139. Moestue S, Sitter B, Bathen TF, Tessem MB, Gribbestad IS. Hr MAS MR Spectroscopy in Metabolic Characterization of Cancer. *Curr Top Med Chem* (2011) 11(1):2–26. doi: 10.2174/156802611793611869
140. Moestue SA, Huuse EM, Lindholm EM, Bofin A, Engebraaten O, Maelandsmo GM, et al. Low-Molecular Contrast Agent Dynamic Contrast-Enhanced (DCE)-MRI and Diffusion-Weighted (DW)-MRI in Early Assessment of Bevacizumab Treatment in Breast Cancer Xenografts. *J Magn Reson Imaging* (2013) 38(5):1043–53. doi: 10.1002/jmri.24079
141. Baccelli I, Schneeweiss A, Riethdorf S, Stenzinger A, Schillert A, Vogel V, et al. Identification of a Population of Blood Circulating Tumor Cells From Breast Cancer Patients That Initiates Metastasis in a Xenograft Assay. *Nat Biotechnol* (2013) 31(6):539–44. doi: 10.1038/nbt.2576
142. Williams ES, Rodriguez-Bravo V, Chippada-Venkata U, De Ia Iglesia-Vicente J, Gong Y, Galsky M, et al. Generation of Prostate Cancer Patient Derived Xenograft Models From Circulating Tumor Cells. *J Vis Exp* (2015) (105):53182. doi: 10.3791/53182
143. Toyoshima K, Hayashi A, Kashiwagi M, Hayashi N, Iwatsuki M, Ishimoto T, et al. Analysis of Circulating Tumor Cells Derived From Advanced Gastric Cancer. *Int J Cancer* (2015) 137(4):991–8. doi: 10.1002/ijc.29455
144. Hodgkinson CL, Morrow CJ, Li Y, Metcalf RL, Rothwell DG, Trapani F, et al. Tumorigenicity and Genetic Profiling of Circulating Tumor Cells in Small-Cell Lung Cancer. *Nat Med* (2014) 20(8):897–903. doi: 10.1038/nm.3600
145. Girotti MR, Gremel G, Lee R, Galvani E, Rothwell D, Viros A, et al. Application of Sequencing, Liquid Biopsies, and Patient-Derived Xenografts for Personalized Medicine in Melanoma. *Cancer Discovery* (2016) 6(3):286–99. doi: 10.1158/2159-8290.CD-15-1336

Conflict of Interest: The authors declare that the research was conducted in the absence of any commercial or financial relationships that could be construed as a potential conflict of interest.

frontiers in Oncology

REVIEW
published: 05 July 2021
doi: 10.3389/fonc.2021.682217

Therapeutic Potential of Targeting Stromal Crosstalk-Mediated Immune Suppression in Pancreatic Cancer

Wenting Du[1], *Marina Pasca di Magliano*[1,2,3*] *and Yaqing Zhang*[1,2*]

[1] Department of Surgery, University of Michigan, Ann Arbor, MI, United States, [2] Rogel Cancer Center, University of Michigan, Ann Arbor, MI, United States, [3] Department of Cell and Developmental Biology, University of Michigan, Ann Arbor, MI, United States

The stroma-rich, immunosuppressive microenvironment is a hallmark of pancreatic ductal adenocarcinoma (PDA). Tumor cells and other cellular components of the tumor microenvironment, such as cancer associated fibroblasts, $CD4^+$ T cells and myeloid cells, are linked by a web of interactions. Their crosstalk not only results in immune evasion of PDA, but also contributes to pancreatic cancer cell plasticity, invasiveness, metastasis, chemo-resistance, immunotherapy-resistance and radiotherapy-resistance. In this review, we characterize several prevalent populations of stromal cells in the PDA microenvironment and describe how the crosstalk among them drives and maintains immune suppression. We also summarize therapeutic approaches to target the stroma. With a better understanding of the complex cellular and molecular networks in PDA, strategies aimed at sensitizing PDA to chemotherapy or immunotherapy through re-programing the tumor microenvironment can be designed, and in turn lead to improved clinical treatment for pancreatic cancer patients.

Keywords: pancreatic cancer, tumor microenvironment, immune suppression, T cells, myeloid cells, cancer-associated fibroblasts

OPEN ACCESS

Edited by:
Takatsugu Ishimoto, Kumamoto University, Japan

Reviewed by:
Joanna Napp, University Medical Center Göttingen, Germany
Davide Melisi, University of Verona, Italy

***Correspondence:**
Yaqing Zhang
yaqingzh@umich.edu
Marina Pasca di Magliano
marinapa@umich.edu

Specialty section:
This article was submitted to Gastrointestinal Cancers, a section of the journal Frontiers in Oncology

Received: *18 March 2021*
Accepted: *21 June 2021*
Published: *05 July 2021*

Citation:
Du W, Pasca di Magliano M, and Zhang Y (2021) Therapeutic Potential of Targeting Stromal Crosstalk-Mediated Immune Suppression in Pancreatic Cancer. Front. Oncol. 11:682217. doi: 10.3389/fonc.2021.682217

INTRODUCTION

Pancreatic ductal adenocarcinoma (PDA) is the most common form of pancreatic cancer, the third leading cause of cancer related death in the United States, with a 5-year survival rate of around 10% (1, 2). Over 80% of PDA patients are diagnosed at a late stage when the tumor is already locally advanced or metastatic to distant organs and therefore do not qualify for surgery (1). Standard chemotherapy, such as Gemcitabine alone or in combination of Albumin-bound paclitaxel (Abraxane) has long been the standard of care for PDA. However, it provides only modest survival benefit since a large percentage of patients are either intrinsically resistant or develop resistance soon after treatment starts (3). Multidrug regimens such as FOLFIRINOX (combination of oxaliplatin, irinotecan, leucovorin, and fluorouracil) have become standard of care for those patients that can tolerate it, as they increase patient median overall survival to 11.1 months. However, FOLFIRINOX is associated with high toxicity (4). Therefore, there is urgent need for the development of novel therapeutic strategies for PDA patients. Immune checkpoint blockade has achieved significant therapeutic success for a subset of cancer patients. Unfortunately, single agent immunotherapy has been ineffective in PDA (5). The reasons for this failure are complex, and likely stem from the nature of the stroma-rich tumor microenvironment (TME) in PDA, with abundant immunosuppressive cells such as cancer associated fibroblasts (CAFs) (6),

$CD4^+$ T cells (7) and myeloid cells including tumor associated macrophages (TAMs) and myeloid derived suppressor cells (MDSCs) (8–11). The stromal and immune compartments are linked by a web of interactions that promotes immune evasion of PDA cancer cells and contributes to the onset and progression of pancreatic carcinogenesis, affecting cell plasticity, metastasis, chemo-resistance and radiotherapy-resistance (3, 7, 12–18). This review summarizes the crosstalk between several key cell types that are dominant within the immunosuppressive TME of pancreatic cancer and discusses the most promising immune regulatory approaches to activate anti-tumor immune responses in PDA.

THE IMMUNOLOGICALLY "COLD" TME IS MODULATED BY ONCOGENIC PATHWAYS IN PDA

PDA initiates with activating mutation of oncogenes such as *KRAS* (mutant in over 90% of tumors, and present in the majority of precursor lesions as well) (19) and followed by inactivation of tumor suppressors such as *CDKN2A* or *P53* (altered in 90% and 70% of PDAs, respectively) (20–23). Pancreatic cancer develops from precursor lesions such as pancreatic intraepithelial neoplasia (PanIN) that over time progress to advanced and metastatic stage (24). Other types of precursor lesions such as intraductal papillary mucinous neoplasms and mucinous cystic neoplasms (25) are less common and have been reviewed elsewhere (20). Genetically engineered mouse models (GEMMs) that harbor pancreas-specific expression of oncogenic *Kras*, such as KC (*LSL-Kras^{G12D}; p48/Pdx-1-Cre*) (26) and iKras* model (*p48-Cre; R26-rtTa-IRES-EGFP; TetO-Kras^{G12D}*) (27), recapitulate the stepwise carcinogenesis process of human PDA. PanIN occurs spontaneously in these models and can progress to metastatic cancer with long latency. Using the KC model, researchers discovered that immunosuppressive cells, including $CD4^+$ $FOXP3^+$ regulatory T cells (Tregs), TAMs, and MDSCs, accumulate both in PanIN and PDA stages compared to normal pancreas (28). $CD8^+$ cytotoxic T cells are scarce in PanIN and only present in a subset of PDA; even when they are present, they lack effector function (28). Similar kinetics of leukocytic infiltration were also described in the more aggressive KPC (*Kras$^{LSL\text{-}G12D/+}$*; *Trp53$^{LSL\text{-}R172H/+}$*; *Pdx-1-Cre*) GEMM (29). Reduced infiltration of $CD8^+$ cytotoxic T cells and increased infiltration of $CD4^+FOXP3^+CD25^+$ Tregs in PDA have also been shown in human patient samples (30, 31). The evidence from both GEMMs and patient samples indicate an immunologically 'cold' TME of PDA. Even when $CD8^+$ T cells are present within the tumor nest in a small cohort of PDA patients, they are dysfunctional or exhausted (32). Recently, our laboratory defined an exhausted $CD8^+$ T cell phenotype in human PDA by expression of T cell immunoglobulin and ITIM domains (TIGIT), an immune checkpoint that is relatively understudied (11). Using a combination of mass cytometry, single-cell RNA sequencing (scRNA-seq) and multiplex immunohistochemistry, we found increased markers of $CD8^+$ T cell dysfunction with an up-regulation of TIGIT in PDA compared to non-malignant pancreas samples; further, the dysfunctional status of $CD8^+$ T cells was more pronounced at later stages of carcinogenesis (11).

Oncogenic *KRAS* is a key mediator of immune suppression in PDA. A recent study using scRNA-seq approaches and TCGA data analysis suggest greater immune infiltration in KRAS independent and KRAS-low tumors compared to KRAS dependent and KRAS-high groups (33). In this model, inactivation of mutant *Kras* in PDA cells did not affect their tumorigenic capacity, but led to failure to evade the host immune system (33). The authors determined that KRAS knockout (KO) PDA cells had a striking up-regulation of major histocompatibility complex I (MHC I) genes compared with KRAS intact control cells, underlying increased susceptibility to anti-tumor immunity. M1-like TAMs, $CD8^+$ cytotoxic T cells and natural killer T (NK T) cells dominated in KRAS KO tumors. Mechanistically, this study identified BRAF and MYC as key downstream regulators of KRAS-driven tumor immune suppression for PDA maintenance (33). MHC I accumulation in the cell is also negatively regulated by autophagy, which is in turn activated by oncogenic KRAS (34).

KRAS activates essential pathways to control the expression and secretion of cytokines and chemokines from tumor cells, thereby regulating the recruitment and development of immune cells. For example, granulocyte–macrophage colony-stimulating factor (GM-CSF) produced by pancreatic cancer cells carrying the *KRAS^{G12D}* mutation recruits immunosuppressive myeloid cells (35, 36). A key downstream effector of *Kras^{G12D}* is the mitogen –activated protein kinase kinase (MEK)/extracellular signal-regulated kinase (ERK) pathway. Mitogen-activated protein kinases (MAPK)/ERK targets include interleukin-10 (IL-10) and transforming growth factor beta (TGF-β), which in turn induce Treg differentiation (37). MAPK/ERK signaling also induces expression of intercellular adhesion molecule (ICAM-1), which acts as chemoattractant for macrophages (38). Besides, growth and differentiation factor 15 (GDF-15), a direct target of nuclear factor kappa B (NF-κB) in tumor cells, suppresses the pro-apoptotic activity of macrophages by inhibiting tumor necrosis factor (TNF) and nitric oxide (NO) production (39). Depletion of GDF-15 in the KPC mouse model delayed tumor development and was accompanied by increased infiltrating antitumor macrophages (39). Extracellular *Kras^{G12D}* in tumor-derived exosomes directly promotes alternatively activated or M2-like macrophage polarization *via* signal transducer and activator of transcription 3 (STAT3)-dependent fatty acid oxidation (40). Blocking *Kras^{G12D}* release from tumor cells and uptake by macrophages suppresses macrophage-mediated pancreatic tumor growth *in vivo* (40). Other inflammatory mediators secreted by PDA cells include granulocyte colony-stimulating factor (G-CSF) (41), IL-6 (42), IL-1α (43), IL-1β (44, 45), ubiquitin specific peptidase 22 (USP22) (46), C-X-C motif chemokine ligand 8 (CXCL8) (47), matrix metallopeptidase 9 (MMP-9) and indoleamine-2,3-dioxygenase (IDO) (48), which all contribute to the establishment of immunosuppressive TME in pancreatic cancer (**Figure 1**).

PDA cells can also induce immune suppression by engaging critical immune checkpoint pathways such as programmed cell death protein 1 (PD1)/programmed death-ligand 1 (PD-L1). In addition, we recently discovered that Poliovirus receptor (PVR), one of the checkpoint TIGIT ligands, is expressed by tumor epithelial cells (11). Previously we showed that expression of PD-L1 in PDA cancer cells is

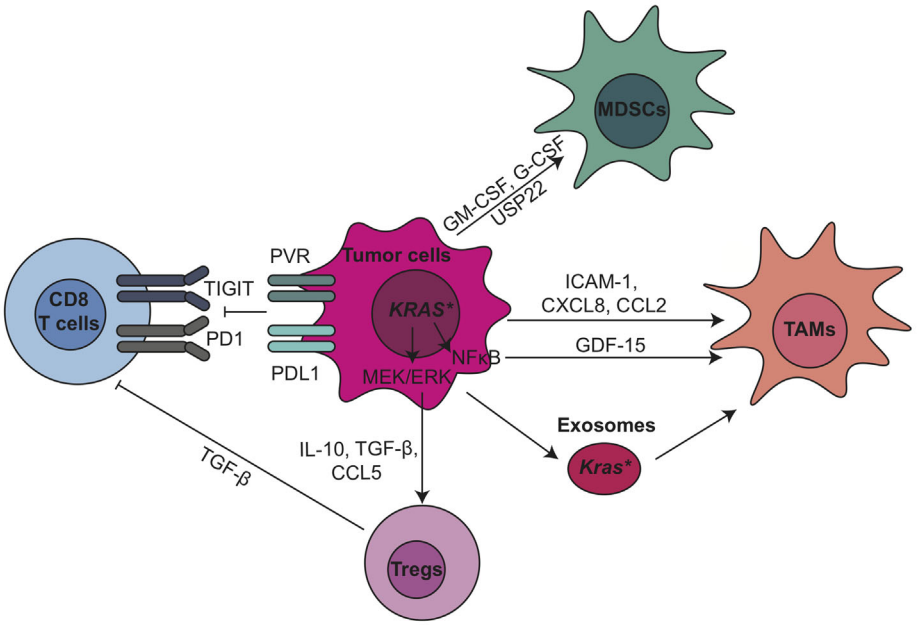

FIGURE 1 | Tumor epithelial cells modulate immunosuppressive tumor microenvironment through oncogenic pathways and immune checkpoint pathways in PDA. CCL, C-C motif chemokine ligand; CXCL, C-X-C motif chemokine ligand; ERK, extracellular signal-regulated kinase; G-CSF, granulocyte-colony stimulating factor; GDF-15, growth/differentiation factor-15; GM-CSF, granulocyte-macrophage colony-stimulating factor; ICAM-1, intercellular adhesion molecule 1; MDSCs, myeloid-derived suppressor cells; MEK, mitogen–activated protein kinase kinase; NF-κB, nuclear factor kappa B; PD-1, anti-programmed cell death 1; PD-L1, programmed cell death ligand 1; PVR, poliovirus receptor; TAMs, tumor associated macrophages; TGF-β, transforming growth factor β; TIGIT, T cell immunoreceptor with Ig and ITIM domains; Tregs, regulatory T cells; USP22, ubiquitin specific peptidase 22.

regulated by epidermal growth factor receptor (EGFR)/MAPK signaling cascade (49). PD-L1 expressed by PDA cells directly induced the apoptosis of PD-1-expressing T cells, and its expression positively correlated with poor prognosis and inversely correlated with tumor-infiltrating T cells, particularly $CD8^+$ T cells, in pancreatic cancer (50). These pre-clinical data have encouraged clinical trials targeting PD-1 and PD-L1, either as monotherapy or in combination with radiation or chemotherapy, in pancreatic cancer (**Table 1**, current active clinical trials, and **Table 2**, past clinical trials targeting pancreatic cancer TME). However, single agent immune checkpoint blockade has thus far been unsuccessful in PDA patients. One potential reason for this failure is the exclusion of active T cells from TME, which reveals an urgent need for strategies transforming the immunologically 'cold' microenvironment into 'hot'. Targeting oncogenic signaling pathways such as KRAS, BRAF and MEK potentially provides an opportunity to alter the TME and sensitize PDA to immune checkpoint blockade (33, 51).

$CD4^+$ T CELLS AND THEIR CROSSTALK WITH STROMAL CELLS NEGATIVELY REGULATE THE TUMOR IMMUNITY IN PDA

$CD4^+$ T cells infiltrate into the pancreas starting at early stages (PanINs) of carcinogenesis (28). Genetic depletion of $CD4^+$ T cells increased tumor infiltrating $CD8^+$ T cells and up-regulated their capacity to produce IFN-γ and granzyme B, therefore inhibiting tumorigenesis in a GEMM of PDA in a $CD8^+$ T cell-dependent manner (7). This highlights that the formation of immunosuppressive microenvironment occurs even at the onset of pancreatic tumorigenesis, and shows that $CD8^+$ T cells mediated anti-tumor immunity during PDA initiation is negatively regulated by $CD4^+$ T cells.

$CD4^+$ T cells include several subtypes, such as T helper 1 (Th1) cells, T helper 2 (Th2) cells, IL-17-producing T helper (Th17) cells, and Tregs (10). Th1 cells secrete pro-inflammatory cytokines such as Interferon gamma (IFN-γ), IL-2, TNF-α, IL-8, and IL-1β and can have anti-tumor effects (52). In contrast, Th2 cells secrete anti-inflammatory cytokines, such as IL-4, IL-5, and IL-10, and are tumor-promoting (53, 54). In human PDA, Th2 ($GATA\text{-}3^+$) cells are predominant over Th1 ($T\text{-}bet^+$) cells and the ratio of Th2/Th1 is an independent predictive marker of reduced patient survival (54). $CD25^+$ Th17 cells express high levels of cytotoxic T-lymphocyte-associated protein 4 (CTLA-4) and mediate $CD8^+$ T cell suppression in an immune checkpoint dependent manner (55). IL-17 secreted by Th17 cells accelerates PanIN initiation and progression by acting directly on epithelial cells that express the IL17 receptor (56). IL17 also recruits neutrophils, triggers neutrophil extracellular traps and excludes cytotoxic $CD8^+$ T cells from tumors (57). Thus, pharmacological and genetical inhibition of IL17/IL17RA signaling in the KPC model increased immune checkpoint blockade sensitivity (57).

TABLE 1 | Currently active clinical trials targeting the microenvironment of PDA.

Target	Agent	Combination	Identifier	Phase	Subjects
CCR2/5	BMS-813160	Chemotherapy or Nivolumab	NCT03184870	1/2	Pancreatic cancer
		GVAX, Nivolumab and SBRT	NCT03767582	1/2	Locally Advanced PDA
CD40	CDX-1140	Pembrolizumab, or chemotherapy	NCT03329950	1	Pancreatic adenocarcinoma
	Selicrelumab	Atezolizumab + Chemotherapy	NCT03193190	1/2	Metastatic pancreatic ductal adenocarcinoma
CSF1R	IMC-CS4	GVAX/CY and Pembrolizumab	NCT03153410	1	Pancreatic cancer
CTLA-4	Ipilimumab	Nab-Paclitaxel/Gemcitabine, Nivolumab and SBRT	NCT04247165	1/2	Locally advanced pancreatic cancer
	Ipilimumab + Nivolumab	Radiotherapy	NCT02866383	2	Pancreatic cancer/Metastastic
			NCT03104439	2	pancreatic cancer
			NCT04361162	2	
	Tremelimumab + Durvalumab	Minimally invasive surgical microwave ablation	NCT04156087	2	Non-resectable pancreatic cancer
CTLA-4 + LAG3	XmAb22841	Monotherapy/Pembrolizumab	NCT03849469	1	Pancreatic cancer
CXCR1/2	SX-682	Nivolumab	NCT04477343	(phase) 1	Pancreatic cancer
DC	DC Vaccine		NCT03592888		Pancreatic adenocarcinoma
			NCT04157127	(phase) 1	
			NCT04627246		
GM-CSF	GVAX/CY		NCT01088789	2	Pancreatic cancer
		Nivolumab	NCT02451982	1/2	Pancreatic cancer
		IDO1 inhibitor (Epacadostat), Pembrolizumab, and CRS-207	NCT03006302	2	Metastatic pancreatic adenocarcinoma
		Nivolumab and SBRT	NCT03161379	2	Pancreatic cancer
		CRS-207, Nivolumab, and Ipilimumab	NCT03190265	2	Pancreatic cancer
	OH2 (oncolytic virus expressing GM-CSF)		NCT04637698	1/2	Locally advanced/metastatic pancreatic cancer
IL-1β	Canakinumab	Spartalizumab, Nab-paclitaxel, and Gemcitabine	NCT04581343	1	Metastatic pancreatic ductal adenocarcinoma
IL-12	Oncolytic adenovirus expression IL-12	Standard chemotherapy	NCT03281382	1	Metastastic pancreatic cancer
IL-6	Siltuximab	Spartalizumab	NCT04191421	1/2	Metastatic pancreatic adenocarcinoma
	Tocilizumab	Nab-Paclitaxel and Gemcitabine	NCT02767557	2	Unresectable panreatic carcinoma
		Ipilimumab, Nivolumab and SBRT	NCT04258150	2	Pancreatic cancer
PD-1	Cemiplimab	Plerixafor	NCT04177810	2	Metastastic pancreatic cancer
		Motixafortide (CXCR4 inhibitor), Nab-paclitaxel, and Gemcitabine	NCT04543071	2	Pancreatic cancer
	Nivolumab	Losartan, Folfirinox and SBRT	NCT03563248	2	Pancreatic cancer
		Tadalafil and vancomycin	NCT03785210	2	Metastatic liver cancer from pancreatic cancer
		FT500 (iPSC-derived NK cell product)	NCT03841110	1	Pancreatic cancer
		Chemotherapy	NCT03970252	1/2	Resectable pancreatic cancer
		Stereotactic radiotherapy	NCT04098432	1/2	Locally advanced non-resectable pancreatic cancer
		Irreversible electroporation	NCT04212026	2	Metastastic pancreatic cancer
		SX-682 (CXCR1/2 inhibitor)	NCT04477343	1	Pancreatic ductal adenocarcinoma
	Pembrolizumab	Neoadjuvant chemoradiation	NCT02305186	1/2	Resectable pancreatic cancer
		CPI-006 (CD73 antibody)	NCT03454451	1	Pancreatic cancer
		SBRT	NCT03716596	1	Pancreatic cancer
		Defactinib	NCT03727880	2	Resectable pancreatic ductal adenocarcinoma
		Lenvatinib (VEGFR inhibitor)	NCT03797326	2	Pancreatic cancer
		GB1275 (CD11b modulator)	NCT04060342	1/2	Pancreatic adenocarcinoma
		NT-I7 (Efineptakin Alfa)	NCT04332653	1/2	Pancreatic cancer
		EGFR/TGFβ Fusion Protein BCA101	NCT04429542	1	Pancreatic cancer
PD-L1	Durvalumab	Stereotactic ablative body radiotherapy (SABR)	NCT03245541	1/2	Pancreatic adenocarcinoma
		Oleclumab (CD73 antibody) and chemotherapy	NCT03611556	1/2	Metastatic pancreatic adenocarcinoma
TGFβR1	PF-06952229		NCT03685591	1	Pancreatic neoplasms

Clinical trial identifier from https://clinicaltrials.gov. CCR, C-C motif chemokine receptor; CSF1R, colony-stimulating factor 1 receptor; CTLA-4, cytotoxic T-lymphocyte-associated protein 4; CXCR, C-X-C motif chemokine receptor; DC, dendritic cell; GM-CSF, granulocyte-macrophage colony-stimulating factor; GVAX, GM-CSF gene transduced irradiated prostate cancer vaccine cells; IDO1, indoleamine 2,3-dioxygenase 1; LAG3, lymphocyte activating 3; PD-1, anti-programmed cell death 1; PDA, pancreatic ductal adenocarcinoma; PD-L1, programmed cell death ligand 1; SBRT, stereotactic body radiation; TGFβR, transforming growth factor β receptor.

TABLE 2 | Past clinical trials targeting the microenvironment of PDA.

Target	Agent	Combination	Identifier	Status	Results
BTK	ACP-196	Pembrolizumab	NCT02362048	Completed	Well tolerated, limited clinical activity
	Ibrutinib	Durvalumab	NCT02403271	Completed	Well tolerated
		Gemcitabine and Nab-Paclitaxel	NCT02562898	Active, not recruiting	Ineffective
CD40	CP-870,893	chemotherapy	NCT00711191	Completed	Partially effective
	RO7009789	Gemcitabine and Nab-Paclitaxel	NCT02588443	Completed	Acceptable toxicity and clinical activity
	APX005M	Gemcitabine and Nab-Paclitaxel with or without Nivolumab	NCT03214250	Active, not recruiting	Manageable toxicity and early efficacy
CSF1R	Pexidartinib	Durvalumab	NCT02777710	Completed	Acceptable toxicity
	Cabiralizumab	Nivolumab	NCT02526017	Completed	Partially effective
		Nivolumab	NCT03336216	Active, not recruiting	Ineffective
DC	DC vaccine		NCT03114631	Completed	Safe with early clinical efficacy
RIPK1	GSK3145095		NCT03681951	Terminated	Serious adverse events
TGFβR1	Galunisertib	Durvalumab	NCT02734160	Completed	Partially effective

Clinical trial identifier from https://clinicaltrials.gov. BTK, Bruton tyrosine kinase; CSF1R, colony-stimulating factor 1 receptor; DC, dendritic cell; Receptor-interacting serine/threonine protein kinase 1 (RIPK1); TGFβR, transforming growth factor β receptor.

Tregs, defined as $CD4^+FOXP3^+CD25^+$ T cells, are the most abundant $CD4^+$ T cell subpopulation in PDA TME (28). High number of Tregs positively correlates with the progression and poor prognosis of PDA patients (31, 58). Tregs can be recruited by C-C chemokine ligand 5 (CCL5) (59). Disrupting CCL5/C-C chemokine receptor 5 (CCR5) signaling inhibited Treg migration to tumor (60). Tregs promoted the development of PDA through the suppression of IFN-γ-producing-$CD8^+$ T cells in an orthotopic implantation model with primary $Kras^{G12D}$-expressing pancreatic ductal epithelial cells (61). In this model, intratumoral Tregs directly interacted with tumor associated $CD11c^+$ dendritic cells (DCs) and reduced their expression of costimulatory molecules necessary for $CD8^+$ T cell activation such as CD40, CD80 and CD86 (61). Ablation of Tregs led to the restoration of immunogenic tumor-associated $CD11c^+$ DCs and increased $CD8^+$ T cell-dependent antitumor immunity, which resulted in an inhibition of tumor growth (61). Interactions between T cells and myeloid cell subsets are summarized in **Figure 2**, and we will further discuss their crosstalk within pancreatic cancer TME in Section 4.

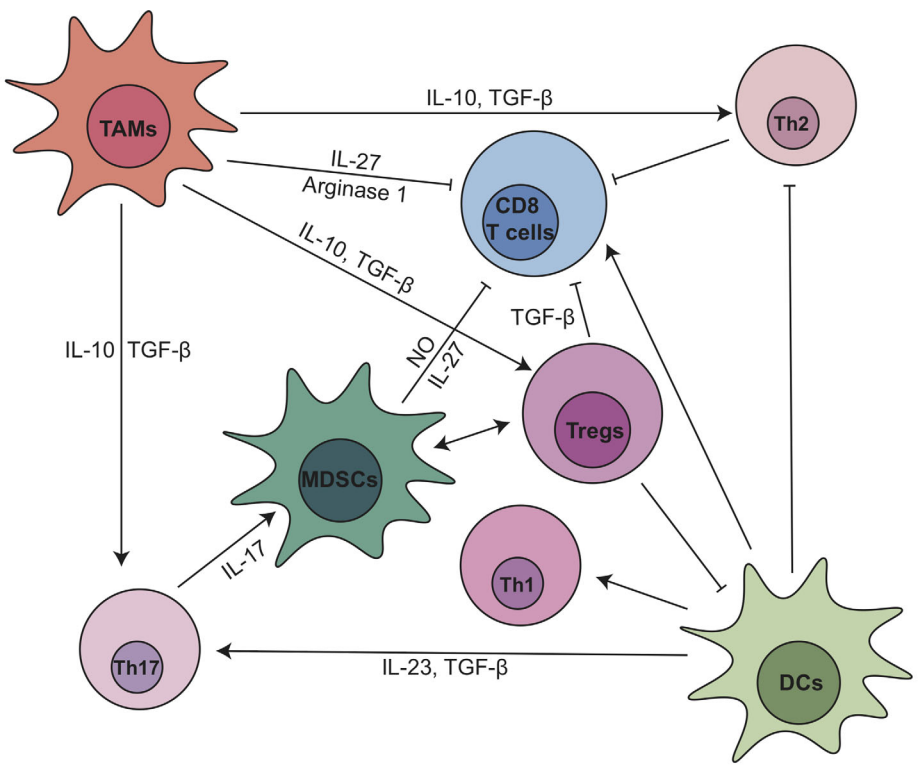

FIGURE 2 | The dynamic cellular and molecular interactions between T cells and myeloid cell subsets in pancreatic cancer. DC, dendritic cell; IL, interleukin; MDSCs, myeloid-derived suppressor cells; NO, nitric oxide; TAMs, tumor associated macrophages; TGF-β, transforming growth factor β; Th, T helper; Tregs, regulatory T cells.

Recently, a new study from our laboratory showed that Treg depletion failed to relieve immunosuppression and accelerated tumor progression in the KC and KPC GEMMs (62). Our study suggests that Tregs are a key source of TGFβ which facilitates the expansion of α-smooth muscle actin $(\alpha SMA)^+$ CAFs. Depletion of Tregs reprogramed the fibroblast populations inducing loss of tumor-restraining αSMA^+ CAFs. The reprogramed fibroblasts secreted increased level of chemokines such as CCL3, CCL6, and CCL8 that act as chemoattractant for suppressive myeloid cells. Therefore, Treg depletion resulted in increased Arginase1 $(Arg1)^+$ and PD-$L1^+$ TAMs, restoring the immunosuppressive TME and promoting carcinogenesis. This effect was inhibited by an inhibitor for the common CCL3/6/8 receptor CCR1. Treg depletion also led to an increase in Th2 cytokine profile, indicating that the absence of Tregs fails to restore immune surveillance, likely because of compensation driven by other subpopulations of $CD4^+$ T cells and immunosuppressive myeloid cells. Thus, a better approach might be reprogramming Tregs rather than depleting them altogether.

TARGETING TUMOR MYELOID CELLS AS A CRUCIAL THERAPEUTIC STRATEGY TO RELIEVE IMMUNOSUPPRESSION IN PDA

Myeloid cells, including immature myeloid cells (also commonly referred to as MDSCs), TAMs and tumor associated neutrophils (TANs) accumulate during the progression of pancreatic cancer (10). Myeloid cells directly promote acinar cell dedifferentiation during the earliest stages of pancreatic cancer (63). Our group has shown that myeloid cells are required for the establishment of an immunosuppressive environment in pancreatic cancer (49). EGFR ligands secreted by tumor infiltrating myeloid cells stimulated EGFR/MAPK signaling and increased the expression of PD-L1 on the epithelial cells to activate the PD-1/PD-L1 checkpoint (49). Depletion of myeloid cells by administration of Diphtheria Toxin (DT) to CD11b-diphtheria toxin receptor (DTR) mice reversed immune suppression and enabled $CD8^+$ T cell activity, thus preventing PanIN formation in the iKras∗; CD11b-DTR GEMM and inhibiting tumor growth in CD11b-DTR mice transplanted with PDA cells (49). Therefore, controlled regulation of myeloid cells is an essential avenue for improvement of clinical efficacy against PDA.

Myeloid-Derived Suppressor Cells in Cooperation With Tregs to Suppress T Cell Activation in PDA

MDSCs are Gr-1^+CD11b^+ myeloid cells that suppress T cell activation. Inducible nitric oxide synthase (64) enzyme in MDSCs regulates the release of nitric oxide from MDSCs, which subsequently causes DNA damage in $CD8^+$ T cells (65). A recent study demonstrated that *in vivo* depletion of MDSCs led to a reduction in Tregs in pancreatic tumors (66). Through light sheet fluorescent microscopy and ex vivo functional assays, the authors showed that MDSCs induced Tregs by cell-cell direct interaction, which was lost in the Transwell system, and Tregs in turn affected the survival and/or proliferation of MDSCs (66). GM-CSF is necessary and sufficient to drive the development of Gr-1^+CD11b^+ cells (35, 36). GM-CSF blockade resulted in reduced MDSC infiltration and higher number of active $CD8^+$ T cells in KPC tumors (36). Further, stroma-derived Dickkopf-1 (DKK1) activates β-catenin in MDSCs and regulates the recruitment and immunosuppressive effects of MDSCs (67). The two main categories of MDSCs are monocytic-MDSCs (Mo-MDSCs), characterized by the surface markers $CD11b^+Ly6G^-Ly6C^{Hi}$, and granulocyte-derived MDSCs (Gr-MDSCs) by $CD11b^+Ly6G^+Ly6C^{Low}$. Selective targeting of Gr-MDSCs was sufficient to induce the activation and proliferation of systemic and intratumoral $CD8^+$ T cells (8).

$CD11b^+Ly6G^+$ cells are also identified as tumor associated neutrophils (TANs). In PDA, the abundance of TANs is strongly associated with poor prognosis (68). High level of CXCL5, a chemokine for the recruitment of neutrophils, as well as its receptor C-X-C chemokine receptor 2 (CXCR2), which is highly expressed on TANs, has been associated with poor outcome in PDA patients (68). CXCR2 inhibition prevented TAN accumulation in PDA TME, potently suppressed tumor growth and metastasis and sensitized PDA tumors to anti-PD-1 therapy (12, 13). The absence of TANs correlated with significant infiltration of activated T cells in the TME (13).Thus, inhibition of trafficking or depletion of MDSCs may offer a potential strategy to enhance the efficacy of immunotherapy for PDA. The role of CXCR2 ligands/CXCR2 biological axis in pancreatic cancer has been studied in a clinical trial (NCT00851955, results are pending). An ongoing clinical trial will evaluate the safety and tolerability of a CXCR1/CXCR2 inhibitor in combination with anti-PD1 as a maintenance therapy in patients with metastatic pancreatic ductal adenocarcinoma and will also assess the immunophenotypic and stromal changes to the tumor microenvironment after treatment (NCT04477343).

Reprogramming of Tumor-Associated Macrophages in PDA as a Strategy to Restore Anti-Tumor Immune Responses

TAMs originate from inflammatory monocytes and tissue resident macrophages with different functions (69). Monocyte-derived TAMs function in antigen presentation whereas embryonically derived TAMs exhibit a pro-fibrotic transcriptional profile (9). TAMs can be recruited by cytokines and chemokines such as colony-stimulating factor-1 (CSF1), CCL2 and CCL5, and polarized into different states (70–76). Pro-inflammatory cytokines such as IFN-γ, TNF-α, and IL-12 secreted by classically activated M1-like macrophages recruit Th1 cells and stimulate anti-tumor activity (77), while alternatively activated M2-like TAMs produce anti-inflammatory cytokines such as IL-10 and TGF-β to promote the expansion of Th2/Th17 cells and Tregs (77–79). M2-like TAMs also produce Arg1 which in turn depletes L-arginine that is necessary for T cell function (80, 81). TAMs can exert opposite roles in cancer, either promoting or

restraining tumorigenesis based on their polarization (82, 83). In PDA, TAMs have a highly dynamic and heterogeneous status, although as a whole they are inclined to be M2-like and have a profound influence on tumorigenesis and metastasis, as well as on immunosuppression and chemotherapeutic resistance. Currently, a growing interest in the field is to disrupt TAM recruitment or to reprogram TAMs to hinder tumor development, boost antitumor immunity and improve clinical therapy.

The CSF1 receptor (CSF1R) is expressed on F4/80$^+$ macrophages and on monocytes in mice. Targeting TAMs through CSF1R inhibitor (CSF1Ri) or a CSF1 neutralizing antibody inhibited tumor growth, reduced metastatic burden and prolonged survival in KPC mice (84, 85). CSF1Ri treatment decreased the number of CD11b$^+$Ly6G$^-$Ly6C^{Lo}F4/80^{Hi}MHCII$^+$ macrophages and CD11b$^+$Ly6G$^-$Ly6C^{Hi} Mo-MDSCs (86). The expression of immunosuppressive molecules, including *Pdcd1lg2*, *Il10*, *Arg1*, *Tgfb1*, and *Ccl22*, was reduced in macrophages while proinflammatory genes, such as *Il12a*, *Ifna*, *Ifnb1*, *Ifng*, *Cxcl10*, and *Nos2*, were upregulated, indicative of reprogramming of TAMs toward a M1-like phenotype (86). Consistently, CD3$^+$CD8$^+$ cytotoxic T cells and CD3$^+$CD4$^+$FOXP3$^-$ effector T (Teff) cells were significantly up-regulated upon treatment with CSF1Ri, while CD4$^+$FOXP3$^+$ Tregs were down-regulated, ending up with a significantly improved Teff/Treg ratio (86). Ex vivo assays also revealed that CSF1 blockade alleviated immunosuppressive activities and enhanced antigen-presenting potential in both TAMs and DCs (86). Moreover, CSF1Ri upregulated PD-1 and CTLA-4 expression on T cells and sensitized PDA to immune checkpoint blockade. CSF1Ri-treated tumors also displayed less prominent αSMA$^+$ stromal expansion, which was partly due to reduction of granulin, a secreted glycoprotein that stimulates fibroblast activation and migration. The expression of granulin is mediated by CSF1/CSF1R signaling in TAMs (87). CSF1R inhibitors Pexidartinib and Cabiralizumab have been tested in clinical trials with standard therapies or immune checkpoint blockade in advanced pancreatic cancer patients (NCT02777710, NCT03336216, NCT02526017). Although the toxicity of CSF1R inhibitor combined with immune checkpoint blockade was generally consistent with monotherapy, and the combination resulted in dose-related reduction of circulating monocytes[1] (88), unfortunately, in phase II study (NCT03336216) the combination of Cabiralizumab and nivolumab (anti-PD1) with or without chemotherapy failed to improve progression-free survival of patients with advanced pancreatic cancer[2]. One possible reason of the unresponsiveness to these immunomodulatory approaches could still be the lack of active T cells in the 'cold' tumors. CSF1R inhibitor IMC-CS4 is currently being tested in combination with pancreatic cancer vaccine and immune checkpoint blockade in pancreatic cancer patients (NCT03153410).

Other approaches developed to reprogram TAMs include targeting Receptor-interacting serine/threonine protein kinase 1 (RIPK1), a critical receptor kinase on TAMs. Targeting RIPK1 with a small molecule GSK3145095 up-regulated STAT1 signaling in TAMs and reprogrammed intratumoral TAMs toward an MHCII^{hi}TNFα$^+$IFNγ$^+$ immunogenic phenotype with a reduction in CD206, IL-10, TGF-β and Arg1 (89). RIPK1-inhibited TAMs induced cytotoxic T cell activation and the differentiation of T helper cells toward a mixed Th1/Th17 phenotype. RIPK1 inhibition thus led to active innate and adaptive immunity in both orthotopic KPC tumors and in organotypic models of human PDA. RIPK1 inhibition also synergized with anti-PD-1 treatment (89). However, the clinical trial of GSK3145095 was terminated because 50% of patients (4/8) involved in part 1 of this phase I/II study developed serious adverse events (NCT03681951).

While targeting TAMs emerges as a potential therapeutic strategy in pancreatic cancer, tumor-associated neutrophils might compensate for the loss of TAMs in PDA. Treatment with a CCR2 inhibitor to target CCR2$^+$ TAMs resulted in a compensatory influx of CXCR2$^+$ TANs in PDA patients (90). Accordingly, combination targeting of both CCR2$^+$ TAMs and CXCR2$^+$ TANs further augmented the anti-tumor immunity and enhanced the efficacy of chemotherapy in PDA. The CCR2/5 inhibitor BMS-813160 is under investigation in combination with chemotherapy or immune checkpoint blockade in advanced PDA patients (NCT03184870, NCT03767582).

Dendritic Cell Scarcity and Insufficient T Cell Priming Contribute to the Cold Tumor of PDA

Increasing evidence points to the possibility that insufficient T cell priming due to lack of dendritic cells in PDA is a root cause of its nature as an immunologically cold tumor. Conventional dendritic cells (cDCs) have been recognized as one of the antigen-presenting cells that mediate T cell priming and cytotoxic T cell activity. A recent study showed that endogenous antigen-specific responses in PDA were aberrant due to a scarcity of DCs and an expansion of Th2/Th17 responses (91). Moreover, dysfunction of type 1 conventional dendritic cells (cDC1s) occurred in the earliest stages of tumorigenesis in KPC mice due to elevated apoptosis induced by IL-6 (92). Neutralization of IL-6 or combination treatment of CD40 agonist and Flt3 ligand rescued cDC1 abundance, leading to the control of tumor outgrowth (92). Restoring cDCs in KPC mice also blocked Th2 and Th17 cells and enhanced Th1 and CD8$^+$ T cell activity, which ultimately resulted in reduced and lower-grade PanIN lesions accompanied by decreased collagen deposition and αSMA$^+$ fibroblast density (91). Another study found that a distinct subset of DCs (CD11b$^+$CD103$^-$) predominated in PDA and induced tumor-promoting FOXP3$^-$ IL-10$^+$IL-17$^+$IFNγ$^+$ regulatory CD4$^+$ T cells through the secretion of IL-23 and TGF-β (93). This DC mediated-CD4$^+$ T-cell differentiation was modulated by retinoic acid signaling (93).

Increasing attention has turned toward restoring T cell priming to overcome checkpoint unresponsiveness. CD40 is a

[1] https://www.businesswire.com/news/home/20171109005417/en/Bristol-Myers-Squibb-and-Five-Prime-Present-Phase-1a1b-Data-Evaluating-Cabiralizumab-anti-CSF-1-receptor-antibody-with-Opdivo-nivolumab-in-Patients-with-Advanced-Solid-Tumors

[2] https://www.businesswire.com/news/home/20200218005144/en/Five-Prime-Therapeutics-Provides-Update-on-Phase-2-Trial-of-Cabiralizumab-Combined-with-Opdivo®-in-Pancreatic-Cancer

cell surface molecule that regulates dendritic cells to promote T cell activation. CD40 on DCs binds to CD154 on $CD4^+$ T helper cells and enables DCs to prime cytotoxic T cells (94). Activation of CD40 reprograms macrophages to destroy tumor stroma (95). Combination of CD40 activating antibody and anti-PD-1/CTLA-4 resulted in tumor regression and immunological memory in KPC mice (96). The T cell activating effect of this combination therapy was dependent on $CD103^+$ DCs without the need for innate immune sensing pathways such as TLR, stimulator of interferon genes (STING) or interferon-α receptor (IFNAR) pathways, indicating that the CD40 pathway represents a distinct and alternative bridge between DCs and adaptive immunity in PDA (96). A previous clinical trial showed CD40 agonist monoclonal antibody (mAb) selicrelumab (formally named as CP-870,893 or RO7009789) with gemcitabine was well tolerated and therapeutic efficacy was observed in a cohort of patients with metastatic PDA (95) (NCT00711191). Another phase 1b study combining agonistic CD40 APX005M (sotigalimab) with gemcitabine plus nab-paclitaxel, with and without nivolumab, in 30 patients with metastatic PDA showed encouraging clinical activity and manageable toxicity (97). A recent phase 1b study used selicrelumab with or without gemcitabine and nab-paclitaxel in 16 resectable PDA patients prior to surgery followed by adjuvant chemotherapy and selicrelumab. The results showed CD40 agonist induced T cell immune response both at the tumor site and systemically in those early-stage PDA patients[3]. Currently, there're more clinical trials exploring the combination of CD40 agonist with immune checkpoint blockade and/or chemotherapy in advanced pancreatic cancer (NCT03193190, NCT03329950).

In addition, there are encouraging results of dendritic cell-based immunotherapy to activate cytolytic T cell responses in pancreatic cancer from preclinical and clinical pilot studies (98, 99). In one study (NCT03114631), DCs generated from blood monocytes and pulsed with tumor lysates or tumor antigens MUC1 and WT1 were injected subcutaneously to 26 patients with stage II–IV pancreatic cancer. The preliminary results indicate DC-based immunotherapy is safe and provides immediate favorable outcome in pancreatic cancer patients (100). More clinical trials of DC vaccines in PDA patients are on-going (NCT04627246, NCT04157127, NCT03592888).

B CELLS CONTRIBUTE TO THE DISFUNCTION OF T CELL-DEPENDENT ANTITUMOR IMMUNE RESPONSES IN PDA

B cells are another immune cell population that plays a significant role in PDA progression, although some controversy regarding their precise function remains. Depletion of B cells using a CD20-specific mAb reduced PanIN formation in KC mice (101). An IL-35 expressing $CD1d^{hi}CD5^+$ B cell subset is required for the pro-tumorigenic effect of B cells in PDA (102). The growth of orthotopic KC cells in B cell-deficient (μMT) mice was significantly inhibited, a phenotype that was rescued by the reconstitution of $CD1d^{hi}CD5^+$ B cells through IL-35 mediated promotion of tumor cell proliferation (102). Bruton tyrosine kinase (BTK), a key B cell and macrophage kinase, contributes to the regulation of T cell-dependent anti-tumor immune responses in PDA (103). Phosphatidylinositol 3-kinase-gamma (PI3Kγ) activated BTK on B cells and Fc receptor γ-chain $(FcRγ)^+$ TAMs, resulting in M2-type macrophage programming that suppressed $CD8^+$ T cell cytotoxicity (103). BTK inhibitors Ibrutinib and ACP-196 were relatively well tolerated in metastatic PDA patients with the combination of chemotherapy or immune checkpoint blockade (NCT02403271, NCT02362048, NCT02562898). However, in the phase III trial patients with metastatic pancreatic cancer treated with Ibrutinib in combination with gemcitabine and nab-paclitaxel didn't show improved progression free survival and overall survival (NCT02562898) (104). Besides, either monotherapy of ACP-196 or combined with pembrolizumab showed limited clinical activity in phase II study despite consistent reduction of MDSCs in peripheral blood (105). Only in two patients treated with combination therapy profound anti-tumor responses were observed, highlighting the necessity of targeting multiple TME components to improve efficacy as well as the need to better understand the complex human pancreatic tumor microenvironment, which may in part contributed to the failure of BTK inhibitors in this disease despite its success in hematologic malignancies (106).

EXTENSIVE NETWORK OF CANCER-ASSOCIATED FIBROBLASTS TO REGULATE IMMUNE SUPPRESSION IN PDA

CAFs are the major contributor to the desmoplastic stroma in PDA (107, 108). Extracellular matrix (ECM) and soluble factors secreted by CAFs are believed to activate key signaling pathways in cancer cells leading to cancer progression, cell survival, metastasis and drug resistance (107, 109, 110). ECM can also act as a physical barrier that prevents drug delivery (111). Sub-populations of CAFs have been noticed by several independent groups (112–115). A subpopulation of CAFs, myofibroblastic CAFs (myCAFs), are found adjacent to cancer cells. They have high expression of αSMA and have been hypothesized to restrict tumor progression. Inflammatory CAFs (iCAFs) are located in the desmoplastic stromal areas of the tumor. They express low level of αSMA but high levels of cytokines and chemokines such as IL-6, IL-11 and leukemia inhibitory factor (LIF) and promote tumor growth. A third sub-population of CAFs is antigen presenting CAFs (apCAFs), also described as mesothelial cells (116, 117). These CAFs express MHC class II related genes and can present antigens to $CD4^+$ T cells. While these subpopulations of CAFs are spatially separated and phenotypically distinct, they still show some dynamic feature since myCAFs and iCAFs are interconvertible and apCAFs can also convert into myCAFs under certain conditions (113, 114).

Due to the heterogeneity of CAFs, they play a complex role in the regulation of PDA progression and TME (**Figure 3**).

[3] https://www.abstractsonline.com/pp8/#!/9325/presentation/5136

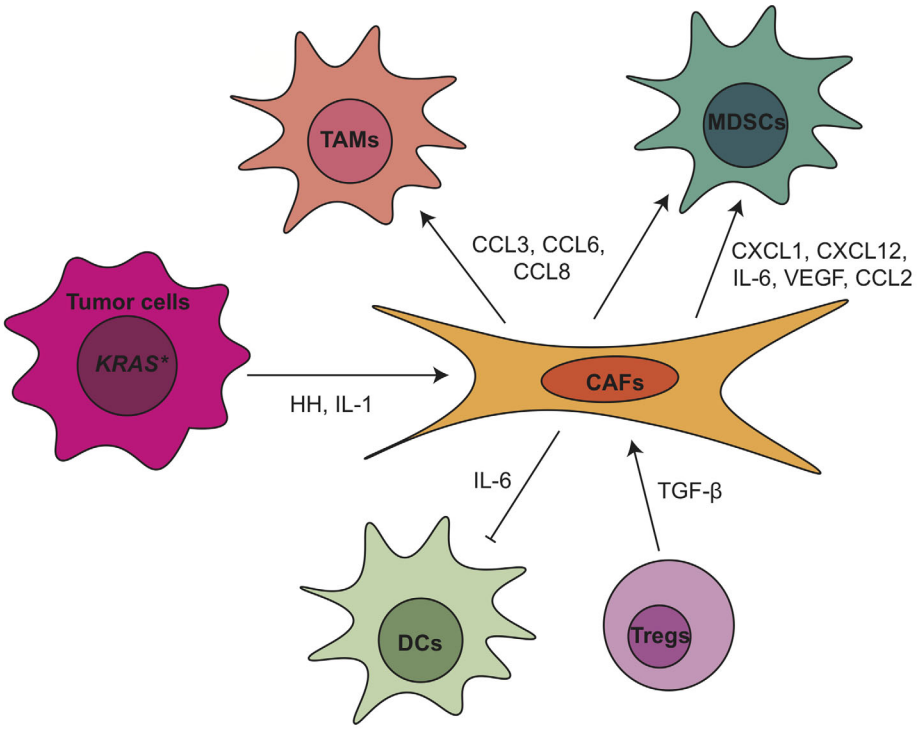

FIGURE 3 | Crosstalk between tumor associated fibroblasts and other TME components within pancreatic cancer. CAF, cancer associated fibroblasts; CCL, C-C motif chemokine ligand; CXCL, C-X-C motif chemokine ligand; DC, dendritic cell; HH, hedgehog; IL, interleukin; MDSCs, myeloid-derived suppressor cells; TAMs, tumor associated macrophages; TGF-β, transforming growth factor β; Tregs, regulatory T cells; VEGF, vascular endothelial growth factor.

Depletion of αSMA$^+$ myofibroblasts starting at either the PanIN or the PDA stage led to invasive, undifferentiated, hypoxic tumors with diminished survival (118). Myofibroblast depletion also decreased overall immune infiltration in PDA but increased CD4$^+$FOXP3$^+$ Tregs, resulting in a reduction in both the Teff/Treg ratio and the cytotoxic CD8$^+$/Treg ratio (118). A similar effect was observed when the Collagen 1 gene *Col1a1* was inactivated in a mouse model of pancreatic cancer (118). Due to the increased CTLA-4 expression following myofibroblast depletion, anti-CTLA4 immunotherapy reversed the disease acceleration caused by myofibroblast depletion and prolonged animal survival in *p48-Cre; LSL-Kras^{G12D}; Tgfbr2$^{flox/flox}$* (PKT) GEMM (118). On the other hand, the depletion of fibroblast activation protein (FAP)$^+$ CAFs reduced the tumor growth and improved the efficacy of anti-CTLA-4 and anti-PD-L1 in KPC GEMM (6). FAP$^+$ CAFs is the main source of CXCL12 in PDA, which coats and protects the cancer cells. Inhibiting CXCR4, a CXCL12 receptor, induced T cell accumulation among cancer cells and synergized with anti-PD-L1 to cause cancer regression (6). Pancreatic stellate cells (PSCs), characterized by lipid droplets in the cytoplasm, were found as a subset of pancreatic CAFs that correlates with increased suppressive immune cell populations and decreased T cells, natural killer (NK) cells, NK T cells and M1-type TAMs in the PDA tumor tissues (119, 120). The infiltration of CD8$^+$ T cells was regulated through NFκB-mediated expression of CXCL12 in PSCs (121). PSCs also enhanced the differentiation and function of MDSCs through the production of MDSC-promoting cytokines IL-6, vascular endothelial growth factor (VEGF), CSF1 and chemokines CXCL12 and CCL2 (122). IL-6 secreted from PSCs led to the phosphorylation of STAT3 in peripheral blood mononuclear cells (PBMCs), which promoted the differentiation of PBMCs into MDSCs (122). Finally, when we inhibited Hedgehog (Hh) signaling, thus shifting the CAF population to a predominant iCAF phenotype, we also observed a decrease in cytotoxic T cells and an expansion of Tregs, indicating increased immunosuppression (123).

As mentioned above, CAFs secrete a variety of soluble factors that in turn shape the PDA TME, including IL-6, which plays multiple roles in the modulation of the immune response in PDA. Il6 not only is responsible for DC disfunction and MDSCs differentiation, as described earlier, but also regulates NK cell activity and Treg infiltration in PDA (124, 125). Combination blockade of IL-6 and PD-L1 led to increased Th1 T cell infiltration and decreased tumor growth (126). In iKras*; IL-6$^{-/-}$ model, we observed deficiency of IL-6 resulted in reduction of tumor infiltrating macrophages and MDSCs (127). Clinical trials targeting IL-6 in PDA patients include IL-6 antibodies Tocilizumab and Siltuximab (NCT02767557, NCT04258150, NCT04191421). Other proteins secreted by CAFs as messenger to crosstalk with immune cells in PDA include but are not limited to CXCL1 (128), CXCL10 (129), IL-33 (130), ETS2 (131), galectin-1 (132), thymic stromal lymphopoietin (TSLP) (54) and βig-h3 (133).

The phenotype and function of CAFs in PDA TME is under control of epithelial cells as well as immune cells. For example, inactivation of oncogenic KRAS in the epithelial cells at the PanIN stage reduced α-SMA expression and inhibited CAF proliferation (14). Hedgehog ligands from tumor cells activated the Hh signaling in CAFs and promoted their expansion (134–136). Further study identified the Hh signaling effector glioma-associated oncogene homolog 1 (GLI1) as a critical transcriptional effector in this process (137). Deletion of a single allele of *Gli1* in iKras∗ GEMM was enough to disrupt the recruitment of immune cells by activated fibroblasts (137). Recently, our laboratory demonstrated that hedgehog signaling inhibition with smoothened antagonist LDE225 altered fibroblast composition with reduced myCAF and increased iCAF numbers in the KPC model (123). Immune cells, such as myeloid cells and Tregs, also participate in the regulation of CAFs. Stromal inactivation and remodeling of ECM were observed in both myeloid cell-depleted PanINs (49) and in CSF1Ri-treated PDA tumors (87). IL-1 and TGF-β have also been identified as ligands to promote CAF heterogeneity (125, 138). Recently, our lab showed that the loss of TGFβ1 upon Treg depletion reprogramed the fibroblast population with loss of αSMA^+ myCAFs (62). Notably, TGFβ receptor inhibitor Galunisertib has been investigated in clinical trial in combination with durvalumab (anti-PD-L1) for metastatic PDA patients (NCT02734160). Newly published results of this trial showed phase II dose of galunisertib co-administered with durvalumab was tolerable and the disease control rate was 25% (8 patients had partial response or stable disease among 32 patients enrolled). The limited clinical benefit might be due in part to the aggressive nature of the advanced stage of disease (139). TGFβ receptor inhibitor PF-06952229 is currently under investigation in advanced solid tumors including pancreatic cancer patients (NCT03685591).

CONCLUDING REMARKS

The stroma-rich, immunosuppressive microenvironment is a hallmark of pancreatic cancer. Tumor evasion of immune surveillance happens at the very early stages of tumorigenesis. Abundant immunosuppressive cells such as macrophages, Tregs and activated fibroblasts are evident even at the onset of acinar-ductal metaplasia (ADM), a key event for PDA initiation (140, 141). In contrast, antitumor effector cells such as $CD8^+$ T cells are either scarce or excluded from the tumor nests. When intratumorally $CD8^+$ T cells are present they are usually exhausted and express checkpoints such as TIGIT (11), lymphocyte-activation gene 3 (LAG-3) and PD-1 (32, 142). Recent research identified intratumoral exhausted T cells ($PD\text{-}1^+Lag3^+Tox^+$) as induced by myeloid cell derived IL-27 in an orthotopic model of PDA (143). Those intratumoral T cells not only produced less IFNγ and Granzyme B but also expressed more IL-10, thus contributing to immune suppression in an autocrine manner. T cell exhaustion in cancer can be self-regulated through cell intrinsic mechanisms, however, the interaction between other cells or cytokines in the TME play an essential role in inducing T cell dysfunction. The TME in pancreatic cancer is composed of various types of cells that secrete abundant cytokines, including tumor cells, immunosuppressive cells, CAFs, inhibitory cytokines such as IL-6, IL-10 and TGF-β. The TME collectively form a complex and integrated immunosuppressive network to limit T cell differentiation, priming and drive T cell exhaustion. Therefore, when tumors have more $CD8^+$ T cells they often also have increased granulocytes, immunosuppressive macrophages, and Tregs, and thus remain immune suppressive (32).

NK cells also play an important role in immune defense and immune regulation in cancer. In addition to their cytolytic activity, NK cells produce cytokines to modulate adaptive immune responses (144). In PDA, NK cells are reported being dysfunctional. NK cells from PDA patients exhibited a significant decrease in cytotoxic degranulation compared with those from healthy controls, a phenomenon that was associated with increased TGF-β1 expression in tumors (145). Future studies are needed to fully understand the mechanisms adopted by the TME to restrain NK cell activity in PDA, which might potentially provide new opportunities to devise new combination treatments for enhanced cancer immunotherapy response.

Significant progress has been made in the application of active immunotherapies including cytokines, immunomodulatory mAbs, and cancer vaccines or passive immunotherapies such as cell-based therapies in cancer (146, 147). Mono-immunotherapies such as single immune checkpoint inhibitor anti-CTLA4 (ipilimumab), anti-PD1 (nivolumab, pembrolizumab) or anti-PD-L1 (duravalumab) have very limited benefits for PDA patients. It is now widely accepted that due to the complicated cellular crosstalk in PDA, targeting one immune-modulating pathway or a single population of stromal cells has very limited efficacy on reactivating immune system and restraining tumor progression. Therefore, simultaneously targeting multiple immunosuppressive components may acquire therapeutic benefits or improve the efficacy of immunomodulating anticancer therapeutics in PDA patients. In fact, a large number of clinical trials have explored the possibility of combination strategy such as the combination of multiple immunotherapy-based treatments, or combining immunotherapy with chemotherapy, radiation, and other cancer targeted therapies. So far, encouraging results from preclinical and clinical studies have demonstrated that combining an immunostimulatory approach, such as T cell priming *via* CD40 activation, with immune checkpoint blockade to prevent negative feedback signals on activated T cells represents the most promising treatment strategy to achieve clinical therapeutic benefit in this immunologically "cold" disease. We summarized a number of promising TME-targeting approaches for pancreatic cancer that are currently under clinical investigation in **Figure 4** and **Table 1**.

The advent of next-generation sequencing technology and large-scale tumor molecular profiling has shed light on the heterogeneous immune infiltration and tumor microenvironment in human PDA both across and within tumors and the heterogeneity in the expression levels of checkpoints on tumor infiltrating T cells (11, 148–150). Based on these considerations, it is important to understand the variety and individual differences in immune

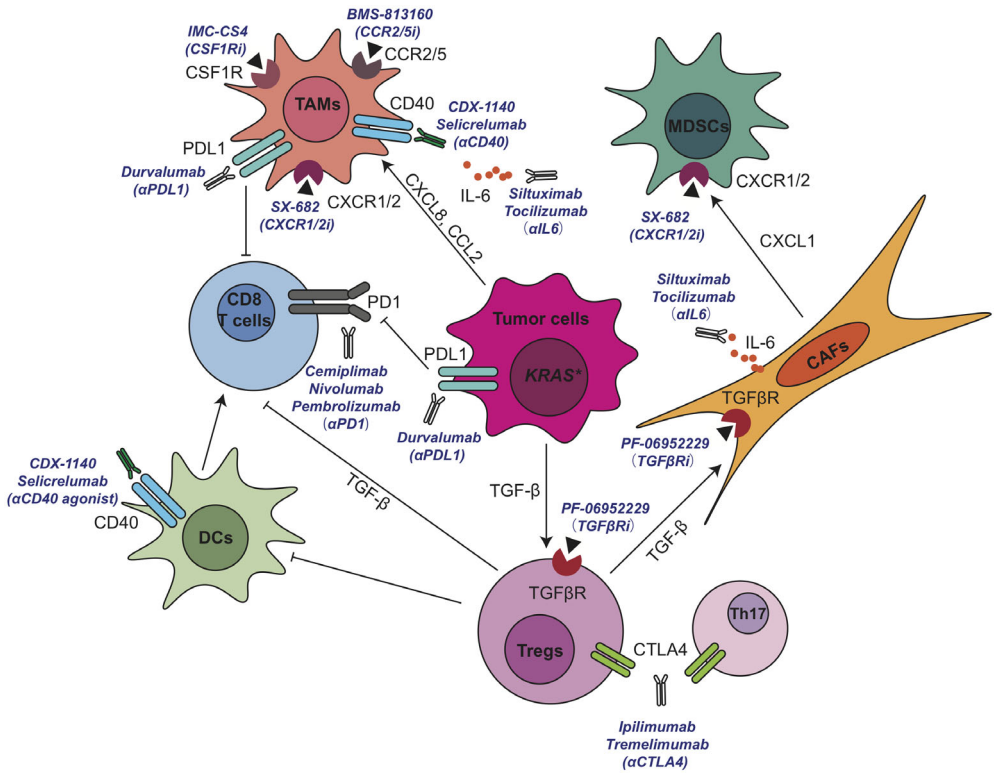

FIGURE 4 | Current active clinical trials targeting immunosuppressive TME in pancreatic cancer. CAF, cancer associated fibroblasts; CCL, C-C motif chemokine ligand; CCR, C-C motif chemokine receptor; CSF1R, colony-stimulating factor 1 receptor; CXCL, C-X-C motif chemokine ligand; DC, dendritic cell; IL, interleukin; MDSCs, myeloid-derived suppressor cells; PD-1, anti-programmed cell death 1; PD-L1, programmed cell death ligand 1; TAMs, tumor associated macrophages; TGF-β, transforming growth factor β; Th, T helper; Tregs, regulatory T cells.

response for future translational studies and clinical trials, including personalized immunotherapy approaches.

With a better dissection of cell heterogeneity and their crosstalk involving cancer and stromal cells within the TME, strategies aimed at targeting multiple mechanisms with synergistic effects may sensitize PDA tumors to chemotherapy or immunotherapy through re-programing the tumor microenvironment of PDA.

AUTHOR CONTRIBUTIONS

WD wrote the manuscript. YZ and MP reviewed and edited the manuscript. All authors contributed to the article and approved the submitted version.

FUNDING

This work was supported by NIH/NCI grants R50 CA232985 to YZ; R01CA151588, R01CA198074, and U01CA224145 to MP. This work was also supported by the University of Michigan Cancer Center support grant (P30CA046592), including an Administrative Supplement to MP.

ACKNOWLEDGMENTS

We apologize to the colleagues whose work could not be included due to space restrictions. We thank the members of the Pasca di Magliano laboratory for critical discussion.

REFERENCES

1. Siegel RL, Miller KD, Jemal A. Cancer Statistics, 2020. *CA Cancer J Clin* (2020) 70(1):7–30. doi: 10.3322/caac.21590
2. Howlader N, Noone AM, Krapcho M, Miller D, Brest A, Yu M, et al. SEER Cancer Statistics Review, (1975-2018). Bethesda, MD: National Cancer Institute. Available at: https://seer.cancer.gov/csr/1975_2018/, based on November 2020 SEER data submission, posted to the SEER web site, April 2021.
3. Liu Q, Liao Q, Zhao Y. Chemotherapy and Tumor Microenvironment of Pancreatic Cancer. *Cancer Cell Int* (2017) 17:68. doi: 10.1186/s12935-017-0437-3
4. Vaccaro V, Sperduti I, Milella M. FOLFIRINOX Versus Gemcitabine for Metastatic Pancreatic Cancer. *N Engl J Med* (2011) 365(8):768–9. doi: 10.1056/NEJMc1107627
5. Martinez-Bosch N, Vinaixa J, Navarro P. Immune Evasion in Pancreatic Cancer: From Mechanisms to Therapy. *Cancers (Basel)* (2018) 10(1):6. doi: 10.3390/cancers10010006
6. Feig C, Jones JO, Kraman M, Wells RJ, Deonarine A, Chan DS, et al. Targeting CXCL12 From FAP-Expressing Carcinoma-Associated Fibroblasts Synergizes With Anti-PD-L1 Immunotherapy in Pancreatic Cancer. *Proc Natl Acad Sci USA* (2013) 110(50):20212–7. doi: 10.1073/pnas.1320318110

7. Zhang Y, Yan W, Mathew E, Bednar F, Wan S, Collins MA, et al. CD4+ T Lymphocyte Ablation Prevents Pancreatic Carcinogenesis in Mice. *Cancer Immunol Res* (2014) 2(5):423–35. doi: 10.1158/2326-6066.CIR-14-0016-T
8. Stromnes IM, Brockenbrough JS, Izeradjene K, Carlson MA, Cuevas C, Simmons RM, et al. Targeted Depletion of an MDSC Subset Unmasks Pancreatic Ductal Adenocarcinoma to Adaptive Immunity. *Gut* (2014) 63 (11):1769–81. doi: 10.1136/gutjnl-2013-306271
9. Zhu Y, Herndon JM, Sojka DK, Kim KW, Knolhoff BL, Zuo C, et al. Tissue-Resident Macrophages in Pancreatic Ductal Adenocarcinoma Originate From Embryonic Hematopoiesis and Promote Tumor Progression. *Immunity* (2017) 47(3):597. doi: 10.1016/j.immuni.2017.08.018
10. Zhang Y, Crawford HC, Pasca di Magliano M. Epithelial-Stromal Interactions in Pancreatic Cancer. *Annu Rev Physiol* (2019) 81:211–33. doi: 10.1146/annurev-physiol-020518-114515
11. Steele NG, Carpenter ES, Kemp SB, Sirihorachai VR, The S, Delrosario L, et al. Multimodal Mapping of the Tumor and Peripheral Blood Immune Landscape in Human Pancreatic Cancer. *Nat Cancer* (2020) 1(11):1097–112. doi: 10.1038/s43018-020-00121-4
12. Sano M, Ijichi H, Takahashi R, Miyabayashi K, Fujiwara H, Yamada T, et al. Blocking CXCLs-CXCR2 Axis in Tumor-Stromal Interactions Contributes to Survival in a Mouse Model of Pancreatic Ductal Adenocarcinoma Through Reduced Cell Invasion/Migration and a Shift of Immune-Inflammatory Microenvironment. *Oncogenesis* (2019) 8(2):8. doi: 10.1038/s41389-018-0117-8
13. Steele CW, Karim SA, Leach JDG, Bailey P, Upstill-Goddard R, Rishi L, et al. CXCR2 Inhibition Profoundly Suppresses Metastases and Augments Immunotherapy in Pancreatic Ductal Adenocarcinoma. *Cancer Cell* (2016) 29(6):832–45. doi: 10.1016/j.ccell.2016.04.014
14. Zhang Y, Yan W, Mathew E, Kane KT, Brannon A, Adoumie M, et al. Epithelial-Myeloid Cell Crosstalk Regulates Acinar Cell Plasticity and Pancreatic Remodeling in Mice. *Elife* (2017) 6:e27388. doi: 10.7554/eLife.27388
15. Halbrook CJ, Pontious C, Kovalenko I, Lapienyte L, Dreyer S, Lee HJ, et al. Macrophage-Released Pyrimidines Inhibit Gemcitabine Therapy in Pancreatic Cancer. *Cell Metab* (2019) 29(6):1390–9.e6. doi: 10.1016/j.cmet.2019.02.001
16. Weizman N, Krelin Y, Shabtay-Orbach A, Amit M, Binenbaum Y, Wong RJ, et al. Macrophages Mediate Gemcitabine Resistance of Pancreatic Adenocarcinoma by Upregulating Cytidine Deaminase. *Oncogene* (2014) 33(29):3812–9. doi: 10.1038/onc.2013.357
17. Azad A, Yin Lim S, D'Costa Z, Jones K, Diana A, Sansom OJ, et al. PD-L1 Blockade Enhances Response of Pancreatic Ductal Adenocarcinoma to Radiotherapy. *EMBO Mol Med* (2017) 9(2):167–80. doi: 10.15252/emmm.201606674
18. Griesmann H, Drexel C, Milosevic N, Sipos B, Rosendahl J, Gress TM, et al. Pharmacological Macrophage Inhibition Decreases Metastasis Formation in a Genetic Model of Pancreatic Cancer. *Gut* (2017) 66(7):1278–85. doi: 10.1136/gutjnl-2015-310049
19. Kanda M, Matthaei H, Wu J, Hong SM, Yu J, Borges M, et al. Presence of Somatic Mutations in Most Early-Stage Pancreatic Intraepithelial Neoplasia. *Gastroenterology* (2012) 142(4):730–3 e9. doi: 10.1053/j.gastro.2011.12.042
20. Ying H, Dey P, Yao W, Kimmelman AC, Draetta GF, Maitra A, et al. Genetics and Biology of Pancreatic Ductal Adenocarcinoma. *Genes Dev* (2016) 30(4):355–85. doi: 10.1101/gad.275776.115
21. Bailey P, Chang DK, Nones K, Johns AL, Patch AM, Gingras MC, et al. Genomic Analyses Identify Molecular Subtypes of Pancreatic Cancer. *Nature* (2016) 531(7592):47–52. doi: 10.1038/nature16965
22. Cancer Genome Atlas Research Network. Electronic Address Aadhe, Cancer Genome Atlas Research N. Integrated Genomic Characterization of Pancreatic Ductal Adenocarcinoma. *Cancer Cell* (2017) 32(2):185–203.e13. doi: 10.1016/j.ccell.2017.07.007
23. Waddell N, Pajic M, Patch AM, Chang DK, Kassahn KS, Bailey P, et al. Whole Genomes Redefine the Mutational Landscape of Pancreatic Cancer. *Nature* (2015) 518(7540):495–501. doi: 10.1038/nature14169
24. Storz P, Crawford HC. Carcinogenesis of Pancreatic Ductal Adenocarcinoma. *Gastroenterology* (2020) 158(8):2072–81. doi: 10.1053/j.gastro.2020.02.059
25. Wilson C, Ye X, Pham T, Lin E, Chan S, McNamara E, et al. AXL Inhibition Sensitizes Mesenchymal Cancer Cells to Antimitotic Drugs. *Cancer Res* (2014) 74(20):5878–90. doi: 10.1158/0008-5472.CAN-14-1009
26. Hingorani SR, Petricoin EF, Maitra A, Rajapakse V, King C, Jacobetz MA, et al. Preinvasive and Invasive Ductal Pancreatic Cancer and its Early Detection in the Mouse. *Cancer Cell* (2003) 4(6):437–50. doi: 10.1016/s1535-6108(03)00309-x
27. Collins MA, Bednar F, Zhang Y, Brisset JC, Galban S, Galban CJ, et al. Oncogenic Kras is Required for Both the Initiation and Maintenance of Pancreatic Cancer in Mice. *J Clin Invest* (2012) 122(2):639–53. doi: 10.1172/JCI59227
28. Clark CE, Hingorani SR, Mick R, Combs C, Tuveson DA, Vonderheide RH. Dynamics of the Immune Reaction to Pancreatic Cancer From Inception to Invasion. *Cancer Res* (2007) 67(19):9518–27. doi: 10.1158/0008-5472.CAN-07-0175
29. Hingorani SR, Wang L, Multani AS, Combs C, Deramaudt TB, Hruban RH, et al. Trp53R172H and KrasG12D Cooperate to Promote Chromosomal Instability and Widely Metastatic Pancreatic Ductal Adenocarcinoma in Mice. *Cancer Cell* (2005) 7(5):469–83. doi: 10.1016/j.ccr.2005.04.023
30. Bernard V, Semaan A, Huang J, San Lucas FA, Mulu FC, Stephens BM, et al. Single-Cell Transcriptomics of Pancreatic Cancer Precursors Demonstrates Epithelial and Microenvironmental Heterogeneity as an Early Event in Neoplastic Progression. *Clin Cancer Res* (2019) 25(7):2194–205. doi: 10.1158/1078-0432.CCR-18-1955
31. Tang Y, Xu X, Guo S, Zhang C, Tang Y, Tian Y, et al. An Increased Abundance of Tumor-Infiltrating Regulatory T Cells is Correlated With the Progression and Prognosis of Pancreatic Ductal Adenocarcinoma. *PloS One* (2014) 9(3):e91551. doi: 10.1371/journal.pone.0091551
32. Stromnes IM, Hulbert A, Pierce RH, Greenberg PD, Hingorani SR. T-Cell Localization, Activation, and Clonal Expansion in Human Pancreatic Ductal Adenocarcinoma. *Cancer Immunol Res* (2017) 5(11):978–91. doi: 10.1158/2326-6066.CIR-16-0322
33. Ischenko I, D'Amico S, Rao M, Li J, Hayman MJ, Powers S, et al. KRAS Drives Immune Evasion in a Genetic Model of Pancreatic Cancer. *Nat Commun* (2021) 12(1):1482. doi: 10.1038/s41467-021-21736-w
34. Yamamoto K, Venida A, Yano J, Biancur DE, Kakiuchi M, Gupta S, et al. Autophagy Promotes Immune Evasion of Pancreatic Cancer by Degrading MHC-I. *Nature* (2020) 581(7806):100–5. doi: 10.1038/s41586-020-2229-5
35. Pylayeva-Gupta Y, Lee KE, Hajdu CH, Miller G, Bar-Sagi D. Oncogenic Kras-Induced GM-CSF Production Promotes the Development of Pancreatic Neoplasia. *Cancer Cell* (2012) 21(6):836–47. doi: 10.1016/j.ccr.2012.04.024
36. Bayne LJ, Beatty GL, Jhala N, Clark CE, Rhim AD , Stanger BZ, et al. Tumor-Derived Granulocyte-Macrophage Colony-Stimulating Factor Regulates Myeloid Inflammation and T Cell Immunity in Pancreatic Cancer. *Cancer Cell* (2012) 21(6):822–35. doi: 10.1016/j.ccr.2012.04.025S1535-6108(12)00167-5[pii
37. Cheng H, Fan K, Luo G, Fan Z, Yang C, Huang Q, et al. Kras(G12D) Mutation Contributes to Regulatory T Cell Conversion Through Activation of the MEK/ERK Pathway in Pancreatic Cancer. *Cancer Lett* (2019) 446:103–11. doi: 10.1016/j.canlet.2019.01.013
38. Liou GY, Doppler H, Necela B, Edenfield B, Zhang L, Dawson DW, et al. Mutant KRAS-Induced Expression of ICAM-1 in Pancreatic Acinar Cells Causes Attraction of Macrophages to Expedite the Formation of Precancerous Lesions. *Cancer Discovery* (2015) 5(1):52–63. doi: 10.1158/2159-8290.CD-14-0474
39. Ratnam NM, Peterson JM, Talbert EE, Ladner KJ, Rajasekera PV, Schmidt CR, et al. NF-kappaB Regulates GDF-15 to Suppress Macrophage Surveillance During Early Tumor Development. *J Clin Invest* (2017) 127 (10):3796–809. doi: 10.1172/JCI91561
40. Dai E, Han L, Liu J, Xie Y, Kroemer G, Klionsky DJ, et al. Autophagy-Dependent Ferroptosis Drives Tumor-Associated Macrophage Polarization *via* Release and Uptake of Oncogenic KRAS Protein. *Autophagy* (2020) 16 (11):2069–83. doi: 10.1080/15548627.2020.1714209
41. Pickup MW, Owens P, Gorska AE, Chytil A, Ye F, Shi C, et al. Development of Aggressive Pancreatic Ductal Adenocarcinomas Depends on Granulocyte Colony Stimulating Factor Secretion in Carcinoma Cells. *Cancer Immunol Res* (2017) 5(9):718–29. doi: 10.1158/2326-6066.CIR-16-0311
42. Flint TR, Janowitz T, Connell CM, Roberts EW, Denton AE, Coll AP, et al. Tumor-Induced IL-6 Reprograms Host Metabolism to Suppress Anti-Tumor Immunity. *Cell Metab* (2016) 24(5):672–84. doi: 10.1016/j.cmet.2016.10.010

43. Wiedemann GM, Knott MM, Vetter VK, Rapp M, Haubner S, Fesseler J, et al. Cancer Cell-Derived IL-1alpha Induces CCL22 and the Recruitment of Regulatory T Cells. *Oncoimmunology* (2016) 5(9):e1175794. doi: 10.1080/2162402X.2016.1175794
44. Das S, Shapiro B, Vucic EA, Vogt S, Bar-Sagi D. Tumor Cell-Derived IL1beta Promotes Desmoplasia and Immune Suppression in Pancreatic Cancer. *Cancer Res* (2020) 80(5):1088–101. doi: 10.1158/0008-5472.CAN-19-2080
45. Takahashi R, Macchini M, Sunagawa M, Jiang Z, Tanaka T, Valenti G, et al. Interleukin-1beta-Induced Pancreatitis Promotes Pancreatic Ductal Adenocarcinoma. *Via B Lymphocyte-Mediated Immune Suppression Gut* (2021) 70(2):330–41. doi: 10.1136/gutjnl-2019-319912
46. Li J, Yuan S, Norgard RJ, Yan F, Yamazoe T, Blanco A, et al. Tumor Cell-Intrinsic USP22 Suppresses Antitumor Immunity in Pancreatic Cancer. *Cancer Immunol Res* (2020) 8(3):282–91. doi: 10.1158/2326-6066.CIR-19-0661
47. Zhang M, Huang L, Ding G, Huang H, Cao G, Sun X, et al. Interferon Gamma Inhibits CXCL8-CXCR2 Axis Mediated Tumor-Associated Macrophages Tumor Trafficking and Enhances Anti-PD1 Efficacy in Pancreatic Cancer. *J Immunother Cancer* (2020) 8(1):e000308. doi: 10.1136/jitc-2019-000308
48. Peng YP, Zhang JJ, Liang WB, Tu M, Lu ZP, Wei JS, et al. Elevation of MMP-9 and IDO Induced by Pancreatic Cancer Cells Mediates Natural Killer Cell Dysfunction. *BMC Cancer* (2014) 14:738. doi: 10.1186/1471-2407-14-738
49. Zhang Y, Velez-Delgado A, Mathew E, Li D, Mendez FM, Flannagan K, et al. Myeloid Cells are Required for PD-1/PD-L1 Checkpoint Activation and the Establishment of an Immunosuppressive Environment in Pancreatic Cancer. *Gut* (2017) 66(1):124–36. doi: 10.1136/gutjnl-2016-312078
50. Nomi T, Sho M, Akahori T, Hamada K, Kubo A, Kanehiro H, et al. Clinical Significance and Therapeutic Potential of the Programmed Death-1 Ligand/Programmed Death-1 Pathway in Human Pancreatic Cancer. *Clin Cancer Res* (2007) 13(7):2151–7. doi: 10.1158/1078-0432.CCR-06-2746
51. Ruscetti M, Morris J, Mezzadra R, Russell J, Leibold J, Romesser PB, et al. Senescence-Induced Vascular Remodeling Creates Therapeutic Vulnerabilities in Pancreas Cancer. *Cell* (2020) 181(2):424–41 e21. doi: 10.1016/j.cell.2020.03.008
52. Geginat J, Paroni M, Maglie S, Alfen JS, Kastirr I, Gruarin P, et al. Plasticity of Human CD4 T Cell Subsets. *Front Immunol* (2014) 5:630. doi: 10.3389/fimmu.2014.00630
53. Ochi A, Nguyen AH, Bedrosian AS, Mushlin HM, Zarbakhsh S, Barilla R, et al. MyD88 Inhibition Amplifies Dendritic Cell Capacity to Promote Pancreatic Carcinogenesis. *Via Th2 Cells J Exp Med* (2012) 209(9):1671–87. doi: 10.1084/jem.20111706
54. De Monte L, Reni M, Tassi E, Clavenna D, Papa I, Recalde H, et al. Intratumor T Helper Type 2 Cell Infiltrate Correlates With Cancer-Associated Fibroblast Thymic Stromal Lymphopoietin Production and Reduced Survival in Pancreatic Cancer. *J Exp Med* (2011) 208(3):469–78. doi: 10.1084/jem.20101876
55. Lang C, Wang J, Chen L. CD25-Expressing Th17 Cells Mediate CD8(+) T Cell Suppression in CTLA-4 Dependent Mechanisms in Pancreatic Ductal Adenocarcinoma. *Exp Cell Res* (2017) 360(2):384–9. doi: 10.1016/j.yexcr.2017.09.030
56. McAllister F, Bailey JM, Alsina J, Nirschl CJ, Sharma R, Fan H, et al. Oncogenic Kras Activates a Hematopoietic-to-Epithelial IL-17 Signaling Axis in Preinvasive Pancreatic Neoplasia. *Cancer Cell* (2014) 25(5):621–37. doi: 10.1016/j.ccr.2014.03.014
57. Zhang Y, Chandra V, Riquelme Sanchez E, Dutta P, Quesada PR, Rakoski A, et al. Interleukin-17-Induced Neutrophil Extracellular Traps Mediate Resistance to Checkpoint Blockade in Pancreatic Cancer. *J Exp Med* (2020) 217(12):e20190354. doi: 10.1084/jem.20190354
58. Hiraoka N, Onozato K, Kosuge T, Hirohashi S. Prevalence of FOXP3+ Regulatory T Cells Increases During the Progression of Pancreatic Ductal Adenocarcinoma and its Premalignant Lesions. *Clin Cancer Res* (2006) 12(18):5423–34. doi: 10.1158/1078-0432.CCR-06-0369
59. Wang X, Lang M, Zhao T, Feng X, Zheng C, Huang C, et al. Cancer-FOXP3 Directly Activated CCL5 to Recruit FOXP3(+)Treg Cells in Pancreatic Ductal Adenocarcinoma. *Oncogene* (2017) 36(21):3048–58. doi: 10.1038/onc.2016.458
60. Tan MC, Goedegebuure PS, Belt BA, Flaherty B, Sankpal N, Gillanders WE, et al. Disruption of CCR5-Dependent Homing of Regulatory T Cells Inhibits Tumor Growth in a Murine Model of Pancreatic Cancer. *J Immunol* (2009) 182(3):1746–55. doi: 10.4049/jimmunol.182.3.1746
61. Jang JE, Hajdu CH, Liot C, Miller G, Dustin ML, Bar-Sagi D. Crosstalk Between Regulatory T Cells and Tumor-Associated Dendritic Cells Negates Anti-Tumor Immunity in Pancreatic Cancer. *Cell Rep* (2017) 20(3):558–71. doi: 10.1016/j.celrep.2017.06.062
62. Zhang Y, Lazarus J, Steele NG, Yan W, Lee HJ, Nwosu ZC, et al. Regulatory T-Cell Depletion Alters the Tumor Microenvironment and Accelerates Pancreatic Carcinogenesis. *Cancer Discov* (2020) 10(3):422–39. doi: 10.1158/2159-8290.CD-19-0958
63. Liou GY, Doppler H, Necela B, Krishna M, Crawford HC, Raimondo M, et al. Macrophage-Secreted Cytokines Drive Pancreatic Acinar-to-Ductal Metaplasia Through NF-kappaB and MMPs. *J Cell Biol* (2013) 202(3):563–77. doi: 10.1083/jcb.201301001
64. O'Bryan JP, Frye RA, Cogswell PC, Neubauer A, Kitch B, Prokop C, et al. Axl, a Transforming Gene Isolated From Primary Human Myeloid Leukemia Cells, Encodes a Novel Receptor Tyrosine Kinase. *Mol Cell Biol* (1991) 11(10):5016–31. doi: 10.1128/MCB.11.10.5016
65. Cartwright ANR, Suo S, Badrinath S, Kumar S, Melms J, Luoma A, et al. Immunosuppressive Myeloid Cells Induce Nitric Oxide-Dependent DNA Damage and P53 Pathway Activation in CD8(+) T Cells. *Cancer Immunol Res* (2021) 9(4):470–85. doi: 10.1158/2326-6066.CIR-20-0085
66. Siret C, Collignon A, Silvy F, Robert S, Cheyrol T, Andre P, et al. Deciphering the Crosstalk Between Myeloid-Derived Suppressor Cells and Regulatory T Cells in Pancreatic Ductal Adenocarcinoma. *Front Immunol* (2019) 10:3070. doi: 10.3389/fimmu.2019.03070
67. D'Amico L, Mahajan S, Capietto AH, Yang Z, Zamani A, Ricci B, et al. Dickkopf-Related Protein 1 (Dkk1) Regulates the Accumulation and Function of Myeloid Derived Suppressor Cells in Cancer. *J Exp Med* (2016) 213(5):827–40. doi: 10.1084/jem.20150950
68. Chao T, Furth EE, Vonderheide RH. CXCR2-Dependent Accumulation of Tumor-Associated Neutrophils Regulates T-Cell Immunity in Pancreatic Ductal Adenocarcinoma. *Cancer Immunol Res* (2016) 4(11):968–82. doi: 10.1158/2326-6066.CIR-16-0188
69. Murray PJ, Allen JE, Biswas SK, Fisher EA, Gilroy DW, Goerdt S, et al. Macrophage Activation and Polarization: Nomenclature and Experimental Guidelines. *Immunity* (2014) 41(1):14–20. doi: 10.1016/j.immuni.2014.06.008
70. Qian BZ, Li J, Zhang H, Kitamura T, Zhang J, Campion LR, et al. CCL2 Recruits Inflammatory Monocytes to Facilitate Breast-Tumour Metastasis. *Nature* (2011) 475(7355):222–5. doi: 10.1038/nature10138
71. Walens A, DiMarco AV, Lupo R, Kroger BR, Damrauer JS, Alvarez JV. CCL5 Promotes Breast Cancer Recurrence Through Macrophage Recruitment in Residual Tumors. *Elife* (2019) 8:e43653. doi: 10.7554/eLife.43653
72. Keophiphath M, Rouault C, Divoux A, Clement K, Lacasa D. CCL5 Promotes Macrophage Recruitment and Survival in Human Adipose Tissue. *Arterioscler Thromb Vasc Biol* (2010) 30(1):39–45. doi: 10.1161/ATVBAHA.109.197442
73. Sanford DE, Belt BA, Panni RZ, Mayer A, Deshpande AD, Carpenter D, et al. Inflammatory Monocyte Mobilization Decreases Patient Survival in Pancreatic Cancer: A Role for Targeting the CCL2/CCR2 Axis. *Clin Cancer Res* (2013) 19(13):3404–15. doi: 10.1158/1078-0432.CCR-13-0525
74. Van Overmeire E, Stijlemans B, Heymann F, Keirsse J, Morias Y, Elkrim Y, et al. M-CSF and GM-CSF Receptor Signaling Differentially Regulate Monocyte Maturation and Macrophage Polarization in the Tumor Microenvironment. *Cancer Res* (2016) 76(1):35–42. doi: 10.1158/0008-5472.CAN-15-0869
75. Wood GW, De M, Sanford T, Choudhuri R. Macrophage Colony Stimulating Factor Controls Macrophage Recruitment to the Cycling Mouse Uterus. *Dev Biol* (1992) 152(2):336–43. doi: 10.1016/0012-1606(92)90140-c
76. Gregory JL, Morand EF, McKeown SJ, Ralph JA, Hall P, Yang YH, et al. Macrophage Migration Inhibitory Factor Induces Macrophage Recruitment *via* CC Chemokine Ligand 2. *J Immunol* (2006) 177(11):8072–9. doi: 10.4049/jimmunol.177.11.8072
77. Arango Duque G, Descoteaux A. Macrophage Cytokines: Involvement in Immunity and Infectious Diseases. *Front Immunol* (2014) 5:491. doi: 10.3389/fimmu.2014.00491

78. Savage ND, de Boer T, Walburg KV, Joosten SA, van Meijgaarden K, Geluk A, et al. Human Anti-Inflammatory Macrophages Induce Foxp3+ GITR+ CD25+ Regulatory T Cells, Which Suppress. *Via Membrane-bound TGFbeta-1 J Immunol* (2008) 181(3):2220–6. doi: 10.4049/jimmunol.181.3.2220
79. Denning TL, Wang YC, Patel SR, Williams IR, Pulendran B. Lamina Propria Macrophages and Dendritic Cells Differentially Induce Regulatory and Interleukin 17-Producing T Cell Responses. *Nat Immunol* (2007) 8 (10):1086–94. doi: 10.1038/ni1511
80. Ellyard JI, Quah BJ, Simson L, Parish CR. Alternatively Activated Macrophage Possess Antitumor Cytotoxicity That is Induced by IL-4 and Mediated by Arginase-1. *J Immunother* (2010) 33(5):443–52. doi: 10.1097/CJI.0b013e3181cd8746
81. Bronte V, Zanovello P. Regulation of Immune Responses by L-Arginine Metabolism. *Nat Rev Immunol* (2005) 5(8):641–54. doi: 10.1038/nri1668
82. Sica A, Larghi P, Mancino A, Rubino L, Porta C, Totaro MG, et al. Macrophage Polarization in Tumour Progression. *Semin Cancer Biol* (2008) 18(5):349–55. doi: 10.1016/j.semcancer.2008.03.004
83. Sica A, Mantovani A. Macrophage Plasticity and Polarization: *In Vivo* Veritas. *J Clin Invest* (2012) 122(3):787–95. doi: 10.1172/JCI59643
84. Candido JB, Morton JP, Bailey P, Campbell AD, Karim SA, Jamieson T, et al. CSF1R(+) Macrophages Sustain Pancreatic Tumor Growth Through T Cell Suppression and Maintenance of Key Gene Programs That Define the Squamous Subtype. *Cell Rep* (2018) 23(5):1448–60. doi: 10.1016/j.celrep.2018.03.131
85. Mitchem JB, Brennan DJ, Knolhoff BL, Belt BA, Zhu Y , Sanford DE, et al. Targeting Tumor-Infiltrating Macrophages Decreases Tumor-Initiating Cells, Relieves Immunosuppression, and Improves Chemotherapeutic Responses. *Cancer Res* (2013) 73(3):1128–41. doi: 10.1158/0008-5472.CAN-12-27310008-5472.CAN-12-2731[pii
86. Zhu Y, Knolhoff BL, Meyer MA, Nywening TM, West BL, Luo J, et al. CSF1/CSF1R Blockade Reprograms Tumor-Infiltrating Macrophages and Improves Response to T-Cell Checkpoint Immunotherapy in Pancreatic Cancer Models. *Cancer Res* (2014) 74(18):5057–69. doi: 10.1158/0008-5472.CAN-13-3723
87. Nielsen SR, Quaranta V, Linford A, Emeagi P, Rainer C, Santos A, et al. Macrophage-Secreted Granulin Supports Pancreatic Cancer Metastasis by Inducing Liver Fibrosis. *Nat Cell Biol* (2016) 18(5):549–60. doi: 10.1038/ncb3340
88. Cassier PA, Garin G, Eberst L, Delord J-P, Chabaud S, Terret C, et al. MEDIPLEX: A Phase 1 Study of Durvalumab (D) Combined With Pexidartinib (P) in Patients (Pts) With Advanced Pancreatic Ductal Adenocarcinoma (PDAC) and Colorectal Cancer (CRC). *Am Soc Clin Oncol* (2019) 37(15_suppl):2579. doi: 10.1200/JCO.2019.37.15_suppl.2579
89. Wang W, Marinis JM, Beal AM, Savadkar S, Wu Y, Khan M, et al. RIP1 Kinase Drives Macrophage-Mediated Adaptive Immune Tolerance in Pancreatic Cancer. *Cancer Cell* (2018) 34(5):757–74 e7. doi: 10.1016/j.ccell.2018.10.006
90. Nywening TM, Belt BA, Cullinan DR, Panni RZ, Han BJ, Sanford DE, et al. Targeting Both Tumour-Associated CXCR2(+) Neutrophils and CCR2(+) Macrophages Disrupts Myeloid Recruitment and Improves Chemotherapeutic Responses in Pancreatic Ductal Adenocarcinoma. *Gut* (2018) 67(6):1112–23. doi: 10.1136/gutjnl-2017-313738
91. Hegde S, Krisnawan VE, Herzog BH, Zuo C, Breden MA, Knolhoff BL, et al. Dendritic Cell Paucity Leads to Dysfunctional Immune Surveillance in Pancreatic Cancer. *Cancer Cell* (2020) 37(3):289–307 e9. doi: 10.1016/j.ccell.2020.02.008
92. Lin JH, Huffman AP, Wattenberg MM, Walter DM, Carpenter EL, Feldser DM, et al. Type 1 Conventional Dendritic Cells are Systemically Dysregulated Early in Pancreatic Carcinogenesis. *J Exp Med* (2020) 217(8): e20190673. doi: 10.1084/jem.20190673
93. Barilla RM, Diskin B, Caso RC, Lee KB, Mohan N, Buttar C, et al. Specialized Dendritic Cells Induce Tumor-Promoting IL-10(+)IL-17(+) FoxP3(neg) Regulatory CD4(+) T Cells in Pancreatic Carcinoma. *Nat Commun* (2019) 10(1):1424. doi: 10.1038/s41467-019-09416-2
94. Vonderheide RH. CD40 Agonist Antibodies in Cancer Immunotherapy. *Annu Rev Med* (2020) 71:47–58. doi: 10.1146/annurev-med-062518-045435
95. Beatty GL, Chiorean EG, Fishman MP, Saboury B, Teitelbaum UR, Sun W, et al. CD40 Agonists Alter Tumor Stroma and Show Efficacy Against Pancreatic Carcinoma in Mice and Humans. *Science* (2011) 331 (6024):1612–6. doi: 10.1126/science.1198443
96. Morrison AH, Diamond MS, Hay CA, Byrne KT, Vonderheide RH. Sufficiency of CD40 Activation and Immune Checkpoint Blockade for T Cell Priming and Tumor Immunity. *Proc Natl Acad Sci USA* (2020) 117 (14):8022–31. doi: 10.1073/pnas.1918971117
97. O'Hara MH, O'Reilly EM, Varadhachary G, Wolff RA, Wainberg ZA, Ko AH, et al. CD40 Agonistic Monoclonal Antibody APX005M (Sotigalimab) and Chemotherapy, With or Without Nivolumab, for the Treatment of Metastatic Pancreatic Adenocarcinoma: An Open-Label, Multicentre, Phase 1b Study. *Lancet Oncol* (2021) 22(1):118–31. doi: 10.1016/S1470-2045(20)30532-5
98. Deicher A, Andersson R, Tingstedt B, Lindell G, Bauden M, Ansari D. Targeting Dendritic Cells in Pancreatic Ductal Adenocarcinoma. *Cancer Cell Int* (2018) 18:85. doi: 10.1186/s12935-018-0585-0
99. Bauer C, Dauer M, Saraj S, Schnurr M, Bauernfeind F, Sterzik A, et al. Dendritic Cell-Based Vaccination of Patients With Advanced Pancreatic Carcinoma: Results of a Pilot Study. *Cancer Immunol Immunother* (2011) 60 (8):1097–107. doi: 10.1007/s00262-011-1023-5
100. Hancharou A, Timohina O, Prokhorov A, Romanovskaya S, Dubuske L. Efficacy of Dendritic Cell Based Immunotherapy for Patients With Pancreatic Cancer. *J Allergy Clin Immunol* (2020) 145(2, Supplement): AB242. doi: 10.1016/j.jaci.2019.12.145
101. Lee KE, Spata M, Bayne LJ, Buza EL, Durham AC, Allman D, et al. Hif1a Deletion Reveals Pro-Neoplastic Function of B Cells in Pancreatic Neoplasia. *Cancer Discovery* (2016) 6(3):256–69. doi: 10.1158/2159-8290.CD-15-0822
102. Pylayeva-Gupta Y, Das S, Handler JS, Hajdu CH, Coffre M, Koralov SB, et al. IL35-Producing B Cells Promote the Development of Pancreatic Neoplasia. *Cancer Discovery* (2016) 6(3):247–55. doi: 10.1158/2159-8290.CD-15-0843
103. Gunderson AJ, Kaneda MM, Tsujikawa T, Nguyen AV, Affara NI, Ruffell B, et al. Bruton Tyrosine Kinase-Dependent Immune Cell Cross-Talk Drives Pancreas Cancer. *Cancer Discov* (2016) 6(3):270–85. doi: 10.1158/2159-8290.CD-15-0827
104. Tempero M, Oh DY, Tabernero J, Reni M, Van Cutsem E, Hendifar A, et al. Ibrutinib in Combination With Nab-Paclitaxel and Gemcitabine for First-Line Treatment of Patients With Metastatic Pancreatic Adenocarcinoma: Phase III RESOLVE Study. *Ann Oncol* (2021) 32(5):600–8. doi: 10.1016/j.annonc.2021.01.070
105. Overman M, Javle M, Davis RE, Vats P, Kumar-Sinha C, Xiao L, et al. Randomized Phase II Study of the Bruton Tyrosine Kinase Inhibitor Acalabrutinib, Alone or With Pembrolizumab in Patients With Advanced Pancreatic Cancer. *J Immunother Cancer* (2020) 8(1):e000587. doi: 10.1136/jitc-2020-000587
106. Wen T, Wang J, Shi Y, Qian H, Liu P. Inhibitors Targeting Bruton's Tyrosine Kinase in Cancers: Drug Development Advances. *Leukemia* (2021) 35 (2):312–32. doi: 10.1038/s41375-020-01072-6
107. Whittle MC, Hingorani SR. Fibroblasts in Pancreatic Ductal Adenocarcinoma: Biological Mechanisms and Therapeutic Targets. *Gastroenterology* (2019) 156(7):2085–96. doi: 10.1053/j.gastro.2018.12.044
108. Thomas D, Radhakrishnan P. Pancreatic Stellate Cells: The Key Orchestrator of The Pancreatic Tumor Microenvironment. *Adv Exp Med Biol* (2020) 1234:57–70. doi: 10.1007/978-3-030-37184-5_5
109. Castells M, Thibault B, Delord JP, Couderc B. Implication of Tumor Microenvironment in Chemoresistance: Tumor-Associated Stromal Cells Protect Tumor Cells From Cell Death. *Int J Mol Sci* (2012) 13(8):9545–71. doi: 10.3390/ijms13089545
110. Neesse A, Bauer CA, Ohlund D, Lauth M, Buchholz M, Michl P, et al. Stromal Biology and Therapy in Pancreatic Cancer: Ready for Clinical Translation? *Gut* (2019) 68(1):159–71. doi: 10.1136/gutjnl-2018-316451
111. Stylianopoulos T, Munn LL, Jain RK. Reengineering the Physical Microenvironment of Tumors to Improve Drug Delivery and Efficacy: From Mathematical Modeling to Bench to Bedside. *Trends Cancer* (2018) 4(4):292–319. doi: 10.1016/j.trecan.2018.02.005
112. Hosein AN, Huang H, Wang Z, Parmar K, Du W, Huang J, et al. Cellular Heterogeneity During Mouse Pancreatic Ductal Adenocarcinoma Progression at Single-Cell Resolution. *JCI Insight* (2019) 5:e129212. doi: 10.1172/jci.insight.129212
113. Elyada E, Bolisetty M, Laise P, Flynn WF, Courtois ET, Burkhart RA, et al. Cross-Species Single-Cell Analysis of Pancreatic Ductal Adenocarcinoma

Reveals Antigen-Presenting Cancer-Associated Fibroblasts. *Cancer Discov* (2019) 9(8):1102–23. doi: 10.1158/2159-8290.CD-19-0094
114. Ohlund D, Handly-Santana A, Biffi G, Elyada E, Almeida AS, Ponz-Sarvise M, et al. Distinct Populations of Inflammatory Fibroblasts and Myofibroblasts in Pancreatic Cancer. *J Exp Med* (2017) 214(3):579–96. doi: 10.1084/jem.20162024
115. Helms E, Onate MK, Sherman MH. Fibroblast Heterogeneity in the Pancreatic Tumor Microenvironment. *Cancer Discov* (2020) 10(5):648–56. doi: 10.1158/2159-8290.CD-19-1353
116. Huang H, Wang Z, Zhang Y, Brekken RA. Mesothelial Cell-Derived Antigen-Presenting Cancer-Associated Fibroblasts Induce Expansion of Regulatory T Cells in Pancreatic Cancer. *bioRxiv* (2021), 2021.02.04.429827. doi: 10.1101/2021.02.04.429827
117. Dominguez CX, Muller S, Keerthivasan S, Koeppen H, Hung J, Gierke S, et al. Single-Cell RNA Sequencing Reveals Stromal Evolution Into LRRC15(+) Myofibroblasts as a Determinant of Patient Response to Cancer Immunotherapy. *Cancer Discovery* (2020) 10(2):232–53. doi: 10.1158/2159-8290.CD-19-0644
118. Ozdemir BC, Pentcheva-Hoang T, Carstens JL, Zheng X, Wu CC, Simpson TR, et al. Depletion of Carcinoma-Associated Fibroblasts and Fibrosis Induces Immunosuppression and Accelerates Pancreas Cancer With Reduced Survival. *Cancer Cell* (2014) 25(6):719–34. doi: 10.1016/j.ccr.2014.04.005
119. Li C, Cui L, Yang L, Wang B, Zhuo Y, Zhang L, et al. Pancreatic Stellate Cells Promote Tumor Progression by Promoting an Immunosuppressive Microenvironment in Murine Models of Pancreatic Cancer. *Pancreas* (2020) 49(1):120–7. doi: 10.1097/MPA.0000000000001464
120. Ene-Obong A, Clear AJ, Watt J, Wang J, Fatah R, Riches JC, et al. Activated Pancreatic Stellate Cells Sequester CD8+ T Cells to Reduce Their Infiltration of the Juxtatumoral Compartment of Pancreatic Ductal Adenocarcinoma. *Gastroenterology* (2013) 145(5):1121–32. doi: 10.1053/j.gastro.2013.07.025
121. Garg B, Giri B, Modi S, Sethi V, Castro I, Umland O, et al. NFkappaB in Pancreatic Stellate Cells Reduces Infiltration of Tumors by Cytotoxic T Cells and Killing of Cancer Cells. *Via Up-Regulation CXCL12 Gastroenterol* (2018) 155(3):880–91 e8. doi: 10.1053/j.gastro.2018.05.051
122. Mace TA, Ameen Z, Collins A, Wojcik S, Mair M, Young GS, et al. Pancreatic Cancer-Associated Stellate Cells Promote Differentiation of Myeloid-Derived Suppressor Cells in a STAT3-Dependent Manner. *Cancer Res* (2013) 73(10):3007–18. doi: 10.1158/0008-5472.CAN-12-4601
123. Steele NG, Biffi G, Kemp SB, Zhang Y, Drouillard D, Syu L, et al. Inhibition of Hedgehog Signaling Alters Fibroblast Composition in Pancreatic Cancer. *Clin Cancer Res* (2021) 27(7):2023–37. doi: 10.1158/1078-0432.CCR-20-3715
124. Feurino LW, Zhang Y, Bharadwaj U, Zhang R, Li F, Fisher WE, et al. IL-6 Stimulates Th2 Type Cytokine Secretion and Upregulates VEGF and NRP-1 Expression in Pancreatic Cancer Cells. *Cancer Biol Ther* (2007) 6(7):1096–100. doi: 10.4161/cbt.6.7.4328
125. Huang H, Zhang Y, Gallegos V, Sorrelle N, Zaid MM, Toombs J, et al. Targeting TGFbetaR2-Mutant Tumors Exposes Vulnerabilities to Stromal TGFbeta Blockade in Pancreatic Cancer. *EMBO Mol Med* (2019) 11(11): e10515. doi: 10.15252/emmm.201910515
126. Mace TA, Shakya R, Pitarresi JR, Swanson B, McQuinn CW, Loftus S, et al. IL-6 and PD-L1 Antibody Blockade Combination Therapy Reduces Tumour Progression in Murine Models of Pancreatic Cancer. *Gut* (2018) 67(2):320–32. doi: 10.1136/gutjnl-2016-311585
127. Zhang Y, Yan W, Collins MA, Bednar F, Rakshit S, Zetter BR, et al. Interleukin-6 is Required for Pancreatic Cancer Progression by Promoting MAPK Signaling Activation and Oxidative Stress Resistance. *Cancer Res* (2013) 73(20):6359–74. doi: 10.1158/0008-5472.CAN-13-1558-T
128. Wen Z, Liu Q, Wu J, Xu B, Wang J, Liang L, et al. Fibroblast Activation Protein Alpha-Positive Pancreatic Stellate Cells Promote the Migration and Invasion of Pancreatic Cancer by CXCL1-Mediated Akt Phosphorylation. *Ann Transl Med* (2019) 7(20):532. doi: 10.21037/atm.2019.09.164
129. Lunardi S, Lim SY, Muschel RJ, Brunner TB. IP-10/CXCL10 Attracts Regulatory T Cells: Implication for Pancreatic Cancer. *Oncoimmunology* (2015) 4(9):e1027473. doi: 10.1080/2162402X.2015.1027473
130. Andersson P, Yang Y, Hosaka K, Zhang Y, Fischer C, Braun H, et al. Molecular Mechanisms of IL-33-Mediated Stromal Interactions in Cancer Metastasis. *JCI Insight* (2018) 3(20):e122375. doi: 10.1172/jci.insight.122375
131. Pitarresi JR, Liu X, Sharma SM, Cuitino MC, Kladney RD, Mace TA, et al. Stromal ETS2 Regulates Chemokine Production and Immune Cell Recruitment During Acinar-To-Ductal Metaplasia. *Neoplasia* (2016) 18 (9):541–52. doi: 10.1016/j.neo.2016.07.006
132. Tang D, Yuan Z, Xue X, Lu Z, Zhang Y, Wang H, et al. High Expression of Galectin-1 in Pancreatic Stellate Cells Plays a Role in the Development and Maintenance of an Immunosuppressive Microenvironment in Pancreatic Cancer. *Int J Cancer* (2012) 130(10):2337–48. doi: 10.1002/ijc.26290
133. Goehrig D, Nigri J, Samain R, Wu Z, Cappello P, Gabiane G, et al. Stromal Protein Betaig-H3 Reprogrammes Tumour Microenvironment in Pancreatic Cancer. *Gut* (2019) 68(4):693–707. doi: 10.1136/gutjnl-2018-317570
134. Spivak-Kroizman TR, Hostetter G, Posner R, Aziz M, Hu C, Demeure MJ, et al. Hypoxia Triggers Hedgehog-Mediated Tumor-Stromal Interactions in Pancreatic Cancer. *Cancer Res* (2013) 73(11):3235–47. doi: 10.1158/0008-5472.CAN-11-1433
135. Hwang RF, Moore TT, Hattersley MM, Scarpitti M, Yang B, Devereaux E, et al. Inhibition of the Hedgehog Pathway Targets the Tumor-Associated Stroma in Pancreatic Cancer. *Mol Cancer Res* (2012) 10(9):1147–57. doi: 10.1158/1541-7786.MCR-12-0022
136. Bailey JM, Swanson BJ, Hamada T, Eggers JP, Singh PK, Caffery T, et al. Sonic Hedgehog Promotes Desmoplasia in Pancreatic Cancer. *Clin Cancer Res* (2008) 14(19):5995–6004. doi: 10.1158/1078-0432.CCR-08-0291
137. Mathew E, Collins MA, Fernandez-Barrena MG, Holtz AM, Yan W, Hogan JO, et al. The Transcription Factor GLI1 Modulates the Inflammatory Response During Pancreatic Tissue Remodeling. *J Biol Chem* (2014) 289 (40):27727–43. doi: 10.1074/jbc.M114.556563
138. Biffi G, Oni TE, Spielman B, Hao Y, Elyada E, Park Y, et al. IL1-Induced JAK/STAT Signaling Is Antagonized by TGFbeta to Shape CAF Heterogeneity in Pancreatic Ductal Adenocarcinoma. *Cancer Discov* (2019) 9(2):282–301. doi: 10.1158/2159-8290.CD-18-0710
139. Melisi D, Oh DY, Hollebecque A, Calvo E, Varghese A, Borazanci E, et al. Safety and Activity of the TGFbeta Receptor I Kinase Inhibitor Galunisertib Plus the Anti-PD-L1 Antibody Durvalumab in Metastatic Pancreatic Cancer. *J Immunother Cancer* (2021) 9(3):e002068. doi: 10.1136/jitc-2020-002068
140. Guerra C, Schuhmacher AJ, Canamero M, Grippo PJ, Verdaguer L, Perez-Gallego L, et al. Chronic Pancreatitis is Essential for Induction of Pancreatic Ductal Adenocarcinoma by K-Ras Oncogenes in Adult Mice. *Cancer Cell* (2007) 11(3):291–302. doi: 10.1016/j.ccr.2007.01.012
141. Kopp JL, von Figura G, Mayes E, Liu FF, Dubois CL, Morris J, et al. Identification of Sox9-Dependent Acinar-to-Ductal Reprogramming as the Principal Mechanism for Initiation of Pancreatic Ductal Adenocarcinoma. *Cancer Cell* (2012) 22(6):737–50. doi: 10.1016/j.ccr.2012.10.025
142. Burrack AL, Spartz EJ, Raynor JF, Wang I, Olson M, Stromnes IM. Combination PD-1 and PD-L1 Blockade Promotes Durable Neoantigen-Specific T Cell-Mediated Immunity in Pancreatic Ductal Adenocarcinoma. *Cell Rep* (2019) 28(8):2140–55 e6. doi: 10.1016/j.celrep.2019.07.059
143. Burrack AL, Rollins MR, Spartz EJ, Mesojednik TD, Schmiechen ZC, Raynor JF, et al. CD40 Agonist Overcomes T Cell Exhaustion Induced by Chronic Myeloid Cell IL-27 Production in a Pancreatic Cancer Preclinical Model. *J Immunol* (2021) 206(6):1372–84. doi: 10.4049/jimmunol.2000765
144. Ben-Shmuel A, Biber G, Barda-Saad M. Unleashing Natural Killer Cells in the Tumor Microenvironment-The Next Generation of Immunotherapy? *Front Immunol* (2020) 11:275. doi: 10.3389/fimmu.2020.00275
145. Jun E, Song AY, Choi JW, Lee HH, Kim MY, Ko DH, et al. Progressive Impairment of NK Cell Cytotoxic Degranulation Is Associated With TGF-Beta1 Deregulation and Disease Progression in Pancreatic Cancer. *Front Immunol* (2019) 10:1354. doi: 10.3389/fimmu.2019.01354
146. Drake CG. Combination Immunotherapy Approaches. *Ann Oncol* (2012) 23 Suppl 8:viii41–6. doi: 10.1093/annonc/mds262
147. Morrissey KM, Yuraszeck TM, Li CC, Zhang Y, Kasichayanula S. Immunotherapy and Novel Combinations in Oncology: Current Landscape, Challenges, and Opportunities. *Clin Transl Sci* (2016) 9(2):89–104. doi: 10.1111/cts.12391
148. Li J, Byrne KT, Yan F, Yamazoe T, Chen Z, Baslan T, et al. Tumor Cell-Intrinsic Factors Underlie Heterogeneity of Immune Cell Infiltration and

Response to Immunotherapy. *Immunity* (2018) 49(1):178–93.e7. doi: 10.1016/j.immuni.2018.06.006

149. Liudahl SM, Betts CB, Sivagnanam S, Morales-Oyarvide V, da Silva A, Yuan C, et al. Leukocyte Heterogeneity in Pancreatic Ductal Adenocarcinoma: Phenotypic and Spatial Features Associated With Clinical Outcome. *Cancer Discov* (2021). doi: 10.1158/2159-8290.Cd-20-0841
150. Grünwald BT, Devisme A, Andrieux G, Vyas F, Aliar K, McCloskey CW, et al. Spatially Confined Sub-Tumor Microenvironments Orchestrate Pancreatic Cancer Pathobiology. *bioRxiv* (2021) 2021.02.18.431890. doi: 10.1101/2021.02.18.431890

Conflict of Interest: The authors declare that the research was conducted in the absence of any commercial or financial relationships that could be construed as a potential conflict of interest.

frontiers in Oncology

ORIGINAL RESEARCH
published: 23 July 2021
doi: 10.3389/fonc.2021.674897

Analysis of Immune-Related Signatures Related to CD4+ T Cell Infiltration With Gene Co-Expression Network in Pancreatic Adenocarcinoma

Zhen Tan[1,2,3,4†], *Yubin Lei*[1,2,3,4†], *Bo Zhang*[1,2,3,4†], *Si Shi*[1,2,3,4], *Jiang Liu*[1,2,3,4], *Xianjun Yu*[1,2,3,4], *Jin Xu*[1,2,3,4*] *and Chen Liang*[1,2,3,4*]

[1] Department of Pancreatic Surgery, Fudan University Shanghai Cancer Center, Shanghai, China, [2] Department of Oncology, Shanghai Medical College, Fudan University, Shanghai, China, [3] Shanghai Pancreatic Cancer Institute, Shanghai, China, [4] Pancreatic Cancer Institute, Fudan University, Shanghai, China

OPEN ACCESS

Edited by:
Takatsugu Ishimoto, Kumamoto University, Japan

Reviewed by:
Chongyi Jiang, Fudan University, China
Jun Zhang, China Medical University, China

***Correspondence:**
Jin Xu
xujin@fudanpci.org
Chen Liang
liangchen@fudanpci.org

[†]*These authors have contributed equally to this work*

Specialty section:
This article was submitted to Gastrointestinal Cancers, a section of the journal Frontiers in Oncology

Received: *02 March 2021*
Accepted: *05 July 2021*
Published: *23 July 2021*

Citation:
Tan Z, Lei Y, Zhang B, Shi S, Liu J, Yu X, Xu J and Liang C (2021) Analysis of Immune-Related Signatures Related to CD4+ T Cell Infiltration With Gene Co-Expression Network in Pancreatic Adenocarcinoma. Front. Oncol. 11:674897. doi: 10.3389/fonc.2021.674897

Background: Pancreatic ductal adenocarcinoma (PDAC) is one of the most invasive solid malignancies. Immunotherapy and targeted therapy confirmed an existing certain curative effect in treating PDAC. The aim of this study was to develop an immune-related molecular marker to enhance the ability to predict Stages III and IV PDAC patients.

Method: In this study, weighted gene co-expression network (WGCNA) analysis and a deconvolution algorithm (CIBERSORT) that evaluated the cellular constituent of immune cells were used to evaluate PDAC expression data from the GEO (Gene Expression Omnibus) datasets, and identify modules related to CD4+ T cells. LASSO Cox regression analysis and Kaplan–Meier curve were applied to select and build prognostic multi-gene signature in TCGA Stages III and IV PDAC patients (N = 126). This was followed by independent Stages III and IV validation of the gene signature in the International Cancer Genome Consortium (ICGC, N = 62) and the Fudan University Shanghai Cancer Center (FUSCC, N = 42) cohort. Inherited germline mutations and tumor immunity exploration were applied to elucidate the molecular mechanisms in PDAC. Univariate and Multivariate Cox regression analyses were applied to verify the independent prognostic factors. Finally, a prognostic nomogram was created according to the TCGA-PDAC dataset.

Results: A four-gene signature comprising NAPSB, ZNF831, CXCL9 and PYHIN1 was established to predict overall survival of PDAC. This signature also robustly predicted survival in two independent validation cohorts. The four-gene signature could divide patients into high and low-risk groups with disparity overall survival verified by a Log-rank test. Expression of four genes positively correlated with immunosuppression activity (PD-L1 and PD1). Immune-related genes nomogram and corresponding calibration curves showed significant performance for predicting 3-year survival in TCGA-PDAC dataset.

Conclusion: We constructed a novel four-gene signature to predict the prognosis of Stages III and IV PDAC patients by applying WGCNA and CIBERSORT algorithm scoring

to transcriptome data different from traditional methods of filtrating for differential genes in cancer and healthy tissues. The findings may provide reference to predict survival and was beneficial to individualized management for advanced PDAC patients.

Keywords: pancreatic ductal adenocarcinoma, immunocytes infiltration, CIBERSORT, WGCNA, bioinformatics

INTRODUCTION

Pancreatic ductal adenocarcinoma (PDAC) is one of the most devastating human invasive solid malignancies in the world. Because of its early metastasis and chemotherapy-resistant, the 5-year survival rate of PDAC is less than 5% (1). However, PDAC patients of the same TNM stage may differ in survival, perhaps by reason of the complex immune microenvironment and the of PDAC. Thus, a better understanding of the pathogenesis of cancer and better signatures to help predict prognosis are imperative for improving individualized treatment for PDAC patients.

In recent decades, advances in high-throughput techniques have provided scientists with new insight into PDAC. Yan et al. revealed a four-gene signature (with LYRM1, KNTC1, IGF2BP2, and CDC6) that predicts OS (overall survival) from a PDAC dataset in TCGA using Cox proportional hazards regression analysis (2). Raman et al. developed a five-gene prognostic model that significantly related to the progression of pancreatic cancer through the same method (3). However, on account of the barrier of overfitting in high-dimensional microarray data, this method is not appropriate at some time. Least Absolute Shrinkage and Selection Operator (LASSO) regression could make up for the defects and has been widely used for optimize selection of genes (4). Additionally, PDAC is highly heterogeneous and the pathological characteristics of PDAC with different stages are quite different. Compared to Stage I patients, conventional chemotherapy and cancer immunotherapies have become the standard for first-line treatment of advanced PDAC patients. However, there was no particularity molecular markers for immunotherapy of Stages III and IV PDAC patients. Therefore, a more accurate prognosis immune-related molecular markers for PDAC patients is important to direct better management strategies.

In this study, we explore the effect of the tumor immune microenvironment and performed a systematic and comprehensive gene signature of PDAC. Weighted gene co-expression network analysis (WGCNA) was performed using PDAC Gene Expression Omnibus (GEO) gene expression data (5). The T-cell compositions of samples were estimated by the Cell type Identification by Estimating Relative Subsets ff RNA Transcripts (CIBERSORT) algorithm (6). A four-gene signature was constructed to predict the prognosis of Stages III and IV PDAC patients using the LASSO Cox regression model and was validated in two independent validation cohorts including the Fudan University Shanghai Cancer Center (FUSCC) and the International Cancer Genome Consortium (ICGC). A prognostic nomogram incorporating the gene signature and clinical prognostic factors was established to predict 3-year survival in advanced PDAC patients.

MATERIAL AND METHODS

Collection of Genomic Data

We downloaded the PDAC RNA expression data from the Gene Expression Omnibus (GEO, http://www.ncbi.nlm.nih.gov/geo/), which contain data related to 36 tumor samples. The dataset of GSE16515 was obtained applying the platform Affymetrix Human Genome U133 Plus 2.0 Array (HG U133 Plus 2.0). R package "limma" was used to normalize the RNA sequencing data (7). A little variation of sequence data often represents noise, so we employed Coefficient of Variation values to screen the most variant genes, which were then applied to construct the network.

Evaluation of Tumor-Infiltrating Immune Cells

In this study, the R package "CIBERSORT" was utilized to estimate the fraction of immune cells of GSE16515 samples. Specifically, the CIBERSORT algorithm was applied to assess the fractions of the 22 types of tumor-infiltrating immune cells (TIICs). The CIBERSORT is thought to be better than previous deconvolution methods for analysis of unrevealed mixture content and noise. This algorithm could be drawn to estimate the relative composition of cell subpopulations from complex tissue expression profiles, making it a practical tool to estimate the abundances of special cells in intricate tissue.

Co-Expression Network Construction

Expression values of 2,537 genes were put into construct a weight co-expression network utilizing the R package "WGCNA" (5). First, according to the Pearson's correlation value among paired genes, the expression levels of microarray data were converted into similarity matrixes. Next, the similarity matrixes were reconstructed to adjacency matrix, on the basis of amn = |cmn| β (cmn = Pearson's correlation between paired genes; amn = adjacency between paired genes). To classify genes with comparable expression patterns into different modules, we applied a dynamic hybrid cutting method, applying a bottom-up algorithm with a module least value cutoff of 30.

Construct Module Trait Relationships

Module eigengenes were used to carry out component analysis of each module. We judge the correlation between module eigengenes and the infiltration level of T cells to conclude the

significance of modules by Pearson test. We picked the interest T cell subtype and module with the highest correlation coefficient and deemed that as a hub module when P <0.05.

Bioinformatic Analysis

The web tool "Metascape" (http://metascape.org) for enrichment analysis was applied to recognize the function of genes in the hub module (8). The top 20 enriched terms were displayed as a bar graph. Aiming to investigate the relationship between terms, a network graph was presented by similarity greater than 0.3 terms.

Identification of Hub Genes

Candidate hub genes were selected determined by the modular connectivity and relationship of gene in the hub module. Module connectivity and is clinical trait relationship identified as the absolute value of the Pearson's correlation (Module Membership) and gene and the trait (Gene Significance). We set the Module Membership >0.6 and the Gene-Significance >0.3 for candidate hub genes. Moreover, we selected genes in the hub module and applied the Search Tool for the Retrieval of Interacting Genes (STRING; https://string-db.org/) online database to construct PPI network and looked for central nodes (9). Genes with a combined score of >0.4 and node connectivity of > 15 were recognized as central nodes. Cytoscape, a free bioinformatics platform, was used to visualize the network (https://cytoscape.org/) (10).

Establishment of the LASSO Regression Model and Calculation of Risk Score

The candidate genes selected by Venn analysis to compare candidate hub genes and central nodes in the PPI network were selected to construct LASSO Cox regression analysis models with the R package "glmnet". The "glmnet" package returned a sequence of models (11). For each model, the tuning parameter λ was conversely related with the complexity of the model and the value of deviance. Kaplan–Meier analysis were employed to calculate predictive differences between the high- and low-risk groups based on a cutoff median risk score in the discovery and other two validation datasets. Additionally, a nomogram and corresponding calibration curves were built according to the TCGA cohort for clinical application.

RNA Extraction, Reverse Transcription, and qRT-PCR Analysis

Total RNA was acquired from 42 patient were diagnosed as Stages III and IV PDAC samples at the FUSCC by using TRIzol Reagent (Invitrogen, USA). TaKaRa PrimeScript RT Reagent Kit (TaKaRa, Japan) was adopted to reverse transcription. ABI 7900HT Real-Time PCR System (Applied Biosystems, USA) was performed to detect the expression of candidate genes. The primers verified in this study are shown in **Supplementary Table S1**.

Statistical Analysis

Statistical analysis was performed in R (version 3.6.2, www.r-project.org). Spearman correlation analysis was used to determine the association of gene signature expression with PD1 and PDL1 expression. Calibration plots were produced to assess whether actual outcomes matched predicted outcomes for the nomogram.

RESULTS

RNA Expression Data

The results of this study are summarized in a flow chart (**Figure 1**). We obtained RNA expression data of 36 PDAC samples in the Gene Expression Omnibus (GEO) database. The median ranking value was used as the expression value if several probes matched a single gene. Approximately 2,568 genes with Coefficient of variation values greater than 0.15 were chosen for the following analysis (**Figure 2A**).

The CIBERSORT Algorithm Evaluation of Tumor-Infiltrating Immune Cells

CIBERSORT is a systematic algorithm that analyzes RNA expression data to estimate the abundance of various cell subtypes for each sample. The fractions of 22 TIICs were evaluated by the R package "CIBERSORT". CD8+ T cell, naive CD4+ T, memory resting CD4 + T cells, activated memory CD4+ T cells were accounted for a large proportion of PDAC samples of immune cell infiltration. Then, four subtypes of T cells of 22 TIICs in tumor sample were chosen as trait data of WGCNA (**Figure 2B**).

Gene Co-Expression Network of PDAC

The expression values of the 2,568 genes were applied to build a co-expression network by the R package "WGCNA" We estimated average linkage and Pearson's relation values to cluster the samples of GSE16515. Soft threshold power analysis revealed the scale-free fit index of the network topology in the WGCNA pipeline. The optimal soft threshold was 7, where the fitting curve approached 0.9 (**Figure 2C**). Dynamic hybrid cutting was adopted to construct hierarchical clustering tree. Each leaf on the tree shows an independent single gene and genes with similar expression data are close together and form a branch of the tree which represent the gene module (**Figure 2D**).

Identification of Hub Modules and Functional Enrichment Analysis

Heatmap of module–trait relationships showing the correlations between module eigengenes and TIICs profile traits. Among the modules, the pink module was highly associated with T cells CD8 (CD8+ T cells) ($R^2 = 0.34$, $P = 0.04$), T cells CD4 naïve ($R^2 = 0.36$, $P = 0.03$) and T cells CD4 memory activated ($R^2 = 0.47$, $P = 0.004$). We were focused specifically on the CD4+ T cells, so the pink module was identified as a hub module due to the high correlation with CD4+ T cells (**Figure 3A**). Genes consisting of pink module were taken into the next analyzation for pathway and process enrichment by the web tool "Matascape". The 20 highest representative enrichment terms were all immune-related terms, and the four most highly enriched terms were

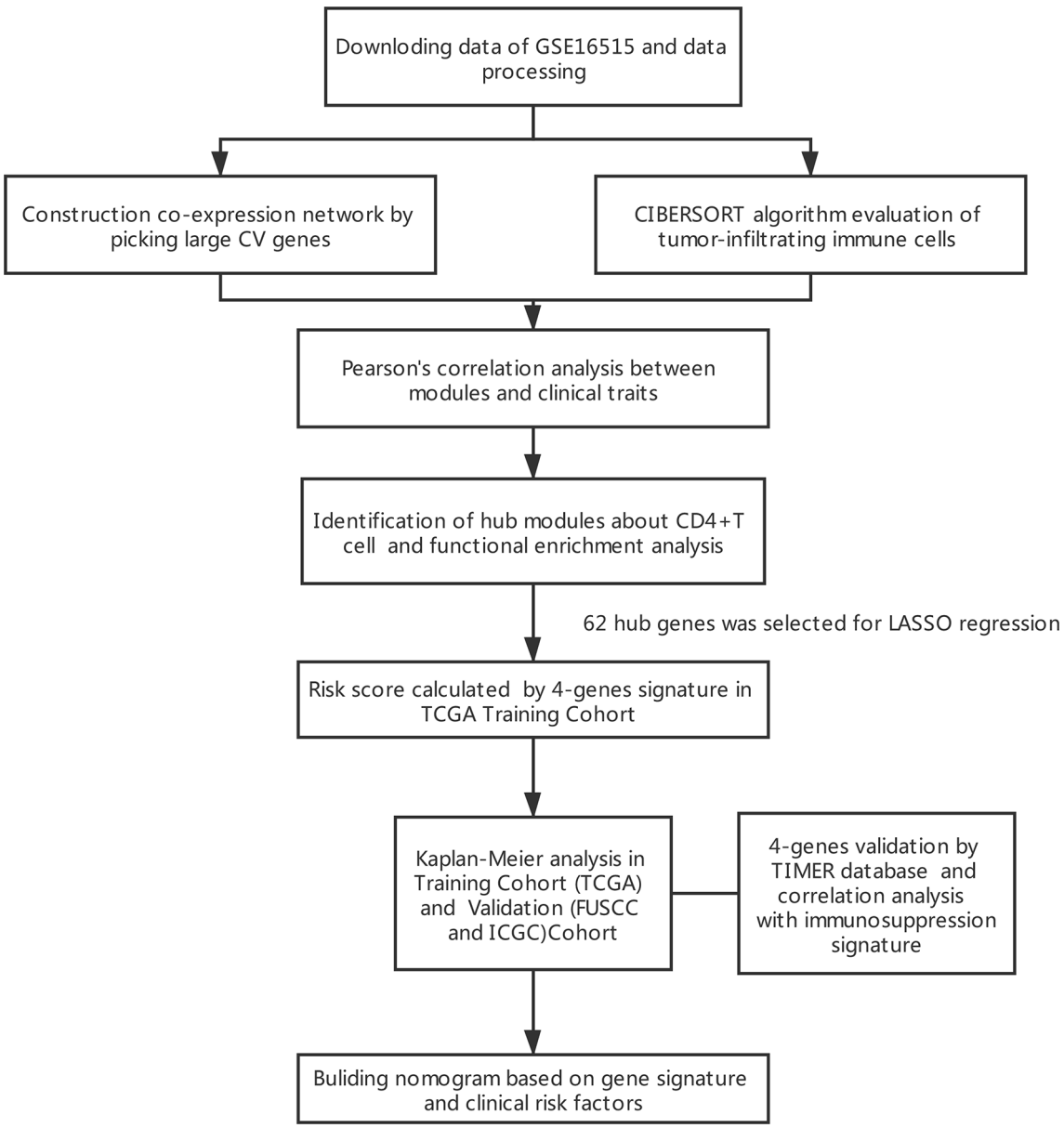

FIGURE 1 | Flowchart presenting the process of establishing the gene signature in this study.

lymphocyte activation, adaptive immune response, antigen receptor-mediated signaling pathway and alpha-beta T cell activation. We then chose a subset of representative terms from this cluster and transformed them into a network layout (**Figure 3B**).

Identification Hub Genes and Establish Prognostic Signature

The highly connected genes consist of pink module were investigated as key factors associated with CD4+ T cell infiltration level. From the protein–protein interactions (PPI) network, the top 100 genes in pink module were selected as central nodes according to Degree rich integrals built using the String database and we visualized these results as network layout using Cytoscape (**Figure 4A**). Furthermore, according to the cut-off standard (Module Membership >0.6 and Gene-Significance >0.3), 77 genes in pink module met these criteria and were selected as candidate hub genes (**Figure 4B**). Finally, 62 genes were selected in both analyses by Venn analysis and designated as hub genes (**Figure 4C**). The LASSO coefficient profiles of the 62 genes are presented in **Figure 5**. The LASSO risk score was obtained as follows:

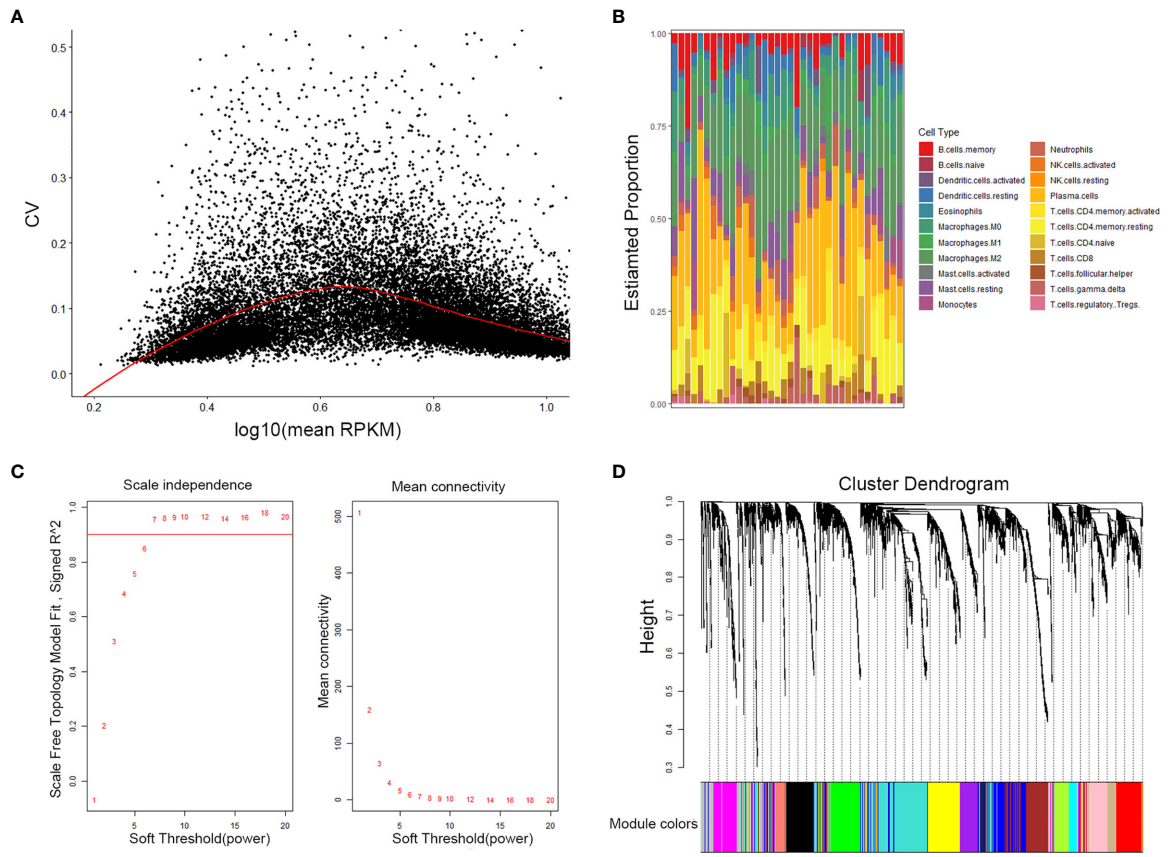

FIGURE 2 | Selection of the appropriate beta value to construct a hierarchical cluster number. **(A)** Selected genes with Coefficient of variation values greater than 0.15. **(B)** Estimate fraction of immune cells by CIBERSORT algorithm in GSE16515. **(C)** Analysis of the scale-free fit index and of the average connectivity of 1–20 soft threshold power. **(D)** Genes are grouped into diverse modules by hierarchical clustering. Different colors represent different modules.

Risk score = (0.32605651 × expression level of CXCL9) − (0.03660404 × expression level of NAPSB) −(0.07097911 × expression level of PYHIN1) − (0.24647254 × expression level of ZNF831)

The samples with low-risk scores showed better overall survival (OS) times than those with high-risk group patients in the TCGA discovery cohort ($P = 0.0011$; **Figure 5E**). The finding was subsequently validated in ICGC ($P = 0.045$; **Figure 5F**) and FUSCC ($P = 0.038$; **Figure 5G**) validation datasets.

Validation of the Expression of and Immunosuppression Alterations in the Four Genes

To explore the association between these hub genes and CD4+ T cells, we investigated the expression data for four genes in the TIMER database. The results revealed positive correlation of the expression values of the four genes with the infiltration levels of CD4+ T cells (**Figure 6A**). To investigate the relation between the expression of four genes and immunosuppression markers (PD1 and PDL1), we use the expression data obtained from the TCGA and ICGC database to validate the correlation test. Furthermore, we collected 42 patients' samples from our center (FUSCC) to test if these expression of four genes was associated with PD1 and PDL1 expression. Taking an unbiased approach, we found that four genes showed a positive and significant correlation with PD1 and PDL1counts in three databases (**Figures 6B–D**).

Correlations Between the Three-Gene Signature and Clinical Characteristics

To validate the reliability of the results of the risk-score of four genes (NAPSB, ZNF831, CXCL9, PYHIN1), their actual expression of 42 PDAC samples were examined with quantitative reverse-transcription polymerase chain reaction (qRT-PCR). The results showed that NAPSB and CXCL9 were upregulated in PDAC tumor tissues with statistical significance (**Figures 7A–D**). Univariate and multivariate Cox proportional hazards regression showed risk score could predict poor survival of PDAC patients, as shown in **Supplementary Table S2** and **Figure 7E** ($P = 0.0013$; 0.00561). The patients from the TCGA dataset were used to establish a prognostic nomogram predicting a 3-year overall survival probability in PDAC patients according to the stepwise Cox regression model (**Figure 7F**). Calibration plots showed that the nomogram presented good agreement at

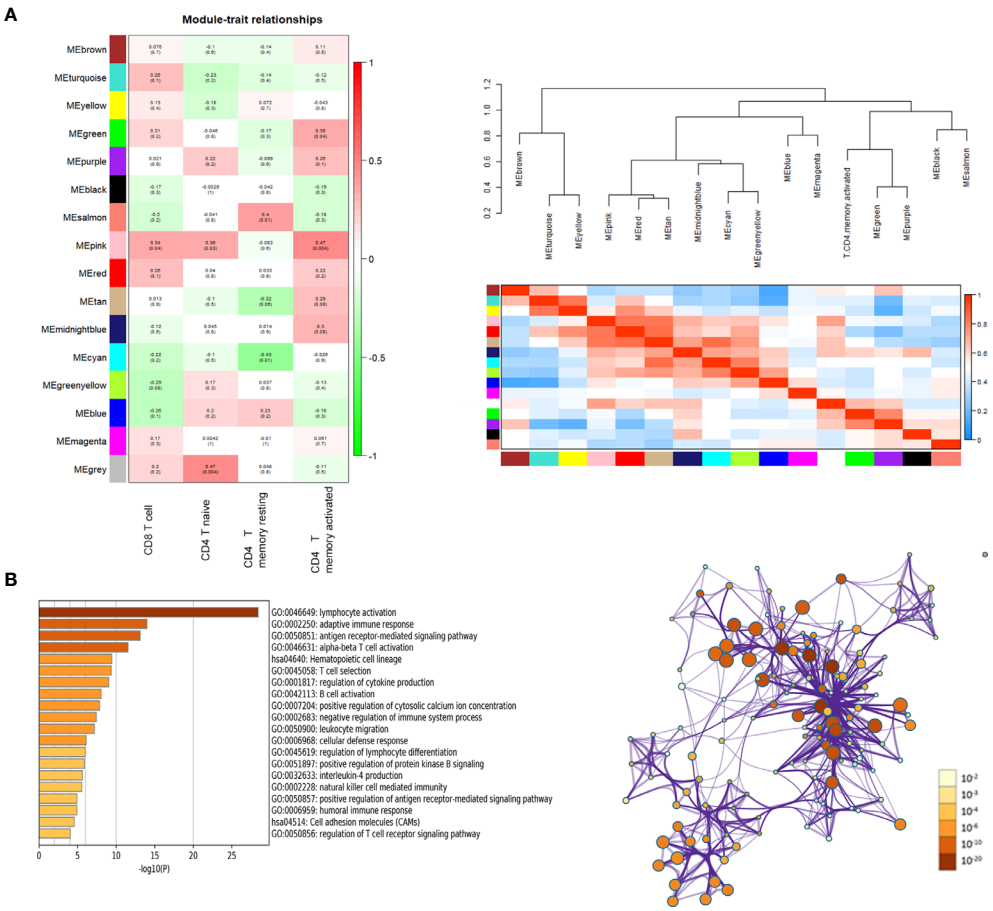

FIGURE 3 | Key modules and feature notes. **(A)** Heatmap and Eigengene-dendrogram show the correlations of module eigengenes with T-cell infiltration. **(B)** The first 20 enriched terms are shown as a bar chart on the left. The protein–protein interaction networks diagram on the right is constructed with each enrichment term as a node and which colored by different cluster ID.

predicting overall survival and the actual proportion in pancreatic cancer patients (**Figure 7G**).

DISCUSSION

PDAC remains a major cause of cancer-related death worldwide, and the incidence and mortality are estimated to increase substantially by 2030 (12). Several studies have reported signatures that could effectively predict overall patient survival, including a five-miRNA signature (13), and a 3-lncRNA signature (14). There are less models that focus on Stages III and IV patients, and the prognosis is rather heterogeneous for these group. In addition, these commonly-used models only incorporate clinical and pathological factors, without considering the role of immune cells from the tumor microenvironment play in tumor progression and prognosis of PDAC patients. Thus, a more precise prognosis model for advanced patients is necessary.

With the rapid development of bioinformatics technology, many tools have been developed to find biomarkers (15). The CIBERSORT is a deconvolution algorithm to quantify the cellular composition of immune cells, such as prostate cancer and kidney cancer (16, 17). The WGCNA is another bioinformatics tool that can be used to recognize correlation modules and hub genes for cancer. Immune checkpoint inhibitors have shown promising initial efficacy in advanced PDAC. This has increased focus on exploring the potential immune-related factors for immunotherapy. CD4+ T cells play a key role in immunotherapy. In the current study, a four-gene signature correlated to CD4+ T cell infiltration level was identified by utilizing the LASSO Cox regression model. In this study, we utilized WGCNA and CIBERSORT algorithms to perform gene expression matrix to establish the co-expression network and estimated the infiltration level of T cells by, and interactions were adopted to identify the genes most related to CD4+ T cells. The gene enrichment analysis of the selected hub module also proves that it is a highly immune-related module. Based on this information, a four-gene signature correlated to CD4+ T cell infiltration level was identified by utilizing the LASSO Cox regression model. Querying the relationship

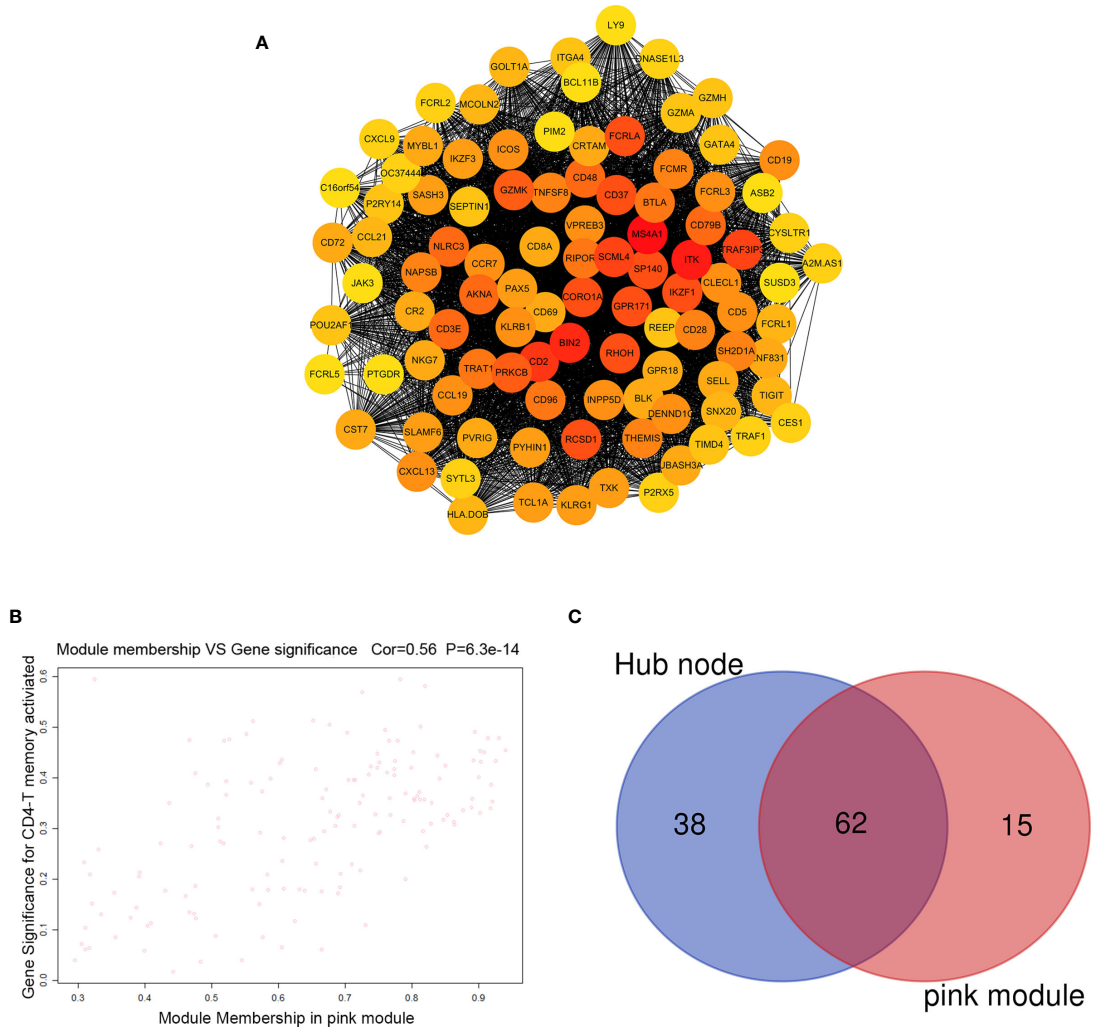

FIGURE 4 | Identification of hub genes. **(A)** PPI network of top 100 genes was selected from the pink module. **(B)** A scatter plot of the genes in the pink module. **(C)** Hub genes were selected according to the overlap between PPI and pink module in co-expression networks.

between these four-genes (NAPSB, ZNF831, CXCL9 and PYHIN1) and immune cells in the TIMER database revealed positively correlated expression of these genes with CD4+ T cells. Positive correlation between four-gene expression and immunosuppression markers (PD1 and PDL1) was proved in the TCGA, ICGC and FUSCC datasets.

Chemokines are a group of small cytokines that can cause directed chemotaxis. Secreted by various types of cells including inflammatory macrophages dendritic cells (particularly the cDC1 subtype), endothelial cells, fibroblasts, and tumor cells themselves, chemokines could be categorized based on their behaviors and structure characteristics (18). The CXC chemokines are a family of 17 α-chemokines that carried out multiple pathological or physiological functions. The role of CXCL9 play in human cancers remains ambiguous and contradictory. It had been found that CXCL9 is expressed in most types of human cancers, such as hepatocellular carcinoma, melanoma, gastric carcinoma, cervical cancer, as well as PDAC (18). Some previous studies have delineated that CXCL9 could be presented as both having promoting and suppressing effects on CD8+ cytotoxic T cells. In prostate tumors it was found out that there is strong positive correlation between CXCL9 and CD8 expression (19). Chow et al. also proved that CXCL9 facilitated the dendritic cell-CTLs interaction and activated the CD8+ T cells response in the tumor microenvironment (20). Additionally, a recent report by Gao et al. shows that CXCL9 activated STAT3 signaling in CD8+ T cells of PDAC cell, and suppression of STAT3 could recover the proliferation and secretion of anti-tumor cytokines of CD8+ T cells (21). The PYHIN1 (Pyrin and HIN Domain Family, Member 1) gene is predicted to encode six different protein isoforms as a result of alternative mRNA splicing (a1, a2, b1, b2, g1, and g2). Each of the isoforms has a common N-terminal region, which contains a PYD and an NLS. Functionally, roles for PYHIN1 in controlling

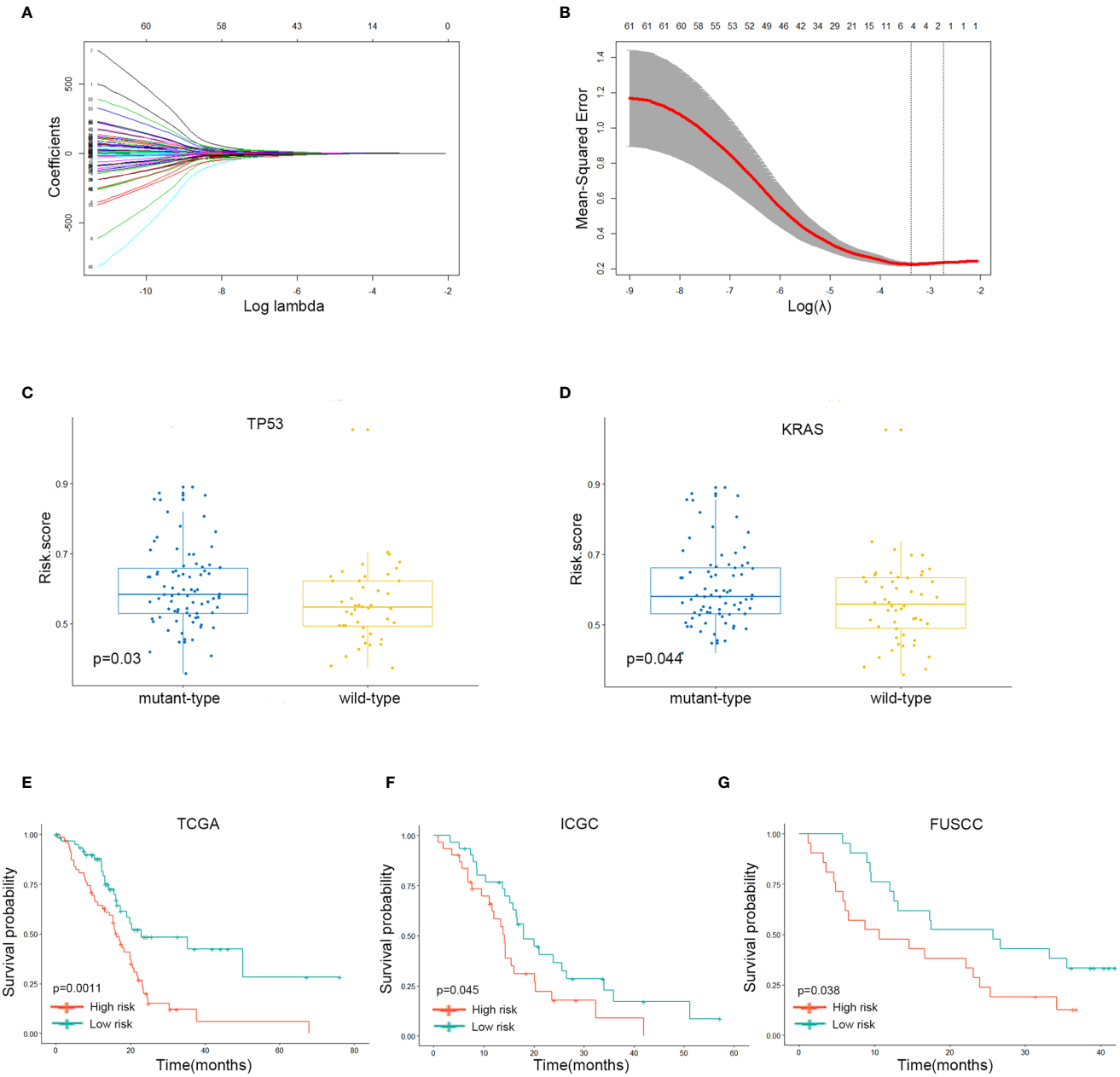

FIGURE 5 | A four-gene signature system was established to predict the overall survival of Stages III and IV PDAC patients in the TCGA discovery and two independent validation cohorts. **(A, B)** LASSO coefficient profiles of the 62 immune-related' genes. LASSO, least absolute shrinkage and selection operator method. **(C)** The expression level of the risk score in mutation status of TP53 in Stages III and IV PDAC patients of TCGA dataset. **(D)** The expression level of the risk score in mutation status of KRAS in Stages III and IV PDAC patients of TCGA dataset. **(E)** The Kaplan–Meier plot of 5-year overall survival in TCGA Stages III and IV PDAC cohort. **(F)** The Kaplan–Meier plot of 5-year overall survival in ICGC Stages III and IV PDAC cohort. **(G)** The Kaplan–Meier plot of 5-year overall survival in FUSCC Stages III and IV PDAC cohort.

cell cycle, differentiation, and apoptosis growth have been reported (22). PYHIN1 expression has been presented to be reduced in breast tumors. Recent studies have delineated that PYHIN1a1 controls tumor suppressive activity mediated by the destabilization of the oncoprotein HDM2 (23). Information about ZNF831 and NAPSB is scarce in the literature.

CONCLUSION

In conclusion, our study successfully identified potential CD4+ T cell related biomarkers and a prognostic nomogram incorporating the gene signature and clinical prognostic factors for prediction of OS in Stages III and IV PDAC patients. Novel

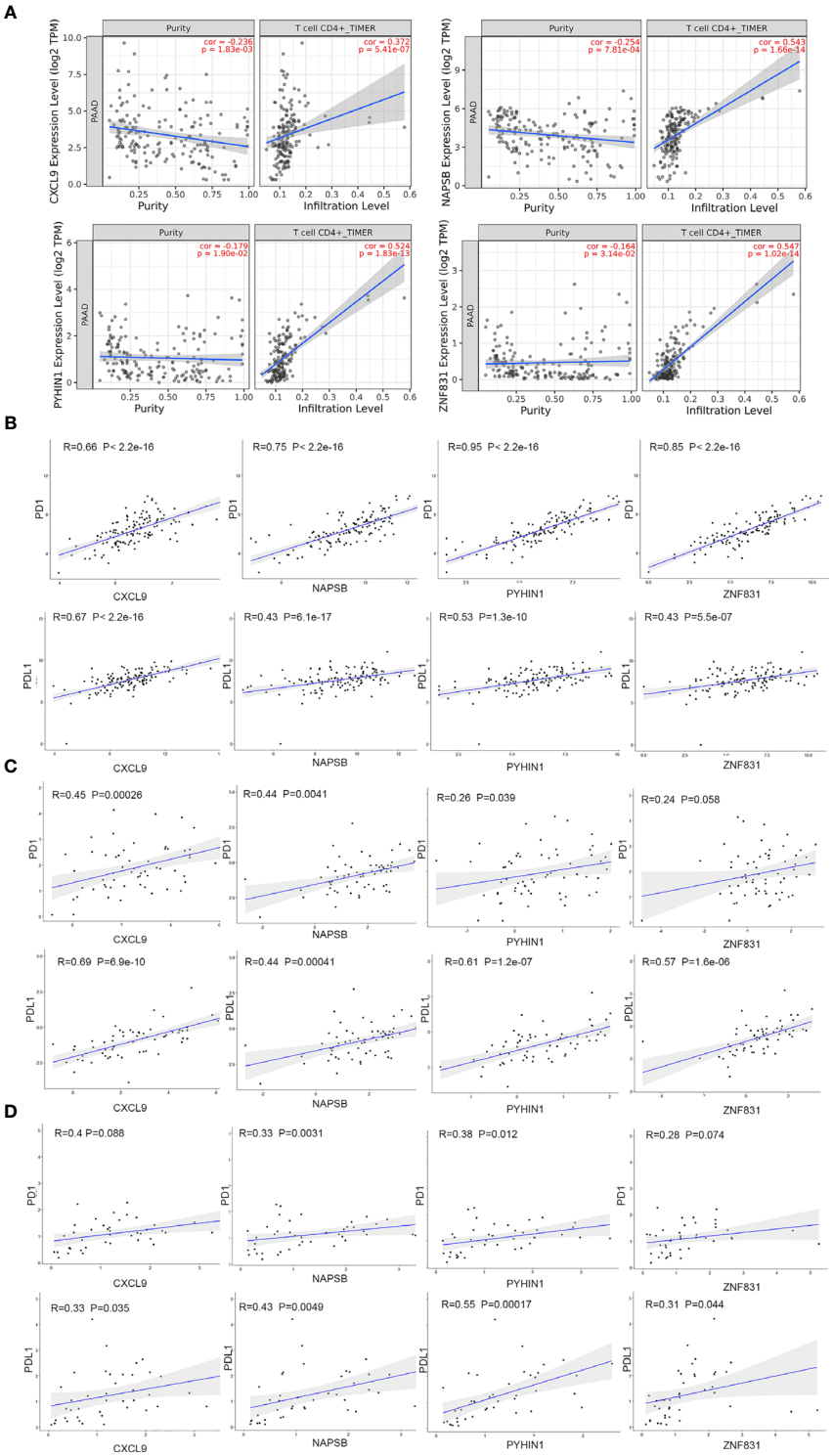

FIGURE 6 | NAPSB, ZNF831, CXCL9 and PYHIN1 associated with CD4+ T lymphocyte infiltration and immunosuppression markers. **(A)** The Timer web tool was performed to estimate the association between the expression levels of four genes with the infiltration level of CD4+ T immune cells in PDAC samples. **(B)** Correlation between four-gene expression and PD1 and PDL1 in PDAC samples of TCGA dataset. Top of Scatter plots depicts R2 and p-values. **(C)** Correlation between four-gene expression and PD1 and PDL1 in PDAC samples of ICGC dataset. **(D)** Correlation between four-gene expression and PD1 and PDL1in PDAC samples of FUSCC dataset.

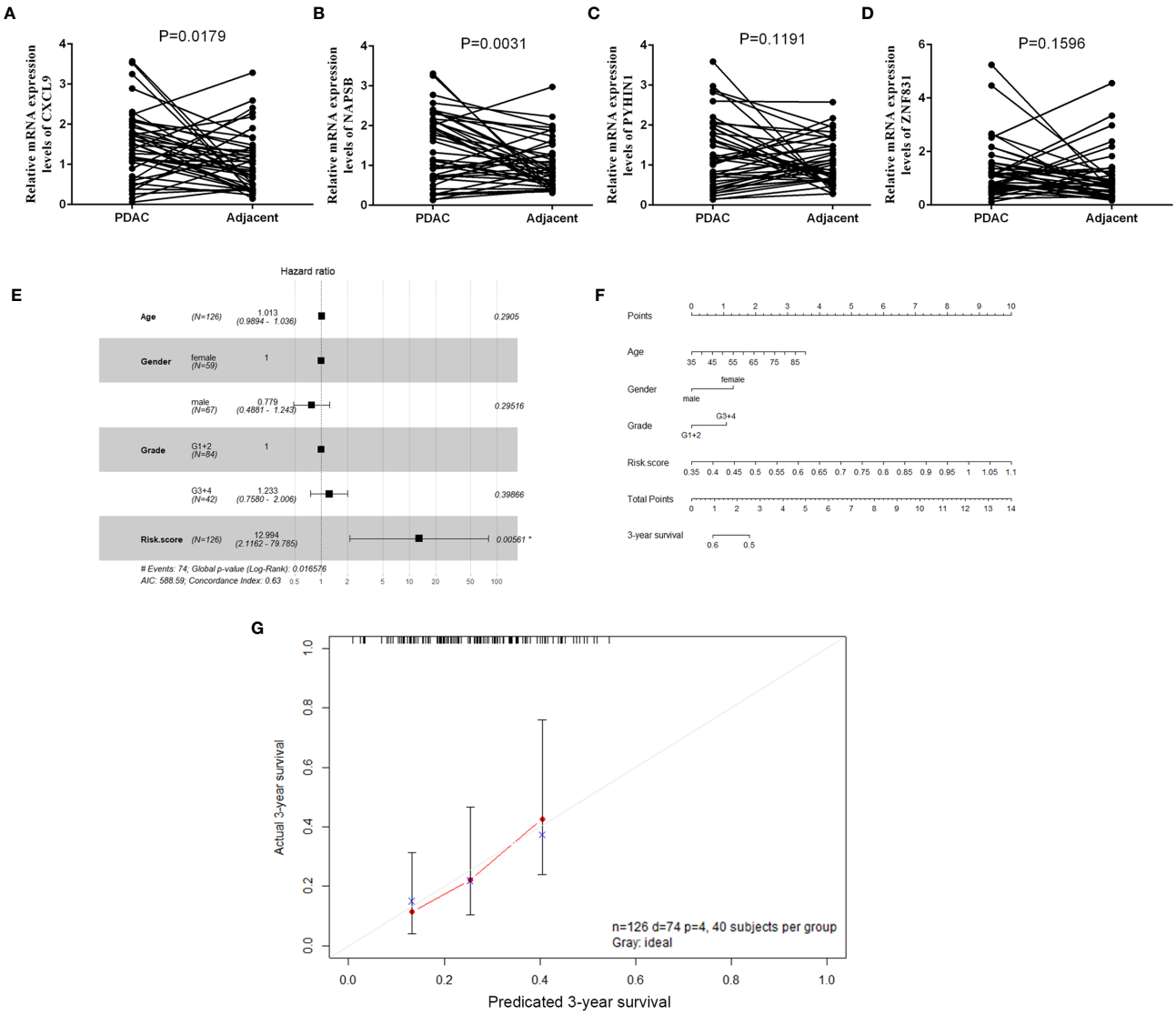

FIGURE 7 | The expression and clinical significance of gene signature in PDAC. **(A–D)** Expression of four genes in tumor and adjacent normal tissues from a cohort of 42 PDAC patients was determined by qPCR. **(E)** Forest plot summary of multivariable Cox regression analyses of the risk score, age, gender and grade on TCGA cohort. The squares represent the hazard ratio (HR), and the transverse lines represent 95% CI. CI, confidence interval. **(F)** A nomogram to predict survival probability at 3-year for PDAC patients based on the results deriving from the TCGA cohort. **(G)** Calibration curve for the nomogram when predicting 3-year overall survival.

insights into the relationship between immune and PDAC were shown in this study. Future investigations on the molecular mechanisms and prospective randomized clinical trials will bring a roadmap for precision medicine.

DATA AVAILABILITY STATEMENT

The original contributions presented in the study are included in the article/**Supplementary Material**. Further inquiries can be directed to the corresponding authors.

ETHICS STATEMENT

The studies involving human participants were reviewed and approved by ethical code: 050432-4-1212B. The patients/participants provided their written informed consent to participate in this study.

AUTHOR CONTRIBUTIONS

CL and JX designed this study; ZT performed the bioinformatics analyses and wrote the manuscript; YL and BZ analysis and

interpretation of data; SS, JL and XY statistical analysis; CL and JX supervised this study. All authors contributed to the article and approved the submitted version.

FUNDING

This study was jointly funded by the national natural Science Foundation of china (No. 81902428, 81802352 and 81772555), the Shanghai Sailing Program (No. 19YF1409400), the national Science Foundation for Distinguished Young Scholars of china (No. 81625016), Clinical and Scientific Innovation Project of Shanghai Hospital Development Center (SHDC12018109), and Scientific Innovation Project of Shanghai Education Committee (2019-01-07-00-07-E00057).

ACKNOWLEDGMENTS

The authors thank all individuals who participated in this study and donated Samples.

SUPPLEMENTARY MATERIAL

The Supplementary Material for this article can be found online at: https://www.frontiersin.org/articles/10.3389/fonc.2021.674897/full#supplementary-material

REFERENCES

1. Siegel RL, Miller KD, Jemal A. Cancer Statistics, 2019. *CA: Cancer J Clin* (2019) 69:7–34. doi: 10.3322/caac.21551
2. Yan X, Wan H, Hao X, Lan T, Li W, Xu L, et al. Importance of Gene Expression Signatures in Pancreatic Cancer Prognosis and the Establishment of a Prediction Model. *Cancer Manage Res* (2019) 11:273–83. doi: 10.2147/CMAR.S185205
3. Raman P, Maddipati R, Lim KH, Tozeren A. Pancreatic Cancer Survival Analysis Defines a Signature That Predicts Outcome. *PloS One* (2018) 13: e0201751. doi: 10.1371/journal.pone.0201751
4. Frost HR, Amos CI. Gene Set Selection via LASSO Penalized Regression (SLPR). *Nucleic Acids Res* (2017) 45:e114. doi: 10.1093/nar/gkx291
5. Langfelder P, Horvath S. WGCNA: An R Package for Weighted Correlation Network Analysis. *BMC Bioinf* (2008) 9:559. doi: 10.1186/1471-2105-9-559
6. Newman AM, Liu CL, Green MR, Gentles AJ, Feng W, Xu Y, et al. Robust Enumeration of Cell Subsets From Tissue Expression Profiles. *Nat Methods* (2015) 12:453–7. doi: 10.1038/nmeth.3337
7. Ritchie ME, Phipson B, Wu D, Hu Y, Law CW, Shi W, et al. Limma Powers Differential Expression Analyses for RNA-Sequencing and Microarray Studies. *Nucleic Acids Res* (2015) 43:e47. doi: 10.1093/nar/gkv007
8. Zhou Y, Zhou B, Pache L, Chang M, Khodabakhshi AH, Tanaseichuk O, et al. Metascape Provides a Biologist-Oriented Resource for the Analysis of Systems-Level Datasets. *Nat Commun* (2019) 10:1523. doi: 10.1038/s41467-019-09234-6
9. Szklarczyk D, Gable AL, Lyon D, Junge A, Wyder S, Huerta-Cepas J, et al. STRING V11: Protein-Protein Association Networks With Increased Coverage, Supporting Functional Discovery in Genome-Wide Experimental Datasets. *Nucleic Acids Res* (2019) 47:D607–13. doi: 10.1093/nar/gky1131
10. Shannon P, Markiel A, Ozier O, Baliga NS, Wang JT, Ramage D, et al. Cytoscape: A Software Environment for Integrated Models of Biomolecular Interaction Networks. *Genome Res* (2003) 13:2498–504. doi: 10.1101/gr.1239303
11. Tibshirani R. The LASSO Method for Variable Selection in the Cox Model. *Stat Med* (1997) 16:385–95. doi: 10.1002/(sici)1097-0258(19970228)16:4<385::aid-sim380>3.0.co;2-3
12. Rahib L, Smith BD, Aizenberg R, Rosenzweig AB, Fleshman JM, Matrisian LM. Projecting Cancer Incidence and Deaths to 2030: The Unexpected Burden of Thyroid, Liver, and Pancreas Cancers in the United States. *Cancer Res* (2014) 74:2913–21. doi: 10.1158/0008-5472.CAN-14-0155
13. Shi XH, Li X, Zhang H, He RZ, Zhao Y, Zhou M, et al. A Five-microRNA Signature for Survival Prognosis in Pancreatic Adenocarcinoma Based on TCGA Data. *Sci Rep* (2018) 8:7638. doi: 10.1038/s41598-018-22493-5
14. Huang GW, Xue YJ, Wu ZY, Xu XE, Wu JY, Cao HH, et al. A three-lncRNA Signature Predicts Overall Survival and Disease-Free Survival in Patients With Esophageal Squamous Cell Carcinoma. *BMC Cancer* (2018) 18:147. doi: 10.1186/s12885-018-4058-6
15. Anslan S, Bahram M, Hiiesalu I, Tedersoo L. PipeCraft: Flexible Open-Source Toolkit for Bioinformatics Analysis of Custom High-Throughput Amplicon Sequencing Data. *Mol Ecol Resour* (2017) 17:e234–40. doi: 10.1111/1755-0998.12692
16. Zhang S, Zhang E, Long J, Hu Z, Peng J, Liu L, et al. Immune Infiltration in Renal Cell Carcinoma. *Cancer Sci* (2019) 110:1564–72. doi: 10.1111/cas.13996
17. Zhao SG, Lehrer J, Chang SL, Das R, Erho N, Liu Y, et al. The Immune Landscape of Prostate Cancer and Nomination of PD-L2 as a Potential Therapeutic Target. *J Natl Cancer Institute* (2019) 111:301–10. doi: 10.1093/jnci/djy141
18. Ding Q, Lu P, Xia Y, Ding S, Fan Y, Li X, et al. CXCL9: Evidence and Contradictions for Its Role in Tumor Progression. *Cancer Med* (2016) 5:3246–59. doi: 10.1002/cam4.934
19. Allen F, Bobanga ID, Rauhe P, Barkauskas D, Teich N, Tong C, et al. CCL3 Augments Tumor Rejection and Enhances CD8(+) T Cell Infiltration Through NK and CD103(+) Dendritic Cell Recruitment. *via IFNgamma Oncoimmunol* (2018) 7:e1393598. doi: 10.1080/2162402X.2017.1393598
20. Chow MT, Ozga AJ, Servis RL, Frederick DT, Lo JA, Fisher DE, et al. Intratumoral Activity of the CXCR3 Chemokine System Is Required for the Efficacy of Anti-PD-1 Therapy. *Immunity* (2019) 50:1498–1512 e1495. doi: 10.1016/j.immuni.2019.04.010
21. Gao HF, Cheng CS, Tang J, Li Y, Chen H, Meng ZQ, et al. CXCL9 Chemokine Promotes the Progression of Human Pancreatic Adenocarcinoma Through STAT3-Dependent Cytotoxic T Lymphocyte Suppression. *Aging* (2020) 12:502–17. doi: 10.18632/aging.102638
22. Ding Y, Wang L, Su LK, Frey JA, Shao R, Hunt KK, et al. Antitumor Activity of IFIX, a Novel Interferon-Inducible HIN-200 Gene, in Breast Cancer. *Oncogene* (2004) 23:4556–66. doi: 10.1038/sj.onc.1207592
23. Ding Y, Lee JF, Lu H, Lee MH, Yan DH. Interferon-Inducible Protein IFIXalpha1 Functions as a Negative Regulator of HDM2. *Mol Cell Biol* (2006) 26:1979–96. doi: 10.1128/MCB.26.5.1979-1996.2006

Conflict of Interest: The authors declare that the research was conducted in the absence of any commercial or financial relationships that could be construed as a potential conflict of interest.

The reviewer CJ declared a shared affiliation, with no collaboration, with the authors, to the handling editor at the time of the review.

Publisher's Note: All claims expressed in this article are solely those of the authors and do not necessarily represent those of their affiliated organizations, or those of the publisher, the editors and the reviewers. Any product that may be evaluated in this article, or claim that may be made by its manufacturer, is not guaranteed or endorsed by the publisher.

frontiers in Oncology

REVIEW
published: 29 July 2021
doi: 10.3389/fonc.2021.700315

Biological Significance of YAP/TAZ in Pancreatic Ductal Adenocarcinoma

Hiromitsu Hayashi, Norio Uemura, Liu Zhao, Kazuki Matsumura, Hiroki Sato, Yuta Shiraishi and Hideo Baba*

Department of Gastroenterological Surgery, Graduate School of Life Sciences, Kumamoto University, Kumamoto, Japan

Pancreatic ductal adenocarcinoma (PDAC) remains one of the most lethal types of cancer. Despite major advances in defining the molecular mutations driving PDAC, this disease remains universally lethal with an overall 5-year survival rate of only about 7–8%. Genetic alterations in PDAC are exemplified by four critical genes (*KRAS*, *TP53*, *CDKN2A*, and *SMAD4*) that are frequently mutated. Among these, *KRAS* mutation ranges from 88% to 100% in several studies. Hippo signaling is an evolutionarily conserved network that plays a key role in normal organ development and tissue regeneration. Its core consists of the serine/threonine kinases mammalian sterile 20-like kinase 1 and 2 (MST1/2) and large tumor suppressor 1 and 2. Interestingly, pancreas-specific *MST1/2* double knockout mice have been reported to display a decreased pancreas mass. Many of the genes involved in the Hippo signaling pathway are recognized as tumor suppressors, while the Hippo transducers Yes-associated protein (YAP) and transcriptional co-activator with PDZ-binding motif (TAZ) are identified as oncogenes. By dephosphorylation, YAP and TAZ accumulate in the nucleus and interact with transcription factors such as TEA domain transcription factor-1, 2, 3, and 4. Dysregulation of Hippo signaling and activation of YAP/TAZ have been recognized in a variety of human solid cancers, including PDAC. Recent studies have elucidated that YAP/TAZ play a crucial role in the induction of acinar-to-ductal metaplasia, an initial step in the progression to PDAC, in genetically engineered mouse models. YAP and TAZ also play a key role in the development of PDAC by both KRAS-dependent and KRAS-independent bypass mechanisms. YAP/TAZ have become extensively studied in PDAC and their biological importance during the development and progression of PDAC has been uncovered. In this review, we summarize the biological significance of a dysregulated Hippo signaling pathway or activated YAP/TAZ in PDAC and propose a role for YAP/TAZ as a therapeutic target.

Keywords: pancreatic cancer, Hippo signaling pathway, Yes-associated protein, TAZ, KRAS mutation, pancreatic ductal adenocarcinoma

OPEN ACCESS

Edited by:
Kanjoormana Aryan Manu, Amala Cancer Research Centre, India

Reviewed by:
Bowen Zhu, Genome Institute of Singapore, Singapore
Jun Zhang, China Medical University, China

****Correspondence:***
Hiromitsu Hayashi
hhayasi@kumamoto-u.ac.jp

Specialty section:
This article was submitted to Gastrointestinal Cancers, a section of the journal Frontiers in Oncology

Received: *26 April 2021*
Accepted: *12 July 2021*
Published: *29 July 2021*

Citation:
Hayashi H, Uemura N, Zhao L, Matsumura K, Sato H, Shiraishi Y and Baba H (2021) Biological Significance of YAP/TAZ in Pancreatic Ductal Adenocarcinoma. Front. Oncol. 11:700315. doi: 10.3389/fonc.2021.700315

Abbreviations: ADM, Acinar-to-ductal metaplasia; CAFs, cancer-associated fibroblasts; CTGF, connective tissue growth factor, CYR61, cysteine-rich angiogenic inducer 61; DKO, double knockout; ECM, extracellular matrix; EMT, epithelial-to-mesenchymal transition; FBXW7, F-box and WD repeat domain containing 7; FOLFIRINOX, 5-fluorouracil, folinic acid, irinotecan, and oxaliplatin; GEMM, genetically engineered mouse model; GnP, gemcitabine plus nab-paclitaxel; ICMT, Isoprenylcysteine carboxylmethyltransferase; LATS1/2, large tumor suppressor 1/2; MST1/2, mammalian sterile 20-like kinase 1/2; MMR, mismatch repair; PDAC, pancreatic ductal adenocarcinoma; TAZ, transcriptional co-activator with PDZ-binding motif; TEAD, TEA domain transcriptional factor; PD-L1, programmed cell death-ligand 1; Pdx-1, pancreatic and duodenal homeobox 1; YAP, Yes-associated protein.

INTRODUCTION

Pancreatic ductal adenocarcinoma (PDAC) remains one of the most lethal types of cancer (1). Genetic alterations in PDAC are exemplified by four critical genes that are frequently mutated (*KRAS*, *TP53*, *CDKN2A*, and *SMAD4*). Some of these mutations occur when the tumors are in a preneoplastic condition (2). Despite major advances in defining the molecular mutations driving PDAC, this disease remains universally lethal, with an overall 5-year survival rate of only about 7–8%. Although recent developments in systemic chemotherapy such as FOLFIRINOX (5-fluorouracil, folinic acid, irinotecan, and oxaliplatin) and GnP (gemcitabine plus nab-paclitaxel) regimens have provided improved survival outcomes of patients with metastatic PDAC (3, 4), chemoresistance to current systemic chemotherapies (FOLFIRINOX and GnP) is a major treatment issue. Furthermore, of the patients who receive surgical treatments, 60% relapse within 12 months; this is most likely due to micro-metastases that were not detected during the diagnostic computed tomography scan (5). Although approximately 25–30% of patients respond to chemotherapeutic drugs, most eventually become resistant. Resistance mechanisms include deficiencies in drug uptake, alteration of drug targets, activation of DNA repair pathways, and resistance to apoptosis (6). Heterogeneity caused by admixture of tumor cells and stromal cells also produces chemoresistance and limits the targeted therapy of PDAC (7). Unfortunately, our knowledge of the genetic and biological backgrounds in this deadly disease has not yet been linked to improved patient survival. Further developments in therapeutic approaches by continued elucidation of the genetics and molecular biology of PDACs may be the next approach to overcoming this poor prognostic disease and improving survival outcomes.

The Hippo signaling pathway was first discovered from studies in *Drosophila melanogaster* (8–10). Hippo signaling is an evolutionarily conserved network that plays a key role in normal organ development and tissue regeneration (11). Multiple inputs control Hippo signaling, ranging from mechanical cues instructed by the cellular microenvironment (mechano-transduction) to soluble factors and metabolic pathways (12, 13). The Hippo pathway also displays extensive crosstalk with other signaling pathways such as transforming growth factor-beta (14, 15), Wnt (16, 17), Sonic hedgehog (18, 19), and Notch (20, 21). Its core consists of the serine/threonine kinases mammalian sterile 20-like kinase 1 and 2 (MST1 and MST2; Hippo in Drosophila) and large tumor suppressor 1 and 2 (LATS1 and LATS2). MST1/2 cooperate with salvador homolog 1 to phosphorylate and activate LATS1/2 kinases. LATS1/2 kinases then combine with the adaptor MOB kinase activator 1 to phosphorylate the Hippo transducers Yes-associated protein (YAP) and transcriptional co-activator with PDZ-binding motif (TAZ) (9, 22) (**Figure 1**). Many of the genes involved in the Hippo signaling pathway are recognized as tumor suppressors, while YAP/TAZ are oncogenes. In addition, YAP and TAZ can be phosphorylated at numerous sites (23, 24). Active LATS1/2 kinases phosphorylate YAP at 5 serine residues (S61, S109, S127, S164, and S381) and TAZ at 4 serine residues (S66, S89, S117, and S311) (23, 24). Among these, S127 (S89 in TAZ; as noted below, the two proteins share moderate sequence similarity) and S381 (S311 in TAZ) are key phosphorylation sites in suppressing YAP/TAZ oncogenic activity (24, 25). Phosphorylation of YAP and TAZ results in their cytoplasmic translocation, sequestration by 14-3-3 proteins, and recruitment of the β-TrCP (SCF) ubiquitin ligase complex (24).

Upon dephosphorylation, YAP and TAZ accumulate in the nucleus and interact with transcription factors such as TEA domain transcriptional factor (TEAD)1, TEAD2, TEAD3, and TEAD4. YAP/TAZ also transcriptionally activate target genes such as connective tissue growth factor (*CTGF*) and cysteine-rich angiogenic inducer 61 (*CYR61*) (11). Deregulation of Hippo signaling has been recognized in a variety of human solid cancers, including PDAC (26–28). YAP/TAZ induce the epithelial-to-mesenchymal transition (EMT) and also induce a more undifferentiated state with malignant behavior in cancer cells (25, 29). YAP/TAZ also contribute to the strongly immunosuppressive microenvironment characteristic of mouse and human PDAC (30). Although YAP and TAZ have very similar structural topologies, share nearly half of their overall amino acid sequences, and are thought to be largely redundant, they may differ in their regulation and downstream functions (31, 32).

YAP/TAZ have become extensively studied in PDAC and their biological importance during the development and progression of PDAC has been uncovered. In this review, we summarize the biological significance of a dysregulated Hippo signaling pathway and activated YAP/TAZ in PDAC, and propose a role for YAP/TAZ as a therapeutic target.

BIOLOGICAL ROLE OF HIPPO SIGNALING PATHWAY DURING NORMAL PANCREAS DEVELOPMENT

The mammalian pancreas is a dual-function organ that is critical for the regulation of basic metabolism. In the mouse, development of the pancreas is divided into two stages, commonly denoted as the primary and secondary transitions (33). In a report using pancreatic *MST1/2* double knockout (DKO) mice, George et al. (34) found that YAP is broadly expressed throughout the pancreatic and duodenal homeobox 1 (Pdx1)-positive embryonic day (E)12.5 mouse pancreas (primary transition) (34) (**Figure 2**). YAP expression then gradually becomes limited to prospective ductal and acinar regions at E16.5 (secondary transition). At E16.5, the productal cells show high YAP expression in the nucleus, whereas acinus-fated cells display expression mainly within the cytoplasm. Strikingly, prospective endocrine cells are negative for YAP expression. Pancreas development at E12.5 is characterized by compartmentalization, whereas E16.5 is characterized by massive cell proliferation and differentiation throughout the pancreas epithelium. In the adult mouse pancreas at 6 weeks (34), YAP expression is markedly decreased and strong expression is largely confined to ductal and terminal-duct centroacinar cells, unlike in the embryonic pancreas.

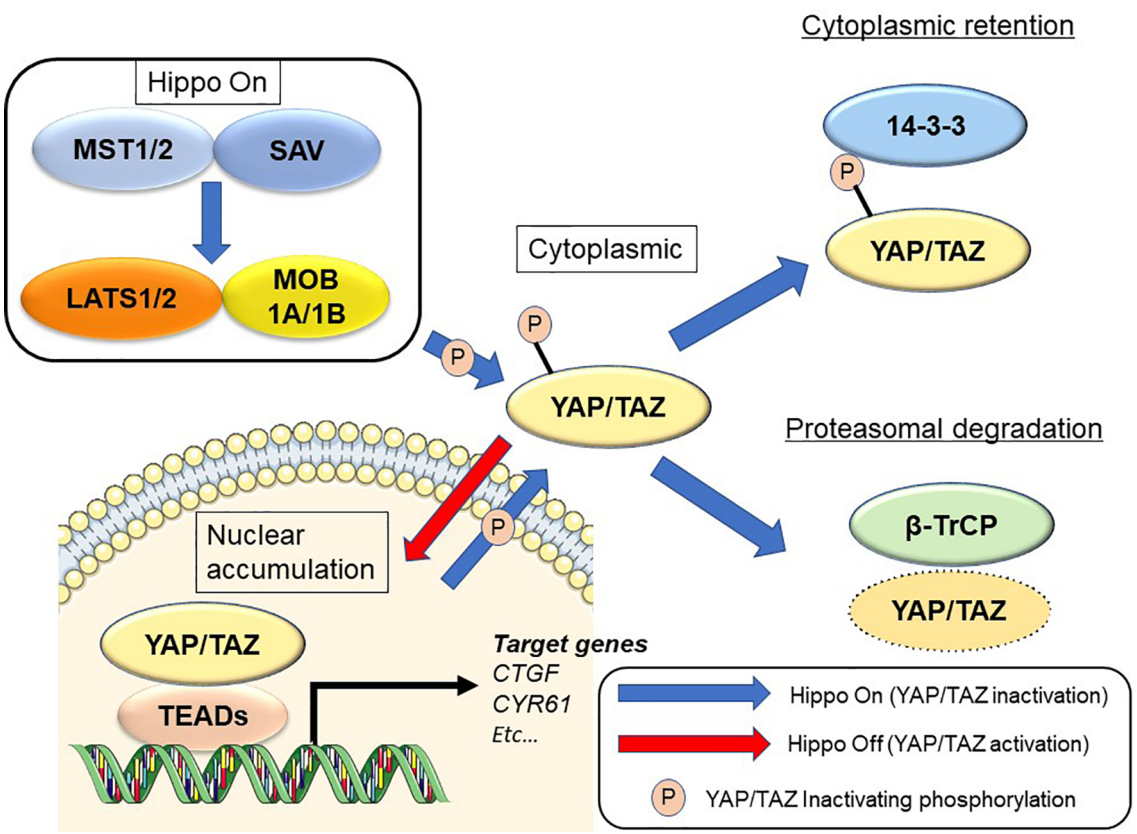

FIGURE 1 | Regulation of the Hippo signaling pathway in mammalian cells. See text for details.

YAP expression in acinar cells displays a weak cytoplasmic staining pattern, and is undetectable within islets. YAP expression in the adult human pancreas mirrors that in the mouse. On the other hand, phosphorylated-MST1/2 expression (indicative of active Hippo signaling) is broadly detectable in adult human pancreas, and islet cells display strong expression of phosphorylated MST1/2 (34). In another report using pancreatic *MST1/2* DKO mice by Gao et al. (35), nuclear YAP staining was observed in the "trunk" regions at E15.5, and was almost undetectable at birth. Thereafter, YAP expression is weak and confined mainly to the ductal compartment at postnatal day (P)7 and later stages. *MST1/2* mRNA levels are highest at E15.5 and lowest at birth; *MST1* mRNA expression reappears at P7 and later stages. Interestingly, YAP expression is decreased and absent during the late embryonic and perinatal periods, raising the possibility that YAP must be silenced for proper pancreas differentiation. Such sequential changes in YAP expression have a crucial role for proper pancreas development (34, 35).

Indeed, in pancreatic *MST1/2* DKO mice, abundant YAP expression was observed in the abnormally numerous duct-like structures from P7 to P14 (35). Furthermore, the duct-like cells in *MST1/2* DKO mice originated from acinar cells. In the absence of MST1/2, acinar cells differentiate normally but fail to maintain their differentiated state and de-differentiate or trans-differentiate into a duct-like state (35). On the other hand, *MST1/2* deletion does not affect perinatal YAP expression, suggesting that perinatal YAP repression occurs *via* an MST1/2-independent mechanism (35).

In addition, pancreatic *MST1/2* DKO mice show the histologic features of acute pancreatitis. While no discernible difference is observed between control and pancreatic *Mst1/2* DKO mice at E12.5 (primary transition), a dramatic reduction in the overall expression of amylase is found in the pancreatic *MST1/2* DKO mice at E16.5 (secondary transition), suggesting a defect in exocrine differentiation (34). In these mice, acini fail to form the classic rosette-like structure (34, 35). Robust immune cell infiltration and TUNEL-positive cell death are also detectable with a pancreatitis-like phenotype (35). These findings further suggest that Hippo signaling becomes active during the secondary transition where it regulates acinar cell proliferation and differentiation.

By 6 weeks, the majority of pancreatic cells are not proliferating in mice (34). In contrast, one-third of amylase-positive acinar cells and cytokeratin 19-positive ductal cells display sustained cell proliferation with BrdU incorporation in the pancreatic *MST1/2* DKO mice (34). Thus, MST1/2 play a role as suppressors of proliferation in the mammalian pancreas.

On the other hand, for endocrine cells, YAP is not expressed in glucagon- or insulin-expressing cells at E12.5 and E16.5, respectively (34). Even at P30, YAP is not detectable in the β-

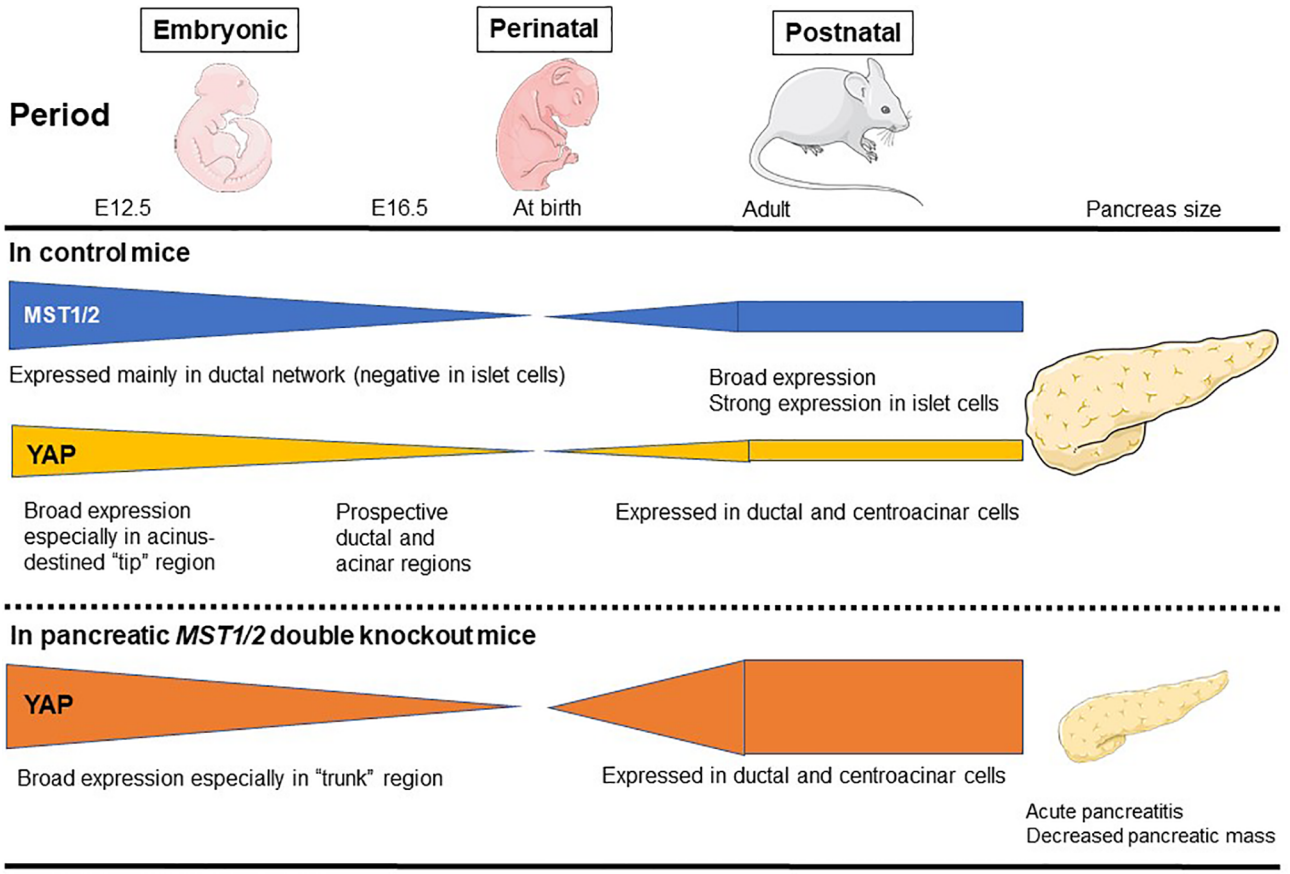

FIGURE 2 | MST1/2 and YAP expression during normal pancreas development. *MST1/2* mRNA levels are highest during the embryonic phase and lowest at birth. *MST1* mRNA expression reappears at postnatal day 7 and later stages. Phosphorylated MST1/2 expression (active Hippo signaling) is broadly detectable in adult human pancreas, and islet cells display strong expression of phosphorylated MST1/2. YAP is broadly expressed throughout the pancreatic and duodenal E12.5 mouse pancreas (primary transition), but then gradually becomes restricted to prospective ductal and acinar regions at E16.5 (secondary transition). In the adult mouse pancreas, YAP expression is markedly decreased and the strong expression is largely confined to ductal and terminal-duct centroacinar cells, unlike in the embryonic pancreas. In pancreatic *MST1/2* double knockout (DKO) mice, nuclear YAP staining is observed in the "trunk" regions during the embryonic phase, but is almost undetectable at birth. Thereafter, YAP expression is weak and confined mainly to the ductal compartment at birth and later postnatal stages. In pancreatic *MST1/2* DKO mice, abundant YAP expression was observed in abnormally numerous duct-like structures during the postnatal phase. YAP remains undetectable within endocrine cells even in the absence of *MST1/2*. Pancreatic *MST1/2* DKO mice show the histologic features of acute pancreatitis and decreased size (an approximately 2-fold decrease in pancreas mass).

cells (35). YAP remains undetectable within endocrine cells even in the absence of MST1/2 (34). Additionally, islet cells are largely Ki-67-negative, in agreement with undetectable YAP expression in both control and pancreatic *MST1/2* DKO mice (34). The ratio of insulin-positive to glucagon-positive cells is not different between control and *MST1/2* DKO mice (34), and blood glucose level also shows no significant difference between them (34, 35). On the other hand, complete loss of YAP in $Yap^{flox/flox}$*:p48-Cre* mice also has no effect on blood glucose level (36). Hippo signaling does not play a crucial role in the pancreatic endocrine compartment.

As a consequence of the above features, the pancreas in pancreatic *MST1/2* DKO mice is smaller (approximately 2-fold decrease in pancreas mass), displaying a pale white color and atrophy (34, 35). While Hippo deficiency in liver results in liver hypertrophy (37, 38), the Hippo-deficient pancreas is reduced in size (34, 35). Thus, pancreas mass and tissue architecture are greatly disrupted in the absence of MST1/2. YAP plays a crucial role downstream of MST1/2 during pancreas development, and dysregulation of Hippo signaling may contribute to human pancreatic disease phenotypes.

BIOLOGICAL ROLE OF THE HIPPO SIGNALING PATHWAY IN PANCREATIC CANCER DEVELOPMENT—LESSONS FROM GENETICALLY ENGINEERED MOUSE MODELS

The genetic landscape of PDAC is characterized by four frequently mutated genes: *KRAS*, *TP53*, *CDKN2A* (p16), and *SMAD4* (39). The four predominant gene mutations appear to

occur sequentially as PanIN progresses. *KRAS* mutations can be found even in normal pancreas and in PanIN1. In PDAC, *KRAS* mutation ranges from 88% to 100% in several studies (40–45). Although the initial step in PDAC development remains to be elucidated, oncogenic *KRAS* mutation is a key event, as evidenced by its presence in PanIN lesions (46, 47) and the development of PanIN lesions in oncogenic *KRAS*-driven genetically engineered mouse models (GEMMs) (48, 49). The oncogenic *KRAS* mutation perturbs the constitutively activated RAS protein, and results in the dysregulated activation of proliferation and survival pathways. GEMMs have provided several insights into the development of PDAC (50–53). Although oncogenic *KRAS* mutations are recognized early events in PDAC development, they are not entirely sufficient for the development of fully invasive PDAC. Indeed, only 5–10% of animals in GEMMs with mutated *KRAS* (without additional genetic alterations) develop frank PDAC, and do so very late (usually after 9 months) (50). PDAC development can be enhanced by the existence of another mutation (e.g., *TP53*) (51, 54). Pancreatic inflammation by administration of cerulein accelerates the formation of PanINs and PDAC in $KRAS^{G12V}$ mice (55). In addition to the role of oncogenic KRAS in development of PDAC, *KRAS* mutations have also been shown to be important for PDAC maintenance (56, 57). Interestingly, inactivation of $KRAS^{G12D}$ in confirmed precursor lesions and during progression to PDAC leads to tumor regression of those lesions, showing that $KRAS^{G12D}$ is required for tumor cell maintenance (56, 58) (**Figure 3**). In an analysis of *KRAS* mutation type, codon G12D mutation was the most frequent (48%), followed by G12V (31%) and G12R (21%) (45).

Acinar-to-ductal metaplasia (ADM) caused by pancreatitis is an initiating step in pancreatic tumor development (55). Cerulein treatment reduces phosphorylation of LATS1, and increases YAP/TAZ protein levels accompanied by strong nuclear localization (59). Following cerulein treatment, cytokeratin 19 (duct cell marker) expression is also increased, consistent with acinar-to-ductal reprogramming (59). Thus, YAP/TAZ activity is accelerated in the injured pancreas, particularly in the subset of cells undergoing ADM (**Figure 3**).

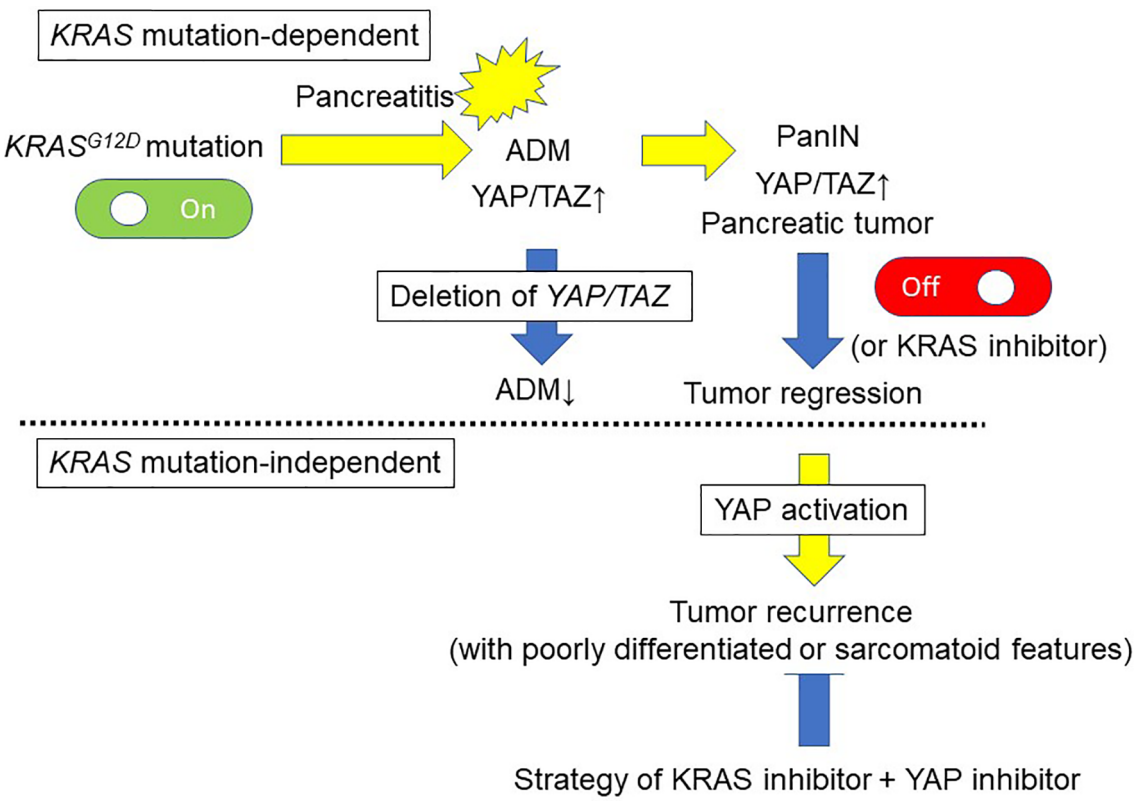

FIGURE 3 | Pancreatic tumor development and maintenance by KRAS-dependent and KRAS-independent mechanisms *via* YAP activation. Oncogenic *KRAS* mutation is a key event of the development of PanIN lesions. Acinar-to-ductal metaplasia (ADM) caused by pancreatitis is an initiating step in pancreatic tumor development. The pancreatic tumor mouse model *LSL-*$KRAS^{G12D}$*; Pdx1-Cre* displays increased ADM lesions and development of PanIN in response to cerulein, accompanied by YAP/TAZ expression. On the other hand, deletion of YAP/TAZ reduces the ability of $KRAS^{G12D}$ mutant mice to develop ADM in response to cerulein, and these mice are free of PanIN lesions even after cerulein-induced pancreatitis. Inactivation of $KRAS^{G12D}$ in established tumor lesions can lead to tumor regression. Although $KRAS^{G12D}$ extinction induces regression of pancreatic tumors, 70% of the mice develop relapsed tumors *via* oncogenic *KRAS*-independent mechanisms involving the *YAP1* oncogene. An anti-YAP1 therapeutic strategy with KRAS-targeting agents may be required for elective tumors.

Recent studies have demonstrated that YAP/TAZ play a crucial role in the induction of ADM, an initial step in the progression to PDAC, in GEMMs (36, 59). The pancreatic tumor mouse model *LSL-KRAS^{G12D};Pdx1-Cre* displays the whole spectrum of preneoplastic lesions (50). In these mice, increased ADM lesions and development of PanIN with strong YAP/TAZ expression are detectable, and YAP/TAZ levels are elevated in pancreatic protein lysates (59). Deletion of *YAP/TAZ* significantly reduced the ability of *KRAS^{G12D}* mice to induce ADM in response to cerulein, and these mice (*KRAS^{G12D};YAP1$^{fl/fl}$;TAZ$^{fl/fl}$*) were free of PanIN lesions at 3 months after the transient induction of pancreatitis by cerulein, similar to control mice (59). Thus, YAP/TAZ are required for *KRAS^{G12D}*-induced ADM in response to pancreatitis *in vivo* (**Figure 3**). Deletion of *YAP/TAZ* in the *KRAS^{G12D}* mice reduced Ras activation even after cerulein treatment (59). In contrast, ectopic YAP/TAZ activation in acinar cells by adenoviral vectors converted the infected acinar cells to duct cell morphology (59). Overexpression of constitutively active YAP1 in primary acinar cells also enhances Ras activity (59). YAP/TAZ are necessary and sufficient for ADM induction (59). Acinar cell-specific YAP/TAZ signaling may be essential for oncogenic *KRAS^{G12D}*-induced PanIN formation in the context of pancreatitis.

Zhang et al. (36) genetically engineered *KRAS$^{G12D/+}$:TP53$^{R172H/+}$:YAP$^{flox/flox}$:p48-Cre* mice to determine whether YAP is involved in PDAC development. In their study, *KRAS$^{G12D/+}$:p48-Cre* or *KRAS$^{G12D/+}$:TP53$^{R172H/+}$:p48-Cre* mice with one or two intact *YAP* alleles developed ADM and early PanINs from 4 to 8 weeks of age, respectively (36). These ADM and early PanINs progressed through late-stage PanINs and eventually to invasive PDAC by 2 to 4 months in *KRAS$^{G12D/+}$:TP53$^{R172H/+}$:p48-Cre* mice, or from 6 months to 2 years in *KRAS$^{G12D/+}$:p48-Cre* or *KRAS$^{G12D/+}$* mice (36). In contrast, when these mice underwent homozygous *YAP* deletion (*KRAS$^{G12D/+}$:YAP$^{flox/flox}$:p48-Cre* and *KRAS$^{G12D/+}$:TP53$^{R172H/+}$:YAP$^{flox/flox}$:p48-Cre*), they entirely lacked any late-stage PanINs or PDAC (36).

Zhang et al. generated *p48-Cre;LSL-KRAS^{G12D};FBXW7$^{fl/fl}$* mice to examine whether loss of the tumor suppressor FBXW7 might be an additional gene alteration in the development of PDAC (60). They found that the mice displayed accelerated tumorigenesis: PDACs were detectable by P14 and all mice yielded PDACs by P40 PDAC in *p48-Cre;LSL-KRAS^{G12D};FBXW7$^{fl/fl}$* mice was preceded by earlier onset of ADM and PanIN lesions, and accompanied by chromosomal instability and the accumulation of YAP (60). Furthermore, in a pancreatic cell line established from *p48-Cre;LSL-KRAS^{G12D};FBXW7$^{fl/fl}$* mice and in *FBXW7*-deficient human pancreatic cancer cells, down-regulation of YAP attenuated cell growth. Thus, deletion of the tumor suppressor FBXW7 accelerates *KRAS*-driven pancreatic tumorigenesis with YAP expression (60).

Kapoor et al. examined the mechanism of *KRAS^{G12D}*-independent PDAC recurrence using a doxycycline-inducible *KRAS^{G12D}* transgene and conditional *p53* null alleles (*p48Cre; tetO_LSL-KRAS^{G12D}; ROSA_rtTA; p53L/+*, designated iKras) (61). In their investigation, *KRAS^{G12D}* extinction by doxycycline withdrawal induced complete regression of pancreatic tumors at three weeks, as determined by MRI imaging. However, 70% of the mice developed relapsed tumors between 9 and 47 weeks after doxycycline withdrawal, with a median survival of 36.6 weeks compared to 15.4 weeks for iKras mice with continued doxycycline treatment (61). Kapoor et al. revealed oncogenic *KRAS*-independent bypass mechanisms involving the *YAP1* oncogene in *KRAS^{G12D}*-independent PDAC recurrence, and emphasized the potential importance of an anti-YAP1 therapeutic strategy for elective tumors in the clinical setting with agents that targeted KRAS and its signaling pathways (61) (**Figure 2**). Shao et al. reported similar mechanisms in *KRAS*-driven lung cancer (62). These findings suggest that murine PDAC cells can survive in the absence of oncogenic *KRAS* signaling and acquire alternative mechanisms to foster their own growth (61, 63). The activity of the transcriptional co-activator YAP plays a critical role in the promotion and maintenance of PDAC by operating as a key downstream target of KRAS signaling. *YAP/TAZ* amplification frequency ranged from 0% to 19% in 9,125 tumor samples among 33 cancer types from The Cancer Genome Atlas (64). Among these 33, the top six cancer types with the highest amplification frequency of *YAP/TAZ* included all five squamous cell-involved cancers (lung squamous cell carcinoma, esophageal squamous cell carcinoma, head and neck squamous cell carcinomas, and bladder urothelial carcinoma), whereas the frequency in PDAC was about 2% and 14th among 33 cancer types (64). Overall, YAP has emerged as a central node of transcriptional convergence in growth-promoting signaling in PDAC cells by both KRAS-dependent and KRAS-independent bypass mechanisms. (**Figure 3**). Collectively, these observations indicate that YAP/TAZ also play a crucial role in the development and recurrence of PDACs.

CLINICAL IMPACT OF YAP/TAZ EXPRESSION IN PDAC PATIENTS

The clinical function of YAP as a prognostic marker has been investigated in several studies (**Table 1**), which have indicated that YAP and/or TAZ are overexpressed in tumor samples from patients with PDACs (61, 65–68). It has been found that nuclear overexpression of YAP is an independent prognostic marker for poor survival and is associated with liver metastasis (68). Furthermore, using public mRNA expression data, YAP was confirmed to be correlated with poor survival (69, 70). The 5-year survival rate was 0% in patients with high *YAP* mRNA expression compared to 32% in those with low expression. Furthermore, multiple YAP/TEAD-regulated genes were associated with poor prognosis, such as transforming growth factor alpha, heparin-binding EGF-like growth factor, integrin subunit alpha 2, P2Y2 receptor, G protein-coupled receptor 87, and mucin 1. On the other hand, YAP-inhibitory pathway components were associated with a favorable prognosis, such as STE20-related kinase adaptor/liver kinase B1, protein kinase

TABLE 1 | YAP/TAZ expression and functional relevance in human pancreatic cancers.

Reference	Number	Target	Location	Positive ratio	Outcomes
Diep et al. (65)					
	64	YAP1	Primary	77%	Not available
Yang et al. (66)					
	38	YAP	Primary	61%	Not available
	25	YAP	Metastatic site	72%	Not available
Xie et al. (67)					
	57	TAZ	Primary	82%*	Not available
Salcedo Allende et al. (68)					
	64	YAP1	Primary	90.62%	Poor OS
Rozengurt et al. (69)**					
	176	*YAP* mRNA	Primary	20%	Poor OS
Zhou et al. (70)***					
	176	*YAP1* mRNA	Primary	50%	Poor OS

Weak, moderate, and strong expression of TAZ were identified as positive.
A published interactive open-access database (www.proteinatlas.org/pathology) was used.
***The cohort of The Cancer Genome Atlas (TCGA) was used.*
OS, overall survival.

A/large tumor suppressor, and tuberous sclerosis complex/mammalian target of rapamycin complex 1.

BIOLOGICAL ROLE OF YAP/TAZ IN CANCER CELLS

There is accumulating evidence that YAP and TAZ promote proliferation and growth of PDAC cells. Treatment of PDAC cells with YAP-targeting small interfering RNA oligonucleotides significantly reduced tumor growth (65). It has been reported that eukaryotic translation initiation factor 5A–pseudopodium-enriched atypical kinase 1 signaling regulates YAP and TAZ expression and pancreatic cancer cell growth (71). Disrupting this signaling in pancreatic cancer cells inhibited YAP/TAZ protein expression, reducing the expression of stem cell-associated transcription factors and tumor sphere growth (71).

In human PDAC cells, YAP functions as a downstream effector of the crosstalk between insulin/IGF-1 receptor and G protein-coupled receptor systems (72). Stimulation with insulin and the G protein-coupled receptor agonist neurotensin induced rapid YAP nuclear import and markedly augmented the mRNA levels of YAP/TEAD-regulated genes, including *CTGF* and *Cyr61*. The growth-promoting agonists regulated YAP activity *via* PI3K and protein kinase D in PANC-1 and MiaPaCa-2 (72), human cell lines that correspond to the squamous/quasi mesenchymal/basal-like sub-type of PDAC. It is of great interest that YAP function has been associated with this PDAC sub-type, considered the most clinically aggressive form.

The epithelial-to-mesenchymal transition (EMT) is a developmental regulatory program defined by the phenotypical transition from an epithelial to a mesenchymal cell state. The EMT is an essential step for metastasis and confers resistance to therapy (73). Active YAP promotes pancreatic cancer cell motility, invasion, and tumorigenesis in a mitotic phosphorylation-dependent manner and contributes to the EMT in pancreatic cancer cells by several mechanisms, including hyperactivation of AKT signaling (66, 67, 74, 75). YAP/TAZ also interact with nuclear factors such as ZEB1 (29) and SMADs (76, 77), both of which are important EMT regulators. TGF-β is a well-known EMT inducer in cancer cells. TGF-β enhances YAP nuclear localization and stabilizes YAP activity, and TGF-β-induced EMT and YAP activity are both blocked by inhibition of AKT signaling in PDAC cells (78). Xie et al. (67) focused on TAZ activation in pancreatic cancer cells and examined its functional roles in the EMT. Aberrant expression and activation of TAZ in pancreatic cancer cells promoted the EMT *via* down-regulation of E-cadherin and up-regulation of vimentin expression. In contrast, depletion of *TAZ* in pancreatic cancer cells suppressed the EMT phenotype (67).

PDAC is characterized by a high degree of chemoresistance. Gemcitabine has been the standard chemotherapeutic agent in PDAC since 1997 (79). Several mechanisms of YAP-induced chemoresistance have been proposed. One mechanism suggests that YAP overexpression induces the EMT in pancreatic cancer cells by activating the AKT cascade, which can cause resistance to gemcitabine (74). Another proposed mechanism involves microRNA, since microRNA 181c was overexpressed in PDAC samples and correlated with poor prognosis. microRNA 181c directly repressed MST1, LATS2, salvador homolog 1, and MOB kinase activator 1, leading to YAP and TAZ activation, and gemcitabine resistance *in vitro* and *in vivo* (80). Isoprenylcysteine carboxylmethyltransferase (ICMT) is the catalytic enzymes in the three step prenylation processing that posttranslationally modifies substrate proteins including RAS isoforms. Suppression of ICMT inhibits cancer stem cell self-renewal and chemoresistance of mutant KRAS pancreatic cancer cells with TAZ protein degradation (81). On the other hand, expression of constitutively active $KRAS^{G12V}$ restores TAZ protein level and the self-renewal ability of pancreatic cancer cells. Thus, mutant KRAS plays a major role in TAZ expression and cancer stem self-renewal in pancreatic cancer cells, and ICMT has potential as a pharmacological target in the treatment of mutant KRAS pancreatic cancer cells (81).

BIOLOGICAL ROLE OF YAP/TAZ IN THE TUMOR MICROENVIRONMENT

An important feature of human and murine PDAC is an extensive desmoplastic stroma (82) that increases the stiffness of the extracellular matrix (ECM) surrounding epithelial cancer cells (83). The Hippo/YAP pathway has been recognized to play a critical role in mechano-transduction (84, 85) and in sensing ECM stiffness (86). High stiffness leads to inhibition of the Hippo tumor suppressive pathway while enhancing the activity of YAP/TAZ. The stroma contains cancer-associated fibroblasts (CAFs), immune cells, endothelial cells, and the ECM. Pancreatic stellate cells are resident mesenchymal cells of the pancreas that represent the major source of CAFs. It has been found that YAP and TAZ are expressed at high levels in activated pancreatic stellate cells in PDAC, as well as in chronic pancreatitis (87).

Transglutaminase 2 secreted by pancreatic cancer cells promotes cross-linking of collagen, which activates CAFs and stimulates their proliferation, and results in higher collagen production by CAFs and further stiffening of the stroma. In turn, such a stiff tumor microenvironment conveys mechanical signals to cancer cells, leading to activation of YAP/TAZ and tumor progression (88). Environmental stimuli, including obesity and metabolic syndrome, also enhance the promotion of invasive PDAC (89, 90).

PDAC is characterized by a profound inflammatory reaction and an immunosuppressive state (91). Pancreatic tumors are associated with immune dysfunction, partly mediated by the recruitment of immunosuppressive cells, such as tumor-associated macrophages and myeloid-derived suppressor cells (92, 93). These cells are recruited to the tumor microenvironment and can inhibit T-cell activity. YAP has been identified as a critical regulator of the immunosuppressive microenvironment in PDAC. YAP inactivation prevented recruitment of myeloid-derived suppressor cells while in turn supporting infiltration of antigen-presenting macrophages and T-cell activation, thereby promoting apoptosis of tumor cells (30). Although T-cell activity is critical for tumor immunity, T-cell fate is governed by Hippo signaling (94–96). Geng et al. reported that TAZ induces Th17 cell differentiation and suppresses the differentiation of immunosuppressive regulatory T-cells (95). Ni et al. reported that immunosuppressive activity of regulatory T-cells was dependent on YAP expression in melanoma, and the anti-tumor immunity was enhanced in the absence of YAP (97). In hepatocellular carcinoma, YAP mediates the migration of macrophages *in vitro* and *in vivo* (98). Thus, YAP/TAZ are capable of regulating the biological activity and function of T-cells and macrophages, which is crucial for tumor immunity. They thereby participate in immune escape by suppressing normal immunological activity.

Whole-genome and whole-exome sequencing of PDACs have revealed a mean mutation load of 1.8 and 1.1 mutations per megabase, respectively, and only 5% of PDACs displayed a hypermutated phenotype (99). The identification of hypermutated PDACs is important because these tumors are sensitive to immunotherapy (99). Furthermore, the prevalence of microsatellite instability was found to be around 5% in many solid tumors, while in PDAC it was only 2% (100). These DNA mismatch repair (MMR)-deficient tumors carried high neo-antigen load and displayed considerably improved responses to programmed cell death 1 blockade (100). These authors reported that solid tumors with MMR deficiency are responsive to immune checkpoint blockade with pembrolizumab. Pembrolizumab has subsequently been approved by the FDA for solid tumors with MMR deficiency, regardless of tissue of origin (101). Furthermore, the clinical benefit of pembrolizumab was confirmed in patients with microsatellite instability high MMR-deficient non-colorectal cancers including pancreatic cancer (102). Thus, immunotherapy is a rapidly progressing field in cancer treatment. Among the immunotherapy modalities, immune checkpoint inhibition has displayed considerable success in several solid tumors, but there is still no significant benefit in PDAC.

In cancers other than PDAC, there is accumulating evidence that YAP/TAZ play a pivotal role in PD-L1 expression. Overexpression of constitutively active YAP or TAZ by the deletion of MST1/2 or LATS1/2 enhances PD-L1 expression in breast and lung cancer cell lines (103). Furthermore, PD-L1 expression is also induced by YAP in BRAF inhibitor-resistant melanoma, and the relationship between YAP and PD-L1 expression was validated in human clinical melanoma tissues (104). In human non-small cell lung cancer, YAP regulated PD-L1 at the transcriptional level, suggesting that YAP has potential as an immunotherapeutic target (105). Lee et al. found that YAP regulates PD-L1 by directly binding to the PD-L1 promoter and that YAP/PD-L1 signaling modulated tumor cell proliferation and migration in EGFR–TKI-resistant lung adenocarcinoma, and also that YAP down-regulation inhibited PD-L1 expression (106). It is worth further exploring the role of YAP/TAZ in tumor immunotherapy. Thus, targeting YAP/TAZ may be an alternative approach for combination with immunotherapy in cancer cells and the tumor microenvironment.

THERAPEUTIC TARGETING OF THE HIPPO SIGNALING PATHWAY IN PDAC

According to the above collected evidence, it is reasonable to develop drugs that target YAP and TAZ activities in PDAC. As indicated above, tumor cells with YAP activation can evade the requirement for *KRAS* mutant expression in PDAC (63). YAP is a key element not only downstream of Ras but also as an alternative route to bypass the need of this oncogene for tumor relapse. Recently, the $KRAS^{G12C}$ inhibitor Sotorasib is effectively developed for solid cancers (107). In 11 PDAC patients with $KRAS^{G12C}$ mutation, one patient had a confirmed partial response, 9 had stable disease, and one had progressive disease in response to Sotorasib (107). Even if Ras could be effectively inhibited by this new therapy, YAP amplification offers a potential pathway to induce tumor recurrence. Recent studies suggest novel approaches to inhibit YAP/TAZ activity with drug repositioning in clinical use, including statins. Statins, which have been used to treat dyslipidemia and prevent heart diseases, selectively inhibit 3-hydroxy-methylglutaryl (HMG) CoA reductase (108), the rate-limiting

enzyme in the generation of mevalonate. Accelerated mevalonate biosynthesis through mutant *p53* (109–111) and AKT/mTORC1 (111) has been reported in cancers. The mevalonate pathway plays an important role in the generation of lipids and lipid intermediates, including farnesyl pyrophosphate, geranylgeranyl pyrophosphate, and cholesterol. In preclinical studies (112, 113), statins delayed the progression of PDAC in mice harboring $KRAS^{G12D}$ mutation. Statins were identified as potential YAP inhibitors by screens of molecules that changed the nuclear/cytoplasmic distribution of YAP (114). In our previous study, statin treatment suppressed cancer cell growth *via* TAZ down-regulation in hepatocellular carcinoma (115). Several epidemiological studies have indicated that statin use correlates with favorable oncologic effects in PDAC (116–124), especially in males (119, 120). A large study demonstrated that statins were associated with a significantly reduced PDAC risk (by 34%), with a stronger effect in males (119). The beneficial effects of statins depend on the type of statins used, with several reports showing positive associations with lipophilic (and not hydrophilic) statins and reduced cancer risk (125–128). On the other hand, Hamada et al. reported that regular statin use was not associated with pancreatic cancer risk in two large prospective cohort studies in the U.S (129). Nevertheless, Hamada et al. also reported increased survival in PDAC patients with regular pre-diagnosis use of statins (130). Recently, a meta-analysis of PDAC risk that included more than 3 million participants and 170,000 PDAC patients has been published (131). This study indicates a significant decrease in PDAC risk with statin use, thus reinforcing the conclusion that statin administration is associated with beneficial effects in PDAC patients. In addition to their potential efficacy in primary prevention and interception, statins may improve the outcome for patients after surgical removal of their primary PDAC (116, 117, 132), indicating a possible role for statins in the prevention of PDAC recurrence. Collectively, accumulating evidence from epidemiological and preclinical studies indicates a protective effect of statins in PDAC. Of the evaluated treatments in PDAC, verteporfin (133, 134) has a direct effect on Hippo signaling by inhibiting YAP–TEAD interactions. Erlotinib (135), FG-3019 (CTGF antagonism) (136), BIS 1 (135), LY3009120 (133) and ICMT small molecule inhibitor (81) indirectly affect YAP and/or TAZ signaling. Although the mechanism is not fully clarified for several natural substances, curcumin (32, 137), resveratrol (138), *Stichopus japonicus* acidic mucopolysaccharide (139), and pseudolaric acid B (140) have been reported to target YAP/TAZ signaling. Also, in our previous study, curcumin, a major component of turmeric and an old Indian spice, successfully suppressed TAZ/YAP expression and exerted anticancer effects in hepatocellular carcinoma cell lines (32). In the future, direct or indirect pharmacological modulation of YAP/TAZ expression may become promising approaches to fight this deadly disease.

CONCLUSIONS

The Hippo pathway is an evolutionarily conserved signaling pathway in mammals, and YAP and TAZ are key downstream regulators in the Hippo pathway that play a crucial role in the development of the normal pancreas and of PDAC in GEMMs. Furthermore, YAP and TAZ play a crucial role in the development of PDAC by both KRAS-dependent and KRAS-independent bypass mechanisms. Also in PDAC progression, aberrant transcriptional activity of YAP and TAZ has a pivotal role in malignant behavior, including cell growth, EMT, and drug resistance. Besides, YAP/TAZ play a tumor-promoting role in the tumor microenvironment. PDAC features an extensive desmoplastic stroma, and the stroma contains CAFs and immune cells. YAP promotes CAF activation and subsequent fibroinflammatory responses, and the resultant high stiffness enhances the malignant behavior of PDAC with high activity of YAP/TAZ. In addition, YAP acts as a critical regulator of the immunosuppressive microenvironment in PDAC. YAP/TAZ have potential as a therapeutic target not only for cancer cells, but also for the tumor microenvironment in PDAC. Thus, accumulating evidence supports the biological importance of YAP/TAZ in the development and progression of PDACs, and the regulation of YAP/TAZ signaling is increasingly recognized as a therapeutic target. In the near future, direct or indirect pharmacological modulation of YAP/TAZ may become promising therapeutic approaches in PDACs. On the other hand, complete deletion of YAP in knockout mice induced embryonic lethality at E8.5 due to severe developmental defects (141). Although TAZ knockout mice show only partial lethality, with 20% of the mice remaining viable, the survivors develop renal cysts and lung emphysema (142–144). Since YAP/TAZ has so many important physiological functions, as evidenced by YAP-null and TAZ-null mice, careful targeting of the YAP/TAZ signaling pathway to minimize systemic effects is clearly a highly desirable goal in PDAC treatment. Anti-YAP/TAZ strategies to selectively block aberrant YAP/TAZ signal activation are attractive and rational. Biomarker analysis to identify aberrant YAP/TAZ signal activation may therefore be the next step to establish an efficient therapeutic approach.

AUTHOR CONTRIBUTIONS

HH and HB conducted the topic investigated in this paper. NU, LS, KM, HS, and YS assisted in the useful discussions and wrote the manuscript. All authors contributed to the article and approved the submitted version.

FUNDING

This work was supported by a Grant-in-Aid for Scientists (C); the Ministry of Education, Culture, Sports, Science, and Technology of Japan, No. 19K09177 (to HH); the Shinnihon Foundation of Advanced Medical Treatment Research (HH), the Takeda Science Foundation, Japan (to HH), and Public Trust Surgery Research Fund (to HH).

REFERENCES

1. Siegel RL, Miller KD, Jemal A. Cancer Statistics, 2019. *CA Cancer J Clin* (2019) 69(1):7–34. doi: 10.3322/caac.21551
2. Notta F, Chan-Seng-Yue M, Lemire M, Li Y, Wilson GW, Connor AA, et al. A Renewed Model of Pancreatic Cancer Evolution Based on Genomic Rearrangement Patterns. *Nature* (2016) 538(7625):378–82. doi: 10.1038/nature19823
3. Conroy T, Desseigne F, Ychou M, Bouche O, Guimbaud R, Becouarn Y, et al. FOLFIRINOX Versus Gemcitabine for Metastatic Pancreatic Cancer. *N Engl J Med* (2011) 364(19):1817–25. doi: 10.1056/NEJMoa1011923
4. Von Hoff DD, Ervin T, Arena FP, Chiorean EG, Infante J, Moore M, et al. Increased Survival in Pancreatic Cancer With Nab-Paclitaxel Plus Gemcitabine. *N Engl J Med* (2013) 369(18):1691–703. doi: 10.1056/NEJMoa1304369
5. Nishio K, Kimura K, Amano R, Yamazoe S, Ohrira G, Nakata B, et al. Preoperative Predictors for Early Recurrence of Resectable Pancreatic Cancer. *World J Surg Oncol* (2017) 15(1):16. doi: 10.1186/s12957-016-1078-z
6. Chand S, O'Hayer K, Blanco FF, Winter JM, Brody JR. The Landscape of Pancreatic Cancer Therapeutic Resistance Mechanisms. *Int J Biol Sci* (2016) 12(3):273–82. doi: 10.7150/ijbs.14951
7. Hayashi H, Higashi T, Miyata T, Yamashita Y-i, Baba H. Recent Advances in Precision Medicine for Pancreatic Ductal Adenocarcinoma. *Ann Gastroenterol Surg* (2021). doi: 10.1002/ags3.12436 [in press]
8. Harvey KF, Pfleger CM, Hariharan IK. The Drosophila Mst Ortholog, Hippo, Restricts Growth and Cell Proliferation and Promotes Apoptosis. *Cell* (2003) 114(4):457–67. doi: 10.1016/S0092-8674(03)00557-9
9. Wu S, Huang J, Dong J, Pan D. Hippo Encodes a Ste-20 Family Protein Kinase That Restricts Cell Proliferation and Promotes Apoptosis in Conjunction With Salvador and Warts. *Cell* (2003) 114(4):445–56. doi: 10.1016/S0092-8674(03)00549-X
10. Huang J, Wu S, Barrera J, Matthews K, Pan D. The Hippo Signaling Pathway Coordinately Regulates Cell Proliferation and Apoptosis by Inactivating Yorkie, the Drosophila Homolog of YAP. *Cell* (2005) 122(3):421–34. doi: 10.1016/j.cell.2005.06.007
11. Maugeri-Sacca M, De Maria R. The Hippo Pathway in Normal Development and Cancer. *Pharmacol Ther* (2018) 186:60–72. doi: 10.1016/j.pharmthera.2017.12.011
12. Dupont S, Morsut L, Aragona M, Enzo E, Giulitti S, Cordenonsi M, et al. Role of YAP/TAZ in Mechanotransduction. *Nature* (2011) 474(7350):179–83. doi: 10.1038/nature10137
13. Dupont S. Role of YAP/TAZ in Cell-Matrix Adhesion-Mediated Signalling and Mechanotransduction. *Exp Cell Res* (2016) 343(1):42–53. doi: 10.1016/j.yexcr.2015.10.034
14. Varelas X, Samavarchi-Tehrani P, Narimatsu M, Weiss A, Cockburn K, Larsen BG, et al. The Crumbs Complex Couples Cell Density Sensing to Hippo-Dependent Control of the TGF-Beta-SMAD Pathway. *Dev Cell* (2010) 19(6):831–44. doi: 10.1016/j.devcel.2010.11.012
15. Fujii M, Toyoda T, Nakanishi H, Yatabe Y, Sato A, Matsudaira Y, et al. TGF-Beta Synergizes With Defects in the Hippo Pathway to Stimulate Human Malignant Mesothelioma Growth. *J Exp Med* (2012) 209(3):479–94. doi: 10.1084/jem.20111653
16. Azzolin L, Zanconato F, Bresolin S, Forcato M, Basso G, Bicciato S, et al. Role of TAZ as Mediator of Wnt Signaling. *Cell* (2012) 151(7):1443–56. doi: 10.1016/j.cell.2012.11.027
17. Varelas X, Miller BW, Sopko R, Song S, Gregorieff A, Fellouse FA, et al. The Hippo Pathway Regulates Wnt/beta-Catenin Signaling. *Dev Cell* (2010) 18(4):579–91. doi: 10.1016/j.devcel.2010.03.007
18. Fernandez LA, Northcott PA, Dalton J, Fraga C, Ellison D, Angers S, et al. YAP1 is Amplified and Up-Regulated in Hedgehog-Associated Medulloblastomas and Mediates Sonic Hedgehog-Driven Neural Precursor Proliferation. *Genes Dev* (2009) 23(23):2729–41. doi: 10.1101/gad.1824509
19. Lin YT, Ding JY, Li MY, Yeh TS, Wang TW, Yu JY. YAP Regulates Neuronal Differentiation Through Sonic Hedgehog Signaling Pathway. *Exp Cell Res* (2012) 318(15):1877–88. doi: 10.1016/j.yexcr.2012.05.005
20. Chen HJ, Wang CM, Wang TW, Liaw GJ, Hsu TH, Lin TH, et al. The Hippo Pathway Controls Polar Cell Fate Through Notch Signaling During Drosophila Oogenesis. *Dev Biol* (2011) 357(2):370–9. doi: 10.1016/j.ydbio.2011.07.003
21. Yu J, Poulton J, Huang YC, Deng WM. The Hippo Pathway Promotes Notch Signaling in Regulation of Cell Differentiation, Proliferation, and Oocyte Polarity. *PLoS One* (2008) 3(3):e1761. doi: 10.1371/journal.pone.0001761
22. Lai ZC, Wei X, Shimizu T, Ramos E, Rohrbaugh M, Nikolaidis N, et al. Control of Cell Proliferation and Apoptosis by Mob as Tumor Suppressor, Mats. *Cell* (2005) 120(5):675–85. doi: 10.1016/j.cell.2004.12.036
23. He M, Zhou Z, Shah AA, Hong Y, Chen Q, Wan Y. New Insights Into Posttranslational Modifications of Hippo Pathway in Carcinogenesis and Therapeutics. *Cell Div* (2016) 11:4. doi: 10.1186/s13008-016-0013-6
24. Zhao B, Li L, Tumaneng K, Wang CY, Guan KL. A Coordinated Phosphorylation by Lats and CK1 Regulates YAP Stability Through SCF (beta-TRCP). *Genes Dev* (2010) 24(1):72–85. doi: 10.1101/gad.1843810
25. Lei QY, Zhang H, Zhao B, Zha ZY, Bai F, Pei XH, et al. TAZ Promotes Cell Proliferation and Epithelial-Mesenchymal Transition and Is Inhibited by the Hippo Pathway. *Mol Cell Biol* (2008) 28(7):2426–36. doi: 10.1128/MCB.01874-07
26. Yu FX, Zhao B, Guan KL. Hippo Pathway in Organ Size Control, Tissue Homeostasis, and Cancer. *Cell* (2015) 163(4):811–28. doi: 10.1016/j.cell.2015.10.044
27. Poma AM, Torregrossa L, Bruno R, Basolo F, Fontanini G. Hippo Pathway Affects Survival of Cancer Patients: Extensive Analysis of TCGA Data and Review of Literature. *Sci Rep* (2018) 8(1):10623. doi: 10.1038/s41598-018-28928-3
28. Moroishi T, Hansen CG, Guan KL. The Emerging Roles of YAP and TAZ in Cancer. *Nat Rev Cancer* (2015) 15(2):73–9. doi: 10.1038/nrc3876
29. Lehmann W, Mossmann D, Kleemann J, Mock K, Meisinger C, Brummer T, et al. ZEB1 Turns Into a Transcriptional Activator by Interacting With YAP1 in Aggressive Cancer Types. *Nat Commun* (2016) 7:10498. doi: 10.1038/ncomms10498
30. Murakami S, Shahbazian D, Surana R, Zhang W, Chen H, Graham GT, et al. Yes-Associated Protein Mediates Immune Reprogramming in Pancreatic Ductal Adenocarcinoma. *Oncogene* (2017) 36(9):1232–44. doi: 10.1038/onc.2016.288
31. Plouffe SW, Lin KC, Moore JL3rd, Tan FE, Ma S, Ye Z, et al. The Hippo Pathway Effector Proteins YAP and TAZ Have Both Distinct and Overlapping Functions in the Cell. *J Biol Chem* (2018) 293(28):11230–40. doi: 10.1074/jbc.RA118.002715
32. Hayashi H, Higashi T, Yokoyama N, Kaida T, Sakamoto K, Fukushima Y, et al. An Imbalance in TAZ and YAP Expression in Hepatocellular Carcinoma Confers Cancer Stem Cell-Like Behaviors Contributing to Disease Progression. *Cancer Res* (2015) 75(22):4985–97. doi: 10.1158/0008-5472.CAN-15-0291
33. Pictet RL, Clark WR, Williams RH, Rutter WJ. An Ultrastructural Analysis of the Developing Embryonic Pancreas. *Dev Biol* (1972) 29(4):436–67. doi: 10.1016/0012-1606(72)90083-8
34. George NM, Day CE, Boerner BP, Johnson RL, Sarvetnick NE. Hippo Signaling Regulates Pancreas Development Through Inactivation of Yap. *Mol Cell Biol* (2012) 32(24):5116–28. doi: 10.1128/MCB.01034-12
35. Gao T, Zhou D, Yang C, Singh T, Penzo-Mendez A, Maddipati R, et al. Hippo Signaling Regulates Differentiation and Maintenance in the Exocrine Pancreas. *Gastroenterology* (2013) 144(7):1543–53.e1. doi: 10.1053/j.gastro.2013.02.037
36. Zhang W, Nandakumar N, Shi Y, Manzano M, Smith A, Graham G, et al. Downstream of Mutant KRAS, the Transcription Regulator YAP Is Essential for Neoplastic Progression to Pancreatic Ductal Adenocarcinoma. *Sci Signal* (2014) 7(324):ra42. doi: 10.1126/scisignal.2005049
37. Dong J, Feldmann G, Huang J, Wu S, Zhang N, Comerford SA, et al. Elucidation of a Universal Size-Control Mechanism in Drosophila and Mammals. *Cell* (2007) 130(6):1120–33. doi: 10.1016/j.cell.2007.07.019
38. Lu L, Li Y, Kim SM, Bossuyt W, Liu P, Qiu Q, et al. Hippo Signaling is a Potent *In Vivo* Growth and Tumor Suppressor Pathway in the Mammalian Liver. *Proc Natl Acad Sci USA* (2010) 107(4):1437–42. doi: 10.1073/pnas.0911427107
39. Aung KL, Fischer SE, Denroche RE, Jang GH, Dodd A, Creighton S, et al. Genomics-Driven Precision Medicine for Advanced Pancreatic Cancer: Early

Results From the COMPASS Trial. *Clin Cancer Res* (2018) 24(6):1344–54. doi: 10.1158/1078-0432.CCR-17-2994
40. Jones S, Zhang X, Parsons DW, Lin JC, Leary RJ, Angenendt P, et al. Core Signaling Pathways in Human Pancreatic Cancers Revealed by Global Genomic Analyses. *Science* (2008) 321(5897):1801–6. doi: 10.1126/science.1164368
41. Biankin AV, Waddell N, Kassahn KS, Gingras MC, Muthuswamy LB, Johns AL, et al. Pancreatic Cancer Genomes Reveal Aberrations in Axon Guidance Pathway Genes. *Nature* (2012) 491(7424):399–405. doi: 10.1038/nature11547
42. Waddell N, Pajic M, Patch AM, Chang DK, Kassahn KS, Bailey P, et al. Whole Genomes Redefine the Mutational Landscape of Pancreatic Cancer. *Nature* (2015) 518(7540):495–501. doi: 10.1038/nature14169
43. Witkiewicz AK, McMillan EA, Balaji U, Baek G, Lin WC, Mansour J, et al. Whole-Exome Sequencing of Pancreatic Cancer Defines Genetic Diversity and Therapeutic Targets. *Nat Commun* (2015) 6:6744. doi: 10.1038/ncomms7744
44. Sausen M, Phallen J, Adleff V, Jones S, Leary RJ, Barrett MT, et al. Clinical Implications of Genomic Alterations in the Tumour and Circulation of Pancreatic Cancer Patients. *Nat Commun* (2015) 6:7686. doi: 10.1158/1538-7445.AM2015-619
45. Cancer Genome Atlas Research Network and Electronic address aadhe. Integrated Genomic Characterization of Pancreatic Ductal Adenocarcinoma. *Cancer Cell* (2017) 32(2):185–203.e13. doi: 10.1016/j.ccell.2017.07.007
46. Murphy SJ, Hart SN, Lima JF, Kipp BR, Klebig M, Winters JL, et al. Genetic Alterations Associated With Progression From Pancreatic Intraepithelial Neoplasia to Invasive Pancreatic Tumor. *Gastroenterology* (2013) 145(5):1098–109.e1. doi: 10.1053/j.gastro.2013.07.049
47. Kanda M, Matthaei H, Wu J, Hong SM, Yu J, Borges M, et al. Presence of Somatic Mutations in Most Early-Stage Pancreatic Intraepithelial Neoplasia. *Gastroenterology* (2012) 142(4):730–3.e9. doi: 10.1053/j.gastro.2011.12.042
48. Hezel AF, Kimmelman AC, Stanger BZ, Bardeesy N, Depinho RA. Genetics and Biology of Pancreatic Ductal Adenocarcinoma. *Genes Dev* (2006) 20(10):1218–49. doi: 10.1101/gad.1415606
49. Perez-Mancera PA, Guerra C, Barbacid M, Tuveson DA. What We Have Learned About Pancreatic Cancer From Mouse Models. *Gastroenterology* (2012) 142(5):1079–92. doi: 10.1053/j.gastro.2012.03.002
50. Hingorani SR, Petricoin EF, Maitra A, Rajapakse V, King C, Jacobetz MA, et al. Preinvasive and Invasive Ductal Pancreatic Cancer and Its Early Detection in the Mouse. *Cancer Cell* (2003) 4(6):437–50. doi: 10.1016/S1535-6108(03)00309-X
51. Hingorani SR, Wang L, Multani AS, Combs C, Deramaudt TB, Hruban RH, et al. Trp53R172H and KrasG12D Cooperate to Promote Chromosomal Instability and Widely Metastatic Pancreatic Ductal Adenocarcinoma in Mice. *Cancer Cell* (2005) 7(5):469–83. doi: 10.1016/j.ccr.2005.04.023
52. Hruban RH, Adsay NV, Albores-Saavedra J, Anver MR, Biankin AV, Boivin GP, et al. Pathology of Genetically Engineered Mouse Models of Pancreatic Exocrine Cancer: Consensus Report and Recommendations. *Cancer Res* (2006) 66(1):95–106. doi: 10.1158/0008-5472.CAN-05-2168
53. Hruban RH, Rustgi AK, Brentnall TA, Tempero MA, Wright CV, Tuveson DA. Pancreatic Cancer in Mice and Man: The Penn Workshop 2004. *Cancer Res* (2006) 66(1):14–7. doi: 10.1158/0008-5472.CAN-05-3914
54. Aguirre AJ, Bardeesy N, Sinha M, Lopez L, Tuveson DA, Horner J, et al. Activated Kras and Ink4a/Arf Deficiency Cooperate to Produce Metastatic Pancreatic Ductal Adenocarcinoma. *Genes Dev* (2003) 17(24):3112–26. doi: 10.1101/gad.1158703
55. Guerra C, Schuhmacher AJ, Canamero M, Grippo PJ, Verdaguer L, Perez-Gallego L, et al. Chronic Pancreatitis Is Essential for Induction of Pancreatic Ductal Adenocarcinoma by K-Ras Oncogenes in Adult Mice. *Cancer Cell* (2007) 11(3):291–302. doi: 10.1016/j.ccr.2007.01.012
56. Collins MA, Bednar F, Zhang Y, Brisset JC, Galban S, Galban CJ, et al. Oncogenic Kras Is Required for Both the Initiation and Maintenance of Pancreatic Cancer in Mice. *J Clin Invest* (2012) 122(2):639–53. doi: 10.1172/JCI59227
57. di Magliano MP, Logsdon CD. Roles for KRAS in Pancreatic Tumor Development and Progression. *Gastroenterology* (2013) 144(6):1220–9. doi: 10.1053/j.gastro.2013.01.071
58. Ying H, Kimmelman AC, Lyssiotis CA, Hua S, Chu GC, Fletcher-Sananikone E, et al. Oncogenic Kras Maintains Pancreatic Tumors Through Regulation of Anabolic Glucose Metabolism. *Cell* (2012) 149(3):656–70. doi: 10.1016/j.cell.2012.01.058
59. Gruber R, Panayiotou R, Nye E, Spencer-Dene B, Stamp G, Behrens A. YAP1 and TAZ Control Pancreatic Cancer Initiation in Mice by Direct Up-Regulation of JAK-STAT3 Signaling. *Gastroenterology* (2016) 151(3):526–39. doi: 10.1053/j.gastro.2016.05.006
60. Zhang Q, Zhang Y, Parsels JD, Lohse I, Lawrence TS, Pasca di Magliano M, et al. Fbxw7 Deletion Accelerates Kras(G12D)-Driven Pancreatic Tumorigenesis *via* Yap Accumulation. *Neoplasia* (2016) 18(11):666–73. doi: 10.1016/j.neo.2016.08.009
61. Kapoor A, Yao W, Ying H, Hua S, Liewen A, Wang Q, et al. Yap1 Activation Enables Bypass of Oncogenic Kras Addiction in Pancreatic Cancer. *Cell* (2014) 158(1):185–97. doi: 10.1016/j.cell.2014.06.003
62. Shao DD, Xue W, Krall EB, Bhutkar A, Piccioni F, Wang X, et al. KRAS and YAP1 Converge to Regulate EMT and Tumor Survival. *Cell* (2014) 158(1):171–84. doi: 10.1016/j.cell.2014.06.004
63. Ying H, Dey P, Yao W, Kimmelman AC, Draetta GF, Maitra A, et al. Genetics and Biology of Pancreatic Ductal Adenocarcinoma. *Genes Dev* (2016) 30(4):355–85. doi: 10.1101/gad.275776.115
64. Wang Y, Xu X, Maglic D, Dill MT, Mojumdar K, Ng PK, et al. Comprehensive Molecular Characterization of the Hippo Signaling Pathway in Cancer. *Cell Rep* (2018) 25(5):1304–17.e5. doi: 10.1016/j.celrep.2018.10.001
65. Diep CH, Zucker KM, Hostetter G, Watanabe A, Hu C, Munoz RM, et al. Down-Regulation of Yes Associated Protein 1 Expression Reduces Cell Proliferation and Clonogenicity of Pancreatic Cancer Cells. *PLoS One* (2012) 7(3):e32783. doi: 10.1371/journal.pone.0032783
66. Yang S, Zhang L, Purohit V, Shukla SK, Chen X, Yu F, et al. Active YAP Promotes Pancreatic Cancer Cell Motility, Invasion and Tumorigenesis in a Mitotic Phosphorylation-Dependent Manner Through LPAR3. *Oncotarget* (2015) 6(34):36019–31. doi: 10.18632/oncotarget.5935
67. Xie D, Cui J, Xia T, Jia Z, Wang L, Wei W, et al. Hippo Transducer TAZ Promotes Epithelial Mesenchymal Transition and Supports Pancreatic Cancer Progression. *Oncotarget* (2015) 6(34):35949–63. doi: 10.18632/oncotarget.5772
68. Salcedo Allende MT, Zeron-Medina J, Hernandez J, Macarulla T, Balsells J, Merino X, et al. Overexpression of Yes Associated Protein 1, an Independent Prognostic Marker in Patients With Pancreatic Ductal Adenocarcinoma, Correlated With Liver Metastasis and Poor Prognosis. *Pancreas* (2017) 46(7):913–20. doi: 10.1097/MPA.0000000000000867
69. Rozengurt E, Sinnett-Smith J, Eibl G. Yes-Associated Protein (YAP) in Pancreatic Cancer: At the Epicenter of a Targetable Signaling Network Associated With Patient Survival. *Signal Transduct Target Ther* (2018) 3:11. doi: 10.1038/s41392-017-0005-2
70. Zhou Q, Bauden M, Andersson R, Hu D, Marko-Varga G, Xu J, et al. YAP1 is an Independent Prognostic Marker in Pancreatic Cancer and Associated With Extracellular Matrix Remodeling. *J Transl Med* (2020) 18(1):77. doi: 10.1186/s12967-020-02254-7
71. Strnadel J, Choi S, Fujimura K, Wang H, Zhang W, Wyse M, et al. Eif5a-PEAK1 Signaling Regulates YAP1/TAZ Protein Expression and Pancreatic Cancer Cell Growth. *Cancer Res* (2017) 77(8):1997–2007. doi: 10.1158/0008-5472.CAN-16-2594
72. Hao F, Xu Q, Zhao Y, Stevens JV, Young SH, Sinnett-Smith J, et al. Insulin Receptor and GPCR Crosstalk Stimulates YAP *via* PI3K and PKD in Pancreatic Cancer Cells. *Mol Cancer Res* (2017) 15(7):929–41. doi: 10.1158/1541-7786.MCR-17-0023
73. Tsai JH, Yang J. Epithelial-Mesenchymal Plasticity in Carcinoma Metastasis. *Genes Dev* (2013) 27(20):2192–206. doi: 10.1101/gad.225334.113
74. Yuan Y, Li D, Li H, Wang L, Tian G, Dong Y. YAP Overexpression Promotes the Epithelial-Mesenchymal Transition and Chemoresistance in Pancreatic Cancer Cells. *Mol Med Rep* (2016) 13(1):237–42. doi: 10.3892/mmr.2015.4550
75. Wei H, Xu Z, Liu F, Wang F, Wang X, Sun X, et al. Hypoxia Induces Oncogene Yes-Associated Protein 1 Nuclear Translocation to Promote Pancreatic Ductal Adenocarcinoma Invasion *via* Epithelial-Mesenchymal Transition. *Tumour Biol* (2017) 39(5):1010428317691684. doi: 10.1177/1010428317691684

76. Narimatsu M, Labibi B, Wrana JL, Attisano L. Analysis of Hippo and TGFbeta Signaling in Polarizing Epithelial Cells and Mouse Embryos. *Differentiation* (2016) 91(4-5):109–18. doi: 10.1016/j.diff.2016.01.003
77. Pefani DE, Pankova D, Abraham AG, Grawenda AM, Vlahov N, Scrace S, et al. TGF-Beta Targets the Hippo Pathway Scaffold RASSF1A to Facilitate YAP/SMAD2 Nuclear Translocation. *Mol Cell* (2016) 63(1):156–66. doi: 10.1016/j.molcel.2016.05.012
78. Gao C, Quan MY, Chen QJ, Yang R, Wu Y, Liu JY, et al. Yap1-2 Isoform Is the Primary Mediator in TGF-Beta1 Induced EMT in Pancreatic Cancer. *Front Oncol* (2021) 11:649290. doi: 10.3389/fonc.2021.649290
79. Burris HA3rd, Moore MJ, Andersen J, Green MR, Rothenberg ML, Modiano MR, et al. Improvements in Survival and Clinical Benefit With Gemcitabine as First-Line Therapy for Patients With Advanced Pancreas Cancer: A Randomized Trial. *J Clin Oncol* (1997) 15(6):2403–13. doi: 10.1200/JCO.1997.15.6.2403
80. Chen M, Wang M, Xu S, Guo X, Jiang J. Upregulation of miR-181c Contributes to Chemoresistance in Pancreatic Cancer by Inactivating the Hippo Signaling Pathway. *Oncotarget* (2015) 6(42):44466–79. doi: 10.18632/oncotarget.6298
81. Chai TF, Manu KA, Casey PJ, Wang M. Isoprenylcysteine Carboxylmethyltransferase Is Required for the Impact of Mutant KRAS on TAZ Protein Level and Cancer Cell Self-Renewal. *Oncogene* (2020) 39 (31):5373–89. doi: 10.1038/s41388-020-1364-7
82. Suklabaidya S, Dash P, Das B, Suresh V, Sasmal PK, Senapati S. Experimental Models of Pancreatic Cancer Desmoplasia. *Lab Invest* (2018) 98(1):27–40. doi: 10.1038/labinvest.2017.127
83. Ren B, Liu X, Suriawinata AA. Pancreatic Ductal Adenocarcinoma and Its Precursor Lesions: Histopathology, Cytopathology, and Molecular Pathology. *Am J Pathol* (2019) 189(1):9–21. doi: 10.1016/j.ajpath.2018.10.004
84. Panciera T, Azzolin L, Cordenonsi M, Piccolo S. Mechanobiology of YAP and TAZ in Physiology and Disease. *Nat Rev Mol Cell Biol* (2017) 18 (12):758–70. doi: 10.1038/nrm.2017.87
85. Low BC, Pan CQ, Shivashankar GV, Bershadsky A, Sudol M, Sheetz M. YAP/TAZ as Mechanosensors and Mechanotransducers in Regulating Organ Size and Tumor Growth. *FEBS Lett* (2014) 588(16):2663–70. doi: 10.1016/j.febslet.2014.04.012
86. Ibar C, Irvine KD. Rapping About Mechanotransduction. *Dev Cell* (2018) 46 (6):678–9. doi: 10.1016/j.devcel.2018.09.007
87. Morvaridi S, Dhall D, Greene MI, Pandol SJ, Wang Q. Role of YAP and TAZ in Pancreatic Ductal Adenocarcinoma and in Stellate Cells Associated With Cancer and Chronic Pancreatitis. *Sci Rep* (2015) 5:16759. doi: 10.1038/srep16759
88. Lee J, Condello S, Yakubov B, Emerson R, Caperell-Grant A, Hitomi K, et al. Tissue Transglutaminase Mediated Tumor-Stroma Interaction Promotes Pancreatic Cancer Progression. *Clin Cancer Res* (2015) 21(19):4482–93. doi: 10.1158/1078-0432.CCR-15-0226
89. Xu M, Jung X, Hines OJ, Eibl G, Chen Y. Obesity and Pancreatic Cancer: Overview of Epidemiology and Potential Prevention by Weight Loss. *Pancreas* (2018) 47(2):158–62. doi: 10.1097/MPA.0000000000000974
90. Abbruzzese JL, Andersen DK, Borrebaeck CAK, Chari ST, Costello E, Cruz-Monserrate Z, et al. The Interface of Pancreatic Cancer With Diabetes, Obesity, and Inflammation: Research Gaps and Opportunities: Summary of a National Institute of Diabetes and Digestive and Kidney Diseases Workshop. *Pancreas* (2018) 47(5):516–25. doi: 10.1097/MPA.0000000000001037
91. von Bernstorff W, Voss M, Freichel S, Schmid A, Vogel I, Johnk C, et al. Systemic and Local Immunosuppression in Pancreatic Cancer Patients. *Clin Cancer Res* (2001) 7(3 Suppl):925s–32s.
92. Mace TA, Ameen Z, Collins A, Wojcik S, Mair M, Young GS, et al. Pancreatic Cancer-Associated Stellate Cells Promote Differentiation of Myeloid-Derived Suppressor Cells in a STAT3-Dependent Manner. *Cancer Res* (2013) 73(10):3007–18. doi: 10.1158/0008-5472.CAN-12-4601
93. Stromnes IM, Brockenbrough JS, Izeradjene K, Carlson MA, Cuevas C, Simmons RM, et al. Targeted Depletion of an MDSC Subset Unmasks Pancreatic Ductal Adenocarcinoma to Adaptive Immunity. *Gut* (2014) 63 (11):1769–81. doi: 10.1136/gutjnl-2013-306271
94. Thaventhiran JE, Hoffmann A, Magiera L, de la Roche M, Lingel H, Brunner-Weinzierl M, et al. Activation of the Hippo Pathway by CTLA-4 Regulates the Expression of Blimp-1 in the CD8+ T Cell. *Proc Natl Acad Sci USA* (2012) 109(33):E2223–9. doi: 10.1073/pnas.1209115109
95. Geng J, Yu S, Zhao H, Sun X, Li X, Wang P, et al. The Transcriptional Coactivator TAZ Regulates Reciprocal Differentiation of TH17 Cells and Treg Cells. *Nat Immunol* (2017) 18(7):800–12. doi: 10.1038/ni.3748
96. Onuora S. Immunology: Hippo Signalling Influences T Cell Fate. *Nat Rev Rheumatol* (2017) 13(7):389. doi: 10.1038/nrrheum.2017.82
97. Ni X, Tao J, Barbi J, Chen Q, Park BV, Li Z, et al. YAP Is Essential for Treg-Mediated Suppression of Antitumor Immunity. *Cancer Discov* (2018) 8 (8):1026–43. doi: 10.1158/2159-8290.CD-17-1124
98. Zhang YL, Li Q, Yang XM, Fang F, Li J, Wang YH, et al. SPON2 Promotes M1-Like Macrophage Recruitment and Inhibits Hepatocellular Carcinoma Metastasis by Distinct Integrin-Rho GTPase-Hippo Pathways. *Cancer Res* (2018) 78(9):2305–17. doi: 10.1158/0008-5472.CAN-17-2867
99. Humphris JL, Patch AM, Nones K, Bailey PJ, Johns AL, McKay S, et al. Hypermutation In Pancreatic Cancer. *Gastroenterology* (2017) 152(1):68–74.e2. doi: 10.1053/j.gastro.2016.09.060
100. Le DT, Durham JN, Smith KN, Wang H, Bartlett BR, Aulakh LK, et al. Mismatch Repair Deficiency Predicts Response of Solid Tumors to PD-1 Blockade. *Science* (2017) 357(6349):409–13. doi: 10.1126/science.aan6733
101. Marcus L, Lemery SJ, Keegan P, Pazdur R. FDA Approval Summary: Pembrolizumab for the Treatment of Microsatellite Instability-High Solid Tumors. *Clin Cancer Res* (2019) 25(13):3753–8. doi: 10.1158/1078-0432.CCR-18-4070
102. Marabelle A, Le DT, Ascierto PA, Di Giacomo AM, De Jesus-Acosta A, Delord JP, et al. Efficacy of Pembrolizumab in Patients With Noncolorectal High Microsatellite Instability/Mismatch Repair-Deficient Cancer: Results From the Phase II KEYNOTE-158 Study. *J Clin Oncol* (2020) 38(1):1–10. doi: 10.1200/JCO.19.02105
103. Janse van Rensburg HJ, Azad T, Ling M, Hao Y, Snetsinger B, Khanal P, et al. The Hippo Pathway Component TAZ Promotes Immune Evasion in Human Cancer Through PD-L1. *Cancer Res* (2018) 78(6):1457–70. doi: 10.1158/0008-5472.CAN-17-3139
104. Kim MH, Kim CG, Kim SK, Shin SJ, Choe EA, Park SH, et al. YAP-Induced PD-L1 Expression Drives Immune Evasion in BRAFi-Resistant Melanoma. *Cancer Immunol Res* (2018) 6(3):255–66. doi: 10.1158/2326-6066.CIR-17-0320
105. Miao J, Hsu PC, Yang YL, Xu Z, Dai Y, Wang Y, et al. YAP Regulates PD-L1 Expression in Human NSCLC Cells. *Oncotarget* (2017) 8(70):114576–87. doi: 10.18632/oncotarget.23051
106. Lee BS, Park DI, Lee DH, Lee JE, Yeo MK, Park YH, et al. Hippo Effector YAP Directly Regulates the Expression of PD-L1 Transcripts in EGFR-TKI-Resistant Lung Adenocarcinoma. *Biochem Biophys Res Commun* (2017) 491 (2):493–9. doi: 10.1016/j.bbrc.2017.07.007
107. Hong DS, Fakih MG, Strickler JH, Desai J, Durm GA, Shapiro GI, et al. KRAS(G12C) Inhibition With Sotorasib in Advanced Solid Tumors. *N Engl J Med* (2020) 383(13):1207–17. doi: 10.1056/NEJMoa1917239
108. Istvan ES, Deisenhofer J. Structural Mechanism for Statin Inhibition of HMG-CoA Reductase. *Science* (2001) 292(5519):1160–4. doi: 10.1126/science.1059344
109. Freed-Pastor WA, Mizuno H, Zhao X, Langerod A, Moon SH, Rodriguez-Barrueco R, et al. Mutant P53 Disrupts Mammary Tissue Architecture via the Mevalonate Pathway. *Cell* (2012) 148(1-2):244–58. doi: 10.1016/j.cell.2011.12.017
110. Clendening JW, Pandyra A, Boutros PC, El Ghamrasni S, Khosravi F, Trentin GA, et al. Dysregulation of the Mevalonate Pathway Promotes Transformation. *Proc Natl Acad Sci USA* (2010) 107(34):15051–6. doi: 10.1073/pnas.0910258107
111. Kuzu OF, Noory MA, Robertson GP. The Role of Cholesterol in Cancer. *Cancer Res* (2016) 76(8):2063–70. doi: 10.1158/0008-5472.CAN-15-2613
112. Mohammed A, Qian L, Janakiram NB, Lightfoot S, Steele VE, Rao CV. Atorvastatin Delays Progression of Pancreatic Lesions to Carcinoma by Regulating PI3/AKT Signaling in p48Cre/+ LSL-KrasG12D/+ Mice. *Int J Cancer* (2012) 131(8):1951–62. doi: 10.1002/ijc.27456
113. Fendrich V, Sparn M, Lauth M, Knoop R, Plassmeier L, Bartsch DK, et al. Simvastatin Delay Progression of Pancreatic Intraepithelial Neoplasia and

Cancer Formation in a Genetically Engineered Mouse Model of Pancreatic Cancer. *Pancreatology* (2013) 13(5):502–7. doi: 10.1016/j.pan.2013.08.002
114. Sorrentino G, Ruggeri N, Specchia V, Cordenonsi M, Mano M, Dupont S, et al. Metabolic Control of YAP and TAZ by the Mevalonate Pathway. *Nat Cell Biol* (2014) 16(4):357–66. doi: 10.1038/ncb2936
115. Higashi T, Hayashi H, Kitano Y, Yamamura K, Kaida T, Arima K, et al. Statin Attenuates Cell Proliferative Ability *via* TAZ (WWTR1) in Hepatocellular Carcinoma. *Med Oncol* (2016) 33(11):123. doi: 10.1007/s12032-016-0845-6
116. Jeon CY, Pandol SJ, Wu B, Cook-Wiens G, Gottlieb RA, Merz CN, et al. The Association of Statin Use After Cancer Diagnosis With Survival in Pancreatic Cancer Patients: A SEER-Medicare Analysis. *PLoS One* (2015) 10(4):e0121783. doi: 10.1371/journal.pone.0121783
117. Wu BU, Chang J, Jeon CY, Pandol SJ, Huang B, Ngor EW, et al. Impact of Statin Use on Survival in Patients Undergoing Resection for Early-Stage Pancreatic Cancer. *Am J Gastroenterol* (2015) 110(8):1233–9. doi: 10.1038/ajg.2015.217
118. Chen MJ, Tsan YT, Liou JM, Lee YC, Wu MS, Chiu HM, et al. Statins and the Risk of Pancreatic Cancer in Type 2 Diabetic Patients–A Population-Based Cohort Study. *Int J Cancer* (2016) 138(3):594–603. doi: 10.1002/ijc.29813
119. Walker EJ, Ko AH, Holly EA, Bracci PM. Statin Use and Risk of Pancreatic Cancer: Results From a Large, Clinic-Based Case-Control Study. *Cancer* (2015) 121(8):1287–94. doi: 10.1002/cncr.29256
120. Carey FJ, Little MW, Pugh TF, Ndokera R, Ing H, Clark A, et al. The Differential Effects of Statins on the Risk of Developing Pancreatic Cancer: A Case-Control Study in Two Centres in the United Kingdom. *Dig Dis Sci* (2013) 58(11):3308–12. doi: 10.1007/s10620-013-2778-7
121. JY E, Lu SE, Lin Y, Graber JM, Rotter D, Zhang L, et al. Differential and Joint Effects of Metformin and Statins on Overall Survival of Elderly Patients With Pancreatic Adenocarcinoma: A Large Population-Based Study. *Cancer Epidemiol Biomarkers Prev* (2017) 26(8):1225–32. doi: 10.1158/1055-9965.EPI-17-0227
122. Iarrobino NA, Gill B, Bernard ME, Mishra MV, Champ CE. Targeting Tumor Metabolism With Statins During Treatment for Advanced-Stage Pancreatic Cancer. *Am J Clin Oncol* (2018) 41(11):1125–31. doi: 10.1097/COC.0000000000000433
123. Jian-Yu E, Graber JM, Lu SE, Lin Y, Lu-Yao G, Tan XL. Effect of Metformin and Statin Use on Survival in Pancreatic Cancer Patients: A Systematic Literature Review and Meta-Analysis. *Curr Med Chem* (2018) 25(22):2595–607. doi: 10.2174/0929867324666170412145232
124. Bang UC, Watanabe T, Bendtsen F. The Relationship Between the Use of Statins and Mortality, Severity, and Pancreatic Cancer in Danish Patients With Chronic Pancreatitis. *Eur J Gastroenterol Hepatol* (2018) 30(3):346–51. doi: 10.1097/MEG.0000000000001060
125. Liu Y, Tang W, Wang J, Xie L, Li T, He Y, et al. Association Between Statin Use and Colorectal Cancer Risk: A Meta-Analysis of 42 Studies. *Cancer Causes Control* (2014) 25(2):237–49. doi: 10.1007/s10552-013-0326-6
126. Manthravadi S, Shrestha A, Madhusudhana S. Impact of Statin Use on Cancer Recurrence and Mortality in Breast Cancer: A Systematic Review and Meta-Analysis. *Int J Cancer* (2016) 139(6):1281–8. doi: 10.1002/ijc.30185
127. Anothaisintawee T, Udomsubpayakul U, McEvoy M, Lerdsitthichai P, Attia J, Thakkinstian A. Effect of Lipophilic and Hydrophilic Statins on Breast Cancer Risk in Thai Women: A Cross-Sectional Study. *J Cancer* (2016) 7(9):1163–8. doi: 10.7150/jca.14941
128. Liu B, Yi Z, Guan X, Zeng YX, Ma F. The Relationship Between Statins and Breast Cancer Prognosis Varies by Statin Type and Exposure Time: A Meta-Analysis. *Breast Cancer Res Treat* (2017) 164(1):1–11. doi: 10.1007/s10549-017-4246-0
129. Hamada T, Khalaf N, Yuan C, Babic A, Morales-Oyarvide V, Qian ZR, et al. Statin Use and Pancreatic Cancer Risk in Two Prospective Cohort Studies. *J Gastroenterol* (2018) 53(8):959–66. doi: 10.1007/s00535-018-1430-x
130. Hamada T, Khalaf N, Yuan C, Morales-Oyarvide V, Babic A, Nowak JA, et al. Prediagnosis Use of Statins Associates With Increased Survival Times of Patients With Pancreatic Cancer. *Clin Gastroenterol Hepatol* (2018) 16(8):1300–6.e3. doi: 10.1016/j.cgh.2018.02.022
131. Zhang Y, Liang M, Sun C, Qu G, Shi T, Min M, et al. Statin Use and Risk of Pancreatic Cancer: An Updated Meta-Analysis of 26 Studies. *Pancreas* (2019) 48(2):142–50. doi: 10.1097/MPA.0000000000001226
132. Lee HS, Lee SH, Lee HJ, Chung MJ, Park JY, Park SW, et al. Statin Use and Its Impact on Survival in Pancreatic Cancer Patients. *Med (Baltimore)* (2016) 95(19):e3607. doi: 10.1097/MD.0000000000003607
133. Zhao X, Wang X, Fang L, Lan C, Zheng X, Wang Y, et al. A Combinatorial Strategy Using YAP and Pan-RAF Inhibitors for Treating KRAS-Mutant Pancreatic Cancer. *Cancer Lett* (2017) 402:61–70. doi: 10.1016/j.canlet.2017.05.015
134. Wei H, Wang F, Wang Y, Li T, Xiu P, Zhong J, et al. Verteporfin Suppresses Cell Survival, Angiogenesis and Vasculogenic Mimicry of Pancreatic Ductal Adenocarcinoma *via* Disrupting the YAP-TEAD Complex. *Cancer Sci* (2017) 108(3):478–87. doi: 10.1111/cas.13138
135. Thongon N, Castiglioni I, Zucal C, Latorre E, D'Agostino V, Bauer I, et al. The GSK3beta Inhibitor BIS I Reverts YAP-Dependent EMT Signature in PDAC Cell Lines by Decreasing SMADs Expression Level. *Oncotarget* (2016) 7(18):26551–66. doi: 10.18632/oncotarget.8437
136. Neesse A, Frese KK, Bapiro TE, Nakagawa T, Sternlicht MD, Seeley TW, et al. CTGF Antagonism With mAb FG-3019 Enhances Chemotherapy Response Without Increasing Drug Delivery in Murine Ductal Pancreas Cancer. *Proc Natl Acad Sci USA* (2013) 110(30):12325–30. doi: 10.1073/pnas.1300415110
137. Zhou X, Su J, Feng S, Wang L, Yin X, Yan J, et al. Antitumor Activity of Curcumin is Involved in Down-Regulation of YAP/TAZ Expression in Pancreatic Cancer Cells. *Oncotarget* (2016) 7(48):79076–88. doi: 10.18632/oncotarget.12596
138. Jiang Z, Chen X, Chen K, Sun L, Gao L, Zhou C, et al. YAP Inhibition by Resveratrol via Activation of AMPK Enhances the Sensitivity of Pancreatic Cancer Cells to Gemcitabine. *Nutrients* (2016) 8(10):546. doi: 10.3390/nu8100546
139. Li X, Liu Y, Zhang C, Niu Q, Wang H, Che C, et al. Stiehopus Japonieus Acidic Mucopolysaccharide Inhibits the Proliferation of Pancreatic Cancer SW1990 Cells Through Hippo-YAP Pathway. *Oncotarget* (2017) 8(10):16356–66. doi: 10.18632/oncotarget.14633
140. Li X, Zhao X, Song W, Tian Z, Yang L, Niu Q, et al. Pseudolaric Acid B Inhibits Proliferation, Invasion and Epithelial-To-Mesenchymal Transition in Human Pancreatic Cancer Cell. *Yonsei Med J* (2018) 59(1):20–7. doi: 10.3349/ymj.2018.59.1.20
141. Morin-Kensicki EM, Boone BN, Howell M, Stonebraker JR, Teed J, Alb JG, et al. Defects in Yolk Sac Vasculogenesis, Chorioallantoic Fusion, and Embryonic Axis Elongation in Mice With Targeted Disruption of Yap65. *Mol Cell Biol* (2006) 26(1):77–87. doi: 10.1128/MCB.26.1.77-87.2006
142. Makita R, Uchijima Y, Nishiyama K, Amano T, Chen Q, Takeuchi T, et al. Multiple Renal Cysts, Urinary Concentration Defects, and Pulmonary Emphysematous Changes in Mice Lacking TAZ. *Am J Physiol Renal Physiol* (2008) 294(3):F542–53. doi: 10.1152/ajprenal.00201.2007
143. Hossain Z, Ali SM, Ko HL, Xu J, Ng CP, Guo K, et al. Glomerulocystic Kidney Disease in Mice With a Targeted Inactivation of Wwtr1. *Proc Natl Acad Sci USA* (2007) 104(5):1631–6. doi: 10.1073/pnas.0605266104
144. Tian Y, Kolb R, Hong JH, Carroll J, Li D, You J, et al. TAZ Promotes PC2 Degradation Through a SCFbeta-Trcp E3 Ligase Complex. *Mol Cell Biol* (2007) 27(18):6383–95. doi: 10.1128/MCB.00254-07

Conflict of Interest: The authors declare that the research was conducted in the absence of any commercial or financial relationships that could be construed as a potential conflict of interest.

Publisher's Note: All claims expressed in this article are solely those of the authors and do not necessarily represent those of their affiliated organizations, or those of the publisher, the editors and the reviewers. Any product that may be evaluated in this article, or claim that may be made by its manufacturer, is not guaranteed or endorsed by the publisher.

frontiers in Oncology

ORIGINAL RESEARCH
published: 29 July 2021
doi: 10.3389/fonc.2021.691685

A First-In-Class, Humanized Antibody Targeting Alternatively Spliced Tissue Factor: Preclinical Evaluation in an Orthotopic Model of Pancreatic Ductal Adenocarcinoma

Clayton S. Lewis[1], Aniruddha Karve[2†], Kateryna Matiash[1†], Timothy Stone[3], Jingxing Li[4], Jordon K. Wang[4], Henri H. Versteeg[5], Bruce J. Aronow[6], Syed A. Ahmad[7], Pankaj B. Desai[2] and Vladimir Y. Bogdanov[1]*

[1] Division of Hematology/Oncology, Department of Internal Medicine, University of Cincinnati College of Medicine, Cincinnati, OH, United States, [2] Division of Pharmaceutical Sciences, University of Cincinnati College of Pharmacy, Cincinnati, OH, United States, [3] Department of Environmental Health, University of Cincinnati College of Medicine, Cincinnati, OH, United States, [4] Technology Development, LakePharma, Inc., Belmont, CA, United States, [5] Einthoven Laboratory for Experimental Vascular Medicine, Department of Internal Medicine, Leiden University Medical Center, Leiden, Netherlands, [6] Department of Biomedical Informatics, Cincinnati Children's Hospital and Medical Center, Cincinnati, OH, United States, [7] Division of Surgical Oncology, Department of Surgery, University of Cincinnati College of Medicine, Cincinnati, OH, United States

In 2021, pancreatic ductal adenocarcinoma (PDAC) is the 3rd leading cause of cancer deaths in the United States. This is largely due to a lack of symptoms and limited treatment options, which extend survival by only a few weeks. There is thus an urgent need to develop new therapies effective against PDAC. Previously, we have shown that the growth of PDAC cells is suppressed when they are co-implanted with RabMab1, a rabbit monoclonal antibody specific for human alternatively spliced tissue factor (asTF). Here, we report on humanization of RabMab1, evaluation of its binding characteristics, and assessment of its *in vivo* properties. hRabMab1 binds asTF with a K_D in the picomolar range; suppresses the migration of high-grade Pt45.P1 cells in Boyden chamber assays; has a long half-life in circulation (~ 5 weeks); and significantly slows the growth of pre-formed orthotopic Pt45.P1 tumors in athymic nude mice when administered intravenously. Immunohistochemical analysis of tumor tissue demonstrates the suppression of i) PDAC cell proliferation, ii) macrophage infiltration, and iii) neovascularization, whereas RNAseq analysis of tumor tissue reveals the suppression of pathways that promote cell division and focal adhesion. This is the first proof-of-concept study whereby a novel biologic targeting asTF has been investigated as a systemically administered single agent, with encouraging results. Given that hRabMab1 has a favorable PK profile and is able to suppress the growth of human PDAC cells *in vivo*, it comprises a promising candidate for further clinical development.

Keywords: pancreatic ductal adenocarcinoma, tissue factor, alternative splicing, monoclonal antibodies, orthotopic tumor model

OPEN ACCESS

Edited by:
Kuzhuvelil B. Harikumar, Rajiv Gandhi Centre for Biotechnology, India

Reviewed by:
Ming Cui, Peking Union Medical College Hospital, China
Ashu Shah, University of Nebraska Medical Center, United States

****Correspondence:***
Vladimir Y. Bogdanov
vladimir.bogdanov@uc.edu

†These authors have contributed equally to this work

Specialty section:
This article was submitted to Gastrointestinal Cancers, a section of the journal Frontiers in Oncology

Received: *06 April 2021*
Accepted: *28 June 2021*
Published: *29 July 2021*

Citation:
Lewis CS, Karve A, Matiash K, Stone T, Li J, Wang JK, Versteeg HH, Aronow BJ, Ahmad SA, Desai PB and Bogdanov VY (2021) A First-In-Class, Humanized Antibody Targeting Alternatively Spliced Tissue Factor: Preclinical Evaluation in an Orthotopic Model of Pancreatic Ductal Adenocarcinoma. Front. Oncol. 11:691685. doi: 10.3389/fonc.2021.691685

INTRODUCTION

Pancreatic ductal adenocarcinoma (PDAC) is a highly lethal malignancy with most patients presenting at stage IV (1). Treatment of PDAC is hindered by its undruggable genomic drivers (mutated Kras, mutated p53), intra-tumoral heterogeneity, and desmoplasia that impedes drug entry into the tumor. The current chemotherapeutic standards of care, Gem-Abraxane and FOLFIRINOX, yield a median overall survival of only 9.6 months underscoring the need for more effective therapies (2).

Recently, we reported on the anti-tumor effects of RabMab1, our monoclonal antibody that binds the alternatively spliced isoform of human tissue factor (asTF), in a setting of orthotopic co-implantation with TF-expressing human PDAC cells (3). In humans and mice, the gene encoding tissue factor (*F3*) produces two protein isoforms: full-length TF (flTF), an integral transmembrane protein, and asTF, which has a unique C-terminus due to a single-nucleotide shift in its open reading frame. asTF lacks the alpha helical transmembrane domain present in flTF, rendering asTF a soluble secreted protein (4). flTF triggers blood coagulation by serving as an enzymatic cofactor for the serine protease fVII(a); flTF can also promote the activation of select protease-activated receptors (PARs) that control intracellular pathways governing platelet activation and wound healing (5). In contrast, asTF promotes cell proliferation, migration, and angiogenesis in a non-proteolytic manner by triggering the activation of PI3K/Akt, MAPK, and FAK pathways through its interactions with $\alpha6\beta1$ and $\alpha v\beta3$ integrins (6). Elevated expression of total TF is positively associated with disease severity in several solid malignancies including breast, prostate, bone, and lower GI. One of the most extensively studied solid cancers with elevated TF expression comprises PDAC, where it was first identified as the protein responsible for PDAC cell-triggered coagulation (7). Elevated TF protein expression was first shown to correlate with the histological grade of PDAC in 1995 (8). Follow-up studies showed that TF promotes PDAC growth and invasion (9). TF localizes to the invasive front of PDAC and patients with higher TF levels in tumors have worse overall survival (10). Earlier studies of TF protein in human tissues were done using antibodies that could not discriminate between flTF and asTF; more recently, we reported that flTF and asTF are both overexpressed in breast cancer and PDAC (11, 12). In breast cancer, asTF fuels cancer cell growth *via* integrin ligation (13). This has also been seen in PDAC, where asTF promotes PDAC cell growth and spread in an orthotopic mouse model *via* $\beta1$ integrin-linked mechanisms (3).

Given TF's ability to drive cancer cell growth and spread, therapeutic targeting of TF is an actively pursued area. Targeting flTF, however, is challenging due to an increased risk of bleeding and flTF's expression in many normal tissues. In contrast to targeting flTF, targeting asTF – which is dispensable to normal hemostasis – is thus a potentially more attractive means to disrupt TF-mediated signaling; moreover, the expression of asTF in normal tissues is minimal compared to that of flTF (12). We have developed a rabbit monoclonal antibody termed RabMab1 that specifically recognizes an epitope unique to human asTF's C-terminus. Tumor-suppressing properties of RabMab1 were evident in the breast cancer and PDAC settings showing that, when asTF-producing cancer cells were exposed to RabMab1, the activation of FAK, Akt, and MAPK pathways was suppressed *in vitro* and co-implanting RabMab1 with tumor cells suppressed their growth *in vivo* (3, 11). In this report, we describe RabMab1's humanization and demonstrate that its humanized variant, termed hRabMab1, has an *in vivo* half-life well in the range of biologics currently used in the clinic. When administered intravenously in athymic nude mice, hRabMab1 is effective at stemming the growth of pre-formed orthotopic PDAC tumors.

MATERIALS AND METHODS

Humanization, Construction, Expression, and Purification of hRabMab1

Antibody design was accomplished at LakePharma by generating a homology modeled antibody 3D structure and creating a profile of the parental antibody based on structure modeling. Acceptor frameworks to utilize were identified based on the overall sequence identity across the framework, matching interface position, similarly classed CDR canonical positions, and presence of N-glycosylation sites that would have to be removed. Two light chain (LC) frameworks IGKV1-39*01 and IGKV1-25*01 and two heavy chain (HC) frameworks IGHV3-23*01 and IGHV3-23*04 were selected for the humanization design. Humanized antibodies were designed by creating multiple hybrid sequences that fuse select parts of the parental antibody sequence with the human framework sequences. Using the 3D model, these humanized sequences were methodically analyzed by eye and computer modeling to isolate the sequences that would most likely retain antigen binding. The goal was to maximize the amount of human sequence in the final humanized antibodies while retaining the original antibody specificity. Back mutations were introduced and a total of three humanized light chains and three humanized heavy chains were designed. Humanness scores, representing how human-like the antibody variable region sequence is, were calculated according to Gao et al. (14). Briefly, an in-depth analysis of the humanness of therapeutic antibodies allowed the creation of a database of human antibody sequences, and increased humanness score was found to be correlated with decreased immunogenicity. Based on this method, heavy chain framework scores of 84 or above were considered human-like; light chain framework scores of 90 or above were considered human-like.

Full-length antibody genes for nine heavy/light chain pairs, as well as those encoding the rabbit chimeric parental, were codon-optimized, synthesized, and cloned into LakePharma's proprietary high expression mammalian vector system and co-transfection of heavy and light chain plasmids at a 1:1 ratio was performed in HEK293 cells (Thermo Fisher Scientific) at 50 mL scale. Starting at 20 hours, and throughout the transient transfection production, antibody titers were measured (Octet QKe, ForteBio). Cultures were harvested at day 5 and antibodies

in the conditioned media were purified using MabSelect SuRe Protein A resin (GE Healthcare).

Assessment of asTF Binding by ELISA

96-well ELISA plates were coated with 5 ug/mL recombinant asTF in 0.05 M sodium bicarbonate buffer, pH 9.6. Serial dilutions of test antibody preparations were added to the pre-blocked plate and incubated for 1.5 hours at room temperature. The plate was then thoroughly washed and HRP conjugated secondary antibodies (Jackson) were added.

Biosensor Affinity Testing

Multi-concentration kinetic experiments were performed on the Octet Red96 system (ForteBio). Anti-huIgG Fc biosensors (ForteBio 18-5064) were hydrated in sample diluent (0.1% BSA in PBS and 0.02% Tween 20) and preconditioned in pH 1.7 glycine. Antibody was diluted to 10 μg/mL with sample diluent and immobilized onto Anti-huIgG Fc biosensors for 120 seconds. After baselines were established for 60 seconds in sample diluent, the biosensors were moved to wells containing the antigen at a series of 7 concentrations, 3-fold serial dilution starting at 300 nM, to measure the association. Association was observed for 90 seconds and dissociation was observed for 90 seconds for each protein of interest in the sample diluent. The binding affinities were assessed by selecting the top 3 or 4 best-fit concentrations with a monovalent binding model (1:1 binding).

Western Blotting

Human PDAC cell lines Pt45.P1 [a kind gift of Prof. Holger Katlthoff (12, 15)], PaCa44 [a kind gift of Prof. Stephan Haas (15)], AsPC1 and MIA-PaCa2 (both – ATCC) were utilized for antibody testing studies. Lysates were prepared with RIPA buffer and loaded into 10% TGX gels (BioRad). Protein was transferred onto PVDF membranes. Blocking was carried out using 2% BSA. RabMab1 and its derivatives were diluted to 1 μg/mL. Silver staining of 10% TGX gels was carried out using ProteoSilver Silver stain kit (Sigma PROTSIL1) according to the manufacturer's instructions. All anti-asTF antibodies tested displayed high signal specificity; a protein species with a higher apparent molecular weight (~60 kDa) was seen in some lysate preparations (not shown).

Cytotoxicity Studies

Antibody-dependent cellular cytotoxicity (ADCC) and cell-mediated cytotoxicity (CMC) assays were carried out using the aCella-TOX bioluminescence cytotoxicity kit (Cell Technology, Hayward, CA) according to the manufacturer's instructions. For ADCC studies, NK cells were purchased from Cell Technology; for CMC studies, lyophilized sera (rabbit and human complement) was purchased from Sigma.

qRT-PCR

RNA was isolated from cell lines and tumor tissue using the RNeasy kit (Qiagen). cDNA was prepared using Transcriptor Reverse Transcriptase (Roche). The primer/probe sets used for mRNA expression analysis are listed in the **Supplementary Material**.

Migration Assay

Pt45.P1 cells were suspended in serum free DMEM and pretreated with the indicated antibody at a concentration of 50 μg/mL for 30 minutes. 1.5 x 10^4 cells were then added to serum free DMEM in 8.0 μm transwells (Corning 353097) precoated with 1 μg laminin (Sigma L4544). 2% FBS in DMEM was used as the source of chemoattractants. ChromPure rabbit IgG (Jackson ImmunoResearch 011-000-003) was used as an isotype control.

Animal Studies

University of Cincinnati's Institutional Animal Care and Use Committee approved all animal studies. Antibody co-implantation studies: Pt45.P1 cells were preincubated with the indicated antibody diluted in PBS to a concentration of 5 mg/mL for 30 minutes prior to surgery. Human IgG1 isotype control (BioXCell, BE0297) was utilized as a negative control. 1x10^6 cells were implanted with antibody into the pancreata of athymic nude mice. Pre-formed orthotopic tumor studies: 1x10^6 Pt45.P1 cells were implanted into the pancreata of athymic nude mice (*Fox1*$^{nu/nu}$; Jackson 002019). Mice were randomized into control and treatment groups. Tumor growth was followed for 7 weeks.

Pharmacokinetic (PK) Assessment

cRabMab-hIgG1 or hRabMab1 were administered intravenously (IV) *via* tail vein to C57Bl/6 mice (n=16 and n=24 mice, respectively). Whole blood was collected at various time points by cardiac puncture method into EDTA coated tubes and centrifuged at 2000 x g for 15 minutes. Plasma was harvested, centrifuged a second time at 2000 x g for 15 minutes, and then frozen at -80°C until samples at all timepoints had been collected. Plasma aliquots were thawed on ice and diluted in the range of 1:1000 to 1:100,000 with PBS depending upon the standard plasma concentration profile for the human IgG1 in mice. Antibody concentration was determined using a human IgG ELISA kit (Abcam 195215). cRabMab1-hIgG1 and hRabMab1 standards were prepared in C57Bl/6 mouse plasma using serial dilution and used to obtain a standard curve.

PK antibody profile (plasma concentrations *vs* time data) after the administration of a single dose were analyzed using Phoenix® WinNonLin® version 8.1 (Certara L.P. (Pharsight), St. Louis, MO). The data were fitted employing a multicompartment PK model based on the apparent biphasic plasma-concentration vs time profile. Accordingly, PK parameters such as distribution and elimination half-life, systemic clearance, volume of distribution, and exposure (measured as the overall area under the plasma concentration-time curve or AUC) were computed. The PK parameters derived from this analysis were then utilized to simulate the multiple-dose PK profile and to predict steady state concentrations of hRabMab1 that may be achieved with repeated dosing. As a part of the pharmacodynamic studies conducted to assess the anti-tumor effects of the hRabMab1 antibody, blood samples collected at the end of the study were also analyzed to determine hRabMab1 concentrations in the plasma and compare the predicted *vs* observed steady-state concentration.

Pharmacodynamic (PD) Assessment

1 x 10^6 Pt45.P1 cells were implanted into the pancreata of athymic nude mice (*Fox1*$^{nu/nu}$; Jackson 002019) and given 10 days to engraft, following which IV administration of hRabMab1, hIgG isotype control, or vehicle began at 18 mg/kg every other day (total of 22 treatment cycles). Mice were then euthanized *via* cardiac puncture while sedated with isoflurane. Whole blood was collected and plasma specimens harvested as detailed above. Tumors were measured with calipers and sectioned into 2 halves, one of which was snap frozen in liquid nitrogen and the other fixed in PBS with 10% formalin. Antibody concentrations in plasma were measured as detailed above.

Immunohistochemistry and Image Analysis

10% formalin fixed tissues were embedded in paraffin and sectioned into 5 μm sections. Sections were stained as previously detailed (3). Briefly, sections were deparaffinized and rehydrated into DAKO wash buffer (Agilent S3006). Antigen retrieval was accomplished using a citrate solution (Biogenex HK086-9K). Native peroxidase activity was squelched using 0.4% hydrogen peroxide. Blocking was carried out with a Power Block solution (Biogenex HK085-5K) and sections were incubated with the following antibodies at the indicated dilution: CD31 (Abcam ab28364, 1:100), CD206 (Abcam ab6493, 0.1 μg/mL), Ki67 (Millipore Sigma ab9260, 1:100), HRP-conjugated anti-human IgG (Jackson ImmunoResearch 109-035-088, 1:500), HBEGF (Cell Signaling 27450, 1:50) and STN1 (Sigma HPA037924, 2.5 μg/mL). An HRP-conjugated anti-rabbit polymer (Agilent/Dako K4010) and DAB+ reagent were used to visualize primary antibody binding for CD31, CD206, Ki67, HBEGF, and STN1. Sections were counterstained with hematoxylin. Staining patterns were evaluated using Olympus BX51 equipped with Olympus DP72 digital camera; representative images were captured and used for statistical analyses. Staining intensity and/or positive staining events were analyzed using ImageJ.

Gene Expression Analysis

RNA was isolated from tumors representing the median tumor volumes from each experimental cohort. RNA library preparation, next generation sequencing, and sequence alignment were performed by the CCHMC DNA Sequencing and Genotyping Core, Cincinnati, OH. 300 ng of total RNA, determined by Invitrogen™ Qubit™ high-sensitivity spectro-fluorometry, was poly-A selected and reverse transcribed using Illumina's TruSeq® stranded mRNA library preparation kit. Each sample was fitted with one of 96 adapters containing a different 8-base molecular barcode for high-level multiplexing. After 15 cycles of PCR amplification, completed libraries were sequenced using Illumina NovaSeq™ 6000, generating 30 million high-quality, 150 base long paired-end reads per sample. A quality control check on the fastq files was performed using FastQC. Upon passing quality metrics, the reads were trimmed to remove adapters and low-quality reads using default parameters in Trimmomatic [Version 0.33] (16). Trimmed reads were then mapped to a reference genome using default parameters with strandness (RF for paired-end) option in Hisat2 [Version 2.0.5] (17). In the next step, transcript/gene abundance was determined using kallisto [Version 0.43.1] (18). We first created a transcriptome index in kallisto using Ensembl cDNA sequences for the reference genome. This index was then used to quantify transcript abundance in raw counts and transcript per million (TPM).

Statistical Analysis

1-way ANOVA was used to determine statistical significance in **Figures 2B, C**, **4A, D–F**, **5B, C** and **Supplementary Figure 1** (GraphPad Prism v6.0). *p ≤ 0.05, **p ≤ 0.01, ***p ≤ 0.001.

RESULTS

Generation of Rabbit-Human Chimeric RabMab1 Antibodies

In our previous studies, hybridoma-derived RabMab1 suppresses tumor cell migration *in vitro* and tumor growth *in vivo* when co-implanted with pancreatic and breast tumor cells (3, 13). To humanize RabMab1, we first sequenced the genomic region of the hybridoma clone encoding RabMab1. The heavy and light chain portions of the variable regions were cloned and inserted into vectors (fee for service, Abcam). These constructs were then introduced into modified HEK-293 cells to generate a recombinant prep of RabMab1 (rRabMab1). Following validation, rRabMab1 served as the reference point for the humanization of RabMab1, the first step of which was the creation of human-rabbit chimeric antibodies and the assessment of their binding kinetics.

Chimeric antibodies comprised of the RabMab1 Fab region and a human Fc region characteristic of either an IgG1 or IgG4 isotype (herein, cRabMab1-hIgG1 and cRabMab1-hIgG4) were assessed by ELISA for their ability to bind recombinant asTF. The chimeras had comparable binding affinities compared to rRabMab1 (**Figure 1A**). The chimeric and parental RabMab1 antibodies were then further analyzed for asTF binding affinity using anti-penta-HIS (HIS1K) biosensors. cRabMab1-hIgG1 and cRabMab1-hIgG4 had asTF equilibrium dissociation constants (K_D) of 430 pM and 1.64 nM, respectively; by comparison, rRabMab1 did not dissociate (**Figure 1B**, SPR sensograms can be found in **Supplementary Figure 1**). When assessed *via* anti-human IgG Fc capture (AHC) biosensors, cRabMab1-hIgG1 and cRabMab1-hIgG4 were found to have an asTF K_D of 4.24 nM and 8.43 nM, respectively (**Figures 1C, D**). Given that hIgG1 isotype antibodies may activate the complement pathway and bind Fc receptors on phagocytic cells (19), as well as its lower K_D, we elected to proceed with further development of cRabMab-hIgG1.

cRabMab1-hIgG1 Binds Native Human asTF and Suppresses PDAC Cell Migration *In Vitro*

cRabMab-hIgG1 was next evaluated for its ability to bind asTF in immobilized, denatured, whole cell lysates of Pt45.P1, PaCa44, AsPC1 and MIA-PaCa2 cells: western blotting revealed that

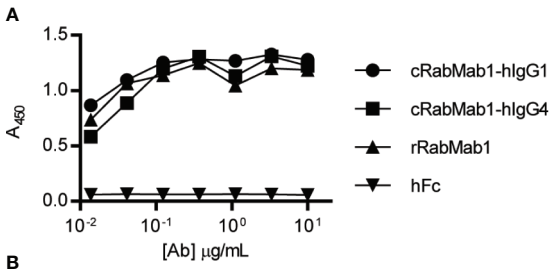

B

Antibody	KD (M)	K_{on} (1/Ms)	K_{dis} (1/s)	Full χ^2	Full R^2
cRabMab1-hIgG1	4.3E-10	2.6E+05	1.1E-04	0.0019	0.9954
cRabMab1-hIgG4	1.6E-09	2.2E+05	3.6E-04	0.0021	0.9952
rRabMab1	<0.4E-12	2.3E+05	<1.0E-07	0.0014	0.9977

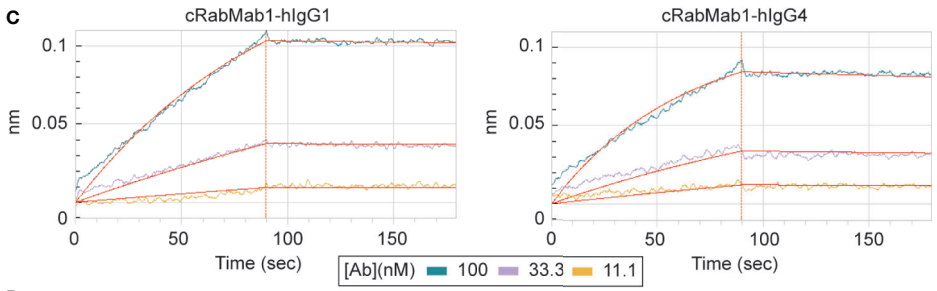

D

Antibody	KD (M)	K_{on} (1/Ms)	K_{dis} (1/s)	Full χ^2	Full R^2
cRabMab1-hIgG1	4.2E-09	3.4E+04	1.6E-04	0.0031	0.9957
cRabMab1-hIgG4	8.4E-09	5.3E+04	4.4E-04	0.0056	0.9871

FIGURE 1 | Chimeric RabMab1 antibodies have asTF binding affinities comparable to rRabMab1. Two human-rabbit chimeric RabMab1 antibodies were compared to parental rRabMab1 for their ability to bind asTF. **(A)** Serial dilutions of recombinant or chimeric RabMab1 were added to asTF-coated ELISA plates. Anti-human or anti-rabbit HRP conjugated secondary antibodies were used to assess antibody binding, hFc = non-targeting human Fc fragment. **(B)** HIS1K biosensor assessment of asTF binding kinetics of each antibody. **(C)** Trace results of AHC biosensor assessment of chimeric antibodies. **(D)** asTF binding kinetics as assessed by AHC biosensor experiments.

cRabMab-hIgG1 recognizes native asTF comparably to RabMab1 [**Figure 2A**; Total TF protein assessed using RabMab95 (20)]. qRT-PCR showed that TF isoform transcript levels for Pt45.P1, PaCa44, and MIA-PaCa2 corresponded to protein expression levels when normalized to TATA Binding Protein (**Figures 2B–D**); interestingly, while AsPC1 express asTF protein at very low levels, qRT-PCR revealed that asTF transcripts are relatively abundant in AsPC1 (**Figures 2A, D**). Our previous studies have shown that RabMab1 suppresses the migration of Pt45.P1 cells in a transwell migration assay (3). We, therefore, assessed the ability of cRabMab1-hIgG1 to inhibit PDAC cell migration in a transwell assay; cRabMab1-hIgG1 significantly suppressed the migration of Pt45.P1 cells (quantification is presented in **Figure 2E**, representative images of transwell inserts are shown in **Supplementary Figure 2**).

We next determined whether cRabMab1-hIgG1 can elicit CMC and/or ADCC. Pt45.P1 cells were pretreated with concentrations of cRabMab1-hIgG1 or human Fc fragment control ranging from 1 μg/mL – 1 mg/mL before being incubated with 25% human complement. Even at the highest concentrations of the antibody, only minimal lysis of the target cells was observed (**Supplementary Figure 3A**). Similarly, when Pt45.P1 cells were pretreated with cRabMab1-hIgG1 (concentrations ranging from 0.02 – 50 μg/mL) followed by 4 hours of incubation with Natural Killer (NK) cells (2:1 ratio NK : Pt45.P1), only minimal lysis of the target cells was observed (**Supplementary Figure 3B**).

cRabMab1-hIgG1 Suppresses Tumor Growth *In Vivo*

Our previous studies have shown RabMab1 to suppress the growth of Pt45.P1 cells *in vivo* when co-implanted in an orthotopic setting (3). To determine whether this effect was preserved post-chimerization, we pre-treated Pt45.P1 cells with 5 mg/mL of cRabMab1-hIgG1 and then implanted $1x10^6$ cells in the pancreata of athymic nude mice. cRabMab1-hIgG1 reduced tumor growth by 78% compared to vehicle control, while no difference was observed between vehicle control and non-targeting antibody control (**Figure 2F**).

To evaluate the PK profile of cRabMab1-hIgG1, we injected it *via* tail vein into 16 C57Bl/6 mice at the dose of 6 mg/kg. Blood was collected at regular intervals for 17 days *via* cardiac puncture. As typically observed for monoclonal antibodies (21), cRabMab1-hIgG1 exhibited a biphasic decline with a short-lived distribution phase and an extended elimination phase. It had a distribution half-life of 1.6 hours and an

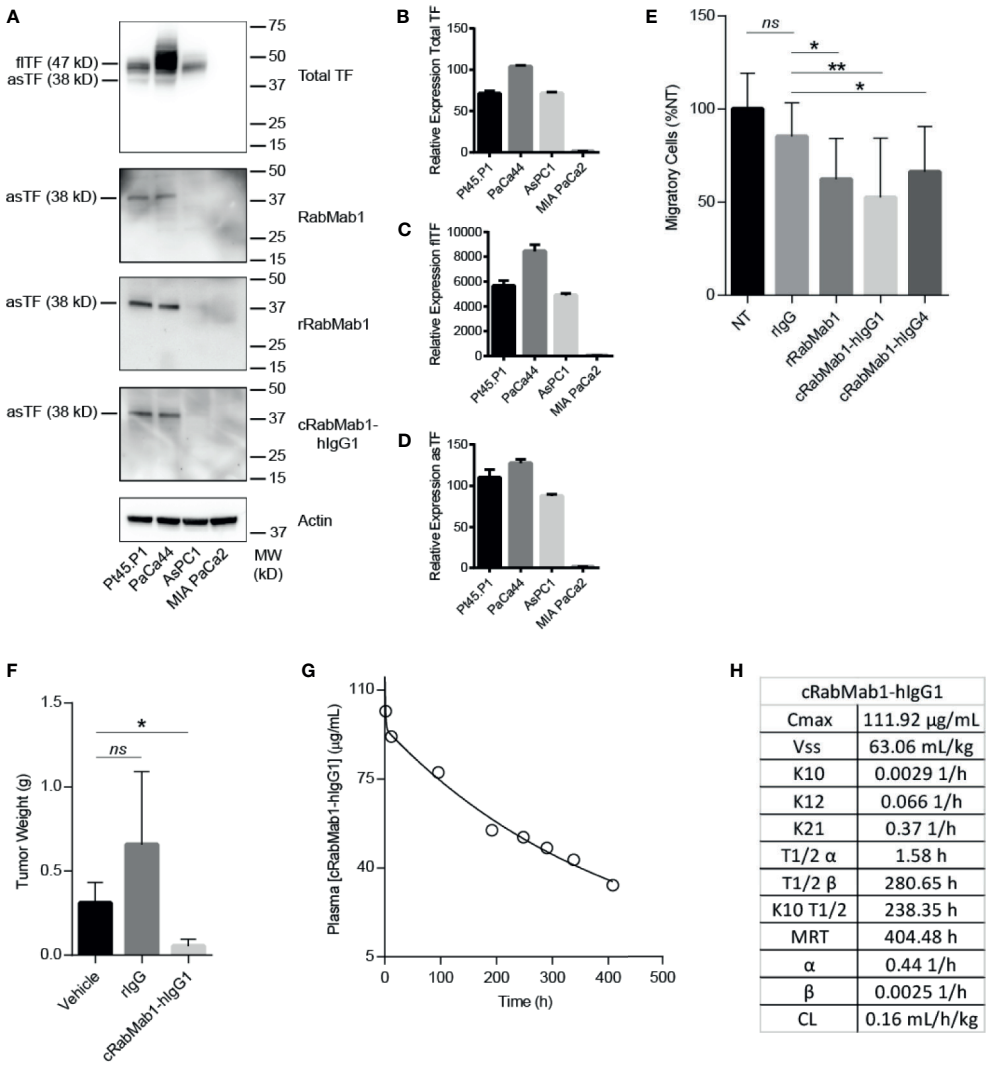

FIGURE 2 | cRabMab1-hIgG1 suppresses tumor growth and has favorable pharmacokinetics. cRabMab1-hIgG1 was assessed for asTF binding *in vitro*, effects on tumor growth, and pharmacokinetics. **(A)** Western blot of Pt45.P1, PaCa44, AsPC1 and MIA-PaCa2 lysates (30 ug each). Each blot was probed with the indicated antibody at 1 µg/mL **(B)** qPCR for total TF transcripts showing relative expression levels. **(C)** qPCR for flTF transcripts showing relative expression levels. **(D)** qPCR for asTF transcripts showing relative expression levels. **(E)** Migration assay with Pt45.P1 cells treated as indicated. **(F)** Tumor weights - $1x10^6$ Pt45.P1 cells were incubated with either 100 µg of rIgG, 100 µg cRabMab1-hIgG1, or an equal volume of vehicle and implanted into the pancreata of athymic nude mice (n = 7/group); tumors grew for 45 days before sacrifice. **(G)** Plasma levels of cRabMab1-hIgG1 resulting from a single injection of 18 mg/kg of the antibody in C57Bl/6 mice. **(H)** PK analysis of cRabMab1-hIgG1. *p ≤ 0.05; **p ≤ 0.01; ns, not significant.

elimination half-life of 281 hours. The steady state volume of distribution (V*ss*) was 63 mL/kg. The area under the concentration-time curve (AUC_{0-t}) was observed to be 24.5 mg/mL/h (**Figures 2G, H**); please also see **Figure 2H** for additional PK findings.

Humanization of cRabMab-hIgG1

Given the encouraging results of our studies comparing cRabMab-hIgG1 and rRabMab1, we proceeded to humanize cRabMab-hIgG1. Plasmids encoding the heavy and light chains of the variable region of cRabMab-hIgG1 were mutagenized to achieve human characteristics. Multiple iterations of this process were performed leading to the creation of three heavy chain and three light chain variants. Combinations of each of these were used to create 9 humanized antibodies; the binding characteristics for each of these were assessed using AHC biosensors (**Figure 3A**, SPR sensograms can be found in **Supplementary Figure 4**). Using this readout, RabMab1-hIgG1-HC3+LC3, hereafter hRabMab1, displayed affinity in the picomolar range (beyond the instrument's detection limit) due to an extremely slow off-rate. hRabMab1's ability to detect asTF *via* western blot was the same as that of cRabMab1-hIgG1 (**Figure 3B**).

A

Antibody	KD (M)	K_{on} (1/Ms)	K_{dis} (1/s)	Full χ^2	Full R^2
cRabMab1-hIgG1	6.4E-09	4.8E+04	3.1E-04	0.0043	0.9992
hRabMab1-hIgG1-(HC1+LC1)	1.7E-08	1.0E+04	1.8E-04	0.0043	0.9993
hRabMab1-hIgG1-(HC1+LC2)	9.8E-09	4.6E+04	4.5E-04	0.0048	0.9993
hRabMab1-hIgG1-(HC1+LC3)	4.4E-09	3.2E+04	1.4E-04	0.0046	0.9992
hRabMab1-hIgG1-(HC2+LC1)	7.7E-10	3.3E+04	2.6E-05	0.0076	0.9991
hRabMab1-hIgG1-(HC2+LC2)	3.8E-09	2.6E+04	9.9E-05	0.0059	0.9994
hRabMab1-hIgG1-(HC2+LC3)	3.9E-09	2.3E+04	8.9E-05	0.0053	0.9994
hRabMab1-hIgG1-(HC3+LC1)	3.0E-08	7.0E+03	2.1E-04	0.0051	0.9995
hRabMab1-hIgG1-(HC3+LC2)	7.9E-10	4.1E+04	3.2E-05	0.0152	0.9982
hRabMab1-hIgG1-(HC3+LC3)	BDL	2.6E+04	BDL	0.0062	0.9993

B

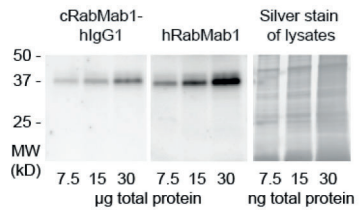

C

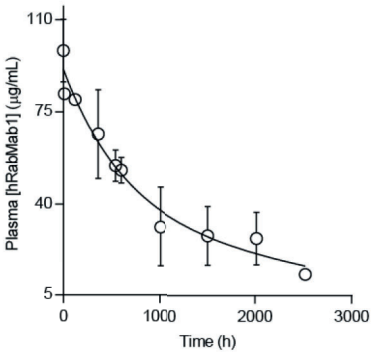

D

hRabMab1	
Cmax	98.36 µg/mL
Vss	75.08 mL/kg
K10	0.00094 1/h
K12	0.0015 1/h
K21	0.0064 1/h
T1/2 α	8.82 h
T1/2 β	907.91 h
K10 T1/2	735.91 h
MRT	1306.86 h
α	0.078 1/h
β	0.00076 1/h
CL	0.057 ml/h/kg

FIGURE 3 | hRabMab1 binds asTF with high affinity and has a favorable PK profile. Nine fully humanized antibodies were produced through mutagenesis of the heavy chain and light chain encoding vectors of the variable region of rRabMab1; HC3+LC3 was chosen for further analysis. **(A)** asTF binding kinetics of humanized RabMab1 antibodies compared to cRabMab1-hIgG1 as determined by AHC biosensor analysis. BDL indicates values were below instrument detection limit. **(B)** Western blot of Pt45.P1 lysates comparing the asTF detection ability of cRabMab1-hIgG1 and hRabMab1 (each diluted to 1 µg/mL); Silver stain of lysates. **(C)** Plasma levels of hRabMab1 resulting from a single injection of the antibody in C57Bl/6 mice. **(D)** PK analysis of hRabMab1.

hRabMab1 Suppresses PDAC Cell Growth *In Vivo*

Given the favorable *in vitro* results, we proceeded to test hRabMab1 *in vivo*. We first assessed the PK properties of hRabMab1 *via* IV administration of hRabMab1 (6 mg/kg) to C57Bl/6 mice. Plasma was collected from 2 mice per time-point as indicated. As with cRabMab1-hIgG1, a biphasic elimination curve was observed with distribution and elimination half-lives of 8.82 hours and 908 hours, respectively (**Figures 3C, D**). The steady state volume of distribution was 75.1 mL/kg. $AUC_{0\text{-}t}$ value for hRabMab1 was observed to be 89.2 mg/mL/h; please also see **Figure 3D** for additional PK findings.

We then proceeded with pharmacodynamic testing of hRabMab1. $1x10^6$ Pt45.P1 cells were implanted into the pancreata of athymic nude mice and given 10 days to engraft prior to the onset of treatment. Mice were then randomly divided into treatment groups receiving either hRabMab1, hIgG1 isotype control, or an equal volume of vehicle control *via* tail vein injection. Based on our previous co-implantation studies and hRabMab1's PK parameters, we arrived at the treatment concentration of 18 mg/kg. hRabMab1 was administered every other day for a total of 22 treatment cycles. Mice treated with hRabMab1 bore tumors that were on average 1/3 the size of those treated with vehicle or isotype control (**Figure 4A**); no differences in average body weight and/or hematological profile were observed between the cohorts (data not shown). Analysis of plasma collected at sacrifice showed that mice treated with hRabMab1 had it circulating at a concentration that was consistent with what we predicted based on simulation of multiple dose administration using the PK parameters derived following single dose administration (**Figure 4B**).

Immunohistochemical analysis demonstrated a statistically significant ~70% reduction in CD31 staining in tumors treated with hRabMab1, pointing to a suppression of neovascularization (6); there was also a ~60% decrease in intratumoral M2-polarized macrophage accumulation (CD206) and a ~25% decrease in the number of actively proliferating cells (Ki67) in the hRabMab1 cohort when compared to the vehicle and/or isotype control cohorts (**Figures 4C–F**). When tumor specimens were stained with an anti-hIgG antibody, there was no signal in tumors treated with vehicle; a minimal, diffuse signal in tumors treated with isotype control; and a pronounced signal in tumors treated with hRabMab1, indicating its accrual in tumor tissue (**Figure 4C**).

Downregulation of Genes Associated With Focal Adhesion, Cytoskeleton Maintenance, and Cell Cycle in hRabMab1-Treated Tumors

Differential gene expression analysis of hRabMab1-treated tumors revealed 955 ENSEMBL transcripts expressed at lower levels when compared to both vehicle and hIgG1 controls, and 458 that were expressed at higher levels (**Figure 5A**). Genelist enrichment analysis using ToppGene indicated that transcripts

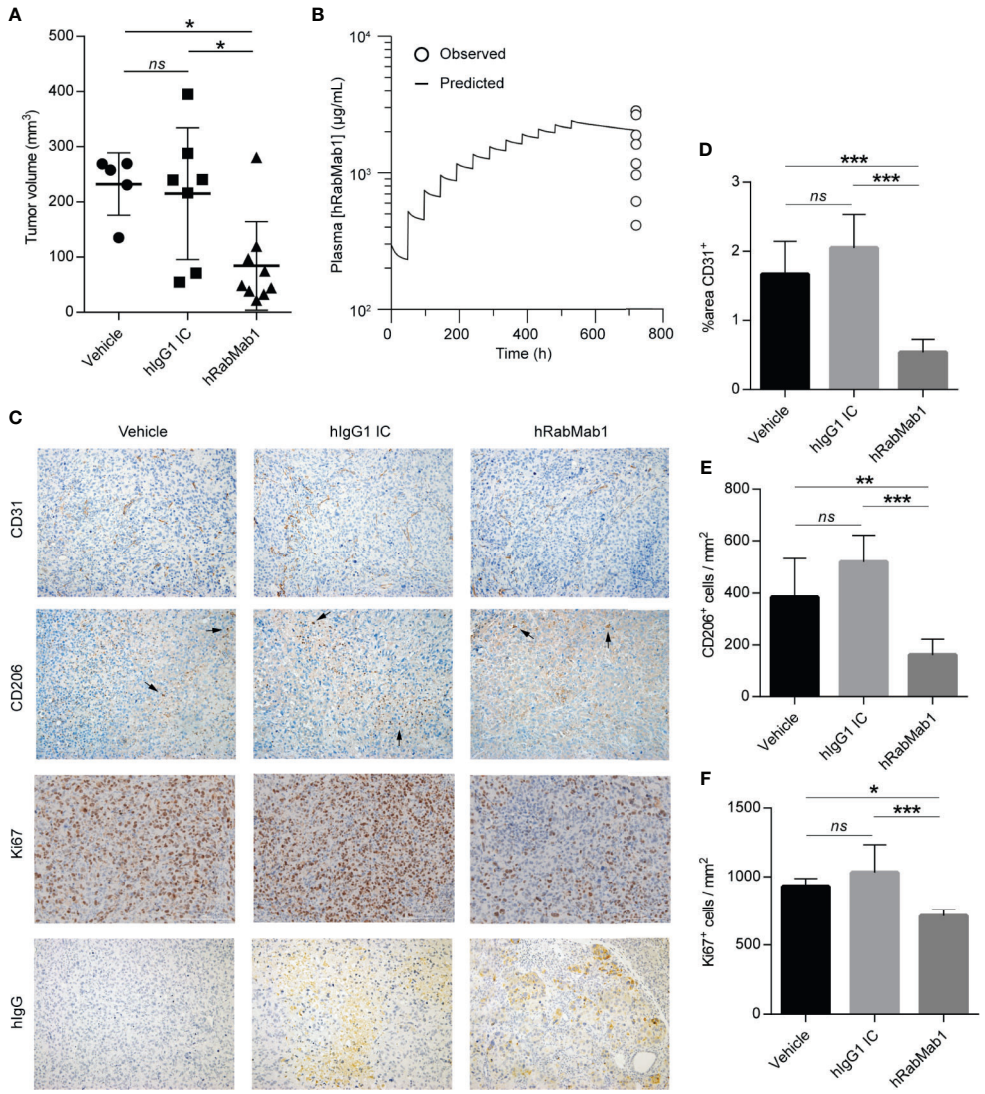

FIGURE 4 | Systemic administration of hRabMab1 suppresses tumor growth. 1x10^6 Pt45.P1 cells were orthotopically implanted into 21 athymic nude mice. Mice were treated every other day with vehicle, 18 mg/kg of hIgG1 IC, or 18 mg/kg of hRabMab1 for a total of 22 treatment cycles. **(A)** Tumor volumes. **(B)** WinNonLin prediction of hRabMab1 accumulation in plasma graphed alongside the amounts detected *via* hIgG1 ELISA at the time of sacrifice. **(C)** Representative images, immunohistochemical analysis of tumor sections as indicated; CD206 panel: arrowheads indicate positive signal (intensely stained single cells); original magnification: 20X. **(D)** Quantification of CD31 positivity in 9 representative images per treatment group. **(E)** The number of CD206$^+$cells/mm^2 in 9 representative images per treatment group. **(F)** The number of Ki67$^+$cells/mm^2 in 9 representative images per treatment group. *p ≤ 0.05; **p ≤ 0.01; ***p ≤ 0.001; ns, not significant.

upregulated in the hRabMab1 group were most significantly associated with mitochondria. In contrast, transcripts that were downregulated in hRabMab1-treated tumors fell in several gene function categories including focal adhesion, cell motility, cell proliferation, cytoskeleton, regulatory proteases, and cell death, many of which are known be TF-associated (**Figures 5** and **6**). Among those most strongly downregulated were heparin binding epidermal growth factor (*HBEGF)*, CST complex subunit *STN1*, epithelial cell transforming 2 (*ECT2)*, phospholipase C delta 3 (*PLCD3)*, and ras homolog family member C (*RHOC)*. To validate our RNAseq findings, the expression levels of *HBEGF* and *STN1* were assessed by qRT-PCR (**Figures 5C, D**). These findings were confirmed on the protein level *via* IHC analysis (**Supplementary Figure 5**).

DISCUSSION

Because hybridoma-derived RabMab1 is effective at stemming tumor growth when co-implanted with cancer cells *in vivo* (3, 11), we pursued humanization of RabMab1. As we show here, target recognition was retained following the engraftment of the variable region of RabMab1 to a human constant region. When administered IV to mice, cRabMab1 had an extended elimination

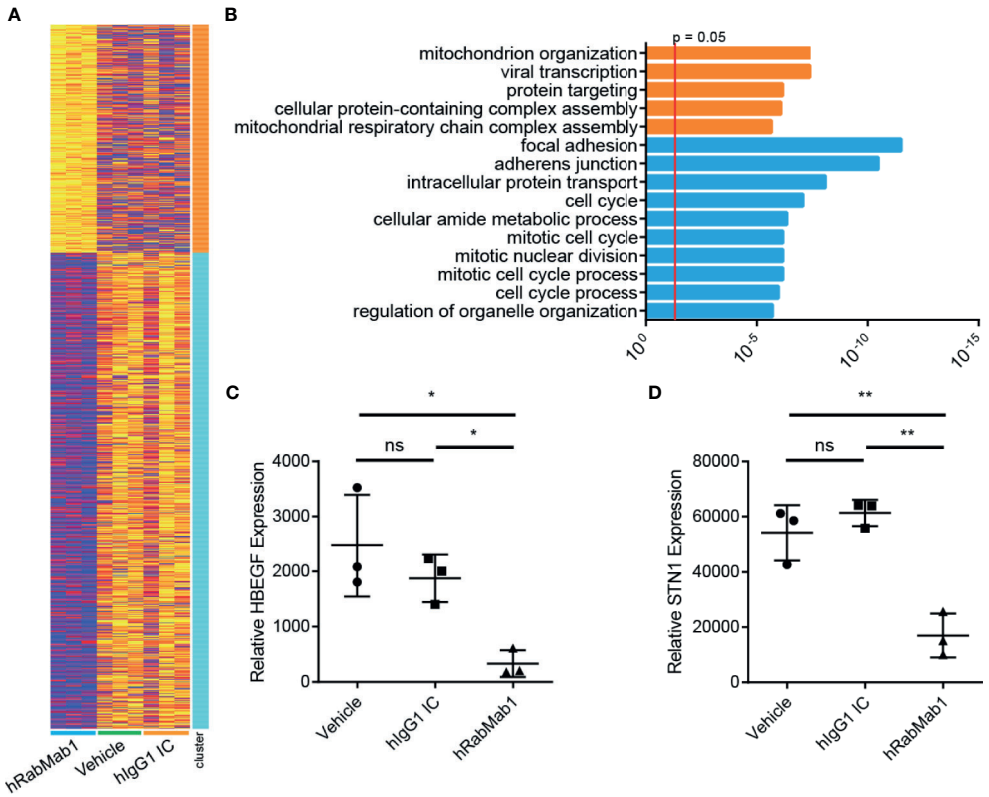

FIGURE 5 | RNAseq analysis of tumor tissue harvested from pharmacodynamic studies. RNA was isolated from 3 tumors from each group representing the median tumors of that group. **(A)** Following library preparation clustering was performed using ToppGene from which a heat map was produced highlighting differences of mRNA expression levels between hRabMab1 treated tumors and those treated with either vehicle or IgG isotype control. **(B)** ToppGene functional enrichment analysis of RNAseq data differentially-expressed genes highlighting strong downregulation of gene transcripts associated with cell cycle and focal adhesion biological processes and cellular component when tumors are treated with hRabMab1. mRNA expression levels of **(C)** HBEGF and **(D)** STN1 in these tumors were quantified by qRT-PCR. *p ≤ 0.05; **p ≤ 0.01; ns, not significant.

half-life, broad systemic exposure (peak plasma concentrations and AUC), and a volume of distribution suggestive of distribution to extravascular spaces. Humanization of the variable regions of RabMab1 yielded hRabMab1; this humanized antibody was verified to recognize native asTF. PK analysis showed that hRabMab1 had an elimination half-life of nearly 35 days in the circulation of C57Bl/6 mice. The observed persistence of high hRabMab1 levels in plasma, when viewed with the *in vitro* efficacy data, suggested that a multiple dosing regimen can be effectively employed to assess anti-tumor efficacy *in vivo*. As such, we implanted asTF-expressing human PDAC cells in the pancreata of athymic nude mice and allowed tumors to establish for 10 days before beginning IV treatment with hRabMab1. A significant reduction in tumor growth was observed, demonstrating hRabMab1's efficacy as a single agent in mice. Consistent with our previous findings showing that asTF promotes neovascularization and macrophage infiltration by binding α6β1 and αvβ3 integrins expressed on endothelial cells, which triggers new vessel formation and, concomitantly, the expression of such cell adhesion molecules as E-selectin, VCAM1, and ICAM1 (3, 6, 22), we found that hRabMab1 suppresses neovascularization as well as macrophage infiltration in the tumor tissue. Blood samples collected to assay hRabMab1 levels at the end of the efficacy study provided a window of opportunity to compare the observed levels with those predicted by PK modelling. Although plasma samples were available only at one time point, the observed plasma concentrations were in good agreement with model-predicted values. This adds confidence that a PK-guided approach can be successfully employed to design efficacious dosing regimens for hRabMab1.

When it was discovered that TF is overexpressed in cancer tissues, systemically targeting it to control tumor growth and spread – as well as cancer-associated coagulopathies – became a goal of those working at the intersection of hematology and oncology. However, targeting "total TF" may result in bleeding due to a disruption of flTF's function of maintaining the hemostatic envelope; we note that these issues may arise with the use of tisotumab vedotin, an "anti-total" TF antibody conjugated to a microtubule-disrupting agent (23). While the precise location of the epitope(s) recognized by tisotumab remain unclear, it does appear to bind flTF (24). Two milestone discoveries have changed the way we think of targeting TF. First, an antibody named 10H10 was invented (25) that binds flTF in a region that does not overlap with the binding sites of FVII and FX as indicated by resolution of the

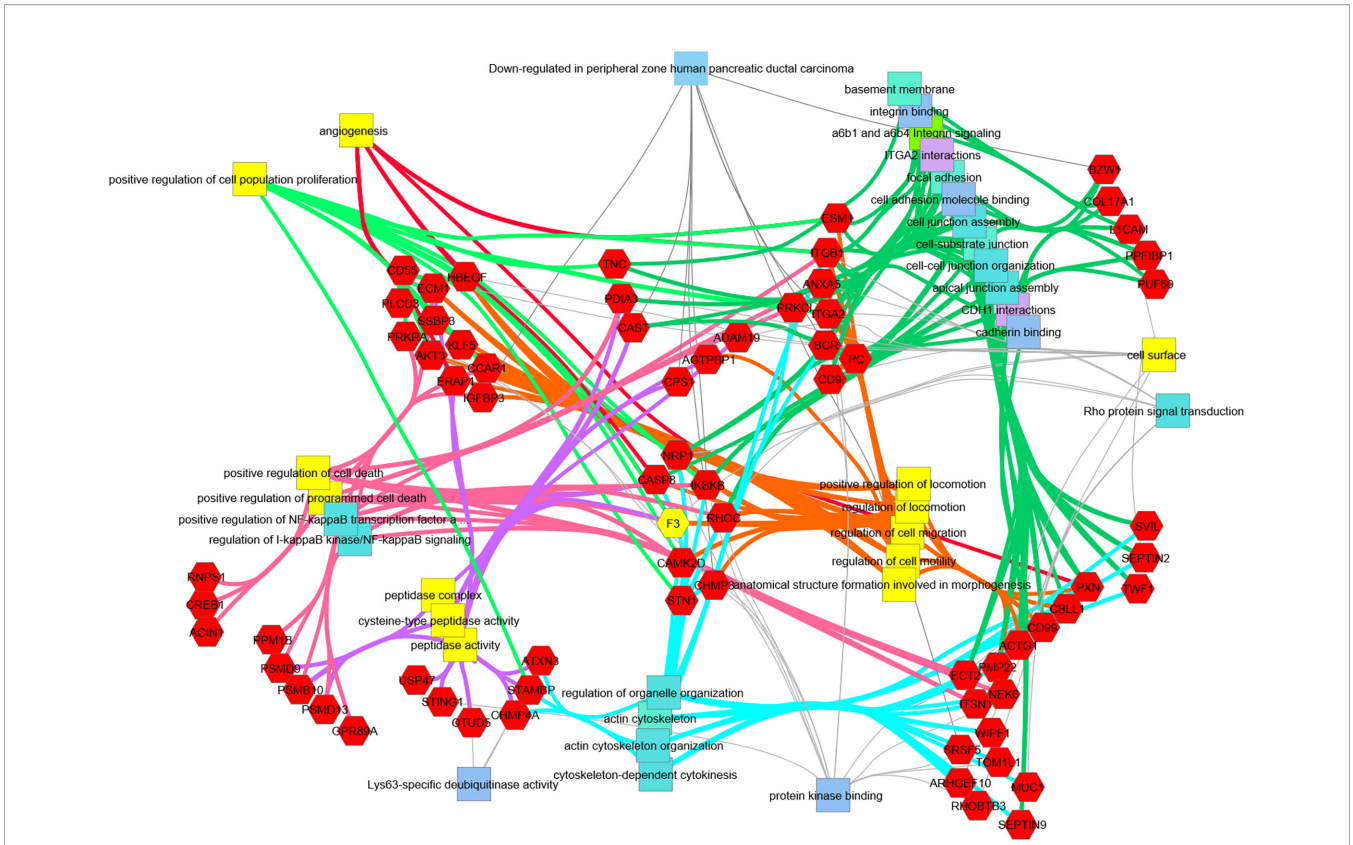

FIGURE 6 | Transcripts downregulated in hRabMab1-treated tumors are associated with a large number of PDAC-relevant biological functions and pathways. Network analysis was performed using ToppCluster, which is based on ToppGene's genelist functions and annotations including GO categories, reactome pathways, protein-protein interactions, and Pubmed manuscript associations. Categories known to be associated with *F3* (highlighted in yellow) also display a strong association with those gene function categories. Of particular interest, there is an extensive downregulation of focal adhesion, cell junction, and cell motility categories; in addition, downregulation of genes associated with positive regulation of proliferation is observed.

crystal structure of the Fab portion of 10H10 bound to the extracellular domain of flTF (26). Thus, 10H10 was believed to bind flTF in a manner that does not interfere with the formation of the extrinsic tenase complex, yet prevents the cleavage of PARs. This has recently come under scrutiny: new evidence showed that even though the 10H10 binding site on flTF does not overlap with the binding sites of FVII or FX, it could still disrupt this binding through steric interference (27); clinical trials have begun with 10H10 but its prospects are uncertain. Second, there was the discovery of asTF and the invention of RabMab1, an antibody that targets asTF's unique C-terminus (4, 11). Given that asTF is dispensable for normal hemostasis, therapeutically targeting this TF isoform is likely to be less risky.

The use of monoclonal antibodies in the treatment of cancer has thus far yielded mixed results. While immunologically targeting the rogue immune cells of hematological malignancies has had great success, targeting solid tumors has only seen partial success, due in part to the inaccessibility of poorly vascularized portions of tumors. This is especially true of PDAC which is characterized by their poor vascularity and dense stroma. Despite this, according to clincaltrials.gov, >160 clinical trials featuring monoclonal antibodies have been launched targeting various aspects of PDAC biology. These can be broadly grouped into those that target glycosylated proteins of the cell-surface, growth factors, growth factor receptors, and checkpoint proteins. Anti-CEA and anti-mucin antibodies performed poorly in these trials; however, four active trials are currently being conducted with anti-CA19-9 antibody, MVT-5873. Anti-EGFR, anti-VEGF, and other antibodies aimed at growth factors and their receptors have also failed to elicit a response, likely owed to the fact that PDAC cells do not rely on any one particular growth factor pathway, but rather engage many such pathways, therefore inhibition of one is easily compensated for. A recent meta-analysis of 9 studies utilizing monoclonal antibodies that target growth factor pathways including cetuximab (anti-EGFR), bevacizumab (anti-VEGF), and ganitumab (anti-IGF1R) found there was no therapeutic benefit of these antibodies when combined with gemcitabine in the treatment of PDAC (28). Disruption of the tumor microenvironment with monoclonals directed against cell adhesion molecules and mucins has also largely been ineffective with the possible exception of anetumab ravtansine, a monoclonal antibody directed against mesothelin and conjugated with the maytansinoid DM4, an inhibitor of microtubule assembly, which is currently being assessed in a phase II trial as a part of a chemotherapeutic regimen (ClinicalTrials.gov Identifier: NCT03816358). The bulk of current clinical trials in PDAC utilizing monoclonal antibodies are focused on inhibiting the

checkpoint pathway, despite the fact that when used as single agents, these have had little effect in the treatment of PDAC (29). There are, however, >100 clinical trials currently focused on assessing how these perform in combination with other chemotherapeutics.

As we show here, systemic administration of hRabMab1 as a single agent strongly suppressed tumor cell growth. RNAseq analysis of resected tumors pointed strongly to an inhibition of the expression of genes associated with focal adhesion and cell cycle progression in the hRabMab1 treated group. Given that the known route of asTF-mediated effects is through integrins, hRabMab1's treatment effect on focal adhesion is to be expected and points to the existence of a positive feedback loop between asTF and integrin signaling. At the same time, downregulation of transcripts involved in cell cycle provides the framework for a mechanistic explanation of hRabMab1-mediated tumor growth inhibition. The fact that the cell cycle regulation genes most strongly suppressed by hRabMab1 are *HBEGF* and *STN1*, is novel and potentially significant because these genes' protein products promote PDAC progression. Heparin-binding epidermal growth factor (HBEGF) is a member of the EGF growth factor family that binds EGFR along other ErbB receptors and acts as a mitogen (30). HBEGF and EGFR are both elevated in PDAC when compared to normal pancreas tissue (31). Hypoxia triggers the expression of *EGFR* through HIF2α in multiple cancer cell lines (32), and it was recently shown that *HBEGF* expression is activated in response to hypoxic conditions by HIF1α in the breast cancer cell line MDA-MB-231 (33). Interestingly, overexpression of asTF in Pt45.P1 cells promotes cell cycle progression and cell motility in hypoxic conditions through a β1 integrin-HIF1α-CAIX signaling cascade (34); thus, it is likely that neutralization of asTF by hRabMab1 mitigates signaling through this pathway leading to a suppression in *HBEGF* expression. Future studies will focus on how hRabMab1 affects the tumor microenvironment and intratumoral hypoxia. STN1 is one of the three components of the CST-complex, which helps maintain telomere integrity (35). The loss of STN1 dramatically impairs telomere replication, leading to rapid telomere shortening and the elicitation of DNA damage response (36). STN1 has also been identified as a mediator of chemotherapeutic resistance to DNA damaging agents; however, its suppression sensitizes cancer cells to these agents (37). In light of this finding, there is a strong rationale for combining hRabMab1 with gemcitabine or FOLFIRINOX in future pre-clinical studies.

In sum, we have shown that our first-in-class, humanized monoclonal antibody directed at asTF exhibits significant anti-PDAC tumor activity *in vivo* when administered intravenously as a single agent. Our findings strongly favor further development of hRabMab1 as a biologic for PDAC management.

DATA AVAILABILITY STATEMENT

The datasets presented in this study can be found in online repositories. The names of the repository/repositories and accession number(s) can be found below: https://www.ncbi.nlm.nih.gov/geo/, GSE158847.

ETHICS STATEMENT

The animal study was reviewed and approved by IACUC, University of Cincinnati.

AUTHOR CONTRIBUTIONS

CSL, AK, KM, TS, JL, and JKW: carried out experiments, analyzed data, and contributed to writing of the manuscript. BJA and PBD: analyzed data and contributed to writing of the manuscript. SAA and HHV: contributed to writing of the manuscript. VYB: conceived the study and contributed to writing of the manuscript. All authors contributed to the article and approved the submitted version.

FUNDING

This work was supported in part by grants R01CA190717 (NCI) and 17-65 BOGD (Pancreatic Cancer Action Network). CSL was supported by grant T32CA236764 (NCI).

ACKNOWLEDGMENTS

The authors are grateful to Dr. Stephan L. Haas, Karolinska University Hospital, Stockholm, Sweden, for the gift of PaCa44 cells.

SUPPLEMENTARY MATERIAL

The Supplementary Material for this article can be found online at: https://www.frontiersin.org/articles/10.3389/fonc.2021.691685/full#supplementary-material

REFERENCES

1. Siegel RL, Miller KD, Jemal A. Cancer Statistics, 2020. *CA Cancer J Clin* (2020) 70:7–30. doi: 10.3322/caac.21590
2. Chan KKW, Guo H, Cheng S, Beca JM, Redmond-Misner R, Isaranuwatchai W, et al. Real-World Outcomes of FOLFIRINOX *vs* Gemcitabine and Nab-Paclitaxel in Advanced Pancreatic Cancer: A Population-Based Propensity Score-Weighted Analysis. *Cancer Med* (2020) 9:160–9. doi: 10.1002/cam4.2705
3. Unruh D, Ünlü B, Lewis CS, Qi X, Chu Z, Sturm R, et al. Antibody-Based Targeting of Alternatively Spliced Tissue Factor: A New Approach to Impede the Primary Growth and Spread of Pancreatic Ductal Adenocarcinoma. *Oncotarget* (2016) 7:25264–75. doi: 10.18632/oncotarget.7955
4. Bogdanov VY, Balasubramanian V, Hathcock J, Vele O, Lieb M, Nemerson Y. Alternatively Spliced Human Tissue Factor: A Circulating, Soluble, Thrombogenic Protein. *Nat Med* (2003) 9:458–62. doi: 10.1038/nm841
5. Hoffman M. The Tissue Factor Pathway and Wound Healing. *Semin Thromb Hemost* (2018) 44:142–50. doi: 10.1055/s-0037-1606181

6. van den Berg YW, van den Hengel LG, Myers HR, Ayachi O, Jordanova E, Ruf W, et al. Alternatively Spliced Tissue Factor Induces Angiogenesis Through Integrin Ligation. *Proc Natl Acad Sci U S A* (2009) 106:19497–502. doi: 10.1073/pnas.0905325106
7. Silberberg JM, Gordon S, Zucker S. Identification of Tissue Factor in Two Human Pancreatic Cancer Cell Lines. *Cancer Res* (1989) 49:5443–7.
8. Kakkar AK, Lemoine NR, Scully MF, Tebbutt S, Williamson RC. Tissue Factor Expression Correlates With Histological Grade in Human Pancreatic Cancer. *Br J Surg* (1995) 82:1101–4. doi: 10.1002/bjs.1800820831
9. Kakkar AK, Chinswangwatanakul V, Lemoine NR, Tebbutt S, Williamson RCN. Role of Tissue Factor Expression on Tumour Cell Invasion and Growth of Experimental Pancreatic Adenocarcinoma. *Br J Surg* (1999) 86:890–4. doi: 10.1046/j.1365-2168.1999.01153.x
10. Nitori N, Ino Y, Nakanishi Y, Yamada T, Honda K, Yanagihara K, et al. Prognostic Significance of Tissue Factor in Pancreatic Ductal Adenocarcinoma. *Clin Cancer Res* (2005) 11:2531–9. doi: 10.1158/1078-0432.CCR-04-0866
11. Kocatürk B, Van den Berg YW, Tieken C, Mieog JSD, de Kruijf EM, Engels CC, et al. Alternatively Spliced Tissue Factor Promotes Breast Cancer Growth in a β1 Integrin-Dependent Manner. *Proc Natl Acad Sci U S A* (2013) 110:11517–22. doi: 10.1073/pnas.1307100110
12. Unruh D, Turner K, Srinivasan R, Kocatürk B, Qi X, Chu Z, et al. Alternatively Spliced Tissue Factor Contributes to Tumor Spread and Activation of Coagulation in Pancreatic Ductal Adenocarcinoma. *Int J Cancer* (2014) 134:9–20. doi: 10.1002/ijc.28327
13. Kocatürk B, Tieken C, Vreeken D, Ünlü B, Engels CC, de Kruijf EM, et al. Alternatively Spliced Tissue Factor Synergizes With the Estrogen Receptor Pathway in Promoting Breast Cancer Progression. *J Thromb Haemost* (2015) 13:1683–93. doi: 10.1111/jth.13049
14. Gao SH, Huang K, Tu H, Adler AS. Monoclonal Antibody Humanness Score and Its Applications. *BMC Biotechnol* (2013) 13(55):1–12. doi: 10.1186/1472-6750-13-55
15. Moore PS, Sipos B, Orlandini S, Sorio C, Real FX, Lemoine NR, et al. Genetic Profile of 22 Pancreatic Carcinoma Cell Lines. *Virchows Arch* (2001) 439:798–802. doi: 10.1007/s004280100474
16. Bolger AM, Lohse M, Usadel B. Trimmomatic: A Flexible Trimmer for Illumina Sequence Data. *Bioinformatics* (2014) 30:2114–20. doi: 10.1093/bioinformatics/btu170
17. Kim D, Langmead B, Salzberg SL. HISAT: A Fast Spliced Aligner With Low Memory Requirements. *Nat Methods* (2015) 12:357–60. doi: 10.1038/nmeth.3317
18. Bray NL, Pimentel H, Melsted P, Pachter L. Near-Optimal Probabilistic RNA-Seq Quantification. *Nat Biotechnol* (2016) 34:525–7. doi: 10.1038/nbt.3519
19. Vidarsson G, Dekkers G, Rispens T. IgG Subclasses and Allotypes: From Structure to Effector Functions. *Front Immunol* (2014) 5:1–17. doi: 10.3389/fimmu.2014.00520
20. Davila M, Robles-Carrillo L, Unruh D, Huo Q, Gardiner C, Sargent IL, et al. Microparticle Association and Heterogeneity of Tumor-Derived Tissue Factor in Plasma: Is It Important for Coagulation Activation? *J Thromb Haemost* (2014) 12:186–96. doi: 10.1111/jth.12475
21. Ovacik M, Lin K. Tutorial on Monoclonal Antibody Pharmacokinetics and Its Considerations in Early Development. *Clin Transl Sci* (2018) 11:540–52. doi: 10.1111/cts.12567
22. Srinivasan R, Ozhegov E, Van Den Berg YW, Aronow BJ, Franco RS, Palascak MB, et al. Splice Variants of Tissue Factor Promote Monocyte-Endothelial Interactions by Triggering the Expression of Cell Adhesion Molecules *Via* Integrin-Mediated Signaling. *J Thromb Haemost* (2011) 9:2087–96. doi: 10.1111/j.1538-7836.2011.04454.x
23. de Bono JS, Concin N, Hong DS, Thistlethwaite FC, Machiels JP, Arkenau HT, et al. Tisotumab Vedotin in Patients With Advanced or Metastatic Solid Tumours (InnovaTV 201): A First-in-Human, Multicentre, Phase 1–2 Trial. *Lancet Oncol* (2019) 20:383–93. doi: 10.1016/S1470-2045(18)30859-3
24. Breij ECW, De Goeij BECG, Verploegen S, Schuurhuis DH, Amirkhosravi A, Francis J, et al. An Antibody-Drug Conjugate That Targets Tissue Factor Exhibits Potent Therapeutic Activity Against a Broad Range of Solid Tumors. *Cancer Res* (2014) 74:1214–26. doi: 10.1158/0008-5472.CAN-13-2440
25. Ahamed J, Versteeg HH, Kerver M, Chen VM, Mueller BM, Hogg PJ, et al. Disulfide Isomerization Switches Tissue Factor From Coagulation to Cell Signaling. *Proc Natl Acad Sci* (2006) 103:13932–7. doi: 10.1073/pnas.0606411103
26. Teplyakov A, Obmolova G, Malia TJ, Wu B, Zhao Y, Taudte S, et al. Crystal Structure of Tissue Factor in Complex With Antibody 10H10 Reveals the Signaling Epitope. *Cell Signal* (2017) 36:139–44. doi: 10.1016/j.cellsig.2017.05.004
27. Rothmeier AS, Marchese P, Langer F, Kamikubo Y, Schaffner F, Cantor J, et al. Tissue Factor Prothrombotic Activity Is Regulated by Integrin-arf6 Trafficking. *Arterioscler Thromb Vasc Biol* (2017) 37:1323–31. doi: 10.1161/ATVBAHA.117.309315
28. Ottaiano A, Capozzi M, De Divitiis C, De Stefano A, Botti G, Avallone A, et al. Gemcitabine Mono-Therapy Versus Gemcitabine Plus Targeted Therapy in Advanced Pancreatic Cancer: A Meta-Analysis of Randomized Phase III Trials. *Acta Oncol (Madr)* (2017) 56:377–83. doi: 10.1080/0284186X.2017.1288922
29. Feng M, Xiong G, Cao Z, Yang G, Zheng S, Song X, et al. PD-1/PD-L1 and Immunotherapy for Pancreatic Cancer. *Cancer Lett* (2017) 407:57–65. doi: 10.1016/j.canlet.2017.08.006
30. Murata T, Mizushima H, Chinen I, Moribe H, Yagi S, Hoffman RM, et al. HB-EGF and PDGF Mediate Reciprocal Interactions of Carcinoma Cells With Cancer-Associated Fibroblasts to Support Progression of Uterine Cervical Cancers. *Cancer Res* (2011) 71:6633–42. doi: 10.1158/0008-5472.CAN-11-0034
31. Kobrin MS, Funatomi H, Friess H, Buchler MW, Stathis P, Korc M. Induction and Expression of Heparin-Binding EGF-Like Growth Factor in Human Pancreatic Cancer. *Biochem Biophys Res Commun* (1994) 202:1705–9. doi: 10.1006/bbrc.1994.2131
32. Franovic A, Gunaratnam L, Smith K, Robert I, Patten D, Lee S. Translational Up-Regulation of the EGFR by Tumor Hypoxia Provides a Nonmutational Explanation for its Overexpression in Human Cancer. *Proc Natl Acad Sci U S A* (2007) 104:13092–7. doi: 10.1073/pnas.0702387104
33. Sethuraman A, Brown M, Krutilina R, Wu Z-H, Seagroves TN, Pfeffer LM, et al. BHLHE40 Confers a Pro-Survival and Pro-Metastatic Phenotype to Breast Cancer Cells by Modulating HBEGF Secretion. *Breast Cancer Res* (2018) 20:117. doi: 10.1186/s13058-018-1046-3
34. Ramchandani D, Unruh D, Lewis CS, Bogdanov VY, Weber GF. Activation of Carbonic Anhydrase IX by Alternatively Spliced Tissue Factor Under Late-Stage Tumor Conditions. *Lab Investig* (2016) 96:1234–45. doi: 10.1038/labinvest.2016.103
35. Miyake Y, Nakamura M, Nabetani A, Shimamura S, Tamura M, Yonehara S, et al. RPA-Like Mammalian Ctc1-Stn1-Ten1 Complex Binds to Single-Stranded DNA and Protects Telomeres Independently of the Pot1 Pathway. *Mol Cell* (2009) 36:193–206. doi: 10.1016/j.molcel.2009.08.009
36. Huang C, Dai X, Chai W. Human Stn1 Protects Telomere Integrity by Promoting Efficient Lagging-Strand Synthesis at Telomeres and Mediating C-Strand Fill-in. *Cell Res* (2012) 22:1681–95. doi: 10.1038/cr.2012.132
37. Zhou Q, Chai W. Suppression of STN1 Enhances the Cytotoxicity of Chemotherapeutic Agents in Cancer Cells by Elevating DNA Damage. *Oncol Lett* (2016) 12:800–8. doi: 10.3892/ol.2016.4676

Conflict of Interest: Authors JL and JKW were employed by LakePharma, Inc.

The remaining authors declare that the research was conducted in the absence of any commercial or financial relationships that could be construed as a potential conflict of interest.

Publisher's Note: All claims expressed in this article are solely those of the authors and do not necessarily represent those of their affiliated organizations, or those of the publisher, the editors and the reviewers. Any product that may be evaluated in this article, or claim that may be made by its manufacturer, is not guaranteed or endorsed by the publisher.

frontiers in Oncology

REVIEW
published: 16 August 2021
doi: 10.3389/fonc.2021.695627

Adjuvant Treatment in Pancreatic Cancer: Shaping the Future of the Curative Setting

Annalisa Pappalardo[1,2†], Emilio Francesco Giunta[1,2†], Giuseppe Tirino[2], Luca Pompella[2], Piera Federico[1], Bruno Daniele[1], Ferdinando De Vita[2] and Angelica Petrillo[1,2]*

[1] Medical Oncology Unit, Ospedale del Mare, Naples, Italy, [2] Division of Medical Oncology, Department of Precision Medicine, School of Medicine, University of study of Campania "L. Vanvitelli", Naples, Italy

Pancreatic ductal adenocarcinoma (PDAC) is a lethal disease even in the early stages, despite progresses in surgical and pharmacological treatment in recent years. High potential for metastases is the main cause of therapeutic failure in localized disease, highlighting the current limited knowledge of underlying pathological processes. However, nowadays research is focusing on the search for personalized approaches also in the adjuvant setting for PDAC, by implementing the use of biomarkers and investigating new therapeutic targets. In this context, the aim of this narrative review is to summarize the current treatment scenario and new potential therapeutic approaches in early stage PDAC, from both a preclinical and clinical point of view. Additionally, the review examines the role of target therapies in localized PDAC and the influence of neoadjuvant treatments on survival outcomes.

Keywords: PDAC - pancreatic ductal adenocarcinoma, biomarkers, ctDNA = circulating tumor DNA, gemcitabine, predictive factors, PARPi, target therapy, neoadjuvant chemotherapy

OPEN ACCESS

Edited by:
Takatsugu Ishimoto, Kumamoto University, Japan

Reviewed by:
Davide Melisi, University of Verona, Italy
Stefan Urbanski, University of Calgary, Canada

****Correspondence:***
Angelica Petrillo
angelic.petrillo@gmail.com

[†]These authors have contributed equally to this work

Specialty section:
This article was submitted to Gastrointestinal Cancers, a section of the journal Frontiers in Oncology

Received: *15 April 2021*
Accepted: *16 June 2021*
Published: *16 August 2021*

Citation:
Pappalardo A, Giunta EF, Tirino G, Pompella L, Federico P, Daniele B, De Vita F and Petrillo A (2021) Adjuvant Treatment in Pancreatic Cancer: Shaping the Future of the Curative Setting. Front. Oncol. 11:695627. doi: 10.3389/fonc.2021.695627

INTRODUCTION

Pancreatic ductal adenocarcinoma (PDAC) is a candidate for the second leading cause of cancer-related death in 2030, with a five-year survival rate of 5-7% (1). Surgical treatment with the goal of radical resection -tumor-free excision margins (so called "R0 resection") is the only potentially curative approach for PDAC. However, only 15-20% of patients with PDAC have localized and potentially resectable disease at diagnosis (2).

In recent years, radiological criteria were developed in order to define tumor resectability and to improve the selection of patients able to receive a curative surgical approach. In detail, according to the degree of contact between the primary tumor and the vessels (portal vein (PV) or superior mesenteric vein (SMV), superior mesenteric artery (SMA), coeliac trunk, and common hepatic artery), PDAC is classified as resectable, borderline resectable, or locally advance unresectable. PDAC is considered resectable when the tumor is free of contact with the SMA, common hepatic artery, coeliac trunk, or contact of < 180° with SMV/PV without vessels' contour irregularity; infiltration of SMA of ≥ 180 or the involvement or occlusion of SMV/PV is generally considered as

locally advanced, unresectable disease. Then, intermediate vascular involvement identifies borderline resectable disease (**Table 1**).

However, a careful multidisciplinary evaluation of those criteria is mandatory in each case in order to perform better patient selection; the multidisciplinary team should consist of a group of physicians from different specialties dedicated to PDAC, highly trained in this regard and working in a high-volume center. It should be assumed that patients with borderline resectable disease have a high probability of residual microscopic resection (R1 resection). For this reason, they should not be considered for upfront surgery and chemotherapy is the first option in the treatment strategy. On the other hand, patients with resectable disease at diagnosis are mainly receive upfront surgery as standard of care.

Nevertheless, despite curative resection, the rate of postoperative tumor recurrence is high and the majority of patients experience a disease relapse (4). On these bases, adjuvant chemotherapy should be offered to all patients who have undergone surgical treatment and maintain an acceptable general condition, regardless of pathological TNM stage, with the aim to improve the poor prognosis of these patients (3, 5). According to this concept, several phase III trials have been developed over the last decades in order to evaluate the more effective chemotherapy regimens, resulting in a radical change of management of resectable PDAC.

Based on this background, the aim of this narrative review is to provide an overview regarding the state of the art of adjuvant treatments in PDAC, alongside the emerging role of perioperative treatment. Lastly, we discuss the role of future perspectives in this field, such as biomarkers and new target therapies.

LOCALIZED PDAC: WHAT WE KNOW IN 2021 AND THE CURRENT TREATMENT SCENARIO

After a suspicion of PDAC, cytological or pathologic diagnosis-usually made with fine-needle biopsy by endoscopic ultrasound guidance or computed tomography (CT)- is mandatory in cases of unresectable and borderline resectable disease (6). Then, an accurate preoperative CT staging and a multidisciplinary evaluation, focused on the assessment of distant metastasis and on the vessels' involvement degree, is recommended in order to identify patients at risk of incomplete resection (R1 or R2 residual macroscopic disease). Those patients have a disappointing survival rate, similar to that of non-resected tumors in case of R2 resections. Additionally, a careful multidisciplinary evaluation might help to decrease the morbidity linked to a non-curative major surgery (5, 7–9).

According to international guidelines, patients with radiological resectable PDAC at diagnosis are candidates for surgery as standard of care, ideally performed in high-volume centers (3, 5). However, the multidisciplinary team should carefully evaluate patients with Ca 19-9 > 500 UI/ml, pain, or histological report of grade 3 tumor (so called "biological criteria of resectability"). In fact, those patients have higher risk of early relapse after surgery also in the case of radiological resectable tumors, underlining the systemic nature of PDAC. In those cases, a systemic treatment followed by curative surgery should be considered as a valid treatment strategy.

Thus, according to the location of the primary tumor, the surgical procedure can be a pancreatoduodenectomy (Whipple technique) in case of head and uncinate tumors and a distal pancreatectomy with en-bloc splenectomy in case of cancers in

TABLE 1 | Criteria of resectability according to NCCN guidelines version 2.2021 (3).

Resectability Status	Venous	Arterial
Resectable	■ No tumor contact with the superior mesenteric vein (SMV) or portal vein (PV) or ≤180° contact without vein contour irregularity.	■ No arterial tumor contact (celiac axis [CA], superior mesenteric artery [SMA], or common hepatic artery [CHA]).
Borderline Resectable	■ Solid tumor contact with the SMV or PV of >180° with contour irregularity of the vein or thrombosis of the vein but with suitable vessel proximal and distal to the site of involvement allowing for safe and complete resection and vein reconstruction. ■ Solid tumor contact with the inferior vena cava (IVC).	Pancreatic head/uncinated process: ■ Solid tumor contact with CHA without extension to CA or hepatic artery bifurcation allowing for safe and complete resection and reconstruction. ■ Solid tumor contact with the SMA of ≤180°. ■ Solid tumor contact with variant arterial anatomy (ex: accessory right hepatic artery, replaced right hepatic artery, replaced CHA, and the origin of replaced or accessory artery) and the presence and degree of tumor contact should be noted if present, as it may affect surgical planning. Pancreatic body/tail: ■ Solid tumor contact with the CA of ≤180°. ■ Solid tumor contact with the CA of >180° without involvement of the aorta and with intact and uninvolved gastroduodenal artery thereby permitting a modified Appleby procedure (some panel members prefer these criteria to be in the locally advanced category).
Locally Advanced	■ Unreconstructible SMV/PV due to tumor involvement or occlusion (can be due to tumor or bland thrombus).	Head/uncinated process: ■ Solid tumor contact with the SMA >180°. ■ Solid tumor contact with the CA >180°.Pancreatic body/tail: ■ Solid tumor contact of >180°with the SMA or CA. ■ Solid tumor contact with the CA and aortic involvement.

the body and tail. Regarding the definition of complete resection, the International Study Group of Pancreatic Surgery (ISGPS) recommends the following: R0 in case of negative resection margins; R1 in case of tumor cells within <1 mm from the margin, considering all seven margins (anterior, posterior, medial, superior mesenteric artery (SMA), pancreatic transection, bile duct, and enteric); and R2 in case of macroscopical residual disease (10). Additionally, surgery should include a standard lymphadenectomy with the removal of > 15 lymph nodes (11).

Currently, open surgery remains the standard of care for the treatment of PDAC, because laparoscopy has been shown to reduce peri-operative morbidity, but with no clear data about oncological results (12, 13). However, despite curative resection, the rate of postoperative tumor recurrence is high, and the majority of patients experience a disease relapse (4). Therefore, PDAC is considered a systemic disease from diagnosis even in cases of localized and resectable tumors. In these cases, a multimodal treatment strategy, such as surgery followed by an adjuvant chemotherapy, can offer more chances of survival (14). However, it is worth mentioning that up to 30% of patient do not receive adjuvant therapy because of the development of comorbidities, the worsening of performance status (PS), post-operative complications, and early recurrence.

Regarding adjuvant chemotherapies, several studies have been developed over the last decades. The European Study Group for Pancreatic cancer (ESPAC)-1 trial showed for the first time that a flourouracil-based adjuvant chemotherapy significantly increased survival compared to surgery alone (median overall survival (OS): 20.1 *versus* 15.5 months, respectively). Additionally, the trial showed a detrimental effect on survival by using an integrate approach with chemoradiotherapy if compared to chemotherapy (15).

Later, the CONKO-001 trial showed significant improvement in disease-free survival (DFS) by using gemcitabine-based adjuvant mono-chemotherapy *versus* observation in resectable PDAC (13.4 *versus* 6.9 months, respectively), whereas median OS was comparable between the gemcitabine and the control group (22.1 *versus* 20.2 months, respectively) (16).

The ESPAC-3 trial did a head-to-head comparison between the two regimens used in ESPAC-1 and in CONKO-001 trials (17). This trial showed no significant differences between the two treatment arms (median OS 23.0 months in the fluorouracil arm and 23.6 months in the gemcitabine arm), with a more acceptable safety profile in the gemcitabine arm (grade 3-4 toxicities: 7.5% *versus* 14% in the fluorouracil arm) (17). However, the ESPAC-3 trial underlined the concept that completing the adjuvant treatment for all six cycles planned, at appropriate dose intensity, has a major impact on survival, rather than an earlier beginning of chemotherapy within the 6-8 weeks after surgery. In fact, it showed that chemotherapy could be postponed for up to 12 weeks after surgery, allowing for a better recovery of patients (18).

More recently, two randomized clinical trials have deeply modified the standard of care for adjuvant chemotherapy for PDAC: ESPAC-4 and PRODIGE 24 trials (19, 20). In 2017, the ESPAC-4 trial showed that the combination of gemcitabine plus capecitabine (GEMCAP) was superior to gemcitabine alone with a significant but modest improvement in median OS (28.0 months in the experimental arm *versus* 25.5 months in the control arm, hazard ratio (HR): 0.82, p=0.032) (19). However, it is important to emphasize the absence of a significant difference in relapse-free survival (RFS) between the two arms, even though a trend in favor of the GEMCAP arm was reported (the 3- and 5-year survival rates were 23.8% and 18.6% with GEMCAP and 20.9% and 11.9% with monotherapy, respectively). The GEMCAP regimen was also associated with a poorer safety profile, with a higher percentage of grade 3-4 adverse events. Methodological limitations of this trial consist of the inclusion of patients with potentially poor prognosis, such as those with post-operative elevation of Ca19.9 serum level, and the absence of planned post-surgical radiological evaluation. Those factors suggest the presence of early metastatic disease in the study population, which might be the reason for the major efficacy of the combination regimen. Nevertheless, international guidelines consider the GEMCAP regimen as a valid option for adjuvant treatment (3, 5).

Then, the PRODIGE 24/CCTG PA.6 trial evaluated the role of a polichemotherapy based on modified fluorouracil/irinotecan/oxaliplatin regimen (mFOLFIRINOX) as adjuvant chemotherapy compared with gemcitabine alone (20). The trial reached its primary endpoint of increasing DFS in the majority of the subgroups (including R0 and R1 resections): after a median follow-up of 33.6 months, median DFS was 21.6 months in the mFOLFIRINOX arm *versus* 12.8 months in the gemcitabine arm (HR: 0.58; p<0.001). In addition, median OS was 54.4 months in the mFOLFIRINOX arm *versus* 35.0 months for gemcitabine arm (HR: 0.64; p=0.003); this was the best achievement in survival in this setting until now. As expected, grade 3-4 toxicities were significantly higher in the mFOLFIRINOX group (75.5% *versus* 51.1%), with higher rates of diarrhea, mucositis, fatigue, peripheral neuropathy, nausea, and vomiting. However, no grade 5 adverse events were reported in the experimental arm. Nevertheless, we should consider two aspects in the analysis of those results: first, only 66% of patients in the mFOLFIRINOX arm received all the planned cycles of chemotherapy compared to 79% in the control arm; second, the population of the PRODIGE 24 trial was very well selected (PS 0-1 according to ECOG, normal post-surgical radiological evaluation and Ca19.9 serum levels < 180 U/ml) with lower risk of early recurrence.

Additionally, the Italian phase III GIP-2 trial showed similar results in this setting, supporting the use of mFOLFIRINOX in the adjuvant setting (21). However, the trial was stopped earlier after the publication of the results of PRODIGE 24 trial, due to the low accrual.

In general, according to international guidelines (3, 5), mFOLFIRINOX is considered the best adjuvant strategy in very well selected and fit patients, with an optimal post-surgical recovery.

Finally, other trials were conducted with the aim to improve the outcomes in this setting. In particular, the APACT trial did not confirm the superiority in DFS of the combination of nab-paclitaxel plus gemcitabine when compared to gemcitabine alone (19.4 *versus* 18.8 months; HR: 0.88; p=0.1824) (22). Likely, the

CONKO-005 trial, that evaluated the efficacy of adding erlotinib to gemcitabine, failed to demonstrate a benefit in DFS and OS in the adjuvant setting in the experimental arm (23).

Lastly, the potential impact of adjuvant radiation therapy to improve the outcome of patients with PDAC is still debated, due to the lack of definitive data evaluating modern radiotherapy doses and techniques. In fact, in the pivotal historical ESPAC-1 and EORT trials (that compared chemoradiotherapy with the observation after surgery alone), radiotherapy has been shown to not improve the survival outcomes in this setting, including in patients who have undergone R1 resection (15, 24).

However, we should consider that those first trials were conducted using suboptimal radiation regimens (such as split-course radiotherapy), without a standardization of doses and comparison groups.

On the other hand, two more recent studies using a national cancer registry database reported that chemordiotherapy was more effective than adjuvant chemotherapy alone, especially in node-positive status or R1 resection (25, 26). However, they were limited by potential inherent biases; therefore, their findings should be carefully interpreted. Thus, to date, the role of post-operative radiation in the modern era of new and more effective systemic therapies remains unanswered. It should be evaluated in phase III trials, at least in some categories of patients with higher risk of local recurrence.

In conclusion, mFOLFIRINOX is considered the best systemic treatment in the adjuvant setting in cases of selected and fit patients. On the other hand, gemcitabine-based monochemotherapy or GEMCAP regimen could be an option in the elderly and for patients with ECOG PS 2.

PDAC EVOLUTION: FROM PANCREATIC GLAND TO METASTASIS

Since the end of the 20th century, important advances in understanding pathological mechanisms beneath PDAC evolution have been made.

As for other human cancer types, a stepwise evolution model has been proposed for PDAC: tumor initiation, as a consequence of driver gene mutations; tumor progression, through clonal expansion and accumulation of new genetic alterations; and tumor dissemination, in which cancer cells reach, through the bloodstream, distant sites (27–29).

First genetic events in tumor initiation concern few loci (**Figure 1**). In particular, four genes (also known as the "Big

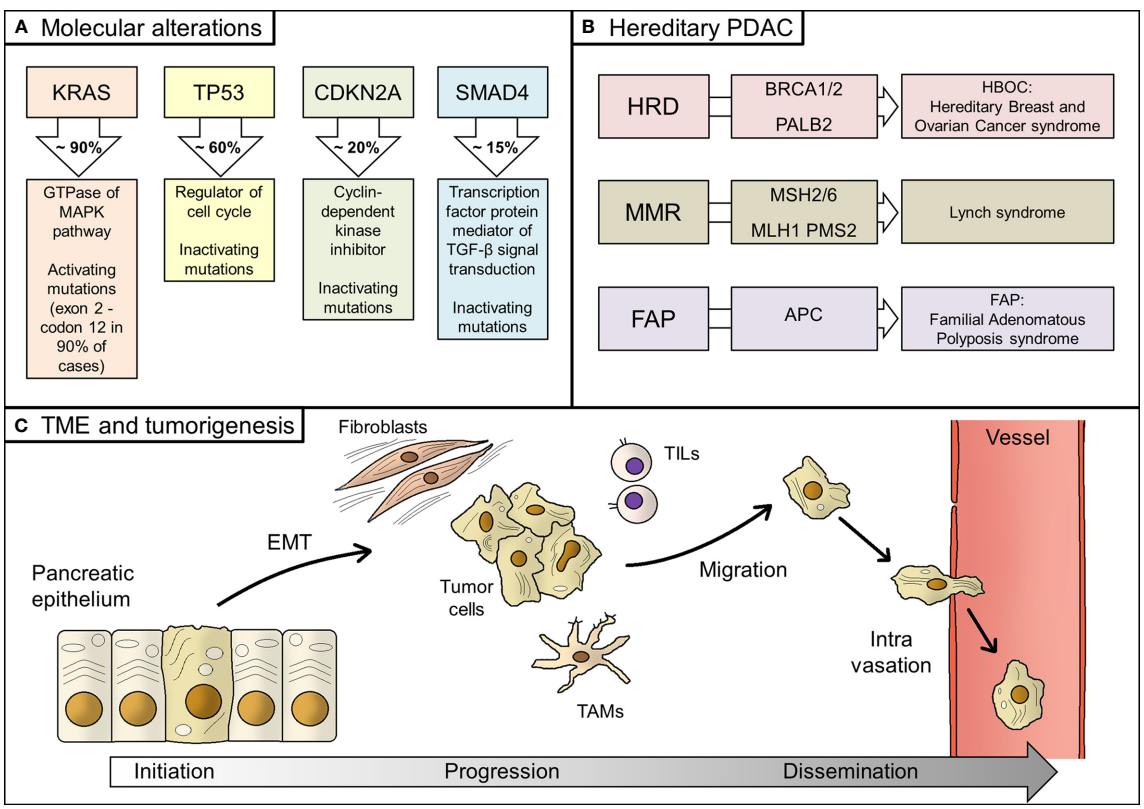

FIGURE 1 | Biology of PDAC. **(A)** Main molecular alterations in PDAC; **(B)** Hereditary alterations, involved genes, and their relative syndromes; **(C)** Main steps of PDAC tumorigenesis, from tumor initiation to tumor progression and, finally, systemic dissemination. PDAC, pancreatic ductal adenocarcinoma; HRD, homologous recombination deficiency; TME, tumor microenvironment; EMT, epithelial-to-mesenchymal transition; TAMs, tumor-associated macrophages; TILs, tumor infiltrating lymphocytes; MMR, mismatch repair.

4") are the most mutated in early pancreatic cancer, namely KRAS, TP53, CDKN2A, and SMAD4 (formerly known as DPC4), with their alterations detected for 94%, 64%, 21%, and 17% of all PDACs, respectively (30). KRAS mutations, which are localized in codon G12 in almost 90% of cases, are the earliest event in pancreatic tumorigenesis; they are activating mutations, unlike the other three genes (30, 31).

Transformation of normal pancreatic epithelium into malignant cells seems to cross in many cases through premalignant lesions, namely the pancreatic intraepithelial neoplasia (PanIN) and intraductal papillary mucinous neoplasm (IPMN) (32). In support of this hypothesis, genomic analysis of PanIN and IPMN showed that they share the same genetic alterations of PDAC, although with lower incidence (33).

Genetic alterations other than the abovementioned could pre-exist the tumor and be responsible for its onset. Hereditary PDAC account for 10% of all PDAC patients, even if a clear predisposition syndrome could be detected in no more than 20% of them (34). Hereditary alterations mainly affect BRCA1/2 genes and other homologous recombination genes, such as PALB2 (hereditary breast and ovarian cancer syndrome, HBOC), mismatch repair (MMR) genes (Lynch syndrome), and APC gene (Familial Adenomatous Polyposis syndrome, FAP) (35). BRCA1/2 and PALB2 alterations are the most frequent inherited mutations in PDAC patients, whilst MMR deficiency is rare, being recorded in less than 1% of patients (36, 37). However, genomic instability might underlie the onset of a significant percentage of PDACs (38, 39).

Epithelial-to-mesenchymal transition (EMT), consisting of the acquisition of migratory properties by epithelial cells, is a common feature in human cancer and it is also described in PDAC, linked to the generation of cancer stem cells, formation of metastasis, and resistance to therapy (40–42).

Then, the tumor microenvironment (TME) plays a fundamental role in PDAC genesis. TME is composed of stromal cells, extracellular matrix, immune cells, and blood vessels (43). It is not merely the physical and cellular support for the tumor growing, but its interactions with tumor cells are responsible for tumor behavior (i.e. promoting EMT), invasiveness, and metastasis (44, 45). In fact, stromal cells should be considered as dynamic elements, therefore representing potential therapeutic targets (46–48). Stromal fibroblasts promoted growth and metastasis in preclinical models of PDAC through production and secretion of soluble factors, whilst composition of immune infiltration has a critical role in tumor progression by regulating immune response against tumor cells (49–51). In detail, immune and inflammatory infiltration consists of several types of cells, from tumor-associated macrophages (TAMs) to bone marrow-derived cells (BMDCs), and from neutrophils to tumor-infiltrating T-cells (TILs) (52). Recent discoveries on antitumor immunity in PDAC have highlighted a peculiar immune microenvironment composition, which explains the evasion from immune surveillance by tumor cells (53). However, specific PDAC mutational signature, such as homologous recombinant deficiency- that results in higher frequency of somatic mutations- could enhance antitumor immunity and be a candidate for new immunotherapy drugs (54).

Tumor dissemination in the bloodstream is not an early event in the genetic evolution of PDAC since the metastatic ability is acquired only years after tumor initiation (55). However, on a clinical point of view, a considerable share of small PDACs (1-5 mm of diameter) are found with synchronous distant metastases, meaning that tumor clinically detectable masses have already accumulated several genetic alterations, thus leading to systemic disease. As support to those assumptions, circulating tumor cells (CTCs) have also been found in blood samples of PDAC patients in earlier stages (56–58). It should be noted that only a few CTCs have the ability to form metastases; however, despite the relative inefficiency of this process, the great amount of tumor cells released in bloodstream explains the high frequency of metastases (59, 60).

There are preferential sites for metastases from PDAC, such as liver, lungs, and peritoneum (61). Interestingly, in the last years several works have suggested the possibility that organs- in particular the liver- could be induced in accepting tumor cells through secreted factors released by primary tumor, such as inhibitor of metalloproteinases or exosomes (so called "pre-metastastic niches") (62, 63). On the other hand, tumor cells could acquire specific characteristics for selective organotropism (64).

TME also plays an important role in the metastatic process. In particular, a similar extracellular matrix composition between primary and metastatic TME has been pointed out, even if metabolic genes in stromal cells are differentially expressed based on metastasis site, highlighting specific regulation in specific contexts (65, 66). Additionally, TME is not a static entity but changes over time in response to tumor behavior (67).

Lastly, on the genomic point of view, it seems that primary PDAC and synchronous/metachronous metastases share similar frequency in main tumor suppressor genes, even if a higher mutational load in cell cycle pathway genes has been observed in metastases (68). That observation supports the hypothesis that main genomic rearrangements involved in tumorigenesis of PDAC occur before bloodstream dissemination, which is indeed a late event in the natural history of this type of human cancer.

NEW DIRECTIONS IN THE ADJUVANT TREATMENT OF PDAC

Better Stratification of Patients: Role of Biomarkers and Prognostic Factors

One of the biggest challenges in early-stage malignant tumors is to assess individual prognosis more accurately, specifically regarding risk of either local or distant relapse. Stratification of these patients is important to avoid unnecessary adjuvant treatment in those who will not experience disease recurrence but also to better tailor post-operative treatment – i.e. number and type of drugs administered or treatment duration – in those who have a high probability of micro-metastases.

Radiological exams currently used in clinical practice are unable to detect micro-metastatic disease; this is why biomarkers, especially those correlating with metastatic burden, have been intensively studied in early PDAC patients in the last decades in order to ideally separate those patients who are at high risk of distant recurrence from those who are not (69).

Among serum biomarkers detectable on blood samples, Ca 19-9 is certainly the most diffused and studied. In fact, elevated levels of Ca19-9 have been associated with poor survival in early stage PDAC patients (70). However, its sensitivity and specificity as a single agent does not allow its use in early detection of PDAC, explaining the clinical need of serological partners to be tested with it (71–73). For example, a recent study pointed out the possibility to predict disease recurrence in PDAC patients through the combination of Ca19-9 and serum metabolomes (74).

Table 2 summarizes novel potential biomarkers and prognostic factors in localized PDAC patients and their potential influence on choosing the best curative approach. Among those, CTCs and circulating tumor DNA (ctDNA) are really promising. CTCs have been detected in early stage PDAC patients. In particular, in clinically and radiologically localized PDAC a cut-off of 3 CTCs per vial (4 ml) was proposed in the literature to discriminate between patients with or without distant micrometastases (75). CTCs are undoubtedly useful in risk stratification, being a candidate for clinical implementation in the near future (76–78).

Regarding ctDNA- which is a hot topic in cancer research worldwide- its role in early stage PDAC has been more finely shaped in very recent years (79). The most important study about ctDNA in early stage PDAC patients has been conducted on 112 subjects suitable for radical resection of primary tumor: pre- and post-operative detection of KRAS mutations in ctDNA was correlated with poor RFS and OS in PDAC patients, also including those who received adjuvant therapy (80). The trial suggested that patients with detectable levels of ctDNA should be treated more aggressively after resection. In order to increase the role of ctDNA as a predictive biomarker, Hussung et al. demonstrated that integration of Ca19-9 and KRAS mutant ctDNA performed better than individual markers for both RFS and OS in PDAC patients undergoing adjuvant treatment (81). Extracellular vesicles are also promising biomarkers for early stage PDAC patients, but optimization of analytical processes is needed for practical use (82).

Beyond tumor biomarkers and moving from the evidence in the metastatic setting, systemic inflammation markers have also been studied in radically resected PDAC patients, such as neutrophil-to-lymphocyte ratio (NLR) and platelet-to-lymphocyte ratio (PLR) (83–85). Recently, a systemic immune-inflammation index, which is the ratio between platelets × neutrophils and lymphocytes, has been proposed as a new prognostic score, predicting poor survival with more accuracy than NLR and PLR (86).

Then, Kim et al. structured a nomogram for early recurrence after pancreatectomy in localized PDAC in order to help clinicians in predicting recurrence risk. The nomogram included some of the abovementioned prognostic (namely, Ca 19-9, NLR, and PLR) and pathological factors (such as tumor size and grade of differentiation) (87). Eventually, in the future, the integration of other biomarkers in some nomograms - such as CTCs and ctDNA –will certainly enhance their predictiveness. Additionally, their use in adjuvant clinical trials should be encouraged for tailoring therapy based on the risk of disseminated microscopic disease.

New Potential Targets in the PDAC Complex Scenario

PDAC is a very complex and heterogeneous disease at the molecular and clinical level. In fact, in the adjuvant context, only a few examples regarding molecular predictive biomarkers exist and no targeted agents are currently used in clinical practice in this setting.

Martinelli P et al. used the large ESPAC-3 trial cohort to classify patients according to the level expression of GATA6 transcription factor, a putative marker of Collisson and Moffitt "Classical" subtype (17, 88–90). They clearly showed that individuals with high GATA6 expression (what we consider as the "classical" type) received the greatest benefit from adjuvant 5-Fluorouracil administration, whereas patients with low-GATA6 did not benefit by using this type of chemotherapy at all. To note, no survival differences based on GATA6 expression were found in the gemcitabine-based adjuvant arm. The hypothesis, also supported by the recent COMPASS trial in advanced disease

TABLE 2 | Potential biomarkers and prognostic factors in localized PDAC patients and their potential influence on choosing the best curative approach.

Biomarker/prognostic factor	Optimal timing for use	Influence on curative approach(es)
CTCs*	■ Detection before surgery indicates a high probability of distant (micro)metastases.	■ Neoadjuvant chemotherapy should be considered.
	■ Detection after surgery indicates a high probability of distant (micro)metastases and/or residual disease.	■ "Adjuvant" chemotherapy should be strengthened.
ctDNA**	■ Detection before surgery indicates a high probability of distant (micro)metastases.	■ Neoadjuvant chemotherapy should be considered.
	■ Detection after surgery indicates a high probability of distant (micro)metastases and/or residual disease.	■ "Adjuvant" chemotherapy should be strengthened.
NLR and PLR §	■ High value after surgery may suggest poor prognosis in frail patients.	■ Adjuvant chemotherapy should be avoided.

**Circulating tumor cells, **Circulating tumor DNA, §Neutrophil-to-lymphocyte ratio (NLR) and platelet-to-lymphocyte ratio.*

setting, is that the classical subtype could be more sensitive to fluoropyrimidine, even in the adjuvant context, making GATA6 an "ideal" (and relatively simple) marker to assess in order to choose the better adjuvant strategy (91).

Buchler's group, again using the data from ESPAC-3 trial (17), showed the potential utility of another marker, hENT1 (human equilibrative nucleoside transporter 1), to predict benefit by using a gemcitabine-based adjuvant therapy (92). In details, hENT1 permits the bidirectional passage into cancer cells of pyrimidine nucleosides (such as gemcitabine, 5-Fluorouracil, and capecitabine), which suggests that higher levels of this transporter could correlate with increased intracellular accumulation of chemotherapy agents, thus causing cancer cell death. Indeed, this retrospective analysis showed that patients who received a gemcitabine-based chemotherapy had a median OS of 26.2 months in case of high hENT1 expression level; on the other hand, patients with low hENT1 levels showed a median OS of 17.1 months after gemcitabine. Nevertheless, there was no difference in hENT1 expression levels in the 5-Fluorouracil-based chemotherapy arm. These preliminary data were also recently confirmed by a Korean study, making hENT1 a possible predictive biomarker for clinical benefit by using a gemcitabine-based adjuvant regimen (93). To explain these results, it is interesting to note that hENT1 has been reported to be the most efficient transporter for gemcitabine but not for other pyrimidine nucleosides (94). Additionally, *in vitro* studies have shown that hENT1 loss could be responsible for resistance to gemcitabine in gastrointestinal human cancer cell lines (95).

More recently, Nicolle R et al. expanded our knowledge about molecular stratification in the adjuvant setting, identifying a molecular signature (the so-called "GemPred" signature) able to predict benefit from adjuvant administration of gemcitabine. Less than 20% of the retrospectively tested patients (~ 430 from different cohorts) were GemPred signature positive, all with "classic" transcriptomic features (96). Interestingly, the median DFS in patients with GemPred positive signature was longer than those with GemPred negative signature (42.5 *versus* 13.4 months); similar results were obtained for the median OS (91.3 *versus* 31.7 months). What kind of molecular intersections there are between GemPred and classic signatures has not been defined yet. However, it is a matter of fact that all patients with GemPred positive signature also had the classic PDAC subtype, whose sensitivity to 5-Fluorouracil was previously shown by Martinelli P et al. (87). Therefore, a better comprehension of the relationship between classic signature and this novel GemPred signature is highly desirable, also in the light of novel single cell data.

A major barrier to precision medicine in PDACs is the inter- and, especially, intra-tumor heterogeneity. Recent data have clearly shown that in a single tumor- defined as classical or basal-like at the bulk level- there is a transcriptional continuum at single cell level between classical and basal-like transcriptional programs (97). Thus, some cells are in a "classical-like state" and others in a "basal-like state", possibly due to different microenvironmental interactions and spatial location within the different tumor regions. This notion complicates the picture further, representing a possible barrier to cytotoxic and/or targeted treatments directed to one specific "bulk" subtype.

Targeted Therapies in the Adjuvant Treatment for PDAC: Hope or Chimera?

Another crucial question in the adjuvant setting for PDAC is the following: beyond classical chemotherapy agents (see *section 2 for additional details*), what specific molecular targets could we imagine in the adjuvant setting? Necessarily we should look at genomic characterizations and at metastatic disease setting.

The first attempt to target metastatic PDAC with a molecular agent was published in 2007, with the combination of gemcitabine and the anti-epithelial growth factor receptor (EGFR)/tyrosine kinases inhibitor (TKI) Erlotinib, based on the observed overexpression of this receptor in tissue from PDAC (98, 99). Although the phase III trial met its primary endpoint with a statistically significant improvement in OS with the combination (6.24 *versus* 5.91 months, respectively), this survival gain was clinically irrelevant. Thus, to date, Erlotinib is not used in the clinical practice for metastatic PDAC. Erlotinib was also tested in the adjuvant setting in combination with gemcitabine and compared to gemcitabine alone (RTOG 0848 trial (100). Preliminary results were negative, showing a lack of survival benefit from the addition of erlotinib to standard chemotherapy. It must be underlined that in both cases (metastatic and adjuvant setting) the study population was not selected by EGFR expression and/or EGFR gene amplification, which could explain – at least in part – the disappointing results.

A recently published retrospective analysis of tumor specimens from CONKO-005 trial has suggested that a specific genetic signature - SMAD4 gene alterations with low MAPK9 expression - could be responsible for erlotinib efficacy in the adjuvant setting, even if these results need to be prospectively validated (101).

In 2015, the consortium led by Biankin and Grimmond identified a small percentage of PDAC (< 15%) with high genomic instability due to serious defects in DNA integrity maintenance (creating the so called "BRCA signature") (102). These patients showed alterations in genes like BRCA1, BRCA2, and PALB2, and the authors could demonstrate a clear clinical usefulness of a platinum-based chemotherapy, at least in two subjects, also assuming a possible role of PARP inhibitors in this context. Based on those preliminary results, the phase III POLO trial evaluated the efficacy of maintenance therapy with Olaparib (a PARP inhibitor) in germline BRCA1/2 mutated metastatic PDAC patients. The trial showed doubled median PFS (from 3.8 to 7.4 months) after an induction first-line therapy platinum-based (103). Although those results were promising, data regarding a possible adjuvant use of Olaparib in radically resected patients are not yet available. Nevertheless, a hypothetic study design as maintenance strategy (up to one year) in ctDNA positive germline BRCA1/2 mutated patients after mFOLFIRINOX standard adjuvant therapy is reported in **Figure 2**; **Table 3** shows the ongoing trials in this field.

A very small percentage of PDAC shows high microsatellite instability (MSI-H), a molecular feature associated with high

response to immune checkpoint inhibitors (ICIs) in advanced disease setting across multiple cancer types (110, 111). However, it is a matter of fact that the objective response rate (ORR) of PDAC to ICIs was lower than that observed in other types of MSI-H cancers (112). However, an adjuvant approach with ICIs in MSI-H patients with ctDNA might be worth investigation in the adjuvant setting in the future.

Nevertheless, with the exception of rare MSI-H patients, PDAC is considered a tumor resistant to ICIs, due to a highly immune-suppressive microenvironment, dominated by extracellular matrix proteins and different cancer associated fibroblast subtypes as well as other immune cell types (113). A very recent report from the NCT02451982 phase I/II Trial is evaluating the combination of GVAX (tumor cell vaccine) plus Nivolumab (anti-PD1) and Urelumab (CD137 agonist). Unfortunately, the results of the adjuvant phase of the trial are not available yet (see *section 4.3 for additional details regarding the results in the neoadjuvant setting*) (114).

Another interesting strategy in the adjuvant setting is to add chloroquine to gemcitabine, thus targeting autophagy, a resistance mechanism to chemotherapy, which has a role in PDAC maintenance, possibly also in a micro-metastatic state (115). In this regard, only the results of the phase II trial in a metastatic setting are available to date (116). The trial did not show any survival benefit for the chloroquine arm; however, a significant improvement in ORR was reported. Based on that consideration, the adding of chloroquine could make even more sense in a pre-operative setting for borderline resectable and/or locally advanced PDAC, where good tumor response could lead to radical surgical resection. However, further prospective evaluations are needed in order to explore this hypothesis.

In conclusion, target therapies are not considered the standard of care in the adjuvant setting for PDAC and they are not used outside clinical trials.

How to Improve the Outcomes for Resectable PDAC: The Role of Neoadjuvant and Perioperative Treatments

The role of neoadjuvant treatment in PDAC is still controversial to date, although several trials and retrospective studies have been conducted in this setting and the general trend is to encourage this approach in the light of the systemic behavior of this malignancy. However, evidence available is still not univocal, as different clinical entities are currently investigated together for primary chemotherapy: locally advanced unresectable, borderline resectable, and resectable tumors (see **Table 1**). All these entities account for 50-60% of the whole newly diagnosed PDAC, but less than half are borderline or upfront resectable tumors.

For borderline/locally advanced tumors, an "induction" treatment should be conceptualized rather than a real "neoadjuvant", even if no robust data have been reported. Preoperative treatment is able to achieve a radical resection in approximately 30% of the cases initially deemed unresectable, while almost 70% of the resectable cases regularly undergo surgery after a neoadjuvant therapy. However, as already discussed in the previous sections, a high percentage of resected patients are bound to relapse despite the best surgical and systemic approach currently available, and not all patients receive chemotherapy after surgery. Potential key points to improve survival outcomes in "curable" settings are the possibility to intensify and individualize pre- and postoperative treatment and the possibility to "adapt" adjuvant regimens in light of neoadjuvant response rate and/or biomarkers expression. This last point is getting more topical the more neoadjuvant treatment is growing in importance in the therapeutic algorithm.

Is it possible to outline a possible perioperative strategy according to specific clinical and biological markers? As a matter of fact, a major reason for treatment failure both in

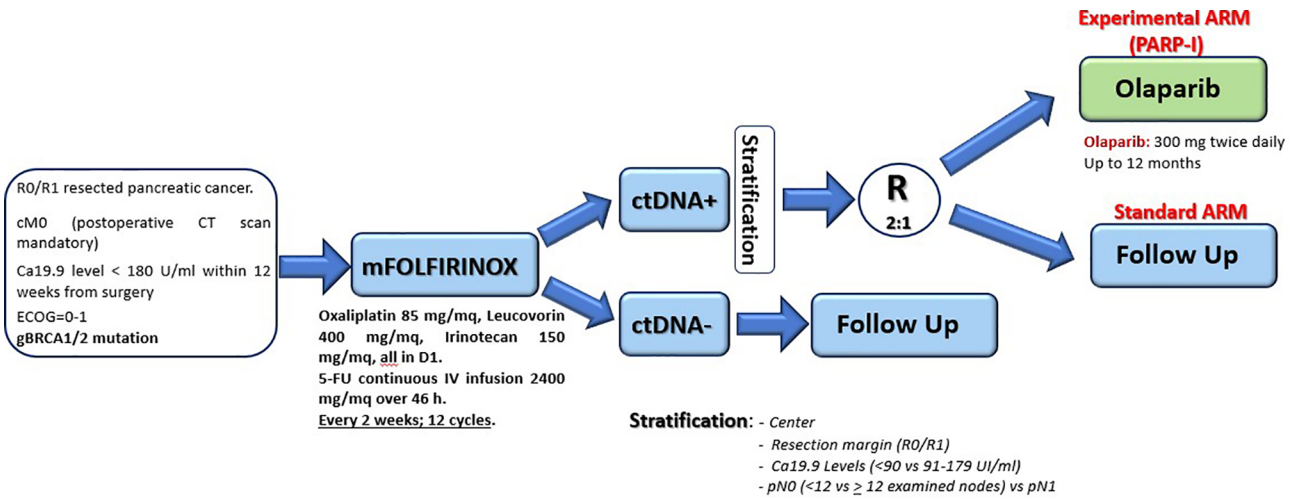

FIGURE 2 | Hypothetic adjuvant study design dedicated to germline BRCA1/2 mutated PDAC patients.

TABLE 3 | Selected major ongoing studies investigating new perioperative/adjuvant approaches .

Study	Phase	*N* of patients	Setting	Experimental arm	Status
NeoPancONE NCT04472910 (104)	II	84*	Perioperative	FOLFIRINOX x 6 periop. (GATA-6 expression)	Recruiting
PROJECTION NCT04246203 (105)	Observational	200*	Neoadjuvant	ctDNA detectable *vs* absent in preoperative	Recruiting
NCT01072981 (HyperAcute-Pancreas Immunotherapy) (106)	III	722	Adjuvant	Gemcitabine or 5FU chemoradiation +/-Algenpantucel-L	Completed
DECIST NCT04157127 (107)	I	43*	Adjuvant	Standard chemo + autologous DC** vaccine	Recruiting
NCT04117087 (Pooled Mutant KRAS-Targeted Long Peptide Vaccine) (108)	I	30*	Adjuvant	KRAS peptide vaccine§ + nivolumab ipilimumab	Recruiting
NCT00733746 (109)	II	123	Perioperative	Erlotinib + gemcitabine periop.	Completed

**estimated, **Dendritic Cells, §Hiltonol® (Poly-ICLC).*

resectable and in locally advanced PDAC is the clinical and biological heterogeneity of different treated tumors, as well as the strong systemic "vocation" of this malignancy since the initial stages. Current neoadjuvant and adjuvant schedules are not able to tackle these issues in most cases.

During the last years, intensified regimens, such as gemcitabine plus nab-paclitaxel and FOLFIRINOX, have been proposed in order to improve resection rate and survival in the neoadjuvant setting.

The use of FOLFIRINOX, established as a standard in adjuvant and metastatic settings, seems suitable and promising according to meta-analytic data, while no prospective phase III data are available in this setting to date (117). In 2019, a meta-analysis of 24 small retrospective and phase I-II prospective studies highlighted the role of this combination in borderline resectable PDAC (1802 patients). The analysis showed a pooled resection rate of 67.8% (95% Confidence Interval (CI): 60.1%-74.6%) and R0-resection rate of 83.9% (95% CI: 76.8% - 89.1%) among all resected patients for the 13/24 studies reporting data about resection margins (117). The median OS ranged from 11.0 to 34.2 months across the studies (to note: lower than phase III PRODIGE-24 with adjuvant FOLFIRINOX). These data are consistent with previously reported meta-analysis (118). Besides the absence of a dedicated randomized controlled trial, the biggest limitation for the use of FOLFIRINOX is the toxicity, with grade 3-4 neutropenia, diarrhea, and fatigue usually reported as the most common adverse events.

With regards to gemcitabine and nab-paclitaxel combination, the Italian phase II GAP trial is the only randomized study comparing this combination *versus* gemcitabine alone (119). In locally advanced tumors, gemcitabine and nab-paclitaxel performed better in terms of distant relapses, also positively affecting PFS and OS, compared to gemcitabine monotherapy. The combination reduced rate of patients who progress after 3 cycles of induction chemotherapy by 20%.

In 2020, the LAPACT phase II single arm trial confirmed the role nab-paclitaxel and gemcitabine (6 cycles) as induction treatment in patients with locally advanced PDAC, with promising PFS (10.9 months, 90% CI; 9.3-11.6) and OS (18.8 months, 90%CI; 15.0- 24.0) and a good tolerability (consistently with data from the metastatic setting) (120). The data reported a better survival compared to historical reference trials. The response rate was 33.6% (90% CI: 26.6 - 41.5), establishing a good activity of this combo for locally advanced PDAC (121, 122).

However, currently no prospective head-to-head comparison between these two schedules (FOLFIRINOX *versus* gemcitabine and nab-paclitaxel) in the "induction" setting for resectable disease is available, whereas the majority of the evidence is retrospective or related to the locally advanced disease (123). The randomized American phase II trial SWOG S1505 compared perioperative treatment using mFOLFIRINOX *versus* gemcitabine and nab-paclitaxel in patients with resectable PDAC (104). The trial enrolled 147 patients and preliminary results, presented at the 2020 ASCO meeting, showed no significant differences in terms of OS (primary endpoint) between the two combinations (22.4 *versus* 23.6 months), with similar resection rates (77% *vs* 73%) (122). The SWOG S1505 and the phase III PREOPANC-1 are currently the most recent and robust evidence supporting the feasibility of perioperative treatment respectively in resectable and borderline resectable PDAC, assuming the use of the same regimens in the postoperative setting (FOLFIRINOX/gemcitabine and nab-paclitaxel versus gemcitabine, respectively) (104, 124). Noteworthy, PREOPANC-1 was not able to demonstrate a significant benefit in OS with the use of preoperative chemoradiotherapy compared to upfront surgery followed by adjuvant gemcitabine (35.2 *versus* 19.8 months; $p = 0.029$), while a significant higher R0-resection rate was reached (71% *versus* 40%, $p < 0.001$) (124).

A further contribution to the evaluation of neoadjuvant chemotherapy in resectable PDAC comes from the Italian phase II PACT-15 trial published in 2018 (106). In this randomized open-label study (93 patients), authors investigated an intensified perioperative approach with PEXG (cisplatin, epirubicin, gemcitabine, and capecitabine) in comparison with the same schedule as adjuvant treatment or a standard adjuvant gemcitabine. In the perioperative arm, 66% of patients were event-free at 1-year (primary endpoint) *versus* 23% and 50% in the other arms, respectively. Although of phase II

design, this study provided further evidence of the feasibility and promising efficacy of neoadjuvant chemotherapy in resectable tumors, and was one of the few direct comparisons with adjuvant treatment.

In summary, according to these trials (SWOG S1505, PREOPANC-1, and PACT-15), the trend should go towards the repurpose of the same regimen, used as neoadjuvant, in the postoperative setting, while both FOLFIRINOX and gemcitabine/nab-paclitaxel should be considered feasible for preoperative treatment in resectable and/or locally advanced tumors (104, 106, 124).

How much adjuvant treatment adds after preoperative treatment and whether it should be selected according to clinical features are interesting points still to be clarified. Some data are available with the use of lymph node ratio (LNR) as a prognostic marker after neoadjuvant treatment followed by surgery, in order to stratify the efficacy of adjuvant therapy according to this factor. From an American registry database, including patients with PDAC who underwent resection following neoadjuvant chemotherapy until 2008, clinicopathologic factors have been retrospectively analyzed (107). Among the 14% of patients who also received postoperative therapy, the treatment was associated with better survival (72 *versus* 33 months, $p = 0.008$) in those with an LNR < 0.15, as confirmed by multivariate analysis. The addition of postoperative chemotherapy after neoadjuvant resulted in improved outcomes (reduced risk of death of 51%, $p = 0.02$, and longer time-to-recurrence) in patients with low LNR. However, this study reported a lack of benefit by the addition of adjuvant treatment in patients with severe lymph node involvement, contradicting other retrospective studies that showed - by contrast - a survival benefit from postoperative chemotherapy especially in patients with node-positive status (105, 107, 108). It is not clear whether the pathological node status plays a stronger prognostic role itself rather than a positive predictive meaning for adjuvant treatment.

No data are available about the role of tumor regression grade (rarely applied for pancreatic cancer) and R0-resection rate in the choice of prosecution and type of adjuvant schedule after neoadjuvant treatment.

All things considered, the open questions for future research in the perioperative context could be the following: the role of adjuvant treatment in pN0 patients, the role of neoadjuvant treatment in upfront resectable tumors (versus the exclusive adjuvant approach), the prosecution of adjuvant treatment in poor responsive patients treated with preoperative chemotherapy (such as switch adjuvant strategy or switch therapy in the non-responders), and the choice of what first line treatment should be used at disease relapse considering all the therapies used in the perioperative approach. In fact, in this challenging scenario, the role of adjuvant chemotherapy after upfront surgery might evolve, since the patients who will undergo immediate pancreatic resection are those in the very early stages who do not need neoadjuvant/perioperative approaches. Additionally, the biologic features and changes in patients who underwent induction chemotherapy followed by surgery should also be considered. About this last point, interesting data are expected from the phase II NeoPancONE trial, which is investigating the molecular features of resectable PDAC that underwent radical surgery after neoadjuvant FOLFIRINOX (109). One of the main aims of this study will be to analyze a potential biomarker already identified in the COMPASS trial, GATA-6, in the perioperative strategy, with the aim to stratify tumor types and responses to treatment (90). This may offer a chance to better select "different regimens for different patients". This study will be the first able to correlate a potential biomarker to a neoadjuvant chemotherapy.

Additionally, considering the promising prognostic role of ctDNA, its detection after surgery could become a biomarker of response to neoadjuvant chemotherapy and help the clinicians to optimize the post-operative approach in case of poor responsive patients (80, 125).

The landscape of targeted therapy and immunotherapy for PDAC is still disappointing, mainly because of the uncomplete knowledge of the complex mechanisms underlying this malignancy and its intricate relations with the tumor microenvironment (as already mentioned in the previous section). With regards to immunotherapy and vaccine research in the neoadjuvant setting, a multi-institutional phase III study has been conducted using algenpantucel-L (a cancer vaccine comprised of irradiated allogeneic transfected pancreatic cancer cells) in addition to adjuvant chemotherapy or chemoradiotherapy (gemcitabine or 5-fluorouracil), based on the results of the phase II in 2013 (126, 127). The transfected cells are able to synthetize a murine enzyme, which is responsible for the production of a cell-surface protein (α-1,3-galactosyl (αGal) carbohydrate) not expressed in humans. The binding of preexisting natural human antibodies (naturally produced against the same proteins of the gut flora, accounting for 1% of all circulating immunoglobulins) results in the activation of antibody-dependent cell-mediated cytotoxicity toward allograft cells and endogenous pancreatic cancer cells. This process, through the so-called "epitope spreading", expands the immune response against other tumor-associated antigens expressed by both injected cells and native cancer cells. The vaccine "drives" a natural preexisting immune weapon against pancreatic cancer, boosting chemotherapy to obtain a response against pancreatic cancer cells, normally resistant to the immune system. In the phase II trial, 70 resected patients have been treated with a 12-month DFS rate of 62% and a 12-month OS of 86%, describing site pain and induration as the most common adverse event. Further definitive efficacy results are expected.

Other phase I/II trials involving vaccine and immunotherapy in the adjuvant setting will provide a further attempt to turn "cold" pancreatic cancer into "hot" immune-sensitive disease (128–130). For additional details regarding ongoing trials in this setting, see **Table 3**.

CONCLUSIONS

PDAC treatment has hugely improved in recent decades. In fact, even if the use of gemcitabine has been the better therapeutic chance for those patients for a long time, both in adjuvant and in

metastatic settings, a lot of new drugs and strategies are appearing in therapeutic armamentarium today. However, PDAC remains a big challenge in the oncological scenario. In fact, even in cases of curative surgery for resectable disease, the rate of recurrence is high, suggesting an early systemic diffusion of cancer cells. A multidisciplinary evaluation of PDAC patients in high volume centers could help to improve the outcomes for those patients, by creating a tailored therapeutic strategy for each patient. According to international guidelines (3, 5), to date, adjuvant chemotherapy based on mFOLFIRINOX or gemcitabine is the recommended treatment in patients with resectable PDAC after curative surgery. However, many changes are ongoing in the current treatment scenario. In particular, use of perioperative and neoadjuvant treatment, even for resectable and borderline resectable PDAC, might allow the adjuvant chemotherapy after upfront surgery to play a marginal role in the future. Additionally, a better understanding of the molecular mechanism of PDAC as well as the research about prognostic and/or predictive biomarkers is urgently needed in order to better select patients who can benefit from different and/or personalized approaches and to design future prospective clinical trials regarding targeted therapies also in this field.

AUTHOR CONTRIBUTIONS

Conceptualization: APa, EG, and APe. Topic: APa, EG, and APe. resources: APa and EG. writing—original draft preparation: APa, EG, and APe. Writing of particular sections: all authors. Writing—review and editing: all authors. Supervision, APe, BD, and FV. All authors contributed to the article and approved the submitted version.

ACKNOWLEDGMENTS

We would like to thank K. El Bairi (Cancer Biomarkers Working Group, Oujda, Morocco) for the editorial assistance.

REFERENCES

1. Rahib L, Smith BD, Aizenberg R, Rosenzweig AB, Fleshman JM, Matrisian LM. Projecting Cancer Incidence and Deaths to 2030: The Unexpected Burden of Thyroid, Liver, and Pancreas Cancers in the United States. *Cancer Res* (2014) 74:2913–21. doi: 10.1158/0008-5472.CAN-14-0155
2. Varadhachary GR, Tamm EP, Abbruzzese JL, Xiong HQ, Crane CH, Wang H, et al. Borderline Resectable Pancreatic Cancer: Definitions, Management, and Role of Preoperative Therapy. *Ann Surg Oncol* (2006) 13(8):1035–46. doi: 10.1245/ASO.2006.08.011
3. Ducreux M, Cuhna S, Caramella C, Hollebecque A, Burtin P, Goéré D, et al. Cancer of the Pancreas: ESMO Clinical Practice Guidelines for Diagnosis, Treatment and Follow-Up. *Ann Oncol* (2005) 26:56–8. doi: 10.1093/annonc/mdv295
4. Katz MH, Wang H, Fleming JB, Sun CC, Hwang RF, Wolff RA, et al. Long-Term Survival After Multidisciplinary Managenement of Resected Pancreatic Adenocarcinoma. *Ann Surg Oncol* (2009) 16:836–47. doi: 10.1245/s10434-008-0295-2
5. National Comprehensive Cancer Networks. *NCCN Guidelines Version 2.2021* (2021). Available at: http://www.nccn.org (Accessed Accesed February 25, 2021).
6. Asbun HJ, Conlon K, Fernandez-Cruz L, Friss H, Shrikhande SV, Adham M, et al. International Study Group of Pancreatic Surgery. When to Perform a Pancreatoduodenectomy in the Absence of Positive Histology? A Consensus Statement by the International Study Group of Pancreatic Surgery. *Surgery* (2014) 155:887–92. doi: 10.1016/j.surg.2013.12.032
7. Tamm EP, Balachandran A, Bhosale PR, Katz MH, Fleming JB, Lee JH, et al. Imaging of Pancreatic Adenocarcinoma: Update on Staging/Resectability. *Radiol Clin North Am* (2012) 50:407–28. doi: 10.1016/j.rcl.2012.03.008
8. Hernandez J, Mullinax J, Clark W, Toomey P, Villadolid D, Morton C, et al. Survival After Pancreaticoduodenectomy is Not Improved by Extending Resections to Achieve Negative Margins. *Ann Surg* (2009) 250:76–80. doi: 10.1002/bjs.11115
9. Bilimoria KY, Talamonti MS, Sener SF, Bilimoria MM, Stewart AK, Winchester DP, et al. Effect of Hospital Volume on Margin Status After Pancreaticoduodenectomy for Cancer. *J Am Coll Surg* (2008) 207:510–9. doi: 10.1016/j.jamcollsurg.2008.04.033
10. Bockhorn M, Uzunoglu FG, Adham M, Imrie C, Milicevic M, SandBerg AA, et al. Borderline Resectable Pancreaticcancer: A Consensus Statement by the International Study Group of PancreaticSurgery (ISGPS). *Surgery* (2014) 155:977–88. doi: 10.1016/j.surg.2014.02.001
11. Tol JA, Gouma DJ, Bassi C, Dervenis C, Montorsi M, Adham M, et al. Definition of a Standard Lymphadenectomy Insurgery for Pancreatic Ductal Adenocarcinoma: A Consensus Statement by Theinternational Study Group on Pancreatic Surgery (ISGPS). *Surgery* (2014) 156:591–600. doi: 10.1016/j.surg.2014.06.016
12. Kooby DA, Hawkins WG, Schmidt CM, Weber SM, Bentrem DJ, Gillespie TW, et al. A Multicenter Analysis of Distalpancreatectomy for Adenocarcinoma: Is Laparoscopic Resection Appropriate? *J Am Coll Surg* (2010) 210:779–785.24. doi: 10.1016/j.jamcollsurg.2009.12.033
13. Ricci C, Casadei R, Taffurelli G, Toscano F, Pacilio CA, Bogoni S, et al. Laparoscopic Versus Open Distalpancreatectomy for Ductal Adenocarcinoma: A Systematic Review and Meta-Analysis. *J Gastrointest Surg* (2015) 19:770–81. doi: 10.1007/s11605-014-2721-z
14. Strobel O NJ, Jäger D, Markus W, Büchler MW. Optimizing the Outcomes of Pancreatic Cancer Surgery. *Nat Rev Clin Oncol* (2018) 16:11–26. doi: 10.1038/s41571-018-0112-1
15. Neoptolemos JP, Dunn JA, Stocken DD, Almond J, Link K, Beger H, et al. Adjuvant Chemoradiotherapy and Chemotherapy in Resectable Pancreatic Cancer: A Randomised Controlled Trial. *Lancet* (2001) 358:1576–85. doi: 10.1016/s0140-6736(01)06651-x
16. Oettle H, Post S, Neuhaus P, Gellert K, Langrehr J, Ridwelski K, et al. Adjuvant Chemotherapy With Gemcitabine *vs* Observation in Patients Undergoing Curative-Intent Resection of Pancreatic Cancer: Arandomized Controlled Trial. *JAMA* (2007) 297:267–77. doi: 10.1001/jama.297.3.267
17. Neoptolemos JP, Stocken DD, Bassi C, Ghaneh P, Cunningam D, Goldstein D, et al. Adjuvant Chemotherapy With Fluorouracil Plus Folinic Acid *vs* Gemcitabine Following Pancreatic Cancer Resection: A Randomized Controlled Trial. *JAMA* (2010) 304:1073–81. doi: 10.1001/jama.2010.1275
18. Valle JW, Palmer D, Jackson R, Cox T, Neoptolemos JP, Ghaneh P, et al. Optimal Duration and Timing of Adjuvant Chemotherapy After Definitive Surgery for Ductal Adenocarcinoma of the Pancreas: Ongoing Lessons From the ESPAC-3 Study. *J Clin Oncol* (2014) 32:504–12. doi: 10.1200/JCO.2013.50.7657
19. Neoptolemos JP, Palmer DH, Ghaneh P, Psarelli EE, Valle JW, Halloran CM, et al. Comparison of Adjuvant Gemcitabine and Capecitabine With Gemcitabinemonotherapy in Patients With Resected Pancreatic Cancer (ESPAC-4): A Multicentre, Open-Label, Randomised, Phase 3 Trial. *Lancet* (2017) 389:1011–24. doi: 10.1016/S0140-6736(16)32409-6
20. Conroy T, Hammel P, Hebbar M, Abdelghani MB, Wei AC, Raoul J, et al. FOLFIRINOX or Gemcitabine as Adjuvant Therapy for Pancreatic Cancer. *N Engl J Med* (2018) 379:2395–406. doi: 10.1056/NEJMoa1809775

21. Vasile E, Vivaldi C, Bianco R, Lonardi S, Di Donato S, Brugnatelli S, et al. Randomized Phase 3 Study of Adjuvant Chemotherapy With Folfoxiri Compared to Gemcitabine in Resected Pancreatic Cancer: The "Gruppo Italiano PANCREAS" GIP-2 Study. *Abstract book 21th Congress Ital Assoc Med Oncol* (2019) 105:1–216. doi: 10.1177/0300891619872589
22. Tempero MA, Reni M, Riess H, Pelzer U, O'Reilly EM, Winter JM, et al. APACT: Phase III, Multicenter, International, Open-Label, Randomized Trial of Adjuvantnab-Paclitaxel Plus Gemcitabine (Nab-P/G) *vs* Gemcitabine (G) for Surgically Resected Pancreatic Adenocarcinoma. *J Clin Oncol* (2019) 37:4000. doi: 10.1093/annonc/mdz247.010
23. Sinn M, Bahra M, Liersch T, Gellert K, Messmann H, Bechstein W, et al. CONKO-005: Adjuvant Chemotherapy With Gemcitabine Plus Erlotinib Versus Gemcitabine Alone in Patients After R0 Resection of Pancreatic Cancer: A Multicenter Randomized Phase III Trial. *J Clin Oncol* (2017) 35:3330–7. doi: 10.1200/JCO.2017.72.6463
24. Klinkenbijl JH, Jeekel J, Sahmoud T, van Pel R, Couvreur ML, Veenhof CH, et al. Adjuvant Radiotherapy and 5-Fluorouracil After Curativeresection of Cancer of the Pancreas and Periampullary Region: Phase III Trial of the EORTC Gastrointestinaltract Cancer Cooperative Group. *Ann Surg* (1999) 230:776–82. doi: 10.1097/00000658-199912000-00006
25. Rutter CE, Park HS, Corso CD, Lester-Coll NH, Mancini BR, Yeboa DN, et al. Addition of Radiotherapy to Adjuvant Chemotherapy is Associated With Improved Overall Survival in Resected Pancreatic Adenocarcinoma: An Analysis of the National Cancer Data Base. *Cancer* (2015) 121:4141–9. doi: 10.1002/cncr.29652
26. Hsieh MC, Chang WW, Yu HH, Lu CY, Chang CL, Chow JM, et al. Adjuvant Radiotherapy and Chemotherapy Improve Survival in Patients With Pancreatic Adenocarcinomareceiving Surgery: Adjuvant Chemotherapy Alone is Insufficient in the Era of Intensity Modulation Radiation Therapy. *Cancer Med* (2018) 7:2328–233. doi: 10.1002/cam4.1479
27. Hruban RH, Goggins M, Parsons J, Kern SE. Progression Model for Pancreatic Cancer. *Clin Cancer Res* (2000) 6:2969–72.
28. Vogelstein B, Kinzler KW. The Multistep Nature of Cancer. *Trends Genet* (1993) 9:138–41. doi: 10.1016/0168-9525(93)90209-Z
29. Makohon-Moore A, Iacobuzio-Donahue CA. Pancreatic Cancer Biology and Genetics From an Evolutionary Perspective. *Nat Rev Cancer* (2016) 16:553–65. doi: 10.1038/nrc.2016.66
30. Waters AM, Der CJ. KRAS: The Critical Driver and Therapeutic Target for Pancreatic Cancer. *Cold Spring Harb Perspect Med* (2018) 8:a031435. doi: 10.1101/cshperspect.a031435
31. Lee KE, Bar-Sagi D. Oncogenic KRas Suppresses Inflammation-Associated Senescence of Pancreatic Ductal Cells. *Cancer Cell* (2010) 18:448–58. doi: 10.1016/j.ccr.2010.10.020
32. Kim JY, Hong SM. Precursor Lesions of Pancreatic Cancer. *Oncol Res Treat* (2018) 41:603–10. doi: 10.1159/000493554
33. Tsuda M, Fukuda A, Takaori K, Seno H. Genetics and Biology of Pancreatic Cancer and its Precursor Lesions: Lessons Learned From Human Pathology and Mouse Models. *Ann Pancreatic Cancer* (2019) 2. doi: 10.21037/apc.2019.07.02
34. Carrera S, Sancho A, Azkona E, Azkuna J, Lopez-Vivanco G. Hereditary Pancreatic Cancer: Related Syndromes and Clinical Perspective. *Hered Cancer Clin Pract* (2017) 15:9. doi: 10.1186/s13053-017-0069-6
35. Grant RC, Selander I, Connor AA, Selvarajah S, Borgida A, Briollais L, et al. Prevalence of Germline Mutations in Cancer Predisposition Genes in Patients With Pancreatic Cancer. *Gastroenterology* (2015) 148:556–64. doi: 10.1053/j.gastro.2014.11.042
36. Wong W, Raufi AG, Safyan RA, Bates SE, Manji GA. BRCA Mutations in Pancreas Cancer: Spectrum, Current Management, Challenges and Future Prospects. *Cancer Manag Res* (2020) 12:2731–42. doi: 10.2147/CMAR.S211151
37. Hu ZI, Shia J, Stadler ZK, Varghese AM, Capanu M, Salo-Mullen E, et al. Evaluating Mismatch Repair Deficiency in Pancreatic Adenocarcinoma: Challenges and Recommendations. *Clin Cancer Res* (2018) 24:1326–36. doi: 10.1158/1078-0432.CCR-17-3099
38. Murphy SJ, Hart SN, Halling GC, Johnson SH, Smadbeck JB, Drucker T, et al. Integrated Genomic Analysis of Pancreatic Ductal Adenocarcinomas Reveals Genomic Rearrangement Events as Significant Drivers of Disease. *Cancer Res* (2016) 76:749–61. doi: 10.1158/0008-5472.CAN-15-2198
39. Hingorani SR, Wang L, Multani AS, Combs C, Deramaudt TB, Hruban RH, et al. Trp53R127H and KrasG12D Cooperate to Promote Chromosomal Instability and Widely Metastatic Pancreatic Ductal Adenocarcinoma in Mice. *Cancer Cell* (2005) 7:469–83. doi: 10.1016/j.ccr.2005.04.023
40. Krebs AM, Mitschke J, Losada ML, Schmalhofer O, Boerries M, Busch H, et al. The EMTactivator Zeb1 is a Key Factor for Cell Plasticity and Promotes Metastasis in Pancreatic Cancer. *Nat Cell Biol* (2017) 19:518–42. doi: 10.1038/ncb3513
41. Rodriguez-Aznar E, Wiesmüller L, Sainz BJr, Hermann PC. EMT and Stemness-Key Players in Pancreatic Cancer Stem Cells. *Cancers (Basel)* (2019) 11:1136. doi: 10.3390/cancers11081136
42. Gaianigo N, Melisi D, Carbone C. EMT and Treatment Resistance in Pancreatic Cancer. *Cancers (Basel)* (2017) 9:122. doi: 10.3390/cancers9090122
43. Baghban R, Roshangar L, Jahanban-Esfahlan R, Seidi K, Ebrahimi-Kalan A, Jaymand M, et al. Tumor Microenvironment Complexity and Therapeutic Implications at a Glance. *Cell Commun Signal* (2020) 1 8:59. doi: 10.1186/s12964-020-0530-4
44. Kikuta K, Masamune A, Watanabe T, Ariga H, Itoh H, Hamada S, et al. Pancreatic Stellate Cells Promote Epithelial-Mesenchymal Transition in Pancreatic Cancer Cells. *Biochem Biophys Res Commun* (2010) 403:380–84. doi: 10.1016/j.bbrc.2010.11.040
45. Rucki AA, Zheng L. Pancreatic Cancer Stroma: Understanding Biology Leads to New Therapeutic Strategies. *World J Gastroenterol* (2014) 20:2237–46. doi: 10.3748/wjg.v20.i9.2237
46. Palumbo AJr, Da Costa Nde O, Bonamino MH, Pinto LF, Nasciutti LE. Genetic Instability in the Tumor Microenvironment: A New Look at an Old Neighbor. *Mol Cancer* (2015) 14:145. doi: 10.1186/s12943-015-0409-y
47. Pure E, Lo A. Can Targeting Stroma Pave the Way to Enhanced Antitumor Immunity and Immunotherapy of Solid Tumors? *Cancer Immunol Res* (2016) 4:269–78. doi: 10.1158/2326-6066.CIR-16-0011
48. Steele NG, Biffi G, Kemp SB, Zhang Y, Drouillard D, Syu L, et al. Inhibition of Hedgehog Signaling Alters Fibroblast Composition in Pancreatic Cancer. *Clin Cancer Res* (2021) 27(7);2023–37. doi: 10.1158/1078-0432.CCR-20-3715
49. Hwang RF, Moore T, Arumugam T, Ramachandran V, Amos KD, Rivera A, et al. Cancer-Associated Stromal Fibroblasts Promot Pancreatic Tumor Progression. *Cancer Res* (2008) 68:918–26. doi: 10.1158/0008-5472.CAN-07-5714
50. Gao Z, Wang X, Wu K, Zhao Y, Hu G. Pancreatic Stellate Cells Increase the Invasion of Human Pancreatic Cancer Cells Through the Stromal Cell-Derived Factor-1/CXCR4 Axis. *Pancreatology* (2010) 10:186–93. doi: 10.1159/000236012
51. Clark CE, Hingorani SR, Mick R, Combs C, Tuveson DA, Vonderheide RH. Dynamics of the Immune Reaction to Pancreatic Cancer From Inception to Invasion. *Cancer Res* (2007) 67:9518–27. doi: 10.1158/0008-5472.CAN-07-0175
52. Javadrashid D, Baghbanzadeh A, Hemmat N, Hajiasgharzadeh K, Nourbakhsh NS, Lotfi Z, et al. Envisioning the Immune System to Determine its Role in Pancreatic Ductal Adenocarcinoma: Culprit or Victim? *Immunol Lett* (2021) 232:48–59. doi: 10.1016/j.imlet.2021.02.009
53. Leinwand J, Miller G. Regulation and Modulation of Antitumor Immunity in Pancreatic Cancer. *Nat Immunol* (2020) 21:1152–9. doi: 10.1038/s41590-020-0761-y
54. Connor AA, Denroche RE, Jang GH, Timms L, Kalimuthu SN, Selander I, et al. Association of Distinct Mutational Signatures With Correlates of Increased Immune Activity in Pancreatic Ductal Adenocarcinoma. *JAMA Oncol* (2017) 3:774–83. doi: 10.1001/jamaoncol.2016.3916
55. Yachida S, Jones S, Bozic I, Antal T, Leary R, Fu B, et al. Distant Metastasis Occurs Late During the Genetic Evolution of Pancreatic Cancer. *Nature* (2010) 467:1114–7. doi: 10.1038/nature09515
56. Ansari D, Bauden M, Bergstrom S, Rylance R, Marko-Varga G, Andersson R. Relationship Between Tumour Size and Outcome in Pancreatic Ductal Adenocarcinoma. *Br J Surg* (2017) 104:600–7. doi: 10.18632/oncotarget.24019
57. Kulemann B, Rosch S, Seifert S, Timme S, Bronsert P, Seifert G, et al. Pancreatic Cancer: Circulating Tumor Cells and Primary Tumors Show Heterogeneous KRAS Mutations. *Sci Rep* (2017) 7:4510. doi: 10.1038/s41598-017-14870-3

58. Martini V, Timme-Bronsert S, Fichtner-Feigl S, Hoeppner J, Kulemann B. Circulating Tumor Cells in Pancreatic Cancer: Current Perspectives. *Cancers Basel* (2019) 11:1659. doi: 10.3390/cancers11111659
59. Pantel K, Speicher MR. The Biology of Circulating Tumor Cells. *Oncogene* (2016) 35:1216–24. doi: 10.1038/onc.2015.192
60. Hasanain A, Blanco BA, Yu J, Wolfgang CL. The Importance of Circulating and Disseminated Tumor Cells in Pancreatic Cancer. *Surg Open Sci* (2019) 1 (2):49–55. doi: 10.1016/j.sopen.2019.08.002
61. Ayres Pereira M, Chio IIC. Metastasis in Pancreatic Ductal Adenocarcinoma: Current Standing and Methodologies. *Genes Basel* (2019) 11:6. doi: 10.3390/genes11010006
62. Grünwald B, Harant V, Schaten S, Frühschütz M, Spallek R, Höchst B, et al. Pancreatic Premalignant Lesions Secrete Tissue Inhibitor of Metalloproteinases-1, Which Activates Hepatic Stellate Cells *via* CD63 Signaling to Create a Premetastatic Niche in the Liver. *Gastroenterology* (2016) 151:1011–24. doi: 10.1053/j.gastro.2016.07.043
63. Costa-Silva B, Aiello NM, Ocean AJ, Singh S, Zhang H, Thakur BK, et al. Pancreatic Cancer Exosomes Initiate Pre-Metastatic Niche Formation in the Liver. *Nat Cell Biol* (2015) 17:816–26. doi: 10.1038/ncb3169
64. Reichert M, Bakir B, Moreira L, Pitarresi JR, Feldmann K, Simon L, et al. Regulation of Epithelial Plasticity Determines Metastatic Organotropism in Pancreatic Cancer. *Dev Cell* (2018) 45:696–711.e8. doi: 10.1016/j.devcel.2018.05.025
65. Whatcott CJ, Diep CH, Jiang P, Watanabe A, LoBello J, Sima C, et al. Desmoplasia in Primary Tumors and Metastatic Lesions of Pancreatic Cancer. *Clin Cancer Res* (2015) 21:3561–8. doi: 10.1158/1078-0432.CCR-141051
66. Chaika NV, Yu F, Purohit V, Mehla K, Lazenby AJ, DiMaio D, et al. Differential Expression of Metabolic Genes in Tumor and Stromal Components of Primary and Metastatic Loci in Pancreatic Adenocarcinoma. *PloS One* (2012) 7:1–10. doi: 10.1371/journal.pone.0032996
67. Aiello NM, Bajor DL, Norgard RJ, Sahmoud A, Bhagwat N, Minh NP, et al. Metastatic Progression is Associated With Dynamic Changes in the Local Microenvironment. *Nat Commun* (2016) 7:12819. doi: 10.1038/ncomms12819
68. Connor AA, Denroche RE, Jang GH, Lemire M, Zhang A, Chan-Seng-Yue M, et al. Integration of Genomic and Transcriptional Features in Pancreatic Cancer Reveals Increased Cell Cycle Progression in Metastases. *Cancer Cell* (2019) 3 5:267–282.e7. doi: 10.1016/j.ccell.2018.12.010
69. Hasan S, Jacob R, Manne U, Paluri R. Advances in Pancreatic Cancer Biomarkers. *Oncol Rev* (2019) 13:410. doi: 10.4081/oncol.2019.410
70. Bergquist JR, Puig CA, Shubert CR, Groeschl RT, Habermann EB, Kendrick ML, et al. Carbohydrate Antigen 19-9 Elevation in Anatomically Resectable, Early Stage Pancreatic Cancer Is Independently Associated With Decreased Overall Survival and an Indication for Neoadjuvant Therapy: A National Cancer Database Study. *J Am Coll Surg* (2016) 223:52–65. doi: 10.1016/j.jamcollsurg.2016.02.009
71. Zhang Y, Yang J, Li H, Wu Y, Zhang H, Chen W, et al. Tumor Markers CA19-9, CA242 and CEA in the Diagnosis of Pancreatic Cancer: A Meta-Analysis. *Int J Clin Exp Med* (2015) 8:11683–91.
72. Gold DV, Gaedcke J, Ghadimi BM, Goggins M, Hruban RH, Liu M, et al. PAM4 Immunoassay Alone and in Combination With CA19-9 for the Detection of Pancreatic Adenocarcinoma. *Cancer* (2013) 119:522–8. doi: 10.1002/cncr.27762
73. Song J, Sokoll LJ, Pasay JJ, Rubin AL, Li H, Bach DM, et al. Identification of Serum Biomarker Panels for the Early Detection of Pancreatic Cancer. *Cancer Epidemiol Biomarkers Prev* (2019) 28:174–82. doi: 10.1158/1055-9965.EPI-18-0483
74. Rho SY, Lee SG, Park M, Lee J, Lee SH, Hwang HK, et al. Developing a Preoperative Serum Metabolome-Based Recurrence-Predicting Nomogram for Patients With Resected Pancreatic Ductal Adenocarcinoma. *Sci Rep* (2019) 9:18634. doi: 10.1038/s41598-019-55016-x
75. Ankeny JS, Court CM, Hou S, Li Q, Song M, Wu D, et al. Circulating Tumour Cells as a Biomarker for Diagnosis and Staging in Pancreatic Cancer. *Br J Cancer* (2016) 114:1367–75. doi: 10.1038/bjc.2016.121
76. Effenberger KE, Schroeder C, Hanssen A, Wolter S, Eulenburg C, Tachezy M, et al. Improved Risk Stratification by Circulating Tumor Cell Counts in Pancreatic Cancer. *Clin Cancer Res* (2018) 24:2844–50. doi: 10.1158/1078-0432.CCR-18-0120
77. Court CM, Ankeny JS, Sho S, Winograd P, Hou S, Song M, et al. Circulating Tumor Cells Predict Occult Metastatic Disease and Prognosis in Pancreatic Cancer. *Ann Surg Oncol* (2018) 25:1000–8. doi: 10.1245/s10434-017-6290-8
78. Poruk KE, Blackford AL, Weiss MJ, Cameron JL, He J, Goggins M, et al. Circulating Tumor Cells Expressing Markers of Tumor-Initiating Cells Predict Poor Survival and Cancer Recurrence in Patients With Pancreatic Ductal Adenocarcinoma. *Clin Cancer Res* (2017) 23:2681–90. doi: 10.1158/1078-0432.CCR-16-1467
79. Jaworski JJ, Morgan RD, Sivakumar S. Circulating Cell-Free Tumour DNA for Early Detection of Pancreatic Cancer. *Cancers Basel* (2020) 12:3704. doi: 10.3390/cancers12123704
80. Lee B, Lipton L, Cohen J, Tie J, Javed AA, Li L, et al. Circulating Tumor DNA as a Potential Marker of Adjuvant Chemotherapy Benefit Following Surgery for Localized Pancreatic Cancer. *Ann Oncol* (2019) 30:1472–8. doi: 10.1093/annonc/mdz200
81. Hussung S, Akhoundova D, Hipp J, Follo M, Klar RFU, Philipp U, et al. Longitudinal Analysis of Cell-Free Mutated KRAS and CA 19-9 Predicts Survival Following Curative Resection of Pancreatic Cancer. *BMC Cancer* (2021) 21:49. doi: 10.1186/s12885-020-07736-x
82. Yee NS, Zhang S, He HZ, Zheng SY. Extracellular Vesicles as Potential Biomarkers for Early Detection and Diagnosis of Pancreatic Cancer. *Biomedicines* (2020) 8:581. doi: 10.3390/biomedicines8120581
83. Ventriglia J, Petrillo A, Huerta Alváro M, Laterza MM, Savastano B, Gambardella V, et al. Neutrophil to Lymphocyte Ratio as a Predictor of Poor Prognosis in Metastatic Pancreatic Cancer Patients Treated With Nab-Paclitaxel Plus Gemcitabine: A Propensity Score Analysis. *Gastroenterol Res Pract* (2018) 2018:2373868. doi: 10.1155/2018/2373868
84. Stotz M, Gerger A, Eisner F, Szkandera J, Loibner H, Ress AL, et al. Increased Neutrophil-Lymphocyte Ratio is a Poor Prognostic Factor in Patients With Primary Operable and Inoperable Pancreatic Cancer. *Br J Cancer* (2013) 109:416–21. doi: 10.1038/bjc.2013.332
85. Smith RA, Bosonnet L, Raraty M, Sutton R, Neoptolemos JP, Campbell F, et al. Preoperative Platelet-Lymphocyte Ratio is an Independent Significant Prognostic Marker in Resected Pancreatic Ductal Adenocarcinoma. *Am J Surg* (2009) 197:466–72. doi: 10.1016/j.amjsurg.2007.12.057
86. Jomrich G, Gruber ES, Winkler D, Hollenstein M, Gnant M, Sahora K, et al. Systemic Immune-Inflammation Index (SII) Predicts Poor Survival in Pancreatic Cancer Patients Undergoing Resection. *J Gastrointest Surg* (2020) 24:610–8. doi: 10.1007/s11605-019-04187-z
87. Kim N, Han IW, Ryu Y, Hwang DW, Heo JS, Choi DW, et al. Predictive Nomogram for Early Recurrence After Pancreatectomy in Resectable Pancreatic Cancer: Risk Classification Using Preoperative Clinicopathologic Factors. *Cancers Basel* (2020) 12:137. doi: 10.3390/cancers12010137
88. Martinelli P, Carrillo-de-Santa Pau E, Cox T, Sainz BJ, Dusetti N, Greenhalf W, et al. GATA6 Regulates EMT and Tumour Dissemination and is a Marker of Response to Adjuvant Chemotherapy in Pancreatic Cancer. *Gut* (2017) 66:1665–76. doi: 10.1136/gutjnl-2015-311256
89. Collisson EA, Sadanandam A, Olson P, Gibb WJ, Truitt M, Gu S, et al. Subtypes of Pancreatic Ductal Adenocarcinoma and Their Differing Responses to Therapy. *Nat Med* (2011) 17:500–3. doi: 10.1038/nm.2344
90. Moffitt RA, Marayati R, Flate EL, Volmar KE, Herrera Loeza SG, Hoadley KA, et al. Virtual Microdissection Identifies Distinct Tumor- and Stroma-Specific Subtypes of Pancreatic Ductal Adenocarcinoma. *Nat Genet* (2015) 47:1168–78. doi: 10.1038/ng.3398
91. O'Kane GM, Grunwald B, Jang G, Masoomian M, Picardo S, Grant RC, et al. GATA6 Expression Distinguishes Classical and Basal-Like Subtypes in Advanced Pancreatic Cancer. *Clin Cancer Res* (2020) 6:4901–10. doi: 10.1158/1078-0432.CCR-19-3724
92. Greenhalf W, Ghane P, Neoptolemos JP, Palmer DH, Cox TF, Lamb RF, et al. Pancreatic Cancer Hent1 Expression and Survival From Gemcitabine in Patients From the ESPAC-3 Trial. *JNCI* (2013) 106:djt347. doi: 10.1093/jnci/djt347
93. Shin DW, Kim MJ, Yang SY, Lee J, Hwang J. Adjuvant Gemcitabine Versus 5-Fluorouracil/Folinic Acid Based on Hent1 Immunostaining in Curative

Resected Pancreatic Adenocarcinoma: A Biomaker Stratified Trial. *JCO* (2019) 37:308–8. doi: 10.1200/JCO.2019.37.4_suppl.308
94. Randazzo O, Papini F, Mantini G, Gregori A, Parrino B, Liu DSK, et al. "Open Sesame?": Biomarker Status of the Human Equilibrative Nucleoside Transporter-1 and Molecular Mechanisms Influencing its Expression and Activity in the Uptake and Cytotoxicity of Gemcitabine in Pancreatic Cancer. *Cancers (Basel)* (2020) 12(11):3206. doi: 10.3390/cancers12113206
95. Spratlin JL, Mackey JR. Human Equilibrative Nucleoside Transporter 1 (Hent1) in Pancreatic Adenocarcinoma: Towards Individualized Treatment Decisions. *Cancers (Basel)* (2010) 2(4):2044–54. doi: 10.3390/cancers2042044
96. Nicolle R, Gayet O, Duconseil P, Vanbrugghe C, Roques J, Bigonnet M, et al. A Transcriptomic Signature to Predict Adjuvant Gemcitabine Sensitivity in Pancreatic Adenocarcinoma. *Ann Onc* (2021) 32:250–60. doi: 10.1016/j.annonc.2020.10.601
97. Chan-Seng-Yue M, Jaeseung CK, Wilson GW, Karen NG, Figueroa EF, O'Kane GM, et al. Transcription Phenotypes of Pancreatic Cancer are Driven by Genomic Events During Tumor Evolution. *Nat Genet* (2020) 52:231–40. doi: 10.1038/s41588-019-0566-9
98. Moore MJ, Golstein D, Hamm J, Figer A, Hecht JR, Gallinger S, et al. Erlotinib Plus Gemcitabine Compared With Gemcitabine Alone in Patients With Advanced Pancreatic Cancer: A Phase III Trial of the National Cancer Institute of Canada Clinical Trials Group. *JCO* (2007) 25:1960–6. doi: 10.1200/JCO.2006.07.9525
99. Oliveira-Cunha M, Newman WJ, Siriwardena AK. Epidermal Growth Factor Receptor in Pancreatic Cancer. *Cancers Basel* (2011) 3:1513–26. doi: 10.3390/cancers3021513
100. Ross A, Winter KA, Safran H, Goodman KA, Regine WF, Berger AC, et al. Results of the NRG Oncology/RTOG 0848 Adjuvant Chemotherapy Question—Erlotinib+Gemcitabine for Resected Cancer of the Pancreatic Head A Phase II Randomized Clinical Trial. *Am J Clin Oncol* (2020) 43:173–9. doi: 10.1097/COC.0000000000000633
101. Hoyer K, Hablesreiter R, Inoue Y, Yoshida K, Briest F, Christen F, et al. A Genetically Defined Signature of Responsiveness to Erlotinib in Early-Stage Pancreatic Cancer Patients: Results From the CONKO-005 Trial. *EBioMedicine* (2021) 66:103327. doi: 10.1016/j.ebiom.2021.103327
102. Waddell N, Pajic M, Patch AM, Chang DK, Kassahn KS, Bailey P, et al. Whole Genomes Redefine the Molecular Landscape of Pancreatic Cancer. *Nature* (2015) 518:495–501. doi: 10.1038/nature14169
103. Golan T, Hammel P, Reni M, Van Cutsem E, Maraculla T, Hall MJ, et al. Maintenance Olaparib for Germline BRCA-Mutated Metastatic Pancreatic Cancer. *N Engl J Med* (2019) 381:317–27. doi: 10.1056/NEJMoa1903387
104. Sohal D, McDonough S, Ahmad SA, Gandhi N, Beg M, Wang-Gillam A, et al. SWOG S1505: Initial Findings on Eligibility and Neoadjuvant Chemotherapy Experience With Mfolfirinox Versus Gemcitabine/Nab-Paclitaxel for Resectable Pancreatic Adenocarcinoma. *JCO* (2019) 37:414. doi: 10.1200/JCO.2019.37.4_suppl.414
105. Skau Rasmussen L, Vittrup B, Ladekarl M, Pfeiffer P, Karen Yilmaz M, Østergaard Poulsen L, et al. The Effect of Postoperative Gemcitabine on Overall Survival in Patients With Resected Pancreatic Cancer: A Nationwide Population-Based Danish Register Study. *Acta Oncol* (2019) 58:864–71. doi: 10.1080/0284186X.2019.1581374
106. Reni M, Balzano G, Zanon S, Zerbi A, Rimassa L, Castoldi R, et al. Safety and Efficacy of Preoperative or Postoperative Chemotherapy for Resectable Pancreatic Adenocarcinoma (PACT-15): A Randomized, Open-Label, Phase 2-3 Trial. *Lancet Gastroenterol Hepatol* (2018) 3(6):30094–3. doi: 10.1016/S2468-1253(18)30081-5
107. Roland CL, Katz MHG, Tzeng C-WD, Lin H, Varadhachary GR, Shroff R, et al. The Addition of Postoperative Chemotherapy is Associated With Improved Survival in Patients With Pancreatic Cancer Treated With Preoperative Therapy. *Ann Surg Oncol* (2015) 22:1221–8. doi: 10.1245/s10434-015-4854-z
108. Van Roessel S, van Veldhuisen E, Klompmaker S, Janssen QP, Abu Hilal M, Alseidi A, et al. Evaluation of Adjuvant Chemotherapy in Patients With Resected Pancreatic Cancer After Neoadjuvant FOLFIRINOX Treatment. *JAMA Oncol* (2020) 6:1–8. doi: 10.1001/jamaoncol.2020.3537
109. *A Phase 0, Pre-Operative, Window-Of-Opportunity Study to Assess Gene Expression in Patients With Resectable, Locally Advanced, or Metastatic Pancreatic Cancer (NEOPANC-01)*. Available at: https://pancreaticcancercanada.ca/press-release-neopancone-clinical-trial-launch/.
110. Luchini C, Brosens L, Wood D, Chatterjee D, Shin J, Sciammarella C, et al. Comprehensive Characterisation of Pancreatic Ductal Adenocarcinoma With Microsatellite Instability: Histology, Molecular Pathology and Clinical Implications. *Gut* (2021) 70:148–56. doi: 10.1136/gutjnl-2020-320726
111. Le DT, Uram JM, Wang H, Bartlett BR, Kerberling H, Eyring AD, et al. PD-1 Blockade in Tumors With Mismatch-Repair Deficiency. *N Engl J Med* (2015) 372:2509–20. doi: 10.1056/NEJMoa1500596
112. Marabelle A, Le DT, Ascierto PA, Di Giacomo AM, De Jesus-Acosta A, Delord JP, et al. Efficacy of Pembrolizumab in Patients With Noncolorectal High Microsatellite Instability/Mismatch Repair-Deficient Cancer: Results From the Phase II KEYNOTE-158 Study. *JCO* (2020) 38:1–10. doi: 10.1200/JCO.19.02105
113. Pompella L, Tirino G, Pappalardo A, Caterino M, Ventriglia A, Nacca V, et al. Pancreatic Cancer Molecular Classifications: From Bulk Genomics to Single Cell Analysis. *Int J Mol Sci* (2020) 21:2814. doi: 10.3390/ijms21082814
114. *Pancreatic Tumor Cell Vaccine (GVAX), Low Dose Cyclophosphamide, Fractionated Stereotactic Body Radiation Therapy (SBRT), and FOLFIRINOX Chemotherapy in Patients With Resected Adenocarcinoma of the Pancreas*. Available at: https://www.clinicaltrials.gov/ct2/show/NCT01595321.
115. Samaras p, Tusup M, Nguyen-Kim TDL, Seifurt B, Bachmann H, von Moos R, et al. Phase I Study of a Chloroquine-Gemcitabine Combination in Patients With Metastatic or Unresectable Pancreatic Cancer. *Cancer Chemother Pharmacol* (2017) 80:1005–12. doi: 10.1007/s00280-017-3446-y
116. Karasic TB, O'hara M, Loaiza-Bonilla A, Reiss KA, Teitelbaum UR, Borazanci E, et al. Effect of Gemcitabine and Nab-Paclitaxel With or Without Hydroxychloroquine on Patients With Advanced Pancreatic Cancer A Phase 2 Randomized Clinical Trial. *JAMA Oncol* (2019) 5:993–8. doi: 10.1001/jamaoncol.2019.0684
117. Janssen QP, Buettner S, Suker M, Beumer BR, Addeo P, Bachellier P, et al. Neoadjuvant FOLFIRINOX in Patients With Borderline Resectable Pancreatic Cancer: A Systematic Review and Patient-Level Meta-Analysis. *J Natl Cancer Inst* (2019) 111:782–94. doi: 10.1093/jnci/djz073
118. Suker M, Beumer BR, Sadot E, Marthey L, Faris JE, Mellon EA, et al. FOLFIRINOX for Locally Advanced Pancreatic Cancer: A Systematic Review and Patient-Level Meta-Analysis. *Lancet Oncol* (2016) 1 7:801–10. doi: 10.1016/S1470-2045(16)00172-8
119. Cascinu S, Berardi R, Bianco R, Bilancia D, Zaniboni A, Ferrari D, et al. Nab-Paclitaxel (Nab) Plus Gemcitabine (G) Is More Effective Than G Alone in Locally Advanced, Unresectable Pancreatic Cancer (LAUPC): The GAP Trial, a GISCAD Phase II Comparative Randomized Trial. *Ann Oncol* (2019) 30:253–v254. doi: 10.1093/annonc/mdz247.001
120. Philip PA, Lacy J, Portales F, Sobrero A, Pazo-Cid R, Manzano Mozo JL, et al. Nab-Paclitaxel Plus Gemcitabine in Patients With Locally Advanced Pancreatic Cancer (LAPACT): A Multicentre, Open-Label Phase 2 Study. *Lancet Gastroenterol Hepatol* (2020) 5:285–94. doi: 10.1016/S2468-1253(19)30327-9
121. Mukherjee S, Hurt CN, Bridgewater J, Falk S, Cummins S, Wasan H, et al. Gemcitabine-Based or Capecitabine-Based Chemoradiotherapy for Locally Advanced Pancreatic Cancer (SCALOP): A Multicentre, Randomised, Phase 2 Trial. *Lancet Oncol* (2013) 14:317–26. doi: 10.1016/S1470-2045(13)70021-4
122. Hammel P, Huguet F, van Laethem JL, Goldstein D, Glimelius B, Artru P, et al. Effect of Chemoradiotherapy *vs* Chemotherapy on Survival in Patients With Locally Advanced Pancreatic Cancer Controlled After 4 Months of Gemcitabine With or Without Erlotinib: The LAP07 Randomized Clinical Trial. *JAMA* (2016) 315:1844–53. doi: 10.1001/jama.2016.4324
123. Williet N, Petrillo A, Roth G, Ghidini M, Petrova M, Forestier J, et al. Gemcitabine/Nab-Paclitaxel Versus FOLFIRINOX in Locally Advanced Pancreatic Cancer: A European Multicenter Study. *Cancers* (2021) 13:2797. doi: 10.3390/cancers13112797
124. Versteijne E, Suker M, Groothuis K, Akkermans-Vogelaar JM, Besselink MG, Bonsing BA, et al. Preoperative Chemoradiotherapy Versus Immediate Surgery for Resectable and Borderline Resectable Pancreatic Cancer: Results

of the Dutch Randomized Phase III PREOPANC Trial. *JCO* (2020) 38:1763–73. doi: 10.1200/JCO.19.02274

125. Lee JS, Rhee TM, Pietrasz D, Bachet JB, Laurent-Puig P, Kong SY, et al. Circulating Tumor DNA as a Prognostic Indicator in Resectable Pancreatic Ductal Adenocarcinoma: A Systematic Review and Meta-Analysis. *Sci Rep* (2019) 18;9(1):16971. doi: 10.1038/s41598-019-53271-6
126. Hewitt DB, Nissen N, Hatoum H, Musher B, Seng J, Coveler AL, et al. A Phase III Trial of Chemotherapy With or Without Algenpantucel-L (HyperAcute-Pancreas) Immunotherapy in Subjets With Bordeline Resectable or Locally Advance Unresectable Pancreatic Cancer. *Ann Sur* (2020). doi: 10.1097/SLA0000000000004669
127. Hardacre JM, Mulcahy M, Small W, Talamonti M, Obel J, Krishnamurthi S, et al. Addition of Algenpantucel-L Immunotherapy to Standard Adjuvant Therapy for Pancreatic Cancer: A Phase 2 Study. *J Gastrointest Surg* (2013) 17:94–100; discussion p. 100-1. doi: 10.1007/s11605-012-2064-6
128. *Th-1 Dendritic Cell Immunotherapy Plus Standard Chemotherapy for Pancreatic Adenocarcinoma (DECIST)*. Available at: https://clinicaltrials.gov/ct2/show/NCT04157127.
129. *Pooled Mutant KRAS-Targeted Long Peptide Vaccine Combined With Nivolumab and Ipilimumab for Patients With Resected MMR-P Colorectal and Pancreatic Cancer* . Available at: https://clinicaltrials.gov/ct2/show/NCT0411708707/s11605-012-2064-6.
130. *Prognostic Role of Circulating Tumor DNA in Resectable Pancreatic Cancer*. Available at: https://clinicaltrials.gov/ct2/show/NCT04246203.

Conflict of Interest: EG had personal fees from Novartis. GT received a travel grant from Servier, Italfarmaco, advisory board: Eli-Lilly. BD received personal fees from Ipsen, Eisai, Eli Lilly, Astra Zeneca, Sanofi, MSD, Bayer, Roche, and Amgen. FV: Scientific consultancy: Servier, Lilly, MSD and BMS; honoraria for speaking: Roche, Bayer, Servier, Lilly, Astellas, MSD and BMS. APe had personal fees with Eli-Lilly, Servier, and MSD. No fees are connected with the submitted paper.

The remaining authors declare that the research was conducted in the absence of any commercial or financial relationships that could be construed as a potential conflict of interest.

frontiers in Oncology

ORIGINAL RESEARCH
published: 19 August 2021
doi: 10.3389/fonc.2021.714527

Fluorescence Imaging Using Enzyme-Activatable Probes for Real-Time Identification of Pancreatic Cancer

Ryugen Takahashi[1], Takeaki Ishizawa[1], Masumitsu Sato[1], Yoshinori Inagaki[1], Mariko Takanka[2], Yugo Kuriki[3], Mako Kamiya[4], Tetsuo Ushiku[2], Yasuteru Urano[3,4] and Kiyoshi Hasegawa[1]**

[1] Hepato-Biliary-Pancreatic Surgery Division, Department of Surgery, Graduate School of Medicine, University of Tokyo, Tokyo, Japan, [2] Department of Pathology, Graduate School of Medicine, The University of Tokyo, Tokyo, Japan, [3] Laboratory of Chemistry and Biology, Graduate School of Pharmaceutical Sciences, The University of Tokyo, Tokyo, Japan, [4] Laboratory of Chemical Biology and Molecular Imaging, Graduate School of Medicine, The University of Tokyo, Tokyo, Japan

OPEN ACCESS

Edited by:
Takatsugu Ishimoto,
Kumamoto University, Japan

Reviewed by:
Kazumichi Kawakubo,
Hokkaido University Hospital, Japan
Tatsunori Miyata,
Cleveland Clinic, United States

***Correspondence:**
Kiyoshi Hasegawa
kihase-tky@umin.ac.jp
Yasuteru Urano
uranokun@m.u-tokyo.ac.jp

Specialty section:
This article was submitted to Gastrointestinal Cancers, a section of the journal Frontiers in Oncology

Received: 25 May 2021
Accepted: 04 August 2021
Published: 19 August 2021

Citation:
Takahashi R, Ishizawa T, Sato M, Inagaki Y, Takanka M, Kuriki Y, Kamiya M, Ushiku T, Urano Y and Hasegawa K (2021) Fluorescence Imaging Using Enzyme-Activatable Probes for Real-Time Identification of Pancreatic Cancer. Front. Oncol. 11:714527. doi: 10.3389/fonc.2021.714527

Introduction: Radical resection is the only curative treatment for pancreatic cancer, which is a life-threatening disease. However, it is often not easy to accurately identify the extent of the tumor before and during surgery. Here we describe the development of a novel method to detect pancreatic tumors using a tumor-specific enzyme-activatable fluorescence probe.

Methods: Tumor and non-tumor lysate or small specimen collected from the resected specimen were selected to serve as the most appropriate fluorescence probe to distinguish cancer tissues from noncancerous tissues. The selected probe was sprayed onto the cut surface of the resected specimen of cancer tissue to acquire a fluorescence image. Next, we evaluated the ability of the probe to detect the tumor and calculated the tumor-to-background ratio (TBR) by comparing the fluorescence image with the pathological extent of the tumor. Finally, we searched for a tumor-specific enzyme that optimally activates the selected probe.

Results: Using a library comprising 309 unique fluorescence probes, we selected GP-HMRG as the most appropriate activatable fluorescence probe. We obtained eight fluorescence images of resected specimens, among which four approximated the pathological findings of the tumor, which achieved the highest TBR. Finally, dipeptidyl-peptidase IV (DPP-IV) or a DPP-IV-like enzyme was identified as the target enzyme.

Conclusion: This novel method may enable rapid and real-time visualization of pancreatic cancer through the enzymatic activities of cancer tissues.

Keywords: pancreatic cancer, pancreatectomy, fluorescence imaging, activatable probe, intraoperative diagnosis, dipeptidyl peptidase-IV (DPP-IV)

INTRODUCTION

Pancreatic cancer is a major life-threatening disease (1–4). Despite recent advances in chemotherapy and radiotherapy, complete resection remains the only curative treatment (5–7). However, it is often difficult to accurately identify the boundaries of cancer tissues during surgery, which may lead to incomplete removal of cancer tissues and unfavorable postoperative survival (6, 7). For patients administered preoperative chemo(radio) therapy (8, 9), it is particularly difficult to identify viable cancer tissues, even in pathological examinations of resected specimens (10).

In 2011, Urano et al. reported a novel fluorescence imaging technique using an "activatable" probe, which is initially nonfluorescent but emits fluorescence immediately after its hydrolysis by γ-glutamyltranspeptidase overexpressed specifically in various cancer cells (11). Subsequently, more than 400 activatable fluorescence probes comprising amino acid or sugar residues that serve as a reactive moiety and target the aminopeptidase or glucosidase have been developed. Furthermore, fluorescently activatable scaffolds such as hydroxymethyl rhodamine-green (HMRG) or hydroxymethyl rhodol with trifluoroethyl group (HMRef) were developed (12), enabling visualization of breast cancer (12–14), esophageal cancer (15, 16), liver cancer (17), lung cancer (18), head and neck cancer (19, 20), colorectal cancer (21), thyroid cancer (22), and glioblastoma (23). Regarding real-time imaging of pancreatic cancer, other approaches using activatable probes can be indicated (24–26), albeit applications of these techniques to fresh human samples have not yet been reported. Here we searched for activatable fluorescence probes for real-time identification of viable pancreatic cancer tissues in resected specimens.

MATERIAL AND METHODS

The Institutional Review Board of the University of Tokyo Hospital approved this study [IRB No. 2957- (11)].

Sample Collection

Fresh tissue samples were collected from resected specimens of patients who underwent radical pancreatectomy for pancreatic adenocarcinoma from April 2017 to December 2020. Written informed consent was obtained from all patients. For the primary and secondary probe selection, 3-5 mm-in-size tissue fragments were obtained from obvious cancerous regions and non-cancerous pancreatic parenchyma with confirmation by the pathologist (M.T.), just after the removal of pancreatic specimens.

Primary Probe Selection

In this study, totally 309 dipeptides-HMRG fluorescence probes were used from our probe library. The concept and synthetic methods of these probes have been described elsewhere (12). Briefly, these probes were synthesized by placing an amino-acid residue selected from 21 amino-acids at P1 and P2 position of Xaa(P2)-Yaa(P1)-HMRG (**Supplementary Table 1**). Among the chemically stable compounds, candidate fluorescence probes were first selected using lysates prepared from cancer and noncancerous tissue samples (12, 15, 23). Briefly, the tissue cut by scissors were homogenized with 1.0 mL of T-per tissue protein in a Lysing Matrix D. After the centrifuge (1,000 rpm x 5 min at 4°C), the supernatant was collected as the lysate. Then, 5 μL of the lysate (0.20 mg/mL protein) was added to the wells of a black 384-well plate, each containing 15 μL of each candidate probe from a library of dipeptide-HMRG compounds (23). The final concentrations of a candidate probe and lysate protein were 1.0 μM and 0.050 mg/dL, respectively. The fluorescence intensity (FI) of each sample was measured using an Envision Multilabel Plate Reader (PerkinElmer, Massachusetts, USA) 0–60 min after the addition of lysates at 37°C. The excitation and emission wavelengths were 485 nm and 535 nm, respectively. The increase of FI was calculated as follows:

$$(FI\ increase) = (FI\ at\ 60\ min) - (FI\ at\ 0\ min)$$

Then, we calculated the difference and the ratio of FI increase between cancer and noncancer lysates, and the probes of which difference or ratio represented the ≥ 90th percentile of all probes was subjected to subsequent evaluations.

Secondary Probe Selection

Candidate fluorescence probes were sprayed directly onto a few millimeters of cancer tissues and noncancerous tissues placed in an eight-well plate. The cancerous and noncancerous tissues were collected as the same way as the primary probe selection, and divided into smaller specimen by scissors respectively. When the size of original tissue samples was insufficient for creating 6 fragments, fluorescence imaging was performed prioritizing candidate probes with better outcomes in the primary screening. The concentration and volume of each fluorescence probe was 50 μM and 200 μL, respectively. Images of fluorescence were obtained using the Maestro *in Vivo* Imaging System (PerkinElmer, Massachusetts, USA), with the blue filter settings (excitation and emission wavelengths of 435–480 nm and 490 nm long pass), respectively, acquired 0 (before), 1, 3, 5, 10, 15, 20, 25, and 30 min after the administration of fluorescence probes. FI was calculated by subtracting the average in the region of interest (ROI) at 1 min from that at 30 min, according to the fluorescence images extracted at 540 nm. Finally, candidate fluorescence probes were refined according to the difference in contrast of FI between cancer tissues and noncancerous tissues.

Macroscopic Evaluation of Cancer Using Whole Surgical Specimens

Immediately after pancreatic resection, the whole specimen was cut to include the maximum diameter of pancreatic cancer tissues. The selected florescence probe (4 mL, 50 μM solution) was sprayed directly onto the cut surfaces, followed by fluorescence imaging using the Maestro *in Vivo* imaging System, as described above. The accuracy of fluorescence imaging to delineate pancreatic cancer was evaluated by a surgeon (R.T.) and a pathologist (M.T.) with reference to histopathological findings of the same planes. The tumor-to-

background ratio (TBR) was calculated as the increase in the mean FI from 1 min to 30 min after administration of the probe to cancer tissues and noncancerous pancreatic tissues, as follows:

$$TBR = \frac{FI\ increase\ of\ the\ cancerous\ tissue}{FI\ increase\ of\ the\ non-cancerous\ tissue}$$

The data were obtained using the Maestro *In Vivo* Imaging System, described above, according to macro- and microscopic pathological findings of the cut surfaces and their corresponding fluorescence images.

Exploration of Target Enzymes

Through the probe screening process, dipeptidyl peptidases were suspected as target enzymes that may be overexpressed specifically in pancreatic cancer tissues. Thus, we first confirmed the ability of DPP-IV and related enzymes to activate candidate fluorescence probes by measuring changes of FI for 1,000 seconds after the addition of human recombinant DPP-IV (0.040 units; D4943, Sigma-Aldrich), DPP-VIII (1.0 μg; ab162872, abcam), or DPP-IX (1.0 μg; ab79621, abcam) to 3.0 mL of probe (1.0 μM) using the F-7000 Hitachi Fluorescence Spectrophotometer (Hitachi, Tokyo, Japan). The excitation and emission wavelengths were 495 nm and 525 nm, respectively. FI in the cancer tissues used in the secondary screening were also measured after administration of DPP-IV inhibitor (K579, CalbioChem) at a dose of 100 μM. Finally, the expression of DPP-IV on cut surfaces of whole surgical specimens was evaluated using immunohistochemical (IHC) analysis with an anti-DPP-IV mouse monoclonal antibody (TA500733; Origene Technologies Inc, Rockville, MD). Antigen retrieval was performed at 110°C for 15 min. The anti-DPP-IV antibody was diluted 1:100, and the tissues were incubated overnight at 4°C. The IHC results were evaluated by a pathologist (M.T.) uninformed about the outcomes of fluorescence imaging.

RESULTS

Primary and Secondary Probe Selection

Primary selection of fluorescence probes employed lysates prepared from five resected specimens, leading to the identification of candidate probes from 309 fluorescence probes (**Supplementary Table 1**). When the differences and ratios of FI increase between cancer and non-cancer lysates were calculated (**Supplementary Table 2**), 14 out of the 19 HMRG-based fluorescence probes with dipeptides with a prolyl residue at the P1 position (XaaP-HMRG) ranked in the upper 90 percentile (**Figure 1A**). Based not only on the FI differences/ratios but also probe stability and the absolute values of FI increase in non-cancer lysates, which could decrease cancer detectability on tissue samples, AcKP- (Acetylated Lysine-Proline-), EP- (Glutamate-Proline-), GP- (Glycine-Proline-), LP- (Leucine-Proline-), PP (Proline-Proline), and YP-HMRG (Tyrosine-Proline-HMRG) were selected in this study (**Figure 1B**) for the second screening using fresh tissue fragments obtained from 11 patients with pancreatic adenocarcinoma. As a result, fluorescence imaging using GP-HMRG yielded the highest intensity differences in FI after 30 min between cancer and noncancerous tissues [median (range), 3.49 (1.03–8.11) a.u. *vs* 1.12 (0.42–2.09) a.u., P = 0.002; Wilcoxon's rank-sum test] (**Figures 1C, D**). GP-HMRG was therefore selected to evaluate fluorescence imaging to specifically detect cancer tissues in whole surgical specimens. Demographic background of the totally 16 patients who provided lysates or tissue samples were demonstrated in **Supplementary Table 3**.

Fluorescence Imaging of Whole Surgical Specimens Using GP-HMRG

Detection of cancer tissues using fluorescence imaging was evaluated by spraying GP-HMRG onto cut surfaces of whole surgical specimens immediately after resection of eight patients with pancreatic adenocarcinoma. Patients' demographic characteristics are summarized in **Table 1**. Neoadjuvant chemotherapy with gemcitabine and nab-paclitaxel was indicated to two patients who underwent surgery. Three patients were treated for diabetes mellitus but were not preoperatively administered DPP-IV inhibitors.

The median TBR of the fluorescence images following the administration of GP-HMRG was 1.96 (range, 1.13–3.44). In five patients with TBRs ranging from 1.93 to 3.44, fluorescence signals in cancer tissues were nearly homogenous and grossly discriminable from the surrounding pancreatic tissues (**Figure 2**). In the remaining three patients, including two who underwent preoperative chemotherapy, cancer tissues emitted heterogenous fluorescence signals, making it difficult to discriminate them from noncancer tissues (**Figure 3**). Fluorescence imaging identified a significant signal increase (TBR, 2.04) in the connective tissues surrounding the splenic artery of one patient in the latter group, which pathological examination subsequently diagnosed as perineural and lymphatic infiltration by viable cancer cells, while the main tumor included fibrosis and mucinous changes with a few viable cancer cells (TBR, 1.13), likely caused by preoperative chemotherapy (**Figure 4**).

Identification of Target Enzymes That Activate GP-HMRG

The *in vitro* fluorescence spectrum of GP-HMRG after adding DPPs indicated that the probe was converted to highly fluorescent HMRG upon reaction with DPP-IV and DPP-IX (**Figure 5**). On the cancer tissue specimens used in the secondary screening (available in 4 cases), FI increase was markedly suppressed when GP-HMRG was administered with the inhibitor (**Figure 6**). In contrast, IHC analysis of the resected specimens of eight patients did not detect an unambiguous difference in the expression levels of DPP-IV between cancer and surrounding pancreatic tissues (**Figures 2**–**4**).

DISCUSSION

Here we screened GP-HMRG, among 309 candidates of activatable fluorescence probes, for its ability to specifically

A

P1 \ P2	G	E	K	Y	L	P	a	d	s	b	sarcosine	-	Ac	AcG	AcE	AcK	AcY	AcL	AcP
G	0.59	0.67	0.57	0.66	0.62	0.35	0.91	0.65	-0.50	0.79	0.01	0.34	0.71	0.41	0.71	0.66	0.40	0.78	0.71
E	-1.58	0.67	0.84	0.57	1.10	-0.67	0.62	0.76	0.40	0.26	0.45	1.74	1.71	0.77	0.66	0.66	0.74	0.64	0.59
K	0.88	1.71	1.54	1.79	2.02	0.96	0.31	0.76	0.94	-0.29	0.47	1.43	1.36	0.50	-0.09	1.04	3.30	1.42	1.58
Y	0.62	0.99	1.95	1.44	1.45	0.69	0.45	-0.60	0.46	-0.36	0.41	1.00	0.12	-0.20	-0.21	0.65	0.37	-0.36	-0.03
L	0.77	2.60	1.00	1.54	1.59	0.86	0.74	0.30	0.76	0.63	0.68	1.45	1.28	0.43	-1.33	1.15	1.21	0.90	0.62
P	2.09	2.14	1.71	1.70	1.81	1.77	0.74	0.77	0.86	5.95	2.52	2.80	0.34	2.90	2.71	2.11	1.66	1.96	2.26
F	0.64	1.02	1.37	1.37	1.32	1.00	-	-	-	-	-	1.21	1.98	0.43	0.22	0.55	0.30	0.29	0.27
R	0.85	2.72	1.24	1.30	1.60	0.81	-	-	-	-	-	1.23	1.12	0.78	0.99	0.98	1.00	0.99	1.00
A	0.53	1.73	1.80	1.91	1.71	0.69	-	-	-	-	-	1.29	1.24	-0.13	0.91	0.64	0.54	0.76	-0.25
H	0.87	0.67	0.99	1.11	0.96	0.85	-	-	-	-	-	0.85	0.21	0.70	0.81	0.91	0.40	0.44	0.62
W	0.64	1.24	2.21	1.04	1.41	0.64	-	-	-	-	-	1.22	0.50	1.82	0.22	0.55	0.99	0.95	0.18
S	0.25	0.71	-0.25	0.21	0.54	0.24	-	-	-	-	-	0.95	2.42	0.09	0.10	-0.34	0.04	-0.82	0.52
M	0.83	2.47	1.68	1.48	1.38	0.97	-	-	-	-	-	1.05	2.27	-0.18	-0.34	1.63	1.75	1.39	0.58
Mo	0.82	1.72	2.10	0.56	0.42	0.67	-	-	-	-	-	0.74	0.64	0.57	0.72	-0.44	2.20	-0.15	0.12
Q	0.38	-0.35	0.41	0.37	0.36	0.33	-	-	-	-	-	0.52	0.28	0.42	0.73	0.68	0.41	0.42	0.54
N	0.27	0.51	0.06	0.83	1.06	0.18	-	-	-	-	-	1.04	1.48	0.53	0.65	0.35	0.56	-0.85	0.53
a	0.17	0.64	-0.29	0.67	-0.01	0.66	0.76	0.70	0.77	0.77	0.55	-	-	-	-	-	-	-	-
d	0.24	0.70	0.72	0.63	0.53	0.28	-0.14	0.68	0.49	0.79	0.66	-	-	-	-	-	-	-	-
s	0.58	0.80	0.70	0.67	0.67	0.84	0.61	0.70	0.46	0.69	0.72	-	-	-	-	-	-	-	-
b	0.77	0.69	0.73	0.09	0.72	0.68	0.85	0.71	0.35	0.82	0.86	-	-	-	-	-	-	-	-
sarcosine	0.82	1.15	1.20	1.32	1.19	1.45	0.76	0.92	0.79	0.74	0.76	-	-	-	-	-	-	-	-

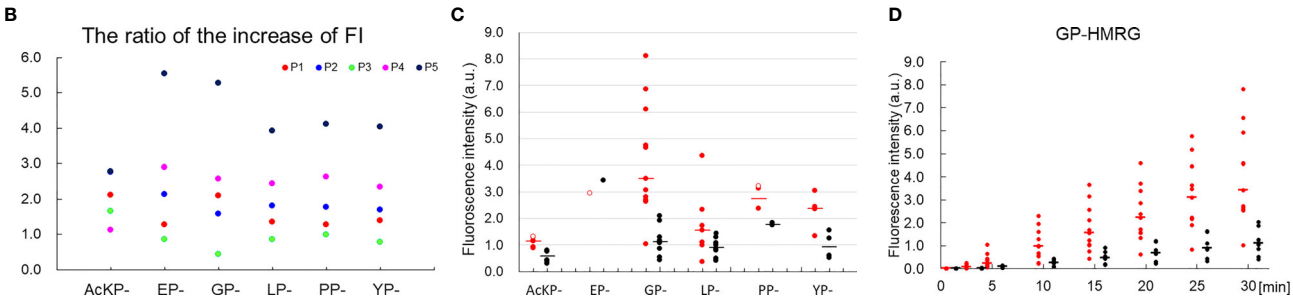

FIGURE 1 | Analysis of FI values of candidate probes in the primary and secondary selections using lysates and tissue fragments obtained from patients with pancreatic cancer. **(A)** The heatmap of the probe library with median differences/ratios of FI increase between cancer and non-cancer lysates for 309 candidate probes. The values ranked in the upper 90 percentile were indicated in yellow (FI differences), orange (FI ratios), or red (both). The number represents the median ratio of FI increase. P1 and P2 correspond the positions of amino acid residues of the probe P2-P1-HMRG. The lowercase letters represent the optical isomers of the amino acids. **(B)** The ratio of the FI increase between cancer and non-cancer lysates obtained from five patients using the selected six HMRG-based fluorescence probes. Probes with a dipeptide with prolyl residue at the P1 position (XaaP-HMRG) tend to show sufficient FI ratios between cancer and non-cancer samples. **(C)** The FI increase 30 min after addition of probe to tissue fragments. The difference in FI increase for 30 minutes tended to be high for GP-HMRG (median [range], 3.49 [1.03–8.11] a.u. *vs* 1.12 [0.42–2.09] a.u., P = 0.002; Wilcoxon's rank-sum test), followed by AcKP-HMRG (1.14 [0.87–1.29] a.u. *vs* 0.58 [0.29–0.78] a.u., P = 0.008), YP-HMRG (2.39 [1.33–3.04] a.u. *vs* 0.93 [0.52–1.54] a.u., P = 0.043), and LP-HMRG (1.55 [0.35–4.35] a.u. *vs* 0.91 [0.40–1.45] a.u., P = 0.093). The number of the cancer/non-cancer fragments (red filled circle/black filled circle) used in this evaluation was: AcKP- (5/6), EP- (0/1), GP- (11/8), LP-HMRG (7/8), PP- (2/2), and YP-HMRG (4/4). In one case, cancerous samples submitted to fluorescence imaging using EP-, PP-, and AcKP-HMRG were proved to be pancreatitis by final pathological evaluations (red empty circle) and excluded from the statistical analyses. Bars indicate median values. **(D)** Trends of FI increases of cancer tissues and noncancerous tissue fragments obtained from the 11 patients after the administration of GP-HMRG. Bars indicate median values.

TABLE 1 | Patients' demographic characteristics and outcomes of fluorescence imaging using GP-HMRG.

Patient	Age (y)	Sex	DM	NAC, (effect*)	Preoperative CA19-9 (IU/mL)	Surgical procedures	Histological type	TBR of FI
1	70	M	–	–	68	DP	Adenosquamous	3.44
2	83	F	+	–	55	DP	tub1 > tub2	2.06
3	63	M	–	–	9	PD	tub2 > tub1 > por	1.98
4	74	M	–	–	39	DP	tub2 > tub1	1.98
5	73	F	+	–	1	DP	tub1 > tub2	1.93
6	68	M	+	–	393	PD	tub2 > tub1	1.47
7	82	F	–	+, (1b*)	25	DP-CAR	tub1 > tub2	1.26
8	84	F	–	+, (1b*)	544	DP	tub1 > tub2**	1.13

DM, diabetic mellitus; NAC, neoadjuvant chemotherapy; PD, pancreaticoduodenectomy; DP, distal pancreatectomy; DP-CAR, distal pancreatectomy with celiac axis resection; TBR, tumor-to-background ratio; tub1/tub2, well/moderately differentiated tubular adenocarcinoma; por, poorly differentiated adenocarcinoma.

**Evans classification.*

***With perineural and lymphatic infiltration of viable cancer cells to the splenic artery.*

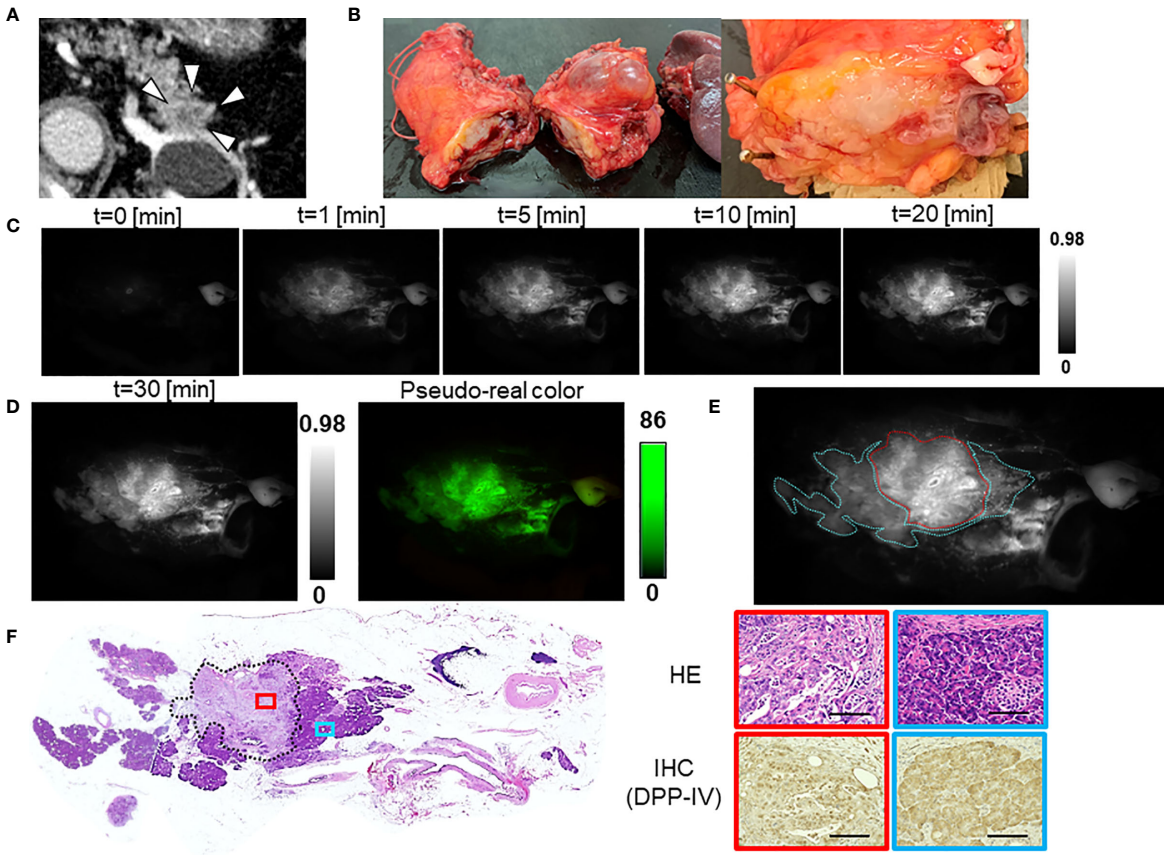

FIGURE 2 | Fluorescence imaging using GP-HMRG to analyze whole surgical specimens demonstrated homogenous increases in fluorescence signals emitted by pancreatic cancer tissues (Patient No. 2). **(A)** Preoperative contrast-enhanced computed tomography of pancreatic tail cancer (arrowheads). **(B)** Macroscopic image of the DP specimen after making cut surfaces of the tumor in the operation room (left). Right indicates magnified view of the cut surface including the tumor. **(C)** Increase of fluorescence signals after spraying GP-HMRG on the cut surface. **(D)** Fluorescence image (left) and its pseudo-real color image (right) of the cut surface 30 min after probe administration. **(E)** Relationships between fluorescence signals and distributions of cancer tissues (red dotted line) and surrounding pancreatic tissues (blue dotted line) according to histological findings. **(F)** Low-magnification histopathological image of hematoxylin–eosin (H&E) staining corresponding to fluorescence images (left, dotted line indicates cancer boundaries). Magnified views of H&E staining and IHC analysis of DPP-IV in cancer (red) and pancreatic (blue) tissues (right). Scale bar = 100 μm.

identify pancreatic cancer tissues. Fluorescence imaging using GP-HMRG sprayed onto cut surfaces of fresh resected specimens visualized cancer tissues as homogenous fluorescing regions with a high (>1.9) TBR in five of eight patients. Among the remaining three patients, fluorescence signals in cancer tissues were heterogenous and therefore insufficient for unambiguous discrimination from surrounding noncancerous tissues. However, in one patient who underwent preoperative chemotherapy, fluorescence imaging visualized grossly-unidentifiable cancer infiltrations around the splenic artery. These results suggest that fluorescence imaging using GP-HMRG potentially visualizes the spread of pancreatic cancer cells in real time, which may be useful for intraoperative diagnosis of surgical margins as well as for preoperative endoscopic evaluations of intraductal lesions.

The major advantage of using activatable probes is their ability to rapidly identify in real-time cancer tissues according to enzymatic activities, which are specifically expressed by cancer cells. Moreover, in the present series, an increase in fluorescence signals emitted by cancer tissues was identified 1 min after the topical administration of GP-HMRG. The FI values of cancer tissues in the remaining three patients may be decreased because of fewer viable cancer cells with fibrosis and mucinous changes, likely caused by preoperative chemotherapy.

Recently developed fluorescence imaging techniques for intraoperative identification of pancreatic cancer employ 5-aminolevulinic acid (27), indocyanine green (28), novel fluorophores targeting carbohydrate antigen 19-9 (CA19-9) (29), carcinoembryonic antigen (CEA) (30–35), epidermal growth factor receptor (EGFR) (36, 37), and insulin-like growth factor 1 receptor (IGF-1R) (38). However, these techniques, most of which involve systemic administration of "non-activatable" probes, usually require longer intervals for washout of fluorescence agents from background tissues, which may lead to lower TBRs compared with those of activatable probes topically administered during surgery.

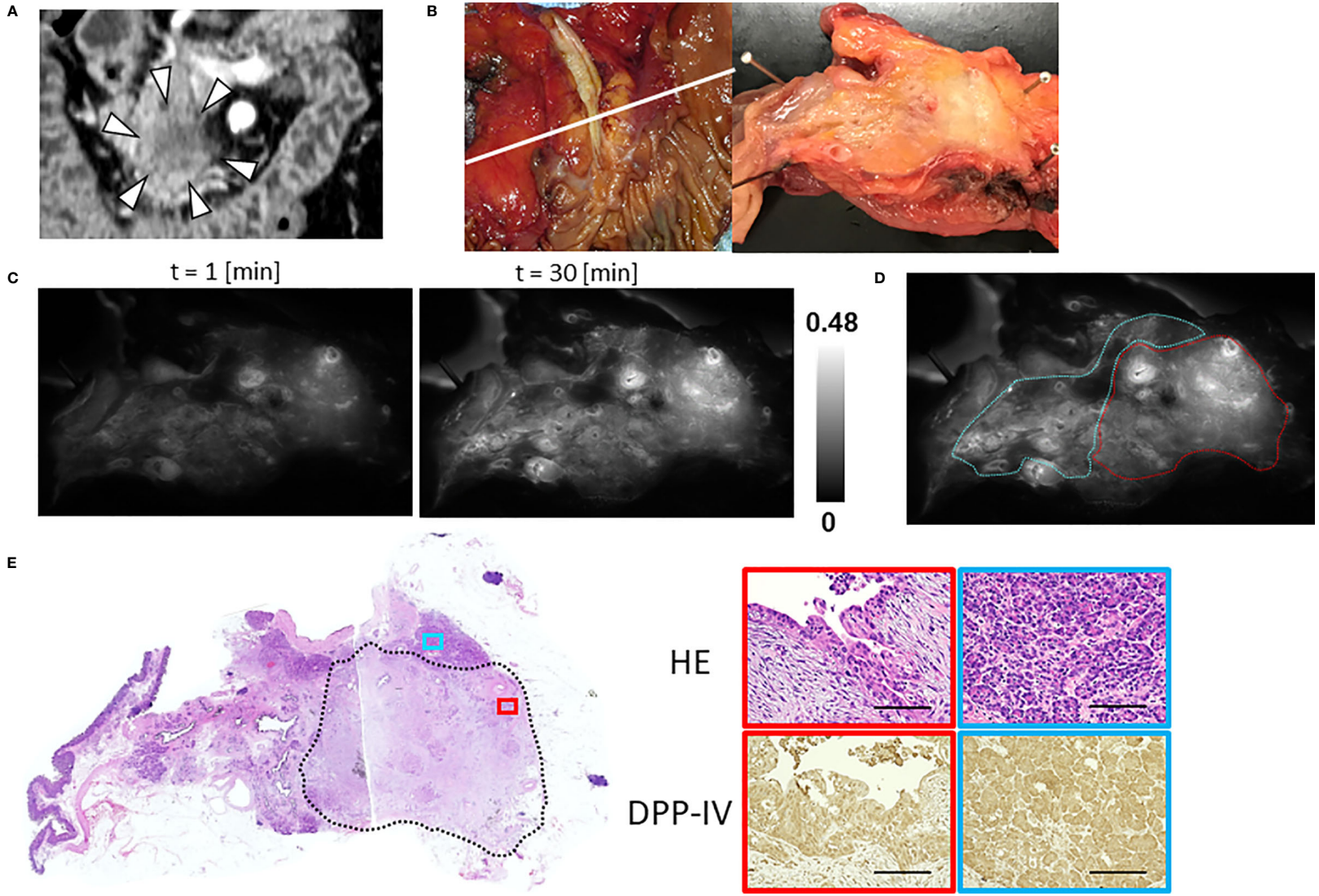

FIGURE 3 | Fluorescence imaging using GP-HMRG to probe whole surgical specimens demonstrates heterogenous increases in fluorescence signals emitted by pancreatic cancer tissues (Patient No. 6). **(A)** Preoperative contrast-enhanced computed tomography of pancreatic head cancer (arrowheads). **(B)** Macroscopic image of the PD specimen (left) and cut surface along the white line including the tumor (right). **(C)** Increase of fluorescence signals after spraying GP-HMRG on the cut surface. **(D)** Relationships between fluorescence signals and distributions of cancer tissues (red dotted line) and surrounding pancreatic tissues (blue dotted line) according to histological findings. **(E)** Low-magnification histopathological image of H&E staining corresponding to fluorescence images (left, dotted line indicates cancer boundaries). Magnified views of H&E staining and IHC analysis of DPP-IV in cancer (red) and pancreatic (blue) tissues (right). Scale bar = 100 μm.

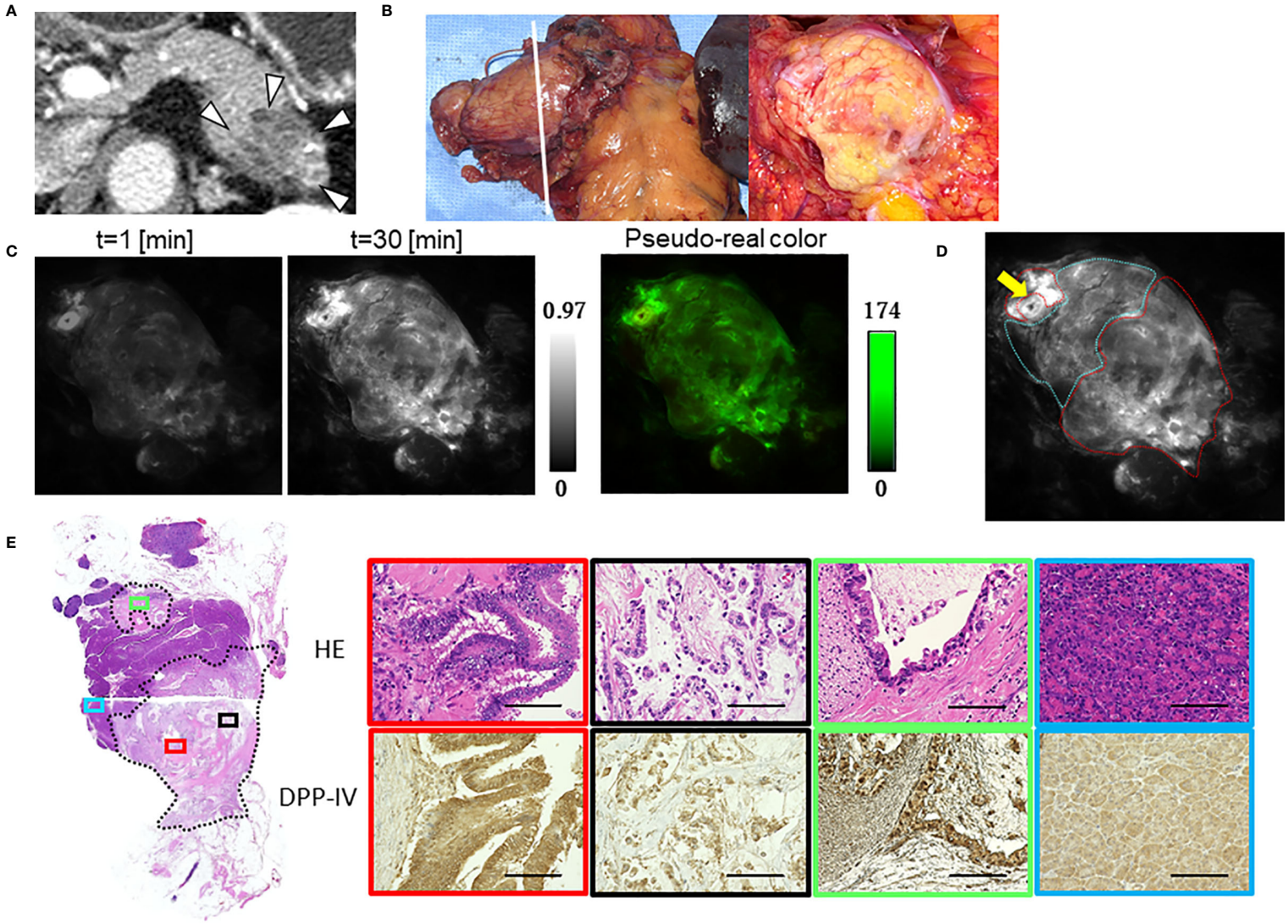

FIGURE 4 | Fluorescence imaging using GP-HMRG to probe whole surgical specimens demonstrates cancer infiltration to the splenic artery (Patient No. 8). **(A)** Preoperative contrast-enhanced computed tomography of pancreatic body cancer (arrowheads). **(B)** Macroscopic images of the DP specimen (left) and cut surface along the dotted line including the tumor (right). **(C)** Increase of fluorescence signals after spraying GP-HMRG on the cut surface and pseudo-real color image at 30 min. **(D)** Relationships between fluorescence signals and distributions of cancer tissues (red dotted line) and surrounding pancreatic tissues (blue dotted line) according to histological findings. Arrow indicates the splenic artery. **(E)** Low-magnification histopathological image of H&E staining corresponding to fluorescence images (left, dotted line indicates cancer boundaries). Magnified views of H&E staining and IHC analysis of DPP-IV showing fluorescence (red) and little fluorescence (black) emitted by parts of the main tumor, viable cancer infiltration around the splenic artery (green), and noncancerous pancreatic tissues (blue), (right). Scale bar = 100 μm.

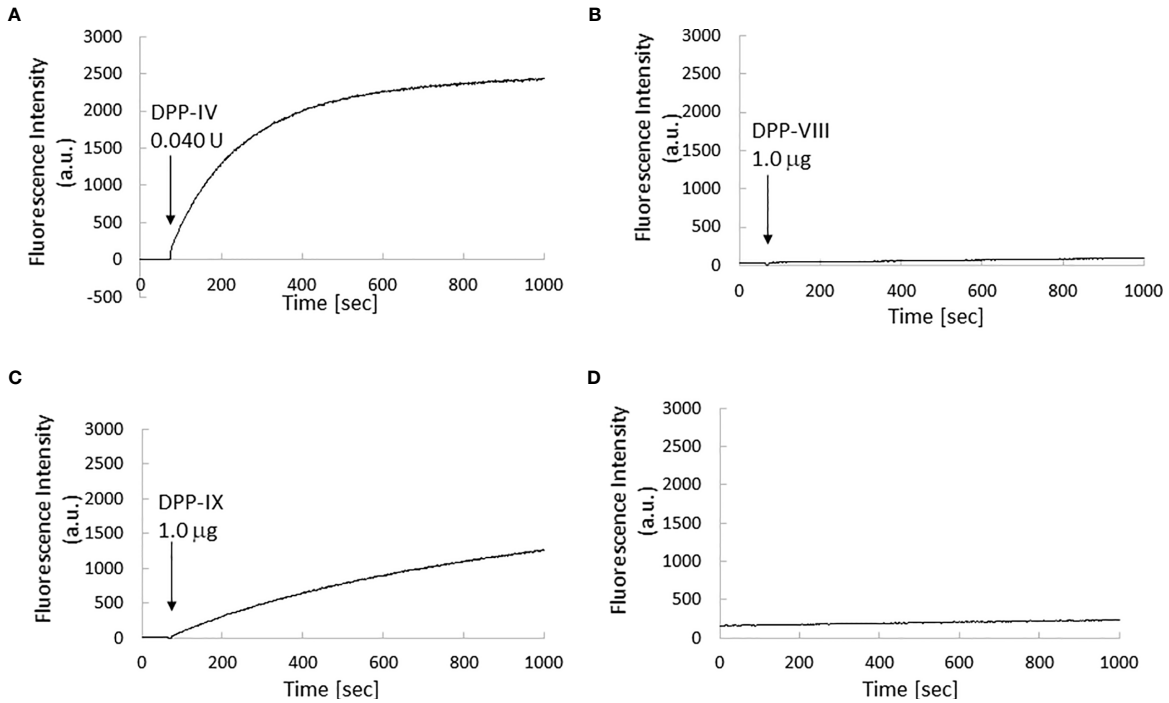

FIGURE 5 | Kinetics of fluorescence intensity of GP-HMRG upon enzyme addition. μ Excitation/emission wavelengths were 495 nm/525 nm. Trends of fluorescence intensities after adding DPP-IV (0.040 units, 0.013 units/ml; **(A)**, DPP-VIII (1.0 μg, 0.033 μg/ml; **(B)**, or DPP-IX (1.0 μg, 0.033 μg/ml; **(C)** to GP-HMRG. Increase of fluorescence intensity of GP-HMRG with no addition of enzymes was also demonstrated in panel **(D)**.

The present technique offers potential advantages for detecting tumor cells with high enzymatic activities specific to cancer tissues, which may facilitate prediction of a patient's sensitivity to chemotherapy and postoperative outcome, as previously suggested in case of fluorescence imaging of colorectal liver metastasis by gGlu-HMRG (17).

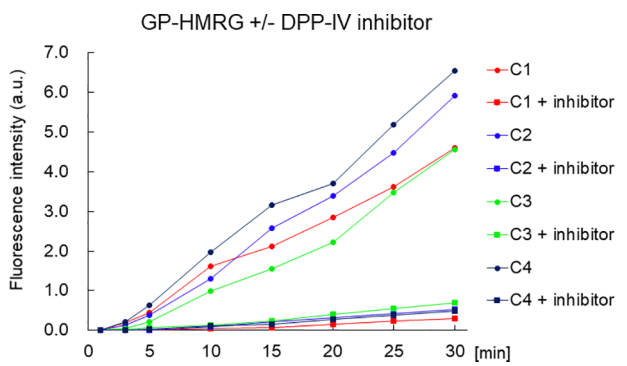

FIGURE 6 | The time course of the increase of FI of small cancer specimen with or without inhibitor. The fluorescence intensity of the pancreatic cancer specimen was decreased with DPP-IV inhibitor. The concentration of the DPP-IV inhibitor (K579, CalbioChem) was 100 μM.

The most likely candidate as a target enzyme of GP-HMRG is DPP-IV that cleaves the N-terminal residue of Xaa-Pro/Ala to regulate the bioavailability of glucose-insulinotropic peptide (GIP) and glucagon-like peptide-1 (GLP-1) (39). Other studies demonstrate the upregulation of DPP-IV in malignancies (40–42) such as pancreatic cancer (43), although IHC analysis here did not demonstrate unambiguous differences in the expression levels of DPP-IV between cancer tissues and noncancerous tissues, likely because of the different antibodies used to detect DPP-IV or for other technical reasons. Another candidate enzyme is DPP-IX, which is upregulated in pancreatic cancer tissues (43) and cleaves GP-HMRG, although IHC staining of DPP-IX expression sufficient for pathological analysis was unavailable.

The limitation of this study lies in its small sample size. With the sufficient number of lysates and tissue samples for robust statistical analyses, more promising fluorophores other than GP-HMRG might have been identified in the initial screening processes. Considering the heterogeneity of pancreatic cancers and factors affecting the enzymatic activities of cancer tissues, we must continue to conduct evaluation of the efficiency of GP-HMRG for fluorescence imaging to identify cancer tissue using an observer-blinded trial, as well as to predict postoperative outcomes of a larger population. Furthermore, the potentially insufficient levels of DPP-IV in cancer cells, as well as in stromal and Langerhans islets (43, 44), may decrease the sensitivity of cancer detection in certain patients. The expression status of

DPP-IV and DPP-IX must therefore be evaluated using IHC and the diced electrophoresis gel assay (DEG-Assay) (45).

In conclusion, fluorescence imaging using GP-HMRG may enable rapid and real-time visualization of pancreatic cancer through the detection of cancer tissue-specific enzymatic activities.

DATA AVAILABILITY STATEMENT

The raw data supporting the conclusions of this article will be made available by the authors, without undue reservation.

ETHICS STATEMENT

The studies involving human participants were reviewed and approved by The Institutional Review Board of the University of Tokyo Hospital (IRB No. 2957-[11]). The patients/participants provided their written informed consent to participate in this study. Written informed consent was obtained from the individual(s) for the publication of any potentially identifiable images or data included in this article.

AUTHOR CONTRIBUTIONS

RT, MS, and TI drafted the initial manuscript. RT and MS collected the samples, acquired the data, and performed the analysis. YK and MK prepared a library of activatable fluorescence probes. RT and MT evaluated the pathological extent of tumor. RT and YI performed immunohistochemistry, and MT evaluated the results. MK, TU, YU, and KH critically evaluated and revised the manuscript. All authors contributed to the article and approved the submitted version.

FUNDING

This work was supported by collaborative research funding between The University of Tokyo and NIPRO Corporation, and grants from the Ministry of Education, Culture, Sports, Science and Technology of Japan [Grant Number 19H05632 to YU]. The funder was not involved in the study design, collection, analysis, interpretation of data, the writing of this article or the decision to submit it for publication.

ACKNOWLEDGMENTS

We thank Drs. Yoshikuni Kawaguchi, Akihiko Ichida, Nobuhisa Akamatsu, Junichi Kaneko, and Junichi Arita for obtaining patients' informed consent; Dr. Eiichi Yasunaga for supporting sample collection; and Edanz Group (https://www.jp.edanz.com/ac) for editing a draft of this manuscript.

SUPPLEMENTARY MATERIAL

The Supplementary Material for this article can be found online at: https://www.frontiersin.org/articles/10.3389/fonc.2021.714527/full#supplementary-material

REFERENCES

1. Hidalgo M. Pancreatic Cancer. *N Engl J Med* (2010) 362(17):1605–17. doi: 10.1056/NEJMra0901557
2. Siegel RL, Miller KD, Jemal A. Cancer Statistics, 2020. *CA Cancer J Clin* (2020) 70(1):7–30. doi: 10.3322/caac.21590
3. Ferlay J, Colombet M, Soerjomataram I, Dyba T, Randi G, Bettio M, et al. Cancer Incidence and Mortality Patterns in Europe: Estimates for 40 Countries and 25 Major Cancers in 2018. *Eur J Cancer* (2018) 103:356–87. doi: 10.1016/j.ejca.2018.07.005
4. Chen W, Zheng R, Baade PD, Zhang S, Zeng H, Bray F, et al. Cancer Statistics in China, 2015. *CA Cancer J Clin* (2016) 66(2):115–32. doi: 10.3322/caac.21338
5. Wagner M, Redaelli C, Lietz M, Seiler CA, Friess H, Büchler MW. Curative Resection is the Single Most Important Factor Determining Outcome in Patients With Pancreatic Adenocarcinoma. *Br J Surg* (2004) 91(5):586–94. doi: 10.1002/bjs.4484
6. Demir IE, Jäger C, Schlitter AM, Konukiewitz B, Stecher L, Schorn S, et al. R0 *Versus* R1 Resection Matters After Pancreaticoduodenectomy, and Less After Distal or Total Pancreatectomy for Pancreatic Cancer. *Ann Surg* (2018) 268 (6):1058–68. doi: 10.1097/SLA.0000000000002345
7. Tummers WS, Groen JV, Sibinga Mulder BG, Farina-Sarasqueta A, Morreau J, Putter H, et al. Impact of Resection Margin Status on Recurrence and Survival in Pancreatic Cancer Surgery. *Br J Surg* (2019) 106(8):1055–65. doi: 10.1002/bjs.11115
8. Gillen S, Schuster T, Meyer Zum Büschenfelde C, Friess H, Kleeff J. Preoperative/neoadjuvant Therapy in Pancreatic Cancer: A Systematic Review and Meta-Analysis of Response and Resection Percentages. *PloS Med* (2010) 7(4):e1000267. doi: 10.1371/journal.pmed.1000267
9. Lutfi W, Talamonti MS, Kantor O, Wang CH, Liederbach E, Stocker SJ, et al. Perioperative Chemotherapy is Associated With a Survival Advantage in Early Stage Adenocarcinoma of the Pancreatic Head. *Surgery* (2016) 160 (3):714–24. doi: 10.1016/j.surg.2016.05.029
10. Verbeke C, Löhr M, Karlsson JS, Del Chiaro M. Pathology Reporting of Pancreatic Cancer Following Neoadjuvant Therapy: Challenges and Uncertainties. *Cancer Treat Rev* (2015) 41(1):17–26. doi: 10.1016/j.ctrv.2014.11.002
11. Urano Y, Sakabe M, Kosaka N, Ogawa M, Mitsunaga M, Asanuma D, et al. Rapid Cancer Detection by Topically Spraying a γ-Glutamyltranspeptidase-Activated Fluorescent Probe. *Sci Transl Med* (2011) 3(110):110ra119. doi: 10.1126/scitranslmed.3002823
12. Fujita K, Kamiya M, Yoshioka T, Ogasawara A, Hino R, Kojima R, et al. Rapid and Accurate Visualization of Breast Tumors With a Fluorescent Probe Targeting α-Mannosidase 2c1. *ACS Cent Sci* (2020) 6(12):2217–27. doi: 10.1021/acscentsci.0c01189
13. Ueo H, Shinden Y, Tobo T, Gamachi A, Udo M, Komatsu H, et al. Rapid Intraoperative Visualization of Breast Lesions With γ-Glutamyl Hydroxymethyl Rhodamine Green. *Sci Rep* (2015) 5:12080. doi: 10.1038/srep12080
14. Shinden Y, Ueo H, Tobo T, Gamachi A, Utou M, Komatsu H, et al. Rapid Diagnosis of Lymph Node Metastasis in Breast Cancer Using a New Fluorescent Method With γ-Glutamyl Hydroxymethyl Rhodamine Green. *Sci Rep* (2016) 6:27525. doi: 10.1038/srep27525
15. Onoyama H, Kamiya M, Kuriki Y, Komatsu T, Abe H, Tsuji Y, et al. Rapid and Sensitive Detection of Early Esophageal Squamous Cell Carcinoma With Fluorescence Probe Targeting Dipeptidylpeptidase IV. *Sci Rep* (2016) 6:26399. doi: 10.1038/srep26399
16. Yamamoto K, Ohnishi S, Mizushima T, Kodaira J, Ono M, Hatanaka Y, et al. Detection of Early Adenocarcinoma of the Esophagogastric Junction by

Spraying an Enzyme-Activatable Fluorescent Probe Targeting Dipeptidyl peptidase-IV. *BMC Cancer* (2020) 20(1):64. doi: 10.1186/s12885-020-6537-9
17. Miyata Y, Ishizawa T, Kamiya M, Yamashita S, Hasegawa K, Ushiku A, et al. Intraoperative Imaging of Hepatic Cancers Using γ-Glutamyltranspeptidase-Specific Fluorophore Enabling Real-Time Identification and Estimation of Recurrence. *Sci Rep* (2017) 7(1):3542. doi: 10.1038/s41598-017-03760-3
18. Hino H, Kamiya M, Kitano K, Mizuno K, Tanaka S, Nishiyama N, et al. Rapid Cancer Fluorescence Imaging Using A γ-Glutamyltranspeptidase-Specific Probe For Primary Lung Cancer. *Transl Oncol* (2016) 9(3):203–10. doi: 10.1016/j.tranon.2016.03.007
19. Mizushima T, Ohnishi S, Shimizu Y, Hatanaka Y, Hatanaka KC, Hosono H, et al. Fluorescent Imaging of Superficial Head and Neck Squamous Cell Carcinoma Using a γ-Glutamyltranspeptidase-Activated Targeting Agent: A Pilot Study. *BMC Cancer* (2016) 16:411. doi: 10.1186/s12885-016-2421-z
20. Mizushima T, Ohnishi S, Shimizu Y, Hatanaka Y, Hatanaka KC, Kuriki Y, et al. Rapid Detection of Superficial Head and Neck Squamous Cell Carcinoma by Topically Spraying Fluorescent Probe Targeting Dipeptidyl peptidase-IV. *Head Neck* (2018) 40(7):1466–75. doi: 10.1002/hed.25126
21. Sato C, Abe S, Saito Y, So Tsuruki E, Takamaru H, Makazu M, et al. A Pilot Study of Fluorescent Imaging of Colorectal Tumors Using a γ-Glutamyl-Transpeptidase-Activatable Fluorescent Probe. *Digestion* (2015) 91(1):70–6. doi: 10.1159/000369367
22. Hino R, Inoshita N, Yoshimoto T, Ogawa M, Miura D, Watanabe R, et al. Rapid Detection of Papillary Thyroid Carcinoma by Fluorescence Imaging Using a γ-Glutamyltranspeptidase-Specific Probe: A Pilot Study. *Thyroid Res* (2018) 11:16. doi: 10.1186/s13044-018-0060-y
23. Kitagawa Y, Tanaka S, Kamiya M, Kuriki Y, Yamamoto K, Shimizu T, et al. A Novel Topical Fluorescent Probe for Detection of Glioblastoma. *Clin Cancer Res* (2021)27(14):3936–47. doi: 10.1158/1078-0432
24. Eser S, Messer M, Eser P, von Werder A, Seidler B, Bajbouj M, et al. *In Vivo* Diagnosis of Murine Pancreatic Intraepithelial Neoplasia and Early-Stage Pancreatic Cancer by Molecular Imaging. *Proc Natl Acad Sci U S A* (2011) 108 (24):9945–50. doi: 10.1073/pnas.1100890108
25. Cruz-Monserrate Z, Abd-Elgaliel WR, Grote T, Deng D, Ji B, Arumugam T, et al. Detection of Pancreatic Cancer Tumours and Precursor Lesions by Cathepsin E Activity in Mouse Models. *Gut* (2012) 61(9):1315–22. doi: 10.1136/gutjnl-2011-300544
26. Li H, Li Y, Cui L, Wang B, Cui W, Li M, et al. Monitoring Pancreatic Carcinogenesis by the Molecular Imaging of Cathepsin E *In Vivo* Using Confocal Laser Endomicroscopy. *PloS One* (2014) 9(9):e106566. doi: 10.1371/journal.pone.0106566
27. Harada K, Murayama Y, Kubo H, Matsuo H, Morimura R, Ikoma H, et al. Photodynamic Diagnosis of Peritoneal Metastasis in Human Pancreatic Cancer Using 5-Aminolevulinic Acid During Staging Laparoscopy. *Oncol Lett* (2018) 16(1):821–8. doi: 10.3892/ol.2018.8732
28. Newton AD, Predina JD, Shin MH, Frenzel-Sulyok LG, Vollmer CM, Drebin JA, et al. Intraoperative Near-Infrared Imaging Can Identify Neoplasms and Aid in Real-Time Margin Assessment During Pancreatic Resection. *Ann Surg* (2019) 270(1):12–20. doi: 10.1097/SLA.0000000000003201
29. McElroy M, Kaushal S, Luiken GA, Talamini MA, Moossa AR, Hoffman RM, et al. Imaging of Primary and Metastatic Pancreatic Cancer Using a Fluorophore-Conjugated Anti-CA19-9 Antibody for Surgical Navigation. *World J Surg* (2008) 32(6):1057–66. doi: 10.1007/s00268-007-9452-1
30. Kaushal S, McElroy MK, Luiken GA, Talamini MA, Moossa AR, Hoffman RM, et al. Fluorophore-Conjugated Anti-CEA Antibody for the Intraoperative Imaging of Pancreatic and Colorectal Cancer. *J Gastrointest Surg* (2008) 12 (11):1938–50. doi: 10.1007/s11605-008-0581-0
31. Lwin TM, Murakami T, Miyake K, Yazaki PJ, Shivley JE, Hoffman RM, et al. Tumor-Specific Labeling of Pancreatic Cancer Using a Humanized Anti-CEA Antibody Conjugated to a Near-Infrared Fluorophore. *Ann Surg Oncol* (2018) 25(4):1079–85. doi: 10.1245/s10434-018-6344-6
32. Lwin TM, Miyake K, Murakami T, DeLong JC, Amirfakhri S, Filemoni F, et al. Fluorescent Humanized Anti-CEA Antibody Specifically Labels Metastatic Pancreatic Cancer in a Patient-Derived Orthotopic Xenograft (PDOX) Mouse Model. *Oncotarget* (2018) 9(99):37333–42. doi: 10.18632/oncotarget.26484
33. Hiroshima Y, Maawy A, Sato S, Murakami T, Uehara F, Miwa S, et al. Hand-Held High-Resolution Fluorescence Imaging System for Fluorescence-Guided Surgery of Patient and Cell-Line Pancreatic Tumors Growing Orthotopically in Nude Mice. *J Surg Res* (2014) 187(2):510–7. doi: 10.1016/j.jss.2013.11.1083
34. Hiroshima Y, Maawy A, Zhang Y, Murakami T, Momiyama M, Mori R, et al. Fluorescence-Guided Surgery, But Not Bright-Light Surgery, Prevents Local Recurrence in a Pancreatic Cancer Patient Derived Orthotopic Xenograft (PDOX) Model Resistant to Neoadjuvant Chemotherapy (NAC). *Pancreatology* (2015) 15(3):295–301. doi: 10.1016/j.pan.2015.02.008
35. Hoogstins CES, Boogerd LSF, Sibinga Mulder BG, Mieog JSD, Swijnenburg RJ, van de Velde CJH, et al. Image-Guided Surgery in Patients With Pancreatic Cancer: First Results of a Clinical Trial Using SGM-101, a Novel Carcinoembryonic Antigen-Targeting, Near-Infrared Fluorescent Agent. *Ann Surg Oncol* (2018) 25(11):3350–7. doi: 10.1245/s10434-018-6655-7
36. Tummers WS, Miller SE, Teraphongphom NT, Gomez A, Steinberg I, Huland DM, et al. Intraoperative Pancreatic Cancer Detection Using Tumor-Specific Multimodality Molecular Imaging. *Ann Surg Oncol* (2018) 25(7):1880–8. doi: 10.1245/s10434-018-6453-2
37. Tummers WS, Miller SE, Teraphongphom NT, van den Berg NS, Hasan A, Longacre TA, et al. Detection of Visually Occult Metastatic Lymph Nodes Using Molecularly Targeted Fluorescent Imaging During Surgical Resection of Pancreatic Cancer. *HPB (Oxford)* (2019) 21(7):883–90. doi: 10.1016/j.hpb.2018.11.008
38. Park JY, Lee JY, Zhang Y, Hoffman RM, Bouvet M. Targeting the Insulin Growth Factor-1 Receptor With Fluorescent Antibodies Enables High Resolution Imaging of Human Pancreatic Cancer in Orthotopic Mouse Models. *Oncotarget* (2016) 7(14):18262–8. doi: 10.18632/oncotarget.7576
39. Lambeir AM, Durinx C, Scharpé S, De Meester I. Dipeptidyl-Peptidase IV From Bench to Bedside: An Update on Structural Properties, Functions, and Clinical Aspects of the Enzyme DPP Iv. *Crit Rev Clin Lab Sci* (2003) 40 (3):209–94. doi: 10.1080/713609354
40. Havre PA, Abe M, Urasaki Y, Ohnuma K, Morimoto C, Dang NH. The Role of CD26/dipeptidyl Peptidase IV in Cancer. *Front Biosci* (2008) 13:1634–45. doi: 10.2741/2787
41. Cordero OJ, Salgado FJ, Nogueira M. On the Origin of Serum CD26 and its Altered Concentration in Cancer Patients. *Cancer Immunol Immunother* (2009) 58(11):1723–47. doi: 10.1007/s00262-009-0728-1
42. Ghersi G, Zhao Q, Salamone M, Yeh Y, Zucker S, Chen WT. The Protease Complex Consisting of Dipeptidyl Peptidase IV and Seprase Plays a Role in the Migration and Invasion of Human Endothelial Cells in Collagenous Matrices. *Cancer Res* (2006) 66(9):4652–61. doi: 10.1158/0008-5472.CAN-05-1245
43. Busek P, Vanickova Z, Hrabal P, Brabec M, Fric P, Zavoral M, et al. Increased Tissue and Circulating Levels of Dipeptidyl Peptidase-IV Enzymatic Activity in Patients With Pancreatic Ductal Adenocarcinoma. *Pancreatology* (2016) 16 (5):829–38. doi: 10.1016/j.pan.2016.06.001
44. Busek P, Hrabal P, Fric P, Sedo A. Co-Expression of the Homologous Proteases Fibroblast Activation Protein and Dipeptidyl Peptidase-IV in the Adult Human Langerhans Islets. *Histochem Cell Biol* (2015) 143(5):497–504. doi: 10.1007/s00418-014-1292-0
45. Komatsu T, Hanaoka K, Adibekian A, Yoshioka K, Terai T, Ueno T, et al. Diced Electrophoresis Gel Assay for Screening Enzymes With Specified Activities. *J Am Chem Soc* (2013) 135(16):6002–5. doi: 10.1021/ja401792d

Conflict of Interest: The authors declare that the research was conducted in the absence of any commercial or financial relationships that could be construed as a potential conflict of interest.

Publisher's Note: All claims expressed in this article are solely those of the authors and do not necessarily represent those of their affiliated organizations, or those of the publisher, the editors and the reviewers. Any product that may be evaluated in this article, or claim that may be made by its manufacturer, is not guaranteed or endorsed by the publisher.

Advantages of publishing in Frontiers

OPEN ACCESS
Articles are free to read for greatest visibility and readership

FAST PUBLICATION
Around 90 days from submission to decision

HIGH QUALITY PEER-REVIEW
Rigorous, collaborative, and constructive peer-review

TRANSPARENT PEER-REVIEW
Editors and reviewers acknowledged by name on published articles

Frontiers
Avenue du Tribunal-Fédéral 34
1005 Lausanne | Switzerland

Visit us: www.frontiersin.org
Contact us: frontiersin.org/about/contact

REPRODUCIBILITY OF RESEARCH
Support open data and methods to enhance research reproducibility

DIGITAL PUBLISHING
Articles designed for optimal readership across devices

FOLLOW US
@frontiersin

IMPACT METRICS
Advanced article metrics track visibility across digital media

EXTENSIVE PROMOTION
Marketing and promotion of impactful research

LOOP RESEARCH NETWORK
Our network increases your article's readership